Errata

Throughout:	replace υ with ν
p iii, line 13	"Hoffman" becomes "Hoffmann"
p vi, line 2	"enthusiasum" becomes "enthusiasm"
p vii	"diphenyllarsino" becomes "diphenylarsino"
	dmba = dimethylbenzylamine-C^2,N
	DPP = differential pulse polarography
p 29, line 2	...coupling of a bridging phosphido...
p 35, line 19	...virtue of having four...
p 40, line 1	"provides" becomes "provide"
p 54, line 5	"Section 1.2.4." becomes "Section 1.2.6.1."
line 8	"excellent reviews" becomes "an excellent review"
p 55, line 13	"isocyanate coordinated" becomes "isocyanide coordinated"
line 15	"Scheme 1.2.25." becomes "Scheme 1.2.56."
line 20	"Scheme 1.2.56." becomes "Scheme 1.2.57."
p 68, line	"label" becomes "labelling"
p 66, line 5	"TPDE" becomes "TPD"
p 78, line 4	"PTol" becomes "PC_6H_4Me-4"
p 83, Table	"Very Miixed" becomes "Very Mixed"
p 85, line 3	insert space after $[Cr(CO)_3]$
line 7	"1.3.5." becomes "1.3.6."
p 87, line 3	"products" becomes "reactions"
line 7	"identifie" becomes "identified"
pp 88-96	"Y. T. Struchov" becomes "Yu. T. Struchov", "O. Y. Okhlobystin" becomes "O. Ya. Okhlobystin", "Y. V Rakitin" becomes "Yu. V Rakitin", "Y. L. Slovokhotov" becomes "Yu. L. Slovokhotov"
p 93	V. F. Kuznetsov
	Ref 133 pp 351-385
	Ref 190 "*IInt.*" becomes "*Int.*"
p 121, line 11	"η^2-cod" becomes "η^4-cod"
pp 121, 124	"pyl" becomes "py"
p 126, line 3	"dpp" becomes "dppee"
p 128, line 1	"A isostructural" becomes "An isostructural"
p 134, line 4	...substitution of carbonyl ligand in **1**...
line 12	"geoemtry" becomes "geometry"
p 139, line 14	"diplaced" becomes "displaced"
p 144	"...(η^5-$P_3C_2Bu^t_2$]" becomes "...(η^5-$P_3C_2Bu^t_2$)]"
p 152, line 18	"are separable" becomes "were separable"
p 158, line 28	...with that of the precursor cluster...
p 157, line 1	"Selected" becomes "selected"
p 159, line 24	"Unversity of Southern Malalysia, Malaysia" becomes "Universiti Sains Malaysia, Minden, Penang"
p 167, line 17	"$[CpWIr_3(\mu\text{-}CO)_3(\mu\text{-}dppb)(CO)_6]$" becomes "$[CpWIr_3(\mu\text{-}CO)_3(\mu\text{-}pdpp)(CO)_6]$"
p 175	Ref 60 "J. Chem. Cryst." becomes "J. Chem. Crystallog."
p 194, line 1	The carbonyl region of the room temperature ^{13}C NMR spectrum...
p 200, line 10	...W-ligated carbonyls a, a'...

p 241, line 10	"they" becomes "the configurations" of **22a** and **22b**"
p 253, line 4	"an" becomes "and"
p 302	Second "Figure 3.2.75." becomes "Figure 3.2.76.", "^{131}P NMR becomes "^{31}P NMR"
p 321,	Ref 9 pp 303-327 Ref 10 pp 471-543
p 322	Ref 49 "Pöe" becomes "Poë"
p 334, line 4	"face capping" becomes "face-capping"
line 5	"bridging" becomes "edge-bridging"
p 335, line 1	"$RuCl_3.3H_20$" becomes "$RuCl_3.3H_2O$"
line 11	"leadsto" becomes "leads to"
pp 379-81	Ref 5 "Vinas" becomes "Viñas" Ref 78 "Srähle" becomes "Strähle" Ref 83 p 188

Some Chemistry of Tungsten-Iridium Carbonyl Clusters

Susan Maree Waterman

B.Sc.(Hons)

A Thesis submitted for the degree of
Doctor of Philosophy
of the
Australian National University
1998

Contents

Summary . . . . . *iii*

Statement v

Acknowledgements . . . . . *vi*

Abbreviations and Comment . . . . . *vii*

Published Results . . . . . *ix*

Chapter 1

"Very Mixed"-Metal Carbonyl Clusters. 1

Chapter 2

Substitution Reactions of Tungsten - Iridium Clusters. 97

Chapter 3

NMR Studies of Tungsten - Iridium Clusters. 176

Chapter 4

Other Chemistry of Tungsten - Iridium Clusters 323

Summary

Transition metal carbonyl clusters have attracted interest for a number of reasons. The oil crisis of the mid-1970's encouraged interest in clusters as pre-catalysts or models for catalysis, and this has been an enduring theme in cluster research since that time. The multimetallic coordination of organic molecules at clusters facilitates substrate transformations not readily achievable at mononuclear complexes. As clusters become progressively larger in size, they may be expected to adopt metallic character, and the intermediacy of a "metametallic" state has been proposed. The preeminent factor controlling the development of areas of cluster chemistry has been the existence or otherwise of efficient routes into the clusters themselves. Most early syntheses were of the "heat it and hope" type which, not surprisingly, has been effective for a range of homometallic clusters but is less useful for mixed-metal clusters. In the last twenty years, general procedures to synthesize mixed-metal clusters have become available, due largely to the poineering theoretical analyses by Hoffman, Mingos and others, and the experimental advances of Stone, Vahrenkamp, and their research groups.

An isostructural series of clusters in which ligated metal fragments are sequentially replaced by isolobal fragments with different metals affords the possibility to assess the impact of heterometal incorporation upon reactivity, product distribution, fluxionality and other properties. The tetrahedral mixed-metal clusters $[CpWIr_3(CO)_{11}]$ and $[Cp_2W_2Ir_2(CO)_{10}]$ are conceptually derived from the "parent" tetrairidium cluster $[Ir_4(CO)_{12}]$ by replacement of one or two $[Ir(CO)_3]$ vertices with one or two $[CpW(CO)_2]$ units, respectively, and a comparison of reactivity and fluxionality across this series of complexes forms the theme of this Thesis.

A focus of the studies described in Chapter 2 is to understand the ligand substitution chemistry of the "very mixed"-metal clusters $[CpWIr_3(CO)_{11}]$ and $[Cp_2W_2Ir_2(CO)_{10}]$ towards a variety of ligands such as phosphines, phosphites, phospholes and isocyanides and benchmark the results against the well-established chemistry of the tetrairidium system. The substitution chemistry of $[CpWIr_3(CO)_{11}]$ and $[Cp_2W_2Ir_2(CO)_{10}]$ reveals greatly enhanced reactivity compared to $[Ir_4(CO)_{12}]$. Ligand substitution proceeds in a stepwise fashion, usually at room temperature, in contrast to $[Ir_4(CO)_{12}]$ where similar ligand replacement requires elevated temperatures to proceed. Introduction of $[CpW(CO)_2]$ into the tetrahedral core introduces possible isomers in the carbonyl-bridged form. Structurally characterized examples of seven different coordination geometries of tetrahedral tungsten-iridium clusters have been obtained.

Fluxionality on ligand-substituted derivatives of $[Ir_4(CO)_{12}]$ has been the subject of extensive investigation. Introduction of a heterometal (as in the ligand-substituted derivatives of $[CpWIr_3(CO)_{11}]$ and $[Cp_2W_2Ir_2(CO)_{10}]$) lowers the molecular symmetry and provides a label to facilitate assignment and to monitor carbonyl scrambling. NMR studies of ligand fluxionality at $[CpWIr_3(CO)_{11}]$ and $[Cp_2W_2Ir_2(CO)_{10}]$ and their derivatives are described in Chapter 3, and compared to the established fluxional processes at $[Ir_4(CO)_{12}]$ derivatives.

Chapter 4 describes some examples of orthometalation of the triphenylphosphine derivatives of $[CpWIr_3(CO)_{11}]$ and some controlled routes to higher nuclearity tungsten-iridium clusters. The reactivity of $[CpWIr_3(CO)_{11}]$ and $[Cp_2W_2Ir_2(CO)_{10}]$ towards terminal acetylenes and metal acetylides is reported, and the chemistry of the two clusters compared and contrasted.

Statement

I certify that the content of this Thesis has never been submitted for any degree and is not currently being submitted for any other degree or qualification, that all the work and results described are original unless due reference is made, and that any help received has been acknowledged.

Susan M Waterman 18/12/98

Susan M. Waterman

Acknowledgements

I wish to express my gratitude to my supervisor, Dr Mark Humphrey, for his guidance, patience, encouragement and unwavering enthusiasum.

My appreciation and gratitude to Dr David C. R. Hockless, Assoc. Prof. Allan H. White and Dr Brian W. Skelton for their crystallographic input.

Thanks are due to Dr Max Keniry and the staff of the University Nuclear Magnetic Resonance Centre for their assistance with the EXSY experiments. Special thanks go to Dr. Graham Ball for assistance with the specialized nuclear magnetic resonance experiments, and for allowing me to work within the NMR Facility at the University of New South Wales. Many thanks go to Prof. Brian Mann (University of Sheffield) for the helpful discussions and advice.

I would also like to personally thank my colleagues Marie, Ian, Andrew, Raina, Nigel, Steve and Joe, and the technical staff of the ANU Chemistry Department.

Lastly, special thanks go to my family and friends for support and encouragement through my years of study.



Abbreviations

General

arphos	1-(diphenyllarsino),-2-(diphenylphosphino)ethane
atm	atmosphere
bipy	2,2'-bipyridyl
Bu^t	tertiary butyl
Bu^n	normal butyl
ca	approximately
cod	1,5-cyclooctadiene
cot	1,3,5,7-cyclooctatraene
Cp	η^5-cyclopentadienyl
Cp'	η^5-methylcyclopentadienyl
Cp^*	η^5-pentamethylcyclopentadienyl
CV	cyclic voltammetry
Cy	cyclohexyl
diars	1,2-bis(dimethylarsino)benzene
DCP	d.c. polarograph
dmat	2-(dimethylethylamino)toluene-*C*,*N*
dmba	dimethyl benzlamine-C^2,*N*
dmpe	1,2-bis(dimethylphosphino)ethane
dpam	bis(diphenylarsino)methane
DPP	different pulse polarography
dppee	1,2-*cis*-bis(diphenylphosphino)ethene
dppa	1,2-bis(diphenylphosphino)acetylene
dppb	1,4-bis(diphenylphosphino)butane
dppe	1,2-bis(diphenylphosphino)ethane
dppm	bis(diphenylphosphino)methane
dppp	1,3-bis(diphenylphosphino)propane
ECE	electrochemical-chemical-electrochemical
ESR	electron spin resonance
Et	ethyl
EXAFS	extended x-ray absorption fine structure
IR	infrared
$[M]^+$	molecular ion
Me	methyl

MePy	methylpyridine
MS	mass spectrometry
nbd	norbornadiene
^{n}Bu	normal butyl
NMR	nuclear magnetic resonance
pdpp	1,2-bis(diphenylphosphino)benzene
	(or phenylene 1,2-diphenylphosphine)
phen	1,10-phenanthroline
Ph	phenyl
Pr	propyl
Pr^{i}	*iso*-propyl
py	2-pyridylphosphine
pz	pyrazolyl
^{t}Bu	tertiary butyl
TEM	Transmission Electron Microscopy
thf	tetrahydrofuran
tlc	thin-layer chromatography
TPD	temperature-programmed desorption/decomposition
TPR	temperature-programmed reduction
XANES	x-ray absorption near-edge spectroscopy
triphos	bis{2-(diphenylphosphino)ethyl}phenylphosphine
Xy	*meta*-xylyl

IR Assignments

br	broad
m	medium
s	strong
sh	shoulder
vs	very strong
vw	very weak

NMR Assignments

br	broad
d	doublet
dd	doublet of doublets
m	multiplet
s	singlet
t	triplet

Published Results

Some of the results presented in this Thesis have been published:

Waterman, S.M., Humphrey, M.G., Tolhurst, V.-A., Hockless, D.C.R., Skelton, B.W. and White, A.H. Organometallics, **1996**, *15*, 934-40.
Mixed-Metal Cluster Chemistry. 2. Site-Selective Substitution of $[CpWIr_3(CO)_{11}]$ by Phosphines; X-ray Crystal Structures of $[CpWIr_3(\mu\text{-}CO)_3(CO)_7(PPh_3)]$, $[CpWIr_3(\mu\text{-}CO)_3(CO)_6(PPh_3)_2]$ and $[CpWIr_3(\mu\text{-}CO)_3(CO)_7(PMe_3)]$.

Waterman, S.M., Humphrey, M.G., Tolhurst, V.-A., Skelton, B.W. and White, A.H. J. Organomet. Chem., **1996**, *515*, 89-98.
Mixed-Metal Cluster Chemistry III. P-C Activation at Tungsten-Triiridium Cores; X-ray Crystal Structures of $[CpWIr_3\{\mu_3\text{-}\eta^2\text{-}PPh(C_6H_4)\}(\mu\text{-}CO)_2(CO)_7]$ and $[CpWIr_3\{\mu_3\text{-}\eta^2\text{--}PPh(C_6H_4)\}(\mu\text{-}CO)_2(CO)_6(PPh_3)]$.

Waterman, S.M., Humphrey, M.G. and Hockless, D.C.R. Organometallics, **1996**, *15*, 1745-48.
Mixed-Metal Cluster Chemistry. 4. Synthesis and X-ray structure of $[Cp_3W_3Ir_4(\mu\text{-}H)(CO)_{12}]$.

Waterman, S.M., Humphrey, M.G. and Hockless, D.C.R. J. Organomet. Chem., **1998**, *555*, 25-33.
Mixed-Metal Cluster chemistry VIII: phosphite substitution at $[CpWIr_3(CO)_{11}]$; X-ray crystal structure of $[CpWIr_3(\mu\text{-}CO)_3(CO)_6\{P(OPh)_3\}_2]$.

Waterman, S.M., Humphrey, M.G. and Hockless, D.C.R. J. Organomet. Chem., **1998**, *565*, 81-95.
Mixed-Metal Cluster Chemistry IX: Alkylarylphosphine Derivatives of $[CpWIr_3(CO)_{11}]$; X-ray structure of $[CpWIr_3(\mu\text{-}CO)_3(CO)_7(PMe_2Ph)]$.

Waterman, S.M. and Humphrey, M.G. Organometallics, *submitted for publication.*
Mixed-Metal Cluster Chemistry. 10. Syntheses, Isomer Distribution and Fluxionality Studies of $[CpWIr_3(\mu\text{-}CO)_3(CO)_{8-n}(PR_3)_n]$ (n = 1, 2; R = Ph, Me).

Waterman, S.M., Humphrey, M.G., Tolhurst, V-A., Bruce, M.I., Low, P.J. and Hockless, D.C.R. Organometallics, *in press.*
Mixed-Metal Cluster Chemistry XI: Reactions of Tungsten-Iridium Clusters with Terminal Alkynes and Tungsten Acetylides; X-ray crystal structures of $[Cp_2W_2Ir_2(\mu_4\text{-}\eta^2\text{-}HC_2Ph)(\mu\text{-}CO)_4(CO)_4]$ *and* $[Cp_2W_2Ir_3(\mu_4\text{-}\eta^2\text{-}C_2C_6H_4Me\text{-}4)(\mu\text{-}CO)(CO)_9]$.

Waterman, S.M., Humphrey, M.G. and Hockless, D.C.R. J. Organomet. Chem., **1998**, *in press.*
Mixed-Metal Cluster Chemistry XII: isocyanide derivatives of $[CpWIr_3(CO)_{11}]$*; X-ray crystal structure of* $[CpWIr_3(CO)_9(CNC_6H_3Me_2\text{-}2,6)_2]$.

Waterman, S.M., Humphrey, M.G., Ball, G.E. and Hockless, D.C.R. Organometallics, *submitted for publication.*
Mixed-Metal Cluster Chemistry. 13. Syntheses, Isomer Distribution and Fluxionality Studies of $[Cp_2W_2Ir_2(\mu\text{-}CO)_3(CO)_{7-n}(PR_3)_n]$ *(n = 1, 2; R = Ph, Me); X-ray Crystal Structure of* $[Cp_2W_2Ir_2(\mu\text{-}CO)_3(CO)_6(PPh_3)]$.

Waterman, S.M., Humphrey, M.G. and Hockless, D.C.R. J. Organomet. Chem., *submitted for publication.*
Mixed-Metal Cluster Chemistry XIV: Reaction of $[Cp_2W_2Ir_2(CO)_{10}]$ *with trimethylphosphite; X-ray crystal structures of* $[Cp_2W_2Ir_2(\mu\text{-}CO)_3(CO)_5\{P(OMe)_3\}_2]$ *and two modifications of* $[CpWIr_3(\mu\text{-}CO)_3(CO)_7\{P(OMe)_3\}]$.

Waterman, S.M., Humphrey, M.G. and Lee, J. J. Organomet. Chem., *submitted for publication.*
Mixed-Metal Cluster Chemistry 15: bidentate phosphine derivatives of $[Cp_2W_2Ir_2(CO)_{10}]$.

Waterman, S. M., Lucas, N. T. and Humphrey M. G. Adv. Organomet. Chem., *in press.*
"Very Mixed"-Metal Carbonyl Clusters.

Chapter 1

"Very Mixed"-Metal Carbonyl Clusters

Chapter 1

"Very Mixed"-Metal Carbonyl Clusters

Contents

1.1. Introduction....3

1.2. Reactivity Studies....4

1.2.1. General Comments....4

1.2.2. Ligand Substitution....4

1.2.2.1. P-Donor Ligands....4

1.2.2.2. Other Ligands....11

1.2.3. Ligand Addition....15

1.2.4. Ligand Tansformations....17

1.2.4.1.C-Donor Ligands....19

1.2.4.2. Other Ligands....25

1.2.5. Core Transformations....29

1.2.5.1. Metal Exchange....30

1.2.5.2. Core Expansion or Core Contraction....40

1.2.6. Catalytic Studies....54

1.2.6.1. Modelling Catalysis....54

1.2.6.2. Homogeneous Catalysis....58

1.2.6.3. Heterogeneous Catalysis....65

1.3. Physical Measurements....68

1.3.1. General Comments....68

1.3.2. Fluxionality....68

1.3.3. Electrochemistry....75

1.3.4. Other Physical Methods....82

1.3.4.1 Magnetic Measurements....82

1.3.4.2 MO Studies....83

1.4. Conclusion and Outlook....87

1.5. References....88

1.1. Introduction

Transition metal carbonyl clusters have attracted interest for a number of reasons.[1] The oil crisis of the mid-1970's encouraged interest in clusters as pre-catalysts or models for catalysis, and this has been an enduring theme in cluster research since that time. The multimetallic coordination of organic molecules at clusters facilitates substrate transformations not readily achievable at mononuclear complexes. As clusters become progressively larger in size, they may be expected to adopt metallic character, and the intermediacy of a "metametallic" state has been proposed.[2]

The preeminent factor controlling the development of areas of cluster chemistry has been the existence or otherwise of efficient routes into the clusters themselves. Most early syntheses were of the "heat it and hope" type which, not surprisingly, has been effective for a range of homometallic clusters but is less useful for mixed-metal clusters. In the last twenty years, general procedures to synthesize mixed-metal clusters have become available, due largely to the pioneering theoretical analyses by Hoffman, Mingos and others, and the experimental advances of Stone, Vahrenkamp, and their research groups.[3-7] Access to a range of mixed-metal clusters affords the possibility to assess the significance of the heterometallic environment on a number of properties (substrate activation, site selectivity, ligand mobility, electrochemical responses, etc) but thus far most reports have focussed on synthetic and structural studies; systematic reactivity studies and investigations of physical properties are comparatively rare.

A significant number of mixed-metal clusters contain metals from the same group or adjacent groups, but far fewer mixed-metal clusters incorporating disparate metals have been reported. This is surprising, as synthetic procedures to afford such clusters are now well-established, and a number of the properties listed above would be expected to show sharp differences to homometallic clusters if the heterometal is very different. For example, coupling an electropositive metal and electronegative metal to give a polar metal-metal bond may enhance substrate activation, and metalloselectivity for a range of reagents, and should affect activation energies for fluxional processes (which may facilitate their discrimination when more than one process is possible). Many heterogeneously-catalyzed transformations couple early to mid-transition metals with late transition metals, and clusters comprised of these metals may be effective pre-catalysts. A number of reviews of heterometallic clusters have appeared,[8-12] but the focus has largely been on mixed-metal clusters containing similar metals, or on synthetic and structural aspects. A review summarizing synthetic and reactivity aspects of group 6 - group 9 heterometallic clusters has recently appeared.[13] This review focuses on the reactivity and physical properties of "very mixed"-metal clusters, defined as those containing transition metals separated by three or more d-block groups, for groups 4-10. While this definition is somewhat arbitrary, it ensures that platinum group metals (PGM) are coupled to non-PGM.

1.2. Reactivity Studies

1.2.1. General Comments

Ligand activation and transformation at heterometallic clusters has been reviewed but, at the time, few examples of "very mixed"-metal clusters effecting the transformations were identified.[14] As mentioned above, major interests in the reactivity of "very mixed"-metal clusters are the possibility of directing reagents to particular sites (metallo-, bond- or face-specificity), enhanced substrate activation, and substrate transformation utilizing the polar metal-metal bonds or unique heterometallic environment. While the reactivity classifications below are self-explanatory, some overlap is unavoidable; substitution reactions frequently proceed by associative mechanisms, with intermediates corresponding to ligand addition, and certain types of metal exchange reactions can occur by way of core-expanded intermediates. A number of studies modelling catalysis involve ligand transformations, and so have been mentioned briefly in both relevant Sections.

1.2.2. Ligand Substitution

The presence of differing metals introduces the possibility of metalloselectivity into ligand substitution; this selectivity should be enhanced upon accentuating the disparity between the metals. The introduction of heterometals into a cluster core also reduces the effective symmetry over that of related homometallic clusters, rendering coordination sites for incoming ligands inequivalent, and affording the prospect of site- as well as metallo-selectivity. Attempts by Vahrenkamp and others to define a "hierachy of site reactivities" in mixed-metal clusters have met with some success but, although a sequence of substitution labilities by core metal can be defined, isolated products often differ from those predicted due to donor ligand mobility.[15] The majority of ligand substitution studies of "very mixed"-metal clusters have involved phosphines, and these are summarized in Section 1.2.1.1. All other ligands are considered in Section 1.2.2.1.

1.2.2.1. P-Donor Ligands

Phosphines are amongst the most fundamental of organometallic reagents. Their availability with a broad range of steric and electronic properties provides the possibility of carrying out systematic investigations of site- and metallo-selectivity, but there are few studies which have defined the substitution sites of a range of phosphines at a "very mixed"-metal cluster; instead, phosphines have frequently been employed solely to enhance the prospects of obtaining samples suitable for single crystal X-ray studies. The results of phosphine substitution at "very mixed"-metal clusters are summarized in Table 1.2.1.

Studies of phosphine substitution have thus far focussed almost exclusively on small (M_n, n = 3 or 4) clusters, with all trimetallic examples pseudotetrahedral by virtue of a μ_3-capping ligand. The group 6 - group 9 clusters $[MCo_2(\mu_3\text{-}CR)(CO)_8(\eta^5\text{-}Cp)]$ (M = Mo, W; R = Me, C_6H_4Me-4, CO_2menthyl; Cp = C_5H_5, $C_5H_4Pr^i$, $C_5H_4SiMe_3$, C_9H_7) have been reacted with phosphites, and monodentate and bidentate phosphines to afford cobalt-ligated products,[16-18] although for most of the derivatives the specific substitution sites were not defined, and $[WCo_2(\mu_3\text{-}CMe)(CO)_7(PHPh_2)(\eta^5\text{-}C_5H_5)]$ was not isolated but is a presumed reaction intermediate *en route* to P-H activation (Section *1.2.4.2.*). NMR studies have clarified the structures of the (+)-methylester-containing derivatives (Figure 1.2.1.), with the bidentate arphos and monodentate $P(OMe)_3$ ligating at equatorial sites (with respect to the $MoCo_2$ plane) and the bulky PCy_3 proposed to ligate at an axial site; significantly, the cobalt atoms are diastereotopic, and metalloselectivity between the cobalt atoms increases on increasing the ligand cone angle from the phosphite (no discrimination) to the phosphine (3 : 1 mixture of diastereomers obtained).

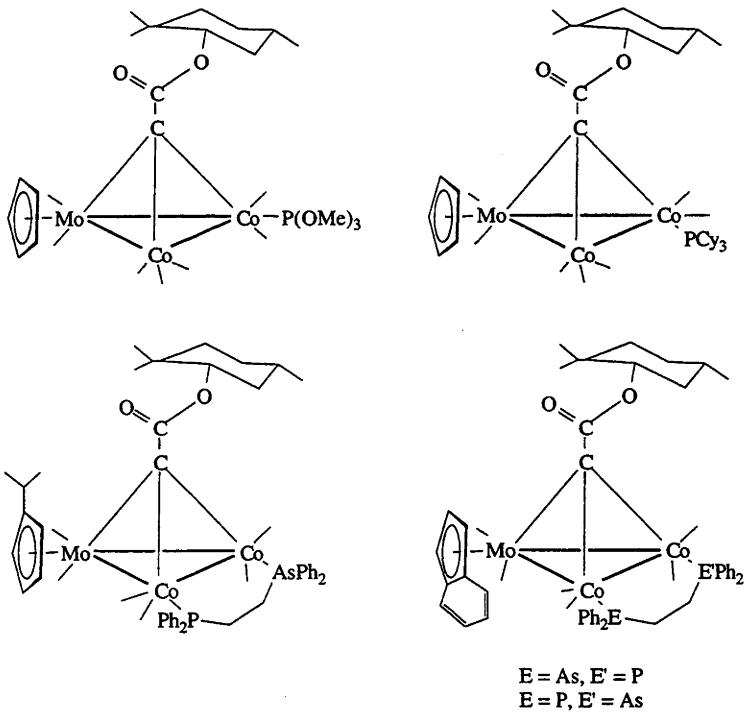


Figure 1.2.1.

$[W_2Ir(\mu_3\text{-}CC_6H_4Me\text{-}4)(\mu\text{-}CC_6H_4Me\text{-}4)(Cl)(CO)_4(\eta^5\text{-}C_5H_5)_2]$ reacted with PPh_3 to afford an iridium-ligated product, but the site of substitution was not determined.[19] The other trimetallic clusters to have been investigated are all chiral by virtue of four differing core constituents. The group 6 - group 8 - group 9 clusters $[MFeCo(\mu_3\text{-}S)(CO)_8(\eta^5\text{-}C_5H_4R)]$ (M = Mo, W; R = H, Me) have been reacted with monodentate and bidentate phosphines

Table 1.2.1.

M_n	*P-donor Ligand Substituted Cluster*	*Comments*	*Ref.(s)*
n = 3	$[MoCo_2(\mu_3\text{-}CCO_2menthyl)(CO)_7(L)(\eta^5\text{-}C_5H_5)]$ [L = $P(OMe)_3$, PCy_3]	Co-ligated, site known	16
	$[MoCo_2(\mu_3\text{-}CCO_2menthyl)(CO)_6(arphos)(\eta^5\text{-}L)]$ (L = $C_5H_4Pr^i$, C_9H_7)	Co-ligated, site known	16
	$[WCo_2(\mu_3\text{-}CMe)(CO)_7(PHPh_2)(\eta^5\text{-}C_5H_5)]$	Co-ligated, site unknown	17
	$[WCo_2(\mu_3\text{-}CC_6H_4Me\text{-}4)(CO)_7(PMe_2Ph)(\eta^5\text{-}L)]$ (L = C_5H_5; L' = $C_5H_4SiMe_3$)	Co-ligated, site unknown	18
	$[WCo_2(\mu_3\text{-}CC_6H_4Me\text{-}4)(CO)_6(L)_2(\eta^5\text{-}L')]$ (L = PMe_2Ph, L' = C_5H_5, $C_5H_4SiMe_3$; L = $P(OMe)_3$, L' = C_5H_5)	Co-ligated, site unknown	18
	$[WCo_2(\mu_3\text{-}CC_6H_4Me\text{-}4)(\mu\text{-}dppm)(CO)_6(\eta^5\text{-}L)]$ (L = C_5H_5, $C_5H_4SiMe_3$)	Co-ligated, site unknown	18
	$[W_2Ir(\mu_3\text{-}CC_6H_4Me\text{-}4)(\mu\text{-}CC_6H_4Me\text{-}4)(Cl)(CO)_3(PPh_3)(\eta^5\text{-}C_5H_5)_2]$	Ir-ligated, site unknown	19
	$[MoFeCo(\mu_3\text{-}S)(CO)_7\{(S)\text{-}PMePhPr)(\eta^5\text{-}C_5H_5)]$	Co-ligated, site known	20
	$[MoFeCo(\mu_3\text{-}S)(\mu\text{-}dppe)(CO)_6(\eta^5\text{-}C_5H_4Me)]$	Fe, Co-ligated, site known	21
	$[MFeCo(\mu_3\text{-}PMe)(CO)_7(L)(\eta^5\text{-}C_5H_5)]$ (M = Mo, W; L = PPh_3, PMe_2Ph)	Co-ligated, site unknown	22
	$[MoCoNi(\mu_3\text{-}CR)(CO)_4(L)(\eta^5\text{-}C_5H_5)_2]$ [L = (*S*)-PMePhPr, PMe_2Ph; R = Me, C(O)Ph]	Co-ligated, site known	23,24
n = 4	$[Mo_2Co_2(\mu_4\text{-}S)(\mu_3\text{-}S)_2(CO)_3(L)(\eta^5\text{-}C_5H_4Me)_2]$ [L = $P(OMe)_3$, PH_2Ph, $PHPh_2$, PPh_3, P^nBu_3]	Co-ligated, site known Adduct for L = $P(OMe)_3$, PMe_3, PPh_3	25
	$[Mo_2Co_2(\mu_4\text{-}S)(\mu_3\text{-}S)_2(CO)_2(PHPh_2)_2(\eta^5\text{-}C_5H_4Me)_2]$	Co-ligated, site known	25

	$[Mo_2Co_2(\mu_4\text{-}S)(\mu_3\text{-}S)_2(CO)_2(\eta^2\text{-}L)(\eta^5\text{-}C_5H_4Me)_2]$	Co-chelated	26
	(L = dppm, dppe, dmpe)		
	$[Mo_2Co_2(\mu_4\text{-}S)(\mu_3\text{-}S)_2(CO)(\eta^1\text{-dmpe})(\eta^2\text{-dmpe})(\eta^5\text{-}C_5H_4Me)_2]$	Co-chelated, Co-ligated	26
	$[MIr_3(\mu\text{-}CO)_3(CO)_{8-n}(L)_n(\eta^5\text{-}C_5H_5)]$	Ir-ligated, site known	27-30,
	[M = Mo, L = PPh_3 or PMe_3, n = 1, 2;		this work
	M = W, L = PPh_3, PMe_3, PMe_2Ph, $PMePh_2$, $P(OPh)_3$, $P(OMe)_3$, n = 1 - 3]		
	$[WIr_3(\mu\text{-}CO)_3(\mu\text{-}L)(CO)_6(\eta^5\text{-}C_5H_5)]$ (L = dppm, dppe, dppa)	Ir-ligated, site known	31
	$[Mo_2Ir_2(\mu\text{-}CO)_3(CO)_{7-n}(L)_n(\eta^5\text{-}C_5H_5)_2]$ (L = PPh_3 or PMe_3, n = 1, 2)	Ir-ligated, site known	32,
			this work
	$[MFeCo_2(\mu_3\text{-}PMe)(\mu\text{-}AsMe_2)(CO)_7(PPh_3)(\eta^5\text{-}C_5H_5)]$ (M = Mo, W)	Co-ligated, site unknown	22
	$[W_2RuPt(\mu_3\text{-}CC_6H_4Me\text{-}4)(\mu\text{-}CC_6H_4Me\text{-}4)(CO)_6(PMe_2Ph)(\eta^5\text{-}C_5H_5)_2]$	Ru-ligated, site known	33
n = 11	$[Mo_2W_3Pt_6(\mu_3\text{-}CC_6H_4Me\text{-}4)_2(\mu_3\text{-}CMe)_3(CO)_{10}(PMe_2Ph)_4(\eta^5\text{-}C_5H_5)_5]$	Pt-ligated, site known	34,35

(Figure 1.2.2.).[20-22]. Initial studies were undertaken with the goal of resolving the cluster enantiomers. A racemic mixture of clusters and the optically active phosphine (*R*)-PMePhPr afforded diastereomeric products which could be separated by crystallization. The phosphine was then removed by carbonylation to give the cluster enantiomers with an optical purity of 98-100 %.[20] More recently, reaction of the (methylcyclopentadienyl)tungsten-containing cluster with dppe has been studied. In contrast to the monodentate phosphine derivative above, in which the phosphine ligates at the cobalt atom *trans* to the Co-Fe vector, the bidentate ligand bridges the Co-Fe linkage and coordinates *trans* to the Fe-Mo and Co-S bonds. The related clusters [$MFeCo(\mu_3$-$PMe)(CO)_7(L)(\eta^5$-$C_5H_5)$] (M = Mo, W; L = PMe_2Ph, PPh_3) resulted from degradation of [$MFeCo_2(\mu_3$-$PMe)(\mu$-$AsMe_2)(CO)_8(\eta^5$-$C_5H_5)$] with the appropriate ligand; cobalt ligation was proposed on the basis of spectral data, but the substitution site was not ascertained.[22] The clusters [$MoCoNi(\mu_3$-$CR)(CO)_8(\eta^5$-$C_5H_5)_2$] [R = Me, C(O)Ph] reacted with both PMe_2Ph [23] and (+)-PMePhPr [24] to afford cobalt-substituted derivatives, with the incoming ligand shown to be *trans* to the Co-C vector for the benzoyl-containing cluster (Figure 1.2.3.).

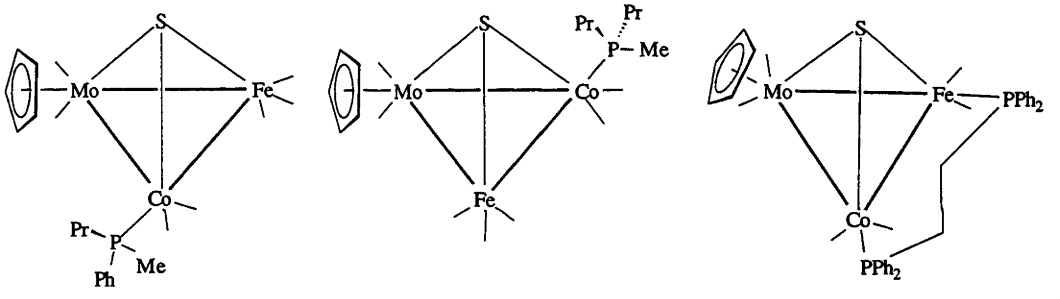
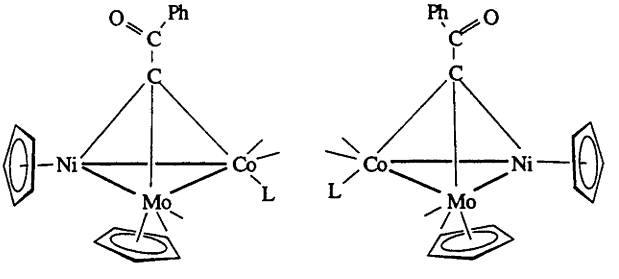


Figure 1.2.2.

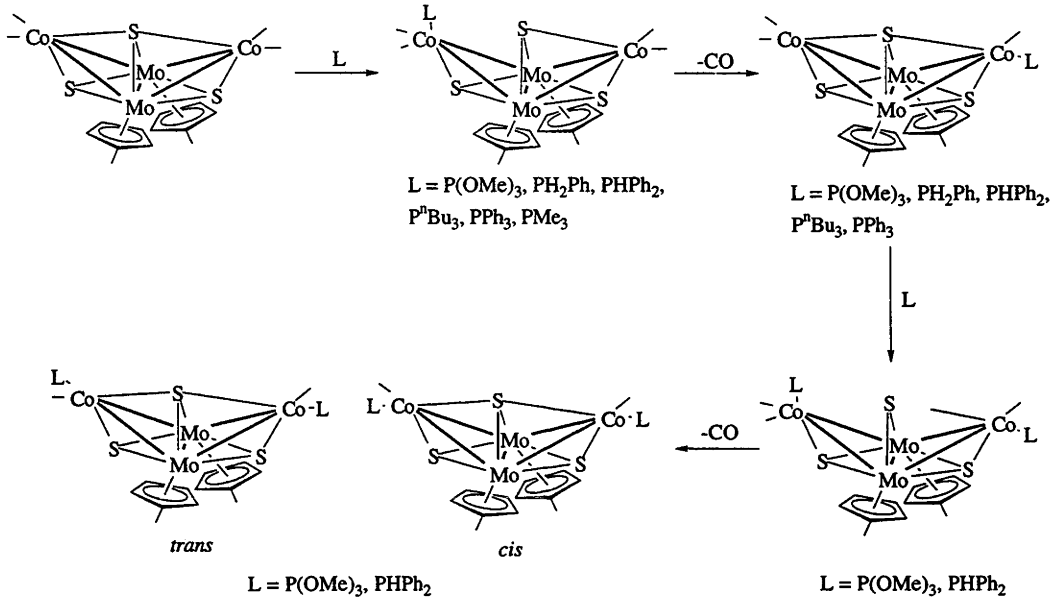


L = (*S*)-PMePhPr, PMe_2Ph

Figure 1.2.3.

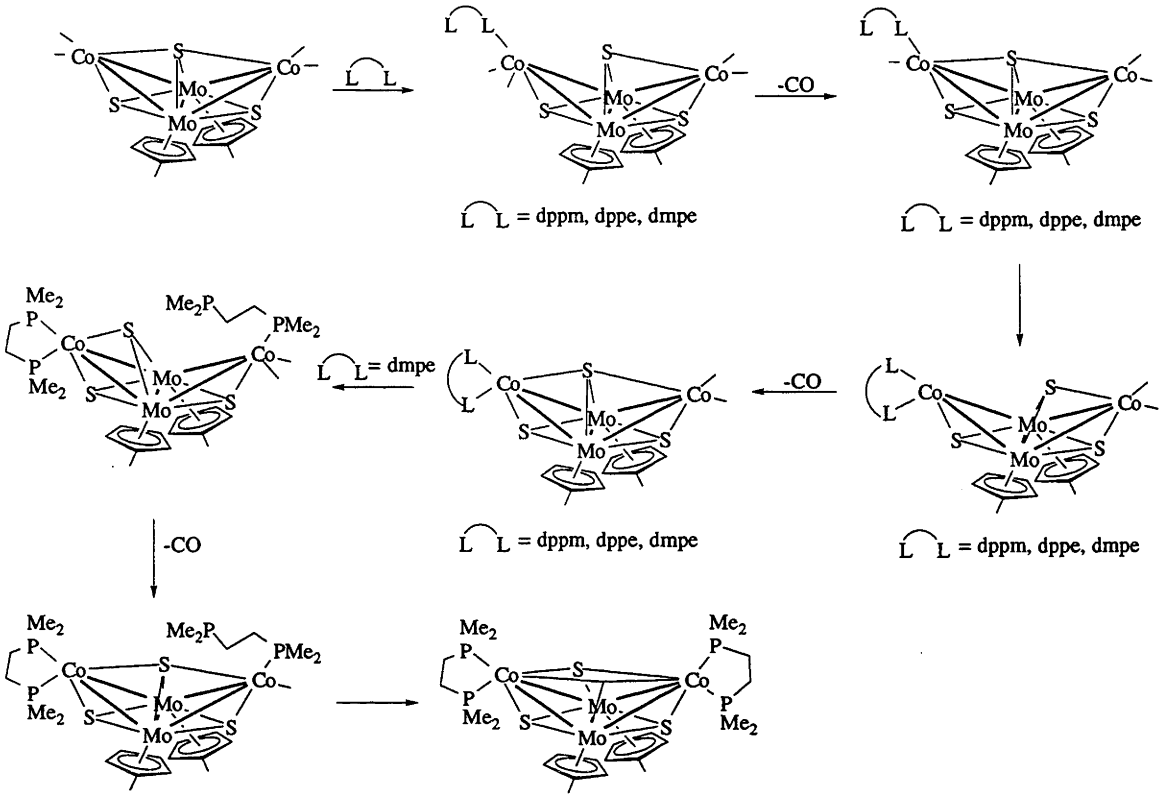
The dimolybenum-dicobalt cluster [$Mo_2Co_2(\mu_4$-$S)(\mu_3$-$S)_2(CO)_4(\eta^5$-$C_5H_4Me)_2$], which desulfurizes organic thiols (Section *1.2.4.2.*), reacted with phosphines by ligand substitution at cobalt.[25] Kinetic studies showed that reaction proceeded by two elementary steps: initial formation of an adduct, followed by loss of CO (Scheme 1.2.1.). The extent of

substitution is dominated by electronic considerations; while phosphine substitution proceeded to give bis-substituted derivatives, reaction with isocyanides afforded tris-substituted products (see Section *1.2.2.2.*). These substitution reactions proceeded at room temperature: heating the PH_2Ph-cluster mixture led to double P-H bond cleavage and coordination of μ_3-phosphinidene (Section *1.2.4.2.*).



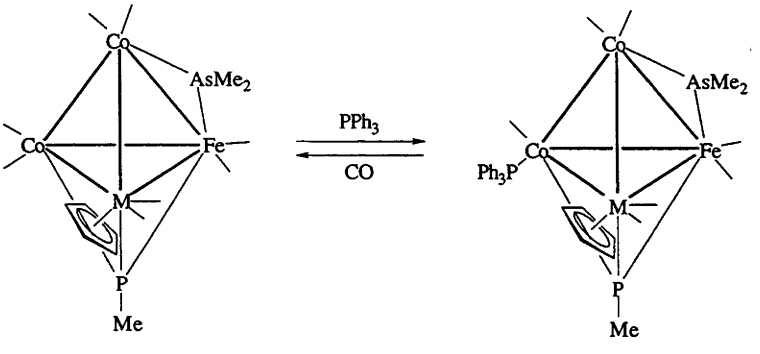
Scheme 1.2.1.

The same cluster reacted with bidentate phosphines to afford cobalt-chelated products (Scheme 1.2.2.), with excess dmpe affording a bis-substituted derivative.[26] In contrast, the related cluster $[Mo_2Co_2(\mu_3\text{-}S)_4(CO)_2(\eta^5\text{-}C_5H_4Me)_2]$ reacted with dppe to form a product in which the bidentate ligand is believed to span the Co-Co vector, and in the presence of excess dppe affords a polymeric product, but the products were incompletely characterized.[26]

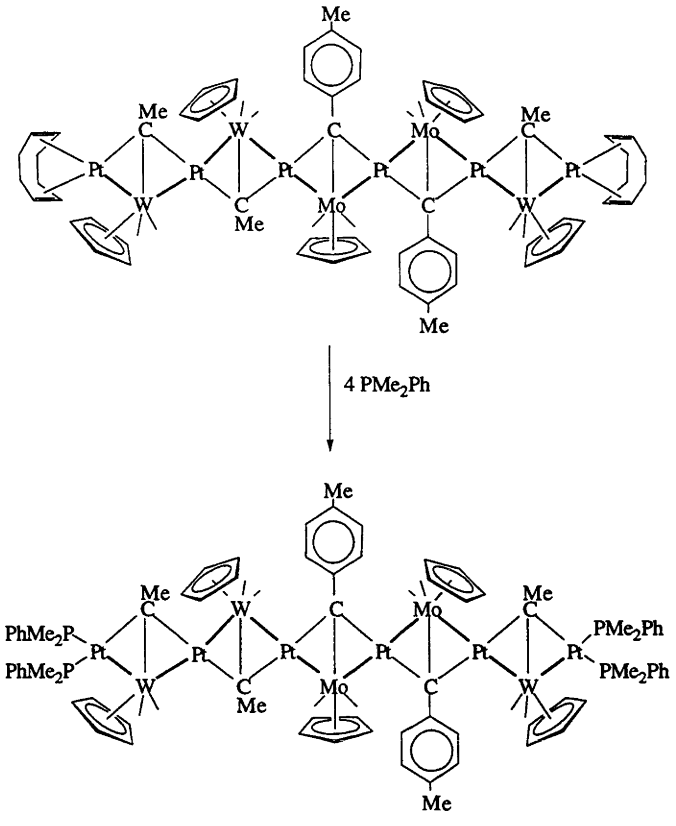


Scheme 1.2.2.

The clusters $[MFeCo_2(\mu_3\text{-}R)(\mu\text{-}AsMe_2)(CO)_8(\eta^5\text{-}C_5H_5)]$ (M = Mo, W; R = S, PMe) reacted with donor ligands RNC, $P(OR)_3$ and PR_3 to afford degradation products; the only products to retain the cluster core nuclearity were the cobalt-ligated $[MFeCo_2(\mu_3\text{-}PMe)(\mu\text{-}AsMe_2)(CO)_7(PPh_3)(\eta^5\text{-}C_5H_5)]$ (Scheme 1.2.3.), although even these clusters were accompanied by other lower nuclearity products,[22] and the incoming phosphine could be readily replaced by CO. Ligand substitution studies on larger "very mixed"-metal clusters are very rare, one example being the formation of $[Mo_2W_3Pt_6(\mu_3\text{-}C_6H_4Me\text{-}4)_2(\mu_3\text{-}CMe)_3(CO)_{10}(PMe_2Ph)_4(\eta^5\text{-}C_5H_5)_5]$ from displacement of the weakly-bound cod ligands in $[Mo_2W_3Pt_6(\mu_3\text{-}C_6H_4Me\text{-}4)_2(\mu_3\text{-}CMe)_3(CO)_{10}(\eta^4\text{-}cod)_2(\eta^5\text{-}C_5H_5)_5]$ by PMe_2Ph (Scheme 1.2.4.).[35]



Scheme 1.2.3.



Scheme 1.2.4.

1.2.2.1. Other Ligands

Almost all other examples of ligand replacement occur at the late transition metal and involve the introduction or replacement of CO (Table 1.2.2.). Carbonylation of clusters occurs with readily displaced ligands. Nitriles are "lightly stabilizing" ligands at transition metal carbonyl clusters; reaction of $[Mn_2Pt(CO)_{10}(NCPh)_2]$ with CO afforded $[Mn_2Pt(CO)_{12}]$ (Figure 1.2.4.).[36] Replacement of the chloro ligand at $[MPd_2(\mu_3\text{-}CO)_2(\mu\text{-}dppm)_2Cl]$ (M = Mo, W) required the assistance of a halo acceptor ($Tl[PF_6]$), proceeding to give $[MPd_2(\mu_3\text{-}CO)_2(\mu\text{-}dppm)_2(CO)]^+$ (Figure 1.2.5.).[37] Both the chloro ligand in the precursor and the terminal carbonyl ligand in the product can be displaced by bromide in the tungsten-containing examples.

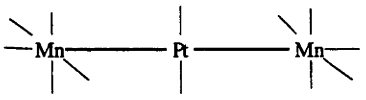


Figure 1.2.4.

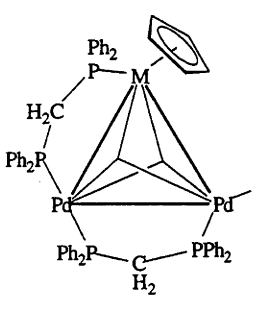
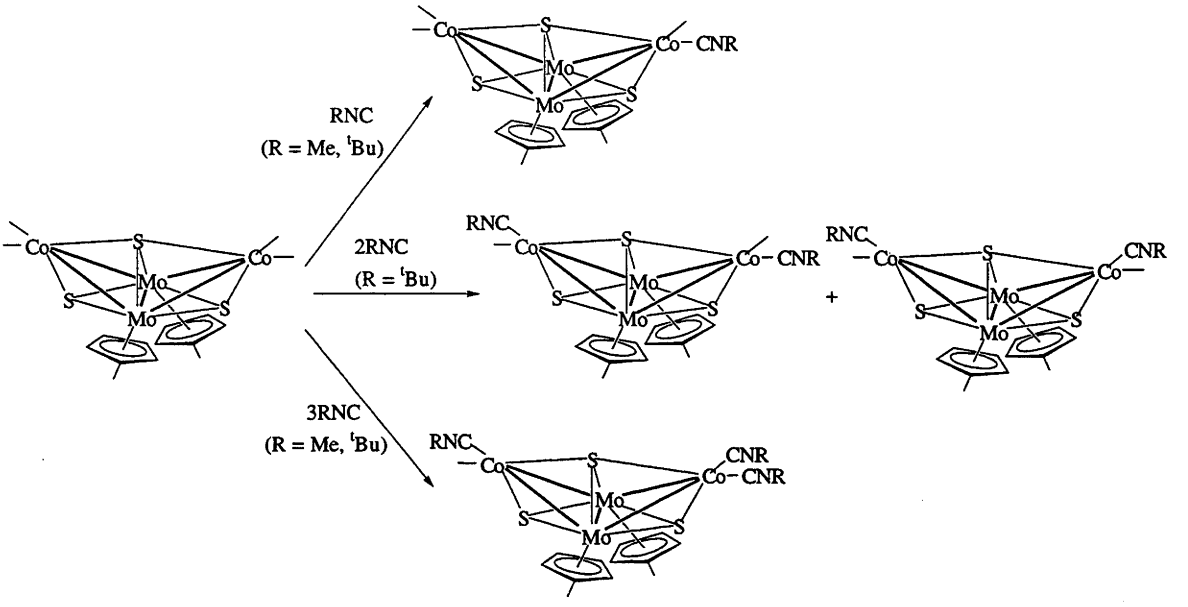


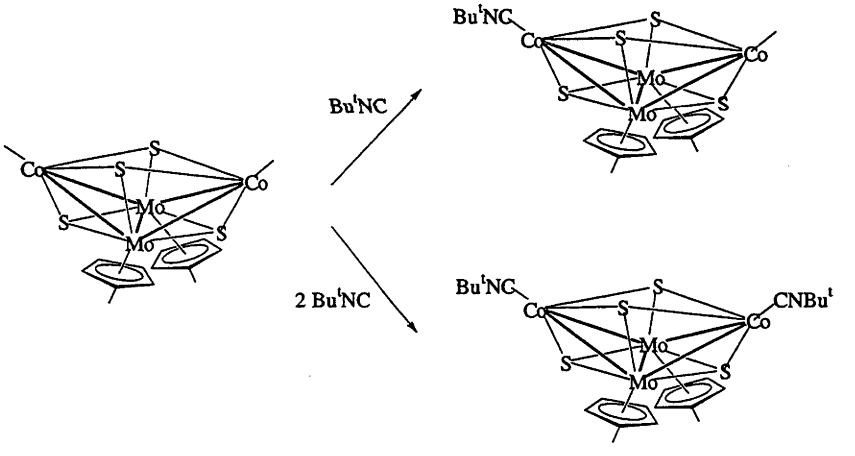
Figure 1.2.5.

Studies of phosphine and phosphite substitution at $[WCo_2(\mu_3\text{-}CC_6H_4Me\text{-}4)(CO)_8(\eta^5\text{-}L)]$ (L = C_5H_5, $C_5H_4SiMe_3$) have been extended to embrace diars.[18] A cobalt-ligated product was obtained, but the specific susbstitution sites were not ascertained. The carbonyl ligands in $[Mo_2Co_2(\mu_4\text{-}S)(\mu_3\text{-}S)_2(CO)_4(\eta^5\text{-}$

$C_5H_4Me)_2]$ and $[Mo_2Co_2(\mu_3\text{-}S)_4(CO)_2(\eta^5\text{-}C_5H_4Me)_2]$ can be displaced by isocyanides,[38-40] though reaction of the former only proceeds to form the tris-substituted product (Schemes 1.2.5. and 1.2.6.)



Scheme 1.2.5.

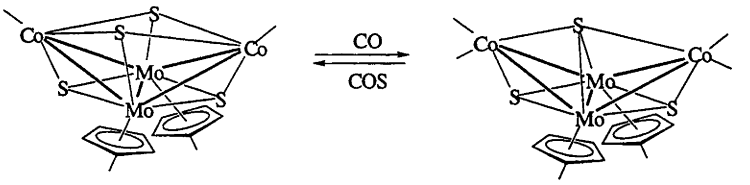


Scheme 1.2.6.

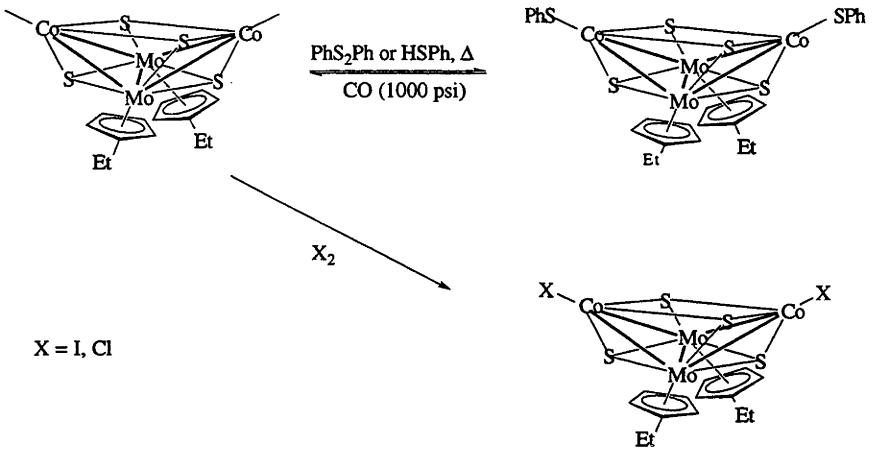
Reaction of $[Mo_2Co_2(\mu_4\text{-}S)(\mu_3\text{-}S)_2(CO)_4(\eta^5\text{-}C_5H_4Me)_2]$ with COS afforded $[Mo_2Co_2(\mu_3\text{-}S)_4(CO)_2(\eta^5\text{-}C_5H_4Me)_2]$, a reaction which can be reversed upon carbonylation (Scheme 1.2.7.).[40] Other reports of ligand replacement at "very mixed"-metal clusters involve a formal oxidation state change. Reaction of $[Mo_2Co_2(\mu_3\text{-}S)_4(CO)_2(\eta^5\text{-}C_5H_4Et)_2]$ with halogens or diphenyldisulfide afforded $[Mo_2Co_2(\mu_3\text{-}S)_4(X)_2(\eta^5\text{-}C_5H_4Et)_2]$ (X = Cl, Br, I, SPh),[41] with a formal oxidation at the cobalt atoms, and cleavage of the Co-Co linkage (Scheme 1.2.8.). All product clusters are paramagnetic in the solid state (but less so in solution), with higher spin states disfavoured as the π-donor ability of X increases.

Table 1.2.2.

Product Cluster(s)	*Formal Replacement*	*Ref.(s)*
$[Mn_2Pt(CO)_{12}]$	PhCN → CO (at Pt)	36
$[MPd_2(\mu_3\text{-}CO)_2(\mu\text{-}dppm)_2(CO)]^+$ (M = Mo, W)	Cl^- → CO (at Pd)	37
$[WPd_2(\mu_3\text{-}CO)_2(\mu\text{-}dppm)_2(Br)(\eta^5\text{-}C_5H_5)]$	CO → Br^- (at Pd) Cl^- → Br^- (at Pd)	37
$[Mo_2Co_2(\mu_4\text{-}S)(\mu_3\text{-}S)_2(CO)_{4-n}(CNR)_n(\eta^5\text{-}C_5H_4Me)_2]$ (R = Bu^t or Me; n =1 - 3)	CO → RNC (at Co)	38,39
$[Mo_2Co_2(\mu_3\text{-}S)_4(CO)_{2-n}(CNR)_n(\eta^5\text{-}C_5H_4Me)_2]$ (n = 1, R = Bu^t or Me; n = 2, R = Bu^t)	CO → RNC (at Co)	39,40
$[Mo_2Co_2(\mu_3\text{-}S)_4(CO)_2(\eta^5\text{-}C_5H_4Me)_2]$	2CO → S (at Co_2Mo face)	40
$[Mo_2Co_2(\mu_3\text{-}S)_4(X)_2(\eta^5\text{-}C_5H_4Et)_2]$ (X = SPh, I, Cl, Br)	2CO → 2X (at Co), formal oxidation state increase	41,42
$[MoRh_3\{\mu_3\text{-}AsRhCl_2(\eta^5\text{-}C_5H_5)\}(\mu_3\text{-}CO)_2(\eta^5\text{-}C_5H_5)_4]$	CO → 2Cl (at non-cluster Rh), formal oxidation state increase	43
$[RePt_3(\mu\text{-}dppm)_3(O)_3]^+$	3CO → 3O (at Re), formal oxidation state increase	44,45

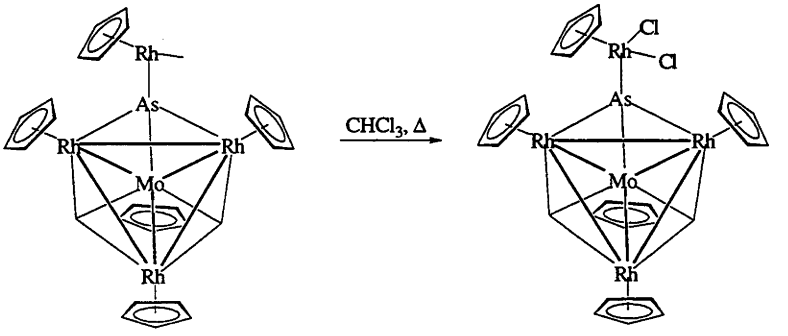


Scheme 1.2.7.

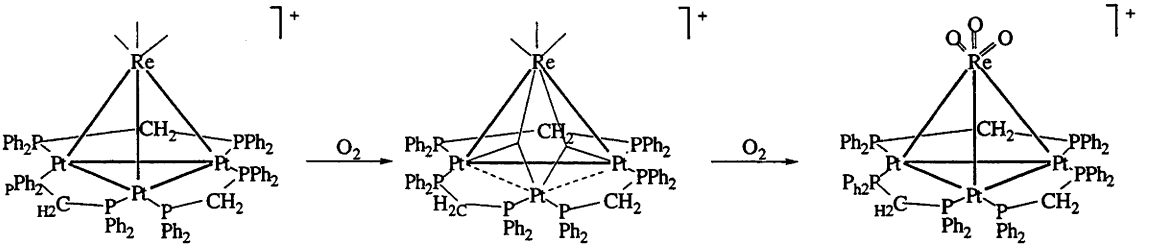


Scheme 1.2.8.

Oxidation at the late transition metal was also seen upon reacting $[MoRh_3\{\mu_3\text{-}AsRh(\eta^5\text{-}C_5H_5)(CO)\}(\mu_3\text{-}CO)_2(\eta^5\text{-}C_5H_5)_4]$ in $CHCl_3$, with the "action" occurring at the non-cluster rhodium atom (Scheme 1.2.9.).[43] In contrast, the earlier transition metal was oxidized in a stepwise fashion upon reacting $[RePt_3(\mu\text{-}dppm)_3(CO)_3]^+$ with molecular oxygen, with (overall) a formal increase of +6 in oxidation state (Scheme 1.2.10.).[44] The oxidation product isolated was sensitive to the reaction conditions, with hydrogen peroxide or molecular oxygen/photolysis affording products lacking metal-metal bonds.[45]



Scheme 1.2.9.

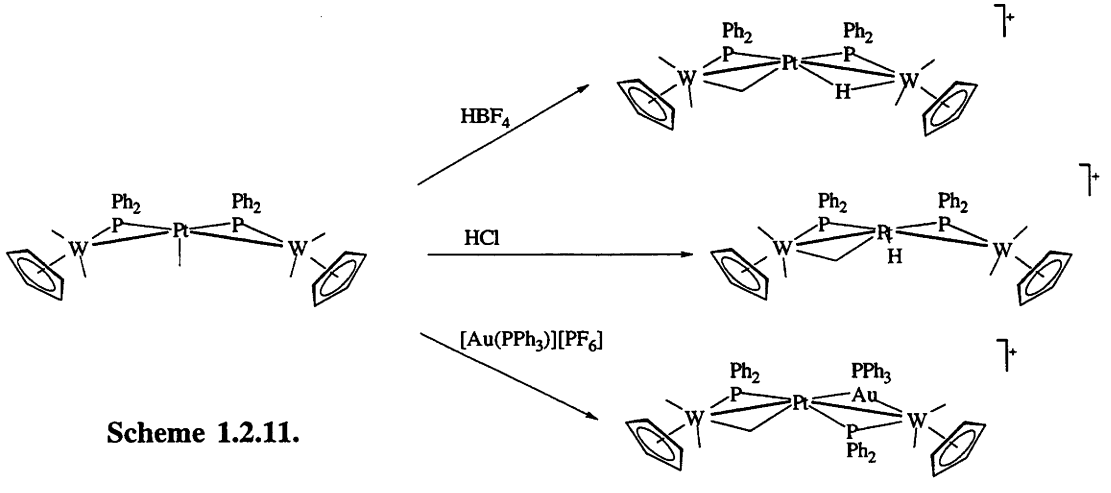


Scheme 1.2.10.

1.2.3. Ligand Addition

The distinction between ligand substitution and ligand addition is frequently arbitrary, with the former often proceeding by way of the latter. Coordinatively unsaturated clusters can, of course, react with ligands without a compensating bond cleavage, but even in these situations the adduct is not always stable. Table 1.2.3. collects examples of ligand addition reactions at "very mixed"-metal clusters.

Most examples of addition involve nucleophiles, reactions with electrophiles being scarce. The reactions of $[W_2Pt(\mu\text{-}PPh_2)(CO)_5(\eta^5\text{-}C_5H_5)_2]$ with two sources of H^+, and the isolobal $[Au(PPh_3)]^+$, have been reported; HBF_4 and $[Au(PPh_3)][PF_6]$ afford adducts with the electrophile bridging a W-Pt linkage, but with differing stereochemistry with respect to the bridging groups across the other W-Pt bond, whereas HCl afforded a product with a terminal Pt-bound hydrido ligand (Scheme 1.2.11.).[46]



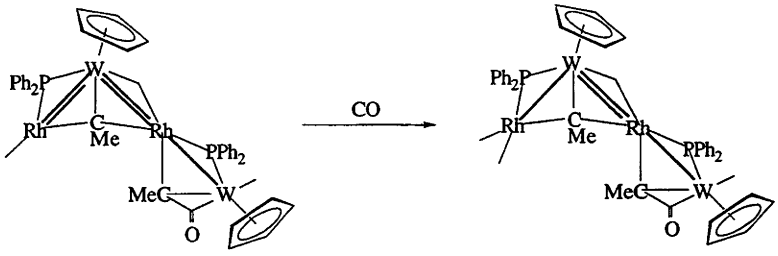
Scheme 1.2.11.

As mentioned in Section *1.2.2.1.*, ligand substitution at $[Mo_2Co_2(\mu_4\text{-}S)(\mu_3\text{-}S)_2(CO)_4(\eta^5\text{-}C_5H_4Me)_2]$ occurs by way of an adduct at cobalt, with a compensating Co-S bond cleavage (Scheme 1.2.1.), although for L = PMe_3 reaction did not proceed past the adduct. The unsaturated cluster $[W_2Rh_2(\mu_3\text{-}CMe)\{\mu\text{-}CMeC(O)\}(\mu\text{-}PPh_2)(\mu\text{-}CO)(CO)_2(\eta^5\text{-}C_5H_5)_2]$, with formal W=Rh double bonds, added one equivalent of CO at the terminal rhodium atom to afford $[W_2Rh_2(\mu_3\text{-}CMe)\{\mu\text{-}CMeC(O)\}(\mu\text{-}PPh_2)(\mu\text{-}CO)(CO)_3(\eta^5\text{-}C_5H_5)_2]$, (Scheme 1.2.12.)

Table 1.2.3.

Product Cluster	*Reagent*	*Site of Reactivity*	*Ref.(s)*
$[W_2Pt(\mu\text{-}H)(\mu\text{-}CO)(\mu\text{-}PPh_2)_2(CO)_4(\eta^5\text{-}C_5H_5)_2]^+$	HBF_4		46
$[W_2Pt(H)(\mu\text{-}CO)(\mu\text{-}PPh_2)_2(CO)_4(\eta^5\text{-}C_5H_5)_2]^+$	HCl		46
$[W_2Pt(\mu\text{-}AuPPh_3)(\mu\text{-}CO)(\mu\text{-}PPh_2)_2(CO)_4(\eta^5\text{-}C_5H_5)_2]^+$	$[AuPPh_3][PF_6]$		46
$[Mo_2Co_2(\mu_4\text{-}S)(\mu_3\text{-}S)_2(CO)_4(PMe_3)(\eta^5\text{-}C_5H_4Me)]$	PMe_3		25,38
$[W_2Rh_2(\mu_3\text{-}CMe)\{\mu\text{-}CMeC(O)\}(\mu\text{-}PPh_2)_2(\mu\text{-}CO)(CO)_3(\eta^5\text{-}C_5H_5)_2]$	CO		47
$[RePt_3(\mu_3\text{-}L)(\mu\text{-}dppm)_3(CO)_3]^+$ (L = Cl^-, Br^-, I^-)	Cl^-, Br^-, I^-	Re	48
$[RePt_3(\mu\text{-}dppm)_3(CO)_3(L)]^+$ [L = CO, $P(OR)_3$ (R = Me, Ph), RNC (R = ^{t}Bu, Me, Cy, Xy), RSH (R = Et, ^{t}Bu, 3-MeC_6H_4), RC_2H (R = H, Ph)]	L = CO, $P(OR)_3$, Cl^-, Br^-, I^-, RNC, RSH, RC_2CH		48-50
$[RePt_3(\mu_3\text{-}X)(\mu\text{-}dppm)_3(CO)_3]^+$ (X = CO, Cl^-, Br^-, I^-)	X	Pt_3 face	48
$[RePt_3(\mu_3\text{-}L)(\mu\text{-}dppm)_3(O)_3]^+$ [L = CO, Hg, Tl(acac), SnX_3^- (X = F, Cl), Cl^-, Br^-, I^-]	CO, Hg, Tl(acac), Cl^-, Br^-, I^-, SnX_3^- (X = F, Cl)		48,49,51
$[RePt_3(\mu\text{-}dppm)_3\{P(OMe)_3\}(O)_3]^+$	$P(OMe)_3$		49,51

which isomerized by P-C formation, and then eliminated CO to regenerate the formal unsaturation.[47]

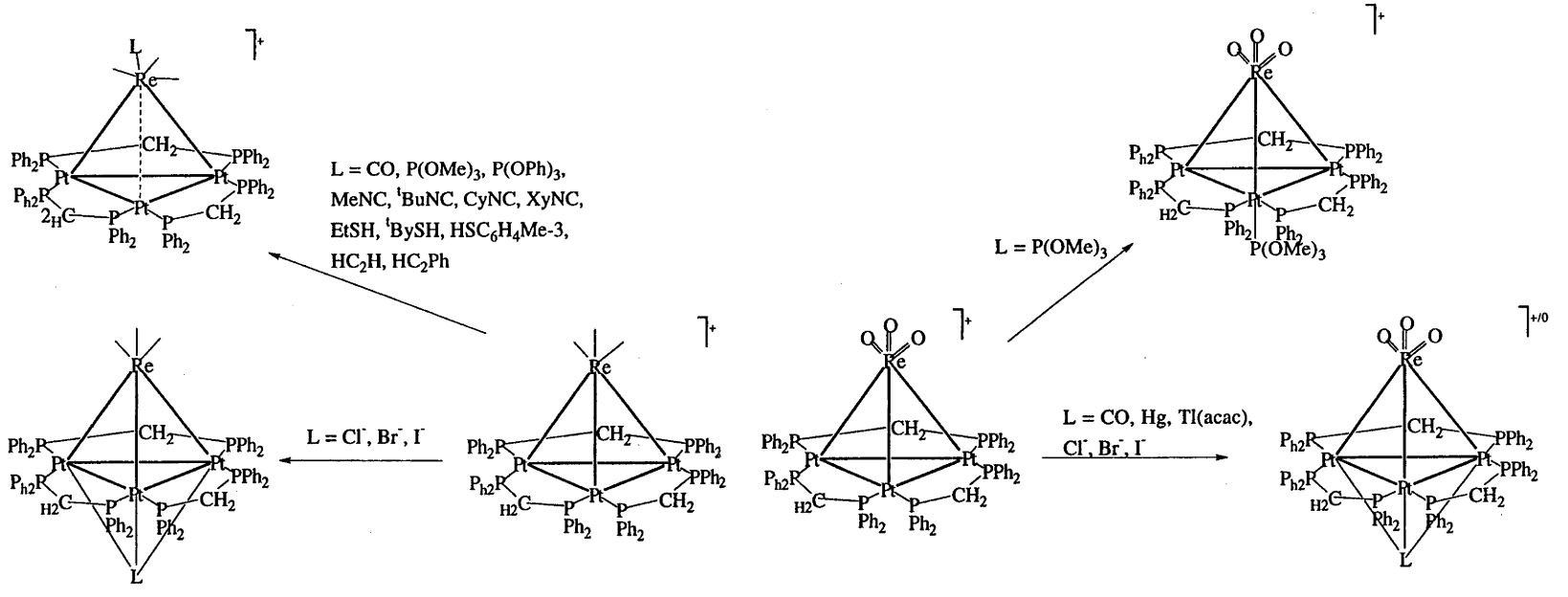


Scheme 1.2.12.

A number of investigations concerning the reactivity of the coordinatively unsaturated (54 e) clusters $[RePt_3(\mu\text{-dppm})_3(CO)_3]^+$ and $[RePt_3(\mu\text{-dppm})_3(O)_3]^+$, in which the apical rheniums differ by 6 in formal oxidation state, have been reported. The cluster $[RePt_3(\mu\text{-dppm})_3(O)_3]^+$ (itself formed by reaction of $[RePt_3(\mu\text{-dppm})_3(CO)_3]^+$ with O_2, via the addition product $[RePt_3(\mu_3\text{-CO})_2(\mu\text{-dppm})_3(CO)_3]^+$ [52]: Section *1.2.2.2.*) was more reactive to ligand addition than the carbonyl-ligated analogue $[RePt_3(\mu\text{-dppm})_3(CO)_3]^+$. $[RePt_3(\mu\text{-dppm})_3(CO)_3]^+$ reacted with neutral donor ligands at the rhenium atom, and with halide ions by capping the triplatinum face (Scheme 1.2.13.).[48-50] Cluster $[RePt_3(\mu\text{-dppm})_3(O)_3]^+$ similarly reacted with halides, and with Hg, Tl(acac) and SnX_3^-, by capping the triplatinum face, but carbonylation also occurred at the triplatinum face, and reaction with phosphite occurred at platinum, the latter two both contrasting with the chemistry at the "low oxidation state" analogue (Scheme 1.2.13.).[48,49,51]

1.2.4. Ligand Transformations

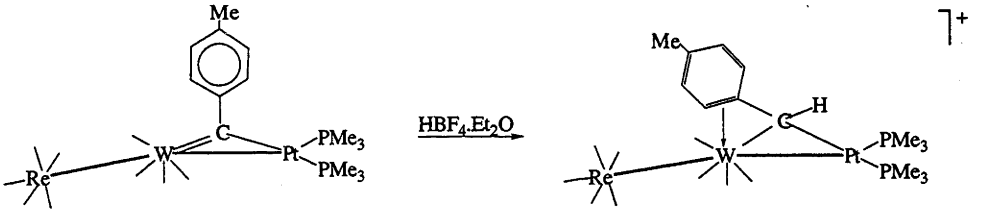
Metal clusters have been shown to transform organic substrates in a large number of ways, many of which are not possible at monometallic complexes;[1,14] two or more metal atoms in specific geometric relationships are required to stabilize ligand fragments and effect bond cleavage and formation. The bond polarity in mixed-metal clusters which may enhance substrate activation should be maximized in progressing to "very mixed"-metal systems. For example, coupling oxophilic and carbophilic metals together in a "very mixed"-metal cluster should facilitate C-heteroatom cleavage by formation of strong M-C and M-heteroatom linkages, but this is one area that has been little-exploited. Ligand transformations at C-ligands are summarized in Section *1.2.4.1.*, while modifications of other ligands are reviewed in Section *1.2.4.2.*


L = CO, P(OMe)3, P(OPh)3,
MeNC, tBuNC, CyNC, XyNC,
EtSH, tBySH, HSC6H4Me-3,
HC2H, HC2Ph
L = P(OMe)3
L = Cl-, Br-, I-
L = CO, Hg, Tl(acac),
Cl-, Br-, I-

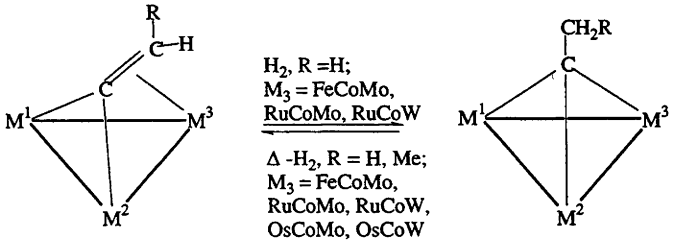
Scheme 1.2.13.

1.2.4.1. C-Donor Ligands

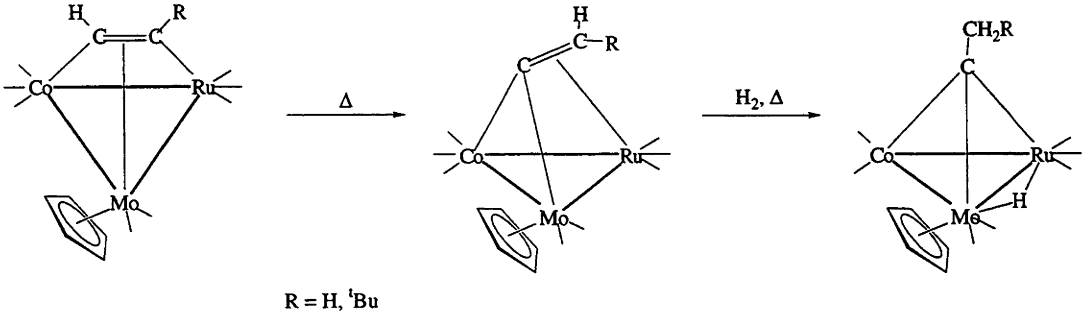
Transformations at C-donor ligands are collected in Table 1.2.4. Several examples of C-H activation or C-H formation at "very mixed"-metal clusters have appeared. Protonation at most clusters occurs at a M-M bond, but in $[WRePt(\mu\text{-}CC_6H_4Me\text{-}4)(CO)_9(PMe_3)_2]$ protonation occurs at the alkylidyne carbon, with the consequent electron deficiency at tungsten relieved by formation of an η^2-aryl linkage (Scheme 1.2.14.).[53] Other examples of C-H formation have utilized H_2 as the hydrogen source.[54,55] Coordinated vinylidene can be converted into alkylidyne at a trimetallic face, but the reverse reaction is the easier, occurring at a much wider range of heterotrimetallic faces (Scheme 1.2.15.).[54] The coordinated vinylidene can be formed by thermolyzing μ_3-η^2-ligated alkyne, the reaction proceeding by a formal 1,2-H shift (Scheme 1.2.16.).[15,55] The remaining example of C-H formation was from formal insertion of an alkyne into an Ru-H bond to form a σ-alkyl linkage (Scheme 1.2.17.); unlike other examples in this Section, the "action" occurred at a single metal.[56]



Scheme 1.2.14.



Scheme 1.2.15.

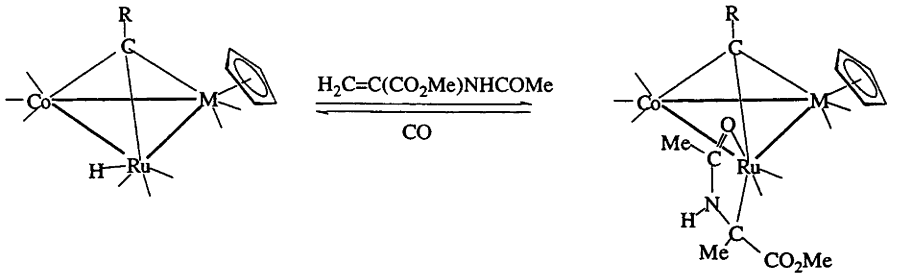


Scheme 1.2.16.

Table 1.2.4.

Transformation	*Product Cluster*	*Face / Bond / Metal Effecting Transformation*	*Ref.(s)*
C-H formation: $CC_6H_4Me\text{-}4 + H \rightarrow CHC_6H_4Me\text{-}4$	$[WRePt(\mu\text{-}\eta^3\text{-}CHC_6H_4Me\text{-}4)(CO)_9(PMe_3)_2]^+$	W-Pt bond	53
C-H formation: $C{=}CHR + H_2 \rightleftarrows CCH_2R + H$	$[M_3(\mu_3\text{-}\eta^2\text{-}C{=}CHR)(CO)_8(\eta^5\text{-}C_5H_5)]$ (for M_3 = MoFeCo, MoRuCo, WRuCo, MoOsCo, WOsCo; for R = H and in one case R = Me)	MM'Co face (M = Mo, W; M' = Fe, Ru, Os)	54
C-H cleavage, C-H formation: $HC{\equiv}CR \rightleftarrows C{=}CHR + H_2 \rightleftarrows CCH_2R + H$	$[MoRuCo(\mu_3\text{-}\eta^2\text{-}CCHR)(CO)_8(\eta^5\text{-}C_5H_5)]$ $[MoRuCo(\mu\text{-}H)(\mu_3\text{-}CCH_2R)(CO)_8(\eta^5\text{-}C_5H_5)]$ (R = H, ^{t}Bu)	MoRuCo face	55
Ru-H cleavage, C-H, Ru-C formation: $Ru\text{-}H + H_2C{=}CRR' \rightarrow Ru\text{-}CRR'Me$	$[MRuCo(CO)_7\{\eta^2\text{-}CMe(CO_2Me)NHC(O)Me\}(\eta^5\text{-}C_5H_5)]$ (M = Mo, W)	Ru	56
C-C formation: $2\ PhC{\equiv}CH \rightarrow CPhCHCHCPh$	$[Mo_2Co_2(\mu_3\text{-}S)_3(\mu_3\text{-}\eta^2\text{-}HC_2Ph)(CO)_2(\eta^5\text{-}C_5H_4Me)_2]$ $[Mo_2Co_2(\mu_3\text{-}S)_3(\mu_3\text{-}\eta^4\text{-}CPhCHCHCPh)(\eta^5\text{-}C_5H_4Me)_2]$	$MoCo_2$ face	57
C-C cleavage, C-C formation: $2\ PhC{\equiv}CPh \rightarrow CPh + CPhCPhCPh$	$[W_2Ir_2(\mu_3\text{-}CPh)(\mu_3\text{-}\eta^2\text{-}CPhCPhCPh)(\mu\text{-}CO)_2(CO)_4(\eta^5\text{-}C_5H_5)_2]$	W_2Ir_2 butterfly	58,59
C-C cleavage, C-C formation: $3\ PhC{\equiv}CPh \rightarrow 2\ CPh +$ $CPhCPhCPhCPh$	$[WIr_3(\mu_3\text{-}CPh)(\mu\text{-}CPh)(\mu\text{-}\eta^4\text{-}CPhCPhCPhCPh)(CO)_5(\eta^5\text{-}C_5H_5)]$	WIr_3 butterfly	60
C-C formation: $CH + PhC{\equiv}CPh \rightarrow CHCPhCPh$	$[Mo_2Co(\mu_3\text{-}\eta^3\text{-}CHCPhCPh)(\mu\text{-}\eta^2\text{-}PhC_2Ph)(\mu_3\text{-}CO)(CO)_2(\eta^5\text{-}C_5H_5)_2]$	Mo_2Co face	61
C-C formation, C-C cleavage: $CH + 2PhC{\equiv}CPh \rightarrow CPhCHCPhCPh$ $+ CPh$	$[Mo_2Co(\mu_3\text{-}CPh)(\mu_3\text{-}\eta^4\text{-}CPhCHCPhCPh)(CO)_2(\eta^5\text{-}C_5H_5)_2]$	Mo_2Co face	61

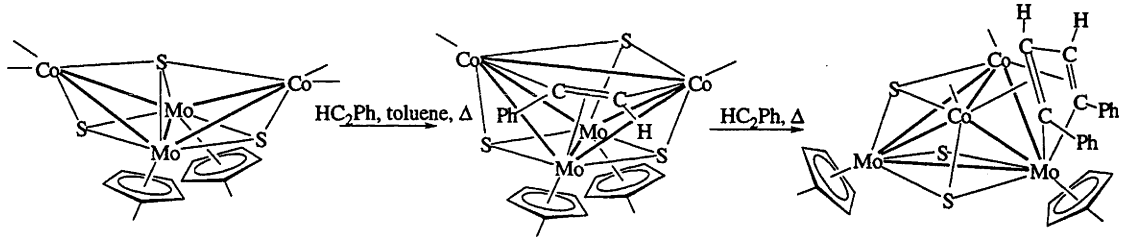
C-C formation: $CH + EtC{\equiv}CEt + CO \rightarrow CHCEtCEtCO$	$[Mo_2Co(CHCEtCEtCO)(CO)_5(\eta^5\text{-}C_5H_5)_2]$	Mo_2Co face	61
C-C formation: $CC_6H_4Me\text{-}4 + RC{\equiv}CR + CO \rightarrow C(C_6H_4Me\text{-}4)CRCRC(O)$ (R = Me, Et)	$[WCo_2\{\mu_3\text{-}C(C_6H_4Me\text{-}4)CEtCEtCO\}(\mu\text{-}CO)(CO)_2\{PPh_2(CR'{=}CHR')\}]$	WCo_2 face	62
N-C activation: $N_2CHCO_2R \rightarrow N_2 + CHCO_2R$ (R = Me, Et)	$[W_2Ir_2\{\mu_3\text{-}\eta^2\text{-}CHC(O)OR\}(\mu\text{-}CHCO_2R)(\mu\text{-}CO)(CO)_6(\eta^5\text{-}C_5H_5)_2]$ (R = Me, Et)	IrIr bond, WIr_2 face	63,64



M = Mo, W;
R = Me, Ph

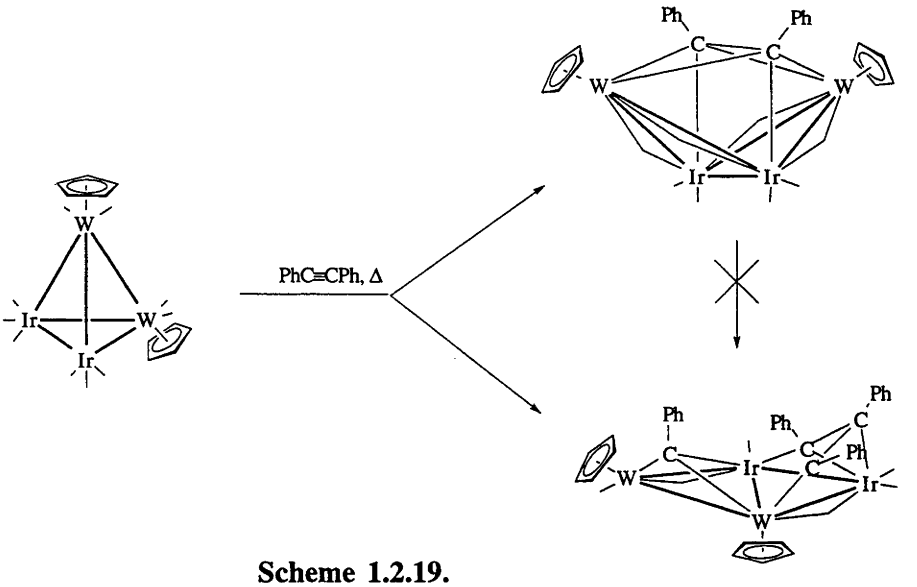
Scheme 1.2.17.

Thus far, all examples of C-C activation and/or C-C formation have employed the prototypical C_2 source, namely alkynes, either alone or in concert with C_1 units such as cluster-bound alkylidyne or CO. Phenylacetylene was dimerized across a Co_2Mo face of a sulfur-rich dicobaltdimolybdenum cluster in a head-to-head fashion, the reaction proceeding by stepwise addition of the C_2 molecules (Scheme 1.2.18.).[57]

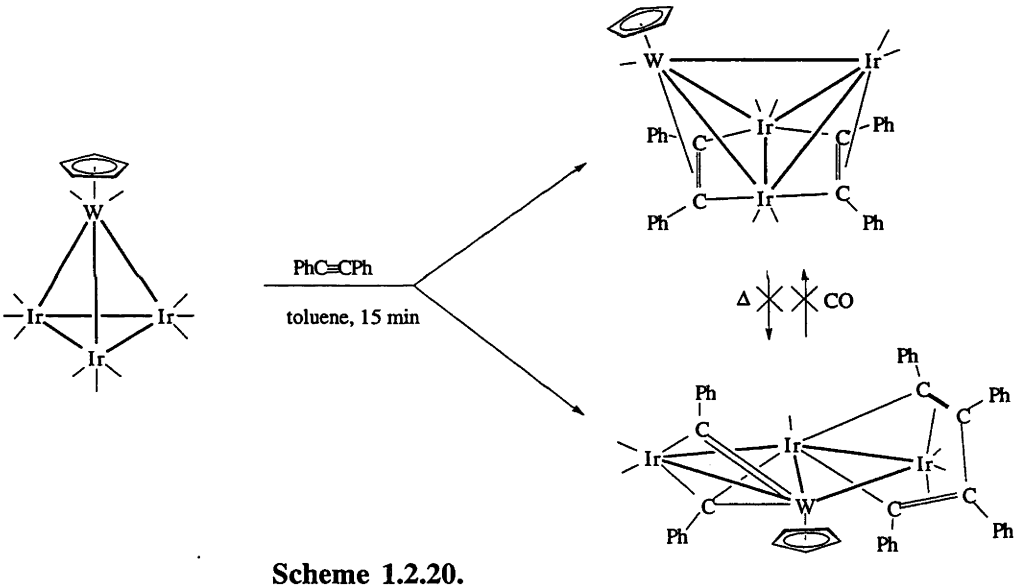


Scheme 1.2.18.

In contrast, reaction of excess internal acetylene PhC≡CPh at a related tetrahedral ditungstendiiridium cluster without bridging sulfur atoms proceeded by C-C cleavage as well as C-C formation to afford a butterfly cluster (resulting from W-Ir cleavage) with cluster-bound C_3 (allyl) and C_1 (alkylidyne) units. The major product of the same reaction was a mono-acetylene adduct resulting from insertion into a W-W bond, which could not be converted to the allyl(alkylidyne)-containing cluster (Scheme 1.2.19.).[58,59] Modification of the cluster core [replacing one $[CpW(CO)_2]$ unit with an isolobal $[Ir(CO)_3]$ fragment] afforded an isostructural cluster which reacted with excess of the same acetylene to afford a product with two cluster-bound acetylenes, and a butterfly cluster resulting from Ir-Ir cleavage with two C_1 and one C_4 ligands; again. these products could not be interconverted (Scheme 1.2.20.).[60] Unlike other examples in this Section, reactions at these tungsten-iridium clusters utilize all four core metals to support the resultant C_x fragments. Clearly, these modifications in core composition have the potential to dramatically affect product selection.

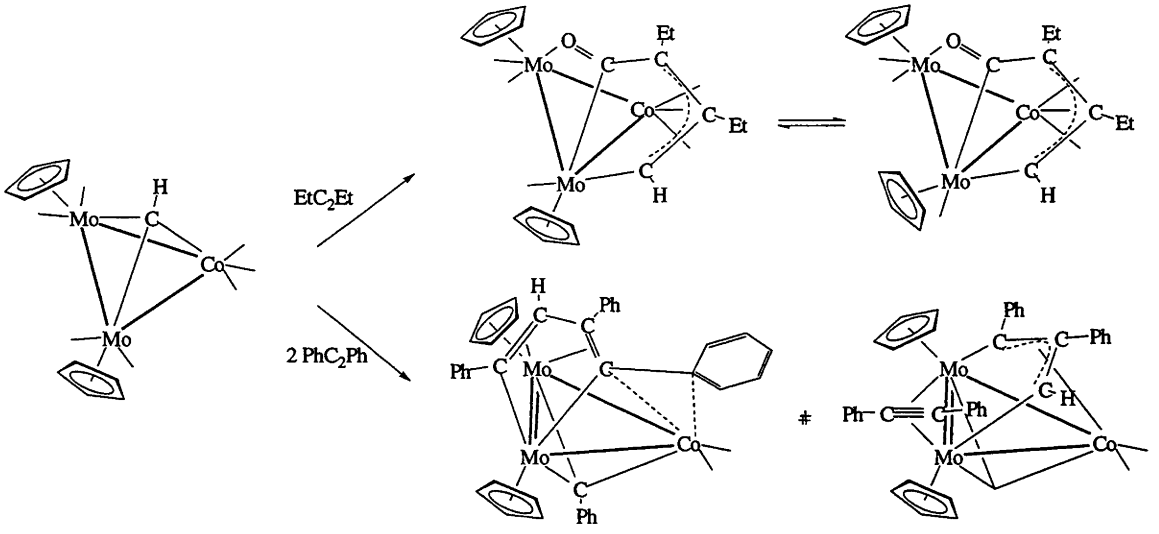


Scheme 1.2.19.

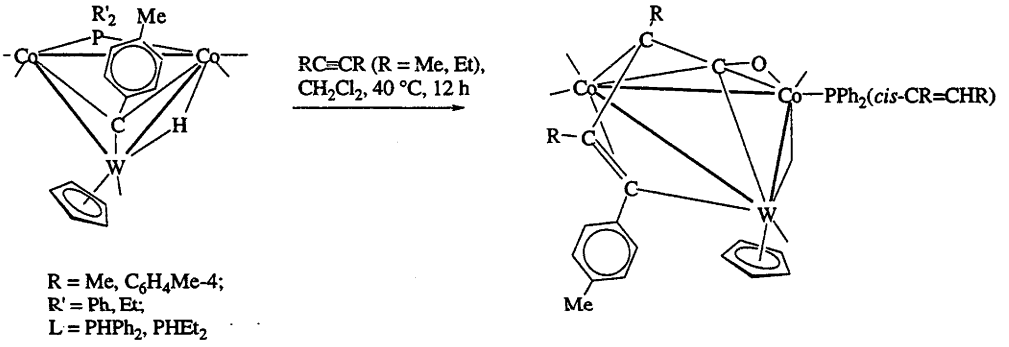


Scheme 1.2.20.

Reactions of alkynes with heterotrimetallic clusters incorporating bridging alkylidyne ligands proceeded by coupling the C_2 and C_1 ligands. Diphenylacetylene and 3-hexyne reacted with $[Mo_2Co(\mu_3\text{-}CH)(CO)_7(\eta^5\text{-}C_5H_5)_2]$ to afford cluster-bound C_3 units, but whereas the former also gave a product resulting from PhC≡CPh cleavage and C-C bond formation, forming a supported C_4 fragment, the latter gave a product from coupling the C_3 unit with CO, also resulting in a C_4 ligand (Scheme 1.2.21.).[61] 2-Butyne and 3-hexyne reacted in a similar fashion at tungsten-dicobalt alkylidyne clusters as at the dimolybdenumcobalt cluster above; coupling of acetylene, CH and CO gave a WCo_2-supported C_4 fragment, although the presence of bridging phosphido led to a side reaction involving P-C formation (Scheme 1.2.22.).[62]

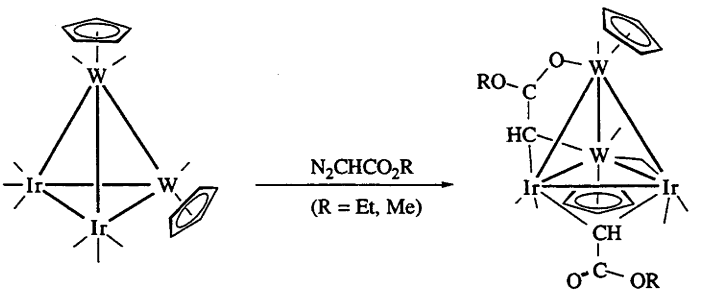


Scheme 1.2.21.



Scheme 1.2.2.22.

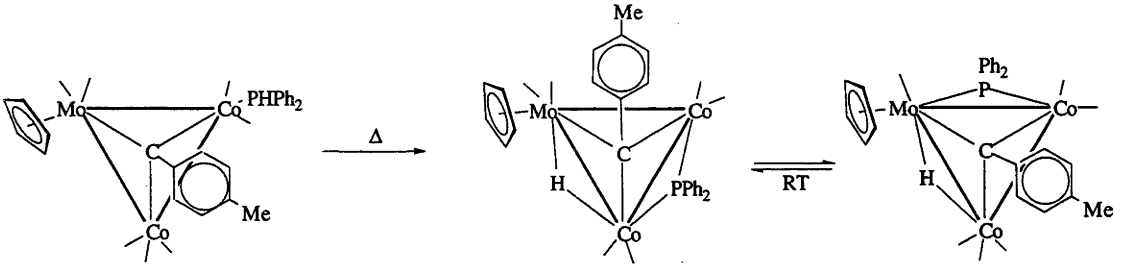
Alkyldiazocarboxylates reacted with $[W_2Ir_2(CO)_{10}(\eta^5\text{-}C_5H_5)_2]$ by C-N cleavage and coordination of the resultant carbene units in two distinct environments; one CHC(O)OR ligand bridges an Ir-Ir bond, while the other capped a W_2Ir face by bridging a W-Ir bond and the ester carbonyl coordinating to the oxophilic tungsten atom (Scheme 1.2.23.).[63] This product could not be obtained by C-C cleavage; both reaction of $[W_2Ir_2(CO)_{10}(\eta^5\text{-}C_5H_5)_2]$ with $RCO_2CH{=}CHCO_2R$, and attempted hydrogenation of $[W_2Ir_2\{\mu_4\text{-}\eta^2\text{-}Et(O)C_2C(O)OEt\}(CO)_8]$ were unsuccessful.



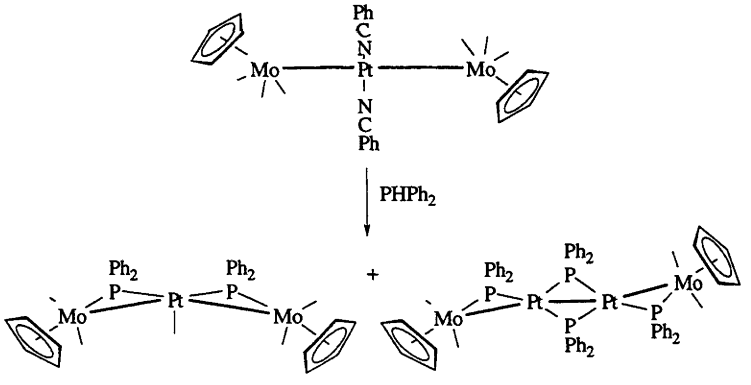
Scheme 1.2.23.

1.2.4.2. Other Ligands

Very few reports concerning transformations of ligands with other donor atoms exist (Table 1.2.5.). P-H activation at secondary phosphines is the most common motif, with heterometallic faces stabilizing the resulting fragments in each case (Schemes 1.2.24. - 1.2.26.).[62,65,66] In the formation of both $[MoCo_2(\mu\text{-}H)(\mu_3\text{-}CC_6H_4Me\text{-}4)(\mu\text{-}PPh_2)(CO)_6(\eta^5\text{-}C_5H_5)]$[65] and $[WCo_2(\mu\text{-}PR_2)_3(CO)_5(\eta^5\text{-}C_5H_5)]$ (R = Et, Ph),[62] prior coordination of phosphine at the later transition metal was observed to precede P-H activation and cleavage. Not surprisingly, double P-H activation at primary phosphines is also possible (Scheme 1.2.27.).[67]



Scheme 1.2.24.

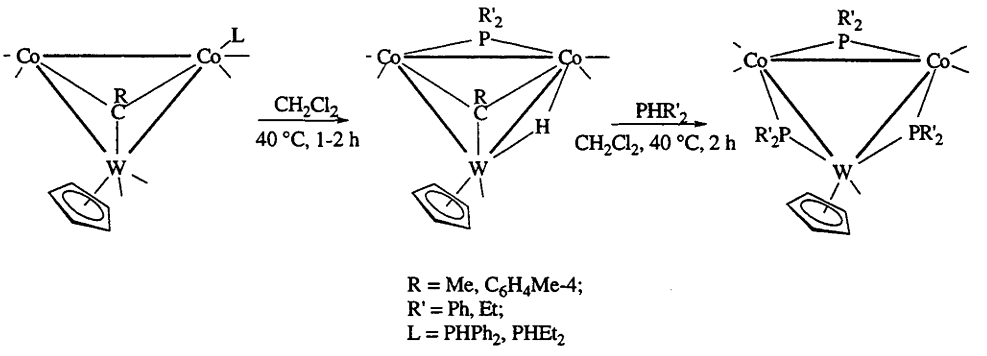


Scheme 1.2.25.

Table 1.2.5.

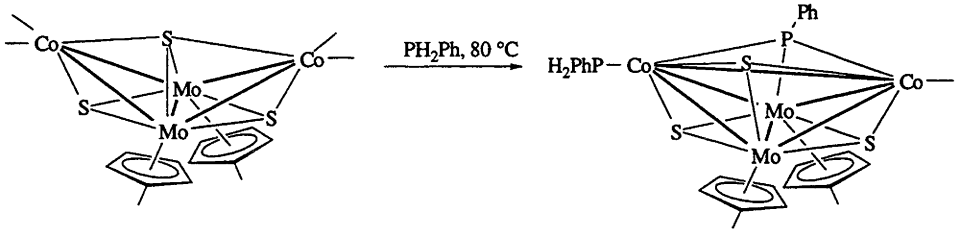
Transformation	*Product Cluster*	*Face / Bond / Metal Effecting Transformation*	*Ref.(s)*
P-H activation: $PHPh_2 \rightarrow PPh_2 + H$	$[MoCo_2(\mu\text{-}H)(\mu_3\text{-}CC_6H_4Me\text{-}4)(\mu\text{-}PPh_2)(CO)_6(\eta^5\text{-}C_5H_5)]$	$MoCo_2$ face	65
P-H activation: $PHPh_2 \rightarrow PPh_2 + H$	$[Mo_2Pt(\mu\text{-}PPh_2)_2(CO)_5(\eta^5\text{-}C_5H_5)_2]$ $[Mo_2Pt_2(\mu\text{-}PPh_2)_4(CO)_4(\eta^5\text{-}C_5H_5)_2]$	Mo_2Pt face	66
P-H activation: $PHR_2 \rightarrow PR_2 + H$ (R = Et, Ph)	$[WCo_2(\mu\text{-}PR_2)_3(CO)_5(\eta^5\text{-}C_5H_5)]$	WCo_2 face	62
P-H activation: $PH_2Ph \rightarrow PPh + H_2$	$[Mo_2Co_2(\mu_3\text{-}PPh)(\mu_3\text{-}S)_3(CO)(PH_2Ph)(\eta^5\text{-}C_5H_4Me)_2]$ $[Mo_2Co_2(\mu_3\text{-}PPh)(\mu_3\text{-}S)_3(CO)_2(\eta^5\text{-}C_5H_4Me)_2]$	$MoCo_2$ face	67
P-C, C-H activation, C-H formation: $PPh_3 \rightarrow PPhC_6H_4\text{-}2 + C_6H_6$	$[WIr_3\{\mu_3\text{-}\eta^2\text{-}PPh(C_6H_4)\}(\mu\text{-}CO)_2(CO)_7(\eta^5\text{-}C_5H_5)]$ $[WIr_3\{\mu_3\text{-}\eta^2\text{-}PPh(C_6H_4)\}(\mu\text{-}CO)_2(CO)_6(PPh_3)(\eta^5\text{-}C_5H_5)]$	Ir_3 face	68, this work

Ar-S activation: Ar-S → Ar + S	$[Mo_2Co_2(\mu_3\text{-}S)_4(CO)_2(\eta^5\text{-}L)_2]^{\cdot}$ (L = C_5H_4Me, C_5Me_4Et) $[Mo_2Co_2(\mu_4\text{-}S)(\mu_3\text{-}S)_2(CO)_3(SR)(\eta^5\text{-}C_5H_4Me)_2]$	MoCo bond / $MoCo_2$ face	69,70
S-R, S-H activation: RSH → S + RH	$[Mo_2Co_2(\mu_3\text{-}S)_4(CO)_2(\eta^5\text{-}C_5H_4Me)_2]$	$MoCo_2$ face	67
P-C, C-H formation: PPh_2 + H + RC≡CR→ PPh_2(CR=CHR) (R = Me, Et)	$[WCo_2\{\mu_3\text{-}C(C_6H_4Me\text{-}4)CEtCEtCO\}(\mu\text{-}CO)(CO)_2\{PPh_2(CR'=CHR')\}]$	WCo_2 face	62
C-C activation, P-C formation CMeCO + PPh_2 → $CMePPh_2$ + CO	$[W_3Rh_2(\mu_3\text{-}CMe)(\mu\text{-}CMe)(\mu\text{-}CMePPh_2)(\mu\text{-}CO)_3(\mu\text{-}PPh_2)(CO)_2(\eta^5\text{-}C_5H_5)_3]$	WRh bond	71,72



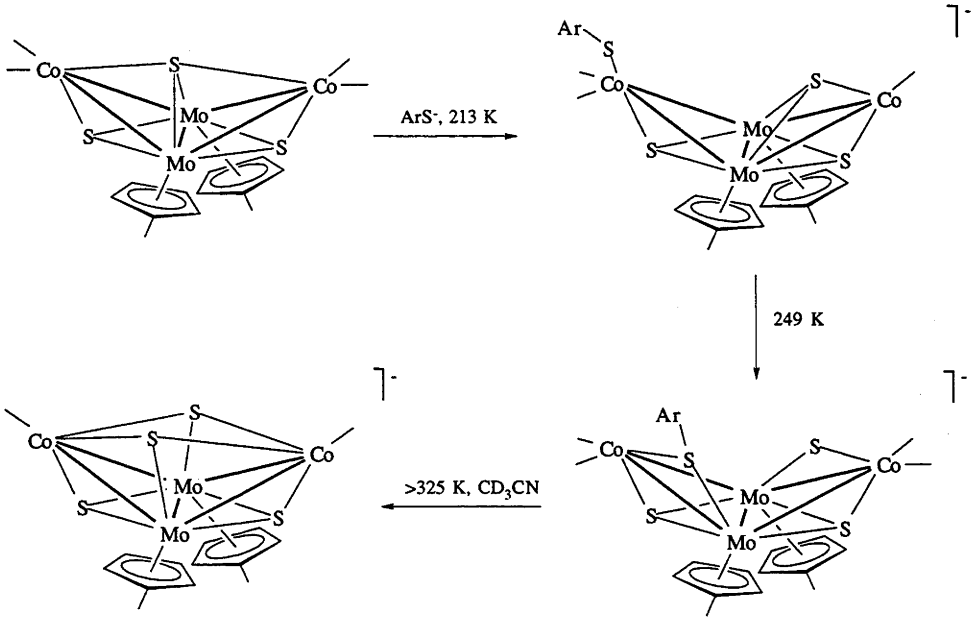
R = Me, C_6H_4Me-4;
R' = Ph, Et;
L = $PHPh_2$, $PHEt_2$

Scheme 1.2.26.

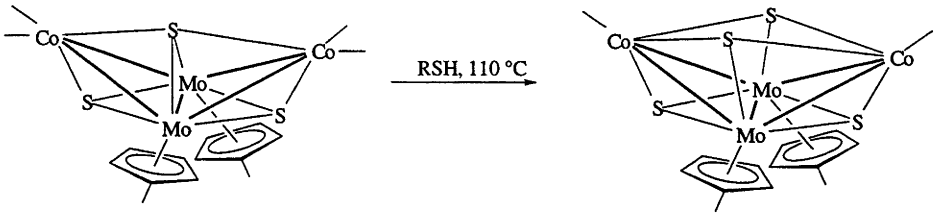


Scheme 1.2.27.

More interesting are examples of C-heteroatom cleavage. C-S cleavage has been reported at mixed molybdenum-cobalt clusters,[67,69,70] which contain a metal combination active for the industrially important hydrodesulfurization of liquid fuels. At low temperatures, coordination of thiophenoxide occurred at a cobalt, but on warming the thiophenoxide bridged a heterometallic linkage and the C-S bond eventually cleaved (Scheme 1.2.28.). At higher temperatures, the same molybdenum-cobalt cluster desulfurized a range of sulfur containing organic compounds (Scheme 1.2.29.).

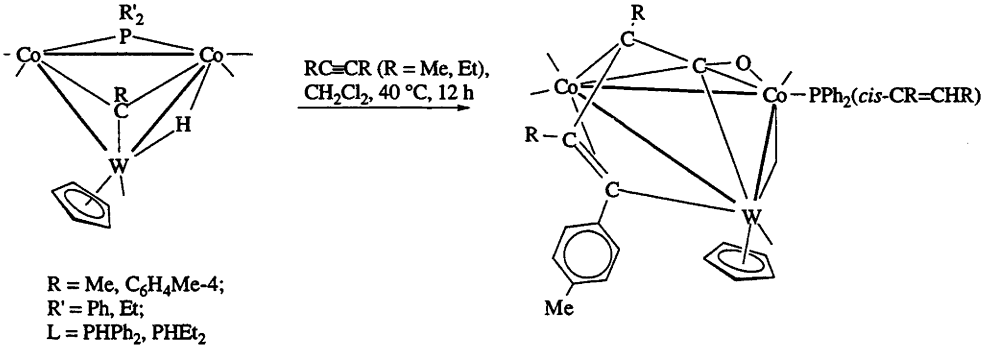


Scheme 2.1.28.

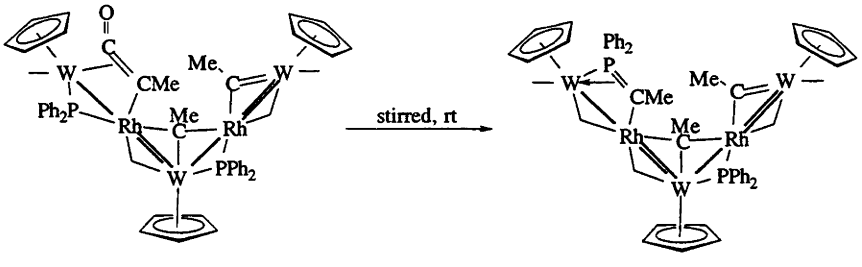


Scheme 1.2.29.

Examples of "very mixed"-metal cluster-assisted C-heteroatom bond formation are still rare, with both literature extant examples involving coupling of bridging phosphido ligand with a C-ligand. Phosphido, hydrido and alkyne were assembled stereospecifically to afford PPh_2(*cis*-CR=CHR) (Scheme 1.2.30.),[62] while an unusual isomerization replaced the bridging phosphido at a W-Rh linkage with a bridging carbonyl, affording the Ph_2P=CMe ligand (Scheme 1.2.31.).[72]



Scheme 1.2.30.



Scheme 1.2.31.

1.2.5. Core Transformations

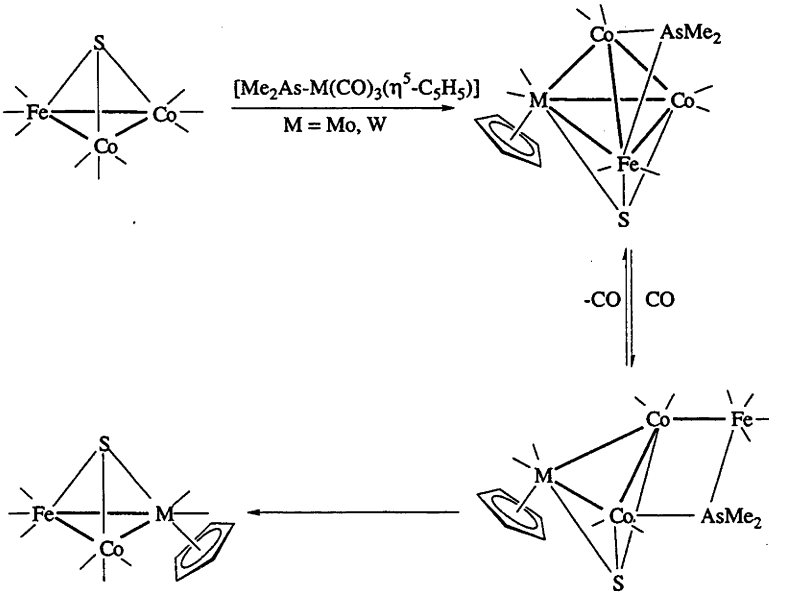
The premise of this review is that synthetic procedures for "very mixed"-metal clusters are comparatively well understood, but that reactivity and physical properties are less well-studied. Metal core transformations (modifications of a pre-existing cluster) fall into both the synthesis and reactivity categories. A summary is presented here but, as they have been reviewed elsewhere,[4,73-75] the account below is necessarily brief. Section *1.2.5.1.* considers core transformations where the cluster core nuclearity is preserved, whereas Section *1.2.5.2.* summarizes reactions involving a change in core size.

1.2.5.1. Metal Exchange

Efficient routes into "very mixed"-metal clusters by metal exchange reactions have been developed, principally by Vahrenkamp and co-workers. Metal exchange reactions are those in which one or more metal-ligand groups of a cluster are replaced by a different metal-ligand group to afford a new cluster containing the same total number of metal atoms.[1] Although metal exchange reactions could be expected to be quite complex, many reactions proceed by one-step processes, with others occurring by multi-step addition and substitution reactions involving systematic addition and incorporation of organometallic units.[4] Specific classes of reagents have been utilized to introduce the heterometal vertices by metal exchange reactions:

A. Metal carbonyl anions / cyclopentadienylmetal carbonyl anions
B. Metal carbonyls / cyclopentadienylmetal carbonyls / nickelocene / $[Pt(\eta^2\text{-}C_2H_4)(PPh_3)_2]$
C. Cyclopentadienylmetal carbonyl arsenides
D. Cyclopentadienyl carbonyl hydrides / chlorides

and Table 1.2.6. contains a classification by each reaction type. The first two types of reagents have been by far the most popular; the arsenides and hydride/chloride routes are considerably more limited in scope, with examples thus far confined to the group 6 metals. The arsenide route has been defined mechanistically (Scheme 1.2.32).



Scheme 1.2.32.

Table 1.2.6.

Compound	*Precursor Cluster, Reagent*	*Reagent Type*	*Ref.(s)*
$[MoFe_2(\mu\text{-}H)(\mu_3\text{-}S)(CO)_8(\eta^5\text{-}C_5H_5)]$	$[MoFeCo(\mu_3\text{-}S)(CO)_8(\eta^5\text{-}C_5H_5)]$, $[Fe(CO)_4]^{2-}$, H_2O	A	76
$[MCo_2(\mu_3\text{-}CR)(CO)_8(\eta^5\text{-}C_5H_5)]$ (M = Cr, Mo, W; R = H, Me, Ph, Cl)	$[Co_3(\mu_3\text{-}CR)(CO)_9]^-$, $[M(CO)_3(\eta^5\text{-}C_5H_5)]^-$ (R = H, Me, Ph); $[Co_3(\mu_3\text{-}CCl)(CO)_9]$, $[Mo(CO)_3(\eta^5\text{-}C_5H_5)]^-[ppn]^+$	A	77,78
$[MCo_2(\mu_3\text{-}CR)(CO)_8(\eta^5\text{-}C_5H_4R)]$ [M = Mo, W, R = CO_2Et, Ph, R' = Me; M = Mo, W, R = Ph, R' = C(O)H, C(O)Me, CO_2Et]	$[Co_3(\mu_3\text{-}CR)(CO)_9]$, $[M(CO)_3(\eta^5\text{-}C_5H_4R)]^-$	A	79-82
$[MCo_2(\mu_3\text{-}CCO_2Et)(CO)_8(\eta^5\text{-}C_5H_4L)]$ (M = Mo, W)	$[Co_3(\mu_3\text{-}CCO_2Et)(CO)_9]$, $[M(CO)_3(\eta^5\text{-}C_5H_4Me)]^-$	A	83
$[MCo_2(\mu_3\text{-}CR)(CO)_8(\eta^5\text{-}C_5H_5)]$ (M = Mo, W; R = Me, $SiEt_3$, H, Cl)	$[Co_3(\mu_3\text{-}CR)(CO)_9]$, $[MoCl(CO)_3(\eta^5\text{-}C_5H_5)]$ (M = Mo, R = Me); $[MoH(CO)_3(\eta^5\text{-}C_5H_5)]$ (R = Me, H, Cl); $[M(CO)_3(\eta^5\text{-}C_5H_5)]^-$ (M = Mo, R = $SiEt_3$, H, Cl; M = W, R = Me, $SiEt_3$, H); $[M(AsMe_2)(CO)_3(\eta^5\text{-}C_5H_5)]$ (M = Mo, W; R = H)	A, C, D	221
$[WCo_2(\mu_3\text{-}CCO_2Pr^i)(CO)_5(\eta^5\text{-}L)]$ (L = C_5H_4Me L = C_5Me_5)	$[Co_3(\mu_3\text{-}CCO_2Pr^i)(CO)_9]$, $[W(CO)_3(\eta^5\text{-}L)]^-$	A	93
$[MoCo_2(\mu_3\text{-}S)\{\mu\text{-}(R)\text{-}CMeNCHMeCy\}(CO)_6(\eta^5\text{-}C_5H_5)]$	$[Co_3(\mu_3\text{-}S)(CO)_7\{\mu\text{-}(R)\text{-}CMeNCHMeCy\}]$, $[Mo(CO)_3(\eta^5\text{-}C_5H_5)]^-$	A	141

$[M_2Co(\mu_3\text{-}CR)(CO)_7(\eta^5\text{-}C_5H_4R')]$ (M = Cr, Mo, W; R = R' = H; M = Mo, W; R = Ph, CO_2Et, R' = Me; M = Mo, R = Cl, R' = H)	$[Co_3(\mu_3\text{-}CCl)(CO)_9]$, $[M(CO)_3(\eta^5\text{-}C_5H_5)]^-$ (K^+, R = H); $[Co_3(\mu_3\text{-}CR)(CO)_9]$, $[M(CO)_3(\eta^5\text{-}C_5H_4Me)]^-$; $[Co_3(\mu_3\text{-}CCl)(CO)_9]$, $[Mo(CO)_3(\eta^5\text{-}C_5H_5)]^-$ [ppn^+, R = Cl]	A	78,79,84
$[MoWCo(\mu_3\text{-}CCl)(CO)_7(\eta^5\text{-}C_5H_5)_2]$	$[MoCo_2(\mu_3\text{-}CCl)(CO)_8(\eta^5\text{-}C_5H_5)]$, $[W(CO)_3(\eta^5\text{-}C_5H_5)]^-$	A	78
$[MM'Fe(\mu_3\text{-}S)(CO)_7(\eta^5\text{-}C_5H_4R)(\eta^5\text{-}C_5H_4R')]$ (M = M'= Mo, W; R = R' = H, CO_2Me, CO_2Et, C(O)Me)	$[MFeCo(\mu_3\text{-}S)(CO)_8(\eta^5\text{-}C_5H_4R)]$, $[M'(CO)_3(\eta^5\text{-}C_5H_4R')]^-$	A	222
$[MFeCo(H)(\mu_3\text{-}CR')(CO)_8(\eta^5\text{-}C_5H_4R)]$ [M = Mo, R' = Ph, R = C(O)H, C(O)Me, CO_2Et; M = Mo, R' = CO_2menthyl, R = H; M = Mo, W, R' = CO_2Et, R = Me]	$[MoCo_2(\mu_3\text{-}CR')(CO)_8(\eta^5\text{-}C_5H_4R)]$, $[Fe(CO)_4]^{2-}$, H^+	A	24,80,83
$[MRuCo(H)(\mu_3\text{-}CR)(CO)_8(\eta^5\text{-}C_5H_5)]$ (M = Mo, W; R = H, Me, Ph)	$[MCo_2(\mu_3\text{-}CR)(CO)_8(\eta^5\text{-}C_5H_5)]$, $[Ru(CO)_4]^{2-}$	A	85,86
$[MOsCo(H)(\mu_3\text{-}CR)(CO)_8(\eta^5\text{-}C_5H_5)]$ (M = Mo, W; R = H, Me, Ph)	$[MCo_2(\mu_3\text{-}CR)(CO)_8(\eta^5\text{-}C_5H_5)]$, $[Os(CO)_4]^{2-}$	A	86
$[MoRuCo(\mu_3\text{-}\eta^2\text{-}RC_2R')(CO)_8(\eta^5\text{-}C_5H_5)]$ (R = R' = Ph, Me)	$[RuCo_2(\mu_3\text{-}\eta^2\text{-}RC_2R')(CO)_9]$, $[Mo(CO)_3(\eta^5\text{-}C_5H_5)]^-$	A	103
$[WRuCo(\mu_3\text{-}PPh)(CO)_8(\eta^5\text{-}C_5H_5)]$	$[RuCo_2(\mu_3\text{-}PPh)(CO)_9]$, $[W(CO)_3(\eta^5\text{-}C_5H_5)]^-$	A	85
$[MFeCo(\mu_3\text{-}E)(CO)_8(\eta^5\text{-}C_5H_5)]$ [M = Mo, E = S, R = C(O)H, C(O)Me, CO_2Et; M = Mo, W, E = S, Se, $PNEt_2$, R = H]	$[FeCo_2(\mu_3\text{-}E)(CO)_9]$, $[M(CO)_3(\eta^5\text{-}C_5H_4R)]^-$	A	87,88
$[MoCo_2(\mu_3\text{-}CCO_2Pr^i)(CO)_9(\eta^5\text{-}L)]$ (L = C_5H_5, C_5H_4Me, C_5Me_5)	$[Co_3(\mu_3\text{-}CCO_2Pr^i)(CO)_9]$, $[Mo(CO)_3(\eta^5\text{-}L)]_2$	B	3,98,99
$[MoCo_2(\mu_3\text{-}CCO_2$menthyl$)(CO)_8(\eta^5\text{-}L)]$ (L = C_5H_5, $C_5H_4Pr^i$, C_9H_7)	$[Co_3(\mu_3\text{-}CCO_2$menthyl$)(CO)_9]$, $[Mo(CO)_3(\eta^5\text{-}L)]_2$	B	16
$[MCo_2(\mu_3\text{-}CMe)(CO)_8(\eta^5\text{-}C_5H_5)]$ (M = Mo, W)	$[Co_3(\mu_3\text{-}CMe)(CO)_9]$, $[M(CO)_3(\eta^5\text{-}C_5H_5)]_2$	B	85,89
$[WCo_2(\mu_3\text{-}CCO_2Pr^i)(CO)_5(\eta^5\text{-}L)]$ (L = C_5H_5)	$[Co_3(\mu_3\text{-}CCO_2Pr^i)(CO)_9]$, $[W(CO)_3(\eta^5\text{-}C_5H_5)]_2$	B	99

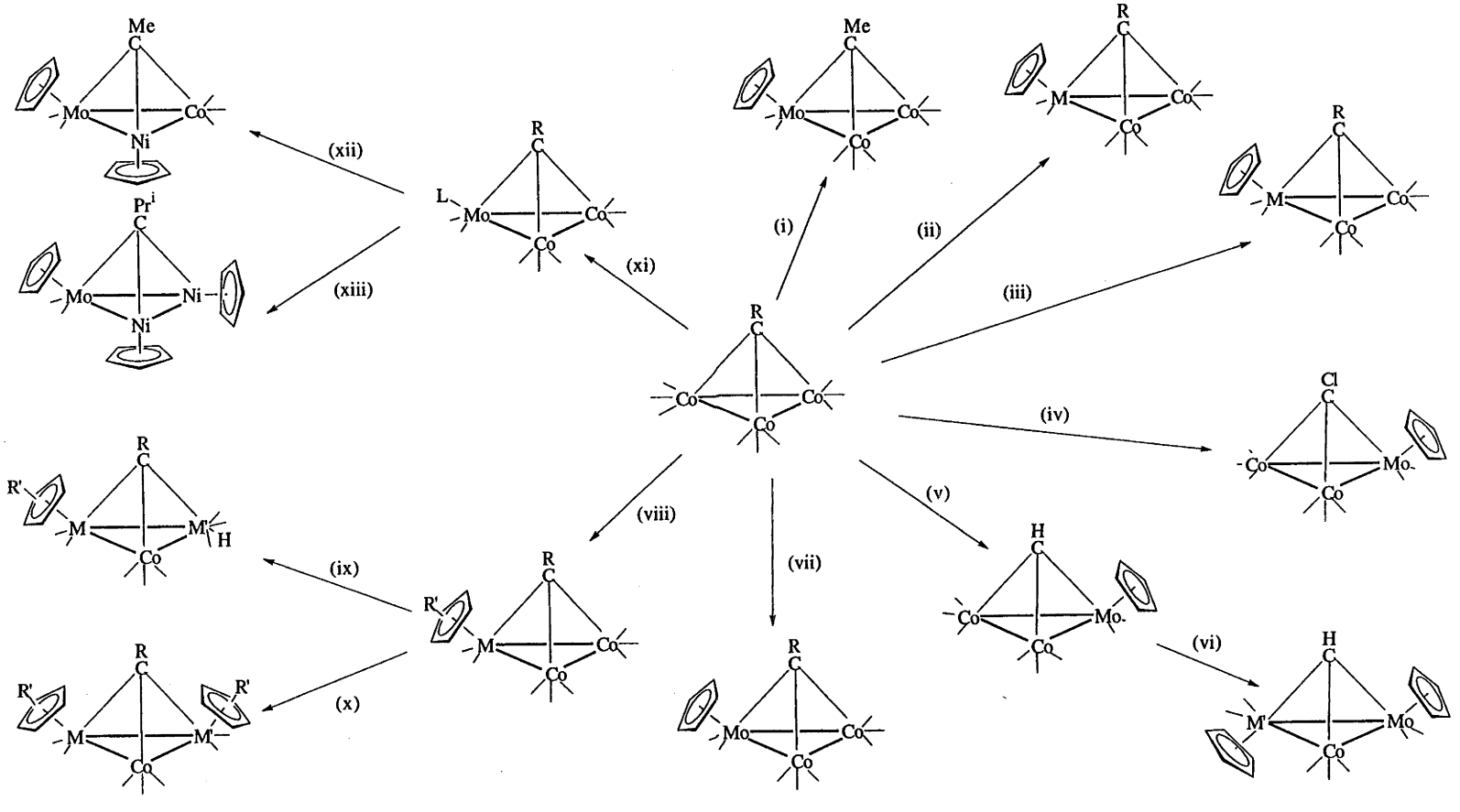
$[MoCo_2(\mu_3\text{-}As)(CO)_3(\eta^5\text{-}C_5H_5)_3]$	$[Mo_3(\mu_3\text{-}As)(CO)_6(\eta^5\text{-}C_5H_5)_3]$, $[Co(CO)_2(\eta^5\text{-}C_5H_5)]$	B	101
$[MoPt_2(\mu_3\text{-}As)(CO)_4(PPh_3)_2]$	$[Mo_3(\mu_3\text{-}As)(CO)_6(\eta^5\text{-}C_5H_5)_3]$, $[Pt(\eta^2\text{-}C_2H_4)(PPh_3)_2]$	B	90
$[Mo_2Ni(\mu_3\text{-}As)(CO)_4(\eta^5\text{-}C_5H_5)_3]$	$[Mo_3(\mu_3\text{-}As)(CO)_6(\eta^5\text{-}C_5H_5)_3]$, $[Ni(CO)(\eta^5\text{-}C_5H_5)]$	B	90
$[MM'Ru(\mu_3\text{-}S)(CO)_7(\eta^5\text{-}C_5H_5)_2]$ (M, M' = Mo, W)	$[MRuCo(\mu_3\text{-}S)(CO)_8(\eta^5\text{-}C_5H_5)]$, $[M'(CO)_3(\eta^5\text{-}C_5H_5)]_2$	B	91
$[MRuCo(\mu_3\text{-}S)(CO)_8(\eta^5\text{-}C_5H_5)]$ (M = Cr, Mo, W)	$[RuCo_2(\mu_3\text{-}S)(CO)_8\{AsMe_2M(CO)_3(\eta^5\text{-}C_5H_5)\}]$	B	92
$[MRuCo(\mu_3\text{-}S)(CO)_8(\eta^5\text{-}C_5H_5)]$ (M = Mo, W)	$[RuCo_2(\mu_3\text{-}S)(CO)_9]$, $[M(CO)_3(\eta^5\text{-}C_5H_5)]_2$	B	92
$[MoRuRh(\mu_3\text{-}\eta^2\text{-}MeC_2Me)(CO)_8(\eta^5\text{-}C_5H_5)]$	$[MoFeRu(\mu\text{-}H)(\mu_3\text{-}\eta^2\text{-}MeC_2Me)(CO)_8(\eta^5\text{-}C_5H_5)]$, base, $[Rh(CO)_2Cl]_2$	B	223
$[MoRuNi(\mu_3\text{-}\eta^2\text{-}MeC_2Me)(CO)_5(\eta^5\text{-}C_5H_5)]$	$[MoRuCo(\mu_3\text{-}\eta^2\text{-}MeC_2Me)(CO)_8(\eta^5\text{-}C_5H_5)]$, $[Ni(CO)(\eta^5\text{-}C_5H_5)]_2$	B	223
$[MoCoNi(\mu_3\text{-}CR)(CO)_5(\eta^5\text{-}C_5H_5)_2]$	$[MoCo_2(\mu_3\text{-}CR)(CO)_8(\eta^5\text{-}C_5H_5)]$ (R = Me, CO_2menthyl, CO_2Pr^i), $[Ni(CO)(\eta^5\text{-}C_5H_5)]_2$; $[Co_2Ni(\mu_3\text{-}CMe)(CO)_6(\eta^5\text{-}C_5H_5)]$, $[Mo(CO)_3(\eta^5\text{-}C_5H_5)]_2$	B	24,89,93
$[MoNi_2(\mu_3\text{-}CCO_2Pr^i)(CO)_2(\eta^5\text{-}C_5H_5)_3]$	$[MoCo_2(\mu_3\text{-}CCO_2Pr^i)(CO)_8(\eta^5\text{-}C_5H_5)$, $[Ni(\eta^5\text{-}C_5H_5)_2]$	B	93
$[MoCo_3(\mu\text{-}CO)_3(CO)_8(\eta^5\text{-}C_5H_5)]$	$[Co_4(CO)_9(\eta^6\text{-mesitylene})]$, $[Mo(CO)_3(\eta^5\text{-}C_5H_5)]_2$	B	224
$[Mo_2Co_2(\mu\text{-}CO)_3(CO)_7(\eta^5\text{-}C_5H_5)_2]$	$[Co_4(CO)_9(\eta^6\text{-mesitylene})]$, $[Mo(CO)_3(\eta^5\text{-}C_5H_5)]_2$	B	224
$[MoCo_2(\mu_3\text{-}CCO_2\text{menthyl})(CO)_8(\eta^5\text{-}C_5H_5)]$	$[Co_3(\mu_3\text{-}CCO_2\text{menthyl})(CO)_9]$, $[Mo(AsMe_2)(CO)_3(\eta^5\text{-}C_5H_5)]$	C	24
$[MCo_2(\mu_3\text{-}CR)(CO)_8\{\eta^5\text{-}C_5H_5\}]$ (M = Cr, Mo, W, R = H, Me, Ph; M = Mo, W, R = C_6H_4Me-4)	$[Co_3(\mu_3\text{-}CR)\{AsMe_2M(CO)_3(\eta^5\text{-}C_5H_5)\}(CO)_8]$	C	94

$[MCo_2(\mu_3\text{-}GeR)(CO)_8(\eta^5\text{-}C_5H_5)]$ (M = Mo, R = Me, Ph, Bu^t; M = W, R = Bu^t)	$[Co_3(\mu_3\text{-}GeR)(CO)_9]$, $[M(AsMe_2)(CO)_3(\eta^5\text{-}C_5H_5)]$	C	102
$[MM'Fe(\mu_3\text{-}S)(CO)_7(\eta^5\text{-}C_5H_5)]$ (M, M' = Mo, W)	$[MFeCo(\mu_3\text{-}S)(CO)_8(\eta^5\text{-}C_5H_5)]$, $[M'(AsMe_2)(CO)_3(\eta^5\text{-}C_5H_5)]$	C	91
$[MFeCo(\mu_3\text{-}S)(CO)_8(\eta^5\text{-}C_5H_5)]$ (M = Mo, W)	$[FeCo_2(\mu_3\text{-}S)(CO)_9]$, $[M(AsMe_2)(CO)_3(\eta^5\text{-}C_5H_5)]$	C	95
$[MoFeCo(\mu_3\text{-}S)(CO)_8(\eta^5\text{-}C_5H_4Me)]$	$[Fe_2Co(\mu\text{-}H)(\mu_3\text{-}S)(CO)_9]$, $[MoCl(CO)_3(\eta^5\text{-}C_5H_4Me)]$	D	100
$[MoRuCo(\mu_3\text{-}\eta^2\text{-}RC_2H)(CO)_8(\eta^5\text{-}C_5H_5)]$ (R = Me, Ph)	$[RuCo_2(\mu_3\text{-}\eta^2\text{-}RC_2H)(CO)_9]$, $[MoCl(CO)_3(\eta^5\text{-}C_5H_5)]$	D	96
$[MCo_3(\mu\text{-}CO)_3(CO)_8(\eta^5\text{-}C_5H_5)]$ (M = Mo, W)	$[Co_4(CO)_{12}]$, $[MH(CO)_3(\eta^5\text{-}C_5H_5)]$	D	170
$[CrWPd_2(\mu_3\text{-}CO)_2(\mu\text{-}CO)_4(PPh_3)_2(\eta^5\text{-}C_5H_5)_2]$	$[Cr_2Pd_2(\mu_3\text{-}CO)_2(\mu\text{-}CO)_4(PPh_3)_2(\eta^5\text{-}C_5H_5)_2]$, $[WH(CO)_3(\eta^5\text{-}C_5H_5)]$	D	132

The trinuclear clusters $[Co_3(\mu_3\text{-}CR)(CO)_9]$ are the most common precursors utilized in the "very mixed"-metal exchange reactions reported thus far (Scheme 1.2.33.), as the $[Co(CO)_3]$ unit is the most readily displaced group in metal exchange reactions.[16,23,77,80,84,86,93,97-99] Early studies in this area have been reviewed;[4] more recently, extensions to the metal exchange procedure have been explored using different μ_3-CR groups, and varying co-ligands on the metal exchange reagents. For example, the reactions between $[Co_3(\mu_3\text{-}CR)(CO)_9]$ (R = $SiEt_3$, H, Cl, Br) and $[M(CO)_3(\eta^5\text{-}C_5H_5)]^-$ (M = Mo, W) afforded $[MCo_2(\mu_3\text{-}CR)(CO)_8(\eta^5\text{-}C_5H_5)]$, the reactivity of the μ_3-CR apical substituent resulting in low yields of the products.[221] The reactions of $[Co_3(\mu_3\text{-}CPh)(CO)_9]$ and $[M(CO)_3(\eta^5\text{-}C_5H_4R)]^-$ [M = Mo, W; R = C(O)H, C(O)Me, CO_2Et] afforded $[MCo_2(\mu_3\text{-}CR)(CO)_8(\eta^5\text{-}C_5H_4R)]$; incorporating an electron-withdrawing group on the cyclopentadienyl ligand reduced the activity of the exchange reagent.[82, 80, 81] An alternative route to $[MCo_2(\mu_3\text{-}CR)(CO)_8(\eta^5\text{-}C_5H_5)]$ (M = Cr, Mo, W; R = H, Me, Ph) involves electron transfer catalysis.[77] Reaction of $[Co_3(\mu_3\text{-}CR)(CO)_9]$, the metal exchange reagent and a catalytic amount of benzophenone ketyl under varying conditions afforded the clusters in good yield. This reaction proceeded rapidly at room temperature, in contrast to the classical metal exchange reaction, which required heating in benzene for three days.[23,97]

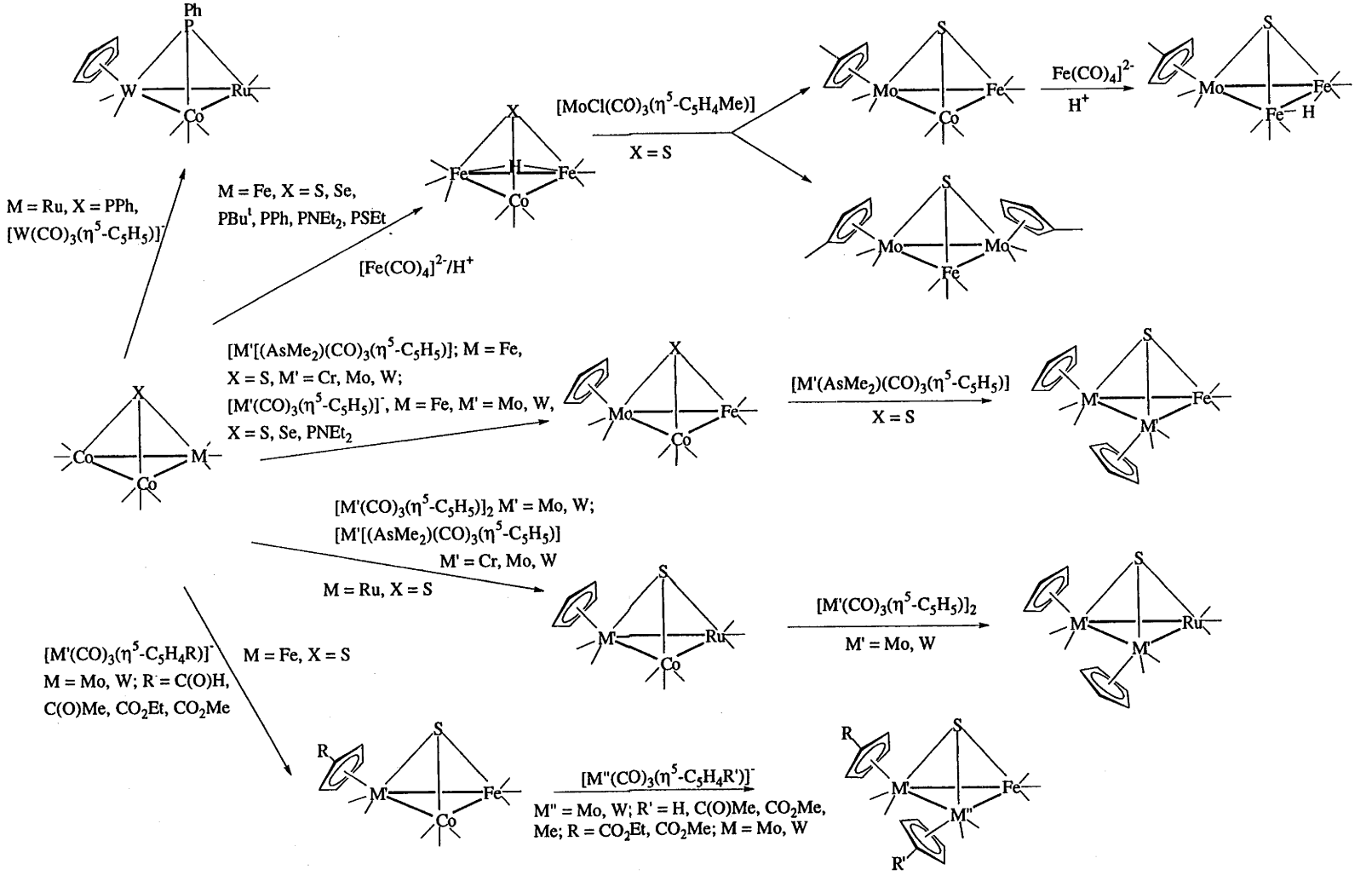
Many examples of sequential metal-exchange at trinuclear clusters have been reported, which can afford tetrahedral clusters which are chiral by virtue of four different core consituents (Scheme 1.2.33.). Metal exchange can proceed by three steps; the cluster $[MoNi_2(\mu_3\text{-}CPr^i)(CO)_2(\eta^5\text{-}C_5H_5)_2]$[93] is an example of metal exchange in which all three $[Co(CO)_3]$ units of the precursor cluster have been replaced with other moieties.

While the apical substituent in these clusters has usually been an alkylidyne group, other face capping ligands have also been successfully employed. For example, the clusters $[MFeCo(\mu_3\text{-}X)(CO)_8(\eta^5\text{-}C_5H_5)]$ (M = Mo, W, X = S, Se, $PNEt_2$),[87] $[MoFeCo(\mu_3\text{-}S)(CO)_8(\eta^5\text{-}C_5H_4L)]$ [L = C(O)H, C(O)Me, C(O)OEt],[88] $[MoFeCo(\mu_3\text{-}S)(CO)_8(\eta^5\text{-}C_5H_5)]$,[91] and $[MoRuCo(\mu_3\text{-}S)(CO)_8(\eta^5\text{-}C_5H_5)]$[91] were formed by metal exchange reactions with $[FeCo_2(\mu_3\text{-}S)(CO)_9]$, itself prepared by metal exchange from the precursor cluster $[Co_3(\mu_3\text{-}X)(CO)_9]$ (Scheme 1.2.34.). $[Fe_2Co(\mu\text{-}H)(\mu_3\text{-}S)(CO)_9]$, prepared from $[FeCo_2(\mu_3\text{-}S)(CO)_9]$, reacted with $[Mo(CO)_3(\eta^5\text{-}C_5H_5)]^-$ to afford $[MoFeCo(\mu_3\text{-}S)(CO)_8(\eta^5\text{-}C_5H_4Me)]$ and $[Mo_2Fe(\mu_3\text{-}S)(CO)_8(\eta^5\text{-}C_5H_4Me)_2]$.[100] A capping arsenic atom has also been employed; one or two $[Mo(CO)_2(\eta^5\text{-}C_5H_5)]$ vertices in the trimolybdenum precursor $[Mo_3(\mu_3\text{-}As)(CO)_6(\eta^5\text{-}C_5H_5)_3]$ were replaced (Scheme 1.2.35.).[101, 90] The flexibility of this procedure has also been demonstrated utilizing clusters with capping germylidyne groups (Scheme 1.2.36.).[102]

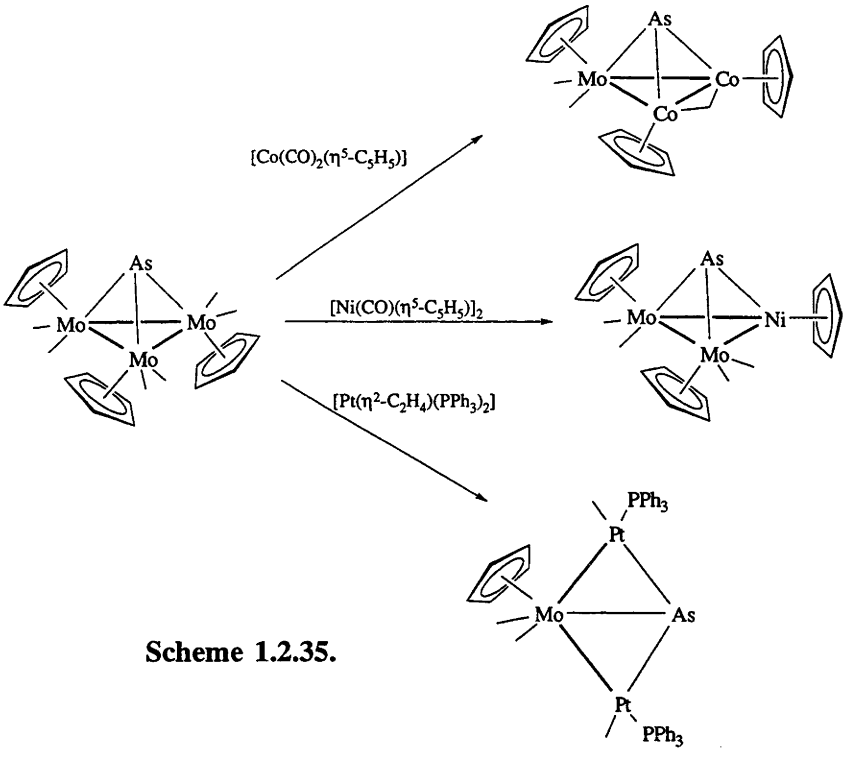


(i) $[MoX(CO)_3(\eta^5\text{-}C_5H_5)]$, X = H, Cl; R = Me. (ii) $[M(CO)_3(\eta^5\text{-}C_5H_5)]^-$, BPK; M = Cr, Mo, W; R = H, Me. (iii) $[M(AsMe_2)(CO)_3(\eta^5\text{-}C_5H_5)]$; M = Cr, Mo, W; R = H, Me, Ph, C_6H_4Me-4. (iv) $[M(CO)_3(\eta^5\text{-}C_5H_5)]^-[ppn]^+$; R = Cl. (v) $[M(CO)_3(\eta^5\text{-}C_5H_5)]^-\ Na^+, K^+$; M = Cr, Mo, W; R = Cl. (vi) $[M'(CO)_3(\eta^5\text{-}C_5H_5)]^-$; M = Mo; M = Mo, W. (vii) $[M(CO)_3(\eta^5\text{-}C_5H_5)]^-$; M = Mo, W; R = $SiEt_3$, H. (viii) $[M(CO)_3(\eta^5\text{-}C_5H_4R')]^-$; M = Mo, W; R' = C(O)H, C(O)Me, CO_2Et; R = Ph; M = Mo, W, R' = H, R = H, Me, Ph; M = Mo, R' = H, R = CO_2menthyl; M = Mo, W, R' = CO_2Et, R = Me; M = Mo, W; R' = Me, R = Ph, CO_2Et. (ix) $[Fe(CO)_4]^{2-}/H^+$; R' = C(O)H, C(O)Me, CO_2Et; R = Ph, M = Mo, M' = Fe; R' = H, R = CO_2menthyl; M = Mo, M' = Fe, R' = Me, R = CO_2Et; M = Mo, W, M' = Fe. (x) $[M'(CO)_4]^{2-}/H^+$; R = H, Me, Ph; M = Mo, W; M' = Ru, Os; M, M' = Mo, W, R = Ph, CO_2Et; R' = Me. (xi) $[M(CO)_3(\eta^5\text{-}L)]_2$; M = W, L = C_5H_5, R = Me; M = Mo, L = $C_5H_4Pr^i$, C_5H_5, C_9H_7, R = CO_2menthyl; M = Mo, L = C_5H_5, C_5H_4Me, C_5Me_5, R = Pr^i. (xii) $[Ni(CO)(\eta^5\text{-}C_5H_5)]_2$; M = Mo, L = $\eta^5\text{-}C_5H_5$; R = Pr^i, Me. (xiii) $[Ni(\eta^5\text{-}C_5H_5)_2]$; M = Mo, L = $\eta^5\text{-}C_5H_5$; R = Pr^i.

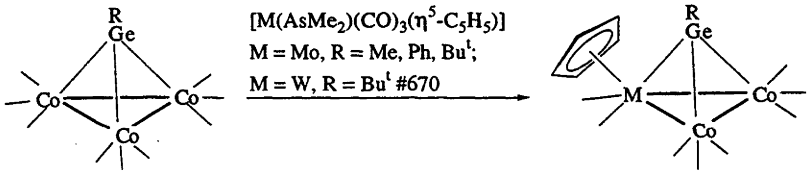
Scheme 1.2.33.


Ph
P
W
Ru
Co
M = Ru, X = PPh,
[W(CO)3(η5-C5H5)]-
M = Fe, X = S, Se,
PBut, PPh, PNEt2, PSEt
[Fe(CO)4]2-/H+
X
Fe
H
Fe
Co
[MoCl(CO)3(η5-C5H4Me)]
X = S
S
Mo
Fe
Co
Fe(CO)4]2-
H+
S
Mo
Fe
Fe
H
S
Mo
Mo
Fe
X
Co
M
Co
[M'[(AsMe2)(CO)3(η5-C5H5)]; M = Fe,
X = S, M' = Cr, Mo, W;
[M'(CO)3(η5-C5H5)]-, M = Fe, M' = Mo, W,
X = S, Se, PNEt2
X
Mo
Fe
Co
[M'(AsMe2)(CO)3(η5-C5H5)]
X = S
S
M'
Fe
M'
[M'(CO)3(η5-C5H5)]2 M' = Mo, W;
[M'[(AsMe2)(CO)3(η5-C5H5)]
M' = Cr, Mo, W
M = Ru, X = S
S
M'
Ru
Co
[M'(CO)3(η5-C5H5)]2
M' = Mo, W
S
M'
Ru
M'
[M'(CO)3(η5-C5H4R)]-
M = Mo, W; R = C(O)H,
C(O)Me, CO2Et, CO2Me
M = Fe, X = S
R
S
M'
Fe
Co
[M''(CO)3(η5-C5H4R')]-
M'' = Mo, W; R' = H, C(O)Me, CO2Me,
Me; R = CO2Et, CO2Me; M = Mo, W
R
S
M'
Fe
M''
R'

Scheme 1.2.34.

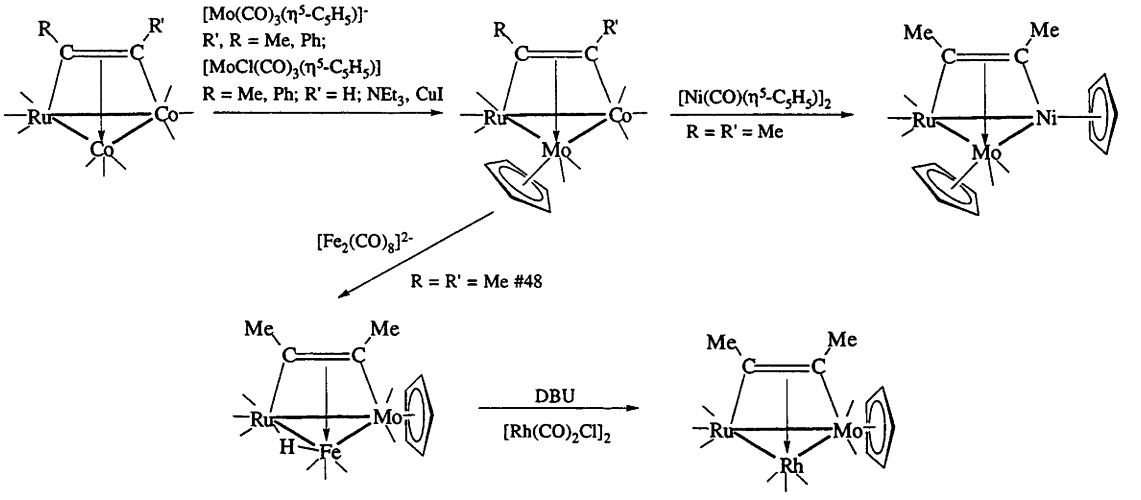


Scheme 1.2.35.



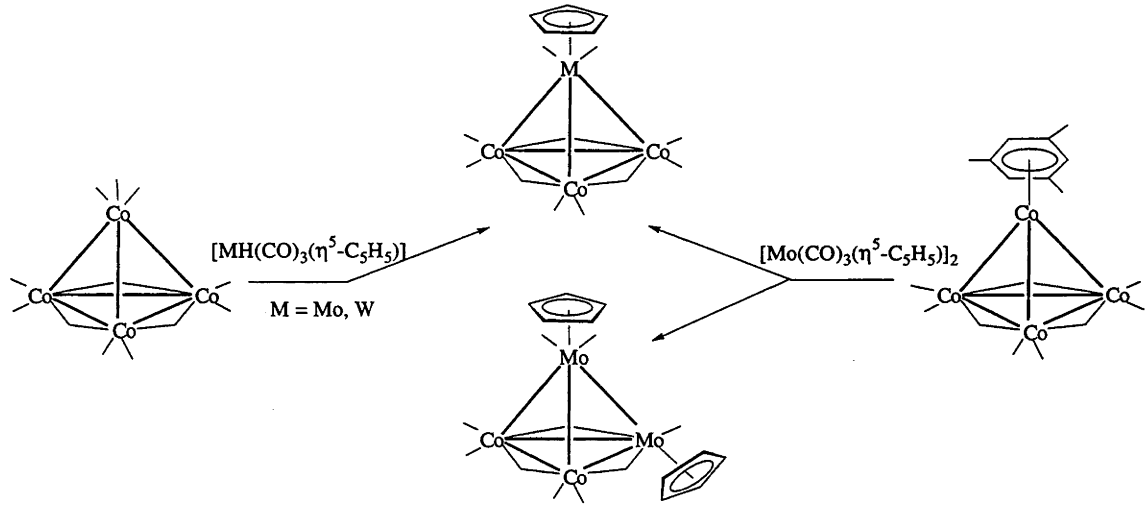
Scheme 1.2.36.

Metal exchange methods have also been utilized with alkyne-bridged clusters. For example, $[RuCo_2(\mu_3\text{-}\eta^2\text{-}RC_2R')(CO)_9]$ was the precursor to $[MRuCo(\mu_3\text{-}\eta^2\text{-}RC_2R')(CO)_8(\eta^5\text{-}C_5H_5)]$ (M = Mo, W; R = Ph, Me, R' = Ph, Me), $[MoRuNi(\mu_3\text{-}\eta^2\text{-}MeC_2Me)(CO)_5(\eta^5\text{-}C_5H_5)]$ and $[RuCoNi(\mu_3\text{-}\eta^2\text{-}RC_2R')(CO)_6(\eta^5\text{-}C_5H_5)]$ (R = Ph, Me, R' = Ph, Me) (Scheme 1.2.37.).[103]

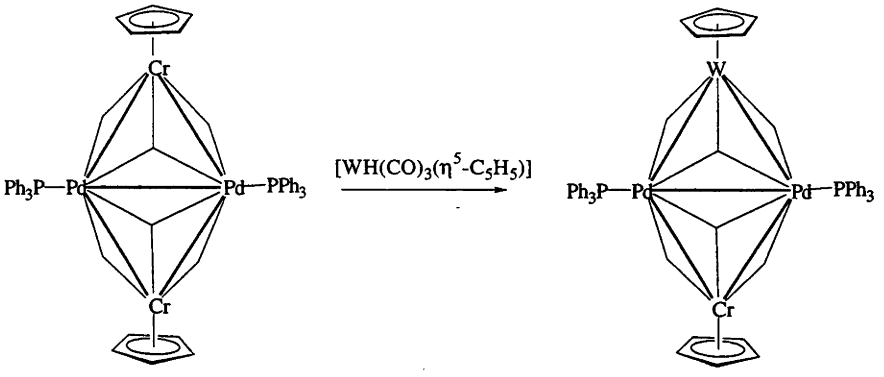


Scheme 1.2.37.

Although metal exchange procedures to afford "very mixed"-metal clusters have been utilized most frequently with trinuclear clusters, reactions involving tetranuclear clusters have also been successful. The reaction of $[Co_4(CO)_{12}]$ with $[MH(CO)_3(\eta^5\text{-}C_5H_5)]$ (M = Mo, W) afforded the tetrahedral cluster $[MCo_3(\mu\text{-}CO)_3(CO)_8(\eta^5\text{-}C_5H_5)]$.[170] A similar reaction between $[Co_4(CO)_9(\eta^6\text{-}1,3,5\text{-}C_6H_3Me)_3]$ and $[Mo(CO)_3(\eta^5\text{-}C_5H_5)]_2$ likewise afforded $[MCo_3(\mu\text{-}CO)_3(CO)_8(\eta^5\text{-}C_5H_5)]$, together with $[Mo_2Co_2(\mu\text{-}CO)_3(CO)_7(\eta^5\text{-}C_5H_5)_2]$ (Scheme 1.2.38.).[224] The butterfly cluster $[Cr_2Pd_2(\mu_3\text{-}CO)_2(\mu\text{-}CO)_4(PPh_3)_2(\eta^5\text{-}C_5H_5)_2]$ reacted with $[WH(CO)_3(\eta^5\text{-}C_5H_5)]$ to afford $[CrWPd_2(\mu_3\text{-}CO)(\mu\text{-}CO)_4(PPh_3)_2(\eta^5\text{-}C_5H_5)_2]$ (Scheme 1.2.39.).[132] Metal exchange to afford higher nuclearity "very mixed"-metal clusters may also be possible, but has yet to be exploited.



Scheme 1.2.38.



Scheme 1.2.39.

1.2.5.2. Core Expansion or Core Contraction

Reactions of clusters with mono or dinuclear metal complexes frequently provides a method of expanding the metal core nuclearity under controlled conditions. The majority of medium- and high-nuclearity homometallic clusters have been prepared from lower-nuclearity cluster precursors by thermolyses ("heat-it-and-hope") reactions. This is less true of the heterometallic clusters in this Section, with three synthetic procedures employed extensively to afford a controlled means of obtaining clusters of different nuclearity. Nucleophilic substitution by a metal complex nucleophile on a cluster, or a cluster nucleophile on a metal complex ("redox condensation"), bridge-assisted procedures employing a variety of flexible ligands, and Stone's systematic stepwise assembly of medium- and high-nuclearity cluster chains and stars have all proved highly successful. Table 1.2.7. collects "very mixed"-metal clusters synthesized by expansion or contraction of pre-existing cluster complexes.

The reaction of $[M_4(\mu\text{-}CO)_3(CO)_9]$ (M = Co, Rh) with $[Cr(CO)_6(\eta^6\text{-}PhC_2Ph)]$ (which has a pendant acetylene linkage) afforded products dependent on the precursor cluster; whereas the lighter cluster fragmented to afford $[Co_2(\mu_3, \eta^2{:}\eta^6\text{-}PhC_2Ph)(CO)_2Cr(CO)_3]$, the heavier cluster $[Rh_4(\mu\text{-}CO)_3(CO)_9]$ reacted with $[Co_2(CO)_2(\mu_3\text{-}\eta^2{:}\eta^6\text{-}PhC_2Ph)Cr(CO)_3]$ by expansion of the cluster core, yielding the crystallographically characterized $[CrRh_4(\mu_5, \eta^2{:}\eta^6\text{-}PhC_2Ph)(\mu\text{-}CO)_2(CO)_{10}]$, with a spiked butterfly coordination geometry (Scheme 1.2.40.).[119]

Table 1.2.7.

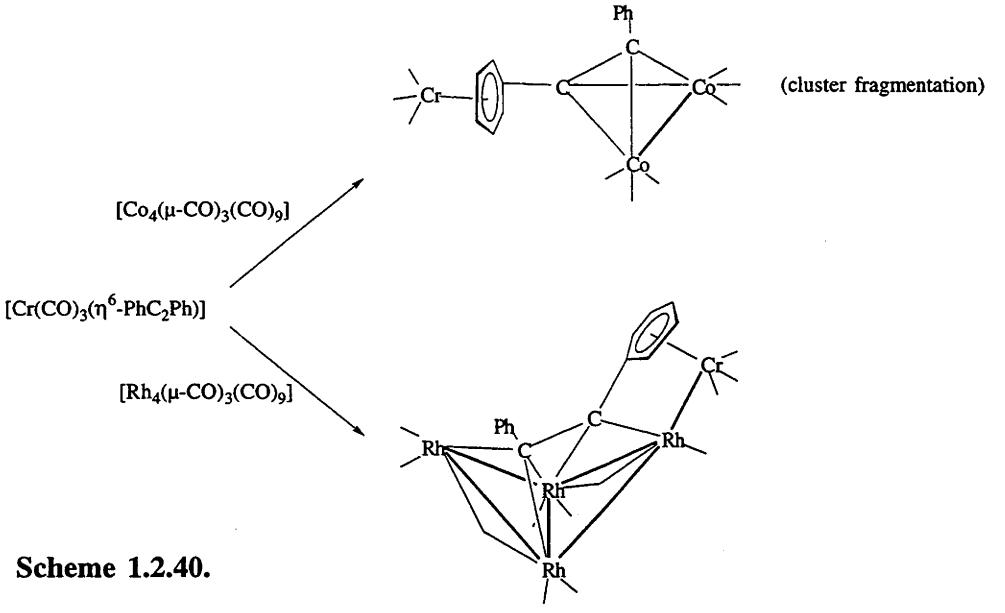
M_n	*Cluster*	*Reactants*	*Ref.(s)*
n = 3	$[MCo_2(\mu_3\text{-CR})(CO)_8(\eta^5\text{-}C_5H_5)]$ (M = Mo, W; R = Me, Ph)	$[MCo_3(\mu_3\text{-CR})(\mu\text{-}AsMe_2)(CO)_8(\eta^5\text{-}C_5H_5)]$, CO	104
	$[MFeCo(\mu_3\text{-PR})(CO)_8(\eta^5\text{-}C_5H_5)]$ (M = Mo, R = Ph, Bu^t; M = W, R = Bu^t)	$[MFeCo_2(\mu_3\text{-PR})(\mu\text{-}AsMe_2)(CO)_8(\eta^5\text{-}C_5H_5)]$, CO	104
	$[MM'Co(\mu_3\text{-S})(CO)_8(\eta^5\text{-}C_5H_5)]$ (M = Mo, W; M' = Fe, Ru)	$[MM'Co_2(\mu_3\text{-S})(\mu\text{-}AsMe_2)(CO)_8(\eta^5\text{-}C_5H_5)]$, CO	104
n = 4	$[M_2M'Pd(\mu\text{-dppm})_2(CO)_5(\eta^5\text{-}C_5H_5)_2]$	$[MM'Pd(\mu_3\text{-}CO)_2(\mu\text{-dppm})_2(Cl)(\eta^5\text{-}C_5H_5)]$ (M = Mo, W; M' = Pd, Pt), $[M(CO)_3(\eta^5\text{-}C_5H_5)]^-$	37,105
	$[Cr_3Co(\mu_3\text{-S})_4(CO)(\eta^5\text{-}C_5H_5)_3]$	$[Cr_2Co(\mu_3\text{-S})_2(\mu\text{-}SBu^t)(CO)_2(\eta^5\text{-}C_5H_5)_2]$, PhC_2Ph	106
	$[Cr_2Co_2(\mu_4\text{-S})(\mu_3\text{-S})_2(CO)_4(\eta^5\text{-}C_5H_5)(\eta^5\text{-}C_5H_4Bu^t)]$	$[Cr_4Ni(\mu_3\text{-S})_4(\mu\text{-}SBu^t)_2(\eta^5\text{-}C_5H_5)_4]$, $[Co_2(CO)_8]$	107
	$[MoCo_3(\mu_4\text{-As})(\mu_3\text{-CO})_2(\eta^5\text{-}C_5H_5)_3(L)]$ (L = η^5-C_5H_5 or η^5-C_5H_4Me)	$[Mo_3(\mu_3\text{-As})(CO)_6(L)_3]$, $[Co(CO)_2(\eta^5\text{-}C_5H_5)]$	101
	$[MoNi_3(\mu_3\text{-CO})_3(\eta^5\text{-}C_5H_5)_4]$	$[Ni_3(\mu_3\text{-CO})_2(\eta^5\text{-}C_5H_5)_3]$, $[Mo(CO)_3(\eta^5\text{-}C_5H_5)]_2$	108
	$[M_2Pt_2(\mu_3\text{-CR})(\mu\text{-CR})(CO)_4(\eta^4\text{-cod})(L)_2]$ (M = Mo, W; R = C_6H_4Me-4, L = η^5-C_5H_5, η^5-C_5Me_5; R = Me, L = η^5-C_5Me_5)	$[M_2Pt(\mu\text{-CR})_2(CO)_4(\eta^5\text{-}C_5H_5)_2]$, $[Pt(\eta^4\text{-cod})_2]$	109-112
	$[MPt_3(\mu\text{-dppm})_3(CO)_3]^+$ (M = Mn, Re)	$[Pt_3(\mu\text{-CO})_3(\mu\text{-dppm})_3]^{2+}$, $[M(CO)_5]^-$	113
	$[Re_3Pt(\mu\text{-H})(CO)_{13}]^{2-}$	$[\{Pt_3(CO)_6\}_n]^{2-}$ ($n \approx 10$), $[Re_2(\mu\text{-H})(H)_2(CO)_8]^-$	114
	$[Mn_2Pd_2(\mu\text{-dppm})_2(CO)_9]$	$[MnPd_2(\mu\text{-dppm})_2(Cl)(CO)_4]$, $[Mn(CO)_5]^-$	105

	$[Re_2Pt(\mu\text{-}H)_2(CO)_9(\eta^4\text{-cod})\{M'\}]$ ($M' = [Mn(CO)_5]^-$, $[ReH(CO)_4(PPh_3)]$, $[ReH(CO)_3(PPh_3)_2]$, $[W(CO)_3(\eta^5\text{-}C_5H_5)]^-$, $[Co(CO)_4]^-$)	$[Re_2Pt(\mu\text{-}H)_2(CO)_8(\eta^4\text{-cod})]$, [M']	115
	$[M_2M'Pt(\mu_3\text{-CR})(\mu\text{-CR})(CO)_4(\eta^4\text{-cod})(L)_2]$ (M = Mo, W; M' = Ni, Pt; L = $\eta^5\text{-}C_5H_5$, $\eta^5\text{-}C_5Me_5$; R = C_6H_4Me-4, Me	$[M_2M'(\mu\text{-CR})_2(CO)_4(L)_2]$, $[Pt(\eta^4\text{-cod})_2]$ (M = Mo, M' = Ni, Pt; M = W, M' = Ni, Pt)	109,111
	$[MoWPt_2(\mu_3\text{-}\sigma\text{:}\eta^6\text{-}7,9\text{-}Me_2\text{-}7,9\text{-}C_2B_{10}H_8\text{-}12\text{-}OC)(\mu_3\text{-}CC_6H_4Me\text{-}4)(CO)_5(PMe_3)_2(\eta^5\text{-}C_5H_5)]$	$[MoW_2Pt_2(\mu_3\text{-}\sigma\text{:}\eta^6\text{-}7,9\text{-}Me_2\text{-}7,9\text{-}C_2B_{10}H_8\text{-}12\text{-}OC)(\mu_3\text{-}CC_6H_4Me\text{-}4)(\mu\text{-}CC_6H_4Me\text{-}4)(\mu\text{-}CO)_2(CO)_5(\eta^5\text{-}C_5H_5)_2]$, PMe_3	116
	$[MoFeCo_2(\mu_3\text{-}CCO_2Pr^i)(CO)_{11}(\eta^5\text{-}C_5H_5)]$	$[MoCo_2(\mu_3\text{-}CCO_2Pr^i)(CO)_8(\eta^5\text{-}C_5H_5)]$, $[Fe_2(CO)_9]$	93
	$[MoFeCo_2(\mu_4\text{-}CCO_2Pr^i)(CO)_5(\eta^5\text{-}C_5H_5)_3]$	$[MoCo_2(\mu_3\text{-}CCO_2Pr^i)(\mu\text{-}CO)(CO)_2(\eta^5\text{-}C_5H_5)_3]$, $[Fe_2(CO)_9]$	93
	$[MoFeRuCo(\mu_3\text{-}\eta^2\text{-}MeC_2Me)(CO)_{10}(\eta^5\text{-}C_5H_5)]$	$[MoRuCo(\mu_3\text{-}\eta^2\text{-}MeC_2Me)(CO)_8(\eta^5\text{-}C_5H_5)]$, $[Fe_2(CO)_9]$	117
	$[MRuCoRh(\mu_3\text{-}\eta^2\text{-}MeC_2Me)(CO)_7(\eta^5\text{-}C_5H_5)_2]$ (M = Mo, W)	$[MRuCo(\mu_3\text{-}\eta^2\text{-}MeC_2Me)(CO)_8(\eta^5\text{-}C_5H_5)]$, $[Rh(CO)_2(\eta^5\text{-}C_5H_5)]$	117
	$[MoFeNi_2(\mu_3\text{-}CCO_2Pr^i)(CO)_5(\eta^5\text{-}C_5H_5)_3]$	$[MoNi_2(\mu_3\text{-}CCO_2Pr^i)(CO)_2(\eta^5\text{-}C_5H_5)_3]$, $[Fe_2(CO)_9]$	93
	$[MoCoMPd(\mu_3\text{-}CO)_2(\mu\text{-dppm})_2(CO)_4(\eta^5\text{-}C_5H_5)]$ (M = Pd, Pt)	$[CoMPd(\mu_3\text{-}CO)_2(\mu\text{-dppm})_2(Cl)(CO)]$, $[Mo(CO)_3(\eta^5\text{-}C_5H_5)]^-$	105
	$[MM'CoPd(\mu_3\text{-}CO)_2(\mu\text{-dppm})_2(CO)_4(\eta^5\text{-}C_5H_5)]$ (M = Pd, Pt; M' = Mo, W; not all combinations)	$[MM'Pd(\mu_3\text{-}CO)_2(\mu\text{-dppm})_2(Cl)(CO)]$, $[Co(CO)_4]^-$	105
	$[MnCoMPd(\mu\text{-}CO)_2(\mu\text{-dppm})_2(CO)_7]$ (M = Pd, Pt; X = Cl, I, not all combinations)	$[CoMPd(\mu_3\text{-}CO)_2(\mu\text{-dppm})_2(X)(CO)]$, $[Mn(CO)_5]^-$; $[PdPtCl_2(\mu\text{-dppm})_2]$, $[Mn(CO)_5]^-$	105,118
	$[MnCoPdPt(\mu\text{-dppm})_2(CO)_8]$	$[CoPdPtCl_2(\mu\text{-dppm})_2]$, $[Mn(CO)_5]^-$	118
n = 5	$[CrRh_4(\mu_5\text{-}\eta^2\text{:}\eta^6\text{-}PhC_2Ph)(CO)_{12}]$	$[Rh_4(CO)_{12}]$, $[Cr(CO)_3(\eta^6\text{-}PhC_2Ph)]$	119
	$[MoRh_4(\mu_3\text{-As})(CO)_3(\eta^5\text{-}C_5H_5)_5]$	$[Mo_3(\mu_3\text{-As})(CO)_6(\eta^5\text{-}C_5H_5)_3]$, $[Rh(CO)_2(\eta^5\text{-}C_5H_5)]$	43

	$[Mo_2Pt_3(\mu_3\text{-}CC_6H_4Me\text{-}4)_2(CO)_4(\eta^4\text{-}cod)_2(\eta^5\text{-}C_5H_5)_2]$	$[Mo_2Pt(\mu\text{-}CC_6H_4Me\text{-}4)_2(CO)_4(\eta^5\text{-}C_5H_5)_2]$, $2[Pt(\eta^4\text{-}cod)_2]$	120
	$[M_2Pt_3(\mu_3\text{-}CR)_2(CO)_4(\eta^4\text{-}cod)_2(\eta^5\text{-}L)_2]$ (M = Mo, W; R = C_6H_4Me-4, Me, L = C_5H_5, C_5Me_5)	$[M_2Pt(\mu\text{-}CR)_2(CO)_4(\eta^5\text{-}L)_2]$, $2.5[Pt(\eta^4\text{-}cod)_2]$	109,112
	$[W_3Pt_2(\mu_3\text{-}CR)(\mu\text{-}CR)_2(CO)_6(L)_3]$ (R = C_6H_4Me-4, Me L = $\eta^5\text{-}C_5H_5$, $\eta^5\text{-}C_5Me_5$; not all combinations)	$[W_2Pt_2(\mu_3\text{-}CR)(\mu\text{-}CR)(CO)_4(\eta^4\text{-}cod)(L)_2]$, $[W(\equiv CR)(CO)_2(\eta^5\text{-}C_5H_5)]$	109,110
	$[W_3Pt_2(\mu_3\text{-}CR)(\mu\text{-}CR')(\mu\text{-}CR'')(CO)_6(L)(L')_2]$ (R, R', R'' = Me, C_6H_4Me-4; L, L' = $\eta^5\text{-}C_5H_5$, $\eta^5\text{-}C_5Me_5$)	$[W_3Pt_2(\mu_3\text{-}CR)(\mu\text{-}CR')(CO)_4(\eta^4\text{-}cod)(L)_2]$, $[W(\equiv CR)(CO)_2(L')]$	109
	$[W_3Pt_2(\mu_3\text{-}CR)_2(\mu\text{-}CR')(\mu\text{-}CR'')(CO)_6(L)(L')_2]$ (R, R', R'' = Me, C_6H_4Me-4; L, L' = $\eta^5\text{-}C_5H_5$, $\eta^5\text{-}C_5Me_5$)	$[W_2Pt_2(\mu_3\text{-}CR)(\mu\text{-}CR')_2(CO)_4(\eta^4\text{-}cod)(L)_2]$, $[W(\equiv CR'')(CO)_2(L)$	109
	$[Re_4Pt(\mu\text{-}H)_6(CO)_{16}]$	$[Re_2Pt(\mu\text{-}H)_2(CO)_8(\eta^4\text{-}cod)]$, $[Re_2(\mu\text{-}H)_2(CO)_8]$	121
	$[Re_4Pt(CO)_{17}]^{2-}$	$[\{Pt_3(CO)_6\}_n]^{2-}$ ($n \approx 10$), $[Re(CO)_5]^-$	114
	$[Cr_2Fe_2M(\mu_3\text{-}S)_4(\mu\text{-}SBu^t)(CO)_6(\eta^5\text{-}L)_2]$	$[Fe_2(\mu\text{-}S)_2(CO)_6]$, $[Cr_2M(\mu_3\text{-}S)_2(\mu\text{-}SBu^t)(L)(\eta^5\text{-}L')_2]$ [M = Co, L = $(CO)_2$, L' = C_5H_4Me; M = Rh, L = η^4-cod, L' = C_5H_5]	122
	$[MoW_2Pt_2(\mu_3\text{-}\sigma\text{:}\eta^6\text{-}7,9\text{-}Me_2\text{-}7,9\text{-}C_2B_{10}H_8\text{-}12\text{-}OC)(\mu_3\text{-}CC_6H_4Me\text{-}4)(\mu\text{-}CC_6H_4Me\text{-}4)(\mu\text{-}CO)_2(CO)_5(\eta^5\text{-}C_5H_5)_2]$	$[MoPt_2(\mu_3\text{-}\sigma\text{-}\sigma'\text{:}\eta^6\text{-}7,9\text{-}Me_2\text{-}7,9\text{-}C_2B_{10}H_8)(\mu\text{-}CO)(CO)_2(\eta^4\text{-}cod)_2]$, $[W(\equiv CC_6H_4Me\text{-}4)(CO)_2(\eta^5\text{-}C_5H_5)]$	116
	$[Mo_2NiPt_2(\mu_3\text{-}CC_6H_4Me\text{-}4)_2(CO)_4(\eta^4\text{-}cod)_2(\eta^5\text{-}C_5H_5)_2]$	$[Mo_2NiPt(\mu_3\text{-}CC_6H_4Me\text{-}4)(\mu\text{-}CC_6H_4Me\text{-}4)(CO)_4(\eta^4\text{-}cod)(\eta^5\text{-}C_5H_5)_2]$, $[Pt(\eta^4\text{-}cod)_2]$	111
n = 6	$[W_3Pt_3(\mu_3\text{-}CMe)_2(\mu\text{-}CMe)(CO)_6(\eta^4\text{-}cod)(\eta^5\text{-}C_5Me_5)_3]$	$[W_3Pt_2(\mu_3\text{-}CMe)(\mu\text{-}CMe)_2(CO)_6(\eta^5\text{-}C_5Me_5)_3]$, $[Pt(\eta^4\text{-}cod)_2]$, C_2H_4	120
	$[RePt_5(\mu\text{-}O)_3(\mu\text{-}OH)(CO)_5(PCy_3)_4]^+$	$[Pt_3(\mu\text{-}CO)_3(PCy_3)_3]$, $[Re_2O_7]$	123
	$[W_2Mn_2Pt_2(\mu_3\text{-}CO)_2(\mu\text{-}CO)_4(CO)_4(\mu\text{-}dppm)_2(\eta^5\text{-}C_5H_4Me)_2]$	$[Mn(\eta^1\text{-}dppm)(CO)_2(\eta^5\text{-}C_5H_4Me)]$, $[W_2Pt(CO)_6(NCPh)_2(\eta^5\text{-}C_5H_4Me)_2]$	124
n = 7	$[W_4Ni_3(\mu_3\text{-}CMe)_2(\mu\text{-}CMe)_2(CO)_8(\eta^5\text{-}C_5Me_5)_4]$	$[W_2Ni(\mu\text{-}CMe)_2(CO)_4(\eta^5\text{-}C_5Me_5)_2]$, $[Ni(\eta^4\text{-}cod)_2]$	120

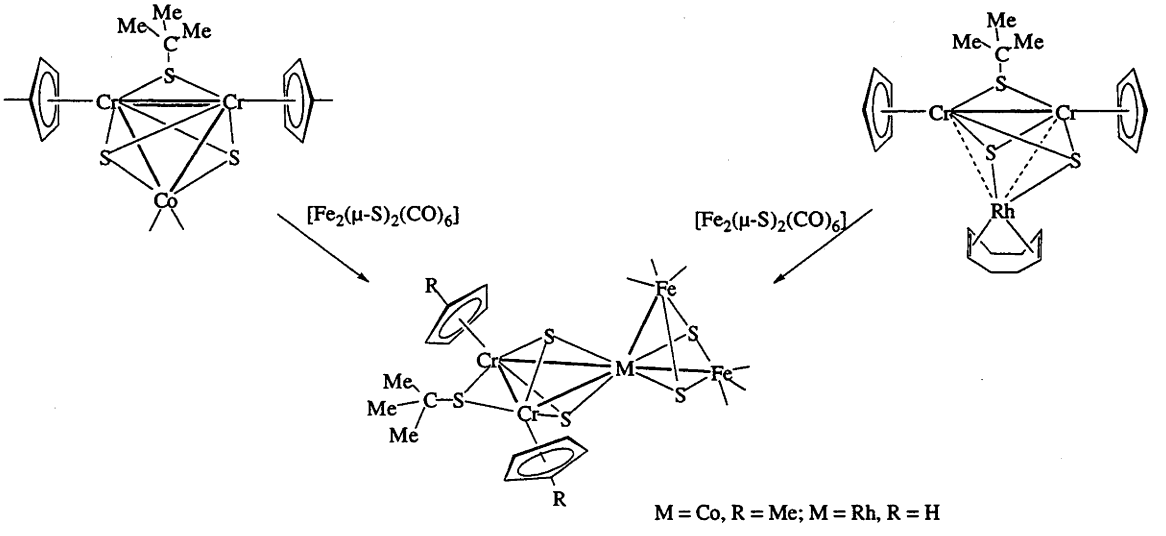
	$[W_4Pt_3(\mu_3\text{-}CC_6H_4Me\text{-}4)_2(\mu\text{-}CC_6H_4Me\text{-}4)_2(CO)_8(\eta^5\text{-}C_5H_5)_4]$	$[W_2Pt_3(\mu_3\text{-}CC_6H_4Me\text{-}4)_2(CO)_4(\eta^4\text{-cod})_2(\eta^5\text{-}C_5H_5)_2]$, $[W(\equiv CC_6H_4Me\text{-}4)(CO)_2(\eta^5\text{-}C_5H_5)]$	120,125
	$[W_4Pt_3(\mu_3\text{-CMe})_2(\mu\text{-CMe})_2(CO)_8(L)(\eta^5\text{-}C_5Me_5)_3]$ (L = η^5-C_5H_5, η^5-C_5Me_5)	$[W_3Pt_3(\mu_3\text{-CMe})_2(\mu\text{-CMe})(CO)_6(\eta^4\text{-cod})(\eta^5\text{-}C_5Me_5)_3]$, $[W(\equiv CMe)(CO)_2(L)]$ (3 atm C_2H_4)	120
	$[Mo_2WPt_3(\mu_3\text{-}CC_6H_4Me\text{-}4)_2(\mu\text{-CMe})(CO)_6(\eta^4\text{-cod})(\eta^5\text{-}C_5H_5)_3]$	$[Mo_2Pt_3(\mu_3\text{-}CC_6H_4Me\text{-}4)_2(CO)_4(\eta^4\text{-cod})_2(\eta^5\text{-}C_5H_5)_2]$, $[W(\equiv CMe)(CO)_2(\eta^5\text{-}C_5H_5)]$ (3 atm C_2H_4)	120
	$[Mo_2WPt_4(\mu_3\text{-}CC_6H_4Me\text{-}4)_2(\mu_3\text{-CMe})(CO)_6(\eta^4\text{-cod})_2(\eta^5\text{-}C_5H_5)_3]$	$[Mo_2WPt_3(\mu_3\text{-}CC_6H_4Me\text{-}4)_2(\mu\text{-CMe})(CO)_6(\eta^4\text{-cod})(\eta^5\text{-}C_5H_5)_3]$, 1.5 $[Pt(\eta^4\text{-cod})_2]$	34,35
	$[Mo_2W_2Pt_3(\mu_3\text{-}CC_6H_4Me\text{-}4)_2(\mu\text{-CMe})_2(CO)_8(\eta^5\text{-}C_5H_5)(L)_2]$ (L = η^5-C_5H_5, η^5-C_5Me_5)	$[Mo_2Pt_3(\mu_3\text{-}CC_6H_4Me\text{-}4)_2(CO)_4(\eta^4\text{-cod})_2(\eta^5\text{-}C_5H_5)_2]$, $[W(\equiv CMe)(CO)_2(L)]$ (3 atm C_2H_4)	120
	$[W_4NiPt_2(\mu_3\text{-CMe})_2(\mu\text{-CMe})_2(CO)_8(\eta^5\text{-}C_5Me_5)_4]$	$[W_2Pt(\mu\text{-CMe})_2(CO)_4(\eta^5\text{-}C_5Me_5)_2]$, $[Ni(\eta^4\text{-cod})_2]$	120
	$[Mo_2W_2NiPt_2(\mu_3\text{-}CC_6H_4Me\text{-}4)_2(\mu\text{-CR})_2(CO)_8(\eta^5\text{-}C_5H_5)_2(\eta^5\text{-L})_2]$	$[Mo_2NiPt_2(\mu_3\text{-}CC_6H_4Me\text{-}4)_2(CO)_4(\eta^4\text{-cod})_2(\eta^5\text{-}C_5H_5)_2]$, $[W(\equiv CPh)(CO)_2(\eta^5\text{-}C_5H_5)]$ (2 atm C_2H_4) (R = Ph, L = C_5H_5); $[MoWPt(\mu\text{-}CC_6H_4Me\text{-}4)(\mu\text{-CMe})(CO)_4(\eta^5\text{-}C_5H_5)(\eta^5\text{-}C_5Me_5)]$, $[Ni(\eta^4\text{-cod})_2]$ (R = Me, L = C_5Me_5)	111
n = 8	$[Mn_2Pd_2(\mu\text{-}\eta^2\text{-CN})_2(CO)_6(\eta^5\text{-}C_5H_4Me)_2]_2$	$[Pd_4(\mu\text{-OAc})_4(CO)_4](AcOH)_2$, $[Mn(CN)(CO)_2(\eta^5\text{-}C_5H_4Me)]^-$	126
	$[Re_7Pd(\mu_6\text{-C})(CO)_{21}(L)]^{2-}$ (L = η^3-1-phenylallyl, η^3-1-C_3H_5)	$[Re_7(\mu_6\text{-C})(CO)_{21}]^{2-}$, $[Pd(L)Cl]_2$	127,128
	$[Re_7Pt(\mu_6\text{-C})(CO)_{21}(L)]^{2-}$ (L = η^3-1-methylallyl, Me_3)	$[Re_7(\mu_6\text{-C})(CO)_{21}]^{2-}$, $[Pt(\eta^3\text{-}C_4H_7)Cl]_2$ or $[PtMe_3I]_4$	128
	$[Mo_4Pd_4(\mu_3\text{-CO})_4(\mu\text{-CO})_8(\eta^5\text{-}C_5H_5)_4]^{2-}$	$[Pd_4(\mu\text{-OAc})_4(CO)_4]$, $[Mo(CO)_3(\eta^5\text{-}C_5H_5)]^-$	129
	$[W_4Ni_2Pt_2(\mu_3\text{-CPh})_4(CO)_8(\eta^5\text{-}C_5H_5)_4]$, $[W_4Ni_2Pt_2(\mu_3\text{-CPh})_3(\mu\text{-CPh})(\mu\text{-CO})(CO)_7(\eta^5\text{-}C_5H_5)_4]$ (two isomers)	$[W_2Pt(\mu\text{-CPh})(CO)_4(\eta^5\text{-}C_5H_5)_2]$, $[Ni(\eta^4\text{-cod})_2]$	130,131

	$[M_4Ni_2Pt_2(\mu_3\text{-}CC_6H_4Me\text{-}4)_3(\mu\text{-}CC_6H_4Me\text{-}4)(\mu\text{-}CO)(CO)_7(\eta^5\text{-}C_5H_5)_4]$ (two isomers) (M = Mo, W)	$[M_2Pt(\mu\text{-}CC_6H_4Me\text{-}4)_2(CO)_4(\eta^5\text{-}C_5H_5)_2]$, $[Ni(\eta^4\text{-}cod)_2]$	111,130,131
	$[W_4Pt_4(\mu_3\text{-}CC_6H_4Me\text{-}4)_3(\mu\text{-}CC_6H_4Me\text{-}4)(\mu\text{-}CO)(CO)_7(\eta^5\text{-}C_5H_5)_4]$	$[W_4Pt_3(\mu_3\text{-}CC_6H_4Me\text{-}4)_2(\mu\text{-}CC_6H_4Me\text{-}4)_2(CO)_8(\eta^5\text{-}C_5H_5)_4]$, $[Pt(\eta^2\text{-}C_2H_4)_3]$ or $[Pt(\eta^4\text{-}cod)_2]$; $[W_2Pt_2(\mu_3\text{-}CC_6H_4Me\text{-}4)(\mu\text{-}CC_6H_4Me\text{-}4)(CO)_4(\eta^5\text{-}C_5H_5)_2]$, C_2H_4	125,131
	$[W_4NiPt_3(\mu_3\text{-}CC_6H_4Me\text{-}4)_3(\mu\text{-}CC_6H_4Me\text{-}4)(\mu\text{-}CO)(CO)_7(\eta^5\text{-}C_5H_5)_4]$ (two isomers)	$[W_4Pt_3(\mu_3\text{-}CC_6H_4Me\text{-}4)_2(\mu\text{-}CC_6H_4Me\text{-}4)_2(CO)_8(\eta^5\text{-}C_5H_5)_4]$, $[Ni(\eta^4\text{-}cod)_2]$	131
	$[M'_2W_2Ni_2Pt_2(\mu_3\text{-}CR)_2(\mu_3\text{-}CR')_2(CO)_8(\eta^5\text{-}C_5H_5)_4]$ (R = Ph, C_6H_4Me-4; R' = Me, C_6H_4Me-4; not all combinations)	$[MM'Pt(\mu\text{-}CR)(\mu\text{-}CR')(CO)_4(\eta^5\text{-}C_5H_5)_2]$, $[Ni(\eta^4\text{-}cod)_2]$ (M, M' = Mo, W)	111,131
n = 9	$[Mo_2W_3Pt_4(\mu_3\text{-}CC_6H_4Me\text{-}4)_2(\mu_3\text{-}CMe)(\mu\text{-}CR)_2(CO)_{10}(\eta^5\text{-}C_5H_5)_5]$ (R = Me, C_6H_4Me-4)	$[Mo_2WPt_4(\mu_3\text{-}CR)_2(\mu_3\text{-}CMe)(CO)_6(\eta^4\text{-}cod)_2(\eta^5\text{-}C_5H_5)_3]$, 2 $[W(\equiv CR)(CO)_2(\eta^5\text{-}C_5H_5)]$	34,35
n = 10	$[Mo_2W_3Pt_5(\mu_3\text{-}CC_6H_4Me\text{-}4)_3(\mu_3\text{-}CMe)(\mu\text{-}CC_6H_4Me\text{-}4)(CO)_{10}(\eta^4\text{-}cod)(\eta^5\text{-}C_5H_5)_5]$	$[Mo_2W_3Pt_4(\mu_3\text{-}CC_6H_4Me\text{-}4)_2(\mu_3\text{-}CMe)(\mu\text{-}CC_6H_4Me\text{-}4)_2(CO)_{10}(\eta^5\text{-}C_5H_5)_5]$, 2.4 $[Pt(\eta^4\text{-}cod)_2]$	35
n =11	$[Mo_2W_3Pt_6(\mu_3\text{-}CC_6H_4Me\text{-}4)_4(\mu_3\text{-}CMe)(CO)_{10}(\eta^4\text{-}cod)_2(\eta^5\text{-}C_5H_5)_5]$	$[Mo_2W_3Pt_4(\mu_3\text{-}CC_6H_4Me\text{-}4)_2(\mu_3\text{-}CMe)(\mu\text{-}CC_6H_4Me\text{-}4)_2(CO)_{10}(\eta^5\text{-}C_5H_5)_5]$, 2.4 $[Pt(\eta^4\text{-}cod)_2]$	35
	$[Mo_2W_3Pt_6(\mu_3\text{-}CC_6H_4Me\text{-}4)_2(\mu_3\text{-}CMe)_3(CO)_{10}(\eta^4\text{-}cod)_2(\eta^5\text{-}C_5H_5)_5]$	$[Mo_2W_3Pt_4(\mu_3\text{-}CC_6H_4Me\text{-}4)_2(\mu_3\text{-}CMe)(\mu\text{-}CMe)_2(CO)_{10}(\eta^5\text{-}C_5H_5)_5]$, 2.4 $[Pt(\eta^4\text{-}cod)_2]$	34,35

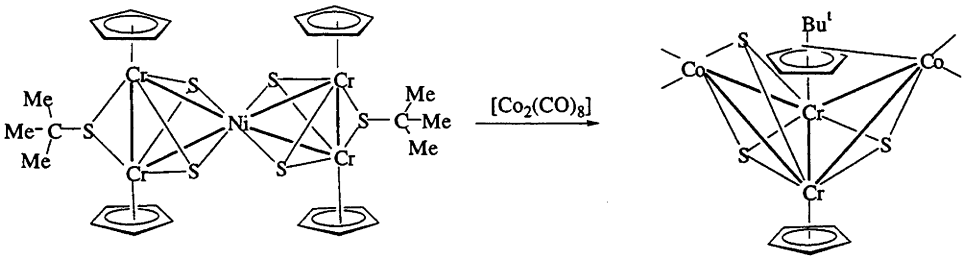


Scheme 1.2.40.

Sulfido bridging ligands can facilitate cluster expansion. Photolysis of the triangular clusters $[Cr_2Co(\mu_3\text{-}S)_2(\mu\text{-}SBu^t)(CO)_2(\eta^5\text{-}C_5H_4Me)_2]$ or $[Cr_2Rh(\mu_3\text{-}S)_2(\mu\text{-}SBu^t)(\eta^4\text{-}cod)(\eta^5\text{-}C_5H_5)_2]$ in the presence of $[Fe_2(\mu\text{-}S)_2(CO)_6]$ afforded the clusters $[Cr_2Fe_2M(\mu_3\text{-}S)_4(\mu\text{-}SBu^t)(CO)_6(\eta^5\text{-}C_5H_4R)_2]$ (M = Co, R = Me; M = Rh, R = H) (Scheme 1.2.41.).[122] Sulfido bridging ligands can also maintain some metal-metal connectivity upon cluster fragmentation. Reaction of the cluster $[Cr_4Ni(\mu_3\text{-}S)_4(\mu\text{-}SBu^t)_2(\eta^5\text{-}C_5H_5)_4]$, with a bow-tie core geometry, and $[Co_2(CO)_8]$ afforded a lower nuclearity cluster $[Cr_2Co_2(\mu_4\text{-}S)(\mu_3\text{-}S)_4(CO)_4(\eta^5\text{-}C_5H_5)(\eta^5\text{-}C_5H_4Me)]$ with a butterfly coordination geometry; this complex reaction also involves an unusual transfer of a tertiary butyl group from the μ-SBu^t ligand to one of the η^5-cyclopentadienyl ligands (Scheme 1.2.42.).[107]

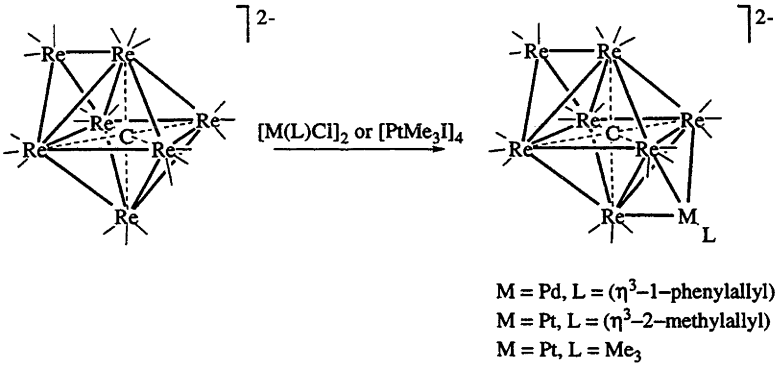


Scheme 1.2.41.



Scheme 1.2.42.

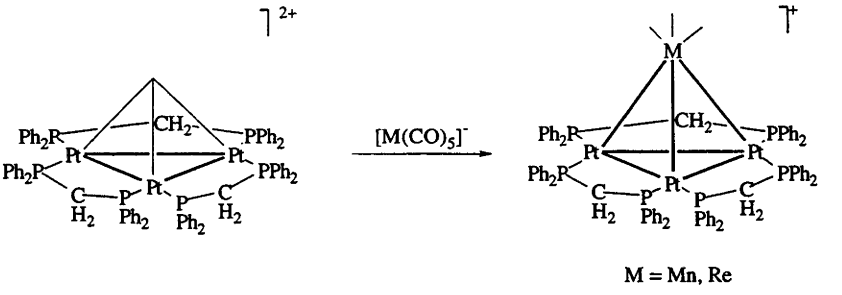
Expansion of the capped octahedral $[Re_7(\mu_6\text{-}C)(CO)_{21}]^{2-}$ with platinum metal electrophiles has afforded the clusters $[Re_7M(\mu_6\text{-}C)(CO)_{21}(L)]^{2-}$ (M = Pd, L = C_3H_5;[128] M = Pd, L = η^2-1-phenylallyl;[127] M = Pt, L = η^3-1-methylallyl;[128] M = Pt, L = Me_3[128]), with 1,4-bicapped octahedral coordination geometries (Scheme 1.2.43.).



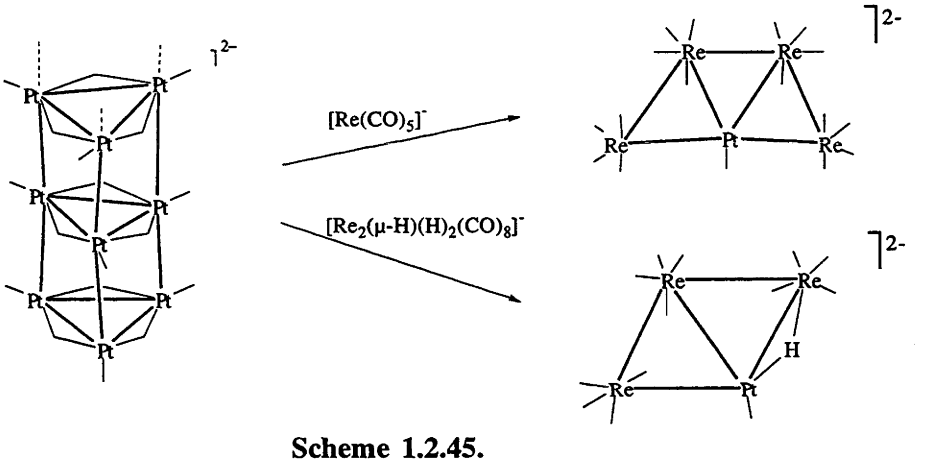
Scheme 1.2.43.

A number of mono and binuclear rhenium complexes have been utilized in the formation and expansion of mixed platinum-rhenium clusters. Reaction of the coordinatively-unsaturated cluster $[Pt_3(\mu_3\text{-}CO)(\mu\text{-}dppm)_3]^{2+}$ with $[M(CO)_5]^-$ (M = Re, Mn) afforded the tetrahedral clusters $[MPt_3(\mu\text{-}dppm)_3(CO)_3]^+$, unusually short metal-metal bond distances being noted for the rhenium example (Scheme 1.2.44.).[113] The Re-Pt clusters formed from the columnar clusters $[\{Pt_3(CO)_6\}_n]^{2-}$ ($n \approx 10$) are dependent on the nature of the rhenium complexes utilized. Reaction of $[\{Pt_3(CO)_6\}_n]^{2-}$ with $[Re(CO)_5]^-$ afforded $[Re_4Pt(CO)_{17}]^{2-}$, with an edge-bridged butterfly ("swallow") core geometry,[114] whereas reaction with $[Re_2(\mu\text{-}H)(H)_2(CO)_8]^-$ afforded $[Re_3Pt(\mu\text{-}H)(CO)_{13}]^{2-}$ with a butterfly core geometry (Scheme 1.2.45.).[114] $[Re_2Pt(\mu\text{-}H)_2(CO)_8]$ was prepared by reaction of $[Pt(\eta^4\text{-}cod)_2]$ and $[Re_2(\mu\text{-}H)H_2(CO)_8]$; it reacted with $[Re_2(\mu\text{-}H)H_2(CO)_8]$ in the presence of H_2 to afford the structurally-characterized $[Re_4Pt(\mu\text{-}H)_6(CO)_{16}]$, with a bow-tie core geometry (Scheme 1.2.46.).[121] In a related series of reactions, reaction of $[Re_2Pt(\mu\text{-}H)_2(CO)_8(\eta^4\text{-}cod)]$ with metal hydrides or metal carbonyl anions caused displacement of the η^4-cod ligand and expansion of the metal core nuclearity, affording the spiked triangular clusters $[Re_2Pt(\mu\text{-}H)_2(CO)_8\{M'\}]$ [{M'} = $Mn(CO)_5$, $Re(CO)_4(PPh_3)$, $Re(CO)_3(PPh_3)_2$, $W(CO)_3(\eta^5\text{-}C_5H_5)$,

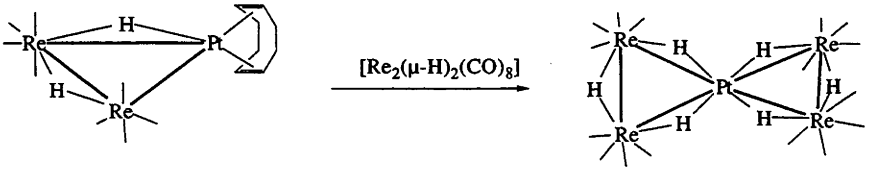
$Co(CO)_4]$ (Scheme 1.2.47.).[115] High oxidation state rhenium precursors can also be successfully employed; reaction of $[Pt_3(\mu\text{-}CO)_3(PCy_3)_3]$ with $[Re_2O_7]$ gave $[Re_2Pt_5(\mu\text{-}O)_3(\mu\text{-}OH)(CO)_4(PCy_3)_4]$, structurally characterized with the unusual bi-butterfly core geometry shown in Scheme 1.2.48.[123]



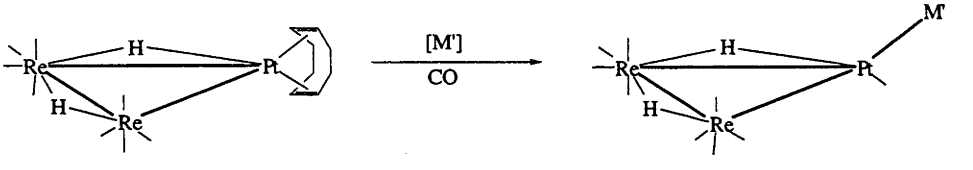
Scheme 1.2.44.



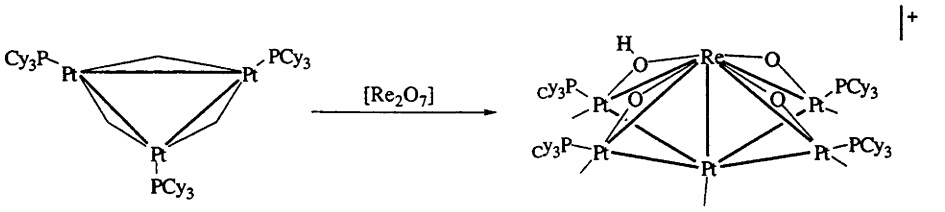
Scheme 1.2.45.



Scheme 1.2.46.

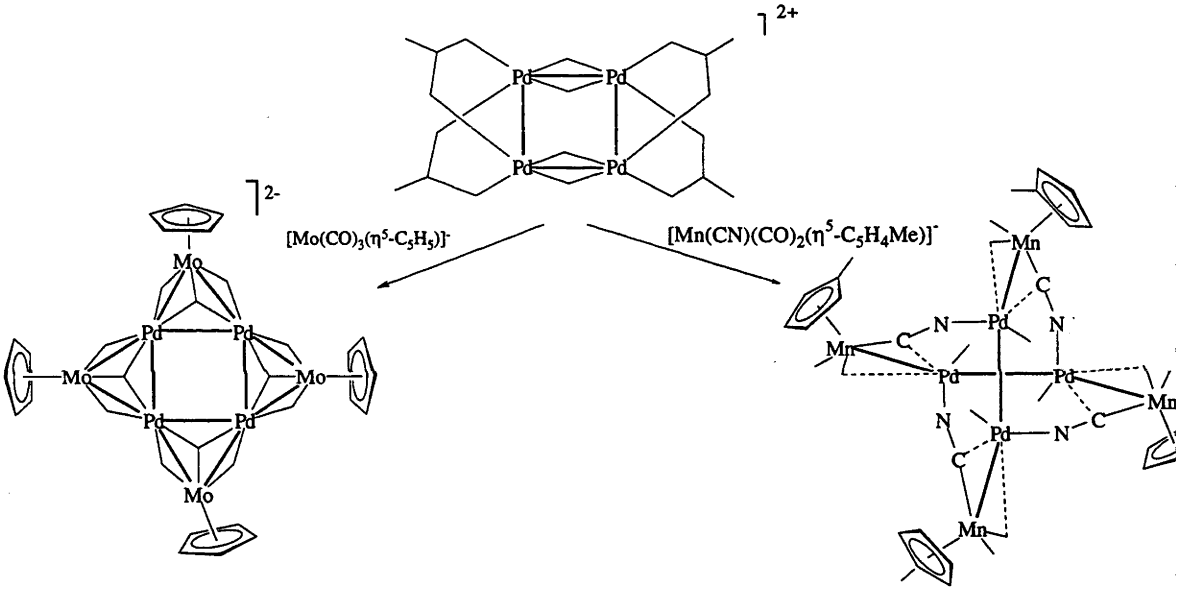


Scheme 1.2.47.



Scheme 1.2.48.

The rectangular cluster $[Pd_4(\mu\text{-}OAc)_4(\mu\text{-}CO)_4]^{2+}$ has acetate groups which are readily displaced; reaction with $[Mo(CO)_3(\eta^5\text{-}C_5H_5)]^-$ afforded $[Mo_4Pd_4(CO)_{12}(\eta^5\text{-}C_5H_5)_4]^{2-}$ with a tetra-edge-bridged square core geometry, and the palladium atoms in the unusual $+\frac{1}{2}$ oxidation state,[129] whereas reaction with $[Mn(CN)(CO)_2(\eta^5\text{-}C_5H_4Me)]^-$ gave $[Mo_4Pd_4(\mu\text{-}NC)_4(CO)_{12}(\eta^5\text{-}C_5H_4Me)_4]$,[126] which consists of two Mn_2Pd_2 chains linked together by bridging CN-moieties (Scheme 1.2.49.).

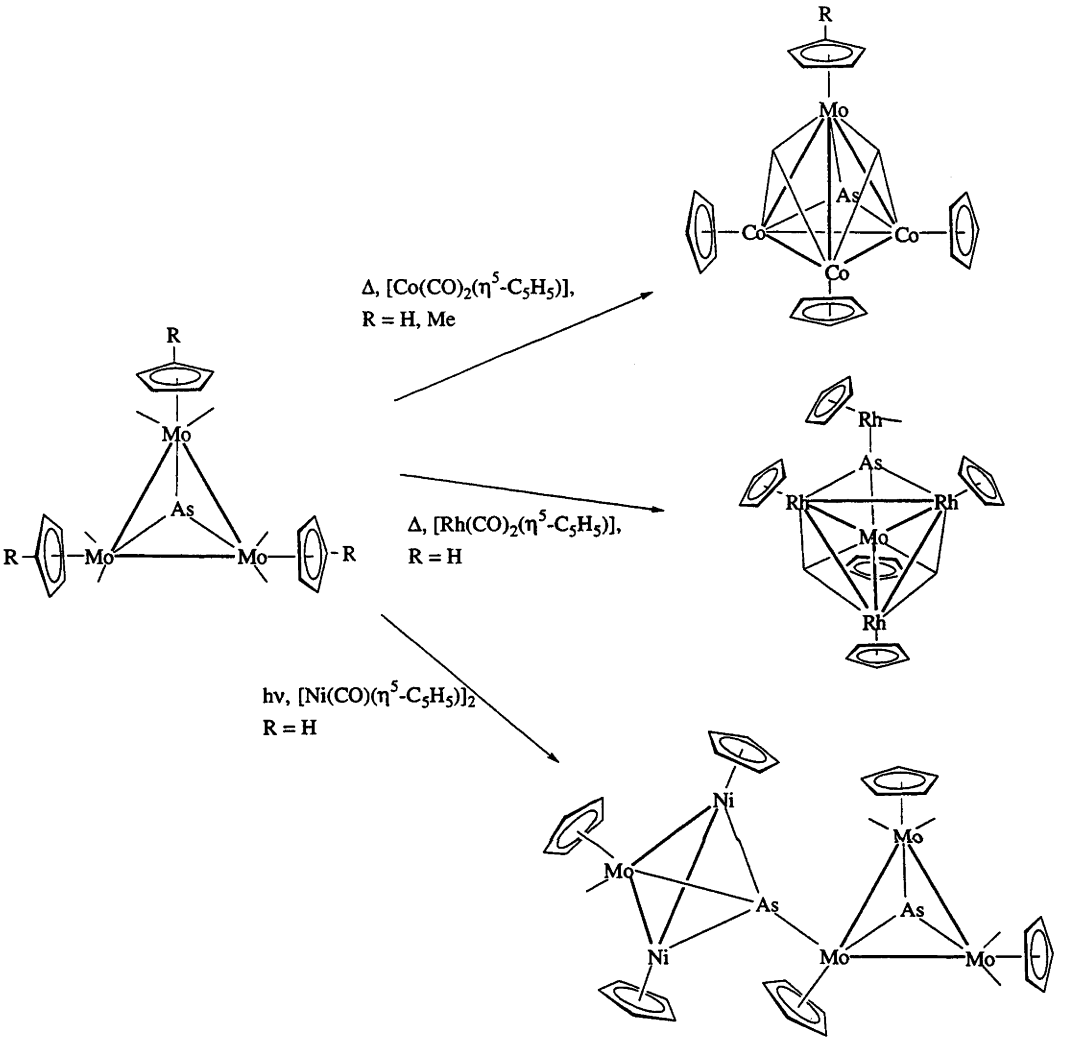


Scheme 1.2.49.

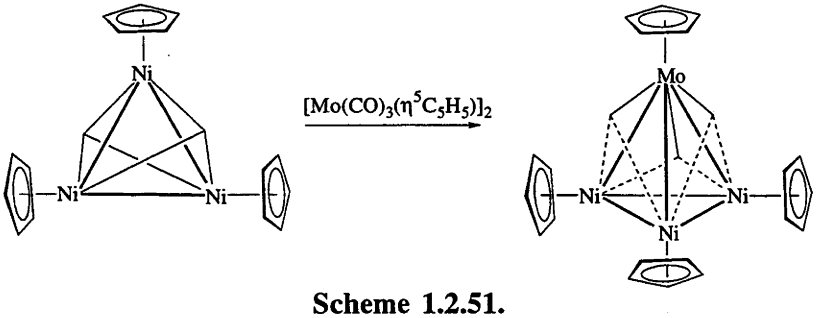
On thermolysis, the clusters $[Mo_3(\mu_3\text{-}As)(CO)_3(\eta^5\text{-}C_5H_4R)_3]$ (R = H, Me) provide a source of "$MoAs(\eta^5\text{-}C_5H_4R)$" fragments which can combine with suitable organometallic reagents; thus, reaction with $[Co(CO)_2(\eta^5\text{-}C_5H_5)]$ afforded $[MoCo_3(\mu_3\text{-}As)(\mu_3\text{-}CO)_2(\eta^5\text{-}C_5H_5)_3(\eta^5\text{-}C_5H_4R)]$,[101] whereas reaction with $[Rh(CO)_2(\eta^5\text{-}C_5H_5)]$ (R = H) gave $[MoRh_4(\mu_3\text{-}As)(\mu_3\text{-}CO)_2(CO)(\eta^5\text{-}C_5H_5)_5]$ (Scheme 1.2.50.).[43] In contrast, photolysis of $[Mo_3(\mu_3\text{-}As)(CO)_6(\eta^5\text{-}C_5H_5)_3]$ in the presence of $[Ni(CO)(\eta^5\text{-}C_5H_5)]_2$ afforded the metal exchange product $[MoNi_2(\mu_3\text{-}As)(CO)_4(\eta^5\text{-}C_5H_5)_3]$ together with $[Mo_4Ni_2(\mu_4\text{-}As)(\mu_3\text{-}As)(CO)_7(\eta^5\text{-}C_5H_5)_6]$, shown crystallographically to consist of Mo_3 and $MoNi_2$ triangles linked by a μ_4-As bridge.[90]

The triangular cluster $[Ni_3(\mu_3\text{-}CO)_2(\eta^5\text{-}C_5H_5)_3]$ reacted with $[Mo(CO)_3(\eta^5\text{-}C_5H_5)]_2$ by core expansion rather than metal exchange, affording the paramagnetic $[MoNi_3(\mu_3\text{-}CO)(\eta^5\text{-}$

$C_5H_5)_4]$ (Scheme 1.2.51.); structural characterization of the analogue $[MoNi_3(\mu_3\text{-}CO)(\eta^5\text{-}C_5H_5)_3(\eta^5\text{-}C_5H_4Me)]$ (prepared by an alternative route from dinuclear precursors) confirmed the tetrahedral core geometry.[108]

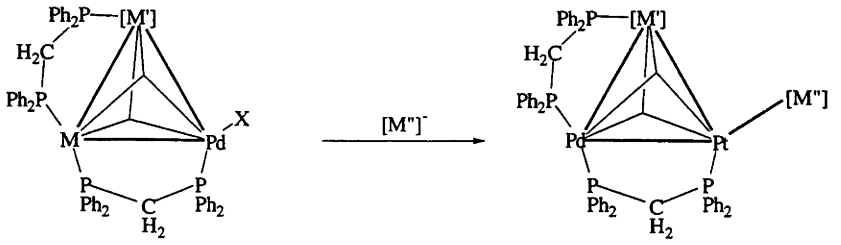


Scheme 1.2.50.



Scheme 1.2.51.

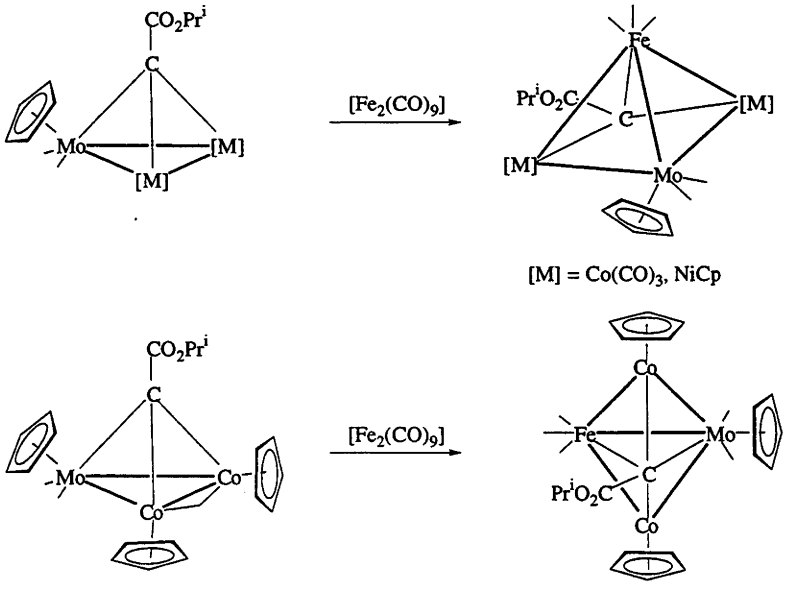
Braunstein and co-workers have demonstrated the utility of carbonylmetalate anions and dppm-stabilized triangular mixed-metal clusters as precursors to clusters with spiked triangular core geometries, with the products retaining the face-capping and bridging ligands of the mixed-metal precursor (Scheme 1.2.52.).[37,105,118]



M = Pd, Pt; [M'] = Mo(η^5-C_5H_5), W(η^5-C_5H_5), $Mn(CO)_2$, Co(CO); [M"] = [$Mo(CO)_3(\eta^5$-C_5H_5)], [$W(CO)_3(\eta^5$-C_5H_5)], [$Mn(CO)_5$], [$Co(CO)_4$]; X = Cl, I; for #646 M" = [Mn(CO)5]-, X = I

Scheme 1.2.52.

As can be seen in Scheme 1.2.33., a significant number of mixed-metal clusters have been derived from the triangular cluster [$Co_3(\mu_3$-CR)$(CO)_9$]. Whereas further treatment with molybdenum, tungsten or nickel complexes usually induces additional metal exchange, treatment of [$MoCo_2(\mu_3$-CCO_2Pr^i)$(CO)_8(\eta^5$-C_5H_5)], [$MoNi_2(\mu_3$-CCO_2Pr^i)$(CO)_2(\eta^5$-$C_5H_5)_3$] or [$MoCo_2(\mu_3$-CCO_2Pr^i)$(\mu$-CO$)(CO)_2(\eta^5$-$C_5H_5)_3$] with [$Fe_2(\mu$-$CO)_3(CO)_6$] resulted in cluster expansion forming [$MoFeCo_2(\mu_3$-CCO_2Pr^i)$(CO)_{11}(\eta^5$-C_5H_5)], [$MoFeNi_2(\mu_3$-CCO_2Pr^i)$(CO)_5(\eta^5$-$C_5H_5)_3$] and [$MoFeCo_2(\mu_3$-CCO_2Pr^i)$(CO)_5(\eta^5$-$C_5H_5)_3$], respectively, with butterfly coordination geometries (Scheme 1.2.53.).[93] Similarly, photolysis of [$MRuCo(\mu_3$-η^2-MeC_2Me)$(CO)_8(\eta^5$-C_5H_5)] (M = Mo) in the presence of [$Fe_2(\mu$-$CO)_3(CO)_6$] afforded [$MoFeRuCo(\mu_3$-η^2-MeC_2Me)$(CO)_{10}(\eta^5$-C_5H_5)], and both the molybdenum and tungsten-containing clusters reacted with [$Rh(CO)_2(\eta^5$-C_5H_5)] to form [$MRuCoRh(\mu_3$-η^2-MeC_2Me)$(CO)_9(\eta^5$-$C_5H_5)_2$] (M = Mo, W) (Figure 1.2.6.).[117]



[M] = $Co(CO)_3$, NiCp

Scheme 1.2.53.

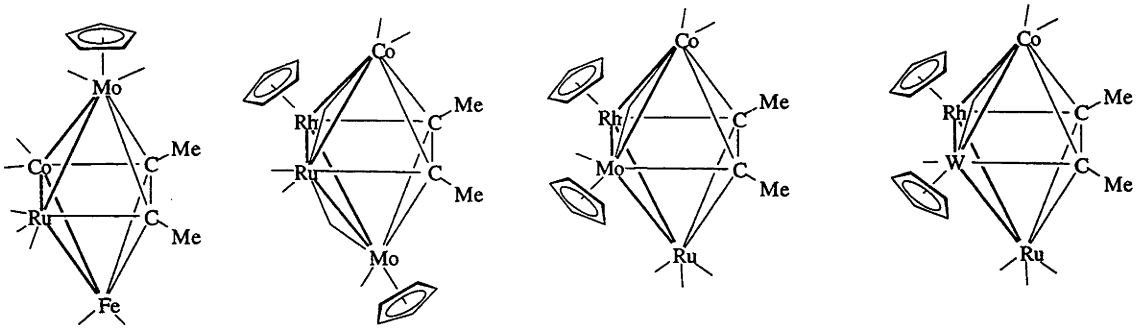
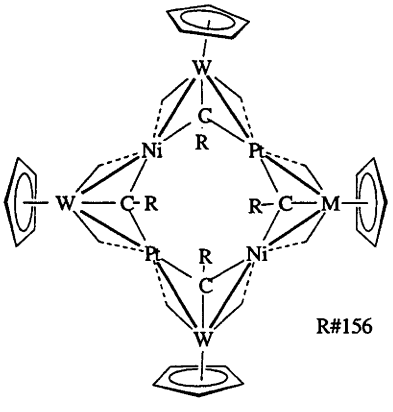
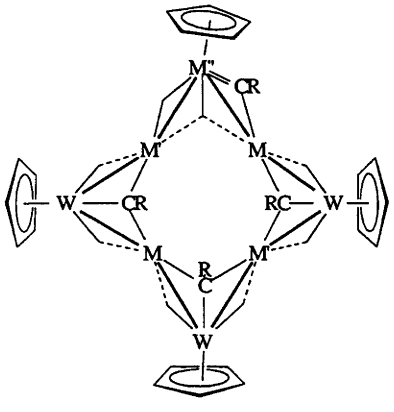


Figure 1.2.6.

Stone and co-workers have reported the systematic expansion of group 6 - group 10 clusters using $[M(\eta^2\text{-cod})_2]$ (M = Ni, Pt) and $[LM'(CO)_2(\equiv CR)]$ (M' = Mo, W; L = η^5-C_5H_5, η^5-C_5Me_5; R = Me, Ph, C_6H_4Me-4). This work has been reviewed elsewhere[3] and will be summarized only briefly here; Scheme 1.2.54. reveals the logical formation of chain complexes of three, four, five, six, seven, nine and eleven metal atoms under mild conditions.[34,35,109-111,116,120,125,131] More recently, this work has been expanded to include metallacarborane cluster compounds with the preparation of $[MoW_2Pt_2(\mu_3\text{-}\eta^6\text{-}7,9\text{-}Me_2\text{-}7,9\text{-}C_2B_{10}H_8\text{-}12\text{-}OC)(\mu_3\text{-}CC_6H_4Me\text{-}4)(\mu\text{-}CC_6H_4Me\text{-}4)(\mu\text{-}CO)_2(CO)_5(\eta^5\text{-}C_5H_5)_2]$ (Scheme 1.2.55.).[116] Attempts to extend the lengths of chains beyond seven metal atoms resulted in chain cyclization to form macrocyclic "star" clusters in instances where the heptametallic precursor has terminal tungsten carbyne groups (Figure 1.2.7.),[111,125,130,131] but the chains can be succesfully extended if the heptametallic intermediate has terminal $[Pt(\eta^4\text{-cod})]$ groups (Scheme 1.2.54.), a result attributed to differing chain conformations.

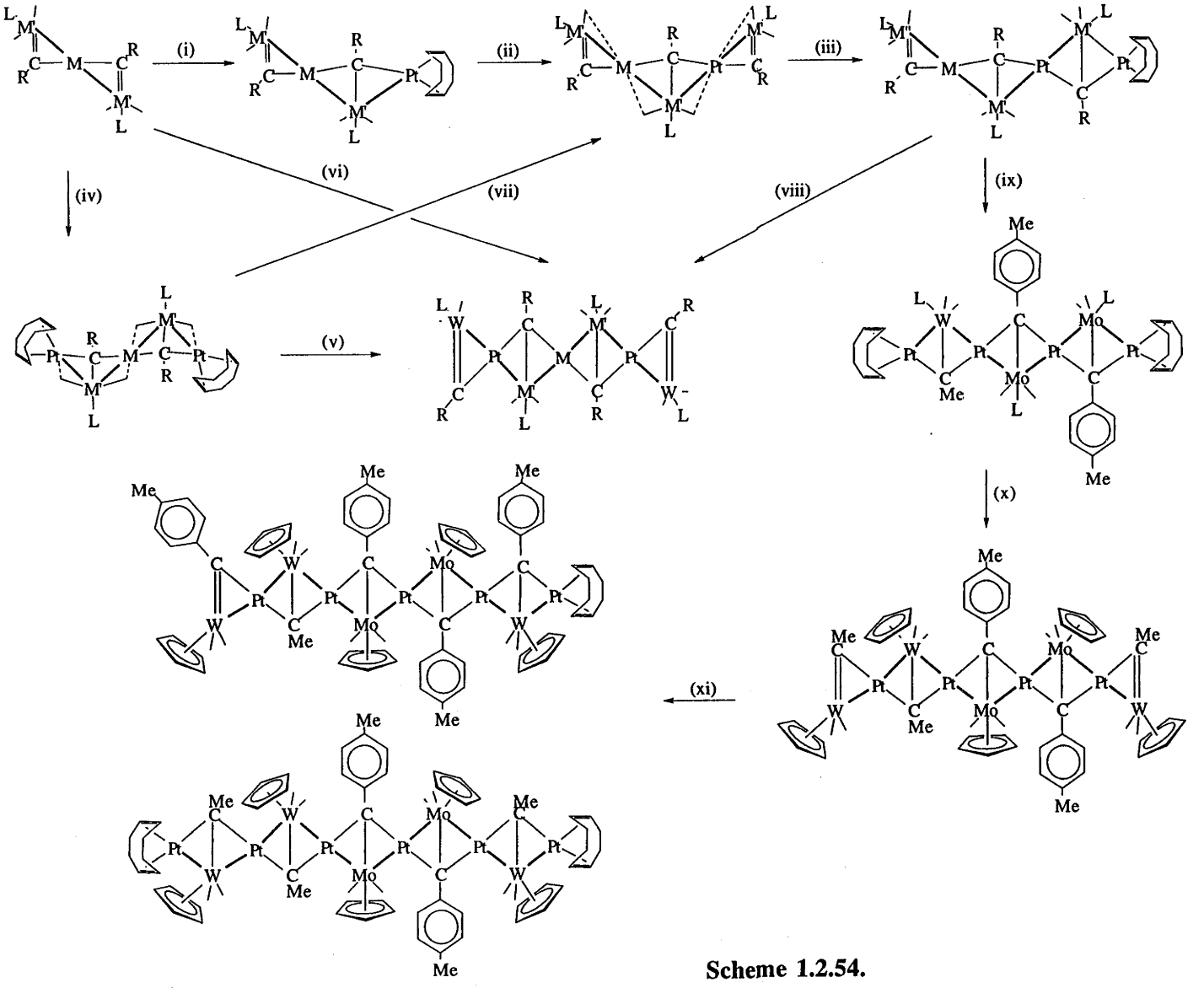


M = Mo, R = C_6H_4Me-4;
M = W, R = Ph



M = Pt, M' = Ni, R = C_6H_4Me-4, Ph
M = Ni, M' = Pt, R = C_6H_4Me-4, Ph
M = Ni, M' = Pt, M" = Mo, R = C_6H_4Me-4

Figure 1.2.7.



(i) $[Pt(\eta^4\text{-cod})_2]$; M = Ni, Pt; M' = Mo, W; R = Me, Ph, C_6H_4Me-4; L = η^5-C_5H_5, η^5-C_5Me_5

(ii) $[W(\equiv CR)(CO)_2(L)]$; M = Ni, Pt; M' = Mo, W; R = C_6H_4Me-4, Me; L = η^5-C_5H_5, η^5-C_5Me_5; not all combinations

(iii) $[Pt(\eta^4\text{-cod})_2]$; M = Ni, Pt, M' = Mo, W; R = Me , L = η^5-C_5Me_5

(iv) 2-2.5$[Pt(\eta^4\text{-cod})_2]$; M = Ni, Pt; M' = Mo, W; R = C_6H_4Me-4, Me; L = η^5-C_5H_5, η^5-C_5Me_5

(v) $[W(\equiv CR)(CO)_2(L)]$, 3 atm C_2H_4; M = Ni, Pt; M' = Mo, W; R = C_6H_4Me-4, Me; L = η^5-C_5H_5, η^5-C_5Me_5; not all combinations

(vi) $[Ni(\eta^4\text{-cod})_2]$; M = Ni, Pt; M' = W; R = Me, L = η^5-C_5Me_5

(vii) $[W(\equiv CR)(CO)_2(L)]$, 3 atm C_2H_4; M = Pt; M' = Mo; R = C_6H_4Me-4; L = η^5-C_5H_5

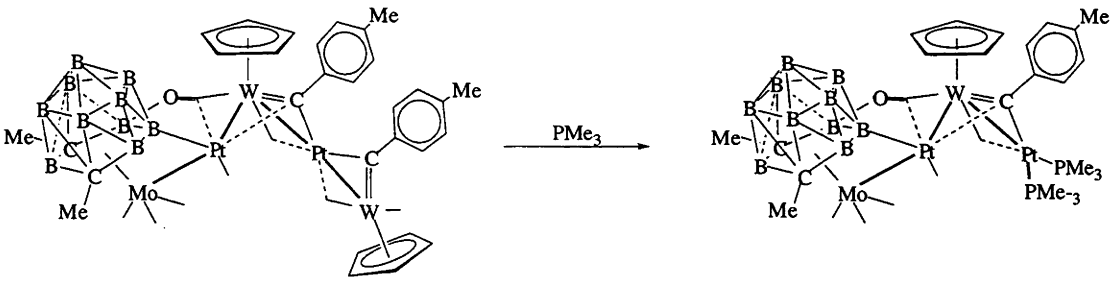
(viii) $[W(\equiv CR)(CO)_2(L)]$, 3 atm C_2H_4; M = Pt; M' = W; R = Me; L = η^5-C_5H_5, η^5-C_5Me_5

(ix) 1.5$[Pt(\eta^4\text{-cod})_2]$; M = Pt; M' = Mo; R = C_6H_4Me-4, Me; L = η^5-C_5H_5, η^5-C_5Me_5

(x) 2$[W(\equiv CMe)(CO)_2(\eta^5\text{-}C_5H_5)]$; M' = Mo, M" = W; L = η^5-C_5H_5

(xi) 2.4$[Pt(\eta^4\text{-cod})_2]$, 3 atm C_2H_4

Scheme 1.2.54.



B-bound H's omitted for clarity

Scheme 1.2.55.

1.2.6. Catalytic Studies

Research into cluster catalysis has been driven by both intrinsic interest and utilitarian potential. Catalysis involving "very mixed"-metal clusters is of particular interest as many established heterogeneously-catalyzed processes couple mid and late transition metals (e.g. hydrodesulfurization and petroleum reforming). Attempts to model catalytic transformations are summarized in Section *1.2.4.*, while the use of "very mixed"-metal clusters as homogeneous and heterogeneous catalysis precursors are discussed in Sections *1.2.6.2.* and *1.2.6.3.*, respectively. The general area of mixed-metal cluster catalysis has been summarized in excellent reviews by Braunstein and Rosé;[133] while the tabulated results are intended to be comprehensive in scope, the discussion below focuses on the more recent results.

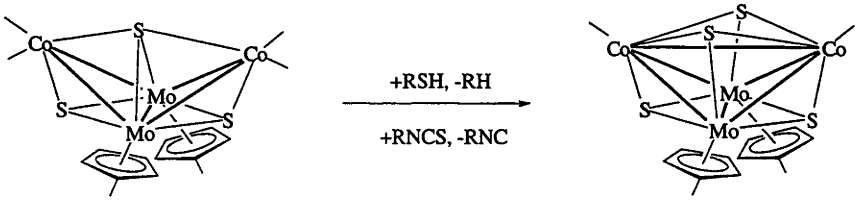
1.2.6.1. Modelling Catalysis

Reactivity studies of organic ligands with mixed-metal clusters have been utilized in an attempt to shed light on the fundamental steps that occur in heterogeneous catalysis (Table 1.2.8.), although the correspondence between cluster chemistry and surface-adsorbate interactions is often poor.[134] While some of these studies have been mentioned above in Section *1.2.4.*, it is useful to to revisit them in the context of the catalytic process for which they are models. Shapley and co-workers have examined the solution chemistry of tungsten-iridium clusters in an effort to understand hydrogenolysis of butane. The reaction of excess diphenylacetylene with $[WIr_3(CO)_{11}(\eta^5\text{-}C_5H_5)]$ gave two addition products which have both been structurally characterized. Coordination of two alkyne units to separate faces of the closed tetrahedral WIr_3 core afforded $[WIr_3(\mu_3\text{-}\eta^2\text{-}PhC_2Ph)_2(CO)_7(\eta^5\text{-}C_5H_5)]$. In contrast, the other adduct, $[WIr_3(\mu_3\text{-}CPh)(\mu\text{-}CPh)(\mu\text{-}\eta^4\text{-}CPhCPhCPhCPh)(CO)_5(\eta^5\text{-}C_5H_5)]$, has an open (butterfly) core with the tungsten atom at the "hinge" position; the alkyne ligands have undergone either C≡C scission to give μ_2- and μ_3-coordinated alkylidyne moieties or dimerization via C–C coupling to give an iridacyclopentadienyl system (see Scheme 1.2.20.).[60] The related cluster $[W_2Ir_2(CO)_{10}(\eta^5\text{-}C_5H_5)_2]$ has also been reacted with diphenylacetylene and yielded a product resulting from intact coordination of

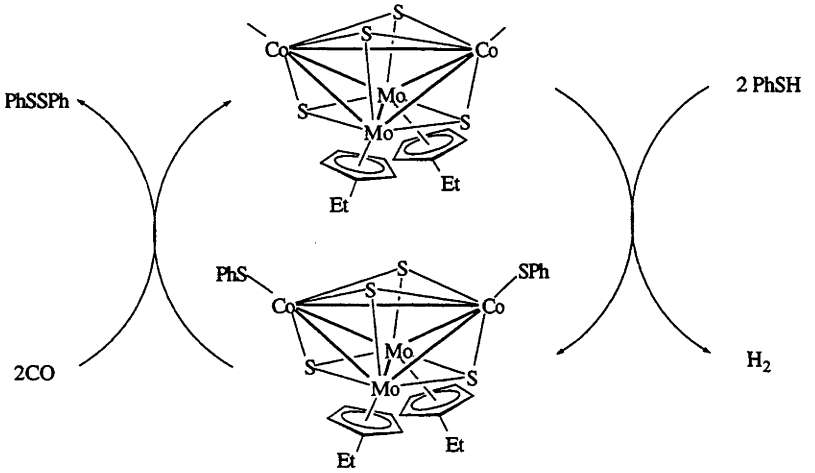
the alkyne together with a cluster exhibiting the effects of C≡C scission and C–C bond formation.[59] These transformations are believed to illustrate processes involved in butane hydrogenolysis over cluster-derived catalysts (experimental studies suggest C–C cleavage of an adsorbed dehydrated intermediate in ethane hydrogenolysis).

Curtis and co-workers have studied the reaction of organosulfur compounds with $[Mo_2Co_2(\mu_4\text{-}S)(\mu_3\text{-}S)_2(CO)_4(\eta^5\text{-}C_5H_4Me)_2]$ and $[Mo_2Co_2(\mu_3\text{-}S)_4(CO)_2(\eta^5\text{-}C_5H_4Et)_2]$ to understand the desulfurization process. The reaction pathways that lead to C-S scission have been compared to the commercial hydrodesulfurization reactions with alumina-supported "MoCoS" catalysts. The bimetallic cluster $[Mo_2Co_2(\mu_4\text{-}S)(\mu_3\text{-}S)_2(CO)_4(\eta^5\text{-}C_5H_4Me)_2]$ desulfurized thiols to parent hydrocarbons and the cubane cluster $[Mo_2Co_2(\mu_3\text{-}S)_4(CO)_2(\eta^5\text{-}C_5H_4Me)_2]$; thiophene desulfurization products were saturated and unsaturated C_1–C_4 hydrocarbons, and isothiocyanates were desulfurized to RNC, which replaced a carbonyl ligand affording isocyanate-coordinated clusters $[Mo_2Co_2(\mu_4\text{-}S)(\mu_3\text{-}S)_2(CO)_3(CNR)(\eta^5\text{-}C_5H_4Me)_2]$ and $[Mo_2Co_2(\mu_3\text{-}S)_4(CNR)(CO)(\eta^5\text{-}C_5H_4Me)_2]$ (Scheme 1.2.25.).[135,136] Kinetic and mechanistic details of the thiol desulfurization reactions have also been investigated.[137]

Reaction of thiophenol with $[Mo_2Co_2(\mu_3\text{-}S)_4(CO)_2(\eta^5\text{-}C_5H_4Et)_2]$ formed the electron-deficient, paramagnetic cluster $[Mo_2Co_2(\mu_3\text{-}S)_4(SPh)_2(\eta^5\text{-}C_5H_4Et)_2]$, which, in the presence of CO, regenerated the original carbonyl cluster and afforded PhSSPh. The combination of these two reactions constitutes the basis of a catalytic cycle (Scheme 1.2.56.).[41,42]



Scheme 1.2.56.



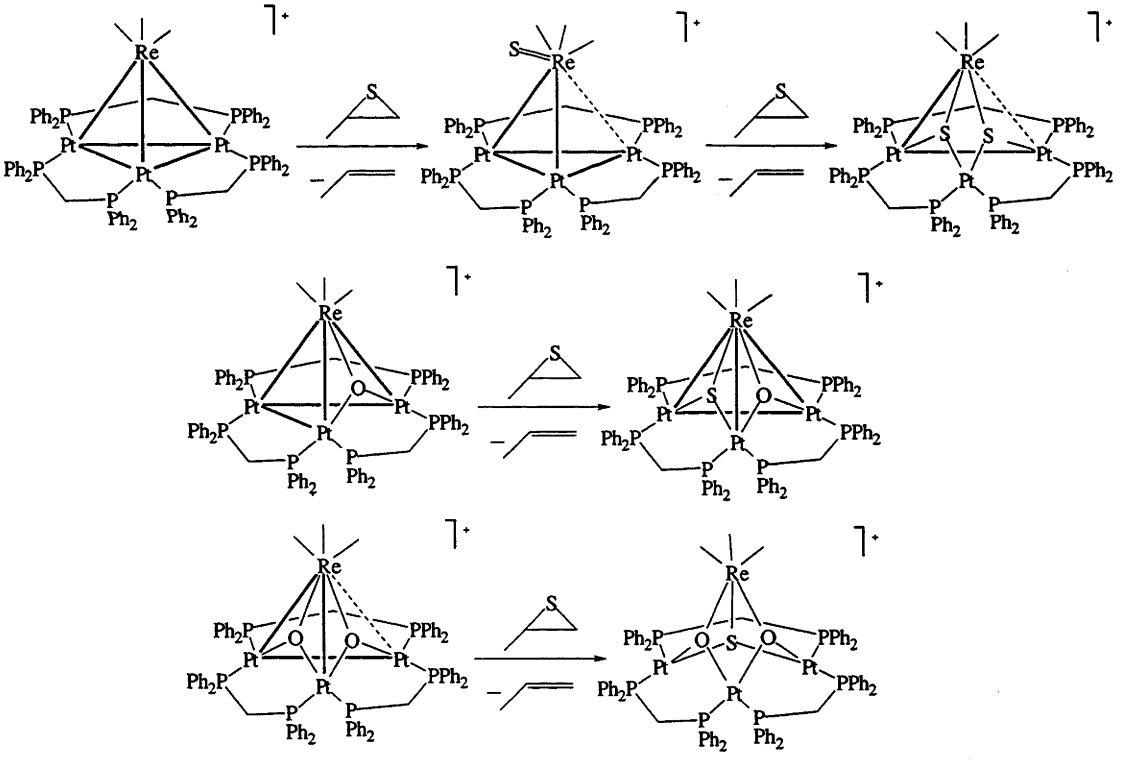
Scheme 1.2.57.

Table 1.2.8.

Metals	*Cluster Precursor*	*Product(s)*	*Reaction Modelled*	*Ref.(s)*
Mo-Co	$[Mo_2Co_2(\mu_4\text{-}S)(\mu_3\text{-}S)_2(CO)_4(\eta^5\text{-}C_5H_4Me)_2]$ + RSH (R = Bu^t, $Me_2CHCH_2CH_2$, Ph)	$[Mo_2Co_2(\mu_3\text{-}S)_4(CO)_2(\eta^5\text{-}C_5H_4Me)_2]$ + RH	Desulfurization	135-137
	$[Mo_2Co_2(\mu_4\text{-}S)(\mu_3\text{-}S)_2(CO)_4(\eta^5\text{-}C_5H_4Me)_2]$ + *cis*-2,3-dimethylthiirane	$[Mo_2Co_2(\mu_3\text{-}S)_4(CO)_2(\eta^5\text{-}C_5H_4Me)_2]$ + *cis*-2-butene	Desulfurization	135,136
	$[Mo_2Co_2(\mu_4\text{-}S)(\mu_3\text{-}S)_2(CO)_4(\eta^5\text{-}C_5H_4Me)_2]$ + diphenylthietane (*cis* or *trans*)	$[Mo_2Co_2(\mu_3\text{-}S)_4(S)(\eta^5\text{-}C_5H_4Me)_2]$ + *cis*-1,3-diphenylpropene	Desulfurization	136
	$[Mo_2Co_2(\mu_4\text{-}S)(\mu_3\text{-}S)_2(CO)_4(\eta^5\text{-}C_5H_4Me)_2]$ + $SCNBu^t$	$[Mo_2Co_2(\mu_3\text{-}S)_4(CO)_2(\eta^5\text{-}C_5H_4Me)_2]$, $[Mo_2Co_2(\mu_3\text{-}S)_4(CNBu^t)(CO)(\eta^5\text{-}C_5H_4Me)_2]$	Desulfurization	135,136
	$[Mo_2Co_2(\mu_4\text{-}S)(\mu_3\text{-}S)_2(CO)_4(\eta^5\text{-}C_5H_4Me)_2]$ + thiophenes	Saturated and unsaturated C_1 - C_4 hydrocarbons	Desulfurization	135,136
	$[Mo_2Co_2(\mu_3\text{-}S)_4(CO)_2(\eta^5\text{-}C_5H_4Et)_2]$ + PhSSPh	$[Mo_2Co_2(\mu_3\text{-}S)_4(SPh)_2(\eta^5\text{-}C_5H_4Et)_2]$	Desulfurization	41,42
	$[Mo_2Co_2(\mu_3\text{-}S)_4(CO)_2(\eta^5\text{-}C_5H_4Et)_2]$ + PhSH	$[Mo_2Co_2(\mu_3\text{-}S)_4(SPh)_2(\eta^5\text{-}C_5H_4Et)_2]$	Desulfurization	41,42
	$[Mo_2Co_2(\mu_3\text{-}S)_4(CO)_2(\eta^5\text{-}C_5H_4Et)_2]$ + PhSH + CO	$[Mo_2Co_2(\mu_3\text{-}S)_4(SPh)_2(\eta^5\text{-}C_5H_4Et)_2]$, PhSSPh, PhS(CO)Ph	Desulfurization	41,42
	$[Mo_2Co_2(\mu_3\text{-}S)_4(SPh)_2(\eta^5\text{-}C_5H_4Et)_2]$ + H_2 + CO	PhSSPh	Desulfurization	41,42
W-Ir	$[WIr_3(CO)_{11}(\eta^5\text{-}C_5H_5)]$ + PhC≡CPh	$[WIr_3(\mu_3\text{-}CPh)(\mu\text{-}CPh)(\mu\text{-}\eta^4\text{-}CPhCPhCPhCPh)(CO)_5(\eta^5\text{-}C_5H_5)]$	Fischer-Tropsch process (CC cleavage and formation)	60

	$[W_2Ir_2(CO)_{10}(\eta^5\text{-}C_5H_5)_2]$ + PhC≡CPh	$[W_2Ir_2(\mu_4\text{-}\eta^2\text{-}PhC_2Ph)(CO)_{10}(\eta^5\text{-}C_5H_5)_2]$ + $[W_2Ir_2(\mu_3\text{-}CPh)(\mu_3\text{-}\eta^3\text{-}CPhCPhCPh)(CO)_{10}(\eta^5\text{-}C_5H_5)_2]$	Fischer-Tropsch process (CC cleavage and formation)	59
Re-Pt	$[RePt_3(\mu\text{-}dppm)_3(CO)_3]^+$ + propylene sulfide	$[RePt_3(\mu\text{-}dppm)_3(CO)_3(S)]^+$ + propene	Desulfurization	138,139
	$[RePt_3(\mu\text{-}dppm)_3(CO)_3]^+$ + excess propylene sulfide	$[RePt_3(\mu_3\text{-}S)_2(\mu\text{-}dppm)_3(CO)_3]^+$ + propene	Desulfurization	138,139
	$[RePt_3(\mu\text{-}dppm)_3(O)_3]^+$ + excess propylene sulfide	$[RePt_3(\mu_3\text{-}S)_2(\mu\text{-}dppm)_3(O)_3]^+$ + propene	Desulfurization	139

Supported bimetallic Re-Pt catalysts are important in selective reforming of petroleum. It is believed that sulfiding the catalyst before use gives ReS units which act as an inert diluent to reduce the size of a local ensemble of platinum atoms. Selectivity for desirable dehydrocyclization and isomerization reactions is increased, and hydrogenolysis of alkanes, which requires several adjacent platinum atoms, is diminished. Metalloselective sulfidation of rhenium in Re-Pt clusters has been studied as evidence for these hypotheses. On reaction with propylene sulfide, one or two sulfur atoms were added to the tetrahedral cluster cation $[RePt_3(\mu\text{-dppm})_3(CO)_3]^+$, to give $[RePt_3(\mu\text{-dppm})_3(S)_n(CO)_3]^+$ (n = 1 or 2). Reaction under mild conditions of one propylene sulfide gave a cluster with a rhenium-coordinated sulfur atom and propene; a second propylene sulfide was then desulfurized to give a cluster with two face-capping sulfur atoms bridging $RePt_2$ faces, and another propene molecule.[138,139] A similar sulfidation of the oxo clusters $[RePt_3(\mu_3\text{-O})(\mu\text{-dppm})_3(CO)_3]^+$ and $[RePt_3(\mu_3\text{-O})_2(\mu\text{-dppm})_3(CO)_3]^+$ with propylene sulfide has recently been studied; an equivalent of propene was generated and the sulfur coordinated in a μ_3-fashion with a decrease in metal-metal bonding in the cluster complexes (Scheme 1.2.58.).[139]



Scheme 1.2.58.

1.2.6.2. Homogeneous Catalysis

Homogeneous catalysis by transition metal clusters has been reviewed from the perspective of the specific transformations.[140] Examples of very mixed-metal clusters catalyzing processes homogeneously are collected in Table 1.2.9.; as is always the case with

homogeneous catalysis, the catalytic precursor is well-defined, but the nature of the active catalyst is often unclear.

Sulfided bimetallic clusters which mimic the metal composition of commercial hydrodesulfurization (HDS) catalysts have been prepared and their homogeneous catalytic behaviour studied. Reaction of thiophenol with $[Mo_2Co_2(\mu_4\text{-}S)(\mu_3\text{-}S)_2(CO)_4(\eta^5\text{-}C_5H_4Me)_2]$ under catalytic conditions (1000 psi CO, 150 °C) afforded only a stoichiometric amount of HDS products; PhSSPh is formed catalytically. The cluster regeneration step involves desulfidation by CO to give COS (Scheme 1.2.7.).[40] Under the same conditions, $[Mo_2Co_2(\mu_3\text{-}S)_4(CO)_2(\eta^5\text{-}C_5H_4Et)_2]$ was reacted with thiophenol to yield PhSSPh (171 %, based on cluster) and PhS(CO)Ph (161 %). The residual organometallic product was recrystallized to give $[Mo_2Co_2(\mu_3\text{-}S)_4(SPh)_2(\eta^5\text{-}C_5H_4Et)_2]$ (57 %)[41,42].

The octanuclear cluster $Na_2[Mo_4Pd_4(\mu_3\text{-}CO)_4(\mu\text{-}CO)_8(\eta^5\text{-}C_5H_5)_4]$ was found to catalyze dehydration of aliphatic (MeOH, EtOH, ^{n}PrOH, ^{t}BuCH$_2$OH) and arylaliphatic (PhCH$_2$OH, Ph$_2$CHOH) alcohols. The accumulation of water took place slowly under mild conditions (60-80 °C) in alcohol solutions containing the catalyst under an argon atmosphere; an acidic medium was not required. Alcohols having no hydrogen atom in the α-position were unable to undergo elimination. All the data available suggest that the reaction proceeded via oxidative addition of the alcohol across the Mo-Pd bond and proton transfer to give an intermediate carbene species (Figure 1.2.8.). The same cluster was inefficient in the hydrogenolysis of alcohols.[151]

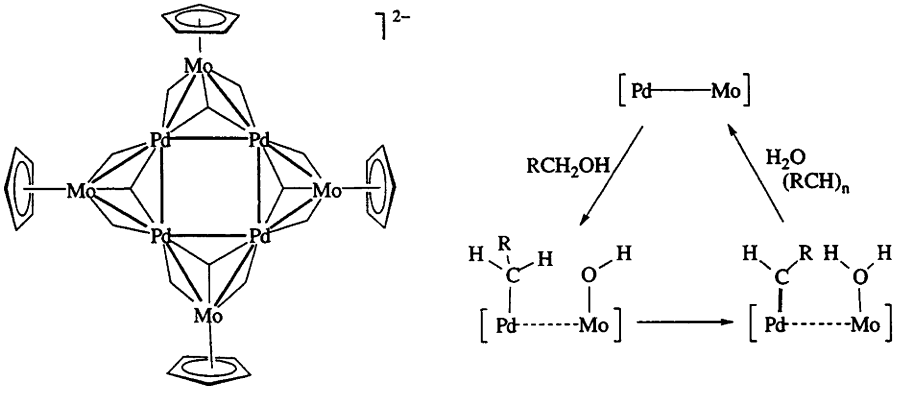


Figure 1.2.8.

Table 1.2.9.

Catalyst	*Precursor Cluster*	*Ref.(s) (Cluster syntheses)*	*Catalyzed Reaction*	*Ref.(s) (Catalysis studies)*
Mo-Co	$[MoCo_2(\mu_3\text{-}CMe)(CO)_7\{P(OMe)_3\}(\eta^5\text{-}C_5H_5)]$	23,141	Hydroformylation of 1-pentene and styrene	142
			Hydrosilation of acetophenone	143
	$[MoCo_2(\mu_3\text{-}CMe)(CO)_8(\eta^5\text{-}C_5H_5)]$	23,141	Hydroformylation of 1-pentene and styrene	142
			Hydrosilation of acetophenone	143
	$[MoCo_2(\mu_3\text{-}S)(CO)_8(\eta^5\text{-}C_5H_5)]$	5	Hydroformylation of 1-pentene and styrene	142
	$[MoCo_2(\mu_3\text{-}S)(\mu\text{-}\eta^2\text{-}MeCNPh)(CO)_6(\eta^5\text{-}C_5H_5)]$	144	Hydroformylation of styrene	144
	$[Mo_2Co_2(\mu_4\text{-}S)(\mu_3\text{-}S)_2(CO)_4(\eta^5\text{-}C_5H_4Me)_2]$	145,146	Hydrodesulfurization of thiophenol	40
	$[Mo_2Co_2(\mu_3\text{-}S)_4(CO)_2(\eta^5\text{-}C_5H_4Et)_2]$	147	Hydrodesulfurization of thiophenol	41,42
W-Co	$[WCo_2(\mu_3\text{-}CH)(CO)_8(\eta^5\text{-}C_5H_5)]$	94	Hydrosilation of acetophenone	143
Cr-Pd	$[Cr_2Pd_2(\mu_3\text{-}CO)_2(\mu\text{-}CO)_4(PEt_3)_2(\eta^5\text{-}C_5H_5)_2]$	148	Hydrogenation of cod	149
Mo-Pd	$[Mo_2Pd_2(\mu_3\text{-}CO)_2(\mu\text{-}CO)_4(PPh_3)_2(\eta^5\text{-}C_5H_5)_2]$	150	Hydrogenation of cod and 1-hexene	149
			Hydrogenation of phenylacetylene and 1-hexyne	149
			Hydroformylation of 1-pentene	149
			Hydrosilation of 1-pentene	149
	$[Mo_2Pd_2(\mu_3\text{-}CO)_2(\mu\text{-}CO)_4(PEt_3)_2(\eta^5\text{-}C_5H_5)_2]$	150	Hydrogenation of cod	149
			Hydrogenation of phenylacetylene and 1-hexyne	149

			Hydrosilation of 1-pentene	149
	$[Mo_4Pd_4(\mu_3\text{-}CO)_4(\mu\text{-}CO)_8(\eta^5\text{-}C_5H_5)_4]$	129	Dehydration/oxidation of alcohols	151
Mo-Pt	$[Mo_2Pt(CNCy)_2(CO)_6(\eta^5\text{-}C_5H_5)_2]$	152	Hydrogenation of alkenes	153
			Hydrogenation of alkynes	153
	$[Mo_2Pt(3\text{-}MePy)_2(CO)_6(\eta^5\text{-}C_5H_5)_2]$	154,155	Hydrogenation of alkynes	153
	$[Mo_2Pt_2(\mu_3\text{-}CO)_2(\mu\text{-}CO)_4(PPh_3)_2(\eta^5\text{-}C_5H_5)_2]$	156,157	Hydrogenation of cod and 1-hexene	149
			Hydrogenation of phenylacetylene	149
			Hydroformylation of 1-pentene	149
			Hydrosilation of 1-pentene	149
	$[Mo_2Pt_2(\mu_3\text{-}CO)_2(\mu\text{-}CO)_4(PEt_3)_2(\eta^5\text{-}C_5H_5)_2$	156,157	Hydrogenation of cod	149
			Hydrogenation of phenylacetylene	149
			Hydrosilation of 1-pentene	149
W-Pd	$[W_2Pd_2(\mu_3\text{-}CO)_2(\mu\text{-}CO)_4(PPh_3)_2(\eta^5\text{-}C_5H_5)_2]$	150	Hydrogenation of cod	149
			Hydrogenation of phenylacetylene	149
			Hydrosilation of 1-pentene	149
	$[W_2Pd_2(\mu_3\text{-}CO)_2(\mu\text{-}CO)_4(PEt_3)_2(\eta^5\text{-}C_5H_5)_2]$	150	Hydrogenation of cod	149
			Hydrogenation of phenylacetylene	149
			Hydrosilation of 1-pentene	149
W-Pt	$[W_2Pt_2(\mu_3\text{-}CO)_2(\mu\text{-}CO)_4(PPh_3)_2(\eta^5\text{-}C_5H_5)_2]$	157	Hydrogenation of cod	149
			Hydrogenation of phenylacetylene	149
	$[W_2Pt_2(\mu_3\text{-}CO)_2(\mu\text{-}CO)_4(PEt_3)_2(\eta^5\text{-}C_5H_5)_2]$	157	Hydrogenation of cod	149

Mo-Fe-Co	$[MoFeCoH(\mu_3\text{-}CMe)(CO)_8(\eta^5\text{-}C_5H_5)]$	20,158	Hydrogenation of styrene	159
			Hydrosilation of acetophenone	143
Mo-Ru-Co	$[MoRuCo(\mu_3\text{-}S)(CO)_8(\eta^5\text{-}C_5H_5)]$	92	Hydrogenation of styrene	159
Mo-Co-Ni	$[MoCoNi(\mu_3\text{-}CMe)(CO)_5(\eta^5\text{-}C_5H_5)_2]$	89	Hydrogenation of styrene	159
			Hydroformylation of 1-pentene and styrene	142
			Hydrosilation of acetophenone	143
W-Fe-Co	$[WFeCo(\mu_3\text{-}PMe)(CO)_8(\eta^5\text{-}C_5H_5)]$	160	Hydrogenation of styrene	159

Table 2.1.10.

Catalyst	*Precursor Cluster*	*Ref.(s) (Cluster syntheses)*	*Support*	*Catalysed Reaction*	*Ref.(s) (Catalysis studies)*
Mo-Co	$[Mo_2Co_2(\mu_4\text{-}S)(\mu_3\text{-}S)_2(CO)_4(\eta^5\text{-}C_5H_4Me)_2]$	166	$\gamma\text{-}Al_2O_3$, SiO_2, TiO_2, MgO	Characterization of catalyst (TPD)	167
			$\gamma\text{-}Al_2O_3$	Hydrodesulfurization	167
Mo-Rh	$[Mo_2Rh(\mu\text{-}CO)(CO)_4(\eta^5\text{-}C_5H_5)_3]$	168	SiO_2	Hydrogenation of CO	169
	$[Mo_2Rh(\mu\text{-}CO)(CO)_4(\eta^5\text{-}C_5H_5)_3]$	168	SiO_2	Hydrogenation of CO	168
Mo-Ir	$[MoIr_3(\mu\text{-}CO)_3(CO)_8(\eta^5\text{-}C_5H_5)]$	170	$\gamma\text{-}Al_2O_3$	Butane hydrogenolysis and catalyst characterization (EXAFS, XANES)	171
	$[Mo_2Ir_2(\mu\text{-}CO)_3(CO)_7(\eta^5\text{-}C_5H_5)_2]$	170,172	$\gamma\text{-}Al_2O_3$	Butane hydrogenolysis and catalyst characterization (EXAFS, XANES)	171
W-Rh	$[W_2Rh(\mu\text{-}CO)(CO)_4(\eta^5\text{-}C_5H_5)_3]$	168		Hydrogenation of CO	169
W-Ir	$[WIr_3(CO)_{11}(\eta^5\text{-}C_5H_5)]$	173	$\gamma\text{-}Al_2O_3$	Butane hydrogenolysis	173
	$[W_2Ir_2(CO)_{10}(\eta^5\text{-}C_5H_5)_2]$	173	$\gamma\text{-}Al_2O_3$	Butane hydrogenolysis	173
Mo-Pd	$[Mo_2Pd_2(\mu_3\text{-}CO)_2(\mu\text{-}CO)_4(PPh_3)_2(\eta^5\text{-}C_5H_5)_2]$	150	$\gamma\text{-}Al_2O_3$	Carbonylation of $ArNO_2$	174
			MgO	Catalyst preparation and characterization (EXAFS, IR, TEM, TPD)	175

W-Pt	$[W_2Pt(CO)_6(NCPh)_2(\eta^5\text{-}C_5H_5)_2]$	176	MgO	Hydrogenation of toluene	176
Re-Pt	$[Re_2Pt(CO)_{12}]$	177	$\gamma\text{-}Al_2O_3$	Catalyst preparation and characterization (EXAFS, IR, TEM, chemisorption)	178
				Catalyst characterization (EXAFS, chemisorption) and methylcyclohexane dehydrogenation	179

1.2.6.3. Heterogeneous Catalysis

Heterogeneous catalysis by metals has been of enduring interest,[161-163] with bimetallic catalysts a particular focus.[164] Transition metal carbonyls have attracted attention as precursors to active catalysts,[165] with heterometallic clusters being examined as precursors to bimetallic particles of controlled stoichiometry. Examples of heterogeneous catalysis by cluster-derived species are collected in Table 1.2.10. A MgO-supported W-Pt catalyst has been prepared from $[W_2Pt(CO)_6(NCPh)_2(\eta^5\text{-}C_5H_5)_2]$ (Figure 1.2.9.) and reduced under a H_2 stream at 400 °C. The sample was characterized by IR, EXAFS, TEM and chemisorption of H_2, CO and O_2. Activity in toluene hydrogenation at 1 atm and 60 °C was more than an order of magnitude less for the bimetallic cluster-derived catalyst, than a catalyst prepared from the two monometallic precursors.[176]

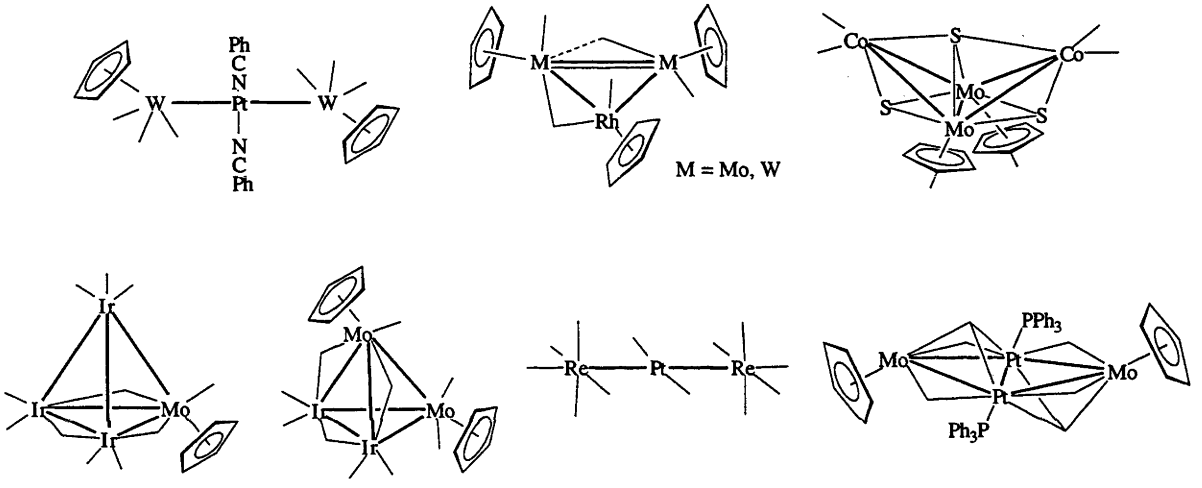


Figure 1.2.9.

A silica-supported catalyst was prepared by anaerobic impregnation of $[Mo_2Rh(\mu\text{-}CO)(CO)_4(\eta^5\text{-}C_5H_5)_2]$ (Figure 1.2.9.) from CH_2Cl_2 solution, then evacuation at room temperature. Decomposition processes were observed at the beginning of the CO hydrogenation at 1 MPa in the flow reactor. At 523 K the decomposition was complete and the catalyst exhibited slightly smaller activity (ca. 50 % conversion) compared with conventionally prepared samples, but higher selectivity towards oxygenated products.[168] This has been extended to include the tungsten-containing homologue. Hydrogenation of carbon monoxide on both molybdenum- and tungsten- promoted silica-supported rhodium catalysts has been investigated using monometallic as well as cluster precursors. The silica-adsorbed clusters $[M_2Rh(\mu\text{-}CO)(CO)_4(\eta^5\text{-}C_5H_5)_3]$ (M = Mo, W) were activated at 473 K in H_2 and the catalyst characterized by FTIR, CO chemisorption, TPR (temperature programmed reduction) and ESR. A significant increase in activity was observed with the presence of a group 6 metal as a promoter, relative to a monometallic-derived rhodium catalyst. The use of these heterometallic clusters as catalyst precursors prevented the

formation of active sites responsible for CH_4 production, increasing the proportion of oxygen-containing products.[169]

Curtis *et al.* have supported $[Mo_2Co_2(\mu_4\text{-}S)(\mu_3\text{-}S)_2(CO)_4(\eta^5\text{-}C_5H_4Me)_2]$ (Figure 1.2.9.) on the refractory oxides Al_2O_3, SiO_2, TiO_2, and MgO, and subjected them to temperature programmed decomposition (TPDE) under H_2. Evolution of CO commenced near 100 °C, followed by evolution of cyclopentadienyl ligands from 180 °C to 400 °C, together with small amounts of CO_2, CH_4 and Me_2S. The alumina-supported catalyst was used in the hydrodesulfurization of thiophene, and its activity compared with the commerical Catalco catalyst. Product distributions and activities of both catalysts were nearly identical; the cluster-derived catalyst showed a greater increase in activity upon presulfiding, while cracking activity was enhanced in the reduced form.[167]

The tetrahedral heterometallic clusters $[MoIr_3(\mu\text{-}CO)_3(CO)_8(\eta^5\text{-}C_5H_5)]$ and $[Mo_2Ir_2(\mu\text{-}CO)_3(CO)_7(\eta^5\text{-}C_5H_5)_2]$ (Figure 1.2.9.) have been deposited on alumina, and methane evolution profiles observed during activation in H_2. Materials with comparable metal compositions were prepared from stoichiometric mixtures of $[Ir_4(CO)_{12}]$ and $[Mo_2(CO)_6(\eta^5\text{-}C_5H_5)_2]$. All the Mo-Ir catalysts were active for the hydrogenolysis of *n*-butane at 215 °C (Table 1.2.11.); the $[MoIr_3]$ catalyst exhibited enhanced activity (5-10 times) over the $[Ir_4 + 2Mo_2]$ sample, but selectivity toward ethane production (70-75 %) was the same for both. In contrast, the $[Mo_2Ir_2]$ catalyst showed greater selectivity for C_1 and C_3 production (ca. 50 %) but activity comparable to $[Ir_4 + 2Mo_2]$. Metal-metal interactions in the activated materials were characterized with the use of Mo K edge X-ray absorption spectra.[171]

A catalyst supported on $\gamma\text{-}Al_2O_3$ was prepared from $[Re_2Pt(CO)_{12}]$ (Figure 1.2.9.) and characterized by IR, X-ray photoelectron spectroscopies (XPS) and temperature-programmed reduction (TPR). The chemisorbed cluster was treated with H_2 at about 150 °C resulting in fragmentation and formation of rhenium subcarbonyls; at 400 °C the sample was completely decarbonylated. A catalyst prepared from a mixture of $[Re_3(\mu\text{-}H)_3(CO)_{12}]$ and $[PtMe_2(\eta^4\text{-cod})]$ and treated under equivalent conditions showed the rhenium present in a high valent cationic form and the platinum in a metallic form. The platinum is believed to facilitate the reduction of rhenium; the platinum is likely to be near the rhenium in the sample prepared from $[Re_2Pt(CO)_{12}]$[178].

Dehydration of methylcyclohexane in the presence of a $[Re_2Pt(CO)_{12}]$-derived catalyst (Figure 1.2.9.) and catalysts derived from $[Pt(NH_3)_2](NO_3)_2$ and $[Pt(NH_3)_2](NO_3)_2 + NH_4[ReO_4]$ has been examined. The alumina-supported cluster was decomposed under flowing H_2 at 400 °C for 4 h. The catalysts were similar to each other in their selectivities for the dehydrogenation of methylcyclohexane, and were characterized by high initial

conversion (>90 %) to toluene. The catalyst made from $[Re_2Pt(CO)_{12}]$ was found to be more resistant to deactivation than catalysts prepared conventionally from rhenium and platinum salt precursors. Characterization by EXAFS revealed the cluster-derived catalyst to be more highly dispersed than the others; its resistance to deactivation was attributed to the role of rhenium in stabilizing the dispersion of the platinum.[179].

MgO-supported model Mo-Pd catalysts have been prepared from the bimetallic cluster $[Mo_2Pd_2(\mu_3\text{-}CO)_2(\mu\text{-}CO)_4(PPh_3)_2(\eta^5\text{-}C_5H_5)_2]$ (Figure 1.2.9.), and monometallic precursors. Each supported sample was treated in H_2 at various temperatures to form metallic palladium, and characterized by chemisorption of H_2, CO, and O_2, transmission electron microscopy, temperature-programmed desorption of adsorbed CO, and EXAFS. The data showed that the presence of molybdenum in the bimetallic precursor helped to maintain the palladium in a highly dispersed form. In contrast, the sample prepared from the monometallic precursors was characterized by larger palladium particles and by weaker Mo-Pd interactions.[175]

1.3. Physical Measurements

The focus of research on "very mixed"-metal clusters has thus far been synthesis and structure. Physical measurements of these clusters are largely restricted to fluxionality and electrochemical investigations. Studies of ligand fluxionality are summarized in Section *1.3.1.* and reports of electrochemical investigations are reviewed in Section *1.3.2.* The few reports of magnetic behaviour of these clusters are discussed in Section *1.3.3.1.*, and theoretical studies are summarized in Section *1.3.3.2.*

1.3.1. Fluxionality

Ligand fluxionality on metal clusters has been the subject of many studies, the majority of reports focussing on carbonyl migration on homometallic tri- and tetranuclear clusters.[1,180-187] Extending fluxionality studies to mixed-metal clusters affords a significant advantage; mechanistic details may be more accessible due to the decreased symmetry and effective label provided by introduction of the heterometal. Additionally, though, activation energies for ligand scrambling in mixed-metal clusters may differ markedly from those of their homometallic analogues, and it would be expected that this difference will be accentuated utilizing "very mixed"-metal clusters. A combination of decreased symmetry, labelled core nuclei, and differing energetics for processes involving metals with disparate electronegativities may permit discrimination of fluxional pathways not possible in homometallic clusters. Despite these significant advantages, comparatively few reports of fluxionality at very mixed-metal clusters have appeared.

Three major classes of fluxional behaviour are commonly observed in clusters:

A. Metal localized scrambling, usually seen in $M(CO)_3$ or $M(CO)_2L$ groups.
B. Intermetallic ligand migrations, usually involving CO or hydrides (although examples with phosphines are extant) and proceeding via edge-bridged or face-capped intermediates.
C. Metal framework rearrangements.

Examples of all three classes of fluxional behaviour have been observed at "very mixed"-metal clusters. It should be emphasized that absolute atomic motions are not accessible; considering ligands rotating around a fixed metal core or a metal core rotating within a fixed ligand polytope are equally valid viewpoints. The former has been utilized far more often in literature reports and, following this convention, this review summarizes specific cases in terms of ligands exchanging by rotating around a metal core where possible.

Table 1.3.1. summarizes reports of ligand fluxionality at "very mixed"-metal clusters. A number of studies[23,51,99,188,189] have reported that both metal-localized and global carbonyl fluxionality occur but give little mechanistic detail. The following discussion focuses on

Table 1.3.1.

M_n	*Cluster*	*Exchange Pathway*	*Comments*	*Ref.(s)*
n = 3	$[ZrRu_2(CO)_4(\eta^5\text{-}C_5H_5)_4]$	A	$CpRu(CO)_2$ rotation ($G^{\ddagger}_{324} = 56.5 \pm 2.1$ kJ mol^{-1})	188
	$[ZrM_2\{\mu\text{-}(NSiMe_3)_2(CH_2)_3\}(CO)_4(\eta^5\text{-}C_5H_5)_2]$ (M = Fe, Ru)	A	$CpM(CO)_2$ rotation	190
	$[ZrCo_2\{\mu\text{-}(NSiMe_3)_2(CH_2)_3\}(CO)_6(PPh_3)_2]$	A	$CpRu(CO)_2$ rotation	190
	$[MM'Rh(\mu\text{-}CO)_2(CO)_5(\eta^5\text{-}C_5Me_5)_2]$ (M = Cr, Mo, W; M' = Co, Rh)	C	$M(CO)_5$ rotation	191,192
	$[MCo_2(\mu_3\text{-}CR'')(CO)_6(L)(\eta^5\text{-}C_5R_4R')]$ [M = Mo, W; R = R' = H, Me; R'' = CO_2Pr^i, C_6H_4Me-4; L = 2CO, $Ph_2ECH_2CH_2PPh_2$ (E = P, As)]	A A B	$Co(CO)_3$ tripodal rotation $CpM(CO)_2$ rotation ($G^{\ddagger}_{233?} = 39 \pm 2.5$ kJ mol^{-1}, M = Mo, R'' = CO_2Pr^i, L = $Ph_2PCH_2CH_2PPh_2$, R = R' = Me) Co-Mo intramolecular CO exchange ($G^{\ddagger}_{353} = 69.0 \pm 2.5$ kcal mol^{-1}, M = Mo, R'' = CO_2Pr^i, L = $Ph_2PCH_2CH_2PPh_2$, R = R' = Me)	98,99,193
	$[MPd_2(\mu\text{-}Cl)(CO)_3(L)_2(\eta^5\text{-}C_5H_5)]$ (M = Cr, Mo, W; L = dimethylbenzylamine-C^2,N (dmba), 2-(dimethylamino)toluene-C,N (dmat)	C	dissociation of $[M(CO)_3(\eta^5\text{-}C_5H_5)]^-$ and reassociation [$G^{\ddagger}$ ~ 70 kJ mol^{-1} (M = Mo, W, L = dmba); $G^{\ddagger}$ ~ 50 kJ mol^{-1} (M = Mo, W, L = dmat)]	194
	$[WCo_2(\mu\text{-}EtC_2Et)(\mu\text{-}\eta^4\text{-}CEtCEtCEtCEt)(CO)_8]$	A C	$Co(CO)_3$ tripodal rotation ligated cobalt "twisting"	195

	$[Re_2Pt(\mu\text{-}H)_2(CO)_8(L)]$ [L = η^4-cod, $(PPh_3)_2$]	A	$Re(CO)_3$ tripodal rotation at $Re(CO)_3(PPh_3)$	196-198
		A	$Re(CO)_2(PPh_3)$ tripodal rotation at $Re(CO)_3(PPh_3)$ ($G^{\ddagger}$ = 74 ± 1.7 kJ mol^{-1} [L = $(PPh_3)_2$])	
		B	hydride exchange across Re-Pt vectors	
	$[MoFeNi(\mu_3\text{-}\eta^2\text{-}PhC_2CO_2Pr^i)(CO)_6(\eta^5\text{-}C_5H_5)_2]$	B	acetylene migration ($G^{\ddagger}$ = 69 ± 4 kJ mol^{-1})	199
n = 4	$[MW_2Co(CO)_9(\eta^5\text{-}C_5H_4Me)_3]$ (M = Mo, W)	B	global MW_2-localized CO exchange	200
	$[Re_3Pt(\mu\text{-}H)_3(L)(CO)_{13}]$ [L = CO, $\{C(O)OMe\}^-$]	B	hydride exchange across Re-Pt vectors [$G^{\ddagger}_{180}$ = 43.0 kJ mol^{-1}, L = CO; $G^{\ddagger}_{243}$ = 70(1) kJ mol^{-1}, L = $\{C(O)OMe\}^-$]	189,201
		C	intermolecular exchange of $ReH(CO)_5$ ($G^{\ddagger}_{180}$ = 41.9 kJ mol^{-1}, L = CO)	
	$[RePt_3(\mu\text{-}dppm)_3(O)_3\{P(OMe)_3\}]^+$	B	migration of phosphite around core	51
n = 5	$[Re_4Pt(\mu\text{-}H)_3(CO)_{18}]^-$	B	hydride exchange across Re-Pt vectors [$G^{\ddagger}_{273}$ = 74(7) kJ mol^{-1}]	201
n = 8	$[Re_7Pt(\mu_6\text{-}C)(L)(CO)_{21}]^{2-}$ (L = Me_3, η^3-2-methylallyl)	A	tripodal rotation at $Re(CO)_3$	128

Footnote to Table Flux: Exchange Pathways: A, Metal localized ligand scrambling; B, Intermetallic ligand migrations; C, Metal framework rearrangements.

the examples for which detailed studies have been undertaken, and/or those for which mechanistic speculation is available.

A number of examples of metal-localized ligand scrambling have been documented. Rotation of the $[Ru(CO)_2(\eta^5\text{-}C_5H_5)]$ units about the Zr-Ru bonds in the V-shaped $[ZrRu_2(CO)_4(\eta^5\text{-}C_5H_5)_4]$ results in equivalence of the carbonyl ligands (Figure 1.3.1.).[188] A similar rotation of the $[W(CO)_2(\eta^5\text{-}C_5Me_5)]$ group in $[WCo_2(\mu_3\text{-}CC_6H_4Me\text{-}4)(CO)_8(\eta^5\text{-}C_5Me_5)]$ has also been noted.[193] A detailed study of the rotation of the $[M(CO)_2(\eta\text{-}C_5R_4R')]$ vertices (M = Mo, W; R, R' = H, Me) in $[MCo_2(\mu_3\text{-}CCO_2Pr^i)(L)(CO)_6(\eta^5\text{-}C_5R_4R')]$ (L = 2CO, $Ph_2PCH_2CH_2PPh_2$, $Ph_2AsCH_2CH_2PPh_2$; not all combinations)[98,99] revealed that the barriers to rotation of the group 6 metal-containing vertices in these clusters (37 - 42 kJ mol^{-1}) are similar to those of the $[M(CO)_2(\eta^5\text{-}C_5H_{5-n}Me_n)]$ vertices in tetrahedral $[M_2(\mu_3\text{-}\eta^2\text{-}RC_2R)(CO)_4(\eta^5\text{-}C_5H_{5-n}Me_n)_2]$.[98] Tripodal $[Co(CO)_3]$ rotation was sufficiently rapid in these clusters $[MoCo_2(\mu_3\text{-}CCO_2Pr^i)(L)(CO)_6(\eta^5\text{-}C_5R_4R')]$ that it could not be frozen out in solution NMR studies. A similarly rapid turnstile motion was observed at one cobalt atom in $[WCo_2(\mu\text{-}EtC_2Et)(\mu\text{-}\eta^4\text{-}CEtCEtCEtCEt)(CO)_8]$, but $Co(CO)_3$ rotation at the other cobalt was retarded by adjacent ethyl groups.[195]

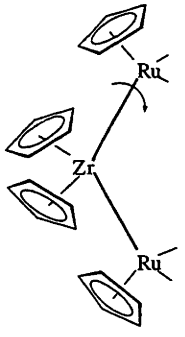
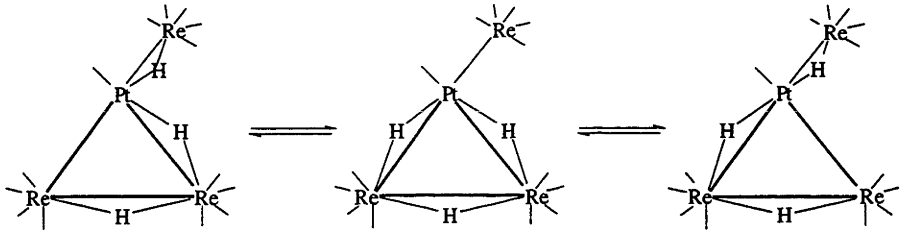


Figure 1.3.1

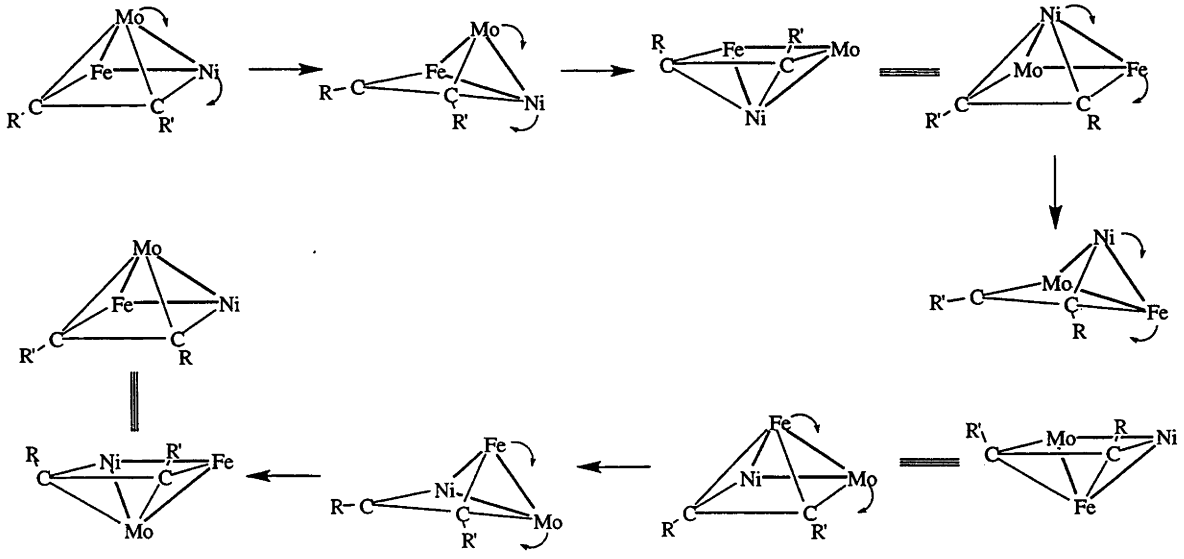
Two localized exchange processes were observed at the triangular $[Re_2Pt(\mu\text{-}H)_2(CO)_8(PPh_3)_2]$; the lower energy process was a scrambling of the three carbonyl ligands in the $[Re(CO)_3(PPh_3)]$ unit, while the higher energy process corresponded to a trigonal twist at the same metal, but involving phosphine as well as carbonyls.[197] Three-fold exchange at $[M(CO)_4]$ groups has been documented previously in homometallic clusters, e.g. $[Os_3(\mu\text{-}H)(\mu_3\text{-}CR)(CO)_{10}]$ (R = H, OMePh).[202] Tripodal $[Re(CO)_3]$ rotation in the bicapped octahedral $[Re_7Pt(\mu_6\text{-}C)(Me)_3(CO)_{21}]^{2-}$ is facile at room temperature.[128] Upon cooling a sample of the cluster, rotation at the three rheniums at the base of the $PtMe_3$ cap was frozen first, followed by cessation at the three rheniums at the base of the $[Re(CO)_3]$ cap. Investigation of the isostructural $[Re_7Pt(\mu_6\text{-}C)(CO)_{21}(\eta^3\text{-}2\text{-methyallyl})]^{2-}$ revealed analogous tripodal rotation; decoalescence of resonances was observed in the reverse order

to that in the $PtMe_3$-containing cluster, but it was not clear if this results from a reversal of relative activation energies, or of chemical shift order. Three independent tripodal exchanges have been similarly observed at the $[Os(CO)_3]$ vertices of the homometallic cluster $[Os_6(CO)_{18}]$.[203]

Several examples of intermetallic hydride migration in rhenium-platinum clusters have been investigated. Hydride hopping between the two Re-Pt edges in triangular $[Re_2Pt(\mu\text{-}H)_2(CO)_8(L)]$ [L = η^4-cod, $(PPh_3)_2$] occurred at a lower energy than rotation of the [Pt(H)(L)] moiety.[198] A similar hydride migration between the two Re-Pt edges was observed in the spiked-triangular $[Re_3Pt(\mu\text{-}H)_3(CO)_{14}]$[189] and $[Re_3Pt(\mu\text{-}H)_3\{C(O)OMe\}(CO)_{13}]^-$,[201] and the "scorpion" $[Re_4Pt(\mu\text{-}H)_3(CO)_{18}]^-$;[201] an intermediate in which both exchanging hydrides are bridging Re-Pt linkages in the triangular fragment of the cluster was proposed (Scheme 1.3.1.).



Scheme 1.3.1.



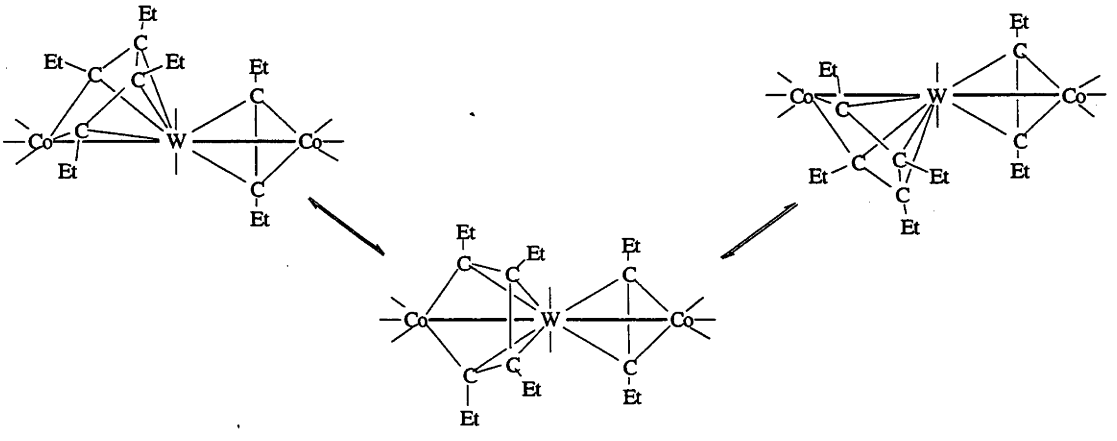
Scheme 1.3.2. other ligands omitted for clarity

Alkyne migration at $[MoFeNi(\mu_3\text{-}\eta^2\text{-}PhC_2CO_2Pr^i)(CO)_6(\eta^5\text{-}C_5H_5)_2]$ has been examined;[199] a formal rotation of the alkyne relative to the metal triangle proceeding by a "modified windscreen wiper" mechanism was proposed (Scheme 1.3.2.).

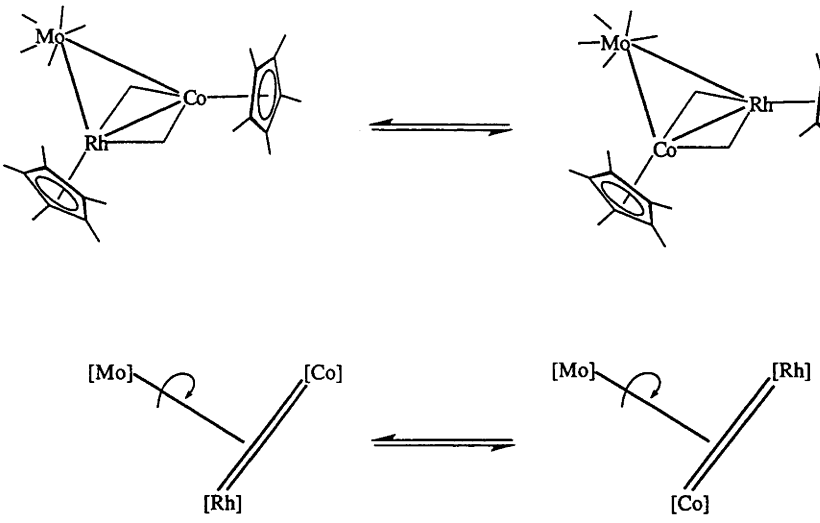
Carbonyl exchange between metals has been the most frequently studied intermetallic ligand migration in homometallic clusters, but the few examples which have been examined in the "very mixed"-metal domain have afforded inconclusive results. In the triangular $[MoCo_2(\mu_3\text{-}CCO_2Pr^i)(\mu\text{-}Ph_2ECH_2CH_2PPh_2)(CO)_6(\eta^5\text{-}C_5Me_5)]$, the mechanism interconverting molybdenum- and cobalt-bound carbonyls was not conclusively established, but rotation of the $[Mo(CO)_2(\eta^5\text{-}C_5Me_5)]$ unit was a critical requirement.[98] Global MW_2-localized CO exchange was noted at the tetrahedral $[MW_2Co(CO)_9(\eta^5\text{-}C_5H_4Me)_3]$,[200] although again the fluxional process or processes were not conclusively established.

Intermetallic phosphite migration has been observed at $[RePt_3(\mu\text{-}dppm)_3(O)_3\{P(OMe)_3\}]^+$;[51] a similar fluxional process to that observed earlier in the homometallic cluster $[Pt_3(\mu_3\text{-}CO)(\mu\text{-}dppm)_3\{P(OMe)_3\}]^{2+}$ was proposed, involving the intermediacy of a phosphite ligand triply bridging the Pt_3 face.

Few examples of metal framework rearrangements have been observed by NMR methods at "very mixed"-metal clusters. A study of the V-shaped cluster $[WCo_2(\mu\text{-}EtC_2Et)(\mu\text{-}\eta^4\text{-}CEtCEtCEtCEt)(CO)_8]$ revealed that the fluxionality on the NMR timescale was not alkyne ligand rotation; rather, a twisting of one ligated cobalt with respect to the other introduced a molecular mirror plane (Scheme 1.3.3.). The triangular clusters $[MM'Rh(\mu\text{-}CO)_2(CO)_5(\eta^5\text{-}C_5Me_5)_2]$ (M = Cr, Mo, W; M' = Co, Rh) underwent a formal rotation of the $[M(CO)_5]$ unit about an axis through M and the midpoint of the M'-Rh vector (Scheme 1.3.4.).[191,192] The cluster is an isolobal analogue of a $d^6\text{-}ML_5$ alkene complex. In this context, it is interesting that the barrier to rotation in $[MoCoRh(\mu\text{-}CO)_2(CO)_5(\eta^5\text{-}C_5Me_5)_2]$ ($G^{\ddagger}_{258}$ = 52.3 ± 1.3 kJ mol^{-1}) is in the range observed for hindered rotation at $d^6\text{-}ML_5$ organic alkene complexes ($G^{\ddagger}$ = 35 - 80 kJ mol^{-1}).

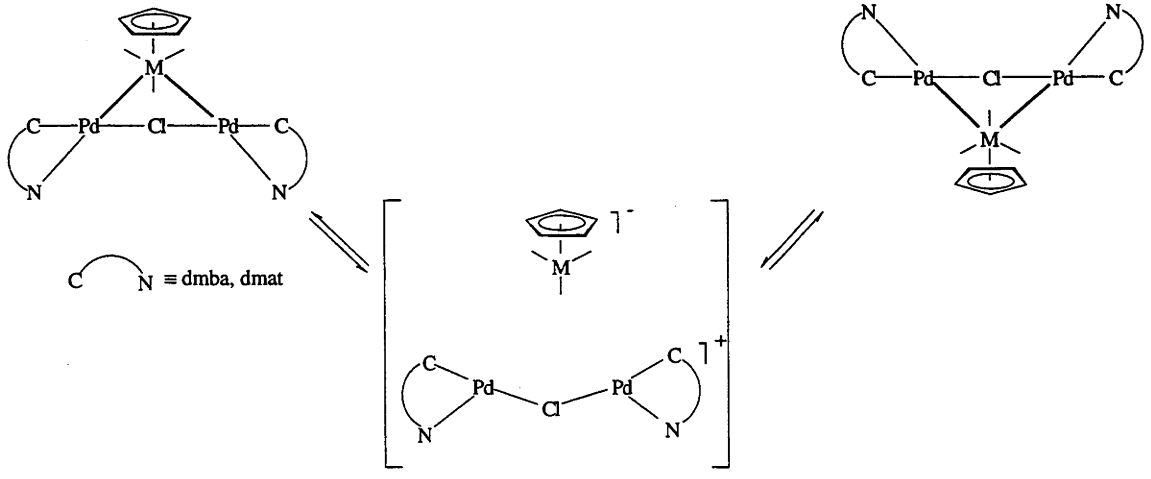


Scheme 1.3.3.

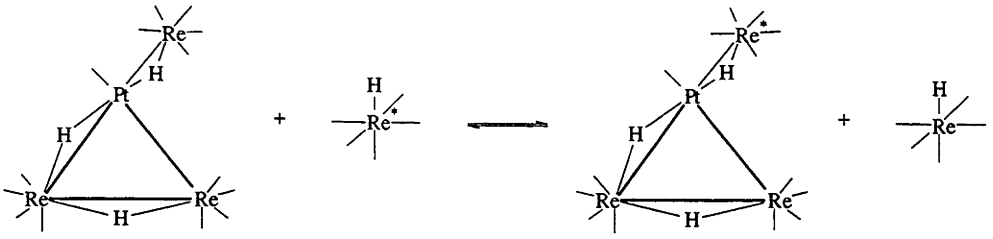


Scheme 1.3.4.

Examples of intermolecular ligated metal exchange are also extant. The V-shaped clusters $[MPd_2(\mu\text{-}Cl)(CO)_3(L)_2(\eta^5\text{-}C_5H_5)]$ (M = Cr, Mo, W; L = dmba, dmat) underwent exchange by dissociation and reassociation of the carbonylmetallate anion $[M(CO)_3(\eta^5\text{-}C_5H_5)]^-$ (Scheme 1.3.5.).[194] The spiked triangular cluster $[Re_3Pt(\mu\text{-}H)_3(CO)_{14}]$ exchanged the "spike" fragment $[ReH(CO)_5]$ in solution, in a process which is a formal substitution at a square planar platinum (Scheme 1.3.6.).[189] Such reactions are usually associative; accordingly, a strong dependence on the concentration of added $[ReH(CO)_5]$ was noted.



Scheme 1.3.5.



Scheme 1.3.6.

"Very mixed"-metal clusters clearly offer significant advantages in fluxionality studies, but these advantages remain to be fully exploited. Studies of tetrahedral rhodium and mixed rhodium-iridium clusters have revealed intermetallic carbonyl ligand site exchange proceeding by way of merry-go-round and change-of-basal-face processes.[181] Substitution of Rh by Ir in the apical site slowed down the former process, rationalized as resulting from the more electronegative Rh inducing a shift of electron density to the basal face and stabilizing the bridging CO-containing ground state. Tetrahedral iridium and mixed rhodium-iridium clusters underwent tripodal rotation at the apical metal. Substitution of Ir by Rh in the basal plane accelerated this process, rationalized as the electronegative Rh removing electron density from the apical 5d orbitals between the apical Ir-CO bonds. Both of these examples involved an electronic effect from a remote metal affecting relative energies of activation. Replacing the vertices in homometallic clusters to afford "very mixed"-metal clusters should accentuate these effects, but this remains to be demonstrated. One problem for fluxional processes involving the heterometal is that isolobal equivalence of ligated metal fragments involves introducing a (formally) higher coordination number metal, and possibly increased steric effects [e.g. replacing $Ir(CO)_3$ by $W(CO)_2(\eta^5\text{-}C_5H_5)$ in proceeding from $[Ir_4(CO)_{12}]$ to isostructural $[WIr_3(CO)_{11}(\eta^5\text{-}C_5H_5)]$ introduces a (formally) eight coordinate tungsten, with a sterically demanding cyclopentadienyl ligand]. However, for fluxional processes remote from the heterometal (such as with the rhodium-iridium examples above), this problem may not be important.

1.3.2. Electrochemistry

The electrochemical behaviour of metal clusters has been reviewed elsewhere.[204] The interest in examining clusters stems from their potential to act as "electron sinks"; in principle, an aggregate of several metal atoms may be capable of multiple redox state changes. The incorporation of heterometals provides the opportunity to tune the electrochemical response, effects which should be maximized in "very mixed"-metal clusters. Few "very mixed"-metal clusters have been subjected to detailed electrochemical studies, the majority of reports dealing with cyclic voltammetry only. Table 1.3.2. contains a summary of electrochemical investigations of "very mixed"-metal clusters.

Table 1.3.2.

M_n	*Cluster*	*Technique(s)*	*Ref.(s)*
n = 3	$[CrCo_2(\mu_3\text{-}CH)(CO)_8(\eta^5\text{-}C_5H_5)]$	ETCS	77
	$[CrCo_2(\mu_3\text{-}CMe)(CO)_8(\eta^5\text{-}C_5H_5)]$	ETCS, CV, DCP, DPP	77,205
	$[CrCo_2(\mu_3\text{-}CPh)(CO)_8(\eta^5\text{-}C_5H_5)]$	ETCS, CV, DCP, DPP, ESR	77,205
	$[MoCo_2(\mu_3\text{-}CH)(CO)_8(\eta^5\text{-}C_5H_5)]$	ETCS	77
	$[MoCo_2(\mu_3\text{-}CR)(CO)_8(\eta^5\text{-}C_5H_5)]$ (R = Me, Ph)	ETCS, CV, DCP, DPP, ESR	77,205,206
	$[MoCo_2(\mu_3\text{-}GeR)(CO)_8(\eta^5\text{-}C_5H_5)]$ (R = Me, Ph)	CV, DCP, DPP, ESR	205
	$[MoCo_2(\mu_3\text{-}PC_6H_4\text{-}4)(\mu\text{-}PPh_2)(CO)_6(\eta^5\text{-}C_5H_5)]^-$ (two isomers)	CV	65
	$[WCo_2(\mu_3\text{-}CH)(CO)_8(\eta^5\text{-}C_5H_5)]$	ETCS	77
	$[WCo_2(\mu_3\text{-}CMe)(CO)_8(\eta^5\text{-}C_5H_5)]$	ETCS, CV, DCP, DPP	77,205,206
	$[WCo_2(\mu_3\text{-}CPh)(CO)_8(\eta^5\text{-}C_5H_5)]$	ETCS, CV, DCP, DPP, ESR	77,205,206
	$[MoFeCo(\mu_3\text{-}P^tBu)(CO)_8(\eta^5\text{-}C_5H_5)]$	CV, DCP, DPP	205
	$[MoFeCo(\mu_3\text{-}PR)(CO)_8(\eta^5\text{-}C_5H_5)]$ (R = Me, Ph)	CV, DCP, DPP, ESR	205,206
	$[MoFeCo(\mu_3\text{-}E)(CO)_8(\eta^5\text{-}C_5H_5)]$ (E = S, Se)	CV	206
	$[MoRuCo(\mu_3\text{-}S)(CO)_8(\eta^5\text{-}C_5H_5)]$	CV	206
	$[WFeCo(\mu_3\text{-}PR)(CO)_8(\eta^5\text{-}C_5H_5)]$ (R = Me, Ph)	CV	206
	$[WFeCo(\mu_3\text{-}S)(CO)_8(\eta^5\text{-}C_5H_5)]$	CV	206
n = 4	$[Cr_3Co(\mu_3\text{-}S)_4(CO)(\eta^5\text{-}C_5H_4Me)_3]$	CV	207
	$[MoCo_3(\mu_3\text{-}\eta^2\text{-}PBu^tC_6H_4\text{-}2\text{-}PBu^t)(\mu\text{-}CO)(CO)_7(\eta^5\text{-}C_5H_5)]$	CV	208

	$[Mo_2Co_2(\mu_3\text{-}\eta^2\text{-}PBu^tC_6H_4\text{-}2\text{-}PBu^t)(\mu\text{-}CO)(CO)_6(\eta^5\text{-}C_5H_5)_2]$	CV	208
	$[Mo_2Co_2(\mu_3\text{-}S)_4(CO)_2(\eta^5\text{-}C_5H_4Et)_2]$	CV	209
	$[Mo_2Co_2(\mu_4\text{-}S)(\mu_3\text{-}S)_2(CO)_4(\eta^5\text{-}C_5H_4Me)_2]$	CV	145
	$[W_2Co_2(\mu_3\text{-}S)_3(CO)_5(\eta^5\text{-}C_5H_4Et)_2]$	CV	209
	$[Cr_2M_2(\mu_3\text{-}CO)_2(\mu\text{-}CO)_4(PR_3)_2(\eta^5\text{-}C_5H_5)_2]$ (M = Pd, Pt; R = Ph, Me, Et, ^{t}Bu)	CV	210,211
	$[Mo_2Ni_2(\mu_3\text{-}S)_4(CO)_2(\eta^5\text{-}C_5H_4Me)_2]$	CV	145
	$[Mo_2M_2(\mu_3\text{-}CO)_2(\mu\text{-}CO)_4(PPh_3)_2(\eta^5\text{-}C_5H_5)_2]$ (M = Pd, Pt; R = Ph, Me, Et, ^{t}Bu)	CV	210,211
	$[W_2Pt_2(\mu_3\text{-}CO)_2(\mu\text{-}CO)_4[PPh_2CH_2PPh_2\{Mn(CO)_2(\eta^5\text{-}C_5H_4Me\}](\eta^5\text{-}C_5H_4Me)_2]$	CV, C	124
	$[W_2M_2(\mu_3\text{-}CO)_2(\mu\text{-}CO)_4(PPh_3)_2(\eta^5\text{-}C_5H_5)_2]$ (M = Pd, Pt; R = Ph, Me, Et, ^{t}Bu)	CV, ESR	210,211
n = 8	$[Re_7Pd(\mu_6\text{-}C)(CO)_{21}(C_3H_5)]^{2-}$	CV	128
	$[Re_7Pt(\mu_6\text{-}C)(CO)_{21}(Me)_3]^{2-}$	CV	128
	$[Re_7Pt(\mu_6\text{-}C)(CO)_{21}(C_4H_7)]^{2-}$	CV	128

C = coulometry; CV = cyclic voltammetry; DCP = d.c. polarography; DPP = differential pulse polarography; ESR = electron spin resonance studies on electrogenerated species; ETCS = electron transfer-catalyzed synthesis.

Not surprisingly, given the success of metal exchange procedures in generating a wide range of systematically varied "very mixed"-metal clusters (Section *1.2.5.1.*), derivatives of $[Co_3(\mu_3\text{-}E)(CO)_9]$ have been studied intensively, especially capped triangular clusters of general formulas $[MCo_2(\mu_3\text{-}E)(CO)_8(\eta^5\text{-}C_5H_5)]$ (M = Cr, Mo or W; E = CH, CMe, CPh, PTol, GeMe or GePh) and $[MM'Co(\mu_3\text{-}E)(CO)_8(\eta^5\text{-}C_5H_5)]$ (M = Mo or W; M' = Fe or Ru; E = CMe, C^{t}Bu, CPh, PMe, S, Se) where the capping group may either be electrochemically active, or provide structural robustness important in subsequent oxidation state changes. Jensen *et al.*[77] have described an electrosynthesis of some alkylidyne examples ($CrCo_2$, $MoCo_2$, WCo_2), with greater yields than the classical thermally-activated route (Scheme 1.3.7.). The direct reaction between $[Co_3(\mu_3\text{-}CPh)(CO)_9]$ and $K[Mo(CO)_3(\eta^5\text{-}C_5H_5)]$ can be initiated by controlled potential electrolysis at the potential for the couple $[Co_3(\mu_3\text{-}CPh)(CO)_9]^{0/-I}$.

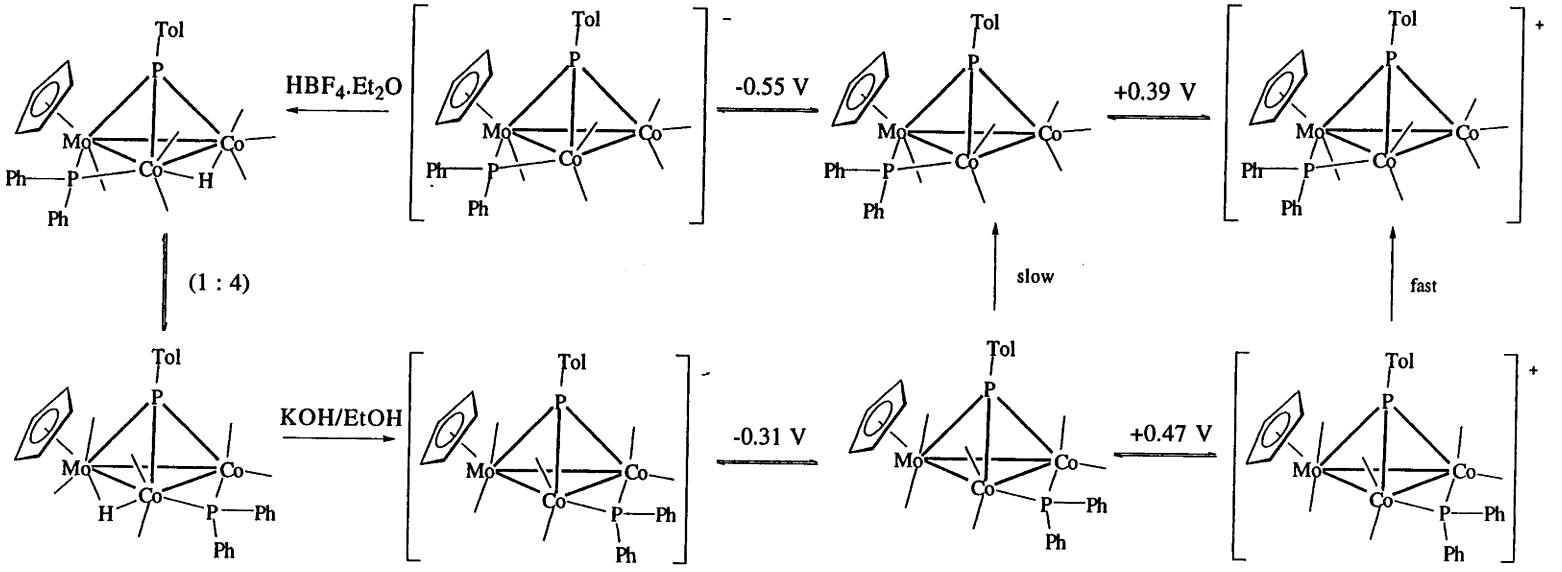
$$[Co_3(\mu_3\text{-}CPh)(CO)_9] + [Mo(CO)_3(\eta^5\text{-}C_5H_5)]^- \xrightarrow[\text{fast}]{-0.40\ V,\ THF} \underset{\text{good yield}}{[MoCo_2(\mu_3\text{-}CPh)(CO)_8]} + [Co(CO)_4]^-$$

$$[Co_3(\mu_3\text{-}CPh)(CO)_9] + {}^1/_2[Mo(CO)_3(\eta^5\text{-}C_5H_5)]_2 \xrightarrow[3\ days]{heat,\ benzene} \underset{\text{low yield}}{[MoCo_2(\mu_3\text{-}CPh)(CO)_8]} + \text{'}[Co(CO)_4]\text{'}$$

Scheme 1.3.7.

Two reduction processes were observed for the $[MCo_2(\mu_3\text{-}CR)(CO)_8(\eta^5\text{-}C_5H_5)]$ (M = Cr, Mo, W; R = Me, Ph) clusters. The first, an electrochemically and chemically irreversible process, was followed by a electrochemically and chemically reversible step; both steps involved cleavage of a M-Co bond accompanied by bridging of these metals by a carbonyl that has moved from a terminal position. The peak separation decreased in the order Cr > W ≈ Mo, with a dependence on apical substituent. ESR data has been used in characterization of the electrogenerated species, with experiments carried out at several temperatures and under argon and CO atmospheres. These clusters are chemically more reactive than their homonuclear tricobalt counterparts, with the $[MoCo_2(\mu_3\text{-}CR)(CO)_8(\eta^5\text{-}C_5H_5)]$ clusters the most chemically reversible.[205,206] The d.c. polarograms and cyclic voltammograms of the related germanium-capped $[MoCo_2(\mu_3\text{-}GeR)(CO)_8(\eta^5\text{-}C_5H_5)]$ (R = Me, Ph) also showed two reduction waves. The first process (reversible) corresponds to formation of the radical anion $[MoCo_2(\mu_3\text{-}GeR)(CO)_8(\eta^5\text{-}C_5H_5)]^{\cdot-}$, an assignment supported by ESR data; the second process is chemically irreversible and has the characteristics of an ECE mechanism.[205]

The anion $[MoCo_2(\mu_3\text{-}PTol)(\mu\text{-}PPh_2)(CO)_6(\eta^5\text{-}C_5H_5)]^-$ underwent two reversible one-electron oxidations to give radical and cationic species sequentially (Scheme 1.3.8.). The structure of the radical was established by a single-crystal X-ray diffraction study, which confirmed that the $\mu\text{-}PPh_2$ ligand bridges a Mo-Co bond. Low-temperature protonation,


Tol
P
Mo
Co
H
Ph
HBF4.Et2O
-0.55 V
+0.39 V
(1 : 4)
slow
fast
KOH/EtOH
-0.31 V
+0.47 V

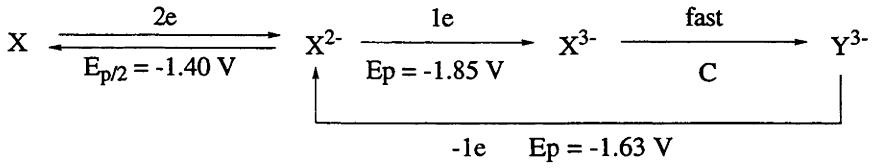
Scheme 1.3.8.

thermally induced migration of the phosphido ligand to the Co-Co bond and subsequent deprotonation gave an isomer of $[MoCo_2(\mu_3\text{-PTol})(\mu\text{-}PPh_2)(CO)_6(\eta^5\text{-}C_5H_5)]^-$. The CV of the deprotonated form of this isomer has been examined and shows two oxidation waves; the first wave was fully reversible and corresponded to the formation of the neutral radical species. Multiple scanning through the second wave, however, showed that rapid isomerization occurs via μ-PPh_2 bridge migration to give the Mo-Co bridging form.[65]

Reduction of the trimetallic clusters $[MoFeCo(\mu_3\text{-}PR)(CO)_8(\eta^5\text{-}C_5H_5)]$ (R = Me, Ph, ^{t}Bu) is chemically and electrochemically irreversible, even at low temperatures, and is believed to arise from a fast fragmentation reaction following radical anion formation. Introduction of a third heterometal makes reduction more difficult than with the related irondicobalt analogues.[205,206] The analogous tungsten-containing clusters $[WFeCo(\mu_3\text{-}PR)(CO)_8(\eta^5\text{-}C_5H_5)]$.(R = Me, Ph) are irreversibly reduced at higher potentials.[206]

The chalcogen-capped clusters $[M_1M_2Co(\mu_3\text{-}S)(CO)_8(\eta^5\text{-}C_5H_5)]$ (M_1M_2 = MoFe, MoRu, WFe) and $[MoFeCo(\mu_3\text{-}Se)(CO)_8(\eta^5\text{-}C_5H_5)]$ underwent a one-electron, quasi-reversible reduction. Addition of an electron proceeds more readily for the clusters with the lighter metals and for the selenium capped cluster relative to the sulfur analogue. An irreversible oxidation occurs at about $Ep_{+/0}$ = +1.0 V.[206]

While trimetallic clusters have been the most intensively studied, research has also been carried out on clusters of higher nuclearity. Cyclic voltammetry of tetrasulfur-capped $[Cr_3Co(\mu_3\text{-}S)_4(CO)(\eta^5\text{-}C_5H_4Me)_3]$ in DMF revealed 4 oxidation waves; three (-1.07, -0.23, +0.23 V) are reversible one-electron transfer steps and the last (+0.80 V) is an irreversible two-electron process. Another tetrasulfur-capped cluster which has been electrochemically studied is $[Mo_2Co_2(\mu_3\text{-}S)_4(CO)_2(\eta^5\text{-}C_5H_4Et)_2]$. Recent work of Mansour *et al.* showed that this compound undergoes a single, reversible, one-electron reduction at -1.04 V, a significantly more positive potential than that of the electron-rich 62-CVE nitrosyl analogue $[Mo_2Co_2(\mu_3\text{-}S)_4(NO)_2(\eta^5\text{-}C_5H_4Et)_2]$ which was also studied (-1.52 V).[209] The electrochemistry of the butterfly cluster $[Mo_2Co_2(\mu_4\text{-}S)(\mu_3\text{-}S)_2(CO)_4(\eta^5\text{-}C_5H_4Me)_2]$ was complicated by an electrode-surface reaction that led to small spurious peaks; starting the reduction sweep at -0.70 V eliminated this problem and produced a well-defined peak with $E_{p/2}$ = -1.40 V (E_p = 30 mV, 2 electron). This is followed by two successive cathodic waves in a EEC process that is coupled to a reverse anodic wave at -1.63 V (Scheme 1.3.9.[145]



$X = [Mo_2Co_2(\mu_4\text{-}S)(\mu_3\text{-}S)_2(CO)_4(\eta^5\text{-}C_5H_4Me)_2]$

Scheme 1.3.9.

The clusters $[MoCo_3(\mu_3\text{-}\eta^2\text{-}P^tBuC_6H_4P^tBu)(\mu\text{-}CO)(CO)_7(\eta^5\text{-}C_5H_5)]$ and $[MoCo_3(\mu_3\text{-}\eta^2\text{-}P^tBuC_6H_4P^tBu)(\mu\text{-}CO)(CO)_6(\eta^5\text{-}C_5H_5)_2]$, with tetrahedral cores, have contrasting electrochemical behaviour; the latter exhibited a quasi-reversible oxidation wave at 0.65 V (E_p = 180 mV), while no oxidation wave was observed for the former (up to 0.75 V). Other studies of these clusters suggested that redox behaviour is an indicator of chemical reactivity.[208]

The sulfur-capped tetrahedral cluster, $[Mo_2Ni_2(\mu_3\text{-}S)_4(CO)_2(\eta^5\text{-}C_5H_4Me)_2]$ displays fairly simple electrochemical behaviour. Reversible, one-electron reduction waves were observed at -1.58 and -2.11 V, while oxidation processes at -0.11 and 0.09 V were irreversible.[145] An uncomplicated reduction cyclic voltammogram of $[W_2Co_2(\mu_3\text{-}S)_3(CO)_2(\eta^5\text{-}C_5H_4Et)_2]$ showed 3 facile electron-transfer processes. The first two reversible reductions (-1.11, -1.71 V) were followed by a third, "quasi-reversible" reduction at -2.23 V (reverse re-oxidation at -2.04 V, E_p = 190 mV). The oxidation behaviour for this cluster is more complex. An inital irreversible oxidation at 0.16 V was followed by four successive oxidations thought to be due to ECE processes.[209] The lower oxidation potential of the tungsten-containing clusters relative to their molybdenum analogues is consistent with tungsten-containing clusters being more electron rich. This trend was confimed by the electrochemical studies on the systematically varied tetrametallic clusters $[M_2M'_2(\mu_3\text{-}CO)_2(\mu\text{-}CO)_4(PR_3)_2(\eta^5\text{-}C_5H_5)_2]$ (M = Cr, Mo, W; M' = Pd, Pt; R = Ph, Me, Et, ^{t}Bu). All combinations underwent an irreversible two-electron reduction leading to the rupture of the metallic core into identified fragments. The $M^1(I)$ centres were formally electroreduced to $M^1(0)$ in one step, accompanied by formation of $[M(CO)_3(\eta^5\text{-}C_5H_5)]^-$ (confirmed by IR). Oxidation occurred in two distinct one-electron transfers, with the second accompanied by some chemical decomposition. The radical cation generated by the first oxidation was reasonably stable and has been studied by ESR as a 106 K frozen solution; results suggested that the HOMO is located on the metals in the cluster. The stability of the dications was dependent on the solvent, with the most stable clusters being $[M_2Pt_2(\mu_3\text{-}CO)_2(\mu\text{-}CO)_4(PPh_3)_2(\eta^5\text{-}C_5H_5)_2]$ (M = Mo or W). While the reduction potentials were sensitive to R substitutent effects, the oxidation potentials were reasonably insensitive. This could indicate that the phosphine only plays a limited role in the HOMO, consistent with the ESR results.[210,211] The related $[W_2Pt_2(\mu_3\text{-}CO)_2(\mu\text{-}CO)_4[PPh_2CH_2PPh_2\{Mn(CO)_2(\eta^5\text{-}C_5H_4Me\}]_2(\eta^5\text{-}C_5H_4Me)_2]$ (Figure

1.3.2.), with pendant manganese metal centres, displayed some similarities to the bis(triphenylphosphine) analogue. In particular, a single irreversible reduction wave was seen at -1.45 V (c.f. -1.44 V); an associated reverse oxidation appeared at -0.18 V. Oxidation of the cluster occurred at 0.86 V and was followed by a reduction peak at -0.67 V in the reverse scan, thought to originate from an ECE process.[124]

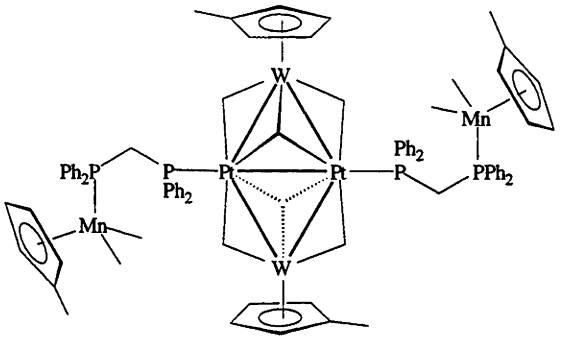


Figure 1.3.2.

The anodic scans of the three related octanuclear anionic clusters $[Re_7Pd(\mu_6\text{-}C)(CO)_{21}(\eta^3\text{-}C_3H_5)]^{2-}$, $[Re_7Pt(\mu_6\text{-}C)(CO)_{21}(Me)_3]^{2-}$ and $[Re_7Pt(\mu_6\text{-}C)(CO)_{21}(\eta^3\text{-}C_4H_7)]^{2-}$ showed two oxidation waves. The first was quasi-reversible while the second was almost completely irreversible. Oxidation potentials for the first process increased in the order $[Re_7Pt(\mu_6\text{-}C)(CO)_{21}(C_4H_7)]^{2-}$ (0.42 V) < $[Re_7Pd(\mu_6\text{-}C)(CO)_{21}(C_3H_5)]^{2-}$ (0.48 V) < $[Re_7Pt(\mu_6\text{-}C)(CO)_{21}(CH_3)_3]^{2-}$ (0.64 V). The large difference between the latter two can be explained based on the oxidation state of platinum in these compounds; in the cluster with the highest oxidation potential, the capping metal is Pt(IV), while in the other clusters the capping metal is Pt(II).[128]

1.3.1. Other Physical Methods

The electronic, optical and magnetic properties of metal clusters are of great current interest.[2] but these properties have been little-studied with "very mixed"-metal clusters. This is to some extent a reflection on the difficulty of preparing high-nuclearity examples; may of these interesting properties become important upon increasing cluster size. The limited magnetic studies to date are summarized in Section *1.3.3.1.*, with complementary MO studies in Section *1.3.3.2.*

1.3.3.1. Magnetic Measurements

The magnetic behaviour of some anti-ferromagnetic "very mixed"-metal carbonyl clusters (Figure 1.3.3.) has been studied by Pasynskii *et al.* Temperature dependences of the magnetic susceptibilies (χ_m) of $[Cr_2Co(\mu_3\text{-}S)_2(\mu\text{-}SCBu^t)(CO)_2(\eta^5\text{-}C_5H_4R)_2]$ (R = H, Me)

have been determined using the Faraday technique.[212,213] From χ_m, the effective magnetic moments (μ_{eff}) were calculated using the formula $\mu_{eff} = (8\chi_m T)$, and plots of μ_{eff} vs T prepared. The plots fitted the Heisenberg-Dirac-Van Vleck (HDVV) model for two exchange-coupled ions in the absence of orbital degeneracy of the complexes in the ground state. The related phosphine-substituted clusters $[Cr_2M(\mu_3\text{-}S)_2(\mu\text{-}SBu^t)(CO)(PPh_3)(\eta^5\text{-}C_5H_5)_2]$ (M = Rh, Ir) also exhibited a decrease in effective magnetic moment with temperature which agreed with the HDVV model. In contrast to the clusters above, the tetrametallic clusters $[Cr_3Co(\mu_3\text{-}S)_4(CO)(\eta^5\text{-}C_5H_4R)_3]$ (R = H, Me) were found to be diamagnetic. This diamagetism correlates with the 18-electron saturation of each metal atom.[106,207]

Table 1.3.3. Magnetic Measurements of "Very Miixed"-Metal Clusters

Cluster	*Measurements*	*Ref.*
$[Cr_2Co(\mu_3\text{-}S)_2(\mu\text{-}SBu^t)(CO)_2(\eta^5\text{-}C_5H_5)_2]$	$\mu_{eff.}$ vs T	212
$[Cr_2Co(\mu_3\text{-}S)_2(\mu\text{-}SBu^t)(CO)_2(\eta^5\text{-}C_5H_4Me)_2]$	$\mu_{eff.}$ vs T	213
$[Cr_2Rh(\mu_3\text{-}S)_2(\mu\text{-}SBu^t)(CO)(PPh_3)(\eta^5\text{-}C_5H_5)_2]$	$\mu_{eff.}$ vs T	214
$[Cr_2Ir(\mu_3\text{-}S)_2(\mu\text{-}SBu^t)(CO)(PPh_3)(\eta^5\text{-}C_5H_5)_2]$	$\mu_{eff.}$ vs T	214
$[Cr_3Co(\mu_3\text{-}S)_4(CO)(\eta^5\text{-}C_5H_5)_3]$	χ	106
$[Cr_3Co(\mu_3\text{-}S)_4(CO)(\eta^5\text{-}C_5H_4Me)_3]$	χ	207

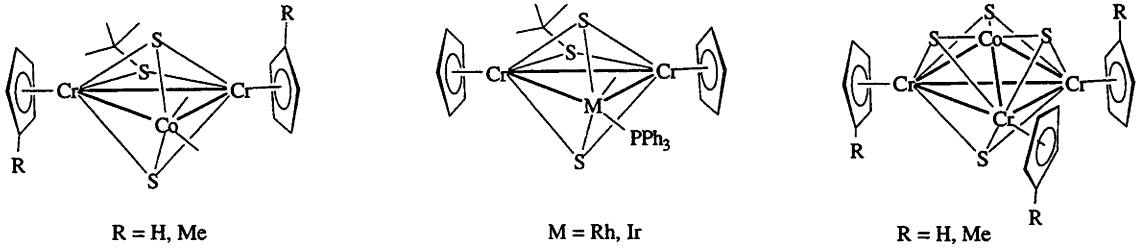


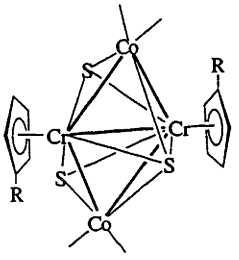
Figure 1.3.3.

1.3.3.2. MO Studies

In order to determine which chromium-based orbitals participated in the metal-metal and metal-ligand interactions of $[Cr_2Co(\mu_3\text{-}S)_2(\mu\text{-}SBu^t)(CO)_2(\eta^5\text{-}C_5H_4R)_2]$ and $[Cr_2Co_2(\mu_4\text{-}S)(\mu_3\text{-}S)_2(CO)_4(\eta^5\text{-}C_5H_4R)_2]$ (R = H, Me) (Figure 1.3.4.), the electronic structure of the fragment $[Cr_2(\mu_3\text{-}S)_2(\mu\text{-}SBu^t)(\eta^5\text{-}C_5H_5)]^-$ was calculated by the Extended Hückel (EH) method.[215]. Interaction of the lower lying p-orbitals of the bridging sulfur atoms with the

Table 1.3.4. MO Calculations of "Very Mixed"-Metal Clusters

Cluster	*MO Calculations*	*Ref.*
$[Cr_2Co(\mu_3\text{-}S)_2(\mu\text{-}SCMe_3)(CO)_2(\eta^5\text{-}C_5H_4R)_2]$ (R = H, Me)	Extended-Hückel	215
$[Cr_2Co(\mu_3\text{-}\eta^7\text{-}B_4H_7)(\mu\text{-}CO)(CO)_2(\eta^5\text{-}C_5Me_5)_2]$	Fenske-Hall	216
$[MoCo_2(\mu_3\text{-}\eta^2\text{-}CCH_2)(CO)_8(\eta^5\text{-}C_5H_5)]^+]$	Extended-Hückel	217
$[Mo_2Rh(CO)_5(\eta^5\text{-}C_5H_5)_3]$	Extended-Hückel	218
$[W_2Rh(CO)_5(\eta^5\text{-}C_5H_5)_3]$	Extended-Hückel	218
$[Cr_2Co_2(\mu_4\text{-}S)(\mu_3\text{-}S)_2(CO)_4(\eta^5\text{-}C_5H_4R)_2]$ (R = H, Me)	Extended-Hückel	215
$[Mo_2Co_2(\mu_3\text{-}S)_4(CO)_2(\eta^5\text{-}C_5H_4Me)_2]$	Extended-Hückel	209
$[Mo_2Ni_2(\mu_4\text{-}CO)(\mu_3\text{-}S)_2(\eta^5\text{-}C_5H_5)_4]$	Extended-Hückel	219



R = H, Me

Figure 1.3.4.

chromium d-orbitals resulted in the destabilization of the d-orbitals; the main localization of Cr-Cr bond orbitals was directed by the greater Cr-S interaction. The use of four half-occupied orbitals of the di-chromium fragment for forming Cr-Co bonds with two $Co(CO)_2$ fragments was thought to explain the diamagnetic behaviour of $[Cr_2Co_2(\mu_4\text{-}S)(\mu_3\text{-}S)_2(CO)_4(\eta^5\text{-}C_5H_4R)_2]$, in contrast to $[Cr_2Co(\mu_3\text{-}S)_2(\mu\text{-}SBu^t)(CO)_2(\eta^5\text{-}C_5H_4R)_2]$ possessing antiferromagnetic properties because of half-occupied orbitals. Bonding of all four (s, p_x, p_y and p_z) orbitals of the sulfide bridges with the chromium atoms corresponded to participation of formally unshared electron pairs of S atoms in "double-bonding"; this is consistent with the decrease in Cr-S distances to 2.25-2.30 Å, significantly less than the sum of covalent radii of Cr (1.46 Å) and S (1.04 Å) atoms.

Fenske-Hall MO calculations were carried out on $[Cr_2Co(\mu_3\text{-}\eta^7\text{-}B_4H_7)(\mu\text{-}CO)(CO)_2(\eta^5\text{-}C_5H_5)_2]$ (Figure 1.3.4.) in order to determine the nature of the interactions between the $[Co(CO)_3]$ and $[(\eta^5\text{-}C_5H_5)Cr]_2B_4H_7$ cluster fragments. The principal changes between the ground state molecule $[(\eta^5\text{-}C_5H_5)Cr]_2B_4H_8$ and the $[(\eta^5\text{-}C_5H_5)Cr]_2B_4H_7$ fragment in the

cluster resulted in the short Cr-Co distance and longer Cr-B distance, and involved increases in energy for those fragment orbitals which are Cr-Cr antibonding and Cr-B bonding. Interaction of an empty σ orbital of the $[Cr(CO)_3]$fragment with a filled B-H-Cr orbital caused the hydrogen atom to become Cr-B-Co face-bridging, rather than edge-bridging.[216]

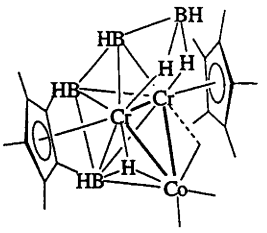
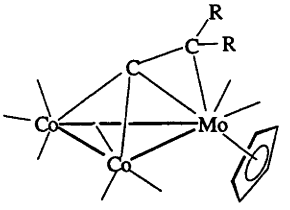


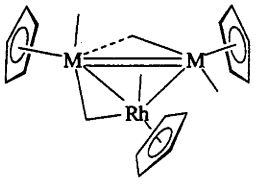
Figure 1.3.5.



R = H, Me

Figure 1.3.6.

In order to explain the preference of the Co-Co bridging vinylidene group of $[MoCo_2(\mu_3\text{-}\eta^2\text{-}CCH_2)(CO)_8(\eta^5\text{-}C_5H_5)]^+$ (Figure 1.3.5.), to lean towards the molybdenum, EHMO calculations have been employed. Results showed that the vinylidene capping unit was particularly well stabilized by direct interaction with the molybdenum atom, where the positive charge is better tolerated. Antarafacial migration of the $C{=}CH_2$ group, possessing a large transition energy barrier, was shown to be severely disfavoured, in accord with NMR experimental data where the $(\mu_3\text{-}\eta^2\text{-}CCMe_2)$ analogue exhibited a sharp methyl singlet over 0 to -90 °C resulting from the higher symmetry molybdenum-bonded vinylidene complex.[217]



M = Mo, W

Figure 1.3.7.

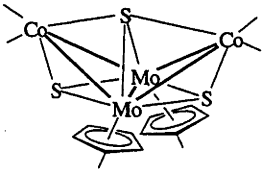


Figure 1.3.8.

The electronic structure of $[M_2Rh(\mu\text{-}CO)(CO)_4(\eta^5\text{-}C_5H_5)_3]$ (M = Mo, W) (Figure 1.3.7.) has been studied utilizing EHMO calculations. The nature of the metal-metal bonds in the clusters have been analyzed in terms of the bonding between the $[M_2(CO)_4(\eta^5\text{-}C_5H_5)_2]$ and $[Rh(CO)(\eta^5\text{-}C_5H_5)]$ fragments. Multiple W=W bonding in $[M_2(CO)_4(\eta^5\text{-}C_5H_5)_2]$ was realized by σ interactions between the orbitals $5d_z2$ and $6p_z$, and π interactions via $5d_{yz}$ and $5d_{xz}$ orbitals. The energetic consequences of the step by step transformation of a terminal CO group, coordinated to M, into a carbonyl ligand bridging one of the M-Rh bonds has been considered; terminal coordination of all carbonyl groups led to an

energetic destabilization of about 11 eV, while the experimentally determined geometry was calculated to have the greatest binding energy.[218]

The calculated EHMO energy levels for $M_2M'_2S_4$ type cubane clusters have been applied to $[Mo_2Co_2(\mu_4\text{-}S)(\mu_3\text{-}S)_2(CO)_2(\eta^5\text{-}C_5H_4Me)_2]$ (Figure 1.3.9.) in order to explain bonding behaviour.[220] It was suggested that the HOMO would have σ(Mo-Mo) character and that the LUMO was most likely σ*(Mo-Mo); addition of electrons to the cluster is believed to result in cleavage of the Mo-Mo, a proposal supported by electrochemical studies (see Section *1.3.3.*).

The butterfly metal core of $[Mo_2Ni_2(\mu_4\text{-}CO)(\mu_3\text{-}S)_2(\eta^5\text{-}C_5H_5)_4]$ is bridged by a crystallographically-confirmed carbonyl with $\mu_4\text{-}\eta^1$-coordination (Figure 1.3.7.). MO calculations have been used to support this assignment.[219] A series of calculations in which the $[NiS(\eta^5\text{-}C_5H_5)]$ unit was rotated about the Mo-Mo axis showed a shallow well with a minimum Ni-CO distance of ca. 2.25 Å. Orbital interactions of the μ_4-CO with the Mo atoms were both σ-bonding and multicentre bonding with the CO π-system. The Ni-CO bonding was best described as a dative bond from Ni to the π^* orbitals of the carbonyl. Low C–O overlap population reflected the additional electron donation into the C–O antibonding orbitals and was reflected with a low ν(CO).

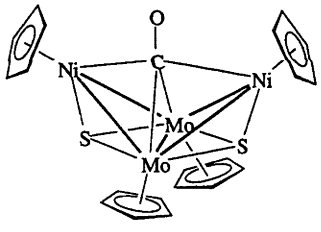


Figure 1.3.9.

1.4. Conclusion and Outlook

With flexible routes into "very mixed"-metal clusters in hand, the time is ripe for systematic investigations of their reactivity and physical properties. Ligand substitution generally proceeds with metalloselectivity, but the products are frequently not site-selective; many of these complexes are highly fluxional, and more than one configuration is often sufficiently stable so that mixtures of isomers are obtained. Characterization of these configurations has largely been crystallographic, which generally results in one configuration only being identifie; comprehensive spectroscopic studies are needed to identify all configurations. A number of examples of C-ligand transformation have been reported and, in almost all instances, this involves a heterometallic bond or face. This likely indicates the importance of heterometallic centres in effecting the transformations, but mechanistic studies to confirm this remain to be carried out; it is always possible, though unlikely in all instances, that the transformation occurs elsewhere on the cluster, and that the heterometallic unit is the favourable centre to stabilize the resulting fragments. Investigations of "very mixed"-metal cluster catalysis have been dominated by clusters with metal combinations effective in heterogeneous catalysis (e.g. Mo-Co in hydrodesulfurization; Re-Pt in petroleum reforming); clearly, there is great scope for exploring the potential of clusters with other metal combinations. The physical properties of "very mixed"-metal clusters have been intensively studied only recently. The significance of heterometals in controlling ligand mobility and tuning electrochemical response has yet to be fully exploited, and other physical properties (e.g. magnetism, nonlinear optical properties) are almost untouched. These are likely to be of increasing importance in the future.

1.5. References

(1) Shriver, D. F.; Kaesz, H. D.; Adams, R. D. *The Chemistry of Metal Cluster Complexes*; V.C.H.: New York, 1990.

(2) de Jongh, L. L. *Physics and Chemistry of Metal Cluster Complexes*; Kluwer: Amster, 1994.

(3) Stone, F. G. A. *Angew. Chem. Int. Ed. Engl.* **1984**, *23*, 89.

(4) Vahrenkamp, H. *Comments. Inorg. Chem.* **1985**, *4*, 253.

(5) Vahrenkamp, H. *Adv. Organomet. Chem.* **1983**, *22*, 169.

(6) Mingos, D. M. P. *Acc. Chem. Res.* **1984**, *17*, 311.

(7) Hoffman, *Angew. Chem., Int. Ed. Eng.* **1982**, *21*, 711.

(8) Gladfelter, W. L.; Geoffroy, G. L. *Adv. Organomet. Chem.* **1981**, *18*, 207.

(9) Farrugia, L. J. In *Comprehensive Organometallic Chemistry II*; Abel, E. W. Stone, F. G. A. Wilkinson, G. Ed.; Pergomon Press: Oxford, U.K., 1994, Vol.10, Ch. 4.

(10) Chi, Y. In *Comprehensive Organometallic Chemistry II*; Abel, E. W. Stone, F. G. A. Wilkinson, G. Ed.; Pergomon Press: Oxford, U.K., 1994, Vol. 6, Ch. 40.

(11) Bruce, M. I. *J. Organomet. Chem.* **1983**, *257*, 417.

(12) Roberts, D. A.; Geoffroy, G. L. In *Comprehensive Organometallic Chemistry*; Abel, E. W. Stone, F. G. A. Wilkinson, G. Ed.; Pergomon Press: Oxford, U.K., 1994, Vol. 6, Ch. 3.

(13) Comstock, M. C.; Shapley, J. R. *Coord. Chem. Rev.* **1995**, *143*, 501.

(14) Sappa, E.; Tiripicchio, A.; Braunstein, P. *Coord. Chem. Rev.* **1985**, *65*, 219.

(15) Vahrenkamp, H. *Pure Appl. Chem.* **1989**, *61*, 1777.

(16) Clark, D. T.; Sutin, K. A.; McGlinchey, M. J. *Organometallics* **1989**, *8*, 155.

(17) Jeffery, J. C.; Lawrence-Smith, J. G. *J. Organomet. Chem.* **1985**, *280*, C34.

(18) Chetcuti, M. J.; Chetcuti, P. A. M.; Jeffery, J. C.; Mills, R. M.; Mitrprachachon, P.; Pickering, S. J.; Stone, F. G. A.; Woodward, P. *J. Chem. Soc., Dalton Trans.* **1982**, 699.

(19) Jeffery, J. C.; Ruiz, M. A.; Stone, F. G. A. *J. Chem. Soc., Dalton Trans.* **1988**, 1131.

(20) Richter, F.; Vahrenkamp, H. *Angew. Chem. Int. Ed. Engl.* **1980**, *19*, 65.

(21) Wang, Q.-L.; Chen, S.-N.; Wang, X.; Sun, W.-H.; Wang, H.-Q.; Yang, S.-Y. *Polyhedron* **1996**, *15*, 2613.

(22) Müller, M.; Schacht, H.-T.; Fischer, K.; Ensling, J.; Gütlich, P.; Vahrenkamp, H. *Inorg. Chem.* **1986**, *25*, 4032.

(23) Beurich, H.; Blumhofer, R.; Vahrenkamp, H. *Chem. Ber.* **1982**, *115*, 2409.

(24) Blumhofer, R.; Vahrenkamp, H. *Chem. Ber.* **1986**, *119*, 683.

(25) Curnow, O. J.; Kampf, J. W.; Curtis, M. D.; Shen, J.-K.; Basalo, F. *J. Am. Chem. Soc.* **1994**, *116*, 224.

(26) Curnow, O. J.; Curtis, M. D.; Kampf, J. W. *Organometallics* **1997**, *16*, 2523.

(27) Waterman, S. M.; Humphrey, M. G.; Tolhurst, V.-A.; Skelton, B. W.; White, A. H.; Hockless, D. C. R. *Organometallics* **1996**, *15*, 934.

(28) Lucas, N. T.; Whittall, I. R.; Humphrey, M. G.; Hockless, D. C. R.; Perera, M. P. S.; Williams, M. L. *J. Organomet. Chem.* **1997**, *540*, 147.

(29) Waterman, S. M.; Humphrey, M. G.; Hockless, D. C. R. *J. Organomet. Chem.* **1997**, *in press*.

(30) Waterman, S. M.; Humphrey, M. G.; Hockless, D. C. R. *J. Organomet. Chem.* **1998**, *565*, 81.

(31) Lee, J.; Humphrey, M. G.; Hockless, D. C. R.; Skelton, B. W.; White, A. H. *Organometallics* **1993**, *12*, 3468.

(32) Lucas, N. T.; Humphrey, M. G.; Healy, P. C.; Williams, M. L. *J. Organomet. Chem.* **1997**, *545-546*, 519.

(33) Davies, S. J.; Howard, J. A. K.; Pilotti, M. U.; Stone, F. G. A. *J. Chem. Soc., Dalton Trans.* **1989**, 2289.

(34) Davies, S. J.; Howard, J. A. K.; Musgrove, R. J.; Stone, F. G. A. *Angew. Chem., Int. Ed. Engl.* **1989**, *28*, 624.

(35) Davies, S. J.; Howard, J. A. K.; Musgrove, R. J.; Stone, F. G. A. *J. Chem. Soc., Dalton Trans.* **1989**, 2269.

(36) Bars, O.; Braunstein, P.; Jud, J.-M. *Nouv. J. Chem.* **1984**, *8*, 771.

(37) Braunstein, P.; Ries, M.; de Méric de Bellefon, C.; Dusausoy, Y.; Mangeot, J.-P. *J. Organomet. Chem.* **1988**, *355*, 533.

(38) Curnow, O. J.; Kampf, J. W.; Curtis, M. D.; Mueller, B. L. *Organometallics* **1992**, *11*, 1984.

(39) Curtis, M. D.; Curnow, O. J. *Organometallics* **1994**, *13*, 2489.

(40) Riaz, U.; Curnow, O.; Curtis, M. D. *J. Am. Chem. Soc.* **1991**, *113*, 1416.

(41) Mansour, M. A.; Curtis, M. D.; Kampf, J. W. *Organometallics* **1995**, *14*, 5460.

(42) Mansour, M. A.; Curtis, M. D.; Kampf, J. W. *Organometallics* **1997**, *16*, 3363.

(43) Neumann, H.-P.; Ziegler, M. L. *J. Organomet. Chem.* **1989**, *377*, 255.

(44) Xiao, J.; Puddephatt, R. J. *J. Am. Chem. Soc.* **1994**, *116*, 1129.

(45) Hao, L.; Xiao, J.; Vittal, J. J.; Puddephatt, R. J. *Angew. Chem., Int. Ed. Engl.* **1995**, *34*, 346.

(46) Braunstein, P.; de Jesús, E.; Tiripicchio, A.; Ugozzoli, F. *Inorg. Chem.* **1992**, *31*, 411.

(47) Davies, S. J.; Stone, F. G. A. *J. Chem. Soc., Dalton Trans.* **1989**, 1865.

(48) Xiao, J.; Hao, L.; Puddephatt, R. J.; Manojlovic-Muir, L.; Muir, K. W.; Torabi, A. A. *Organometallics* **1995**, *14*, 2194.

(49) Xiao, J.; Hao, L.; Puddphatt, R. J.; Manojlovic-Muir, L.; Muir, K. W.; Torabi, A. A. *J. Chem. Soc., Chem. Commun.* **1994**, 2221.

(50) Xiao, J.; Hao, L.; Puddephatt, R. J.; Manojlovic-Muir, L.; Muir, K. W.; Torabi, A. A. *Organometallics* **1995**, *14*, 4183.

(51) Hao, L.; Xiao, J.; Vittal, J.; Puddephatt, R. J.; Manojlovic-Muir, L.; Muir, K. W.; Torabi, A. A. *Inorg. Chem.* **1996**, *35*, 658.

(52) Xiao, J.; Vittal, J. J.; Puddephatt, R. J. *J. Am. Chem. Soc.* **1993**, *115*, 7882.

(53) Jeffery, J. C.; Lewis, D. B.; Lewis, G. E.; Parrott, M. J.; Stone, F. G. A. *J. Chem. Soc., Dalton Trans.* **1986**, 1717.

(54) Bernhardt, W.; Schacht, H.-T.; Vahrenkamp, H. *Z. Naturforsch.* **1989**, *44b*, 1060.

(55) Bernhardt, W.; von, Schering, C.; Vahrenkamp, H. *Angew. Chem., Int. Ed. Engl.* **1986**, *25*, 279.

(56) Mani, D.; Schacht, H.-T.; Powell, A.; Vahrenkamp, H. *Organometallics* **1987**, *6*, 1360.

(57) Riaz, U.; Curtis, M. D.; Rheingold, A.; Haggerty, B. S. *Organometallics* **1990**, *9*, 2647.

(58) Churchill, M. R.; Biondi, L. V. *J. Organomet. Chem.* **1989**, *366*, 265.

(59) Shapley, J. R.; McAteer, C. H.; Churchill, M. R.; Biondi, L. V. *Organometallics* **1984**, *3*, 1595.

(60) Shapley, J. R.; Humphrey, M. G.; McAteer, C. H. In *Selectivity in Catalysis*; Davis, M. E. and. Suib, S. L. Ed.; American Chemical Society: Washington, DC, 1993; Vol. 517; p 127.

(61) Adams, R. D.; Belinski, J. A. *Organometallics* **1991**, *10*, 2114.

(62) Dunn, P.; Jeffery, J. C.; Sherwood, P. *J. Organomet. Chem.* **1986**, *311*, C55.

(63) Churchill, M. R.; Biondi, L. V.; Shapley, J. R.; McAteer, C. H. *J. Organomet. Chem.* **1985**, *280*, C63.

(64) Churchill, M. R.; Biondi, L. V. *J. Organomet. Chem.* **1988**, *353*, 73.

(65) Bradford, M. R.; Connelly, N. G.; Harrison, N. C.; Jeffery, J. C. *Organometallics* **1989**, *8*, 1829.

(66) Blum, T.; Braunstein, P.; Tiripicchio, A.; Tiripicchio Camellini, M. *Organometallics* **1989**, *8*, 2504.

(67) Curtis, M. D.; Riaz, U.; Curnow, O. J.; Kampf, J. W.; Rheingold, A. L.; Haggerty, B. S. *Organometallics* **1995**, *14*, 5337.

(68) Waterman, S. M.; Tolhurst, V.-A.; Humphrey, M. G.; Skelton, B. W.; White, A. H. *J. Organomet. Chem.* **1996**, *515*, 89.

(69) Druker, S. H.; Curtis, M. D. *J. Am. Chem. Soc.* **1995**, *117*, 6366.

(70) Curtis, M. D.; Druker, S. H.; Goossen, L.; Kampf, J. W. *Organometallics* **1997**, *16*, 231.

(71) Davies, S. J.; Howard, J. A. K.; Pilotti, M. U.; Stone, F. G. A. *J. Chem. Soc., Chem. Commun.* **1989**, 190.

(72) Davies, S. J.; Howard, J. A. K.; Pilotti, M. U.; Stone, F. G. A. *J. Chem. Soc., Dalton Trans.* **1989**, 1855.

(73) Vahrenkamp, H. *Phil. Trans. R. Soc. Lond. A* **1982**, *308*, 17.

(74) Stone, F. G. A. *Phil. Trans. R. Soc. Lond. A* **1982**, *308*, 87.

(75) Stone, F. G. A. *Pure Appl. Chem.* **1986**, *58*, 529.

(76) Fischer, K.; Deck, W.; Schwarz, M.; Vahrenkamp, H. *Chem. Ber.* **1985**, *118*, 4946.

(77) Jensen, S.; Robinson, B. H.; Simpson, J. *J. Chem. Soc., Chem. Commun.* **1983**, 1081.

(78) Duffy, D. N.; Kassis, M. M.; Rae, A. D. *J. Organomet. Chem.* **1993**, *460*, 97.

(79) Heping, W.; Zhuanyun, Z.; Yuanqi, Y.; Daosen, J.; Xiaoying, H. *Polyhedron* **1995**, *14*, 1543.

(80) Wu, H.-P.; Yin, Y.-Q.; Huang, X.-Y.; Yu, K.-B. *J. Organomet. Chem.* **1995**, *498*, 119.

(81) Wu, H.-P.; Yin, Y.-Q.; Huang, X.-Y. *Polyhedron* **1995**, *14*, 2993.

(82) Wu, H.-P.; Yin, Y.-Q.; Huang, X.-Y. *Inorg. Chim. Acta* **1997**, *255*, 167.

(83) Wu, H.-P.; Zhao, Z.-Y.; Liu, S.-M.; Ding, E.-R.; Yin, Y.-Q. *Polyhedron* **1996**, *15*, 4117.

(84) Duffy, D. N.; Kassis, M. M.; Rae, A. D. *Acta Cryst.* **1991**, *C47*, 2343.

(85) Mani, D.; Vahrenkamp, H. *Chem. Ber.* **1986**, *119*, 3639.

(86) Schacht, H.-T.; Vahrenkamp, H. *Chem. Ber.* **1989**, *122*, 2239.

(87) Honrath, U.; Vahrenkamp, H. *Z. Naturforsch.* **1984**, *39b*, 559.

(88) Heping, W.; Yuanqi, Y.; Qingchuan, Y. *Polyhedron* **1996**, *15*, 43.

(89) Beurich, H.; Vahrenkamp, H. *Angew. Chem. Int. Ed. Engl.* **1981**, *20*, 98.

(90) Gorzellik, M.; Nuber, B.; Bohn, T.; Ziegler, M. L. *J. Organomet. Chem.* **1992**, *429*, 173.

(91) Richter, F.; Roland, E.; Vahrenkamp, H. *Chem. Ber.* **1984**, *117*, 2429.

(92) Roland, E.; Vahrenkamp, H. *Chem. Ber* **1984**, *117*, 1039.

(93) Mlekuz, M.; Bougeard, P.; Sayer, B. G.; Faggiani, R.; Lock, C. J. L.; McGlinchey, M. J.; Jaouen, G. *Organometallics* **1985**, *4*, 2046.

(94) Beurich, H.; Vahrenkamp, H. *Angew. Chem., Int. Ed. Engl.* **1978**, *17*, 863.

(95) Richter, F.; Vahrenkamp, H. *Organometallics* **1982**, *1*, 756.

(96) Bernhardt, W.; Vahrenkamp, H. *J. Organomet. Chem.* **1988**, *355*, 427.

(97) Richter, F.; Beurich, H.; Vahrenkamp, H. *J. Organomet. Chem.* **1979**, *166*, C5.

(98) Sutin, K. A.; Kolis, J. W.; Mlekuz, M.; Bougeard, P.; Sayer, B. G.; Quilliam, M. A.; Faggiani, R.; Lock, C. J. L.; McGlinchey, M. J.; Jaouen, G. *Organometallics* **1987**, *6*, 439.

(99) Sutin, K. A.; Li, L.; Frampton, C. S.; Sayer, B. G.; McGlinchey, M. J. *Organometallics* **1991**, *10*, 2362.

(100) Sun, W.-H.; Wang, H.-Q.; Yang, S.-Y.; Zhou, Q.-F. *Polyhedron* **1994**, *13*, 389.

(101) Ziegler, M. L.; Neumann, H.-P. *Chem. Ber.* **1989**, *122*, 25.

(102) Gusbeth, P.; Vahrenkamp, H. *Chem. Ber.* **1985**, *118*, 1758.

(103) Bantel, H.; Powell, A. K.; Vahrenkamp, H. *Chem. Ber.* **1990**, *123*, 1607.

(104) Richter, F.; Müller, M.; Gärtner, N.; Vahrenkamp, H. *Chem. Ber.* **1984**, *117*, 2438.

(105) Braunstein, P.; de Méric de Bellefon, C.; Ries, M. *Inorg. Chem.* **1990**, *29*, 1181.

(106) Pasynskii, A. A.; Eremenko, I. L.; Orazsakhatov, B.; Kalinnikov, V. T.; Aleksandrov, G. G.; Struchkov, Y. T. *J. Organomet. Chem.* **1981**, *214*, 367.

(107) Eremenko, I. L.; Pasynskii, A. A.; Katugin, A. S.; Orazsakhatov, B.; Shirokii, V. L.; Shklover, V. E.; Struchkov, Y. T. *J. Organomet. Chem.* **1988**, *345*, 177.

(108) Chetcuti, M. J.; Huffman, J. C.; McDonald, S. R. *Inorg. Chem.* **1989**, *28*, 238.

(109) Elliot, G. P.; Howard, J. A. K.; Mise, T.; Moore, I.; Nunn, C. M.; Stone, F. G. A. *J. Chem. Soc., Dalton Trans.* **1986**, 2091.

(110) Awang, M. R.; Carriedo, G. A.; Howard, J. A. K.; Mead, K. A.; Moore, I.; Nunn, C. M.; Stone, F. G. A. *J. Chem. Soc., Chem. Commun.* **1983**, 964.

(111) Davies, S. J.; Stone, F. G. A. *J. Chem. Soc., Dalton Trans.* **1989**, 785.

(112) Chetcuti, M. J.; Fanwick, P. E.; Gordon, J. C. *Inorg. Chem.* **1991**, *30*, 4710.

(113) Xiao, J.; Kristof, E.; Vittal, J. J.; Puddephatt, R. J. *J. Organomet. Chem.* **1995**, *490*, 1.

(114) Beringhelli, T.; Ceriotti, A.; Ciani, G.; D'Alfonso, G.; Garlaschelli, L.; Della Pergola, R.; Moret, M.; Sironi, A. *J. Chem. Soc., Dalton Trans.* **1993**, 199.

(115) Bergamo, M.; Beringhelli, T.; Ciani, G.; D'Alfonso, G.; Moret, M.; Sironi, A. *Inorg. Chim. Acta* **1997**, *259*, 291.

(116) Carr, N.; Mullica, D. F.; Sappenfield, E. L.; Stone, F. G. A.; Went, M. J. *Organometallics* **1993**, *12*, 4350.

(117) Bantel, H.; Powell, A. K.; Vahrenkamp, H. *Chem. Ber.* **1990**, *123*, 677.

(118) Braunstein, P.; de Méric de Bellefon, C.; Ries, M. *J. Organomet. Chem.* **1984**, *262*, C14.

(119) Tunik, S. P.; Shipil, P. N.; Vlasov, A. V.; Denisov, V. R.; Nikols'kii, A. B.; Dolgushin, F. M.; Yanovsky, A. I.; Struchkov, Y. T. *J. Organomet. Chem.* **1996**, *515*, 11.

(120) Davies, S. J.; Elliot, G. P.; Howard, J. A. K.; Nunn, C. M.; Stone, F. G. A. *J. Chem. Soc., Dalton Trans.* **1987**, 2177.

(121) Ciani, G.; Moret, M.; Sironi, A.; Antognazza, P.; Beringhelli, T.; D'Alfonso, G.; Della Pergola, R.; Minoja, A. *J. Chem. Soc., Chem. Commun.* **1991**, 1255.

(122) Eremenko, I. L.; Pasynskii, A. A.; Katugin, A. S.; Zalmanovitch, V. R.; Orazsakhatov, B.; Sleptsova, S. A.; Nekhaev, A. I.; Kaverin, V. V.; Ellert, O. G.; Novotortsev, V. M.; Yanovsky, A. I.; Shklover, V. E.; Struchkov, Y. T. *J. Organomet. Chem.* **1989**, *365*, 325.

(123) Hao, L.; Vittal, J. J.; Xiao, J.; Puddephatt, R. J. *J. Am. Chem. Soc.* **1995**, *117*, 8035.

(124) Braunstein, P.; Knorr, M.; Strampfer, M.; Dusausoy, Y.; Bayeul, D.; DeCian, A.; Fischer, J.; Zanello, P. *J. Chem. Soc., Dalton Trans.* **1994**, 1533.

(125) Elliot, G. P.; Howard, J. A. K.; Nunn, C. M.; Stone, F. G. A. *J. Chem. Soc. Chem. Commun.* **1986**, 431.

(126) Braunstein, P.; Oswald, B.; Tiripicchio, A.; Tiripicchio-Camellini, M. *Angew. Chem. Int. Ed., Engl.* **1990**, *29*, 1140.

(127) Henly, T. J.; Wilson, S. R.; Shapley, J. R. *Inorg. Chem.* **1988**, *27*, 2551.

(128) Henly, T. J.; Shapley, J. R.; Rheingold, A. L.; Gelb, S. J. *Organometallics* **1988**, *7*, 441.

(129) Stromonova, T. A.; Busygina, I. N.; Katser, S. B.; Antsyshkina, A. S.; Porai-Koshits, M. A.; Moiseev, I. I. *J. Chem. Soc. Chem. Commun.* **1988**, 114.

(130) Elliot, G. P.; Howard, J. A. K.; Mise, T.; Nunn, C. M.; A., Stone, F. G. A. *Angew. Chem. Int., Ed. Engl.* **1986**, *25*, 190.

(131) Elliot, G. P.; Howard, J. A. K.; Mise, T.; Nunn, C. M.; Stone, F. G. A. *J. Chem. Soc., Dalton Trans.* **1987**, 2189.

(132) Kuznetsov, Bensimon, C. Facey, G. A. Grushin, V. V. Alper, H. *Organometallics* **1997**, *16, 97.*

(133) *Heterometallic Clusters in Catalysis*; Braunstein, P.; Rose, J., Ed.; Elsevier: Amsterdam, 1989; Vol. 3.

(134) Johnson, B. F. G.; Gallup, M.; Roberts, Y. V. *J. Mol. Catal.* **1994**, *86*, 51.

(135) Riaz, U.; Curnow, O. J.; Curtis, M. D. *J. Am. Chem. Soc.* **1994**, *116*, 4357.

(136) Curtis, M. D. *J. Cluster Sci.* **1996**, *7*, 247.

(137) Curtis, M. D.; Druker, S. H. *J. Am. Chem. Soc.* **1997**, *119*, 1027.

(138) Hao, L.; Xiao, J.; Vittal, J. J.; Puddephatt, R. J. *J. Chem. Soc., Chem. Commun.* **1994**, 2183.

(139) Hao, L.; Xiao, J.; Vittal, J. J.; Puddephatt, R. J. *Organometallics* **1997**, *16*, 2165.

(140) Süss-Fink, G.; Meister, G. *Adv. Organomet. Chem.* **1993**, *35*, 41.

(141) Beurich, H.; Vahrenkamp, H. *Chem. Ber.* **1982**, *115*, 2385.

(142) Richmond, M. G.; Absi-Halbi, M.; Pittman Jr., C. U. *J. Mol. Catal.* **1984**, *22*, 367.

(143) Pittman, C. U.; Richmond, M. G.; Absi-Halabi, M.; Beurich, H.; Richter, F.; Vahrenkamp, H. *Angew. Chem. Int. Ed. Engl.* **1982**, *21*, 786.

(144) Mahe, C.; Patin, H.; Le Marouille, J.-Y.; Benoit, A. *Organometallics* **1983**, *2*, 1051.

(145) Curtis, M. D.; Williams, P. D.; Butler, W. M. *Inorg. Chem.* **1988**, *27*, 2853.

(146) Li, P.; Curtis, D. *Inorg. Chem.* **1990**, *29*, 1242.

(147) Brunner, H.; Wachter, J. *J. Organomet. Chem.* **1982**, *240*, C41.

(148) Bender, R.; Braunstein, P.; Dusausoy, Y.; Protas, J. *Angew. Chem. Int. Ed. Engl.* **1978**, *17*, 596.

(149) Pittman, C. U.; Honnick, W.; Absi-Halabi, M.; Richmond, M. G.; Bender, R.; Braunstein, P. *J. Mol. Catal.* **1985**, *32*, 177.

(150) Bender, R.; Braunstein, P.; Jud, J.-M.; Dusausoy, Y. *Inorg. Chem.* **1983**, 3394.

(151) Moiseev, I. I.; Stromnova, T. A.; Vargaftik, M. N. *J. Mol. Catal.* **1994**, *86*, 71.

(152) Barbier, J.-P.; Braunstein, P. *J. Chem. Res. (S)* **1978**, 412.

(153) Fusi, A.; Ugo, R.; Psaro, R.; Braunstein, P.; Dehand, J. *J. Mol. Catal.* **1982**, *16*, 217.

(154) Braunstein, P.; Dehand, J. *J. Organomet. Chem.* **1970**, *24*, 497.

(155) Braunstein, P.; Dehand, J. *J. Chem. Soc., Chem. Commun.* **1972**, 164.

(156) Bender, R.; Braunstein, P.; Dusausoy, Y.; Protas, J. *J. Organomet. Chem.* **1979**, *172*, C51.

(157) Bender, R.; Braunstein, P.; Jud, J.-M.; Dusausoy, Y. *Inorg. Chem.* **1984**, *23*, 4489.

(158) Richter, F.; Vahrenkamp, H. *Angew. Chem. Int. Ed. Engl.* **1978**, *17*, 864.

(159) Mani, D.; Vahrenkamp, H. *J. Mol. Catal.* **1985**, *29*, 305.

(160) Müller, M.; Vahrenkamp, H. *Chem. Ber.* **1983**, *116*, 2748.

(161) Sinfelt, J. H. *Prog. Solid-State Chem.* **1975**, *10*, 55.

(162) Boudart, M. *J. Mol. Catal.* **1965**, *30*, 27.

(163) Biswas, J.; Bickle, G. M.; Gray, P. G.; Do, D. D.; Barbier, J. *Catal. Rev. - Sci. Eng.* **1988**, *30*, 161.

(164) Sinfelt, J. H. *Sci. Am.* **1985**, *253*, 96.

(165) Bailey, D. C.; Langer, S. H. *Chem. Rev.* **1981**, *81*, 109.

(166) Curtis, M. D.; Williams, P. D. *Inorg. Chem.* **1983**, *22*, 2661.

(167) Curtis, M. D.; Penner-Hahn, J. E.; Schwank, J.; Baralt, O.; McCabe, D. J.; Thompson, L.; Waldo, G. *Polyhedron* **1988**, *7*, 2411.

(168) Walthur, B.; Scheer, M.; Böttcher, H.-C.; Trunschke, A.; Ewald, H.; Gutschick, D.; Miessner, H.; Skupin, M.; Vorbeck, G. *Inorg. Chim. Acta* **1989**, *156*, 285.

(169) Trunschke, A.; Ewald, H.; Gutschick, D.; Miessner, H.; Skupin, M.; Walthur, B.; Böttcher, H.-C. *J. Molec. Catal.* **1989**, *56*, 95.

(170) Churchill, M. R.; Li, Y.-J.; Shapley, J. R.; Foose, D. S.; Uchiyama, W. S. *J. Organomet. Chem.* **1986**, *312*, 121.

(171) Shapley, J. R.; Uchiyama, W. S.; Scott, R. A. *J. Phys. Chem.* **1990**, *94*, 1190.

(172) Lucas, N. T.; Humphrey, M. G.; Hockless, D. C. R. *J. Organomet. Chem.* **1997**, *535*, 175.

(173) Shapley, J. R.; Hardwick, S. J.; Foose, D. S.; Stucky, G. D. *J. Am. Chem. Soc.* **1981**, *103*, 7383.

(174) Braunstein, P.; Bender, R.; Kervennal, J. *Organometallics* **1982**, *1*, 1236.

(175) Kawi, S.; Alexeev, O.; Shelef, M.; Gates, B. C. *J. Phys. Chem.* **1995**, *99*, 6296.

(176) Alexeev, O.; Shelef, M.; Gates, B. C. *J. Catal.* **1996**, *164*, 1.

(177) Urbanic, M. A.; Wilson, S. R.; Shapley, J. R. *Inorg. Chem.* **1984**, *23*, 2954.

(178) Fung, A. S.; McDevitt, M. R.; Tooley, P. A.; Kelley, M. J.; Koningsberger, D. C.; Gates, B. C. *J. Mol. Catal.* **1993**, *140*, 190.

(179) Fung, A. S.; Kelley, M. J.; Koningsberger, D. C.; Gates, B. C. *J. Am. Chem. Soc.* **1997**, *119*, 5877.

(180) Farrugia, L. J. *J. Chem. Soc., Dalton Trans.* **1997**, 1783.

(181) Roulet, R. *Chimia* **1996**, *50*, 629.

(182) Johnson, B. F. G.; Roberts, Y. V.; Parisini, E.; Benfield, R. E. *J. Organomet. Chem.* **1994**, *478*, 21.

(183) Orrell, K.; Sik, V. *Ann. Rep. NMR Spectroscopy* **1993**, *27*, 103.

(184) Orrell, K.; Sik, V. *Ann. Rep. NMR Spectroscopy* **1987**, *19*, 79.

(185) Mann, B. E. *Ann. Rep. NMR Spectroscopy* **1982**, *12*, 263.

(186) Band, E.; Muetterties, E. L. *Chem. Rev.* **1978**, *78*, 639.

(187) Johnson, B. F. G.; Benfield, R. E. *J. Chem. Soc., Dalton Trans.* **1978**, 1554.

(188) Casey, C. P.; Jordan, R. F.; Rheingold, A. L. *Organometallics* **1984**, *3*, 504.

(189) Beringhelli, T.; D'Alfonso, G.; Minoja, A. P. *Organometallics* **1994**, *13*, 663.

(190) Friedrich, S.; Gade, L. H.; Scowan, I. J.; McPartlin, M. *Angew. Chem., IInt. Ed. Engl.* **1996**, *35*, 1338.

(191) Barr, R. D.; Green, M.; Howard, J. A. K.; Marder, T. B.; Stone, F. G. A. *J. Chem. Soc., Chem. Commun.* **1983**, 759.

(192) Barr, R. D.; Green, M.; Marsden, K.; Stone, F. G. A.; Woodward, P. *J. Chem. Soc., Dalton Trans.* **1983**, 507.

(193) Delgado, E.; Hein, J.; Jeffrey, J. C.; Ratermann, A. L.; Stone, F. G. A.; Farrugia, L. J. *J. Chem. Soc., Dalton Trans.* **1987**, 1191.

(194) Pfeffer, M.; Fischer, J.; Mitschler, A. *Organometallics* **1984**, *3*, 1531.

(195) Scott, I. D.; Smith, D. O.; Went, M. J. *J. Chem. Soc., Dalton Trans.* **1989**, 1375.

(196) Beringhelli, T.; Ceriotti, A.; D'Alfonso, G.; Della Pergola, R. *Organometallics* **1990**, *9*, 1053.

(197) Beringhelli, T.; D'Alfonso, G.; Minoja, A. P. *Organometallics* **1991**, *10*, 394.

(198) Antognazza, P.; Beringhelli, T.; D'Alfonso, G.; Minoja, A..; Ciani, G..; Moret, M.; Sironi, A. *Organometallics* **1992**, *11*, 1777.

(199) Mlekuz, M.; Bougeard, P.; Sayer, B. G.; Peng, S.; McGlinchy, M. J.; Marinetti, A.; Saillard, J.-Y.; Naceur, J. B.; Mentzen, B.; Jaouen, G. *Organometallics* **1985**, *4*, 1123.

(200) Chetcuti, M. J.; Gordon, J. C.; Fanwick, P. E. *Inorg. Chem.* **1990**, *29*, 3781.

(201) Bergamo, M.; Beringhelli, T.; D'Alfonso, G.; Cian, G.; Moret, M.; Sironi, A. *Organometallics* **1996**, *15*, 1637.

(202) Yeh, W.-Y.; Shapley, J. R. *Organometallics* **1985**, *4*, 767.

(203) Eady, C. R.; Jackson, W. G.; Johnson, B. F. G.; Lewis, J.; Matheson, T. W. *J. Chem. Soc., Chem. Commun.* **1975**,

(204) Zanello, P. *Structure and Bonding* **1992**, *79*, 101.

(205) Lindsay, P. N.; Peake, B. M.; Robinson, B. H.; Simpson, J.; Honrath, U.; Vahrenkamp, H.; Bond, A. M. *Organometallics* **1984**, *3*, 413.

(206) Honrath, U.; Vahrenkamp, H. *Z. Naturforsch.* **1984**, *39b*, 545.

(207) Pasynskii, A. A.; Eremenko, I. L.; Katugin, A. S.; Gasanov, G. S.; Turchanova, E. A.; Ellert, O. G.; Struchkov, Y. T.; Shklover, V. E.; Berberova, N. T.; Sogomonova, A. G.; Okhlobystin, O. Y. *J. Organomet. Chem.* **1988**, *344*, 195.

(208) Kyba, E. P.; Kerby, M. C.; Kashyap, R. P.; Mountzouris, J. A.; Davis, R. E. *J. Am. Chem. Soc.* **1990**, *112*, 905.

(209) Mansour, M. A.; Curtis, M. D.; Kampf, J. W. *Organometallics* **1997**, *16*, 275.

(210) Jund, R.; Lemoine, P.; Gross, M.; Bender, R.; Braunstein, P. *J. Chem. Soc., Chem. Commun.* **1983**, 86.

(211) Jund, R.; Lemoine, P.; Gross, M.; Bender, R.; Braunstein, P. *J. Chem. Soc., Dalton Trans.* **1985**, 711.

(212) Pasynskii, A. A.; Eremenko, I. L.; Orazsakhatov, B.; Rakitin, Y. V.; Novotortsev, V. M.; Ellert, O. G.; Kalinnikov, V. T.; Aleksandrov, G. G.; Struchkov, Y. T. *J. Organomet. Chem.* **1981**, *214*, 351.

(213) Pasynskii, A. A.; Eremenko, I. L.; Orazsakhatov, B.; Gasanov, G. S.; Novotortsev, V. M.; Ellert, O. G.; Seifulina, Z. M.; Shklover, V. E.; Struchkov, Y. T. *J. Organomet. Chem.* **1984**, *270*, 53.

(214) Pasynskii, A. A.; Eremenko, I. L.; Zalmanovitch, V. R.; Kaverin, V. V.; Orazsakhatov, B.; Nefedov, S. E.; Ellert, O. G.; Novotortsev, V. M.; Yanovsky, A. I.; Struchkov, Y. T. *J. Organomet. Chem.* **1991**, *414*, 55.

(215) Eremenko, I. L.; Pasynskii, A. A.; Orazsakhatov, B.; Shestakov, A. F.; Gasanov, G. S.; Katugin, A. S.; Struchkov, Y. T.; Shklover, V. E. *J. Organomet. Chem.* **1988**, *338*, 369.

(216) Aldridge, S.; Hashimoto, H.; Kawamura, K.; Shang, M.; Fehlner, T. P. *Inorg. Chem.* **1998**, *37*, 928.

(217) D'Agostino, M. F.; Frampton, C. S.; McGlinchey, M. J. *J. Organomet. Chem.* **1990**, *394*, 145.

(218) Winter, G.; Schultz, B.; Trunschke, A.; Miessner, H.; Böttcher, H.-C.; Walther, B. *Inorg. Chim. Acta* **1991**, *184*, 27.

(219) Li, P.; Curtis, M. D. *J. Am. Chem. Soc.* **1989**, *111*, 8279.

(220) Harris, S. *Polyhedron* **1989**, *8*, 2843.

(221) Schacht, H. T.; Vahrenkamp, H. *J. Organomet. Chem.* **1990**, *381*, 261.

(222) Song, L.-C.; Shen, J.-Y.; Hu, Q-M.; Qin, X.-D. *Polyhedron*, **1995**, *14*, 2079.

(223) Albiez, J.; Bantel, H.; Vahrenkamp, H. *Chem. Ber.* **1990**, *123*, 1805.

(224) Kaganovich, V. S.; Slovokhotov, Y. L.; Mironov, A. V.; Struchkov, Y. T.; Rybinskaya, M. I. *J. Organomet. Chem.* **1989**, *373*, 339.

Chapter 2

Substitution Reactions of Tungsten - Iridium Clusters

Chapter 2

Substitution Reactions of Tungsten - Iridium Clusters

Contents

2.1. Phosphine substitution of tetrairidium clusters and related derivatives 102

2.1.1. Coordination Geometries for Mono-substituted Derivatives of $[Ir_4(CO)_{12}]$ (**1**).....102

2.1.2. Ligand Substitution at $[Ir_4(CO)_{12}]$ (**1**).....103

2.1.3. Summary.....127

2.2. Synthesis and characterization of phosphine, phosphite and isocyanide derivatives of $[CpWIr_3(CO)_{11}]$ (**2**) and $[Cp_2W_2Ir_2(CO)_{10}]$ (**3**).....128

2.2.1. Reaction of $[CpWIr_3(CO)_{11}]$ (**2**) with PPh_3 or PMe_3.....129

2.2.2. Reaction of $[CpWIr_3(CO)_{11}]$ (**2**) with $PMePh_2$ or PMe_2Ph.....136

2.2.3. Reaction of $[CpWIr_3(CO)_{11}]$ (**2**) with $P(OPh)_3$ or $P(OMe)_3$.....138

2.2.4. Reaction of $[CpWIr_3(CO)_{11}]$ (**2**) with 1,2-bis(diphenylphosphino)benzene...144

2.2.5. Attempted reaction of $[CpWIr_3(CO)_{11}]$ (**2**) with $[Fe(\eta^5\text{-}C_5H_5)(\eta^5\text{-}P_3C_2Bu^t_2)]$.....144

2.2.6. Reaction of $[CpWIr_3(CO)_{11}]$ (**2**) with XyNC or Bu^tNC.....145

2.2.7. Reaction of $[Cp_2W_2Ir_2(CO)_{10}]$ (**3**) with PPh_3 or PMe_3.....148

2.2.8. Reaction of $[Cp_2W_2Ir_2(CO)_{10}]$ (**3**) with $P(OMe)_3$.....152

2.2.9. Reaction of $[Cp_2W_2Ir_2(CO)_{10}]$ (**3**) with dppm or dppe.....155

2.3. Conclusions.....158

2.4. Experimental.....159

2.4.1. General Conditions, Instruments, Reagents and Chromatography.....159

2.4.2. Crystal Preparation.....160

2.4.3. Reaction of $[CpWIr_3(CO)_{11}]$ (**2**) with one equivalent of PPh_3.....161

2.4.4. Reaction of $[CpWIr_3(CO)_{11}]$ (**2**) with two equivalents of PPh_3.....161
2.4.5. Reaction of $[CpWIr_3(CO)_{11}]$ (**2**) with three equivalents of PPh_3.....161
2.4.6. Reaction of $[CpWIr_3(CO)_{11}]$ (**2**) with one equivalent of PMe_3.....162
2.4.7 Reaction of $[CpWIr_3(CO)_{11}]$ (**2**) with two equivalents of PMe_3.....162
2.4.8. Reaction of $[CpWIr_3(CO)_{11}]$ (**2**) with three equivalents of PMe_3.....162
2.4.9. Reaction of $[CpWIr_3(CO)_{11}]$ (**2**) with one equivalent of $PMePh_2$.....163
2.4.10. Reaction of $[CpWIr_3(CO)_{11}]$ (**2**) with two equivalents of $PMePh_2$.....163
2.4.11. Reaction of $[CpWIr_3(CO)_{11}]$ (**2**) with three equivalents of $PMePh_2$.....163
2.4.12. Reaction of $[CpWIr_3(CO)_{11}]$ (**2**) with one equivalent of PMe_2Ph.....164
2.4.13. Reaction of $[CpWIr_3(CO)_{11}]$ (**2**) with two equivalents of PMe_2Ph.....164
2.4.14. Reaction of $[CpWIr_3(CO)_{11}]$ (**2**) with three equivalents of PMe_2Ph.....165
2.4.15. Reaction of $[CpWIr_3(CO)_{11}]$ (**2**) with one equivalent of $P(OPh)_3$.....165
2.4.16. Reaction of $[CpWIr_3(CO)_{11}]$ (**2**) with two equivalents of $P(OPh)_3$.....165
2.4.17. Reaction of $[CpWIr_3(CO)_{11}]$ (**2**) with three equivalents of $P(OPh)_3$.....166
2.4.18. Reaction of $[CpWIr_3(CO)_{11}]$ (**2**) with one equivalent of $P(OMe)_3$.....166
2.4.19. Reaction of $[CpWIr_3(CO)_{11}]$ (**2**) with two equivalents of $P(OMe)_3$.....166
2.4.20. Reaction of $[CpWIr_3(CO)_{11}]$ (**2**) with three equivalents of $P(OMe)_3$.....167
2.4.21. Reaction of $[CpWIr_3(CO)_{11}]$ (**2**) with pddp.....167
2.4.22. Attempted reaction of $[CpWIr_3(CO)_{11}]$ (**2**) with
$[Fe(\eta^5\text{-}C_5H_5)(\eta^5\text{-}P_3C_2Bu^t_2)]$.....167
2.4.23. Reaction of $[CpWIr_3(CO)_{11}]$ (**2**) with one equivalent of XyNC.....168
2.4.24. Reaction of $[CpWIr_3(CO)_{11}]$ (**2**) with two equivalents of XyNC.....168
2.4.25. Reaction of $[CpWIr_3(CO)_{11}]$ (**2**) with three equivalents of XyNC.....168
2.4.26. Reaction of $[CpWIr_3(CO)_{11}]$ (**2**) with one equivalent of Bu^tNC.....169
2.4.27. Reaction of $[CpWIr_3(CO)_{11}]$ (**2**) with two equivalents of Bu^tNC.....169
2.4.28. Reaction of $[CpWIr_3(CO)_{11}]$ (**2**) with three equivalents of Bu^tNC.....169
2.4.29. Reaction of $[Cp_2W_2Ir_2(CO)_{10}]$ (**3**) with one equivalent of PPh_3.....170
2.4.30. Reaction of $[Cp_2W_2Ir_2(CO)_{10}]$ (**3**) with two equivalents of PPh_3.....170
2.4.31. Reaction of $[Cp_2W_2Ir_2(CO)_{10}]$ (**3**) with one equivalent of PMe_3.....171
2.4.32. Reaction of $[Cp_2W_2Ir_2(CO)_{10}]$ (**3**) with two equivalents of PMe_3.....171
2.4.33. Reaction of $[Cp_2W_2Ir_2(CO)_{10}]$ (**3**) with one equivalent of $P(OMe)_3$.....171
2.4.34. Reaction of $[Cp_2W_2Ir_2(CO)_{10}]$ (**3**) with two equivalents of $P(OMe)_3$.....172
2.4.35. Reaction of $[Cp_2W_2Ir_2(CO)_{10}]$ (**3**) with dppm.....172
2.4.36. Reaction of $[Cp_2W_2Ir_2(CO)_{10}]$ (**3**) with dppe.....172

2.5. References 174

List of Figures

Figure 2.1.1. Solid-state structures of $[M_4(CO)_{12}]$ (M = Co, Rh, Ir).....102
Figure 2.1.2. Sites of substitution for derivatives of $[Ir_4(CO)_{12}]$ (**1**).....103
Figures 2.1.3.-2.1.20. Coordination geometries of derivatives of $[Ir_4(CO)_{12}]$ (**1**)....119-127
Figure 2.2.1. Coordination geometries of $[Ir_4(CO)_{12}]$ (**1**), $[CpWIr_3(CO)_{11}]$ (**2**) and $[Cp_2W_2Ir_2(CO)_{10}]$ (**3**).....128
Figure 2.2.2. Molecular structure and atomic labelling scheme for $[CpWIr_3(\mu\text{-}CO)_3(CO)_7(PPh_3)]$ (**4**).....130
Figure 2.2.3. Molecular structure and atomic labelling scheme for $[CpWIr_3(\mu\text{-}CO)_3(CO)_6(PPh_3)_2]$ (**5**).....131
Figure 2.2.4. Molecular structure and atomic labelling scheme for $[CpWIr_3(\mu\text{-}CO)_3(CO)_7(PMe_3)]$ (**7**).....134
Figure 2.2.5. Molecular structure and atomic labelling scheme for $[CpWIr_3(\mu\text{-}CO)_3(CO)_7(PMe_2Ph)]$ (**13**).....137
Figure 2.2.6. Molecular structure and atomic labelling scheme for $[CpWIr_3(\mu\text{-}CO)_3(CO)_6\{P(OPh)_3\}_2]$ (**17**).....139
Figure 2.2.7. Molecular structure and atomic labelling scheme for $[CpWIr_3(\mu\text{-}CO)_3(CO)_7\{P(OMe)_3\}]$ (**19**).....141
Figure 2.2.8. Molecular structure and atomic labelling scheme for $[CpWIr_3(CO)_9(CNXy)_2]$ (**24**).....146
Figure 2.2.9. $[Fe_3(\mu\text{-}CO)_2(CNBu^t)_2(CO)_8]$.....148
Figure 2.2.10. Molecular structure and atomic labelling scheme for $[Cp_2W_2Ir_2(\mu\text{-}CO)_3(CO)_6(PPh_3)]$ (**29**).....150
Figure 2.2.11. Molecular structure and atomic labelling scheme for $[Cp_2W_2Ir_2(\mu\text{-}CO)_3(CO)_5\{P(OMe)_3\}]$ (**34**).....153
Figure 2.2.12. Molecular structure and atomic labelling scheme for $[Cp_2W_2Ir_2(\mu\text{-}CO)_3(\mu\text{-}dppm)(CO)_5]$ (**35**).....156

List of Tables

Table 2.1.1. Coordination Geometries of Ligand-substituted Derivatives of $[Ir_4(CO)_{12}]$ (**1**).....104

Table 2.2.1. Selected Bond Lengths (Å) for $[CpWIr_3(\mu\text{-}CO)_3(CO)_7(PPh_3)]$ (**4**) and $[CpWIr_3(\mu\text{-}CO)_3(CO)_6(PPh_3)_2]$ (**5**).....132

Table 2.2.2. Selected Bond Angles (°) for $[CpWIr_3(\mu\text{-}CO)_3(CO)_7(PPh_3)]$ (**4**) and $[CpWIr_3(\mu\text{-}CO)_3(CO)_6(PPh_3)_2]$ (**5**).....133

Table 2.2.3. Selected Bond Lengths (Å) for $[CpWIr_3(\mu\text{-}CO)_3(CO)_7(PMe_3)]$ (**7**) and $[CpWIr_3(\mu\text{-}CO)_3(CO)_7(PMe_2Ph)]$ (**13**).....135

Table 2.2.4. Selected Bond Angles (°) $[CpWIr_3(\mu\text{-}CO)_3(CO)_7(PMe_3)]$ (**7**) and $[CpWIr_3(\mu\text{-}CO)_3(CO)_7(PMe_2Ph)]$ (**13**).....136

Table 2.2.5. Selected Bond Lengths (Å) for $[CpWIr_3(\mu\text{-}CO)_3(CO)_6\{P(OPh)_3\}_2]$ (**17**).....140

Table 2.2.6. Selected Bond Angles (°) for $[CpWIr_3(\mu\text{-}CO)_3(CO)_6\{P(OPh)_3\}_2]$ (**17**).....140

Table 2.2.7. Selected Bond Lengths (Å) for $[CpWIr_3(\mu\text{-}CO)_3(CO)_7\{P(OMe)_3\}]$ (**19**).....143

Table 2.2.8. Selected Bond Angles (°) for $[CpWIr_3(\mu\text{-}CO)_3(CO)_7\{P(OMe)_3\}]$ (**19**).....144

Table 2.2.9. Selected Bond Lengths (Å) for $[CpWIr_3(CO)_7(CNXy)_2]$ (**24**) 147

Table 2.2.10. Selected Bond Angles (°) for $[CpWIr_3(CO)_7(CNXy)_2]$ (**24**) 147

Table 2.2.11. Selected Bond Lengths (Å) for $[Cp_2W_2Ir_2(\mu\text{-}CO)_3(CO)_6(PPh_3)]$ (**29**).....151

Table 2.2.12. Selected Bond Angles (°) for $[Cp_2W_2Ir_2(\mu\text{-}CO)_3(CO)_6(PPh_3)]$ (**29**).....151

Table 2.2.13. Selected Bond Lengths (Å) for $[Cp_2W_2Ir_2(\mu\text{-}CO)_3(CO)_6\{P(OMe)_3\}_2]$ (**34**).....154

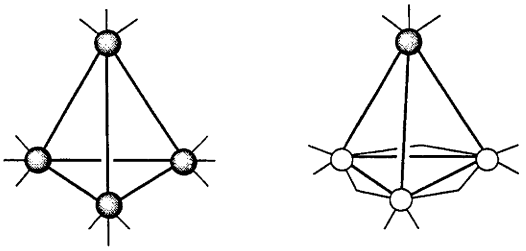
Table 2.2.14. Selected Bond Angles (°) for $[Cp_2W_2Ir_2(\mu\text{-}CO)_3(CO)_6\{P(OMe)_3\}_2]$ (**34**).....154

Chapter 2

Substitution Reactions of Tungsten - Iridium Clusters

2.1. Phosphine substitution of tetrairidium clusters and related derivatives

The chemistry of $[Ir_4(CO)_{12}]$ (**1**) has been studied extensively, and has been reviewed recently in some detail;[1] in the review the substitution chemistry of **1** is summarized, but the coordination geometries of the products are not discussed in detail, although at each stage of substitution (mono-, bis-, etc.) several isomers are possible. The short summary below explores more specifically the site-selective substitution of **1** and its derivatives. The solid-state structure of **1**[2] differs from the analogous group 9 clusters $[Co_4(CO)_{12}]$ and $[Rh_4(CO)_{12}]$ in that it comprises a regular tetrahedron of iridium atoms with an all-terminal carbonyl ligand geometry (Figure 2.1.1.). Due to the relative inertness of **1**, the substituted tetranuclear carbonyl clusters were found to be excellent candidates for studying the stereochemical arrangement of ligands around the metal core and the fluxional processes in solution.



$[Ir_4(CO)_{12}]$ T_d $[Co_4(CO)_{12}]$, $[Rh_4(CO)_{12}]$ C_{3v}

Figure 2.1.1. Solid-state structures of $[M_4(CO)_{12}]$ (M = Co, Rh, Ir)

2.1.1. Coordination Geometries for Mono-substituted Derivatives of $[Ir_4(CO)_{12}]$ (1)

The site at which the ligand substitutes leads to different geometries of the resultant clusters. In a few cases, the ligand may coordinate in a manner such that the complex retains its all-terminal geometry [for which the all-carbonyl form has T_d symmetry, Figure

2.1.2. (i)]. The majority of clusters are derived from the C_{3v} structure with the basal plane containing three bridging carbonyls. In these circumstances, ligands may substitute in a radial site [Figure 2.1.2. (ii)], axial site [Figure 2.1.2. (iii)] or an apical site [Figure 2.1.2. (iv)], with respect to the plane of bridging carbonyls. Some ligands are also capable of occupying a bridging site [Figure 2.1.2. (v)]. When ligands capable of coordinating to more than one site are involved (bidentate, tridentate ligands) the coordinating ligands may bridge a M-M bond at two of the sites mentioned above for monodentate two-electron donor ligands, or chelate two sites on the one iridium atom [Figure 2.1.2. (vi)].

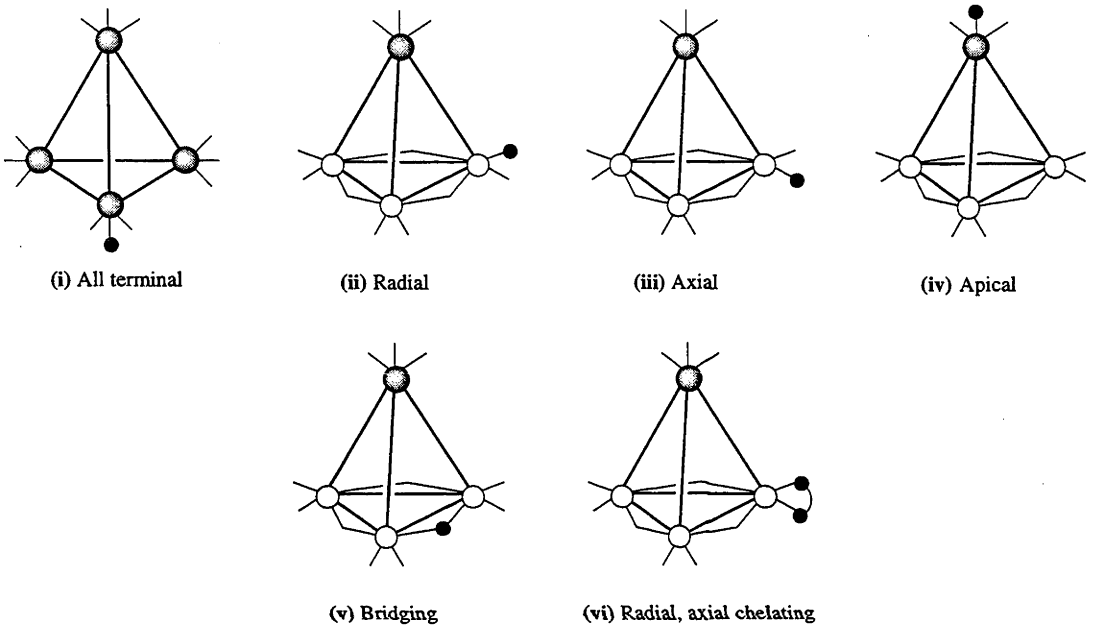
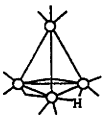
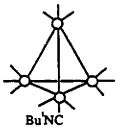
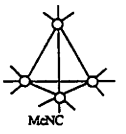
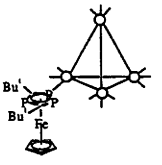
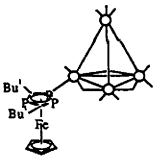
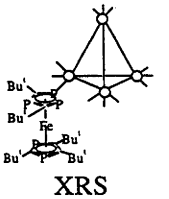
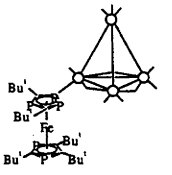
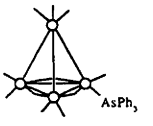


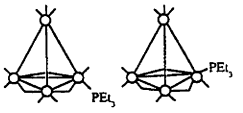
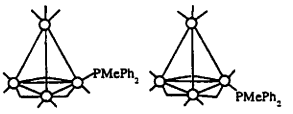
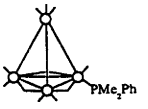
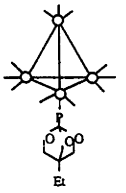
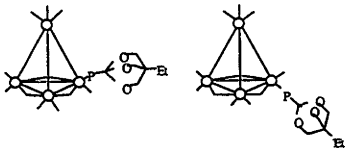
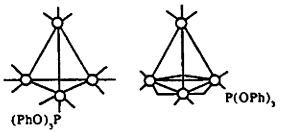
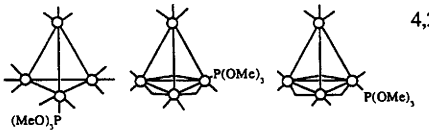
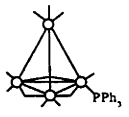
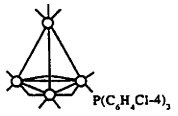
Figure 2.1.2. Sites of substitution for derivatives of $[Ir_4(CO)_{12}]$ (**1**)

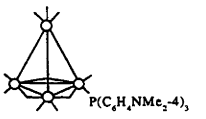
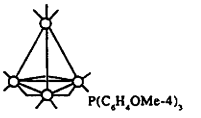
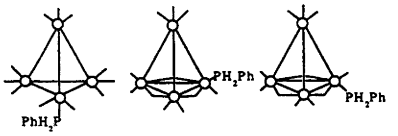
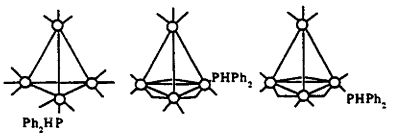
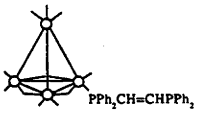
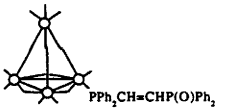
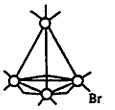
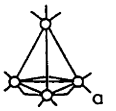
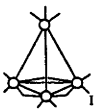
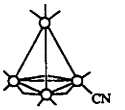
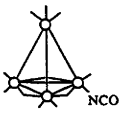
2.1.2. Ligand Substitution at $[Ir_4(CO)_{12}]$ (1)

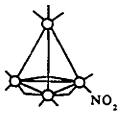
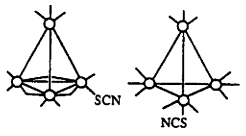
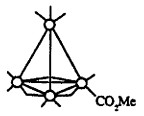
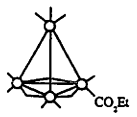
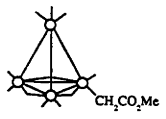
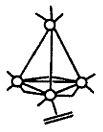
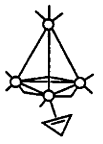
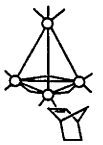
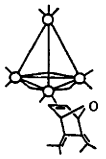
The ligand-substituted derivatives of **1** are listed in Table 2.1.1. Substituted tetrairidium clusters with all-terminal geometries may result from derivatives with ligands that are good π-acceptors. A number of monosubstituted derivatives of **1** have been structurally characterized. The complexes $[Ir_4(CO)_{11}(CNBu^t)]$,[3] $[Ir_4(CO)_{11}\{P(OCH_2)_3CEt\}]$,[4] $[Ir_4(CO)_{11}(\overline{COCH_2CH_2O})]$,[5] $[Ir_4(CO)_{11}\{\eta^1\text{-}P\text{-}[Fe(\eta^5\text{-}C_5H_5)(\eta^5\text{-}P_2C_3Bu^t_3)]\}]$[6,7] and $[Ir_4(CO)_{11}(SCN)]^-$ [8] are all examples of clusters of the type $[Ir_4(CO)_{11}(L)]$ adopting a pseudo-T_d geometry in the solid state. A number of other $[Ir_4(CO)_{11}(L)]$ clusters (L = CNMe, $PHPh_2$, PH_2Ph)[9,10] are believed to have an all-terminal geometry on the basis of IR or NMR spectroscopic evidence. The complexes $[Ir_4(CO)_{11}(PHPh_2)]$ and $[Ir_4(CO)_{11}(PH_2Ph)]$ were proposed to exist as interconverting mixtures of all-terminal isomers and isomers with pseudo C_{3v} geometry. Clusters with the ligand distribution of the C_{3v} structure of $[M_4(\mu\text{-}CO)_3(CO)_9]$ (M = Co or Rh) were observed in the majority of

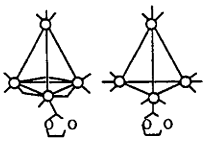
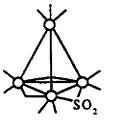
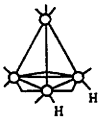
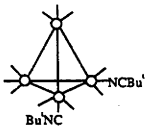
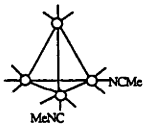
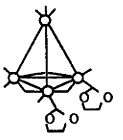
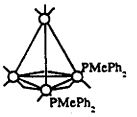
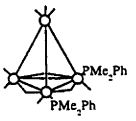
Table 2.1.1. Coordination Geometries of Ligand-substituted Derivatives of $[Ir_4(CO)_{12}]$ (**1**)

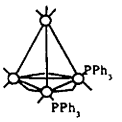
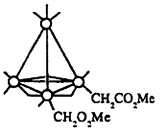
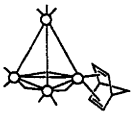
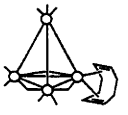
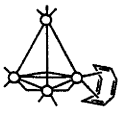
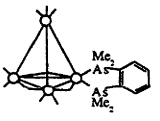
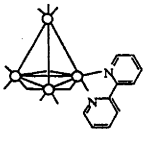
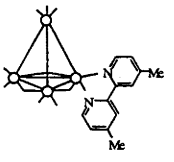
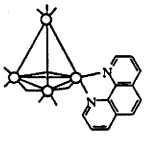
Complex	Geometries[a]	Reference
$[Ir_4(\mu\text{-}H)(\mu\text{-}CO)_2(CO)_9]^-$	 XRS	18,20-22
$[Ir_4(CO)_{11}(CNBu^t)]$	 XRS	3,9
$[Ir_4(CO)_{11}(CNMe)]$		9
$[Ir_4(CO)_{11}\{\eta^1\text{-}P\text{-}[Fe(\eta^5\text{-}C_5H_5)(\eta^5\text{-}P_2C_3Bu^t_3)]\}]$		6
$[Ir_4(\mu\text{-}CO)_3(CO)_8\{\eta^1\text{-}P\text{-}[Fe(\eta^5\text{-}C_5H_5)(\eta^5\text{-}P_2C_3Bu^t_3)]\}]$		6
$[Ir_4(CO)_{11}\{\eta^1\text{-}P\text{-}[Fe(\eta^5\text{-}P_3C_2Bu^t_2)(\eta^5\text{-}P_2C_3Bu^t_3)]\}]$	 XRS	6
$[Ir_4(\mu\text{-}CO)_3(CO)_8\{\eta^1\text{-}P\text{-}[Fe(\eta^5\text{-}P_3C_2Bu^t_2)(\eta^5\text{-}P_2C_3Bu^t_3)]\}]$		6
$[Ir_4(\mu\text{-}CO)_3(CO)_8(AsPh_3)]$		17

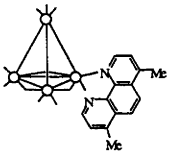
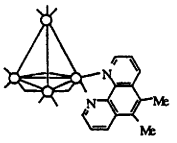
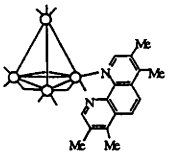
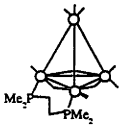
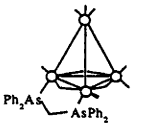
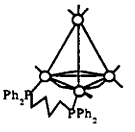
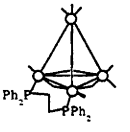
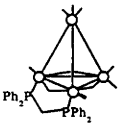
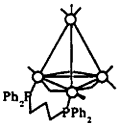
Complex	Geometries[a]	Reference
$[Ir_4(\mu\text{-}CO)_3(CO)_8(PEt_3)]$		23-25
$[Ir_4(\mu\text{-}CO)_3(CO)_8(PMePh_2)]$		17,26
$[Ir_4(\mu\text{-}CO)_3(CO)_8(PMe_2Ph)]$		23
$[Ir_4(\mu\text{-}CO)_3(CO)_8\{P(C_6H_4Me\text{-}4)_3\}]$	Geometry not assigned	23
$[Ir_4(CO)_{11}\{P(OCH_2)_3CEt\}]$	 XRS	4
$[Ir_4(\mu\text{-}CO)_3(CO)_8\{P(OCH_2)_3CEt\}]$		4
$[Ir_4(\mu\text{-}CO)_3(CO)_8\{P(OPh)_3\}]$ $[Ir_4(CO)_{11}\{P(OPh)_3\}]$		4,23
$[Ir_4(\mu\text{-}CO)_3(CO)_8\{P(OMe)_3\}]$ $[Ir_4(CO)_{11}\{P(OMe)_3\}]$		4,23
$[Ir_4(\mu\text{-}CO)_3(CO)_8(PPh_3)]$		17,23,27,28
$[Ir_4(\mu\text{-}CO)_3(CO)_8\{P(C_6H_4Cl\text{-}4)_3\}]$		28

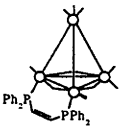
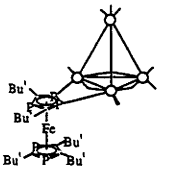
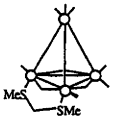
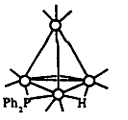
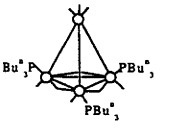
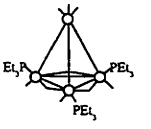
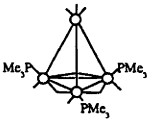
Complex	Geometries[a]	Reference
$[Ir_4(\mu\text{-}CO)_3(CO)_8\{P(C_6H_4NMe_2\text{-}4)_3\}]$		28
$[Ir_4(\mu\text{-}CO)_3(CO)_8\{P(C_6H_4OMe\text{-}4)_3\}]$		28
$[Ir_4(\mu\text{-}CO)_3(CO)_8(PH_2Ph)]$ $[Ir_4(CO)_{11}(PH_2Ph)]$		10
$[Ir_4(\mu\text{-}CO)_3(CO)_8(PHPh_2)]$ $[Ir_4(CO)_{11}(PHPh_2)]$		10
$[Ir_4(\mu\text{-}CO)_3(CO)_8(\textit{trans}\text{-}Ph_2PCH{=}CHPPh_2)]$		17
$[Ir_4(\mu\text{-}CO)_3(CO)_8(\textit{trans}\text{-}$ $Ph_2PCH{=}CHP(O)Ph_2)]$		17
$[Ir_4(\mu\text{-}CO)_3(CO)_8Br]^-$	 XRS	14,28-30
$[Ir_4(\mu\text{-}CO)_3(CO)_8Cl]^-$		14
$[Ir_4(\mu\text{-}CO)_3(CO)_8I]^-$		14,28
$[Ir_4(\mu\text{-}CO)_3(CO)_8(CN)]^-$		14
$[Ir_4(\mu\text{-}CO)_3(CO)_8(NCO)]^-$		28,31

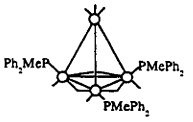
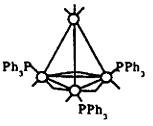
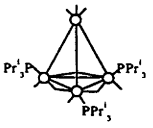
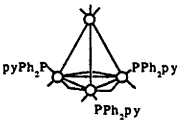
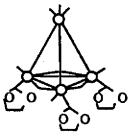
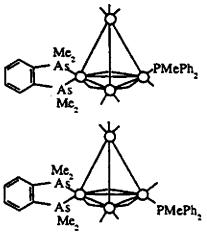
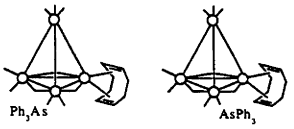
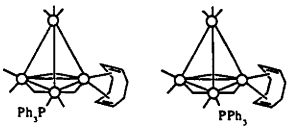
Complex	Geometries[a]	Reference
$[Ir_4(\mu\text{-}CO)_3(CO)_8(NO_2)]^-$		28
$[Ir_4(\mu\text{-}CO)_3(CO)_8(SCN)]^-$ $[Ir_4(CO)_{11}(SCN)]^-$	 XRS XRS	8,11,14,28
$[Ir_4(\mu\text{-}CO)_3(CO)_8(CO_2Me)]^-$	 XRS	16
$[Ir_4(\mu\text{-}CO)_3(CO)_8(CO_2Et)]^-$		16
$[Ir_4(\mu\text{-}CO)_3(CH_2CO_2Me)(CO)_8]^-$	 XRS	15
$[Ir_4(\mu\text{-}CO)_3(CO)_8(\eta^2\text{-}C_2H_4)]$		32,33
$[Ir_4(\mu\text{-}CO)_3(CO)_8(\eta^2\text{-}\overline{CH=CHCH_2})]$		33
$[Ir_4(\mu\text{-}CO)_3(CO)_8(\eta^2\text{-}C_7H_{10})]$		32,33
$[Ir_4(\mu\text{-}CO)_3(CO)_8(\eta^2\text{-}C_8H_8O)]$		33

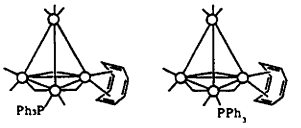
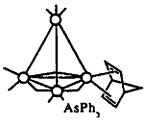
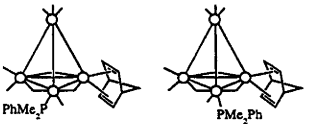
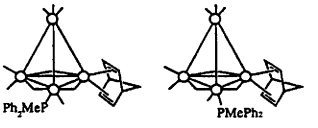
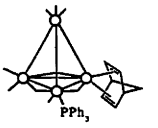
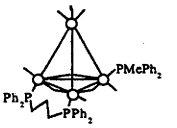
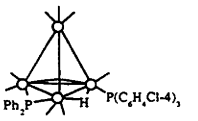
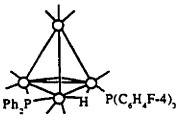
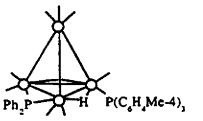
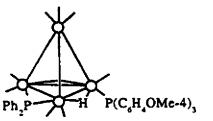
Complex	Geometries[a]	Reference
$[Ir_4(\mu\text{-}CO)_3(CO)_8(\overline{COCH_2CH_2O})]$ $[Ir_4(CO)_{11}(\overline{COCH_2CH_2O})]$	 XRS	5
$[Ir_4(\mu\text{-}CO)_2(\mu\text{-}SO_2)(CO)_9]$	 XRS	34
$[Ir_4(H)_2(\mu\text{-}CO)_3(CO)_7]^{2-}$	 XRS	35
$[Ir_4(CO)_{10}(CNBu^t)_2]$		9
$[Ir_4(CO)_{10}(CNMe)_2]$		9
$[Ir_4(\mu\text{-}CO)_3(CO)_7(\overline{COCH_2CH_2O})_2]$	 XRS	5
$[Ir_4(\mu\text{-}CO)_3(CO)_7(PEt_3)_2]$	Geometry not assigned	23
$[Ir_4(\mu\text{-}CO)_3(CO)_7(PMePh_2)_2]$		17,26,28
$[Ir_4(\mu\text{-}CO)_3(CO)_7(PMe_2Ph)_2]$		17,23
$[Ir_4(\mu\text{-}CO)_3(CO)_7\{P(C_6H_4Me\text{-}4)_3\}_2]$	Geometry not assigned	23
$[Ir_4(\mu\text{-}CO)_3(CO)_7\{P(OMe)_3\}_2]$	Geometry not assigned	23
$[Ir_4(\mu\text{-}CO)_3(CO)_7\{P(OPh)_3\}_2]$	Geometry not assigned	23

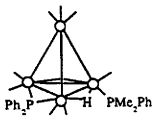
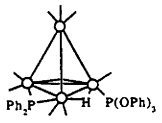
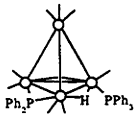
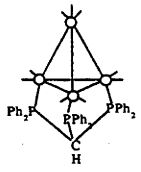
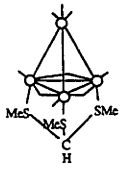
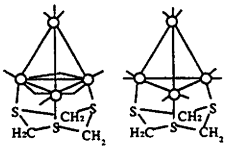
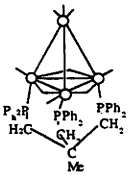
Complex	Geometries[a]	Reference
$[Ir_4(\mu\text{-}CO)_3(CO)_7(PPh_3)_2]$	 XRS	17,23,36-38
$[Ir_4(\mu\text{-}CO)_3(CH_2CO_2Me)_2(CO)_7]^{2-}$		15
$[Ir_4(\mu\text{-}CO)_3(CO)_7(\eta^4\text{-nbd})]$		32,33
$[Ir_4(\mu\text{-}CO)_3(CO)_7(\eta^4\text{-cod})]$		33,39
$[Ir_4(\mu\text{-}CO)_3(CO)_7(\eta^4\text{-cot})]$		33
$[Ir_4(\mu\text{-}CO)_3(CO)_7(\eta^2\text{-diars})]$	 XRS	39-41
$[Ir_4(\mu\text{-}CO)_3(CO)_7(2,2'\text{-bipy})]$		42
$[Ir_4(\mu\text{-}CO)_3(CO)_7(4,4';\text{-}Me_2\text{-bipy})]$	 XRS	42
$[Ir_4(\mu\text{-}CO)_3(CO)_7(\eta^2\text{-phen})]$	 XRS	42

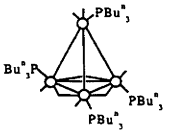
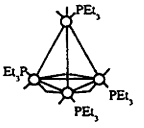
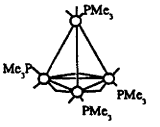
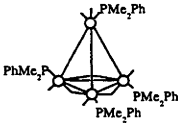
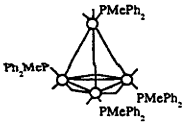
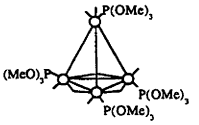
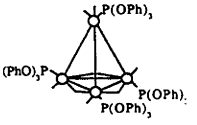
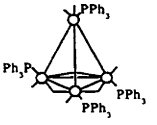
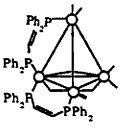
Complex	Geometries[a]	Reference
$[Ir_4(\mu\text{-}CO)_3(CO)_7(\eta^2\text{-}4,7\text{-}Me_2\text{-}phen)]$		42
$[Ir_4(\mu\text{-}CO)_3(CO)_7(\eta^2\text{-}5,6\text{-}Me_2\text{-}phen)]$		42
$[Ir_4(\mu\text{-}CO)_3(CO)_7(\eta^2\text{-}3,4,7,8\text{-}Me_4\text{-}phen)]$		42
$[Ir_4(\mu\text{-}CO)_3(\mu\text{-}dmpe)(CO)_7]$	 XRS	17
$[Ir_4(\mu\text{-}CO)_3(\mu\text{-}dpam)(CO)_7]$		28
$[Ir_4(\mu\text{-}CO)_3(\mu\text{-}dppb)(CO)_7]$	 XRS	17,43
$[Ir_4(\mu\text{-}CO)_3(\mu\text{-}dppe)(CO)_7]$		17
$[Ir_4(\mu\text{-}CO)_3(\mu\text{-}dppm)(CO)_7]$		17,28,44
$[Ir_4(\mu\text{-}CO)_3(\mu\text{-}dppp)(CO)_7]$		17,28

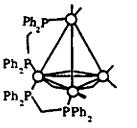
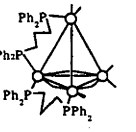
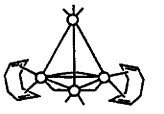
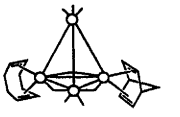
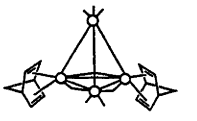
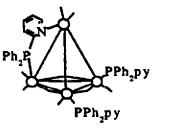
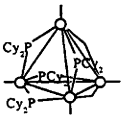
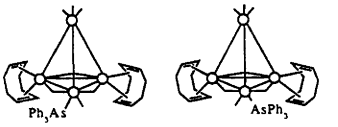
Complex	Geometries[a]	Reference
$[Ir_4(\mu\text{-}CO)_3(\mu\text{-dppee})(CO)_7]$	 XRS	17,45,46
$[Ir_4(\mu\text{-}CO)_3(CO)_7\{\eta^1\text{-}[Fe(\eta^5\text{-}C_5H_5)(\eta^5\text{-}P_2C_3Bu^t_3)]\}]$	Geometry not assigned	6
$[Ir_4(\mu\text{-}CO)_3(CO)_7\{\eta^1\text{-}[Fe(\eta^5\text{-}P_3C_2Bu^t_2)(\eta^5\text{-}P_2C_3Bu^t_3)]\}]$	Geometry not assigned	6
$[Ir_4(\mu\text{-}CO)_3(CO)_7\{\mu\text{-}\eta^2\text{-}[Fe(\eta^5\text{-}P_3C_2Bu^t_2)(\eta^5\text{-}P_2C_3Bu^t_3)]\}]$		6
$[Ir_4(\mu\text{-}CO)_3(\mu\text{-}MeSCH_2SMe)(CO)_7]$		28
$[HIr_4(\mu\text{-}CO)_3(\mu\text{-}PPh_2)(CO)_7]$	 XRS	47
$[Ir_4(CO)_9(CNBu^t)_3]$	Geometry not assigned T_d and C_{3v} isomers	9
$[Ir_4(CO)_9(CNMe)_3]$	Geometry not assigned T_d isomers	9
$[Ir_4(\mu\text{-}CO)_3(CO)_6(PBu^n_3)_3]$		37,48
$[Ir_4(\mu\text{-}CO)_3(CO)_6(PEt_3)_3]$		37,48
$[Ir_4(\mu\text{-}CO)_3(CO)_6(PMe_3)_3]$		48

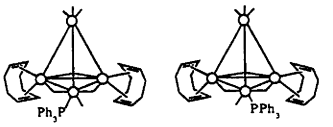
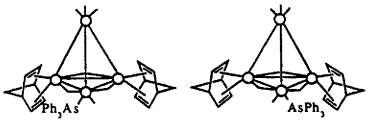
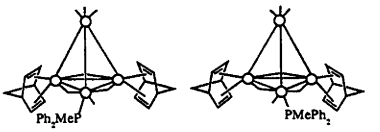
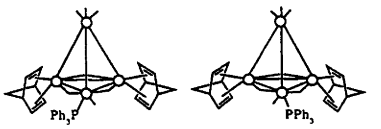
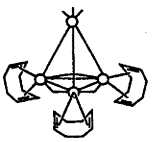
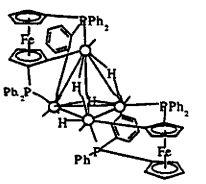
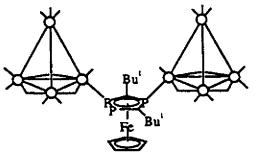
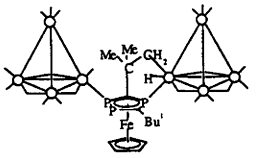
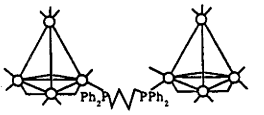
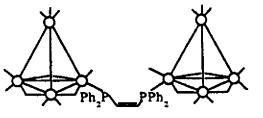
Complex	Geometries[a]	Reference
$[Ir_4(\mu\text{-}CO)_3(CO)_6(PMe_2Ph)_3]$	Geometry not assigned	17
$[Ir_4(\mu\text{-}CO)_3(CO)_6(PMePh_2)_3]$		26
$[Ir_4(\mu\text{-}CO)_3(CO)_6(PPh_3)_3]$	 XRS	17,23,36,37,4 8,49
$[Ir_4(\mu\text{-}CO)_3(CO)_6(PPr^i_3)_3]$		37,48
$[Ir_4(\mu\text{-}CO)_3(CO)_6(PPr^n_3)_3]$	Geometry not assigned	37
$[Ir_4(\mu\text{-}CO)_3(CO)_6\{P(C_6H_4Me\text{-}4)_3\}_3]$	Geometry not assigned	37,49
$[Ir_4(\mu\text{-}CO)_3(CO)_6(PPh_2py)_3]$	 XRS	50,51
$[Ir_4(\mu\text{-}CO)_3(CO)_6(\overline{COCH_2CH_2O})_3]$	 XRS	5
$[Ir_4(\mu\text{-}CO)_3(CO)_6(PMePh_2)(\eta^2\text{-diars})]$		52
$[Ir_4(\mu\text{-}CO)_3(AsPh_3)(CO)_6(\eta^4\text{-cod})]$		53
$[Ir_4(\mu\text{-}CO)_3(CO)_6(PPh_3)(\eta^4\text{-cod})]$		53

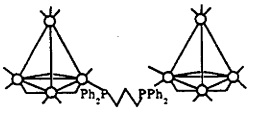
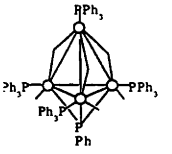
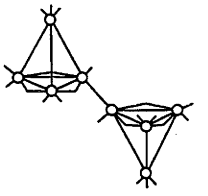
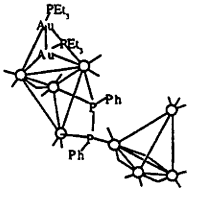
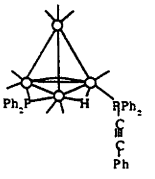
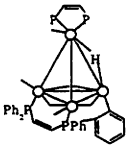
Complex	Geometries[a]	Reference
$[Ir_4(\mu\text{-}CO)_3(PPh_3)(CO)_6(\eta^4\text{-}cot)]$		53
$[Ir_4(\mu\text{-}CO)_3(AsPh_3)(CO)_6(\eta^4\text{-}nbd)]$		53
$[Ir_4(\mu\text{-}CO)_3(CO)_6(PMe_2Ph)(\eta^4\text{-}nbd)]$	 XRS	32,53
$[Ir_4(\mu\text{-}CO)_3(CO)_6(PMePh_2)(\eta^4\text{-}nbd)]$		32,52,53
$[Ir_4(\mu\text{-}CO)_3(CO)_6(PPh_3)(\eta^4\text{-}nbd)]$	 XRS	32,52,53
$[Ir_4(\mu\text{-}CO)_3(\mu\text{-}dppp)(CO)_6(PMePh_2)]$		52
$[Ir_4(\mu\text{-}H)(\mu\text{-}CO)(\mu\text{-}PPh_2)(CO)_8\{P(C_6H_4Cl\text{-}4)_3\}]$		47
$[Ir_4(\mu\text{-}H)(\mu\text{-}CO)(\mu\text{-}PPh_2)(CO)_8\{P(C_6H_4F\text{-}4)_3\}]$		47
$[Ir_4(\mu\text{-}H)(\mu\text{-}CO)(\mu\text{-}PPh_2)(CO)_8\{P(C_6H_4Me\text{-}4)_3\}]$		47
$[Ir_4(\mu\text{-}H)(\mu\text{-}CO)(\mu\text{-}PPh_2)(CO)_8\{P(C_6H_4OMe\text{-}4)_3\}]$		47

Complex	Geometries[a]	Reference
$[Ir_4(\mu\text{-}H)(\mu\text{-}CO)(\mu\text{-}PPh_2)(CO)_8(PMe_2Ph)]$		47
$[Ir_4(\mu\text{-}H)(\mu\text{-}CO)(\mu\text{-}PPh_2)(CO)_8\{P(OPh)_3\}]$		47
$[Ir_4(\mu\text{-}H)(\mu\text{-}CO)(\mu\text{-}PPh_2)(CO)_8(PPh_3)]$		47
$[Ir_4\{\mu_3\text{-}HC(PPh_2)_3\}(CO)_9]$	 XRS	54,55
$[Ir_4\{\mu_3\text{-}HC(SMe)_3\}(\mu\text{-}CO)_3(CO)_6]$		52
$[Ir_4\{\mu_3\text{-}3S\text{-}c\text{-}(SCH_2)_3\}(\mu\text{-}CO)_3(CO)_6]$ $[Ir_4\{\mu_3\text{-}3S\text{-}c\text{-}(SCH_2)_3\}(CO)_9]$	 XRS XRS	56,57
$[Ir_4(\mu_3\text{-triphos})(\mu\text{-}CO)_3(CO)_6]$		52
$[Ir_4(CO)_8(CNBu^t)_4]$ $[Ir_4(\mu\text{-}CO)_3(CO)_5(CNBu^t)_4]$	Geometry not assigned T_d and C_{3v} isomers	9
$[Ir_4(CO)_8(CNMe)_4]$	Geometry not assigned T_d isomers	9
$[Ir_4(\mu\text{-}CO)_3(AsMe_2Ph)_4(CO)_5]$	Geometry not assigned	58
$[Ir_4(\mu\text{-}CO)_3(AsMePh_2)_4(CO)_5]$	Geometry not assigned	58

Complex	Geometries[a]	Reference
$[Ir_4(\mu\text{-}CO)_3(CO)_5(PBu^n{}_3)_4]$		48
$[Ir_4(\mu\text{-}CO)_3(CO)_5(PEt_3)_4]$		48
$[Ir_4(\mu\text{-}CO)_3(CO)_5(PEt_2Ph)_4]$	Geometry not assigned	36,58
$[Ir_4(\mu\text{-}CO)_3(CO)_5(PMe_3)_4]$	 XRS	48,59
$[Ir_4(\mu\text{-}CO)_3(CO)_5(PMe_2Ph)_4]$	 XRS	58,60
$[Ir_4(\mu\text{-}CO)_3(CO)_5(PMePh_2)_4]$		23,26,58,59
$[Ir_4(\mu\text{-}CO)_3(CO)_5\{P(OMe)_3\}_4]$		48,59
$[Ir_4(\mu\text{-}CO)_3(CO)_5\{P(OPh)_3\}_4]$		48,58,59
$[Ir_4(\mu\text{-}CO)_3(CO)_5(PPh_3)_4]$		61
$[Ir_4(\mu\text{-}CO)_3(\mu\text{-}dppe)_2(CO)_5]$	Geometry not assigned	36
$[Ir_4(\mu\text{-}CO)_3(\mu\text{-}dppee)_2(CO)_5]$		45,46

Complex	Geometries[a]	Reference
$[Ir_4(\mu\text{-}CO)_3(\mu\text{-}dppm)_2(CO)_5]$	 XRS	52,58,62,63
$[Ir_4(\mu\text{-}CO)_3(\mu\text{-}dppp)_2(CO)_5]$		52
$[Ir_4(\mu\text{-}CO)_3(CO)_5(\eta^4\text{-}cod)_2]$		33,52,62
$[Ir_4(\mu\text{-}CO)_3(CO)_5(\eta^4\text{-}cod)(\eta^4\text{-}nbd)]$		52
$[Ir_4(\mu\text{-}CO)_3(CO)_5(\eta^4\text{-}nbd)_2]$		52
$[Ir_4(\mu\text{-}CO)_3(\mu\text{-}PPh_2py)(CO)_5(PPh_2py)_2]$	 XRS	51
$[HIr_4(\mu\text{-}CO)_3(\mu\text{-}PPh_2)(CO)_5\{P(C_6H_4Cl\text{-}4)_3\}_2]$	Geometry not assigned	47
$[HIr_4(\mu\text{-}CO)_3(\mu\text{-}PPh_2)(CO)_5\{P(C_6H_4Me\text{-}4)_3\}_2]$	Geometry not assigned	47
$[HIr_4(\mu\text{-}CO)_3(\mu\text{-}PPh_2)(CO)_5(PPh_3)_2]$	Geometry not assigned	47
$[Ir_4(\mu\text{-}CO)_2(\mu\text{-}PCy_2)_4(CO)_4]$	 XRS	64
$[Ir_4(\mu\text{-}CO)_3(AsPh_3)(CO)_4(\eta^4\text{-}cod)_2]$		53

Complex	Geometries[a]	Reference
$[Ir_4(\mu\text{-}CO)_3(CO)_4(PPh_3)(\eta^4\text{-}cod)_2]$		53
$[Ir_4(\mu\text{-}CO)_3(AsPh_3)(CO)_4(\eta^4\text{-}nbd)_2]$		53
$[Ir_4(\mu\text{-}CO)_3(CO)_4(PMePh_2)(\eta^4\text{-}nbd)_2]$		52
$[Ir_4(\mu\text{-}CO)_3(CO)_4(PPh_3)(\eta^4\text{-}nbd)_2]$		53
$[Ir_4(\mu\text{-}CO)_3(CO)_3(\eta^4\text{-}cod)_3]$		62
$[Ir_4(\mu\text{-}H)_4(CO)_4\{Fe(\eta^5\text{-}C_5H_3PPh_2(\eta^5\text{-}C_5H_4PPhC_6H_4)\}_2]$	 XRS	65
$[Ir_4(\mu\text{-}CO)_3(CO)_8\{\mu\text{-}\eta^1\text{:}\eta^1\text{-}[Fe(\eta^5\text{-}C_5H_5)(\eta^5\text{-}P_3C_2Bu^t_2)]\}Ir_4(\mu\text{-}CO)_3(CO)_8]$		6
$[Ir_4(H)(\mu\text{-}CO)_3(CO)_8\{Fe(\eta^5\text{-}C_5H_5)[\eta^5\text{-}P_3C(CMe_2CH_2)CBu^t)]\}Ir(\mu\text{-}CO)_3(CO)_7]$	 XRS	6
$[\{Ir_4(\mu\text{-}CO)_3(CO)_8\}_2(\mu\text{-}dppb)]$		17
$[\{Ir_4(\mu\text{-}CO)_3(CO)_8\}_2(\mu\text{-}dppee)]$		17

Complex	Geometries[a]	Reference
$[\{Ir_4(\mu\text{-}CO)_3(CO)_8\}_2(\mu\text{-dppp})]$		17
$[Ir_4(\mu_3\text{-}PPh)(\mu\text{-}CO)_3(CO)_3(PPh_3)_4]$	 XRS	61
$[Ir_8(\mu\text{-}CO)_6(CO)_{16}]^{2-}$	 XRS	66
$[\{Ir_4(\mu\text{-}CO)_3(CO)_8\}(\mu\text{-PhPPh})\{Ir_4(\mu\text{-}CO)(CO)_8(AuPEt_3)_2\}]$	 XRS	67
$[Ir_4(\mu\text{-H})(\mu\text{-}PPh_2)(\mu\text{-CO})(CO)_8(Ph_2PC_2Ph)]$		68
$[Ir_4(\mu\text{-H})(\mu_3\text{-}\eta^3\text{-}P, P', C\text{-}PPhC_6H_4CH{=}CHPPh_2)(\eta^2\text{-dppee})(\mu\text{-}CO)_3(CO)_7]$	 XRS	45

[a]XRS ≡ structurally characterized

monosubstituted derivatives of **1** (Table 2.1.1). Ligands which are good σ- or π-donors or which are sterically cumbersome afford this structure. One interesting case was revealed with $[Ir_4(\mu\text{-}CO)_3(CO)_8(SCN)]^-$; $[NMe_2(CH_2Ph)_2][Ir_4(CO)_{11}(SCN)]$ [8] has all-terminal ligands in the solid state, whereas $[N(PPh_3)_2][Ir_4(\mu\text{-}CO)_3(CO)_8(SCN)]$ [11] exhibited a geometry with a basal plane, three bridging carbonyls and an axially ligated thiocyanate (Figure 2.1.3), providing an interesting example of solid-state packing considerations driving the observed ligand distribution.

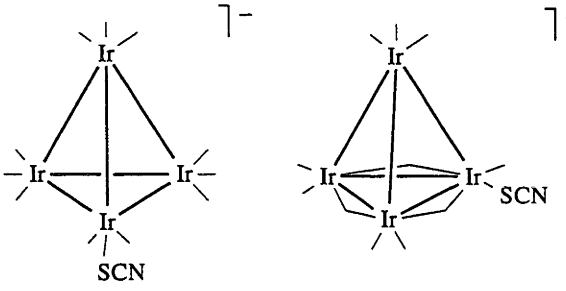
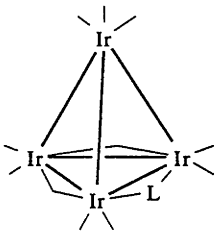


Figure 2.1.3.

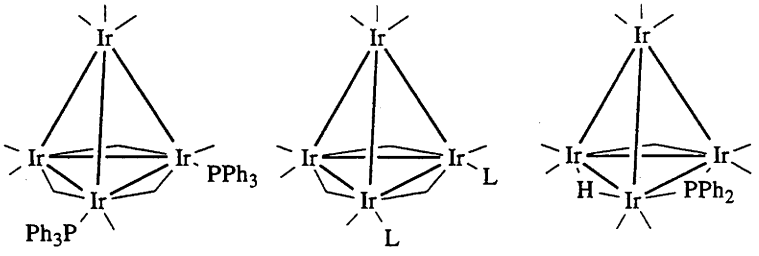
Calculations have shown that the radial sites are the least sterically hindered in clusters with pseudo C_{3v} geometry.[12] Despite this, most monosubstituted clusters $[Ir_4(\mu\text{-}CO)_3(CO)_8(L)]$ have ligands in an axial site, below the plane of bridging carbonyls and formally *trans* to the M_{apical}-M_{basal} bond (Table 2.1.1.).[13] Structurally characterized axially-ligated complexes include $[Ir_4(CO)_{11}(Br)]^-$,[14] $[Ir_4(CO)_{11}(CH_2CO_2Me)]^-$ [15] and $[Ir_4(CO)_{11}(CO_2Me)]^-$.[16] A considerable number of other clusters have also been assigned this coordination geometry utilizing information from the crystallographically-verified isomers, chemical shifts in the ^1H, ^{13}C or ^{31}P NMR spectra and/or ν(CO) bands in the IR spectra. An established NMR chemical shift sequence states that in the ^1H, ^{13}C or ^{31}P NMR spectra of tetrairidium cluster compounds, the chemical shifts of the ligands decrease in the positional sequence: bridging > radial > axial ≈ apical[17] (note that the isomer assignment in tetrairidium clusters will be discussed more thoroughly in Chapter 3). Complexes with carbonyls in radial-ligated sites were also found in isomers of $[Ir_4(\mu\text{-}CO)_3(CO)_8(L)]$, although less frequently. This geometry has not been structurally characterized, isomer assignment being based on spectroscopic evidence. Complexes usually exist as interconverting isomers in solution. The remaining monosubstituted derivatives of **1** have the geometry $[Ir_4(\mu\text{-}CO)_2(\mu\text{-}L)(CO)_9]$ [(v) in Figure 2.1.2.] The complexes $[Ir_4(\mu\text{-}H)(\mu\text{-}CO)_2(CO)_9]^-$ [18] and $[Ir_4(\mu\text{-}CO)_2(\mu\text{-}SO_2)(CO)_9]$[19] have been structurally characterized with their unique ligands occupying bridging sites in the basal plane (Figure 2.1.4.).



L = H, SO_2

Figure 2.1.4.

When more than one carbonyl group is replaced, complexes with pseudo-C_{3v} symmetry generally result. All-terminal coordination geometries for the clusters $[Ir_4(CO)_{10}(CNBu^t)_2]$ and $[Ir_4(CO)_{10}(CNMe)_2]$ [9] were proposed on the basis of their spectral data. Tetrairidium cluster substitution with monodentate ligands invariably proceeded at a different basal metal to afford bis-substituted derivatives with three bridging carbonyls, and usually a radial, axial configuration. X-ray structural characterizations of $[Ir_4(\mu\text{-}CO)_3(CO)_7(PPh_3)_2]$[36,38] (Figure 2.1.5.) revealed that the phosphines are ligated in a radial, axial coordination mode. This geometry was also proposed, on the basis of the similarity of the NMR spectra, for the other bis-phosphine derivatives investigated.[17,26,28] The complex $[Ir_4(H)_2(\mu\text{-}CO)_3(CO)_7]^{2-}$ is considered to have its hydride ligands terminally bound and axially ligated; although the hydride ligands were not found in the structural characterization,[35] their locations below the basal plane were postulated from the positions of carbonyl ligands. Structural characterizations of the alkyl-ligated cluster $[Ir_4(\mu\text{-}CO)_3(CO)_7(CH_2CO_2Me)_2]^{2-}$ [15] and the carbene-ligated $[Ir_4(\mu\text{-}CO)_3(CO)_7(\overline{COCH_2CH_2O})_2]$[5] (Figure 2.1.5.) also revealed geometries with diaxially coordinated ligands. The disubstituted phosphido cluster $[Ir_4(\mu\text{-}H)(\mu\text{-}PPh_2)(\mu\text{-}CO)(CO)_9]$ has been structurally characterized with a novel mode of coordination (Figure 2.1.5.); the cluster has a bridging hydride, a bridging phosphido ligand and one bridging carbonyl in the basal plane.

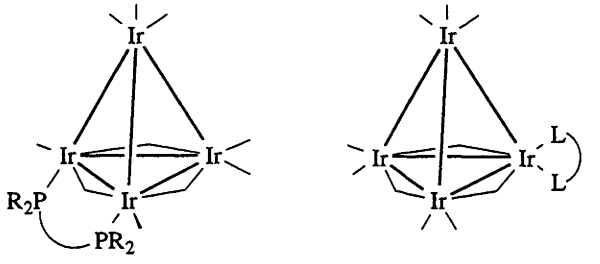


L = H, CH_2CO_2Me, $COCH_2CH_2O$

Figure 2.1.5.

Two new modes of coordination are introduced when bidentate ligands are considered. In most cases the bidentate ligand bridged an Ir-Ir edge below the basal plane. The complexes $[Ir_4(\mu\text{-}CO)_3(\mu\text{-dmpe})(CO)_7]$,[17] $[Ir_4(\mu\text{-}CO)_3(\mu\text{-dppb})(CO)_7]$,[43] and $[Ir_4(\mu\text{-}CO)_3(\mu\text{-}$

dppee)$(CO)_7$][45] (Figure 2.1.6.) have been structurally characterized with a diaxially bridging geometry. This geometry is also proposed for the diphosphine complexes [Ir_4(μ-$CO)_3$(μ-dppe)$(CO)_7$], [Ir_4(μ-$CO)_3$(μ-dppm)$(CO)_7$] and [Ir_4(μ-$CO)_3$(μ-dppp)$(CO)_7$],[17,28] the diarsine complex [Ir_4(μ-$CO)_3$(μ-dpam)$(CO)_7$],[28] the bis(methylthio)methane complex [Ir_4(μ-$CO)_3$(μ-$MeSCH_2SMe$)$(CO)_7$],[28] and the phosphole derivative [Ir_4(μ-$CO)_3${μ-η^4-[Fe(η^5-$P_3C_2Bu^t_2$)(η^5-$P_2C_3Bu^t$)]}$(CO)_7$].[6] Molecular models have previously shown that a diradially coordinated geometry may only occur with diphosphines when the aliphatic chain of the diphosphine is at least four C-atoms in length.[28] In a few cases these bidentate ligands chelate to one iridium in a radial, axial configuration (Figure 2.1.6.). This has been structurally characterized with [Ir_4(μ-$CO)_3(CO)_7$(η^2-diars)][41] and [Ir_4(μ-$CO)_3(CO)_7$(η^2-cod)].[39]



[Ir_4(μ-$CO)_3$(μ-dmpe)$(CO)_7$], [Ir_4(μ-$CO)_3$(μ-dppb)$(CO)_7$], [Ir_4(μ-$CO)_3$(μ-dppee)$(CO)_7$]

[Ir_4(μ-$CO)_3(CO)_7$(η^2–diars)], [Ir_4(μ-$CO)_3(CO)_7$(η^2–cod)]

Figure 2.1.6.

Isomer interconversion between the diaxial bridging form and the radial, axial chelating form in the bis(diphenylphosphino)ethene-derived cluster has been proposed from NMR kinetic evidence (Figure 2.1.7.).[46] The clusters [Ir_4(μ-$CO)_3(CO)_7$(η^2-phen)][42] and [Ir_4(μ-$CO)_3(CO)_7$(η^2-4,4-Me_2-bipy)][42] were also characterized with radial, axial chelating geometries. The di-olefin substituted clusters [Ir_4(μ-$CO)_3(CO)_7$(η^4-L)] (L = nbd, cot) are also believed to adopt this coordination mode (on the basis of spectral data). The first substitution takes place at an axial site giving [Ir_4(μ-$CO)_3(CO)_8$(η^2-L)], followed by chelation at a radial site of the same iridium.

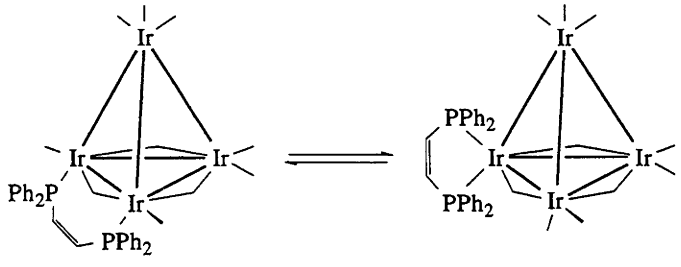


Figure 2.1.7. Isomer interconversion of [Ir_4(μ-$CO)_3$(μ-dppee)$(CO)_7$] and [Ir_4(μ-$CO)_3(CO)_7$(*cis*-dppee)]

For trisubstituted derivatives of **1**, isomers with an all-terminal coordination geometry were postulated for $[Ir_4(CO)_9(L)_3]$ (L = $CNBu^t$, CNMe),[9] but an additional isomer with bridging carbonyls was suggested for the more sterically demanding $CNBu^t$ derivative. The majority of clusters with monodentate ligands have the third ligand situated in the basal plane to minimize steric effects. Phosphines and similar ligands progressively substitute on different basal metal atoms, affording clusters with diradial, axial geometries. This geometry is demonstrated in the crystallographic characterizations of $[Ir_4(\mu\text{-}CO)_3(CO)_6(PPh_3)_3]$[36] and $[Ir_4(\mu\text{-}CO)_3(CO)_6(PPh_2pyl)_3]$.[50] The carbene-ligated cluster $[Ir_4(\mu\text{-}CO)_3(CO)_6(\overline{COCH_2CH_2O})_3]$[5] has a unique solid-state structure for monodentate ligand-substituted clusters, with a triaxial geometry (Figure 2.1.8). Phosphines and phosphites substitute the cluster $[Ir_4(\mu\text{-}H)(\mu\text{-}CO)(\mu\text{-}PPh_2)(CO)_9]$ affording $[Ir_4(\mu\text{-}H)(\mu\text{-}CO)(\mu\text{-}PPh_2)(CO)_8(L)]$ with the incoming ligand coordinating in an axial position, as revealed by a structural study of $[Ir_4(\mu\text{-}H)(\mu\text{-}CO)(\mu\text{-}PPh_2)(CO)_8(PPh_3)]$[47] (Figure 2.1.8.).

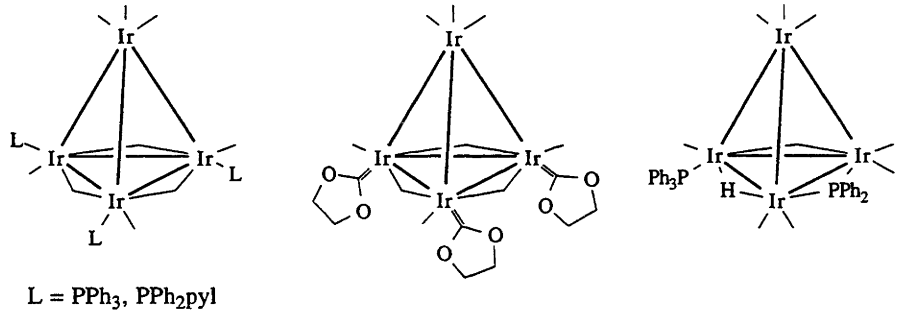
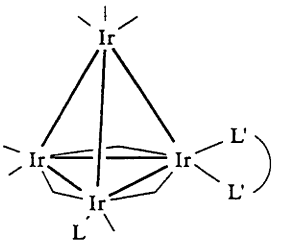
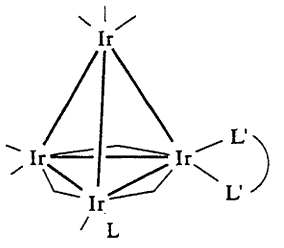


Figure 2.1.8.

Substitution by a diars, nbd or dppp ligand at the complexes $[Ir_4(\mu\text{-}CO)_3(CO)_8(L)]$ (L = PMe_2Ph, $PMePh_2$, PPh_3, $AsPh_3$) gives complexes with the geometries shown in Figure 2.1.9. The complexes $[Ir_4(\mu\text{-}CO)_3(CO)_6(PMe_2Ph)(\eta^4\text{-nbd})]$ and $[Ir_4(\mu\text{-}CO)_3(CO)_6(PPh_3)(\eta^4\text{-nbd})]$ have been structurally characterized.[53] Substitution of **1** by a tridentate ligand generally lead to coordination of the ligand below the iridium basal plane. The complexes $[Ir_4(CO)_9\{\mu_3\text{-}HC(PPh_2)_3\}]$[55] and $[Ir_4(CO)_9\{\mu_3\text{-c-}(SCH_2)_3\}]$[56] are unusual in that all carbonyls are bound in a terminal fashion. A second isomer of the cyclo-trithiane substituted cluster $[Ir_4(\mu\text{-}CO)_3(CO)_6\{\mu_3\text{-c-}(SCH_2)_3\}]$[56] was structurally characterized, with a plane of bridging carbonyls and the cyclo-trithiane group ligated triaxially. Similarly, the clusters $[Ir_4(\mu\text{-}CO)_3(CO)_6\{\mu_3\text{-}HC(\mu\text{-}SMe)_3\}]$[52] and $[Ir_4(\mu\text{-}CO)_3(CO)_6\{\mu_3\text{-triphos}\}]$[52] have been assigned triaxial coordination geometries.



L = PMe_2Ph, $PMePh_2$, L'∩L' = nbd;
L = PPh_3, $AsPh_3$, L'∩L' = cod, cot;
L = $PMePh_2$, L'∩L' = diars



L = PMe_2Ph, $PMePh_2$, PPh_3, $AsPh_3$,
L'∩L' = nbd;
L = PPh_3, $AsPh_3$, L'∩L' = cod, cot;
L = $PMePh_2$, L'∩L' = diars

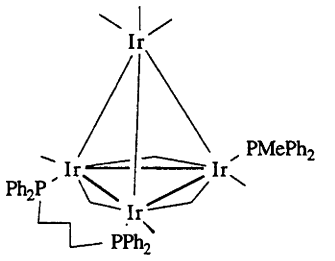
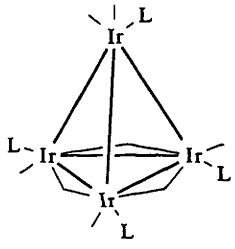


Figure 2.1.9.

The fourth ligand substitutes at the apical metal, resulting in the two ligands on the basal metals on that $M_{apical}(M_{basal})_2$-triangular face moving into axial sites and the other ligand into a radial site. Crystallographic studies of $[Ir_4(\mu\text{-}CO)_3(CO)_5(L)_4]$ (L = PMe_2Ph[60] and PMe_3,[59] Figure 2.1.10.) show the radial, diaxial, apical geometry exhibited most frequently in these tetra-substituted clusters.



L = PMe_2Ph, PMe_3

Figure 2.1.10.

The tetrakis(isocyanide) derivatives are again proposed to adopt configurations with all-terminal coordination geometries, with the $CNBu^t$ derivative also having one or more isomers with a plane of bridging carbonyls. A cluster with radial, apical bridging, radial, axial coordination geometry has been identified in a structural study of $[Ir_4(\mu\text{-}CO)_3(\mu\text{-}P\text{-}N\text{-}PPh_2pyl)(CO)_6(PPh_2pyl)_2]$.[51] This was formed from $[Ir_4(\mu\text{-}CO)_3(CO)_6(PPh_2pyl)_3]$, by transformation of one of the radial 2-pyridylphosphine ligands into a bridging ligand. An NMR study suggests the complexes interconvert in solution (Figure 2.1.11.).

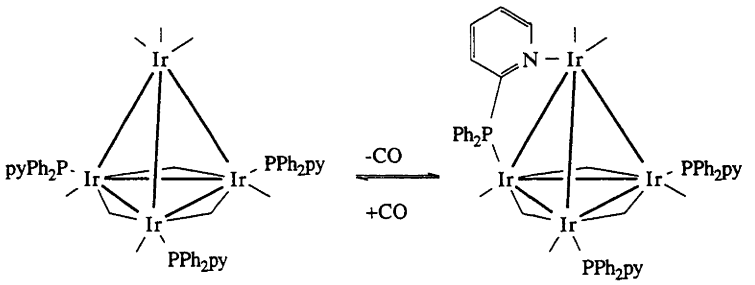


Figure 2.1.11. Interconversion of $[Ir_4(\mu\text{-}CO)_3(CO)_6(PPh_2py)_3]$ and $[Ir_4(\mu\text{-}CO)_3(\mu\text{-}P\text{-}N\text{-}PPh_2pyl)(CO)_5(PPh_2py)_2]$

Three bis-substituted alkylarylphosphine complexes of the type $[Ir_4(\mu\text{-}CO)_3(\mu\text{-}L)_2(CO)_5]$ (L = dppm,[52,58,63] dppee[45,46] dppe,[36] and dppp[52]) are known, with structural characterizations of the first two examples confirming a geometry with one bidentate phosphine bridging two basal iridiums ligated in a diaxial fashion, and the other bidentate phosphine bridging the remaining basal iridium and the apical iridium in a radial, apical manner (Figure 2.1.12.).

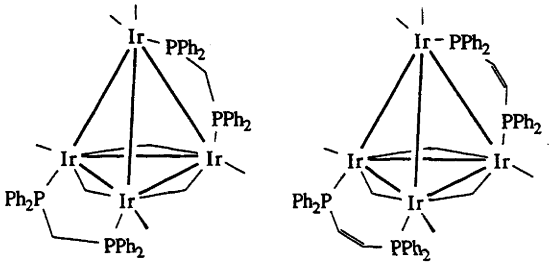


Figure 2.1.12.

The geometries of the tetrasubstituted chelating complexes $[Ir_4(\mu\text{-}CO)_3(CO)_5(\eta^4\text{-}L)(\eta^4\text{-}L')]$ (L = L' =cod,[33,52,62] L = cod, L' = nbd,[52] L = L' = nbd,[52] Figure 2.1.15.) were proposed as bis(radial, axial) chelating from extensive NMR investigations. One interesting tetrasubsituted tetrairidium cluster is the structurally characterized $[Ir_4(\mu\text{-}CO)_2(\mu\text{-}PCy_2)_4(CO)_4]$[64] (Figure 2.1.13.) with four bridging phosphido ligands; the bulky phosphido ligand was found to dramatically alter the usual geometry of these complexes. A crystallographic study of the arsino complex $[Ir_4(\mu\text{-}AsBu^t_2)_4(\mu\text{-}CO)_2(CO)_4]$[64] revealed that the sterically demanding $AsBu^t_2$ ligand forces the cluster into a planar tetrairidium arrangement. An attempt to prepare the tetrasubstituted triphenylphosphine complex produced the novel complex $[Ir_4(\mu_3\text{-}PPh)(\mu\text{-}CO)_3(CO)_3(PPh_3)_4]$[61] with a face-capping phosphido ligand and four triphenylphosphine ligands (Figure 2.1.14.).

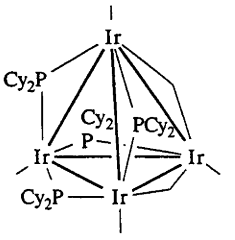


Figure 2.1.13.

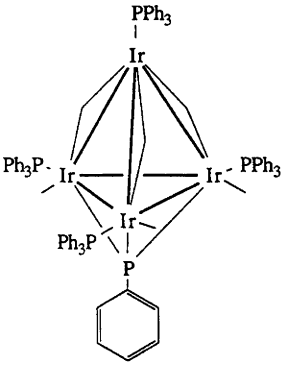


Figure 2.1.14.

Two isomers of the pentasubstituted tetrairidium cluster $[Ir_4(\mu\text{-}CO)_3(CO)_4(PMePh_2)(\eta^4\text{-}nbd)_2]$[52] (Figure 2.1.15.) have been identified by NMR, with the phosphine ligand in either an axial or radial position. The isomers of the NMR studies do not interconvert in solution over the temperature range 183 - 333 K. Analogous triphenylphosphine and triphenylarsine nbd or cod substituted clusters have also been characterized by NMR. The (formally) hexasubstituted cluster $[Ir_4(\mu\text{-}CO)_3(CO)_3(\eta^4\text{-}cod)_3]$[62] has been assigned a geometry with three radial, axial chelating cod on the basis of spectral evidence.

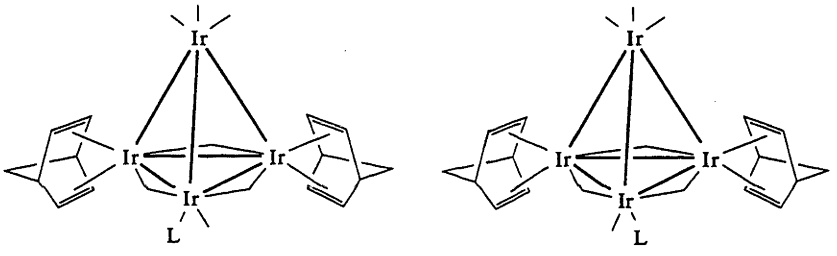


Figure 2.1.15.

A (formally) octa-substituted derivative of **1**, $[Ir_4(\mu\text{-}H)_4(CO)_4\{Fe(\eta^5\text{-}C_5H_3PPh_2(\eta^5\text{-}C_5H_4PPhC_6H_4)\}_2]$ was formed by thermolysis of **1** with dppf. Two dehydrogenated dppf ligands were formed upon orthometalation of a cyclopentadienyl ligand and a phenyl ring, as shown in Figure 2.1.16.[65]

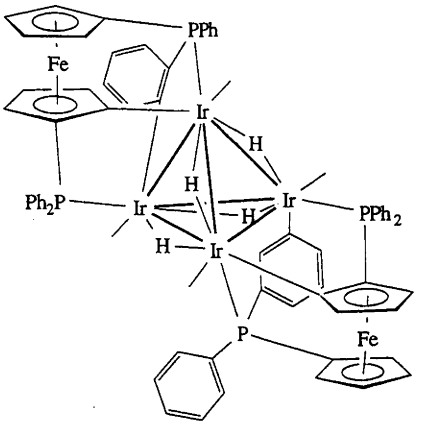
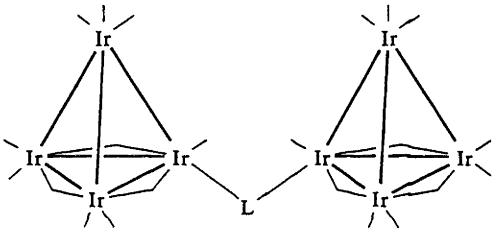


Figure 2.1.16.

When the reaction conditions employed for bidentate phosphine or phosphole substitution were altered, another class of compounds results. The diphosphine-substituted complexes $[\{Ir_4(\mu\text{-}CO)_3(CO)_8\}_2(\mu\text{-}L)]$ (L= dpp, dppp, dppb)[17] as well as $[\{Ir_4(\mu\text{-}CO)_3(CO)_8\}_2\{\mu\text{-}\eta^1\text{:}\eta^1\text{-}[Fe(\eta^5\text{-}C_5H_5)(\eta^5\text{-}P_3C_2Bu^t_2)]\}]$ [6] (Figure 2.1.17.) have been reported with the *P*-donor atoms of the phosphine or phosphole, ligating axially to differing tetrairidium cores.



L = dpp, dppp, dppb
$\{\mu\text{-}\eta^1\text{:}\eta^1\text{-}[Fe(\eta^5\text{-}C_5H_5)(\eta^5\text{-}P_3C_2Bu^t_2)]\}$

Figure 2.1.17.

Carbonyl loss and oxidative addition of a C-H bond in the phosphole-coordinated complex afforded the $[HIr_4(\mu\text{-}CO)_3(CO)_7[\mu\text{-}P, P', C\text{-}\{Fe(\eta^5\text{-}C_5H_5)[\eta^5\text{-}P_3C(CMe_2H_2)CBu^t]\}]]Ir_4(\mu\text{-}CO)_3(CO)_8]$ [6,7] (Figure 2.1.18.), with a structural study confirming the C-H activation.

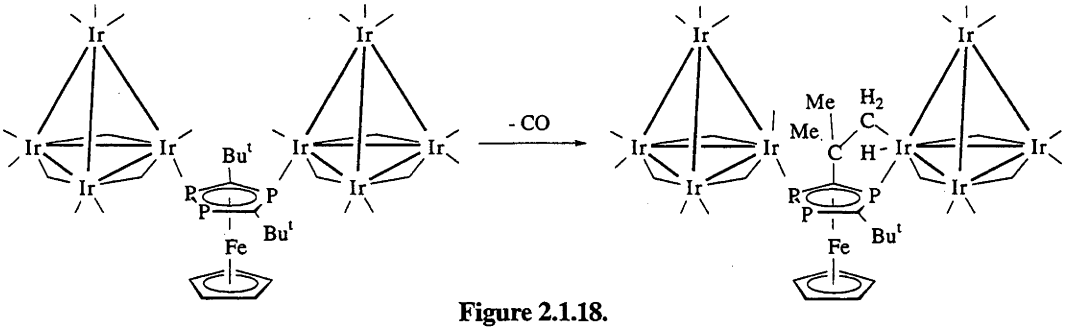


Figure 2.1.18.

Deprotonation and subsequent oxidation of $[Ir_4(CO)_{11}(PH_2Ph)]$ afforded the novel complex $[\{Ir_4(\mu\text{-}CO)_3(CO)_8\}(\mu\text{-}PhPPPh)\{Ir_4(\mu\text{-}CO)(CO)_8(AuPEt_3)_2\}]$.[67] A crystallographic study revealed that the two tetrairidium units are linked by a diphosphane (PhPPPh) ligand (Figure 2.1.19.) in an unusual coordination mode. The final cluster complex described is also a dimer of two Ir_4 units; the dianion $[Ir_8(\mu\text{-}CO)_6(CO)_{16}]^{2-}$ has an Ir-Ir bond linking the two $[Ir_4(\mu\text{-}CO)_3(CO)_8]^-$ fragments via formal axial sites (Figure 2.1.20.).

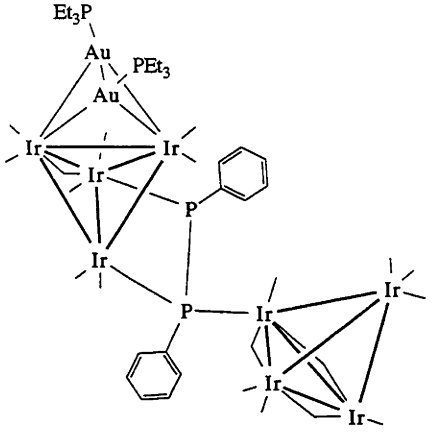


Figure 2.1.19.

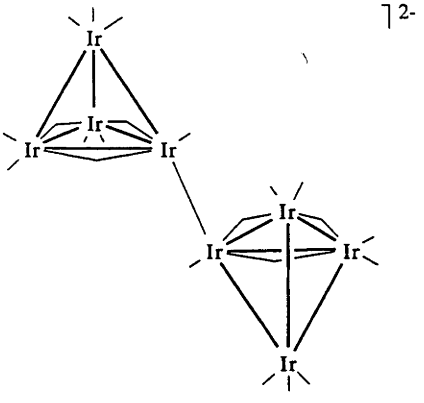


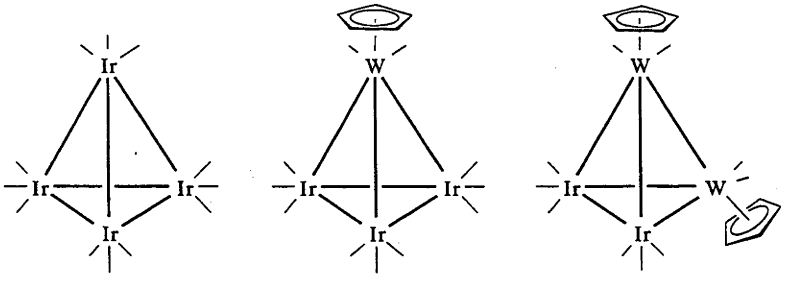
Figure 2.1.20.

2.1.3. Summary

Despite requiring elevated temperatures or halide activation to proceed, the substitution chemistry of **1** has been extensively investigated. Twenty five different coordination modes have been identified crystallographically, the majority of which are (formally) derived from those with the substitution sites shown in Figure 2.1.2. Many of the clusters exist as isomers, which have been verified by NMR spectroscopic investigations; these are discussed more fully in Chapter 3.

2.2. Synthesis and characterization of phosphine, phosphite and isocyanide derivatives of $[CpWIr_3(CO)_{11}]$ (2) and $[Cp_2W_2Ir_2(CO)_{10}]$ (3)

A isostructural series of clusters in which ligated metal fragments are sequentially replaced by isolobal fragments with different metals affords the possibility to assess the impact of heterometal incorporation upon reactivity, product distribution, fluxionality and other properties. The tetrahedral mixed-metal clusters $[CpWIr_3(CO)_{11}]$ (2) and $[Cp_2W_2Ir_2(CO)_{10}]$ (3) (Figure 2.2.1.) are conceptually derived from the "parent" tetrairidium cluster **1** by replacement of one or two $[Ir(CO)_3]$ vertices with one or two $[CpW(CO)_2]$ units, respectively. Iridium and tungsten are sufficiently different for the polar metal-metal bonds, formed between carbophilic iridium and oxophilic tungsten, to have a noticeable effect on reactivity. Compounds of tungsten and iridium (both 5d metals) have a greater bond strength than their 3d and 4d counterparts. While a significant body of work exists for the chemistry of mixed-metal clusters incorporating metals from the same or adjacent groups, significantly less is known of "very mixed"-metal clusters incorporating disparate metals (Chapter 1) . The particular focus of the studies described in this Chapter is to understand the ligand substitution chemistry of the "very mixed"-metal clusters **2** and **3** towards a variety of ligands such as phosphines, phosphites, phospholes and isocyanides and benchmark the results against the well-established chemistry of the tetrairidium system described above.



(1) (2) (3)

Figure 2.2.1.

2.2.1. Reaction of [CpWIr$_3$(CO)$_{11}$] (2) with PPh$_3$ or PMe$_3$

The reactions of [CpWIr$_3$(CO)$_{11}$] (**2**) with n equivalents of PPh$_3$ (n = 1, 2 or 3) or PMe$_3$ (n = 1, 2 or 3) proceeded in dichloromethane at room temperature to afford the clusters [CpWIr$_3$(μ-CO)$_3$(CO)$_{8-n}$(PPh$_3$)$_n$] [n = 1, (**4**); n = 2, (**5**); n = 3, (**6**)] or [CpWIr$_3$(μ-CO)$_3$(CO)$_{8-n}$(PMe$_3$)$_n$] [n = 1, (**7**); n = 2, (**8**); n = 3, (**9**)], respectively, as the major or sole reaction products in fair to excellent yields (38 - 63 %). The products have been characterized by a combination of IR, ^{1}H, ^{13}C and ^{31}P NMR spectroscopies, FAB MS and satisfactory microanalyses. Infrared spectra suggest the presence of edge-bridging carbonyl ligands in all complexes [υ(CO) 1840 - 1807 cm^{-1}], which contrasts with the all-terminal precursor **2**. In combination with the X-ray structural results detailed below, the number of bands in the terminal carbonyl ligand υ(CO) region is indicative of the presence of isomers. The ^{1}H and ^{13}C NMR (where appropriate) spectra contain signals assigned to Cp and Ph groups for **4**, **5** and **6**, and Cp and Me groups for **7**, **8** and **9**. Discussion of the ^{13}C and ^{31}P NMR spectra is deferred until Chapter 3 (as with the ^{13}C and ^{31}P NMR spectra of all complexes characterized in this Chapter), but the spectra indicate the presence of interconverting isomers in solution. The FAB mass spectra of complexes **4**, **5** and **7** have molecular ions, stepwise loss of carbonyls, and isotope patterns consistent with the presence of three iridium atoms and one tungsten atom; in some cases, loss of Ph is competitive with loss of the last few carbonyl ligands. The FAB mass spectra of derivatives **6**, **8** and **9** do not contain molecular ions. Although mass spectra for **7** and **8** exhibit loss of carbonyls from the molecular ion, that of **6** shows initial loss of a phosphine ligand, followed by loss of carbonyls, possibly a result of steric factors.

The molecular structures of **4**, **5** and **7** as determined by single-crystal X-ray studies are consistent with the formulations given above, define the substitution sites for these derivatives, and aid interpretation of the ^{13}C and ^{31}P NMR spectra (see Chapter 3). Selected bond distances and angles are listed in Tables 2.2.1. and 2.2.2. (**4** and **5**) and Tables 2.2.3. and 2.2.4. (**7**). ORTEP plots showing the molecular geometry and atomic numbering scheme are shown in Figure 2.2.2. (**4**), Figure 2.2.3. (**5**) and Figure 2.2.4. (**7**).

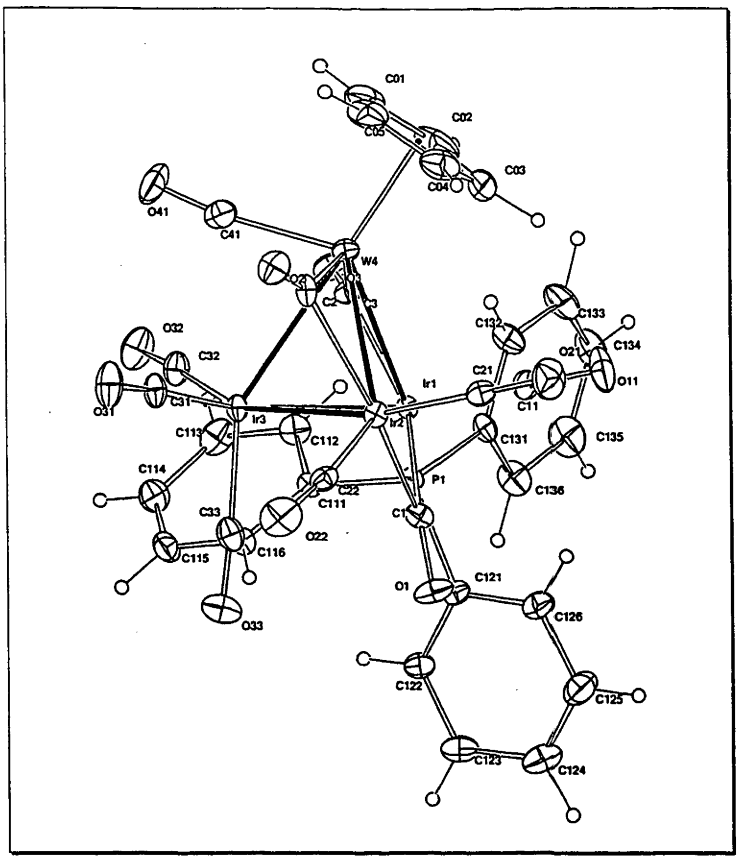


Figure 2.2.2. Molecular structure and atomic labelling scheme for $[CpWIr_3(\mu\text{-}CO)_3(CO)_7(PPh_3)]$, (**4**). Thermal envelopes of 20 % probability are shown for the non-hydrogen atoms; hydrogen atoms have arbitrary radii of 0.1 Å.

(By Brian W. Skelton, Vicki-Anne Tolhurst and Allan H. White)

Complexes **4** and **5** have the WIr_3 pseudotetrahedral framework of the precursor cluster **2** and possess η^5-cyclopentadienyl groups, three bridging carbonyls arranged about a WIr_2 plane, six (**5**) or seven (**4**) terminal carbonyl ligands, and one (**4**) or two (**5**) iridium-ligated triphenylphosphine ligands. The WIr_3 core distances ($W\text{-}Ir_{av}$ = 2.85 Å **4**, 2.86 Å **5**, $Ir\text{-}Ir_{av}$ = 2.699 Å **4**, 2.737 Å **5**) can be compared to those of **2** ($W\text{-}Ir_{av}$ = 2.82 Å, $Ir\text{-}Ir_{av}$ = 2.699 Å), and possibly suggest some slight core expansion upon phosphine substitution; core distances of the diphosphine-substituted complexes $[CpWIr_3(\mu\text{-}CO)_3(\mu\text{-dppe})(CO)_6]$, $[CpWIr_3(\mu\text{-}CO)_3(\mu\text{-dppm})(CO)_6]$ and $[CpWIr_3(\mu\text{-}CO)_3(\mu\text{-dppa})(CO)_6]$ are also larger than those of **2**.[69] As previously observed with the diphosphine clusters, the longest W-Ir distance in **4** is effectively *trans* to the Cp group, although that in **5** is on the WIr_2 face to which the Cp group is inclined. In **5**, the shortest Ir - Ir bonds are between the phosphine-coordinated iridiums, the longest Ir-Ir vector in both $[CpWIr_3(\mu\text{-dppe})(\mu\text{-}CO)_3(CO)_6]$ and $[CpWIr_3(\mu\text{-dppm})(\mu\text{-}CO)_3(CO)_6]$. The cyclopentadienyl groups in **4** and **5** are inclined toward the WIr_2 faces containing the bridging carbonyl ligands. Carbonyl distances and angles for **5** are relatively imprecise, and will not be discussed here. Ir-CO(terminal) interactions for **4** [1.85(1) - 1.94(1) Å] and the W-CO(terminal) distance [1.97(1) Å] are

comparable to those reported in other tungsten-iridium carbonyl complexes; the M-C-O angles are in the normal range for terminal carbonyl groups [171(1)-178(1)°]. In **2**, carbonyls 1 and 3 bridge asymmetrically toward Ir(1), with Ir(1) -CO(1) 2.08(1) Å, Ir(2)-CO(1) 2.14(1) Å, and Ir(1)-CO(3) 2.10(1) Å, W(4)-CO(3) 2.17(1) Å; CO(2) is displaced towards tungsten [W(4)-CO(2) 2.09(1) Å, Ir(2)-CO(2) 2.17(1) Å]. The asymmetry in bridging carbonyls presumably reflects the increase in electron density (and capacity for back donation) at Ir(1) resultant upon phosphine substitution. Complexes **4** and **5** are the first examples from the tungsten-iridium system with bridging carbonyls at a WIr_2 face. The Ir-P distances [2.330(3) Å (**3**), 2.33 Å (**4**) (av)] are unexceptional, as are the intraphosphine bond lengths and angles. Formal electron counting reveals that **3** and **4** have 60 e, electron precise for tetrahedral clusters.

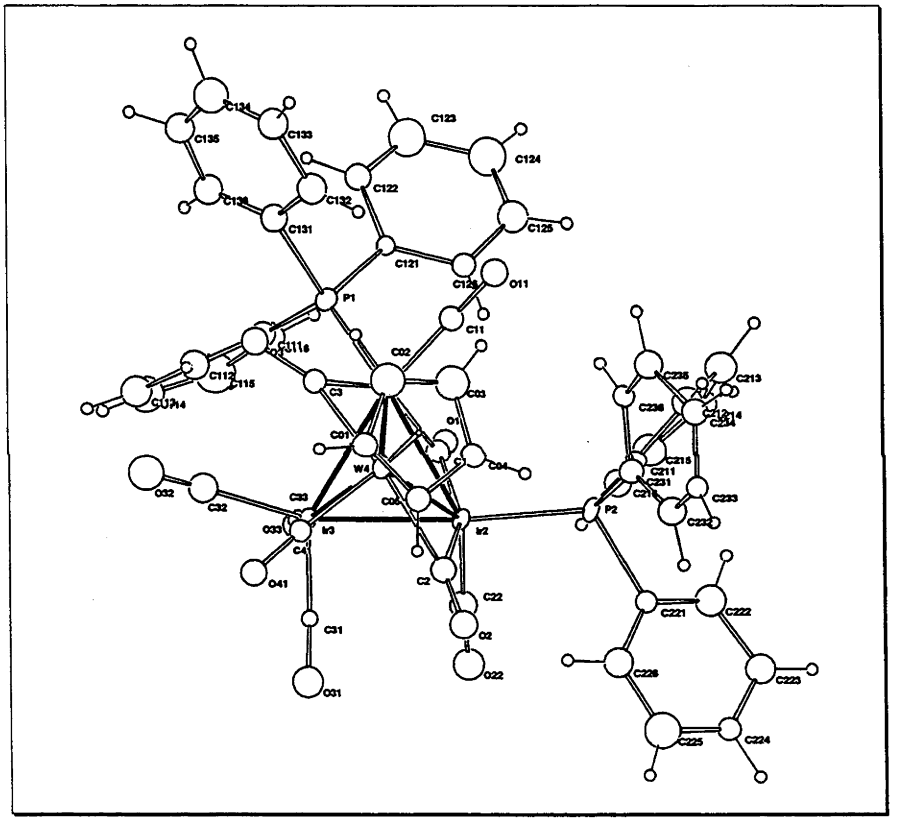


Figure 2.2.3. Molecular structure and atomic labelling scheme for $[CpWIr_3(\mu\text{-}CO)_3(CO)_6(PPh_3)_2]$, (**5**). Thermal envelopes of 20 % probability are shown for the non-hydrogen atoms; hydrogen atoms have arbitrary radii of 0.1 Å.

(By Brian W. Skelton, Vicki-Anne Tolhurst and Allan. H. White)

Table 2.2.1. Selected Bond Lengths (Å) for $[CpWIr_3(\mu\text{-}CO)_3(CO)_7(PPh_3)]$ (**4**) and $[CpWIr_3(\mu\text{-}CO)_3(CO)_6(PPh_3)_2]$ (**5**).

Bond Distance	4	5
Ir (1) - Ir (2)	2.6775 (9)	2.708 (3)
Ir (1) - Ir (3)	2.734 (1)	2.778 (3)
Ir (2) - Ir (3)	2.685 (1)	2.725 (3)
Ir (1) - W (4)	2.813 (1)	2.785 (3)
Ir (2) - W (4)	2.841 (1)	2.918 (3)
Ir (3) - W (4)	2.896 (1)	2.869 (3)
Ir (1) - P (1)	2.330 (3)	2.34 (1)
Ir (2) - P (2)		2.32 (1)
Ir (1) - C (1)	2.08 (1)	2.12 (4)
Ir (1) - C (3)	2.10 (1)	2.04 (4)
Ir (1) - C (11)	1.85 (1)	1.74 (5)
Ir (2) - C (1)	2.14 (1)	2.00 (4)
Ir (2) - C (2)	2.17 (1)	2.09 (5)
Ir (2) - C (21)	1.87 (1)	
Ir (2) - C (22)	1.87 (1)	1.73 (5)
Ir (3) - C (31)	1.94 (1)	1.82 (4)
Ir (3) - C (32)	1.92 (1)	1.97 (5)
Ir (3) - C (33)	1.90 (1)	1.81 (5)
W (4) - C (2)	2.09 (1)	2.19 (5)
W (4) - C (3)	2.17 (1)	2.09 (5)
W (4) - C (41)	1.97 (1)	1.88 (4)
W (4) - C (01)	2.31 (2)	2.29 (5)
W (4) - C (02)	2.32 (1)	2.24 (7)
W (4) - C (03)	2.34 (2)	2.30 (7)
W (4) - C (04)	2.30 (2)	2.26 (5)
W (4) - C (05)	2.27 (2)	2.23 (5)

Table 2.2.2. Selected Bond Angles (°) for $[CpWIr_3(\mu\text{-}CO)_3(CO)_7(PPh_3)]$ (**4**) and $[CpWIr_3(\mu\text{-}CO)_3(CO)_6(PPh_3)_2]$ (**5**).

Bond Angle	4	5
Ir (2) - Ir (1) - Ir (3)	59.48 (3)	59.54 (7)
Ir (1) - Ir (2) - Ir (3)	61.32 (3)	61.52 (7)
Ir (1) - Ir (3) - Ir (2)	59.21 (3)	58.94 (7)
Ir (1) - Ir (2) - W (4)	61.22 (3)	59.19 (7)
Ir (1) - Ir (3) - W (4)	59.87 (3)	59.07 (7)
Ir (2) - Ir (1) - W (4)	62.25 (3)	64.17 (7)
Ir (3) - Ir (1) - W (4)	62.93 (3)	62.08 (7)
Ir (2) - Ir (3) - W (4)	61.05 (2)	62.84 (7)
Ir (1) - W (4) - Ir (3)	57.21 (3)	58.85 (7)
Ir (1) - W (4) - Ir (2)	56.53 (3)	56.63 (6)
Ir (2) - W (4) - Ir (3)	55.80 (3)	56.17 (6)
Ir (2) - Ir (1) - P (1)	149.21 (7)	142.7 (3)
Ir (3) - Ir (1) - P (1)	109.06 (8)	109.6 (3)
W (4) - Ir (1)- P (1)	142.00 (7)	146.8 (3)
Ir (1) - Ir (2) - P (2)		113.8 (3)
Ir (3) - Ir (2) - P (2)		174.4 (3)
W (4) - Ir (2) - P (2)		114.4 (3)
W (4) - Ir (2) - P (2)		114.4 (3)

A single-crystal X-ray diffraction study of **7** reveals the presence of four independent molecules per asymmetric unit, each molecule differing only slightly from the others. No chemically significant differences exist in the four independent molecules; a representative molecule is depicted in Figure 2.2.4. As with **4**, complex **7** also possesses a WIr_3 pseudotetrahedral framework with η^5-cyclopentadienyl groups, phosphine ligand, and seven terminal carbonyl ligands, but in contrast to **4** has three bridging carbonyls arranged around the triiridium plane, a structural type found previously with the bidentate ligand derivatives $[CpWIr_3(\mu\text{-}CO)_3(\mu\text{-}L)(CO)_6]$ (L = dppm, dppe, dppa).[69] The WIr_3 core distances ($W\text{-}Ir_{av}$ 2.863 Å, $Ir\text{-}Ir_{av}$ 2.749 Å) are comparable to **4** and **5**; as with **4**, the longest W-Ir distance for **7** is effectively *trans* to the Cp group, and the shortest Ir-Ir bond is that effectively *trans* to the phosphine ligand. The cyclopentadienyl group is inclined towards a WIr_2 face; three W-C distances (av. 2.30 Å) are shorter than the two W-C distances (av. 2.40 Å) involving the carbons closest to the Ir-Ir vector. Ir-CO(terminal) interactions [1.81(5) - 1.94(1) Å] and W-CO interactions [1.98(2) - 1.99(3) Å] are normal. Cluster **7** is also electron precise with 60 e.

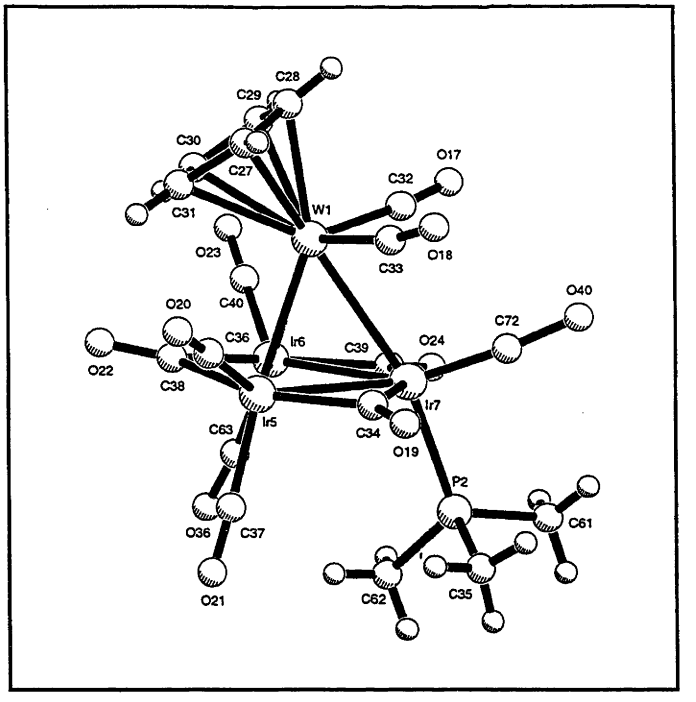


Figure 2.2.4. Molecular structure and atomic labelling scheme for $[CpWIr_3(\mu\text{-}CO)_3(CO)_7(PMe_3)]$, (**7**). Thermal envelopes of 50 % probability are shown for the non-hydrogen atoms; hydrogen atoms have arbitrary radii of 0.1 Å.

(By David C. R. Hockless)

As discussed in Section *2.1.*, the reactions of the tetrahedral homometallic cluster **1** with phosphines have been extensively investigated. Studies have concentrated on stereochemistry and ligand fluxionality. Comparison with the isolobally related **2** is useful. Substitution of carbonyl ligands by phosphine required elevated temperatures or halide activation to proceed. By contrast, phosphine substitution reactions on **2** proceeded at room temperature affording di, tri and tetrasubstituted products in good yields. In both the homometallic and bimetallic systems, substitution of carbonyl by phosphine converted the all-terminal carbonyl ligand geometry to one in which a MIr_2 plane (M = Ir, W) has three edge-bridging carbonyl groups; substitution by phosphine occurred at iridium atoms in both these systems. The radial, axial and radial, diaxial coordination geometries of **4** and **5**, respectively, have been identified previously in the tetrairidium system, however, the axial, apical coordination geometry of **7** is an unknown geoemtry for tetrahedral clusters.

Table 2.2.3. Selected Bond Lengths (Å) for $[CpWIr_3(\mu\text{-}CO)_3(CO)_7(PMe_3)]$ (**7**) and $[CpWIr_3(\mu\text{-}CO)_3(CO)_7(PMe_2Ph)]$ (**13**).

Bond Distance	7	13
Ir (1) - Ir (2)	2.756 (1)	2.740(1)
Ir (1) - Ir (3)	2.739 (1)	2.752(1)
Ir (2) - Ir (3)	2.753 (2)	2.744(1)
Ir (1) - W (1)	2.855 (1)	2.823(1)
Ir (2) - W (1)	2.839 (1)	2.838(1)
Ir (3) - W (1)	2.894 (1)	2.9004(9)
Ir (3) - P (1)	2.312 (7)	2.327(4)
Ir (1) - C (1)	2.10 (2)	2.13(2)
Ir (1) - C (3)	2.13 (2)	2.02(2)
Ir (1) - C (11)	1.85 (2)	
Ir (2) - C (11)		1.87(2)
Ir (1) - C (12)	1.93 (3)	
Ir (2) - C (12)		1.87(2)
Ir (2) - C (1)	2.12 (2)	2.11(2)
Ir (2) - C (2)	2.13 (3)	2.13(2)
Ir (2) - C (21)	1.81 (3)	
Ir (1) - C (21)		1.88(2)
Ir (2) - C (22)	1.94 (2)	
Ir (1) - C (22)		1.91(2)
Ir (3) - C (2)	2.11 (2)	2.06(2)
Ir (3) - C (3)	2.12 (2)	2.06(2)
Ir (3) - C (31)	1.81 (3)	1.84(2)
W (1) - C (41)	1.98 (2)	1.96(2)
W (1) - C (42)	1.99 (3)	2.01(2)
W (1) - C (01)	2.30 (2)	2.27(2)
W (1) - C (02)	2.28 (2)	2.28(2)
W (1) - C (03)	2.38 (3)	2.33(2)
W (1) - C (04)	2.41 (3)	2.36(2)
W (1) - C (05)	2.31 (3)	2.36(2)

Tables 2.2.4. Selected Bond Angles (°) $[CpWIr_3(\mu\text{-}CO)_3(CO)_7(PMe_3)]$ (**7**) and $[CpWIr_3(\mu\text{-}CO)_3(CO)_7(PMe_2Ph)]$ (**13**).

Bond Angle	7	13
Ir (2) - Ir (1) - Ir (3)	60.14 (4)	59.94(3)
Ir (1) - Ir (2) - Ir (3)	59.63 (3)	60.25(2)
Ir (1) - Ir (3) - Ir (2)	60.23 (3)	59.81(3)
Ir (1) - Ir (2) - W (1)	61.35 (3)	60.79(3)
Ir (1) - Ir (3) - W (1)	60.83 (3)	59.87(3)
Ir (2) - Ir (1) - W (1)	60.75 (3)	61.32(3)
Ir (3) - Ir (1) - W (1)	62.27 (3)	62.67(3)
Ir (2) - Ir (3) - W (1)	60.29 (4)	62.67(3)
Ir (1) - W (1) - Ir (3)	56.90 (3)	57.46(2)
Ir (1) - W (1) - Ir (2)	57.90 (3)	57.90(3)
Ir (2) - W (1) - Ir (3)	57.40 (3)	57.11(2)
Ir (3) - Ir (2) - W (1)	62.31 (4)	62.59(3)
Ir (1) - Ir (3) - P (1)	106.1 (2)	108.1(1)
Ir (2) - Ir (3) - P (1)	107.0 (2)	108.2(1)
W (1) - Ir (3)- P (1)	164.6 (2)	165.9(1)

2.2.2. Reaction of $[CpWIr_3(CO)_{11}]$ (2) with $PMePh_2$ or PMe_2Ph

The reactions of $[CpWIr_3(CO)_{11}]$ (**2**) with *n* equivalents of $PMePh_2$ or PMe_2Ph (*n* = 1-3) proceeded in dichloromethane at room temperature to afford the clusters $[CpWIr_3(\mu\text{-}CO)_3(CO)_{8-n}(PMePh_2)_n]$ [*n* = 1 (**10**), 2 (**11**) or 3 (**12**)] or $[CpWIr_3(\mu\text{-}CO)_3(CO)_{8-n}(PMe_2Ph)_n]$ [*n* = 1 (**13**), 2 (**14**) or 3 (**15**)], respectively, as the major or sole reaction products in good to excellent yields (40 - 76 %). The clusters **10 - 15** have been characterized by a combination of IR, ^1H, ^{13}C and ^{31}P NMR spectroscopies, mass spectrometry and satisfactory microanalyses. Infrared spectra suggest the presence of edge-bridging carbonyl ligands in all complexes [υ(CO) 1801-1891 cm^{-1}], which contrasts with the all-terminal geometry of the precursor **2**. In combination with the X-ray structural results detailed below, the number of bands in the terminal carbonyl ligand υ(CO) regions of the IR spectra of **10 - 14** is indicative of the presence of isomers. The ^1H NMR spectra contain signals assigned to cyclopentadienyl, phenyl and methyl groups for **10 - 15** in the appropriate ratios. The mass spectra of complexes **10 - 15** contain molecular ions, and all spectra contain fragment ions corresponding to stepwise loss of carbonyls; isotope patterns are consistent with the presence of three iridium atoms and one tungsten atom in all complexes.

The molecular structure of **13** as determined by a single-crystal X-ray diffraction study is consistent with the formulation given above, defines the substitution site of the phosphine, and aids interpretation of the ^{31}P NMR spectra (see Chapter 3). Selected bond distances are shown in Table 2.2.3. and angles are listed in Table 2.2.4. An ORTEP plot showing the molecular geometry and atomic numbering scheme is shown in Figure 2.2.5.

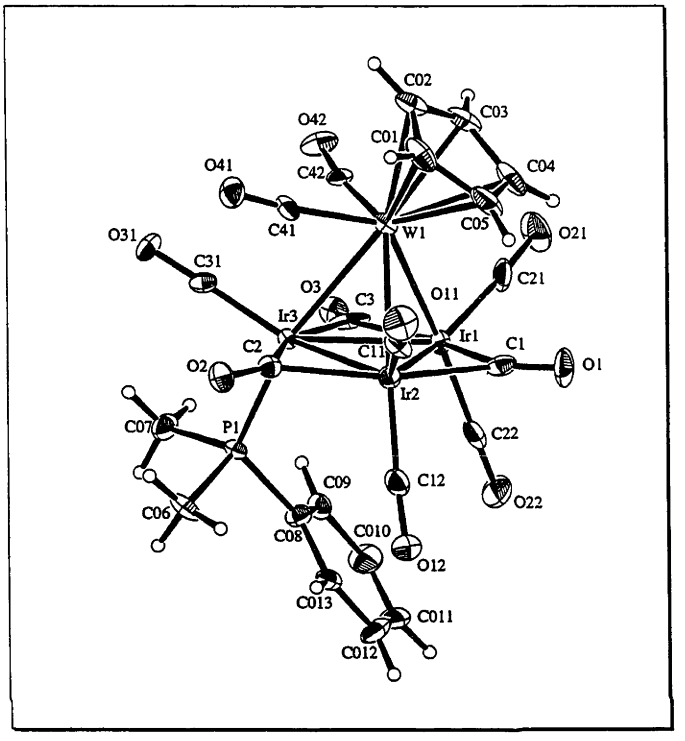


Figure 2.2.5. Molecular structure and atomic labelling scheme for [$CpWIr_3(\mu$-$CO)_3(CO)_7(PMe_2Ph)$], (**13**). Thermal envelopes of 50 % probability are shown for the non-hydrogen atoms; hydrogen atoms have arbitrary radii of 0.1 Å.

(By David C. R. Hockless)

Complex **13** has the WIr_3 pseudotetrahedral framework of the precursor cluster **2** and possesses an η^5-cyclopentadienyl group, three bridging carbonyls arranged about the triiridium plane, seven terminal carbonyl ligands, and an iridium-ligated dimethylphenylphosphine ligand. The WIr_3 core distances ($W\text{-}Ir_{av}$ = 2.85 Å, $Ir\text{-}Ir_{av}$ = 2.75 Å) are slightly longer than those of **2** ($W\text{-}Ir_{av}$ = 2.82 Å, $Ir\text{-}Ir_{av}$ = 2.70 Å); core distances of the mono(phosphine)-substituted complexes **4** and **7** are also consistent with core expansion upon introduction of *P*-donor ligands. The longest W-Ir distance for **13** is effectively *trans* to the Cp group. The cyclopentadienyl group is inclined towards a WIr_2 face; three W-C distances (average 2.29 Å) are shorter than the two W-C distances (average 2.36 Å) involving the carbons closest to the Ir-Ir vector. Ir-CO(terminal) interactions [1.84(2) - 1.91(2) Å] and W-CO interactions [1.96(2), 2.01(2) Å] for **13** are

unexceptional. The disposition of ligands in **13** is similar to that found in **7**. Formal electron counting reveals that **13** has 60 e, electron precise for a tetrahedral cluster.

2.2.3. Reaction of [CpWIr$_3$(CO)$_{11}$] (2) with P(OPh)$_3$ or P(OMe)$_3$

The reactions of [CpWIr$_3$(CO)$_{11}$] (**2**) with *n* equivalents of P(OPh)$_3$ or P(OMe)$_3$ (*n* = 1 or 2) proceeded in dichloromethane at room temperature to afford the clusters [CpWIr$_3$(μ-CO)$_3$(CO)$_{8-n}${P(OPh)$_3$}$_n$] [*n* = 1 (**16**) or *n* = 2 (**17**)] or [CpWIr$_3$(μ-CO)$_3$(CO)$_{8-n}${P(OMe)$_3$}$_n$] [*n* = 1 (**19**) or *n* = 2 (**20**)], respectively, as the major or sole reaction products in good yields (41-71 %). Although low yields are obtained upon reaction of **1** with three equivalents of the phosphites at room temperature, better yields of [CpWIr$_3$(μ-CO)$_3$(CO)$_5${P(OPh)$_3$}$_3$] (**18**) and [CpWIr$_3$(μ-CO)$_3$(CO)$_5${P(OMe)$_3$}$_3$] (**21**) were obtained by heating **2** with a slight excess of the appropriate phosphite in refluxing dichloromethane for three hours. The clusters **16 - 21** have been characterized by a combination of IR, ^{1}H, ^{13}C and ^{31}P NMR spectroscopies, mass spectrometry and satisfactory microanalyses. Infrared spectra suggest the presence of edge-bridging carbonyl ligands in all complexes [υ(CO) 1801-1854 cm^{-1}], which contrasts with the all-terminal geometry of the precursor **2**, but is similar to that seen for analogous triphenylphosphine and trimethylphosphine derivatives; the number of bands in the terminal carbonyl ligand υ(CO) region is indicative of the presence of isomers. The ^{1}H NMR spectra contain signals assigned to cyclopentadienyl and phenoxy groups for **16**, **17** and **18**, and cyclopentadienyl and methoxy groups for **19**, **20** and **21**, in the appropriate ratios. The mass spectra of complexes **16** and **19** contain molecular ions, and all spectra contain fragment ions corresponding to stepwise loss of carbonyls; isotope patterns are consistent with the presence of three iridium atoms and one tungsten atom in each complex.

The molecular structures of **17** and **19** as determined by single-crystal X-ray diffraction studies are consistent with the formulations given above, define the substitution sites of the phosphites, and aid interpretation of the ^{31}P NMR spectra (see Chapter 3). Selected bond distances and angles for complex **17** are listed in Tables 2.2.5. and 2.2.6., respectively. An ORTEP plot showing the molecular geometry and atomic numbering scheme is shown in Figure 2.2.6. Selected bond distances and angles for complex **19** are listed in Tables 2.2.7. and 2.2.8, and an ORTEP plots showing the molecular geometry and atomic numbering scheme is shown in Figure 2.2.7. (**19**).

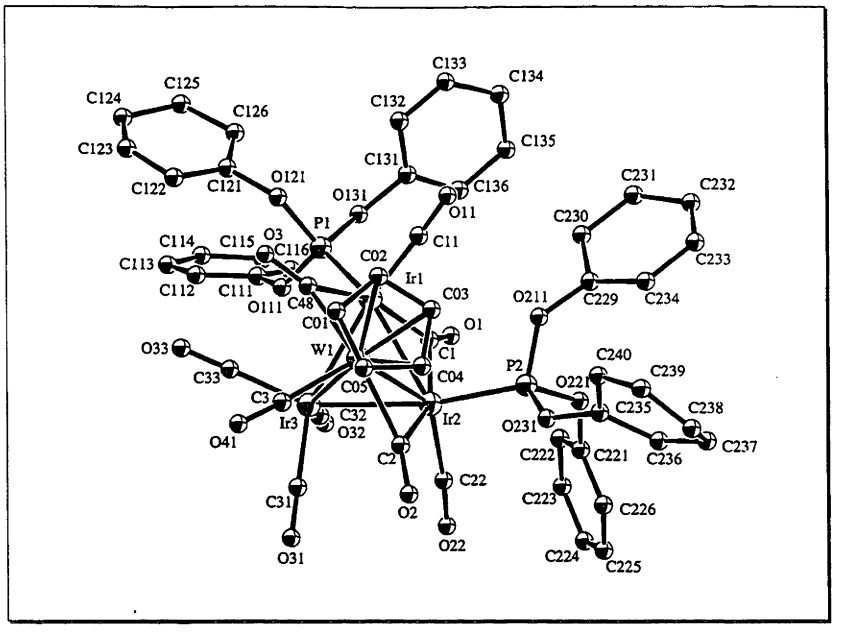


Figure 2.2.6. Molecular structure and atomic labelling scheme for $[CpWIr_3(\mu\text{-}CO)_3(CO)_6\{P(OPh)_3\}_2]$, (**17**). Thermal envelopes of 50 % probability are shown for the non-hydrogen atoms; hydrogen atoms have arbitrary radii of 0.1 Å.

(By David C. R. Hockless)

Complex **17** has the WIr_3 pseudotetrahedral framework of the precursor cluster **2** and possesses an η^5-cyclopentadienyl group, three bridging carbonyls arranged about a WIr_2 plane, six terminal carbonyl ligands, and two iridium-ligated triphenylphosphite ligands. The WIr_3 core distances ($W\text{-}Ir_{av}$ = 2.85 Å, $Ir\text{-}Ir_{av}$ = 2.71 Å) are slightly longer than those of **2** ($W\text{-}Ir_{av}$ = 2.82 Å, $Ir\text{-}Ir_{av}$ = 2.699 Å); core distances of the bis(phosphine)- or diphosphine-substituted complexes $[CpWIr_3(\mu\text{-}CO)_3(CO)_6(PPh_3)_2]$ (**5**), $[CpWIr_3(\mu\text{–}dppe)(\mu\text{-}CO)_3(CO)_6]$ [69], $[CpWIr_3(\mu\text{–}dppm)(\mu\text{-}CO)_3(CO)_6]$ [69] and $[CpWIr_3(\mu\text{–}dppa)(\mu\text{-}CO)_3(CO)_6]$ [69] are also consistent with core expansion upon introduction of *P*-donor ligands. The shortest Ir-Ir bond in **17** [Ir(1)-Ir(2) 2.6941(5) Å] is between the phosphite-coordinated iridiums; a short Ir-Ir linkage between the phosphine-ligated iridiums is also seen in **5**. The cyclopentadienyl group is inclined towards the WIr_2 face containing the bridging carbonyl ligands. Ir-CO(terminal) interactions for **17** [1.830(9)-1.918(9) Å] and ∠Ir-C-O(terminal) [174.5(8) - 180(1)°] are unexceptional. Carbonyls CO(1) and CO(48) bridge somewhat asymmetrically, both being diplaced towards Ir(1) which bears the radially - ligated phosphite; it is possible that this asymmetry maximizes backbonding. The Ir-P distances [2.230(3), 2.239(3) Å] and intraphosphite bond lengths and angles are not unusual. The disposition of ligands in **17** is similar to that found in **5**.

Table 2.2.5. Selected Bond Lengths (Å) for $[CpWIr_3(\mu\text{-}CO)_3(CO)_6\{P(OPh)_3\}_2]$ (**17**)

Bond	Length	Bond	Length
Ir(1)-Ir(2)	2.6941(5)	Ir(1)-Ir(3)	2.7281(6)
Ir(2)-Ir(3)	2.7125(6)	Ir(1)-W(1)	2.8042(6)
Ir(2)-W(1)	2.8485(5)	Ir(3)-W(1)	2.8990(8)
Ir(1)-P(1)	2.230(3)	Ir(2)-P(2)	2.239(3)
Ir(1)-C(1)	2.048(9)	Ir(1)-C(11)	1.830(9)
Ir(1)-C(48)	2.080(8)	Ir(2)-C(1)	2.139(9)
Ir(2)-C(2)	2.157(9)	Ir(2)-C(22)	1.89(1)
Ir(3)-C(31)	1.89(1)	Ir(3)-C(32)	1.909(9)
Ir(3)-C(33)	1.918(9)	W(1)-C(01)	2.276(9)
W(1)-C(02)	2.30(1)	W(1)C-(03)	2.33(1)
W(1)-C(04)	2.29(1)	W(1)-C(05)	2.282(9)
W(1)-C(2)	2.134(9)	W(1)-C(3)	1.978(9)
W(1)-C(48)	2.146(9)		

Table 2.2.6. Selected Bond Angles (°) for $[CpWIr_3(\mu\text{-}CO)_3(CO)_6\{P(OPh)_3\}_2]$ (**17**)

Bond	Angle	Bond	Angle
Ir(2)-Ir(1)-Ir(3)	60.03(1)	Ir(2)-Ir(1)-W(1)	62.37(1)
Ir(3)-Ir(1)-W(1)	63.19(2)	Ir(3)-Ir(2)-W(1)	62.79(2)
Ir(1)-Ir(2)-Ir(3)	60.61(1)	Ir(1)-Ir(2)-W(1)	60.71(1)
Ir(1)-Ir(3)-Ir(2)	59.36(1)	Ir(1)-Ir(3)-W(1)	59.69(1)
Ir(2)-Ir(3)-W(1)	60.90(2)	Ir(1)-W(1)-Ir(2)	56.92(1)
Ir(1)-W(1)-Ir(3)	57.12(1)	Ir(2)-W(1)-Ir(3)	56.31(1)
Ir(2)-Ir(1)-P(1)	139.12(7)	Ir(3)-Ir(1)-P(1)	100.44(7)
W(1)-Ir(1)-P(1)	144.54(7)	Ir(1)-Ir(2)-P(2)	109.38(8)
Ir(3)-Ir(2)-P(2)	167.18(7)	W(1)-Ir(2)-P(2)	105.90(7)

The formation of crystals of **19**, grown from a solution of **34** (see Section *2.2.8.*), revealed that the ditungsten-diiridium cluster framework of **34** slowly decomposes in solution at room temperature to afford the tungsten-triiridium framework of cluster **19**. A structural study of one crystal of **19** at 183 K (crystal modification **19a**) was observed to have a different unit cell and slightly different bond length and angle parameters from that of a structural study of a second crystal of **19** at 298 K (crystal modification **19b**). A unit cell

determination of the second crystal of **19** at 183 K revealed that the cell parameters were temperature invariant and that no structural modifications to the crystals of **19** were occurring on raising or lowering the temperature.

Complex **19** has the pseudotetrahedral framework of the related cluster **2**,[70] and possesses an η^5-cyclopentadienyl group, three bridging carbonyls arranged around a WIr_2 plane, seven terminal carbonyls, and an iridium-ligated trimethylphosphite ligand. The WIr_3 core distances ($W\text{-}Ir_{av}$ = 2.87 Å **19a**, 2.86 Å **19b**; $Ir\text{-}Ir_{av}$ = 2.72 Å **19a**, 2.71 Å **19b**) are slightly longer than those of **2** ($W\text{-}Ir_{av}$ = 2.82 Å; $Ir\text{-}Ir_{av}$ = 2.70 Å [70]); core distances of the related mono-phosphine substituted clusters $[CpWIr_3(\mu\text{-}CO)_3(CO)_7(PPh_3)]$ (**4**), $[CpWIr_3(\mu\text{-}CO)_3(CO)_7(PMe_3)]$ (**7**) and $[CpWIr_3(\mu\text{-}CO)_3(CO)_7(PMe_2Ph)]$ (**10**) are also consistent with core expansion upon introduction of a *P*-donor ligand. The longest W-Ir core distance for **19a** and **19b** is effectively *trans* to the Cp group. Ir-CO(terminal) interactions [1.87(1) - 1.94(2) Å **19a**; 1.86(1) - 1.93(2) Å **19b**] and W-CO(terminal) interactions [1.98(1) Å **19a**, 1.97(1) Å **19b**] are unexceptional. The Ir-P distances [2.251(3) Å **19a**, 2.247(3) Å **4b**] are comparable to those of **17** [2.230(3), 2.239(3)] and slightly shorter than those in the phosphine-substituted tungsten-triiridium clusters **4**, **5**, **7** and **10** [2.312(7) - 2.34(1) Å]. Intraphosphite bond lengths and angles are not unusual. The diaxial disposition of ligands in **19a** and **19b** has not been structurally identified previously in the tungsten-iridium cluster system. Formal electron counting reveals that the clusters **17**, **19a** and **19b** have 60 e, electron precise for tetrahedral clusters.

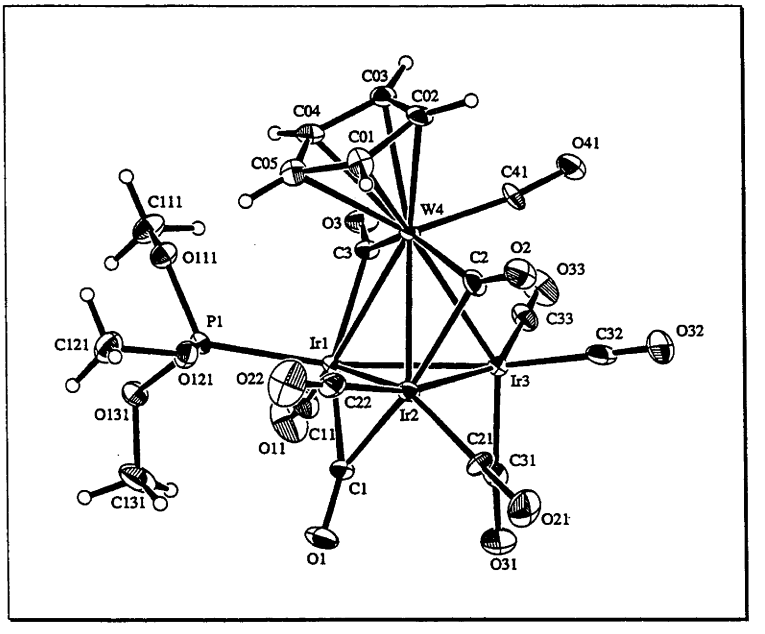


Figure 2.2.7. Molecular structure and atomic labelling scheme for $[CpWIr_3(\mu\text{-}CO)_3(CO)_7\{P(OMe)_3\}]$, (**19**). Thermal envelopes of 50 % probability are shown for the non-hydrogen atoms; hydrogen atoms have arbitrary radii of 0.1 Å.

(By David C. R. Hockless)

The diaxial coordination geometry of **19** is favourable only because of the small cone angle of the $P(OMe)_3$ ligand. Diaxial coordination geometries are unusual in the homometallic system, with $[Ir_4(H)_2(\mu\text{-}CO)_3(CO)_7]^{2-}$,[35] $[Ir_4(\mu\text{-}CO)_3(CO)_7(\overline{COCH_2CH_2O})_2]$,[5] and $[Ir_4(\mu\text{-}CO)_3(CO)_7(CH_2CO_2Me)_2]^{2-}$,[15] crystallographically confirmed in the "parent" tetrairidium system and $[Co_4(\mu\text{-}CO)_3(CO)_7\{P(OMe)_3\}_2]$ [71] structurally characterized in the related tetracobalt system (in each case, the cone angle of the entering ligand is small). Amongst heterometallic clusters, diaxial coordination geometries have been crystallographically confirmed for $[FeCo_3(\mu_3\text{-}H)(\mu\text{-}CO)_3(CO)_7(PPh_3)_2]$, [72] $[RuCo_3(\mu_3\text{-}H)(\mu\text{-}CO)_3(CO)_7(PPh_3)_2]$,[73] $[RuRh_3(\mu_3\text{-}H)(\mu\text{-}CO)_3(CO)_7(PPh_3)_2]$,[73] and $[RuCoRh_2(\mu_3\text{-}H)(\mu\text{-}CO)_3(CO)_7(PPh_3)_2]$,[74] but in all cases a face-capping hydride lies below the basal plane; this has been reported to cause the radial carbonyls to be displaced towards the apical metal, providing more room for the incoming ligand to occupy the axial sites.

Table 2.2.7. Selected Bond Lengths (Å) for $[CpWIr_3(\mu\text{-}CO)_3(CO)_7\{P(OMe)_3\}]$ (**19**)

Bond	**19a**	**19b**
Ir(1)-Ir(2)	2.6885(8)	2.7005(9)
Ir(1)-Ir(3)	2.7453(7)	2.7196(6)
Ir(2)-Ir(3)	2.7148(8)	2.717(1)
Ir(1)-W(1/4)	2.8640(7)	2.8699(6)
Ir(2)-W(1/4)	2.8470(7)	2.8167(6)
Ir(3)-W(1/4)	2.9043(8)	2.9020(7)
Ir(1)-P(1)	2.251(3)	2.247(3)
Ir(1)-C(1)	2.08(1)	2.10(1)
Ir(1)-C(3)	2.13(1)	2.10(1)
Ir(1)-C(11)	1.87(1)	1.86(1)
Ir(2)-C(1)	2.12(1)	2.14(1)
Ir(2)-C(2)	2.19(1)	2.22(1)
Ir(2)-C(21)	1.90(1)	1.88(2)
Ir(2)-C(22)	1.90(2)	1.88(1)
Ir(3)-C(31)	1.87(2)	1.89(2)
Ir(3)-C(32)	1.94(2)	1.93(2)
Ir(3)-C(33)	1.94(2)	1.91(1)
W(1/4)-C(01)	2.31(1)	2.33(1)
W(1/4)-C(02)	2.27(1)	2.32(1)
W(1/4)-C(03)	2.33(1)	2.30(1)
W(1/4)-C(04)	2.32(1)	2.31(1)
W(1/4)-C(05)	2.36(1)	2.33(1)
W(1/4)-C(2)	2.11(1)	2.13(1)
W(1/4)-C(3)	2.15(1)	2.14(1)
W(1/4)-C(41)	1.98(1)	1.97(1)

Table 2.2.8. Selected Bond Angles (°) for $[CpWIr_3(\mu\text{-}CO)_3(CO)_7\{P(OMe)_3\}]$ (**19**)

Angle	19a	19b
Ir(2)-Ir(1)-Ir(3)	59.94(2)	60.16(2)
Ir(2)-Ir(1)-W(1/4)	61.60(2)	60.66(2)
Ir(3)-Ir(1)-W(1/4)	62.32(2)	62.49(2)
Ir(3)-Ir(2)-W(1/4)	62.91(2)	63.23(2)
Ir(1)-Ir(2)-Ir(3)	61.07(2)	60.27(3)
Ir(1)-Ir(2)-W(1/4)	62.23(2)	62.65(2)
Ir(1)-Ir(3)-Ir(2)	58.99(2)	59.57(2)
Ir(1)-Ir(3)-W(1/4)	60.84(2)	61.29(2)
Ir(2)-Ir(3)-W(1/4)	60.77(2)	60.07(2)
Ir(1)-W(1/4)-Ir(2)	56.17(2)	56.70(2)
Ir(1)-W(1/4)-Ir(3)	56.84(2)	56.22(2)
Ir(2)-W(1/4)-Ir(3)	56.32(2)	56.70(2)
Ir(2)-Ir(1)-P(1)	106.34(9)	109.12(8)
Ir(3)-Ir(1)-P(1)	162.55(9)	166.20(8)
W(1/4)-Ir(1)-P(1)	102.41(8)	105.29(8)

2.2.4. Reaction of $[CpWIr_3(CO)_{11}]$ (2) with 1,2-bis(diphenylphosphino)benzene

The reaction of $[CpWIr_3(CO)_{11}]$ (**2**) with the bidentate phosphine 1,2-bis(diphenylphosphino)benzene (pdpp) proceeded in dichloromethane at room temperature to afford the cluster $[CpWIr_3(\mu\text{-}CO)_3(\mu\text{-pdpp})(CO)_6]$ (**22**) as the sole reaction product in excellent yield (75 %). The cluster was characterized by a combination of IR, ^1H and ^{31}P NMR spectroscopies, mass spectrometry and satisfactory microanalyses. The infrared spectrum suggests the presence of edge-bridging carbonyl ligands. The ^1H NMR spectrum contains signals assigned to Cp and Ph groups in the appropriate ratio. The FAB mass spectrum contains a molecular ion followed by sequential loss of eight carbonyls. The above data are consistent with the formulation above; it is likely that the complex adopts an analogous structure to those of the crystallographically verified clusters $[CpWIr_3(\mu\text{-}CO)_3(\mu\text{-L})(CO)_6]$ (L = dppm, dppe, dppa[69]), i.e. a diaxially ligated bidentate diphosphine and apically-situated cyclopentadienyl ligand.

2.2.5. Attempted reaction of $[CpWIr_3(CO)_{11}]$ (2) with $[Fe(\eta^5\text{-}C_5H_5)(\eta^5\text{-}P_3C_2Bu^t_2)]$

Reaction of $[Ir_4(CO)_{11}Br]^-$ with a stoichiometric amount of the phosphole complex $[Fe(\eta^5\text{-}C_5H_5)(\eta^5\text{-}P_3C_2Bu^t_2]$ was reported to afford the cluster $[Ir_4(CO)_{11}(\eta^1\text{-}[Fe(\eta^5\text{-}C_5H_5)(\eta^5\text{-}$

$P_3C_2Bu^t_2]$)].[6] Similar attempts at reacting $[CpWIr_3(CO)_{11}]$ (**2**) with the phosphole complex at room temperature were unsuccessful; heating **2** and the phosphole complex in refluxing thf caused decomposition of the cluster, and no reaction was observed under more mild conditions.

2.2.6. Reaction of [CpWIr$_3$(CO)$_{11}$] (2) with XyNC or ^{t}BuNC

The reactions of $[CpWIr_3(CO)_{11}]$ (**2**) with *n* equivalents of 2,6-dimethylphenylisocyanide (CNXy) or *t*-butylisocyanide proceeded in dichloromethane at room temperature to afford the clusters $[CpWIr_3(CO)_{11-n}(CNXy)_n]$ [*n* = 1 (**23**), 2 (**24**) or 3 (**25**)] or $[CpWIr_3(CO)_{11-n}(CNBu^t)_n]$ [*n* = 1 (**26**), 2 (**27**) or 3 (**28**)], respectively, as the major or sole reaction products in good to excellent yields (47 - 63 %). The clusters **23 - 28** have been characterized by a combination of IR, ^1H and ^{13}C NMR (for **5 - 7**) spectroscopies, mass spectrometry and satisfactory microanalyses. Infrared spectra suggest the presence of edge-bridging carbonyl ligands in the more highly substituted clusters, **24**, **25**, **27** and **28** [υ(CO) 1898-1816 cm^{-1}]. In combination with the X-ray structural results detailed below, the number of bands in the terminal carbonyl ligand υ(CO) regions of the IR spectra of **24 - 25** and **27 - 28** are indicative of the presence of isomers. Complexes **23** and **26** have infrared absorptions arising from terminal carbonyls only, suggesting a ligand disposition similar to the precursor **2**. The ^1H NMR spectra contain signals assigned to cyclopentadienyl, phenyl and methyl groups for **23 - 25** and cyclopentadienyl and methyl groups for **26 - 28**, in the appropriate ratios. The mass spectra of all complexes contain molecular ions, and all spectra contain fragment ions corresponding to stepwise loss of carbonyls; in all cases the base peak is $[M-3CO]^+$. Isotope patterns are consistent with the presence of three iridium atoms and one tungsten atom.

The molecular structure of **24** as determined by a single-crystal X-ray study is consistent with the formulation given above and defines the substitution sites of the isocyanides. Selected bond distances are listed in Table 2.2.9. and selected bond angles in Table 2.2.10. An ORTEP plot showing the molecular geometry and atomic numbering scheme is shown in Figure 2.2.8. Complex **24** has the WIr_3 pseudotetrahedral framework of the precursor cluster **2** and possesses an η^5-cyclopentadienyl group, nine terminal carbonyl ligands, and two iridium-ligated 2,6-dimethylphenylisocyanide ligands. The WIr_3 core distances [W-Ir 2.781(1), 2.8282(9), 2.8502(1); Ir-Ir 2.682(1), 2.695(1), 2.7229(8) Å] are similar to those of **2** [W-Ir 2.7920(10), 2.8151(10), 2.8648(10); Ir-Ir 2.6967(9), 2.6985(10), 2.7018(9) Å]. The longest W-Ir distance for **24** is effectively *trans* to the Cp group. Ir-CO(terminal) [1.88(2) - 1.94(2) Å] and W-CO interactions [1.96(1), 1.98(2) Å] for **24** are unexceptional. The Ir-CN [1.96(2), 2.01(1)], IrC-N [1.13(2), 1.14(2)] and N-C(aryl) [1.39(2), 1.40(2) Å] distances and Ir-C-N [174(1), 176(1)°] and C-N-C(aryl) [174(2), 168(2)°] angles are consistent with the expected valence bond structure [Ir-C≡N-Xy]. The

Ir-CN linkages are (on average) longer than the Ir-CO distances, consistent with the enhanced Ir→CO π^* backbonding of the carbonyl ligand. Ir(1) is in a unique environment, being linked to one terminal carbonyl ligand and two terminal 2,6-dimethylphenylisocyanide ligands. The isocyanide ligands are *trans* to Ir-Ir linkages, and the unique carbonyl ligand at Ir(1) is *trans* to the W-Ir linkage. This site selection may be determined by the nature of the *trans*-disposed ligand; the isocyanides are *trans* to CO groups, and the CO ligand is *trans* to the Cp ligand, both of which should maximize back-bonding to the carbonyls, and consistent with the site selection being driven by electronic considerations. It is perhaps surprising that both isocyanides ligate the same iridium. Although steric considerations may disfavour coordination at the site occupied by CO(21) and CO(31), it is not clear why coordination at CO(22) and CO(33) does not proceed.

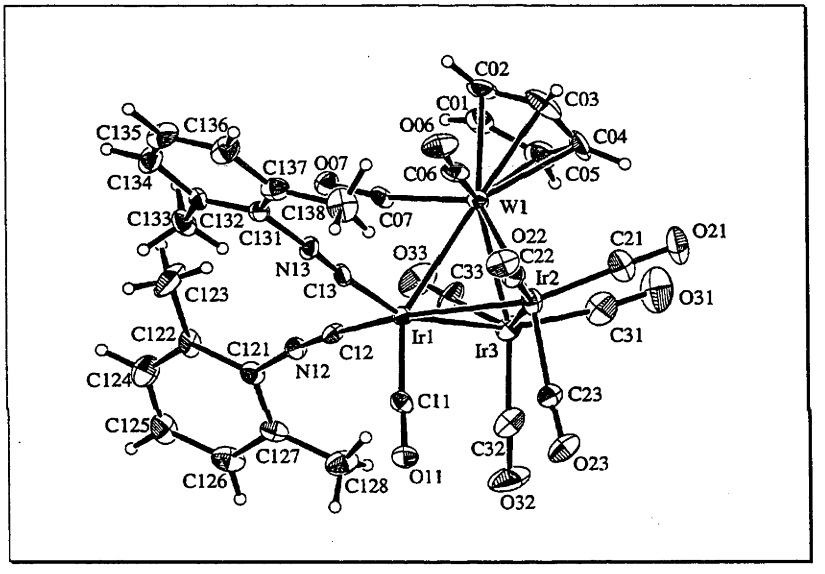


Figure 2.2.8. Molecular structure and atomic labelling scheme for $[CpWIr_3(CO)_9(CNXy)_2]$, (**24**). Thermal envelopes of 50 % probability are shown for the non-hydrogen atoms; hydrogen atoms have arbitrary radii of 0.1 Å.

(By David C. R. Hockless)

Table 2.2.9. Selected Bond Lengths (Å) for $[CpWIr_3(CO)_9(CNXy)_2]$

Bond	Distance	Bond	Distance
Ir(1)-Ir(2)	2.7229(8)	Ir(1)-Ir(3)	2.682(1)
Ir(2)-Ir(3)	2.695(1)	Ir(1)-W(1)	2.8502(8)
Ir(2)-W(1)	2.8282(9)	Ir(3)-W(1)	2.781(1)
Ir(1)-C(11)	1.86(2)	Ir(1)-C(12)	1.96(2)
Ir(1)-C(13)	2.01(1)	Ir(2)-C(21)	1.88(2)
Ir(2)-C(22)	1.90(2)	Ir(2)-C(23)	1.94(2)
Ir(3)-C(31)	1.89(2)	Ir(3)-C(32)	1.91(2)
Ir(3)-C(33)	1.95(2)	W(1)-C(01)	2.36(2)
W(1)-C(02)	2.26(2)	W(1)-C(03)	2.31(2)
W(1)-C(04)	2.36(2)	W(1)-C(05)	2.35(2)
W(1)-C(06)	1.98(2)	W(1)-C(07)	1.94(1)

Table 2.2.10. Selected Bond Angles (°) for $[CpWIr_3(CO)_9(CNXy)_2]$

Bond	Angle	Bond	Angle
Ir(2)-Ir(1)-Ir(3)	59.81(2)	Ir(2)-Ir(1)-W(1)	60.94(2)
Ir(3)-Ir(1)-W(1)	60.27(3)	Ir(1)-Ir(2)-Ir(3)	59.35(2)
Ir(1)-Ir(2)-W(1)	61.75(2)	Ir(3)-Ir(2)-W(1)	60.42(3)
Ir(1)-Ir(3)-Ir(2)	60.84(2)	Ir(1)-Ir(3)-W(1)	62.86(3)
Ir(2)-Ir(3)-W(1)	62.16(3)	Ir(1)-W(1)-Ir(2)	57.31(2)
Ir(1)-W(1)-Ir(3)	56.87(2)	Ir(2)-W(1)-Ir(3)	57.42(2)
Ir(2)-Ir(1)-C(11)	89.6(5)	Ir(3)-Ir(1)-C(11)	97.3(4)
W(1)-Ir(1)-C(11)	148.8(4)	Ir(2)-Ir(1)-C(12)	155.4(4)
Ir(2)-Ir(1)-C(13)	105.2(4)	Ir(3)-Ir(1)-C(12)	95.6(4)
Ir(3)-Ir(1)-C(13)	158.2(4)	W(1)-Ir(1)-C(12)	109.4(4)
W(1)-Ir(1)-C(13)	99.2(4)	C(11)-Ir(1)-C(12)	93.2(6)
C(11)-Ir(1)-C(13)	93.8(6)	C(12)-Ir(1)-C(13)	98.5(6)
Ir(1)-C(11)-O(11)	177(1)	Ir(1)-C(12)-N(12)	174(1)
Ir(1)-C(13)-N(13)	176(1)		

Stuntz and Shapley have examined isocyanide substitution at $[Ir_4(CO)_{12}]$ (**1**).[9] Introduction of Bu^tNC into the tetrairidium cluster necessitates significantly more forcing conditions (refluxing chlorobenzene or prior activation with $Me_3NO.2H_2O$) than are

required to effect substitution at $[CpWIr_3(CO)_{11}]$ (**2**); a similar rate enhancement was noted for phosphine substitution in proceeding from the homometallic to the heterometallic system. IR and ^{13}C NMR spectra for $[Ir_4(CO)_{12-n}(CNR)_n]$ are consistent with isomers with terminal carbonyls only for n = 1 or 2, and isomers possessing bridging carbonyls for n = 3 or 4. A similar result is apparent for the tungsten-triiridium derivatives if the Cp group is considered as the first incoming ligand. Low temperature limiting spectra were achievable for the tetrairidium system at 183 K, but could not be obtained for the mixed-metal derivatives to 143 K (Chapter 3), consistent with significantly enhanced fluxionality from the homometallic to the heterometallic system. The structural study of $[Ir_4(CO)_{11}(CNBu^t)]$ revealed a derivative with no bridging carbonyl ligands, as expected from the solution spectral data.[3] The structural study of $[CpWIr_3(CO)_9(CNXy)_2]$ (**24**) similarly revealed an isomeric form with no bridging carbonyls, although the spectral data for this derivative indicate that other isomers with bridging carbonyls are also present in solution.

Cluster **24** was the first structurally characterized tetrahedral cluster with two terminal isocyanide groups ligated to the same metal vertex, although a precedent exists in trinuclear cluster chemistry: a structural characterization of the triangular $[Fe_3(\mu\text{-}CO)_2(CO)_8(CNBu^t)_2]$ reveals a related ligand disposition to **24** [75], with two Bu^tNC ligated to the same iron vertex, but with two bridging carbonyls ligating the Fe-Fe bond opposite the bis(isocyanide)-ligated iron vertex (Figure 2.2.9.).

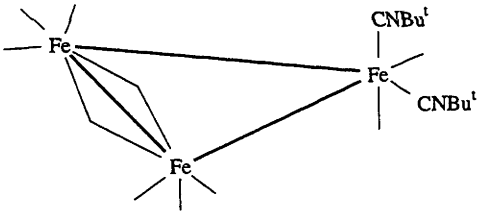


Figure 2.2.9. $[Fe_3(\mu\text{-}CO)_2(CO)_8(CNBu^t)_2]$

2.2.7. Reaction of $[Cp_2W_2Ir_2(CO)_{10}]$ (3) with PPh_3 or PMe_3

The reactions of $[Cp_2W_2Ir_2(CO)_{10}]$ (**3**) with n equivalents of PPh_3 or PMe_3 (n = 1, 2) proceeded in dichloromethane at room temperature to afford the clusters $[Cp_2W_2Ir_2(\mu\text{-}CO)_3(CO)_{7-n}(PPh_3)_n]$ [n = 1 (**29**) or 2 (**30**)] or $Cp_2W_2Ir_2(\mu\text{-}CO)_3(CO)_{7-n}(PMe_3)_n$ [n = 1 (**31**) or 2 (**32**)], respectively, as the major or sole reaction products in good to excellent yields (38 - 63 %). The bis-triphenylphosphine substituted product $Cp_2W_2Ir_2(\mu\text{-}CO)_3(CO)_5(PPh_3)_2$ (**30**) was found to be unstable above 273 K; work-up of reaction between **3** and two equivalents of PPh_3 revealed that decomposition of **30** occurred on the thin-layer chromatographic plate to afford **29**, but a swift work-up afforded sufficient **30** to permit spectroscopic characterization. The products were characterized by a

combination of IR, ^{1}H, ^{13}C and ^{31}P NMR spectroscopies and mass spectrometry, and satisfactory microanalyses for the mono-phosphine clusters. Infrared spectra suggest the presence of edge-bridging carbonyl ligands in all complexes [υ(CO) 1840 - 1803 cm^{-1}], which contrasts with the all-terminal geometry of the precursor **3**. In combination with the X-ray structural results detailed below, the numbers of bands in the terminal carbonyl ligand υ(CO) regions of the IR spectra are indicative of the presence of isomers. The ^{1}H NMR spectra contain signals assigned to cyclopentadienyl and phenyl groups for **29** and **30** and cyclopentadienyl and methyl groups for **31** and **32**, in the appropriate ratios. Discussion of the ^{13}C and ^{31}P NMR spectra is deferred until Chapter 3. The mass spectra of the complexes **31** and **32** contain molecular ions and all complexes contain fragment ions corresponding to stepwise loss of carbonyls; isotope patterns are consistent with the presence of two iridium atoms and two tungsten atoms.

The molecular structure of **29** as determined by a single-crystal X-ray study is consistent with the formulation given above and defines the substitution site of the phosphine. A summary of crystal and refinement data is shown in Table 2.2.11., and selected bond distances and angles are listed in Table 2.2.12. Figure 2.2.10. contains an ORTEP plot showing the molecular geometry and atomic numbering scheme.

Complex **29** has the pseudotetrahedral framework of the precursor cluster **3**.[76] Each tungsten atom bears one η^5-cyclopentadienyl group and three bridging carbonyls span a WIr_2 face. Six terminal carbonyl ligands and an iridium-ligated triphenylphosphine ligand complete the coordination sphere. The W_2Ir_2 core distances [W-Ir_{av} 2.866, W-W 3.0604(6), Ir-Ir 2.7348(6) Å] are all slightly longer than those of **3** [W-Ir_{av} 2.835, W-W 2.991(1), Ir-Ir 2.722(1) Å]; core distances of the related mono(phosphine)-substituted tungsten-triiridium clusters [$CpWIr_3(\mu\text{-}CO)_3(CO)_7(L)$] (L = PPh_3, PMe_3, PMe_2Ph) compared to the precursor [$CpWIr_3(CO)_{11}$] are also consistent with core expansion upon introduction of *P*-donor ligands. Intracore bond angles are all close to 60° as expected. As was observed with **3**, angles centred at iridium for **29** are slightly larger [60.01(2) - 64.78(2)°] than those centred at tungsten [56.66(1) - 59.08(1)°]. The Ir-P distance [2.3483(3) Å] and intraphosphine bond lengths and angles are not unusual. With respect to the plane of bridging carbonyls, PPh_3 occupies an axial coordination site with the cyclopentadienyl groups in axial and apical positions. Formal electron counting reveals that **2** has 60 e, electron precise for a tetrahedral cluster.

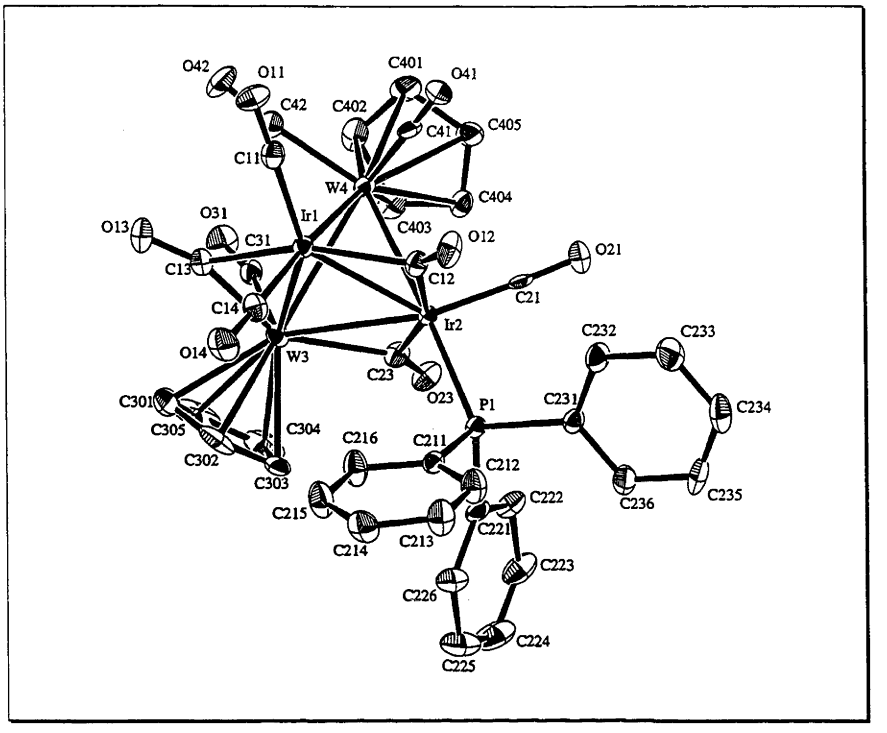


Figure 2.2.10. Molecular structure and atomic labelling scheme for $[Cp_2W_2Ir_2(\mu\text{-}CO)_3(CO)_6(PPh_3)]$, (**29**). Thermal envelopes of 50 % probability are shown for the non-hydrogen atoms; hydrogen atoms have arbitrary radii of 0.1 Å.

(By David C. R. Hockless)

Table 2.2.11. Selected Bond Lengths (Å) for $[Cp_2W_2Ir_2(\mu\text{-}CO)_3(CO)_6(PPh_3)]$ (**29**)

Bond	Length	Bond	Length
Ir(1)-Ir(2)	2.7348(6)	Ir(1)-W(3)	2.8294(7)
Ir(1)-W(4)	2.8833(6)	Ir(2)-W(3)	2.823(1)
Ir(2)-W(1)	2.838(1)	Ir(2)-W(3)	2.9146(6)
Ir(2)-W(4)	2.831(6)	W(3)-W(4)	3.0604(6)
Ir(2)-P(1)	2.348(3)	Ir(1)-C(11)	1.88(1)
Ir(1)-C(12)	2.13(1)	Ir(1)-C(13)	2.25(1)
Ir(2)-C(21)	1.83(1)	Ir(2)-C(23)	2.11(1)
W(3)-C(31)	1.94(1)	W(3)-C(301)	2.29(1)
W(3)-C(302)	2.32(1)	W(3)-C(303)	2.30(1)
W(3)-C(304)	2.28(1)	W(3)-C(305)	2.30(1)
W(4)-C(41)	1.98(1)	W(4)-C(42)	1.98(1)
W(4)-C(401)	2.28(1)	W(4)-C(402)	2.31(1)
W(4)-C(403)	2.37(1)	W(4)-C(404)	2.39(1)
W(4)-C(405)	2.31(1)		

Table 2.2.12. Selected Bond Angles (°) for $[Cp_2W_2Ir_2(\mu\text{-}CO)_3(CO)_6(PPh_3)]$ (**29**)

Bond	Angle	Bond	Angle
Ir(2)-Ir(1)-W(3)	63.15(1)	Ir(2)-Ir(1)-W(4)	60.62(1)
W(3)-Ir(1)-W(4)	64.78(2)	Ir(1)-Ir(2)-W(3)	60.01(2)
Ir(1)-Ir(2)-W(4)	62.28(1)	W(3)-Ir(2)-W(4)	64.26(1)
Ir(1)-W(3)-Ir(2)	56.84(2)	Ir(1)-W(3)-W(4)	58.46(1)
Ir(2)-W(3)-W(4)	56.66(1)	Ir(1)-W(4)-Ir(2)	57.10(1)
Ir(1)-W(4)-W(3)	56.76(1)	Ir(2)-W(4)-W(3)	59.08(1)
Ir(1)-Ir(2)-P(1)	118.74(7)	W(3)-Ir(2)-P(1)	113.01(6)
W(4)-Ir(2)-P(1)	176.49(6)		

2.2.8. *Reaction of $[Cp_2W_2Ir_2(CO)_{10}]$ (3) with $P(OMe)_3$*

The reactions of $[Cp_2W_2Ir_2(CO)_{10}]$ (**3**) with n equivalents of $P(OMe)_3$ (n = 1 or 2) proceed in dichloromethane at room temperature to afford the clusters $[Cp_2W_2Ir_2(\mu\text{-}CO)_3(CO)_{7-n}\{P(OMe)_3\}_n]$ [n = 1, (**33**); n = 2, (**34**)] as the major or sole reaction products in excellent yields (54 - 76 %). The products have been characterized by a combination of IR, ^1H, ^{13}C and ^{31}P NMR spectroscopies, MS and satisfactory microanalyses. Infrared spectra suggest the presence of edge-bridging carbonyl ligands in both complexes [υ(CO) 1869 - 1807 cm^{-1}], in contrast to the all-terminal precursor **3**. The number of bands in the carbonyl ligand υ(CO) region for clusters **33** and **34** are consistent with the presence of one configuration only for each cluster, in contrast to most of the previously studied ligand-substituted tungsten-iridium clusters which have IR spectra suggestive of more than one configuration in solution (Sections *2.2.1.* - *2.2.7.*). The ^1H NMR spectra contain signals assigned to Cp and Me groups in the expected ratios. The FAB mass spectra of the complexes do not contain molecular ions; instead, $[M\text{-}2CO]^+$ is the largest fragment observed. These ions fragment by stepwise loss of carbonyls, with particularly intense $[M\text{-}3CO]^+$ ions. The isotope patterns are consistent with the presence of two iridium atoms and two tungsten atoms.

Crystallization of a dichloromethane / octane solution of **34** by slow evaporation afforded three different types of crystals suitable for X-ray diffraction studies which are separable by hand. An X-ray study of the red, prismatic crystals confirmed the molecular composition of **34**. Two single-crystal X-ray studies of pale orange, plate-like crystals revealed that **34** slowly decomposes in solution to afford $[CpWIr_3(\mu\text{-}CO)_3(CO)_7\{P(OMe)_3\}]$ (**19**).

The single-crystal X-ray study of **34** is consistent with the formulation given above, defines the substitution sites of the phosphites and the η^5-cyclopentadienyl ligands, and aids interpretation of the ^{13}C and ^{31}P NMR spectra (Chapter 3). Selected bond lengths and angles are shown in Tables 2.2.13. and 2.2.14., respectively. Figure 2.2.11. contains an ORTEP plot of **3** showing the molecular geometry and atomic numbering scheme.

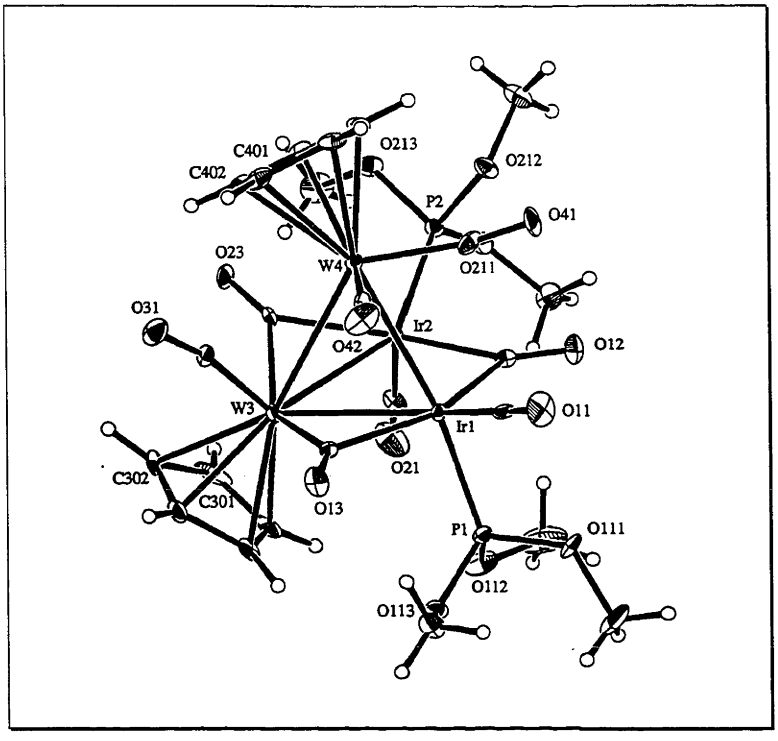


Figure 2.2.11. Molecular structure and atomic labelling scheme for $[Cp_2W_2Ir_2(\mu\text{-}CO)_3(CO)_5\{P(OMe)_3\}_2]$, (**34**). Thermal envelopes of 50 % probability are shown for the non-hydrogen atoms; hydrogen atoms have arbitrary radii of 0.1 Å.

(By David C. R. Hockless)

Table 2.2.13. Selected Bond Lengths (Å) for $[Cp_2W_2Ir_2(\mu\text{-}CO)_3(CO)_5\{P(OMe)_3\}_2]$, (**34**)

Bond	Length	Bond	Length
Ir(1)-Ir(2)	2.7108(8)	Ir(1)-W(3)	2.8722(9)
Ir(1)-W(4)	2.8885(9)	Ir(2)-W(3)	2.8167(8)
Ir(2)-W(4)	2.8607(8)	W(3)-W(4)	3.0702(9)
Ir(1)-P(1)	2.241(4)	Ir(2)-P(2)	2.250(4)
Ir(1)-C(11)	1.90(2)	Ir(1)-C(12)	2.11(1)
Ir(1)-C(13)	2.16(1)	Ir(2)-C(12)	2.06(2)
Ir(2)-C(21)	1.85(2)	Ir(2)-C(23)	2.12(2)
W(3)-C(13)	2.11(2)	W(3)-C(23)	2.13(2)
W(3)-C(31)	1.93(2)	W(3)-C(301)	2.32(2)
W(3)-C(302)	2.30(2)	W(3)-C(303)	2.30(1)
W(3)-C(304)	2.32(1)	W(3)-C(305)	2.34(1)
W(4)-C(41)	1.98(2)	W(4)-C(42)	2.02(2)
W(4)-C(401)	2.30(1)	W(4)-C(402)	2.35(2)
W(4)-C(403)	2.36(2)	W(4)-C(404)	2.31(1)
W(4)-C(405)	2.28(1)		

Table 2.2.14. Selected Bond Angles (°) for $[Cp_2W_2Ir_2(\mu\text{-}CO)_3(CO)_5\{P(OMe)_3\}_2]$, (**34**)

Bond	Angle	Bond	Angle
Ir(2)-Ir(1)-W(3)	60.52(2)	Ir(2)-Ir(1)-W(4)	61.35(2)
W(3)-Ir(1)-W(4)	64.41(2)	Ir(1)-Ir(2)-W(3)	62.58(2)
Ir(1)-Ir(2)-W(4)	62.39(2)	W(3)-Ir(2)-W(4)	65.47(2)
Ir(1)-W(3)-Ir(2)	56.90(2)	Ir(1)-W(3)-W(4)	58.05(2)
Ir(2)-W(3)-W(4)	57.96(2)	Ir(1)-W(4)-Ir(2)	56.26(2)
Ir(1)-W(4)-W(3)	57.54(2)	Ir(2)-W(4)-W(3)	56.57(2)
Ir(2)-Ir(1)-P(1)	108.6(1)	W(3)-Ir(1)-P(1)	103.8(1)
W(4)-Ir(1)-P(1)	166.9(1)	Ir(1)-Ir(2)-P(2)	137.6(1)
W(3)-Ir(2)-P(2)	148.1(1)	W(4)-Ir(2)-P(2)	99.7(1)

Complex **34** has the pseudotetrahedral framework of the precursor cluster **3**. Each tungsten atom bears one η^5-cyclopentadienyl group; three bridging carbonyls span a WIr_2 face, and five terminal carbonyl ligands and two iridium-ligated trimethylphosphite ligands complete the coordination sphere. The W_2Ir_2 core distances [$W\text{-}Ir_{av}$ = 2.86 Å, W-W = 3.0702(9) Å]

are slightly longer than those of **3** [76] [W-Ir_{av} 2.835, W-W 2.991(1)] while the Ir-Ir distance [2.7108(8) Å for **34** compared with 2.722(1) Å for **3**] is marginally shorter, consistent with a core expansion on introduction of phosphite; core distances of the related mono(phosphine)-substituted cluster $[Cp_2W_2Ir_2(\mu\text{-}CO)_3(CO)_6(PPh_3)]$ (**29**) are also consistent with core expansion upon introduction of a *P*-donor ligand. The longest W-Ir core distance for **34** is effectively *trans* to both the apical Cp group and the axially ligating $P(OMe)_3$. Ir-CO(terminal) interactions for **34** [1.85(2), 1.90(2) Å] and Ir-C-O(terminal) angles [176(2), 177(2) °] are unexceptional. Intracore bond angles are all close to 60° as expected. As was observed with **3**, and the related **29**, angles centred at iridium for **34** [60.52(2) - 65.47(2)°] are slightly larger than those centred at tungsten [56.90(2) - 58.05(2)°]. The Ir-P distances [2.250(4), 2.241(4) Å] are, as expected, slightly shorter than those in the **29** [2.348(3) Å]. Intraphosphite bond lengths and angles are not unusual. With respect to the plane of bridging carbonyls, the $P(OMe)_3$ ligands occupy radial and axial coordination sites with the cyclopentadienyl groups in axial and apical positions. This radial, diaxial, apical disposition of ligands in **34** has not been structurally identified previously with tungsten-iridium clusters, but is the tetra-substituted configuration which is predicted to be of lowest energy on steric grounds (the apical ligand is inclined to the face containing the two axial ligands).

The formation of crystals of **19**, grown from a solution of **34**, reveals that the ditungsten-diiridium cluster framework of **34** slowly decomposes in solution at room temperature to afford the tungsten-triiridium framework of cluster **19**. This work has afforded an unusual instance of two crystal modifications of a cluster from the same solvent mixture. The single-crystal X-ray studies of **19a** and **19b** confirm that the decomposition product of **34** was in fact the cluster $[CpWIr_3(\mu\text{-}CO)_3(CO)_7\{P(OMe)_3\}]$ (**19**) [prepared in Section *2.2.3.* by reaction of $[CpWIr_3(CO)_{11}]$ with one equivalent of $P(OMe)_3$]. The structural study for **19** is described in Section *2.2.3.*

2.2.9. Reaction of $[Cp_2W_2Ir_2(CO)_{10}]$ (3) with dppm or dppe

The reactions of $[Cp_2W_2Ir_2(CO)_{10}]$ (**3**) with dppm or dppe proceeded rapidly in dichloromethane at room temperature to afford the clusters $[Cp_2W_2Ir_2(\mu\text{-dppm})(\mu\text{-}CO)_3(CO)_5]$ (**35**) and $[Cp_2W_2Ir_2(\mu\text{-dppe})(\mu\text{-}CO)_3(CO)_5]$ (**36**), respectively, as the major reaction products in excellent yields (76 % and 80 %, respectively). The products were characterized by a combination of IR, ^1H, ^{13}C and ^{31}P NMR spectroscopies, mass spectrometry and satisfactory microanalyses. Infrared spectra suggest the presence of edge-bridging carbonyl ligands in both complexes [υ(CO) 1859-1870 cm^{-1}], which contrasts with the all-terminal geometry of the precursor **3**. In combination with the X-ray structural results detailed below, the number of bands in the terminal carbonyl ligand υ(CO) regions of the IR spectra is indicative of the presence of isomers. The ^1H NMR

spectra contain signals assigned to cyclopentadienyl, phenyl and methylene groups for **35** and **36** in the appropriate ratios. Discussion of the ^{13}C and ^{31}P NMR spectra is deferred until the solid state structure is presented (see below). The mass spectra of the complexes contain molecular ions and fragment ions corresponding to stepwise loss of carbonyls; isotope patterns are consistent with the presence of two iridium atoms and two tungsten atoms.

The molecular structure of **35** as determined by a single-crystal X-ray study is consistent with the formulation given above and defines the substitution sites of the diphosphine and coordination sites of the other ligands. An ORTEP plot showing the molecular geometry and atomic numbering scheme is shown in Figure 2.2.12. It was not possible to satisfactorily conclude the structural determination. The study, however, is sufficient to define the atom connectivity and spatial disposition of the constituent atoms.

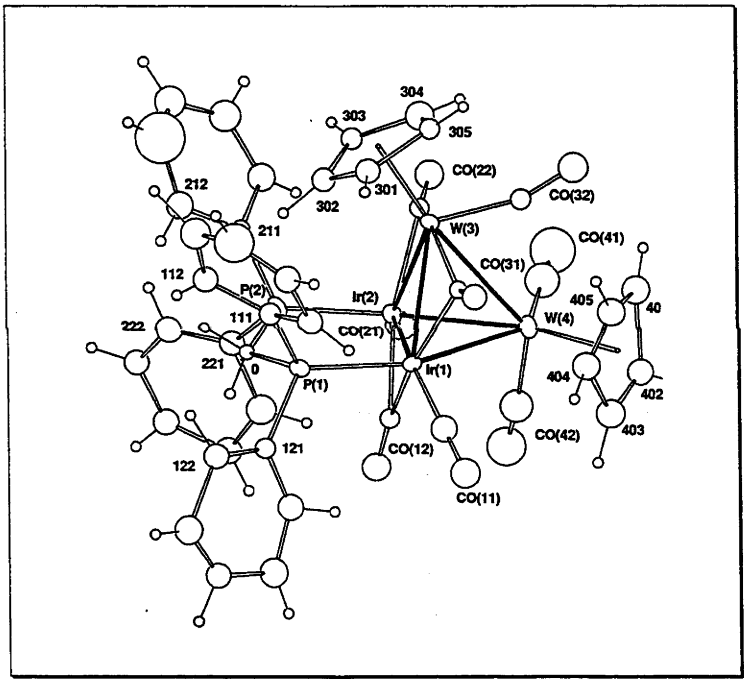


Figure 2.2.12. Molecular structure and atomic labelling scheme for $[Cp_2W_2Ir_2(\mu\text{-}CO)_3(\mu\text{-}dppm)(CO)_5]$, (**35**). Thermal envelopes of 20 % probability are shown for the non-hydrogen atoms; hydrogen atoms have arbitrary radii of 0.1 Å.

(By Brian W. Skelton and Allan H. White)

Complex **35** has the W_2Ir_2 pseudotetrahedral framework of the precursor cluster **1** and possesses three bridging carbonyls arranged about the basal WIr_2 plane, five terminal carbonyl ligands, two η^5-cyclopentadienyl groups (one of which is axially-ligated and the other of which is apically-coordinated) and a diaxially-coordinated dppm ligand spanning an iridium-iridium vector. While no comment on bond length or angle parameters is

possible, the structural study is Selected in facilitating interpretation of the NMR data (see Chapter 3). Formal electron counting reveals that **35** has 60 e, electron precise for a tetrahedral cluster.

2.3. Conclusions

The substitution chemistry of the tetrahedral homometallic cluster **1** has been extensively investigated in previous work. The analogous chemistry at **2** and **3** has revealed greatly enhanced reactivity compared to **1**. Ligand substitution at **2** and **3** proceeded in a stepwise fashion, usually at room temperature, in contrast to **1** where similar ligand replacement requires refluxing toluene or halide activation to proceed.

Differences extend to product configuration: replacement of $[Ir(CO)_3]$ by isolobal $[CpW(CO)_2]$ in the tetrahedral core immediately introduces possible isomers in the carbonyl-bridged form. The Cp ligand can occupy axial, radial or apical sites, and structurally characterized examples of the axial and apical forms have been shown, although the radial has proved elusive.

Related structurally-characterized mixed-metal clusters containing one metal from group 6 and three metals from group 9 in the carbonyl-bridged form, i.e. $[CpMoCo_3(\mu\text{-}CO)_3(CO)_8]$[77] and $[CpMoIr_3(\mu\text{-}CO)_3(CO)_8]$,[78] have the basal plane containing the lighter metals, i.e. $[Co_3(\mu\text{-}CO)_3]$ for the former, $[MoIr_2(\mu\text{-}CO)_3]$ for the latter. Neither tungsten nor iridium favour the carbonyl-bridged geometry (which in general becomes increasingly less likely on descending a group); as a consequence, $[WIr_2(\mu\text{-}CO)_3]$ and $[Ir_3(\mu\text{-}CO)_3]$ basal planes are accessible in this system for derivatives of **2**, and $[W_2Ir(\mu\text{-}CO)_3]$ and $[WIr_2(\mu\text{-}CO)_3]$ basal planes are accessible for derivatives of **3**. This Chapter has shown seven structurally characterized clusters with $[WIr_2(\mu\text{-}CO)_3]$ basal planes (complex **4** with radial, axial coordination geometry, complex **19** with diaxial coordination geometry, complexes **5** and **17** with radial, diaxial coordination geometries, complex **29** with diaxial, apical coordination geometry, complex **34** with radial, diaxial, apical coordination geometry and complex **35** with radial, diaxial bridging, apical coordination geometry), two structurally characterized clusters with $[Ir_3(\mu\text{-}CO)_3]$ basal planes (complexes **7** and **13** with axial, apical coordination geometries) and one structurally characterized cluster with an all-terminal geometry (**24**). The structurally characterized clusters all reveal slight core expansion upon the introduction of *P*-donor ligands. Comparison of the crystal structure of the bis(isocyanide) derivative **24** with the precursor cluster **2** revealed similar core distances .

2.4. Experimental

2.4.1. General Conditions, Instruments, Reagents and Chromatography

2.4.1.1. General Conditions

Reactions were carried out using standard Schlenk techniques[79] under an inert atmosphere; subsequent workup was carried out without any precautions to exclude air. The reaction solvents dichloromethane (calcium hydride) and tetrahydrofuran (sodium/benzophenone) were dried and distilled under an inert atmosphere prior to use. Petroleum ether refers to a fraction of boiling point range 60-80 °C.

2.4.1.2. Instruments

IR spectra were recorded using a Perkin-Elmer 1600 or System 2000 fourier-transform spectrophotometer using a solution cell with NaCl windows. Unless otherwise stated, all IR bands correspond to ν(CO). Frequencies for the bands are in cm^{-1}.

NMR spectra were recorded on either a Varian Gemini-300 or a Varian VXR300S spectrometer, the ^{1}H spectra at 300 MHz, the ^{13}C at 75 MHz using approximately 0.02 M $Cr(acac)_3$ as the relaxation agent and the recycle delay set to 0.5 s. References for the ^{1}H and ^{13}C NMR spectra were set to residual solvent peaks; the latter were proton decoupled.

Mass spectra were obtained at the Australian National University on a VG ZAB 2SEQ instrument (30 kV Cs^+ ions, current 1 mA, accelerating potential 8 kV, matrix 3-nitrobenzyl alcohol). Peaks are reported as *m/z* (assignment, relative intensity).

Elemental analyses were performed by the Microanalytical Service, Research School of Chemistry, Australian National University.

2.4.1.3. Reagents

$[CpWIr_3(CO)_{11}]$ (**2**) and $[Cp_2W_2Ir_2(CO)_{10}]$ (**3**) were prepared by literature methods.[80] Commercial reagents PPh_3 (Aldrich), PMe_3 (Aldrich, 1M solution in thf), $PMePh_2$ (Aldrich), PMe_2Ph (Aldrich), $P(OPh)_3$ (BDH), $P(OMe)_3$ (Aldrich), dppm (Aldrich), dppe (Aldrich), pdpp (Strem) and ^{t}BuNC (Aldrich) were used as received. $[Fe(\eta^5\text{-}C_5H_5)(\eta^5\text{-}P_3C_2Bu^t_2)]$ was obtained from Prof. John Nixon (University of Sussex, U.K.). 2,6-dimethylphenylisocyanide was obtained from Assoc. Prof. Omar b. Shawkataly (University of Southern Malaysia, Malaysia).

2.4.1.4. Chromatography

Thin layer chromatography was on glass plates (20 × 20 cm) coated with Merck GF_{254} silica gel (0.5 mm). Column chromatography utilized Merck Silica Gel 60 (70 - 230 mesh).

2.4.2. Crystal Preparation

Crystals suitable for diffraction analyses were grown as follows:

• $[CpWIr_3(\mu\text{-}CO)_3(CO)_7(PMe_3)]$ (**7**) by slow diffusion of methanol into chloroform at room temperature.

• $[CpWIr_3(\mu\text{-}CO)_3(CO)_7(PMe_2Ph)]$ (**13**) by slow diffusion of methanol into dichloromethane at -5 °C.

• $[CpWIr_3(\mu\text{-}CO)_3(CO)_6\{P(OPh)_3\}_2]$ (**17**) by slow diffusion of hexane into dichloromethane at -5 °C.

• $[CpWIr_3(\mu\text{-}CO)_3(CO)_7\{P(OMe)_3\}]$ (**19**) by slow evaporation of dichloromethane from a solution of $[Cp_2W_2Ir_2(\mu\text{-}CO)_3(CO)_6\{P(OMe)_3\}_2]$ (**34**) in dichloromethane/octane at room temperature.

• $[CpWIr_3(CO)_9(CNXy)_2]$ (**24**) by slow diffusion of methanol into dichloromethane at -5 °C.

• $[Cp_2W_2Ir_2(\mu\text{-}CO)_3(CO)_6(PPh_3)]$ (**29**) by slow diffusion of hexane into a dichloromethane solution of $[Cp_2W_2Ir_2(\mu\text{-}CO)_3(CO)_5(PPh_3)_2]$ (**30**) at room temperature.

• $[Cp_2W_2Ir_2(\mu\text{-}CO)_3(CO)_6\{P(OMe)_3\}_2]$ (**34**) by slow evaporation of dichloromethane from a dichloromethane/octane solution at room temperature.

• $[Cp_2W_2Ir_2(\mu\text{-}CO)_3(\mu\text{-}dppm)(CO)_5]$ (**35**) by slow diffusion of methanol into dichloromethane at room temperature.

• $[CpWIr_3(\mu\text{-}CO)_3(CO)_7(PPh_3)]$ (**4**) were obtained by V.-A. Tolhurst by slow diffusion of methanol into dichloromethane at room temperature.

• $[CpWIr_3(\mu\text{-}CO)_3(CO)_7(PPh_3)_2]$ (**5**) were obtained by V.-A. Tolhurst by slow diffusion of methanol into dichloromethane at room temperature.

2.4.3. *Reaction of [CpWIr$_3$(CO)$_{11}$] (2) with one equivalent of PPh$_3$*

Complex **4** was prepared following the literature procedure.[69] IR (c-C_6H_{12}) 2075vs, 2063m, 2039vs, 2024vs, 2010vs, 1994vs, 1984m, 1962m, 1926s cm^{-1}.

2.4.4. *Reaction of [CpWIr$_3$(CO)$_{11}$] (2) with two equivalents of PPh$_3$ (with V.-A. Tolhurst)*

An orange solution of [CpWIr$_3$(CO)$_{11}$] (30.3 mg, 0.0267 mmol) and PPh_3 (14.0 mg, 0.0534 mmol) in CH_2Cl_2 (20 mL) was stirred at room temperature for 24 h. The dark orange solution obtained was evaporated to dryness. The resultant orange residue was dissolved in CH_2Cl_2 (*ca* 1 mL) and chromatographed (3 CH_2Cl_2 : 2 petroleum ether eluant). Three bands were obtained. The contents of the first band were identified as **4** (2.3 mg, 6 %) by solution IR spectroscopy. The second band contained a small amount of an unidentified green compound. Crystallization of the contents of the third band, R_f 0.48, from CH_2Cl_2/MeOH afforded orange crystals of [CpWIr$_3$(μ-CO)$_3$(CO)$_6$(PPh$_3$)$_2$], **5** (12.0 mg, 45%). Analytical data for **5**: IR (c-C_6H_{12}) 2059vs, 2027w, 2009s, 2001vs, 1986s, 1958m, 1904m, 1815m cm^{-1}; ^{1}H NMR ($CDCl_3$) δ 7.58-7.29 (m, 30H, Ph), 4.87 (s (br), 5H, C_5H_5); ^{13}C NMR ($CDCl_3$) δ 133.9-128.0 (Ph), 87.5 (C_5H_5); MS 1602 ([M]$^+$, 57), 1574 ([M-CO]$^+$, 54), 1546 ([M-2CO]$^+$, 69), 1518 ([M-3CO]$^+$, 100), 1490 ([M-4CO]$^+$, 42) 1462 ([M-5CO]$^+$, 100), 1434 ([M-6CO]$^+$, 64), 1406 ([M-7CO]$^+$, 58), 1378 ([M-8CO]$^+$, 40). Anal. Calcd: C 37.48, H 2.20. Found: C 37.44, H 2.22 %.

2.4.5. *Reaction of [CpWIr$_3$(CO)$_{11}$] (2) with three equivalents of PPh$_3$ (with V.-A. Tolhurst)*

Following the method of Section 2.4.4., [CpWIr$_3$(CO)$_{11}$] (21.5 mg, 0.0190 mmol) and PPh_3 (14.9 mg, 0.0568 mmol) in CH_2Cl_2 (20 mL) afforded two products after chromatography (3 CH_2Cl_2 : 2 petroleum ether eluant), one of which was in trace amounts. The major product, R_f 0.29, was crystallized ($CHCl_3$/EtOH at -20 °C) to afford red crystals of [CpWIr$_3$(μ-CO)$_3$(CO)$_5$(PPh$_3$)$_3$], **6** (16.2 mg, 46 %). Analytical data for **6**: IR (c-C_6H_{12}) 2059m, 2027w, 2009s, 2000vs, 1986s, 1958m, 1904m, 1815m cm^{-1}; ^{1}H NMR (acetone-d_6) δ 8.02 (s, 0.66H, $CHCl_3$), 7.57-7.37 (m, 45H, Ph), 4.82 (s, 5H, C_5H_5); MS 1420 ([M-PPh_3-2Ph]$^+$, 43), 1392 ([M-PPh_3-2Ph-CO]$^+$, 39), 1364 ([M-PPh_3-2Ph-2CO]$^+$, 100), 1336 ([M-PPh_3-2Ph-3CO]$^+$, 84), 1308 ([M-PPh_3-2Ph-4CO]$^+$, 58). Anal. Calcd: C 42.42; H 2.67. Found: C 42.16; H 2.38 %.

2.4.6. Reaction of [CpWIr$_3$(CO)$_{11}$] (2) with one equivalent of PMe$_3$ (with V.-A. Tolhurst)

Following the method of Section 2.4.4., [CpWIr$_3$(CO)$_{11}$] (21.0 mg, 0.0185 mmol) and PMe$_3$ (20 μL, 1 M solution in THF, 0.020 mmol) in THF (20 mL) afforded two products after chromatography (3 CH_2Cl_2: 2 petroleum ether eluant), one of which was in trace amounts. The major product, R_f 0.19, was crystallized ($CHCl_3$/MeOH) to afford orange crystals of [CpWIr$_3$(μ-CO)$_3$(CO)$_8$(PMe$_3$)], **7** (8.2 mg, 38 %). Analytical data for **7**: IR (c-C_6H_{12}) 2070s, 2040vs, 2030m, 2021s, 2003s, 1992vs, 1958w, 1920m, 1840w cm^{-1}; ^{1}H NMR ($CDCl_3$) δ 5.03 (s, 5H, C_5H_5), 1.91 (d, J_{HP} = 11 Hz, 9H, Me), ^{13}C NMR: (acetone-d_6) δ 84.0 (s, C_5H_5), 20.4 (d, J_{CP} = 36 Hz, Me); MS 1182 ([M]$^+$, 6), 1154 ([M-CO]$^+$, 38), 1126 ([M-2CO]$^+$, 42), 1098 ([M-3CO]$^+$, 69), 1070 ([M-4CO]$^+$, 100), 1042 ([M-5CO]$^+$, 31), 1028 ([M-5CO-CH$_3$]$^+$, 10), 1012 ([M-5CO-2CH$_3$]$^+$, 55), 997 ([M-5CO-3CH$_3$]$^+$, 11), 984 ([M-6CO-2CH$_3$]$^+$, 46), 969 ([M-6CO-3CH$_3$]$^+$, 32), 954 ([M-6CO-4CH$_3$]$^+$, 15). Anal. Calcd: C 18.29, H 1.19. Found: C 18.24, H 0.80 %.

2.4.7 Reaction of [CpWIr$_3$(CO)$_{11}$] (2) with two equivalents of PMe$_3$ (with V.-A. Tolhurst)

Following the method of Section 2.4.4., [CpWIr$_3$(CO)$_{11}$] (22.9 mg, 0.0203 mmol) and PMe$_3$ (40 μL, 1 M solution in THF, 0.040 mmol) in THF (20 mL) afforded two products after chromatography (3 CH_2Cl_2: 2 petroleum ether eluant), one of which was in trace amounts. The major product, R_f 0.40, was crystallized ($CHCl_3$/MeOH) to afford orange crystals of [CpWIr$_3$(μ-CO)$_3$(CO)$_6$(PMe$_3$)$_2$], **8** (9.6 mg, 41 %). Analytical data for **8**: IR (c-C_6H_{12}) 2044m, 2004vs, 1988vs, 1977m, 1965m, 1955m, 1807w cm^{-1}; ^{1}H NMR ($CDCl_3$) δ 5.06 (s, 5H, C_5H_5), 1.97 (d, J_{HP} = 10 Hz, 18H, Me); ^{13}C NMR (acetone-d_6) δ 88.3 (s, C_5H_5), 20.6 (s, J_{HP} = 36 Hz, Me); MS 1202 ([M-CO]$^+$, 12), 1174 ([M-2CO]$^+$, 24), 1146 ([M-3CO]$^+$, 100), 1118 ([M-4CO]$^+$, 37), 1090 ([M-5CO]$^+$, 14), 1062 ([M-6CO]$^+$, 37), 1034 ([M-7CO]$^+$, 23). Anal. Calcd: C 19.55, H 1.89. Found: C 19.49; H 1.91 %.

2.4.8. Reaction of [CpWIr$_3$(CO)$_{11}$] (2) with three equivalents of PMe$_3$ (with V.-A. Tolhurst)

Following the method of Section 2.4.4., [CpWIr$_3$(CO)$_{11}$] (22.3 mg, 0.0198 mmol) and PMe$_3$ (60 μL, 1 M solution in THF, 0.060 mmol) in THF (20 mL) afforded one product after chromatography (3 CH_2Cl_2: 2 petroleum ether eluant).The orange band, R_f 0.56, was crystallized ($CHCl_3$/MeOH) to afford orange crystals of [CpWIr$_3$(μ-CO)$_3$(CO)$_5$(PMe$_3$)$_3$], **9** (8.2 mg, 63 %). Analytical data for **9**: IR (c-C_6H_{12}) 2002s, 1966vs, 1957s, 1949vs, 1815vw cm^{-1}; ^{1}H NMR ($CDCl_3$) δ 4.89 (s, 5H, C_5H_5), 1.54 (d, J_{HP} = 10 Hz, 27H, Me); MS 1222 ([M-2CO]$^+$, 80), 1194 ([M-3CO]$^+$, 75), 1166 ([M-4CO]$^+$, 100), 1138 ([M-5CO]$^+$, 45), 1110 ([M-6CO]$^+$, 80), 1082 ([M-7CO]$^+$, 40), 1067 ([M-7CO-CH$_3$]$^+$, 50), 1052 ([M-7CO-

$2CH_3]^+$, 45), 1037 ([M-7CO-$3CH_3]^+$, 30), 1024 ([M-8CO-$2CH_3]^+$, 25), 1009 ([M-8CO-$3CH_3]^+$, 21), 994 ([M-8CO-$4CH_3]^+$, 20). Satisfactory analyses could not be obtained due to sample decomposition over days.

2.4.9. Reaction of [CpWIr$_3$(CO)$_{11}$] (2) with one equivalent of PMePh$_2$

Following the method of Section 2.4.4., [$CpWIr_3(CO)_{11}$] (20.0 mg, 0.0176 mmol) and $PMePh_2$ (3.5 μL, 0.0175 mmol) in CH_2Cl_2 (20 mL) afforded two bands after chromatography (3 CH_2Cl_2 : 2 petroleum ether eluant). The contents of the first band were identified as **2** (1.3 mg, 6%) by solution IR spectroscopy. Crystallization of the contents of the second band, R_f 0.55, from CH_2Cl_2/MeOH afforded orange crystals of [$CpWIr_3(\mu\text{-}CO)_3(CO)_7(PMePh_2)$], **10** (12.4 mg, 54 %). Analytical data for **10**: IR (c-C_6H_{12}) 2074s, 2063m, 2042vs, 2031m, 2023vs, 2013vs, 2007vs, 1994vs, 1983m, 1970m, 1924m, 1878w, 1850w, 1825m, 1801m cm^{-1}; ^{1}H NMR ($CDCl_3$) δ 7.56-7.42 (m, 10H, Ph), 4.90 (s (br), 5H, C_5H_5), 2.18 (d, J_{HP} = 10 Hz, 3H, Me); ^{13}C NMR ($CDCl_3$) δ 134.2-128.7 (s, Ph), 85.8 (s, C_5H_5), 20.3 (s, Me); MS 1306 ([M]$^+$, 10), 1278 ([M-CO]$^+$, 12), 1250 ([M-2CO]$^+$, 50), 1222 ([M-3CO]$^+$, 42), 1194 ([M-4CO]$^+$, 47), 1166 ([M-5CO]$^+$, 100), 1138 ([M-6CO]$^+$, 65), 1110 ([M-7CO]$^+$, 62), 1082 ([M-8CO]$^+$, 40). Anal. Calcd: C 25.75, H 1.39. Found: C 25.48, H 1.63 %.

2.4.10. Reaction of [CpWIr$_3$(CO)$_{11}$] (2) with two equivalents of PMePh$_2$

Following the method of Section 2.4.4., [$CpWIr_3(CO)_{11}$] (20.0 mg, 0.0176 mmol) and $PMePh_2$ (7.0 μL, 0.036 mmol) in CH_2Cl_2 (20 mL) afforded two bands after chromatography (3 CH_2Cl_2 : 2 petroleum ether eluant). The contents of the first band were identified as **10** (3.3 mg, 12 %) by solution IR spectroscopy. Crystallization of the contents of the second band, R_f 0.40, from CH_2Cl_2/MeOH afforded orange crystals of $CpWIr_3(\mu\text{-}CO)_3(CO)_6(PMePh_2)_2$, **11** (11.2 mg, 43 %). Analytical data for **11**: IR (c-C_6H_{12}) 2059s, 2048m, 2036w, 2092m, 2001vs, 1992s, 1987vs, 1967m, 1901br m, 1869w, 1844w, 1810w cm^{-1}; ^{1}H NMR ($CDCl_3$) δ 7.60-7.38 (m, 20H, Ph), 4.71 (s (br), 5H, C_5H_5), 2.06 (d, J_{HP} = 10 Hz, 6H, Me); ^{13}C NMR ($CDCl_3$) δ 131.9-128.3 (m, Ph), 87.1 (s, C_5H_5), 20.2 (s, Me); MS 1602 ([M]$^+$, 57), 1574 ([M-CO]$^+$, 54), 1546 ([M-2CO]$^+$, 69), 1518 ([M-3CO]$^+$, 100), 1490 ([M-4CO]$^+$, 42) 1462 ([M-5CO]$^+$, 100), 1434 ([M-6CO]$^+$, 64), 1406 ([M-7CO]$^+$, 58), 1378 ([M-8CO]$^+$, 40). Anal. Calcd: C 32.50, H 2.11. Found: C 32.56, H 1.91 %.

2.4.11. Reaction of [CpWIr$_3$(CO)$_{11}$] (2) with three equivalents of PMePh$_2$

Following the method of Section 2.4.4., [$CpWIr_3(CO)_{11}$] (20.3 mg, 0.0178 mmol) and $PMePh_2$ (11 μL, 0.072 mmol) in CH_2Cl_2 (20 mL) afforded one band (R_f 0.51) after

chromatography (2 CH_2Cl_2 : 1 petroleum ether eluant). Crystallization from CH_2Cl_2/MeOH afforded orange crystals of $[CpWIr_3(\mu\text{-}CO)_3(CO)_5(PMePh_2)_3]$, **12** (20.0 mg, 76 %). Analytical data for **12**: IR (c-C_6H_{12}) 2012m, 1996s, 1992s, 1973vs, 1971vs, 1969sh, 1931br m, 1891m, 1869m cm^{-1}; ^1H NMR ($CDCl_3$, 230K) δ 7.66-7.14 (m, 30H, Ph), 5.28 (s, 1H, $0.5CH_2Cl_2$), 4.37 (s, 5H, C_5H_5), 2.65-1.65 (m, 9H, Me), ^{13}C NMR ($CDCl_3$) δ 131.9-128.3 (m, Ph), 87.1 (s, C_5H_5), 53.4 (s, CH_2Cl_2), 20.7 (s, Me); MS 1602 ($[M]^+$, 57), 1574 ($[M\text{-}CO]^+$, 54), 1546 ($[M\text{-}2CO]^+$, 69), 1518 ($[M\text{-}3CO]^+$, 100), 1490 ($[M\text{-}4CO]^+$, 42), 1462 ($[M\text{-}5CO]^+$, 100), 1434 ($[M\text{-}6CO]^+$, 64), 1406 ($[M\text{-}7CO]^+$, 58), 1378 ($[M\text{-}8CO]^+$, 40). Anal. Calcd: C 32.50, H 2.11. Found: C 32.56, H 1.91 %.

2.4.12. Reaction of $[CpWIr_3(CO)_{11}]$ (2) with one equivalent of PMe_2Ph

Following the method of Section 2.4.4., $[CpWIr_3(CO)_{11}]$ (20.0 mg, 0.0176 mmol) and PMe_2Ph (2.5 μL, 0.0175 mmol) in CH_2Cl_2 (20 mL) afforded two bands after chromatography. The contents of the first band were identified as **2** (1.9 mg, 9 %) by solution IR spectroscopy. Crystallization of the contents of the second band, R_f 0.61, from CH_2Cl_2/MeOH afforded orange crystals of $[CpWIr_3(\mu\text{-}CO)_3(CO)_7(PMe_2Ph)]$, **13** (14.8 mg, 64 %). Analytical data for **13**: IR (c-C_6H_{12}) 2071s, 2064w, 2042vs, 2032m, 2022vs, 2007vs, 1998m, 1993vs, 1960m, 1922m, 1824br m, 1801m cm^{-1}; ^1H NMR ($CDCl_3$) δ 7.55-7.39 (m, 5H, Ph), 4.96 (s (br), 5H, C_5H_5), 2.18 (d, J_{HP} = 10 Hz, 6H, Me); ^{13}C NMR ($CDCl_3$) δ 130.5-128.6 (Ph), 86.3 (C_5H_5), 20.0 (Me); MS 1244 ($[M]^+$, 43), 1216 ($[M\text{-}CO]^+$, 74), 1188 ($[M\text{-}2CO]^+$, 45), 1160 ($[M\text{-}3CO]^+$, 51), 1132 ($[M\text{-}4CO]^+$, 37), 1104 ($[M\text{-}5CO]^+$, 100), 1076 ($[M\text{-}6CO]^+$, 73), 1048 ($[M\text{-}7CO]^+$, 80), 1020 ($[M\text{-}8CO]^+$, 51). Anal. Calcd: C 22.21, H 1.30. Found: C 22.35, H 1.14 %.

2.4.13. Reaction of $[CpWIr_3(CO)_{11}]$ (2) with two equivalents of PMe_2Ph

Following the method of Section 2.4.4., $[CpWIr_3(CO)_{11}]$ (20.0 mg, 0.0176 mmol) and PMe_2Ph (4.8 μL, 0.0355 mmol) in CH_2Cl_2 (20 mL) afforded two bands after chromatography. The contents of the first band were identified as **13** (2.8 mg, 12 %) by solution IR spectroscopy. Crystallization of the contents of the second band, R_f 0.47, from CH_2Cl_2/MeOH afforded orange crystals of $[CpWIr_3(\mu\text{-}CO)_3(CO)_6(PMe_2Ph)_2]$, **14** (10.5 mg, 40 %). Analytical data for **14**: IR (c-C_6H_{12}) 2047m, 2043s, 2029w, 2010s, 1994vs, 1990m, 1977m, 1970m, 1956m, 1973w, 1899m, 1803w cm^{-1}; ^1H NMR ($CDCl_3$) δ 7.66-7.35 (m, 10H, Ph), 4.89 (s (br), 5H, Cp), 2.23 (d, J_{HP} = 10 Hz, 12H, Me); ^{13}C NMR ($CDCl_3$) δ 132.2-123.4 (m, Ph), 86.3 (s, C_5H_5), 20.4 (m, Me); MS 1354 ($[M]^+$, 3), 1326 ($[M\text{-}CO]^+$, 10), 1298 ($[M\text{-}2CO]^+$, 25), 1270 ($[M\text{-}3CO]^+$, 100), 1242 ($[M\text{-}4CO]^+$, 12), 1214 ($[M\text{-}5CO]^+$, 60), 1186 ($[M\text{-}6CO]^+$, 79), 1158 ($[M\text{-}7CO]^+$, 50), 1130 ($[M\text{-}8CO]^+$, 20). Anal. Calcd: C 26.61, H 1.67. Found: C 26.82, H 1.67 %.

2.4.14. Reaction of [CpWIr$_3$(CO)$_{11}$] (2) with three equivalents of PMe$_2$Ph

Following the method of Section 2.4.4., [CpWIr$_3$(CO)$_{11}$] (20.3 mg, 0.0178 mmol) and PMe$_2$Ph (7.0 μL, 0.071 mmol) in CH_2Cl_2 (20 mL) afforded one band (R_f 0.43) after chromatography (2 CH_2Cl_2 : 1 petroleum ether eluant). Crystallization from CH_2Cl_2/Me OH afforded orange crystals of [CpWIr$_3$(μ-CO)$_3$(CO)$_5$(PMe$_2$Ph)$_3$], **15** (13.5 mg, 52%). Analytical data for **15**: IR (c-C_6H_{12}) 2006s, 1992w, 1968sh, 1967vs, 1952s, 1915w, 1861w, 1825w cm^{-1}; ^{1}H NMR ($CDCl_3$, 230K) δ 7.72-7.20 (m, 15H, Ph), 5.28 (s, 1H, 0.5CH_2Cl_2), 4.38 (s, 5H, C_5H_5), 2.26-1.17 (m, 18H, Me); ^{13}C NMR ($CDCl_3$) δ 129.5-127.8 (m, Ph), 87.1 (s, C_5H_5), 53.4 (s, CH_2Cl_2), 20.4 (m, Me); MS 1464 ([M]$^+$, 10), 1408 ([M-2CO]$^+$, 29), 1380 ([M-3CO]$^+$, 100), 1353 ([M-4CO]$^+$, 17), 1324 ([M-5CO]$^+$, 53), 1296 ([M-6CO]$^+$, 61), 1268 ([M-7CO]$^+$, 10). Anal. Calcd: C 29.90, H 2.61. Found: C 29.68, H 1.19 %.

2.4.15. Reaction of [CpWIr$_3$(CO)$_{11}$] (2) with one equivalent of P(OPh)$_3$

Following the method of Section 2.4.4., [CpWIr$_3$(CO)$_{11}$] (20.1 mg, 0.0177 mmol) and P(OPh)$_3$ (4.6 μL, 0.0177 mmol) in CH_2Cl_2 (20 mL) afforded two bands after chromatography (3 CH_2Cl_2 : 2 petroleum ether eluant). The contents of the first band were identified as **2** by IR spectroscopy. Crystallization of the contents of the second band, R_f 0.51, from CH_2Cl_2/MeOH afforded orange crystals of [CpWIr$_3$(μ-CO)$_3$(CO)$_7${P(OPh)$_3$}], **16** (11.2 mg, 45 %). Analytical data for **16**: IR (c-C_6H_{12}) 2080vs, 2071w, 2047vs, 2029vs, 2020s, 2008m, 1997m, 1967m, 1927w, 1925br w, 1854w, 1825w, 1802w cm^{-1}; ^{1}H NMR (acetone-d_6) δ 8.02 (s, 0.66H, $CHCl_3$), 7.33-7.02 (m, 15H, OPh), 5.04 (s, 5H, C_5H_5); MS 1416 ([M]$^+$, 5), 1388 ([M-CO]$^+$ 7), 1360 ([M-2CO]$^+$, 12), 1332 ([M-3CO]$^+$, 15), 1304 ([M-4CO]$^+$, 13), 1276 ([M-5CO]$^+$, 100), 1248 ([M-6CO]$^+$, 35), 1220 ([M-7CO]$^+$, 14), 1192 ([M-8CO]$^+$, 57), 1164 ([M-9CO]$^+$, 34), 1136 ([M-10CO]$^+$, 27). Anal. Calcd: C 27.04, H 139. Found: C 27.08, H 1.42 %.

2.4.16. Reaction of [CpWIr$_3$(CO)$_{11}$] (2) with two equivalents of P(OPh)$_3$

Following the method of Section 2.4.4., [CpWIr$_3$(CO)$_{11}$] (20.2 mg, 0.0178 mmol) and P(OPh)$_3$ (9.3 μL, 0.0356 mmol) in CH_2Cl_2 (20 mL) afforded two products after chromatography (2 CH_2Cl_2 : 1 petroleum ether eluant), one of which was in trace amounts. The major product, R_f 0.35, was crystallized from CH_2Cl_2/MeOH to afford orange crystals of [CpWIr$_3$(μ-CO)$_3$(CO)$_6${P(OPh)$_3$}$_2$], **17** (12.3 mg, 41 %). Analytical data for **17**: IR (c-C_6H_{12}) 2069vs, 2045w, 2021vs, 2008s, 1987m, 1957m, 1917m, 1906m, 1830w cm^{-1}; ^{1}H NMR ($CDCl_3$) δ 7.30–7.00 (m, 30H, OPh), 4.99 (s, 5H, C_5H_5); MS 1558 ([M-5CO]$^+$, 68), 1530 ([M-6CO]$^+$, 28), 1502 ([M-7CO]$^+$, 75), 1474 ([M-8CO]$^+$, 100), 1446 ([M-9CO]$^+$, 64). Anal. Calcd: C 35.36, H 2.08. Found: C 35.95, H 1.83 %.

2.4.17. Reaction of [CpWIr$_3$(CO)$_{11}$] (2) with three equivalents of P(OPh)$_3$

An orange solution of [CpWIr$_3$(CO)$_{11}$] (20.2 mg, 0.0178 mmol) and P(OPh)$_3$ (23.3 μL, 0.089 mmol) in CH_2Cl_2 (20 mL) was refluxed for 3 h. The dark orange solution obtained was evaporated to dryness. The resultant orange residue was dissolved in CH_2Cl_2 (*ca* 1 mL) and chromatographed (2 CH_2Cl_2 : 1 petroleum ether eluant) to afford two products, the contents of the first band being characterized as **17** by IR spectroscopy. The third band, R_f 0.18, was crystallized from CH_2Cl_2/MeOH to afford orange crystals of [CpWIr$_3$(μ-CO)$_3$(CO)$_5${P(OPh)$_3$}$_3$], **18** (11.2 mg, 32 %). Analytical data for **18**: IR (c-C_6H_{12}) 2069s, 2043m, 2021s, 2013vs, 1989m, 1954m, 1912m, 1909m, 1843br w cm^{-1}; ^{1}H NMR ($CDCl_3$) δ 7.31–7.01 (m, 45H, Ph), 4.97 [s (br), 5H, C_5H_5]; MS 1896 ([M-3CO]$^+$, 41), 1868 ([M-4CO]$^+$, 6), 1840 ([M-5CO]$^+$, 10), 1812 ([M-6CO]$^+$, 11), 1784 ([M-7CO]$^+$, 20) . Satisfactory analyses could not be obtained due to sample decomposition over days.

2.4.18. Reaction of [CpWIr$_3$(CO)$_{11}$] (2) with one equivalent of P(OMe)$_3$

Following the method of Section 2.4.4., [CpWIr$_3$(CO)$_{11}$] (20.0 mg, 0.0176 mmol) and P(OMe)$_3$ (2.1 μL, 0.0175 mmol) in CH_2Cl_2 (20 mL) afforded two bands after chromatography (3 CH_2Cl_2 : 2 petroleum ether eluant). The contents of the first band were identified as **2** (1.5 mg, 7.5 %) by solution IR spectroscopy. Crystallization of the contents of the second band, R_f 0.42, from CH_2Cl_2/MeOH afforded orange crystals of [CpWIr$_3$(μ-CO)$_3$(CO)$_7${P(OMe)$_3$}], **19** (15.4 mg, 71 %). Analytical data for **19**: IR (c-C_6H_{12}) 2078s, 2070w, 2060w, 2046vs, 2033m, 2022s, 2017vs, 1999m, 1995m, 1970m, 1959w, 1921m, 1841w, 1830w, 1825m, 1801w cm^{-1}; ^{1}H NMR ($CDCl_3$) δ 4.98 (s, 5H, C_5H_5), 3.71 (d, J_{HP} = 12 Hz, 9H, Me); MS 1230 ([M]$^+$, 15), 1202 ([M-CO]$^+$, 14), 1174 ([M-2CO]$^+$, 20), 1146 ([M-3CO]$^+$, 100), 1118 ([M-4CO]$^+$, 33) 1090 ([M-5CO]$^+$, 5). Anal. Calcd: C 17.58, H 1.15. Found: C 18.58, H 0.58 %.

2.4.19. Reaction of [CpWIr$_3$(CO)$_{11}$] (2) with two equivalents of P(OMe)$_3$

Following the method of Section 2.4.4., [CpWIr$_3$(CO)$_{11}$] (20.0 mg, 0.0176 mmol) and P(OMe)$_3$ (4.3 μL, 0.0352 mmol) in CH_2Cl_2 (20 mL) afforded two products after chromatography (2 CH_2Cl_2 : 1 petroleum ether eluant), one of which was in trace amounts. The major product, R_f 0.35, was crystallized from CH_2Cl_2/MeOH to afford orange crystals of [CpWIr$_3$(μ-CO)$_3$(CO)$_6${P(OMe)$_3$}$_2$], **20** (9.7 mg, 41 %). Analytical data for **20**: IR (c-C_6H_{12}) 2065vs, 2042w, 2012vs, 1997m, 1983s, 1948m, 1910m, 1908w, 1819m cm^{-1}; ^{1}H NMR ($CDCl_3$) δ 4.93 (s, 5H, C_5H_5), 3.73 (d, J_{HP} = 12 Hz, 18H, Me); MS 1270 ([M-2CO]$^+$, 20), 1242 ([M-3CO]$^+$, 100), 1214 ([M-4CO]$^+$, 20), 1186 ([M-5CO]$^+$, 17). Anal. Calcd: C 18.12, H 1.75. Found: C 18.23, H 1.40 %.

2.4.20. *Reaction of $[CpWIr_3(CO)_{11}]$ (2) with three equivalents of $P(OMe)_3$*

An orange solution of $[CpWIr_3(CO)_{11}]$ (20.0 mg, 0.0176 mmol) and $P(OMe)_3$ (10 μL, 0.083 mmol) in CH_2Cl_2 (20 mL) was refluxed for 3 h. The resultant dark orange solution was evaporated to dryness, the orange residue dissolved in CH_2Cl_2 (*ca* 1 mL) and chromatographed (2 CH_2Cl_2 : 1 petroleum ether eluant) to afford three products. The contents of the first two bands were characterized as **19** and **20** by IR spectroscopy. The third band, R_f 0.16, was crystallized from CH_2Cl_2/MeOH to afford orange crystals of $[CpWIr_3(\mu\text{-}CO)_3(CO)_5\{P(OMe)_3\}_3]$, **21** (7.2 mg, 29 %). Analytical data for **21**: IR (c-C_6H_{12}) 2008s, 1992vs, 1974s, 1940m, 1901m, 1898w, 1908w, 1844w, 1802m cm^{-1}; ^1H NMR ($CDCl_3$) δ 4.71 (s (br), 5H, C_5H_5), 3.91-3.78 (m, 27H, Me); MS 1338 ($[M\text{-}3CO]^+$, 100), 1310 ($[M\text{-}4CO]^+$, 11), 1282 ($[M\text{-}5CO]^+$, 8), 1254 ($[M\text{-}6CO]^+$, 35). Anal. Calcd: C 18.58, H 2.27. Found: C 18.90, H 1.91 %.

2.4.21. *Reaction of $[CpWIr_3(CO)_{11}]$ (2) with pddp*

Following the method of Section 2.4.4., $[CpWIr_3(CO)_{11}]$ (20.0 mg, 0.0176 mmol) and pdpp (7.9 mg, 0.0177 mmol) in CH_2Cl_2 (20 mL) afforded two bands after chromatography (3 CH_2Cl_2 : 2 petroleum ether eluant). The contents of the first band were identified as **2** (1.5 mg, 7.5 %) by solution IR spectroscopy. Crystallization of the contents of the second band, R_f 0.51, from CH_2Cl_2/MeOH afforded orange crystals of $[CpWIr_3(\mu\text{-}CO)_3(\mu\text{-dppb})(CO)_6]$, **22** (16.6 mg, 62 %). Analytical data for **22**: IR (c-C_6H_{12}) 2062w, 2054w, 2047vs, 2023vs, 1987s, 1984s, 1961w, 1921w, 1811w cm^{-1}; ^1H NMR ($CDCl_3$) δ 7.62 – 7.27 (m, 24H, Ph), 4.99 (s, 5H, C_5H_5); MS 1524 ($[M]^+$, 15), 1496 ($[M\text{-}CO]^+$, 40), 1468 ($[M\text{-}2CO]^+$, 14), 1440 ($[M\text{-}3CO]^+$, 100), 1412 ($[M\text{-}4CO]^+$, 18), 1384 ($[M\text{-}5CO]^+$, 28), 1356 ($[M\text{-}6CO]^+$, 57), 1328 ($[M\text{-}7CO]^+$, 40), 1300 ($[M\text{-}8CO]^+$, 7). Anal. Calcd: C 34.15, H 1.93. Found: C 34.72, H 2.01 %.

2.4.22. *Attempted reaction of $[CpWIr_3(CO)_{11}]$ (2) with $[Fe(\eta^5\text{-}C_5H_5)(\eta^5\text{-}P_3C_2Bu^t_2)]$*

Attempt I: A dark orange solution of $[CpWIr_3(CO)_{11}]$ (20.0 mg, 0.0176 mmol) and $[Fe(\eta^5\text{-}C_5H_5)(\eta^5\text{-}P_3C_2Bu^t_2)]$ (6.2 mg, 0.0176 mmol) in CH_2Cl_2 (20 mL) was stirred at room temperature for 24 h. No apparent reaction was observed. The solution was slowly heated and refluxed for 16h. An IR spectrum indicated no reaction had occurred.

Attempt II: A dark orange solution of $[CpWIr_3(CO)_{11}]$ (20.0 mg, 0.0176 mmol) and $[Fe(\eta^5\text{-}C_5H_5)(\eta^5\text{-}P_3C_2Bu^t_2)]$ (10.0 mg, 0.0284 mmol) in thf (20 mL) was refluxed for 20 h. Monitoring the reaction by IR showed a decrease in the intensity of the ν(CO) bands, but with no other changes in the pattern. Chromatography yielded no tractable products.

2.4.23. Reaction of [CpWIr$_3$(CO)$_{11}$] (2) with one equivalent of XyNC

Following the method of Section 2.4.4., [CpWIr$_3$(CO)$_{11}$] (20.0 mg, 0.0176 mmol) and XyNC (2.3 mg, 0.0176 mmol) in CH_2Cl_2 (20 mL) afforded two bands after chromatography (2 CH_2Cl_2 : 1 petroleum ether eluant). The contents of the first band were identified as **2** (2.6 mg, 12 %) by solution IR spectroscopy. Crystallization of the contents of the second band, R_f 0.60, from CH_2Cl_2/MeOH afforded orange crystals of [CpWIr$_3$(CO)$_{10}$(CNXy)], **23** (13.6 mg, 60 %). Analytical data for **23**: IR (c-C_6H_{12}) υ(C≡N) 2153m, υ(C≡O) 2067s, 2037vs, 2014s, 2001w, 1987w, 1986m, 1950w cm^{-1}; ^{1}H NMR ($CDCl_3$) δ 7.17-7.09 (m, 3H, Ph), 5.21 (s, 5H, C_5H_5), 2.38 (s, 6H, Me); MS 1237 ([M]$^+$, 10), 1202 ([M-CO]$^+$, 12), 1181 ([M-2CO]$^+$, 25), 1153 ([M-3CO]$^+$, 100), 1125 ([M-4CO]$^+$, 55), 1097 ([M-5CO]$^+$, 39), 1069 ([M-6CO]$^+$, 45), 1041 ([M-7CO]$^+$, 52), 1013 ([M-8CO]$^+$, 56), 985 ([M-9CO]$^+$, 26). Anal. Calcd: C 23.31, H 1.14, N 1.13. Found: C 24.22, H 1.08, N 1.26 %.

2.4.24. Reaction of [CpWIr$_3$(CO)$_{11}$] (2) with two equivalents of XyNC

Following the method of Section 2.4.4., [CpWIr$_3$(CO)$_{11}$] (20.0 mg, 0.0176 mmol) and XyNC (4.6 mg, 0.0352 mmol) in CH_2Cl_2 (20 mL) afforded two bands after chromatography (2 CH_2Cl_2 : 1 petroleum ether eluant). The contents of the first band were identified as **23** (6.5 mg, 30 %) by solution IR spectroscopy. Crystallization of the contents of the second band, R_f 0.38, from CH_2Cl_2/MeOH afforded orange crystals of [CpWIr$_3$(CO)$_9$(CNXy)$_2$], **24** (11.1 mg, 47 %). Analytical data for **24**: IR (c-C_6H_{12}) υ(C≡N) 2152m, 2118m, υ(C≡O) 2051s, 2046m, 2027vs, 2007s, 2001s, 1994m, 1901m, 1984m, 1978m, 1898w, 1847w cm^{-1}; ^{1}H NMR ($CDCl_3$) δ 7.30-7.03 (m, 6H, Ph), 5.08 (s, 5H, C_5H_5), 2.35 (s, 12H, Me); MS 1340 ([M]$^+$, 5), 1312 ([M-CO]$^+$, 6), 1284 ([M-2CO]$^+$, 14), 1256 ([M-3CO]$^+$, 100), 1228 ([M-4CO]$^+$, 58), 1200 ([M-5CO]$^+$, 42), 11172 ([M-6CO]$^+$, 23), 1144 ([M-7CO]$^+$, 19), 1116 ([M-8CO]$^+$, 16). Anal. Calcd: C 28.68, H 1.73, N 2.09. Found: C 28.19, H 1.83, N 2.04 %.

2.4.25. Reaction of [CpWIr$_3$(CO)$_{11}$] (2) with three equivalents of XyNC

Following the method of Section 2.4.4., [CpWIr$_3$(CO)$_{11}$] (20.0 mg, 0.0176 mmol) and XyNC (7.0 mg, 0.0530 mmol) in CH_2Cl_2 (20 mL) afforded two bands after chromatography (3 CH_2Cl_2 : 1 petroleum ether eluant). The contents of the first band were identified as **24** (6.6 mg, 28 %) by solution IR spectroscopy. Crystallization of the contents of the second band, R_f 0.55, from CH_2Cl_2/MeOH afforded orange crystals of [CpWIr$_3$(CO)$_8$(CNXy)$_3$], **25** (16.0 mg, 63%). Analytical data for **25**: IR (c-C_6H_{12}) υ(C≡N) 2150s, 2131s, 2115s υ(C≡O) 2031s, 2022m, 2027vs, 1995vs, 1986s, 1972m, 1898w, 1879m, 1844m cm^{-1}; ^{1}H NMR ($CDCl_3$) δ 7.12-7.00 (m, 9H, Ph), 5.01 (s, 5H, C_5H_5), 2.31 (s, 18H, Me); MS 1443 ([M]$^+$, 8), 1415 ([M-CO]$^+$, 4), 1387 ([M-2CO]$^+$, 10), 1359 ([M-

$3CO]^+$, 100), 1331 ($[M-4CO]^+$, 53), 1303 ($[M-5CO]^+$, 69), 1275 ($[M-6CO]^+$, 13), 1247 ($[M-7CO]^+$, 30). Satisfactory microanalyses could not be obtained due to sample decomposition in solution over days.

2.4.26. Reaction of [CpWIr$_3$(CO)$_{11}$] (2) with one equivalent of ^{t}BuNC

Following the method of Section 2.4.4., [CpWIr$_3$(CO)$_{11}$] (**2**) (20.0 mg, 0.0176 mmol) and ^{t}BuNC (2 μL, 0.0176 mmol) in CH_2Cl_2 (20 mL) afforded two bands after chromatography (3 CH_2Cl_2 : 2 petroleum ether eluant). The contents of the first band were identified as **1** (1.8 mg, 9 %) by solution IR spectroscopy. Crystallization of the contents of the second band, R_f 0.78, from CH_2Cl_2/MeOH afforded orange crystals of [CpWIr$_3$(CO)$_{10}$(CNBu^t)], **26** (12.1 mg, 58 %). Analytical data for **26**: IR (c-C_6H_{12}) υ(C≡N) 2178m, υ(C≡O) 2069s, 2036vs, 2026s, 2012s, 1999w, 1989sh, 1984m, 1964w cm^{-1}; ^{1}H NMR (acetone-d^6) δ 5.44 (s, 5H, C_5H_5), 1.52 (s, 9H, Me); ^{13}C NMR (acetone-d^6) 180.4 (s, CO), 87.6 (s, C_5H_5), other signals not observed; MS 1189 ($[M]^+$, 5), 1161 ($[M-CO]^+$, 10), 1133 ($[M-2CO]^+$, 20), 1105 ($[M-3CO]^+$, 100), 1077 ($[M-4CO]^+$, 55), 1049 ($[M-5CO]^+$, 30), 1021 ($[M-6CO]^+$, 37), 993 ($[M-7CO]^+$, 35), 965 ($[M-8CO]^+$, 22), 937 ($[M-9CO]^+$, 13). Anal. Calcd: C 20.21, H 1.19, N 1.13. Found: C 21.14, H 1.42, N 1.32 %.

2.4.27. Reaction of [CpWIr$_3$(CO)$_{11}$] (2) with two equivalents of ^{t}BuNC

Following the method of Section 2.4.4., [CpWIr$_3$(CO)$_{11}$] (**2**) (20.0 mg, 0.0176 mmol) and ^{t}BuNC (4 μL, 0.0352 mmol) in CH_2Cl_2 (20 mL) afforded two bands after chromatography (3 CH_2Cl_2 : 2 petroleum ether eluant). The contents of the first band were identified as **26** (5.6 mg, 28 %) by solution IR spectroscopy. Crystallization of the contents of the second band, R_f 0.39, from CH_2Cl_2/MeOH afforded orange crystals of [CpWIr$_3$(CO)$_9$(CNBu^t)$_2$], **27** (12.6 mg, 58 %). Analytical data for **27**: IR (c-C_6H_{12}) υ(C≡N) 2177m, 2152m, υ(C≡O) 2049s, 2045s, 2022vs, 2005s, 1996s, 1986s, 1974m, 1925w, 1890m, 1854w, 1838w cm^{-1}; ^{1}H NMR (acetone-d^6) δ 5.18 (s, 5H, C_5H_5), 1.49 (s, 18H, Me); ^{13}C NMR (CS_2/CD_2Cl_2) 182.0 (s, CO), 86.2 (s, C_5H_5), 28.5 (s, Me), other signals not observed; MS 1244 ($[M]^+$, 5), 1216 ($[M-CO]^+$, 7), 1188 ($[M-2CO]^+$, 17), 1160 ($[M-3CO]^+$, 100), 1132 ($[M-4CO]^+$, 65), 1104 ($[M-5CO]^+$, 47), 1076 ($[M-6CO]^+$, 28), 1048 ($[M-7CO]^+$, 23), 1020 ($[M-8CO]^+$, 21), 992 ($[M-9CO]^+$, 20). Anal. Calcd: C 23.17, H 1.86, N 2.25. Found: C 23.51, H 1.98, N 2.00 %.

2.4.28. Reaction of [CpWIr$_3$(CO)$_{11}$] (2) with three equivalents of ^{t}BuNC

Following the method of Section 2.4.4., [CpWIr$_3$(CO)$_{11}$] (**2**) (20.0 mg, 0.0176 mmol) and ^{t}BuNC (6 μL, 0.0530 mmol) in CH_2Cl_2 (20 mL) afforded two bands after chromatography (2 CH_2Cl_2 : 1 petroleum ether eluant). The contents of the first band were identified as **27**

(6.1 mg, 28 %) by solution IR spectroscopy. Crystallization of the contents of the second band, R_f 0.38, from CH_2Cl_2/MeOH afforded orange crystals of $[CpWIr_3(CO)_8(CNBu^t)_3]$, **28** (13.5 mg, 59 %). Analytical data for **28**: IR (CH_2Cl_2) υ(C≡N) 2179m, 2155m, υ(C≡O) 2056vw, 2021vs, 1982vs, 1867w, 1816m cm^{-1}; ^1H NMR (acetone-d^6) δ 4.99 (s, 5H, C_5H_5), 1.46 (s, 27H, Me); ^{13}C NMR (CS_2/CD_2Cl_2) 182.6 (s, CO), 85.9 (s, C_5H_5), 29.0 (s, Me), other signals not observed; MS 1299 ($[M]^+$, 10), 1271 ($[M\text{-}CO]^+$, 6), 1243 ($[M\text{-}2CO]^+$, 13), 1215 ($[M\text{-}3CO]^+$, 100), 1187 ($[M\text{-}4CO]^+$, 60), 1159 ($[M\text{-}5CO]^+$, 75), 1131 ($[M\text{-}6CO]^+$, 18), 1103 ($[M\text{-}7CO]^+$, 35), 1075 ($[M\text{-}8CO]^+$, 30). Satisfactory microanalyses could not be obtained due to sample decomposition in solution over days.

2.4.29. Reaction of $[Cp_2W_2Ir_2(CO)_{10}]$ (3) with one equivalent of PPh_3 (with J. Lee)

A deep red solution of $[Cp_2W_2Ir_2(CO)_{10}]$ (20.0 mg, 0.0172 mmol) and PPh_3 (4.5 mg, 0.0175 mmol) in CH_2Cl_2 (20 mL) was stirred at room temperature for 18 h. The red-brown solution obtained was evaporated to dryness. The resultant brown residue was dissolved in CH_2Cl_2 (*ca* 1 mL) and chromatographed (3 CH_2Cl_2 : 2 petroleum ether eluant). Two bands were obtained, one in trace amounts. Crystallization of the contents of the second band, R_f 0.42, from CH_2Cl_2/MeOH or CH_2Cl_2/n-hexane afforded deep red crystals of $[Cp_2W_2Ir_2(\mu\text{-}CO)_3(CO)_6(PPh_3)]$, **29** (16 mg, 62 %). Analytical data for **29**.CH_2Cl_2: IR (c-C_6H_{12}) 2041vs, 2023w, 2002m, 1987s, 1980m, 1958m, 1921m, 1840m cm^{-1}. ^1H NMR ($CDCl_3$, 298 K) δ 7.44-7.37 (m, 15H, Ph), 5.32 (s, 2H, CH_2Cl_2), 4.68 [s (br), 10H, C_5H_5]; MS 1340 ($[M\text{-}2CO]^+$, 29), 1284 ($[M\text{-}3CO]^+$, 61), 1255 ($[M\text{-}4CO]^+$, 36), 1228 ($[M\text{-}5CO]^+$, 36), 1200 ($[M\text{-}6CO]^+$, 50), 1170 ($[M\text{-}7CO]^+$, 21). Anal. Calcd: C 30.81, H 1.84. Found: C 31.04, H 1.30 %.

2.4.30. Reaction of $[Cp_2W_2Ir_2(CO)_{10}]$ (3) with two equivalents of PPh_3

Following the method of Section 2.4.29., $[Cp_2W_2Ir_2(CO)_{10}]$ (20.0 mg, 0.0172 mmol) and PPh_3 (9.0 mg, 0.0344 mmol) in CH_2Cl_2 (20 mL) afforded one product after chromatography (2 CH_2Cl_2 : 1 petroleum ether eluant). The band, R_f 0.30, was crystallized (CH_2Cl_2/MeOH at -20 °C) to afford red crystals of $[Cp_2W_2Ir_2(\mu\text{-}CO)_3(CO)_5(PPh_3)_2]$, **30** (9 mg, 32 %). Analytical data for **30**: IR (c-C_6H_{12}) 2041s, 2024w, 2003vs, 1987m, 1980vs, 1969m, 1950vs, 1921m, 1909m, 1896s, 1850m, 1803m cm^{-1}; ^1H NMR (CD_2Cl_2, 203 K) 7.80-7.31 (m, 30H, Ph), 4.68 (s, 5H, C_5H_5, both isomers), 4.55 (s, 4H, C_5H_5, major isomer), 4.42 (s, 1H, C_5H_5, minor isomer); MS 1340 ($[M\text{-}PPh_3\text{-}CO]^+$, 29), 1311 ($[M\text{-}PPh_3\text{-}2CO]^+$, 10), 1284 ($[M\text{-}PPh_3\text{-}3CO]^+$, 67), 1255 ($[M\text{-}PPh_3\text{-}4CO]^+$, 37), 1228 ($[M\text{-}PPh_3\text{-}5CO]^+$, 38), 1200 ($[M\text{-}PPh_3\text{-}6CO]^+$, 50), 1170 ($[M\text{-}PPh_3\text{-}7CO]^+$, 22), 1142 ($[M\text{-}PPh_3\text{-}8CO]^+$, 40). Satisfactory microanalyses could not be obtained due to sample decomposition at room temperature.

2.4.31. *Reaction of $[Cp_2W_2Ir_2(CO)_{10}]$ (3) with one equivalent of PMe_3*

Following the method of Section 2.4.29., $[Cp_2W_2Ir_2(CO)_{10}]$ (21.0 mg, 0.0181 mmol) and PMe_3 (19 μL, 1 M solution in THF, 0.019 mmol) in THF (20 mL) afforded two products after chromatography (3 CH_2Cl_2: 2 petroleum ether eluant), one of which was in trace amounts. The major product, R_f 0.45, was crystallized ($CHCl_3$/MeOH) to afford orange crystals of $[Cp_2W_2Ir_2(\mu\text{-}CO)_3(CO)_6(PMe_3)]$, **31** (8.2 mg, 38 %). Analytical data for **31**: IR (c-C_6H_{12}) 2026s, 2001w, 1986vs, 1957m, 1922w, 1895w, 1867w, 1833 br w cm^{-1}; ^1H NMR ($CDCl_3$, 298 K) δ 4.90 (s, 10H, C_5H_5), 1.87 (d, J_{HP} = 9 Hz, 9H, Me); MS 1210 ($[M]^+$, 10), 1182 ($[M\text{-}CO]^+$, 44), 1154 ($[M\text{-}2CO]^+$, 61), 1126 ($[M\text{-}3CO]^+$, 90), 1098 ($[M\text{-}4CO]^+$, 74), 1070 ($[M\text{-}5CO]^+$, 100), 1042 ($[M\text{-}6CO]^+$, 62). Anal. Calcd: C 21.83, H 1.58. Found: C 21.78, H 1.65 %.

2.4.32. *Reaction of $[Cp_2W_2Ir_2(CO)_{10}]$ with two equivalents of PMe_3*

Following the method of Section 2.4.29., Following method A, $[Cp_2W_2Ir_2(CO)_{10}]$ (20.2 mg, 0.0174 mmol) and PMe_3 (18 μL, 1 M solution in THF, 0.038 mmol) in THF (20 mL) afforded two products after chromatography (3 CH_2Cl_2: 2 petroleum ether eluant), one of which was in trace amounts. The major product, R_f 0.31, was crystallized ($CHCl_3$/MeOH) to afford orange crystals of $[Cp_2W_2Ir_2(\mu\text{-}CO)_3(CO)_5(PMe_3)_2]$, **32** (9.3 mg, 42 %). Analytical data for **32**: IR (c-C_6H_{12}) 2054w, 2048m, 2029w, 1994m, 1982s, 1972s, 1958vs, 1948s, 1873 br m, 1839 m cm^{-1}; ^1H NMR ($CDCl_3$, 298 K) δ 4.78 (s, 10H, C_5H_5), 1.83 (d, J_{HP} = 12 Hz, 18H, Me); MS 1258 ($[M]^+$, 11), 1231 ($[M\text{-}CO]^+$, 12), 1202 ($[M\text{-}2CO]^+$, 76), 1174 ($[M\text{-}3CO]^+$, 95), 1146 ($[M\text{-}4CO]^+$, 100), 1118 ($[M\text{-}5CO]^+$, 83). Satisfactory microanlyses could not be obtained due to sample decomposition over a number of days.

2.4.33. *Reaction of $[Cp_2W_2Ir_2(CO)_{10}]$ (3) with one equivalent of $P(OMe)_3$*

Following the method of Section 2.4.29., $[Cp_2W_2Ir_2(CO)_{10}]$ (20.0 mg, 0.0172 mmol) and $P(OMe)_3$ (4.5 mg, 0.0175 mmol) in CH_2Cl_2 (20 mL) afforded two bands after chromatography (3 CH_2Cl_2 : 2 petroleum ether eluant), one in trace amounts. Crystallization of the contents of the first band, R_f 0.60, from CH_2Cl_2/MeOH afforded orange crystals of $[Cp_2W_2Ir_2(\mu\text{-}CO)_3(CO)_6\{P(OMe)_3\}]$, **33** (11.9 mg, 54 %). Analytical data for **33**: IR (c-C_6H_{12}) 2049w, 2031s, 2007vs, 2004w, 1978s, 1959m, 1922s, 1869m. 1834m cm^{-1}; ^1H NMR ($CDCl_3$) δ 4.82 [s (vbr), 10H, C_5H_5], 3.74 (d, J_{HP} = 12 Hz, 9H, OMe); MS 1202 ($[M\text{-}2CO]^+$, 42), 1174 ($[M\text{-}3CO]^+$, 100), 1146 ($[M\text{-}4CO]^+$, 79) 1118 ($[M\text{-}5CO]^+$, 97), 1090 ($[M\text{-}6CO]^+$, 33), 1072 ($[M\text{-}7CO]^+$, 30), 1044 ($[M\text{-}8CO]^+$, 50), 1016 ($[M\text{-}9CO]^+$, 28). Anal. Calcd: C 21.00, H 1.52. Found: C 20.59, H 1.73 %.

2.4.34. Reaction of $[Cp_2W_2Ir_2(CO)_{10}]$ (3) with two equivalents of $P(OMe)_3$

Following the method of Section 2.4.29., $]Cp_2W_2Ir_2(CO)_{10}]$ (20.0 mg, 0.0172 mmol) and $P(OMe)_3$ (8.8 mg, 0.0344 mmol) in CH_2Cl_2 (20 mL) afforded two bands after chromatography (3 CH_2Cl_2 : 2 petroleum ether eluant), one in trace amounts. Crystallization of the contents of the first band, R_f 0.60, from CH_2Cl_2/MeOH afforded orange crystals of $[Cp_2W_2Ir_2(\mu\text{-}CO)_3(CO)_5(P(OMe)_3)_2]$, **34** (18.1 mg, 76 %). Analytical data for **34**: IR (c-C_6H_{12}) 2002vs, 2031s, 1983w, 1949m, 1914s, 1858m. 1807m cm^{-1}; ^1H NMR ($CDCl_3$) δ 4.670 [s (br), 5H, C_5H_5], 3.80 - 3.61 (m, 18H, OMe); MS 1298 ([M-2CO]$^+$, 32), 1270 ([M-3CO]$^+$, 100), 1242 ([M-4CO]$^+$, 65) 1214 ([M-5CO]$^+$, 90), 1186 ([M-6CO]$^+$, 23), 1158 ([M-7CO]$^+$, 35);. Anal. Calcd: C 21.28, H 2.08. Found: C 21.68, H 1.98 %.

2.4.35. Reaction of $[Cp_2W_2Ir_2(CO)_{10}]$ (3) with dppm (with J. Lee)

Following the method of Section 2.4.29., $[Cp_2W_2Ir_2(CO)_{10}]$ (20.0 mg, 0.0172 mmol) and dppm (6.6 mg, 0.0172 mmol) in CH_2Cl_2 (20 mL) afforded two bands after chromatography (3 CH_2Cl_2 : 1 petroleum ether eluant). The contents of the first band were identified as **3** (2.1 mg, 11 %). Crystallization of the contents of the second band, R_f 0.65, from CH_2Cl_2/MeOH afforded dark brown crystals of $[Cp_2W_2Ir_2(\mu\text{-}CO)_3(\mu\text{-dppm})(CO)_5]$, **35** (19.4 mg, 76%). Analytical data for **35**: IR (c-C_6H_{12}) 2003vs, 1990s, 1979s, 1971m, 1960s, 1952m, 1911m, 1870w cm^{-1}; ^1H NMR ($CDCl_3$, 298 K) δ 7.54-7.39 (m, 20H, Ph), 4.56 (s (br), 10H, C_5H_5), 3.48 (s, 2H, CH_2); ^{13}C NMR (CD_2Cl_2, 213 K) δ 133.2-127.9 (m, Ph), 88.7 (s, C_5H_5), 87.6 (s, C_5H_5), other signals not observed; MS 1491 ([M]$^+$, 33), 1463 ([M-CO]$^+$, 22), 1435 ([M-2CO]$^+$, 35), 1407 ([M-3CO]$^+$, 100), 1379 ([M-4CO]$^+$, 47), 1351 ([M-5CO]$^+$, 92), 1323 ([M-6CO]$^+$, 36). Anal. Calcd.: C 34.64, H 2.16. Found: C 34.89, H 2.26 %.

2.4.36. Reaction of $[Cp_2W_2Ir_2(CO)_{10}]$ (3) with dppe (with J. Lee)

Following the method of Section 2.4.29., $[Cp_2W_2Ir_2(CO)_{10}]$ (20.0 mg, 0.0172 mmol) and dppe (6.9 mg, 0.0173 mmol) in CH_2Cl_2 (20 mL) afforded two bands after chromatography (4 CH_2Cl_2 : 1 petroleum ether eluant). The contents of the first band were identified as **3** (1.6 mg, 8 %). Crystallization of the contents of the second band, R_f 0.60, from CH_2Cl_2/MeOH afforded dark brown crystals of $[Cp_2W_2Ir_2(\mu\text{-}CO)_3(\mu\text{-dppe})(CO)_5]$, **36** (20.3 mg, 80 %). Analytical data for **36**: IR (c-C_6H_{12}) 2007s, 2002vs, 1992w, 1978s, 1973s, 1954m, 1916s, 1859m cm^{-1}; ^1H NMR ($CDCl_3$, 298 K) δ 7.53-7.38 (m, 20H, Ph), 4.73 (s (br), 10H, C_5H_5), 3.98 (s, 4H, CH_2); ^{13}C NMR (CD_2Cl_2, 213 K) δ 131.3-128.5 (m, Ph), 88.7 (s, C_5H_5), 88.4 (s, C_5H_5), 87.9 (s, C_5H_5), 87.6 (s, C_5H_5), 20.2 (s, Me); MS 1505 ([M]$^+$, 45), 1477 ([M-CO]$^+$, 13), 1449 ([M-2CO]$^+$, 20), 1421 ([M-3CO]$^+$, 100), 1393 ([M-4CO]$^+$,

28), 1365 ([M-5CO]$^+$, 60), 1337 ([M-6CO]$^+$, 45), 1309 ([M-7CO]$^+$, 50). Anal. Calcd.: C 35.12, H 2.28. Found: C 34.72, H 1.91%.

2.5. References

(1) Barnes, C. In *Comprehensive Organometallic Chemistry II*; Abel, E. W.; Stone, F. G. A.; Wilkinson, G., Eds.; Pergamon Press, Oxford, U.K.: 1995; Vol. 8, Ch. 4.

(2) Churchill, M. R.; Hutchinson, J. P. *Inorg. Chem.* **1978**, *17*, 3528.

(3) Churchill, M. R.; Hutchinson, J. P. *Inorg. Chem.* **1979**, *18*, 2451.

(4) Besançon, K.; Laurenczy, G.; Lumini, T.; Roulet, R. *Helv. Chim. Acta* **1993**, *76*, 2926.

(5) Bondietti, G.; Ros, R.; Roulet, R.; Musso, F.; Gervasio, G. *Inorg. Chim. Acta* **1993**, *213*, 301.

(6) Benvenutti, M. H. A.; Hitchcock, P. B.; Nixon, J. F.; Vargas, M. D. *J. Chem. Soc., Dalton Trans.* **1996**, 739.

(7) Benvenutti, M. H. A.; Hitchcock, P. B.; Nixon, J. F.; Vargas, M. D. *J. Chem. Soc., Chem. Commun.* **1996**, 441.

(8) Della Pergola, R.; Garlaschelli, L.; Martinengo, S.; Demartin, F.; Manassero, M.; Sansoni, M. *Gazz. Chim. Ital.* **1987**, *117*, 245.

(9) Stuntz, G. F.; Shapley, J. R. *J. Organomet. Chem.* **1981**, *213*, 389.

(10) Mann, B. E.; Vargas, M. D.; Khadar, R. *J. Chem. Soc., Dalton Trans.* **1992**, 1725.

(11) Brown, M. P.; Burns, D.; Harding, M. M.; Maginn, S.; Smith, A. K. *Inorg. Chim. Acta* **1989**, *162*, 287.

(12) May, A. S., PhD Thesis, University of Western Australia, 1986.

(13) Bojczuk, M.; Heaton, B. T.; Johnson, S.; Ghilardi, C. A.; Orlandini, A. *J. Organomet. Chem.* **1988**, *341*, 473.

(14) Chini, P.; Ciani, G.; Garlaschelli, L.; Manassero, M.; Martinengo, S.; Sironi, A. *J. Organomet. Chem.* **1978**, *152*, C35.

(15) Ragaini, F.; Porta, F.; Demartin, F. *Organometallics* **1991**, *10*, 185.

(16) Garlaschelli, L.; Martinengo, S.; Chini, P.; Canziani, F.; Bau, R. *J. Organomet. Chem.* **1981**, *213*, 379.

(17) Ros, R.; Scrivanti, A.; Albano, V. G.; Braga, D. *J. Chem. Soc., Dalton Trans.* **1986**, 2411.

(18) Bau, R.; Chiang, M. Y.; Wei, C.-Y.; Garlaschelli, L.; Martinengo, S.; Koetzle, T. F. *Inorg. Chem.* **1984**, *23*, 4758.

(19) Braga, D.; Grepioni, F.; Livotto, F. S.; Vargas, M. D. *J. Organomet. Chem.* **1990**, *391*, C28.

(20) Malatesta, L.; Caglio, G. J. *Chem. Commun.* **1967**, 420.

(21) Vandenberg, D. M.; Chin-Choy, T.; Ford, P. C. *J. Organomet. Chem.* **1989**, *366*, 257.

(22) Davis, M. J.; Roulet, R. *Inorg. Chim. Acta.* **1992**, *197*, 15.

(23) Stuntz, G. F.; Shapley, J. R. *Inorg. Chem.* **1976**, *15*, 1994.

(24) Mann, B. E.; Spencer, C. M.; Smith, A. K. *J. Organomet. Chem.* **1983**, *244*, C17.

(25) Mann, B. E.; Pickup, B. T.; Smith, A. K. *J. Chem. Soc., Dalton Trans.* **1989**, 889.

(26) Stuntz, G. F.; Shapley, J. R. *J. Am. Chem. Soc.* **1977**, *99*, 607.

(27) Karel, K. J.; Norton, J. R. *J. Am. Chem. Soc.* **1974**, *96*, 6812.

(28) Strawczynski, A.; Suardi, G.; Ros, R.; Roulet, R. *Helv. Chim. Acta* **1993**, *76*, 2210.

(29) Ciani, G.; Manassero, M.; Sironi, A. *J. Organomet. Chem.* **1980**, *199*, 271.

(30) Strawczynski, A.; Ros, R.; Roulet, R. *Helv. Chim. Acta* **1988**, *71*, 867.

(31) Stevens, R. E.; Liu, P. C. C.; Gladfelter, W. L. *J. Organomet. Chem.* **1985**, *287*, 133.

(32) Ros, R.; Canziani, F.; Roulet, R. *J. Organomet. Chem.* **1984**, *267*, C9.

(33) Ros, R.; Scrivanti, A.; Roulet, R. *J. Organomet. Chem.* **1986**, *303*, 273.

(34) Braga, D.; Ros, R.; Roulet, R. *J. Organomet. Chem.* **1985**, *286*, C8.

(35) Ciani, G.; Manassero, M.; Albano, V. G.; Canziani, F.; Giordano, G.; Martinengo, S.; Chini, P. *J. Organomet. Chem.* **1978**, *150*, C17.

(36) Albano, V.; Bellon, P.; Scatturin, V. *Chem. Commun.* **1967**, 730.

(37) Drakesmith, A. J.; Whyman, R. *J. Chem. Soc., Dalton Trans.* **1973**, 362.

(38) Flörke, U.; Haupt, H.-J. *Z. Kristallogr.* **1990**, *191*, 149.

(39) Strawczynski, A.; Ros, R.; Roulet, R. *Helv. Chim. Acta* **1988**, *71*, 1885.

(40) Shapley, J. R.; Stuntz, G. F.; Churchill, M. R.; Hutchinson, J. P. *J. Am. Chem. Soc.* **1979**, *101*, 7425.

(41) Churchill, M. R.; Hutchinson, J. P. *Inorg. Chem.* **1980**, *19*, 2765.

(42) Ros, R.; Bertani, R.; Tassan, A.; Braga, D.; Grepioni, F. *Inorg. Chim. Acta* **1996**, *244*, 11.

(43) Strawczynski, A.; Ros, R.; Roulet, R.; Braga, D.; Gradella, C.; Grepioni, F. *Inorg. Chim. Acta* **1990**, *170*, 17.

(44) Foster, D. F.; Nicholls, B. S.; Smith, A. K. *J. Organomet. Chem.* **1982**, *236*, 395.
(45) Albano, V. G.; Braga, D.; Ros, R.; Scrivanti, A. *J. Chem. Soc., Chem. Commun.* **1985**, 866.
(46) Laurenczy, G.; Bondietti, G.; Ros, R.; Roulet, R. *Inorg. Chim. Acta* **1996**, *247*, 65.
(47) Livotto, F. S.; Raithby, P. R.; Vargas, M. D. *J. Chem. Soc., Dalton Trans.* **1993**, 1797.
(48) Darensbourg, D. J.; Baldwin-Zuschke, B. J. *J. Am. Chem. Soc.* **1982**, *104*, 3906.
(49) Whyman, R. *J. Organomet. Chem.* **1970**, *24*, C35.
(50) Galdecka, E.; Galdecki, Z.; Wajda-Hermanowicz, K.; Pruchnik, F. P. *J. Chem. Cryst.* **1995**, *25*, 717.
(51) Wajda-Hermanowicz, K.; Pruchnik, F.; Zuber, M.; Rusek, G.; Galdecka, E.; Galdecki, Z. *Inorg. Chim. Acta* **1995**, *232*, 207.
(52) Strawczynski, A.; Hall, C.; Bondietti, G.; Ros, R.; Roulet, R. *Helv. Chim. Acta* **1994**, *77*, 754.
(53) Braga, D.; Grepioni, F.; Guadalupi, G.; Scrivanti, A.; Ros, R.; Roulet, R. *Organometallics* **1987**, *6*, 56.
(54) Arduini, A. A.; Bahsoun, A. A.; Osborn, J. A.; Voelker, C. *Angew. Chem. Int. Ed. Engl.* **1980**, *19*, 1024.
(55) Clucas, J. A.; Harding, M. M.; Nicholls, B. S.; Smith, A. K. *J. Chem. Soc., Chem. Commun.* **1984**, 319.
(56) Suardi, G.; Strawczynski, A.; Ros, R.; Roulet, R. *Helv. Chim. Acta* **1990**, *73*, 154.
(57) Orlandi, A.; Frey, U.; Suardi, G.; Merbach, A. E.; Roulet, R. *Inorg. Chem.* **1992**, *31*, 1304.
(58) Cattermole, P. E.; Orrell, K. G.; Osborne, A. G. *J. Chem. Soc., Dalton Trans.* **1974**, 328.
(59) Darensbourg, D. J.; Baldwin-Zuschke, B. J. *Inorg. Chem.* **1981**, *20*, 3846.
(60) Blake, A. J.; Osborne, A. G. *J. Organomet. Chem.* **1984**, *260*, 227.
(61) Demartin, F.; Manassero, M.; Sansoni, M.; Garlaschelli, L.; Sartorelli, U. *J. Organomet. Chem.* **1981**, *204*, C10.
(62) Stuntz, G. F.; Shapley, J. R.; Pierpoint, C. G. *Inorg. Chem.* **1978**, *17*, 2596.
(63) Harding, M. M.; Nicholls, B. S.; Smith, A. K. *Acta. Cryst.* **1984**, *C40*, 790.
(64) Arif, A. M.; Jones, R. A.; Schwab, S. T.; Whittlesey, B. R. *J. Am. Chem. Soc.* **1986**, *108*, 1703.
(65) Ueng, C.-H.; Lu, S.-M. *Inorg. Chim. Acta* **1997**, *262*, 113.
(66) Demartin, F.; Manassero, M.; Sansoni, M.; Garlaschelli, L.; Raimondi, C.; Martinengo, S.; Canziani, F. *J. Chem. Soc., Chem. Commun.* **1981**, 528.
(67) Nicholls, J. N.; Raithby, P. R.; Vargas, M. D. *J. Chem. Soc., Chem. Commun.* **1986**, 1617.
(68) Benvenutti, M. H. A.; Vargas, M. D.; Braga, D.; Grepioni, F.; Mann, B. E.; Naylor, S. *Organometallics* **1993**, *12*, 2947.
(69) Lee, J.; Humphrey, M. G.; Hockless, D. C. R.; Skelton, B. W.; White, A. H. *Organometallics* **1993**, *12*, 3468.
(70) Churchill, M. R.; Hutchinson, J. P. *Inorg. Chem.* **1981**, *20*, 4112.
(71) Darensbourg, D. J.; Incorvia, M. J. *Inorg. Chem.* **1981**, *20*, 1911.
(72) Iiskola, E.; Pakkanen, T. *Acta Chem. Scand. A* **1984**, *38*, 731.
(73) Pursiainen, J.; Pakkanen, T. A.; Jääskeläinen, J. *J. Organomet. Chem.* **1985**, *290*, 85.
(74) Pursiainen, J.; Ahlgren, M.; Pakkanen, T.; Valkonen, J. *J. Chem. Soc., Dalton Trans.* **1990**, 1147.
(75) Murray, J. B.; Nicholson, B. K.; Whitton, A. J. *J. Organomet. Chem.* **1990**, *385*, 91.
(76) Churchill, M. R.; Bueno, C.; Hutchinson, J. P. *Inorg. Chem.* **1982**, *21*, 1359.
(77) Schmidt, G.; Bartl, K.; Boese, R. *Z. Naturforsch, B* **1977**, *32*, 1277.
(78) Churchill, M. R., Li, Y.-J., Shapley, J. R., Foose, D. S., Uchiyama, W. S. *J. Organomet. Chem.* **1986**, *312*, 121.
(79) Shriver, D. F.; Drezdzon, M. A. *The Manipulation of Air Sensitive Compounds;* 2nd ed.; John Wiley and Sons: New York **1986**.
(80) Shapley, J. R.; Hardwick, S. J.; Foose, D. S.; Stucky, G. D. *J. Am. Chem. Soc.* **1981**, *103*, 7383.

Chapter 3

NMR Studies on Tungsten - Iridium Clusters

Chapter 3

NMR Studies on Tungsten-Iridium Clusters

Contents

3.1. Carbonyl Migration on Tetrairidium Clusters.....184

3.2. NMR Studies of Tungsten-Iridium Clusters.....194

3.2.1. NMR Spectra of $[CpWIr_3(CO)_{11}]$ (**2**) and $[Cp_2W_2Ir_2(CO)_{10}]$ (**3**).....194

3.2.2. NMR studies of PPh_3 and PMe_3 derivatives of $[CpWIr_3(CO)_{11}]$ (**2**).....197

3.2.3. NMR studies of $PMePh_2$ and PMe_2Ph derivatives of $[CpWIr_3(CO)_{11}]$ (**2**).....225

3.2.4. NMR studies of $P(OPh)_3$ and $P(OMe)_3$ derivatives of $[CpWIr_3(CO)_{11}]$ (**2**).....231

3.2.5. NMR studies of dppe, dppm and pdpp derivatives of $[CpWIr_3(CO)_{11}]$ (**2**).....238

3.2.6. NMR studies of isocyanide derivatives of $[CpWIr_3(CO)_{11}]$ (**2**).....255

3.2.7. NMR studies of PPh_3 and PMe_3 derivatives of $[Cp_2W_2Ir_2(CO)_{10}]$ (**3**) 256

3.2.8. NMR studies of $P(OMe)_3$ derivatives of $[Cp_2W_2Ir_2(CO)_{10}]$ (**3**).....281

3.2.9. NMR studies of dppm and dppe derivatives of $[Cp_2W_2Ir_2(CO)_{10}]$ (**3**).....289

3.3. Conclusions.....300

3.4. Experimental.....309

3.4.1. Instruments and Reagents.....313

3.4.2. Spectroscopic Data for $[CpWIr_3(\mu\text{-}CO)_3(CO)_7(PPh_3)]$ (**4**).....313

3.4.3. Spectroscopic Data for $[CpWIr_3(\mu\text{-}CO)_3(CO)_6(PPh_3)_2]$ (**5**).....314

3.4.4. Spectroscopic Data for [CpWIr$_3$(μ-CO)$_3$(CO)$_5$(PPh$_3$)$_3$] (**6**).....315

3.4.5. Spectroscopic Data for [CpWIr$_3$(μ-CO)$_3$(CO)$_7$(PMe$_3$)] (**7**).....315

3.4.6. Spectroscopic Data for [CpWIr$_3$(μ-CO)$_3$(CO)$_6$(PMe$_3$)$_2$] (**8**).....315

3.4.7. Spectroscopic Data for [CpWIr$_3$(μ-CO)$_3$(CO)$_5$(PMe$_3$)$_3$] (**9**).....315

3.4.8. Spectroscopic Data for [CpWIr$_3$(μ-CO)$_3$(CO)$_7$(PMePh$_2$)] (**10**).....316

3.4.9. Spectroscopic Data for [CpWIr$_3$(μ-CO)$_3$(CO)$_6$(PMePh$_2$)$_2$] (**11**).....316

3.4.10. Spectroscopic Data for [CpWIr$_3$(μ-CO)$_3$(CO)$_5$(PMePh$_2$)$_3$] (**12**).....316

3.4.11. Spectroscopic Data for [CpWIr$_3$(μ-CO)$_3$(CO)$_7$(PMe$_2$Ph)] (**13**)..... 316

3.4.12. Spectroscopic Data for [CpWIr$_3$(μ-CO)$_3$(CO)$_6$(PMe$_2$Ph)$_2$] (**14**).....316

3.4.13. Spectroscopic Data for [CpWIr$_3$(μ-CO)$_3$(CO)$_5$(PMe$_2$Ph)$_3$] (**15**).....317

3.4.14. Spectroscopic Data for [CpWIr$_3$(μ-CO)$_3$(CO)$_7${P(OPh)$_3$}] (**16**).....317

3.4.15. Spectroscopic Data for [CpWIr$_3$(μ-CO)$_3$(CO)$_6${P(OPh)$_3$}$_2$] (**17**).....317

3.4.16. Spectroscopic Data for [CpWIr$_3$(μ-CO)$_3$(CO)$_5${P(OPh)$_3$}$_3$] (**18**).....317

3.4.17. Spectroscopic Data for [CpWIr$_3$(μ-CO)$_3$(CO)$_7${P(OMe)$_3$}] (**19**).....317

3.4.18. Spectroscopic Data for [CpWIr$_3$(μ-CO)$_3$(CO)$_6${P(OMe)$_3$}$_2$] (**20**).....317

3.4.19. Spectroscopic Data for [CpWIr$_3$(μ-CO)$_3$(CO)$_5${P(OMe)$_3$}$_3$] (**21**).....317

3.4.20. Spectroscopic Data for [CpWIr$_3$(μ-dppe)(μ-CO)$_3$CO)$_6$] (**22**).....317

3.4.21. Spectroscopic Data for [CpWIr$_3$(μ-dppm)(μ-CO)$_3$(CO)$_6$] (**23**).....317

3.4.22. Spectroscopic Data for [CpWIr$_3$(μ-pdpp)(μ-CO)$_3$(CO)$_6$] (**24**).....318

3.4.23. Spectroscopic Data for [Cp$_2$W$_2$Ir$_2$(μ-CO)$_3$(CO)$_6$(PPh$_3$)] (**31**).....318

3.4.24. Spectroscopic Data for [Cp$_2$W$_2$Ir$_2$(μ-CO)$_3$(CO)$_5$(PPh$_3$)$_2$] (**32**).....318

3.4.25. Spectroscopic Data for [Cp$_2$W$_2$Ir$_2$(μ-CO)$_3$(CO)$_6$(PMe$_3$)] (**33**).....318

3.4.26. Spectroscopic Data for [Cp$_2$W$_2$Ir$_2$(μ-CO)$_3$(CO)$_5$(PMe$_3$)$_2$] (**34**).....319

3.4.27. Spectroscopic Data for [Cp$_2$W$_2$Ir$_2$(μ-CO)$_3$(CO)$_6${P(OMe)$_3$}] (**35**).....319

3.4.28. Spectroscopic Data for [Cp$_2$W$_2$Ir$_2$(μ-CO)$_3$(CO)$_5${P(OMe)$_3$}$_2$] (**36**).....320

3.4.29. Spectroscopic Data for [Cp$_2$W$_2$Ir$_2$(μ-dppm)(μ-CO)$_3$(CO)$_5$] (**37**).....320

3.4.30. Spectroscopic Data for [Cp$_2$W$_2$Ir$_2$(μ-dppe)(μ-CO)$_3$(CO)$_5$] (**38**).....320

3.5. References.....321

List of Figures

Figure 3.2.1. Variable temperature ^{13}C NMR spectroscopic study of $[CpWIr_3(CO)_{11}]$ (**2**) 195

Figure 3.2.2. Variable temperature ^{13}C NMR spectroscopic study of $[Cp_2W_2Ir_2(CO)_{10}]$ (**3**).....196

Figure 3.2.3. Variable temperature ^{31}P NMR spectroscopic study of $[CpWIr_3(\mu\text{-}CO)_3(CO)_7(PPh_3)]$ (**4**).....198

Figure 3.2.4. Variable temperature ^{13}C NMR spectroscopic study of $[CpWIr_3(\mu\text{-}CO)_3(CO)_7(PPh_3)]$ (**4**).....199

Figure 3.2.5. Configurations of $[CpWIr_3(\mu\text{-}CO)_3(CO)_{8-n}(L)_n]$ (L = PPh_3, PMe_3; n = 1-3).....201

Figure 3.2.6. ^{13}C NMR COSY spectrum of $[CpWIr_3(\mu\text{-}CO)_3(CO)_7(PPh_3)]$ (**4**).....202

Figure 3.2.7. ^{13}C NMR spectrum of $[CpWIr_3(\mu\text{-}CO)_3(CO)_7(PPh_3)]$ (**4**).....203

Figure 3.2.8. ^{13}C NMR EXSY spectrum of $[CpWIr_3(\mu\text{-}CO)_3(CO)_7(PPh_3)]$ (**4**).....204

Figure 3.2.9. Variable temperature ^{31}P NMR spectroscopic study of $[CpWIr_3(\mu\text{-}CO)_3(CO)_6(PPh_3)_2]$ (**5**) 207

Figure 3.2.10. Variable temperature ^{13}C NMR spectroscopic study of $[CpWIr_3(\mu\text{-}CO)_3(CO)_6(PPh_3)_2]$ (**5**).....208

Figure 3.2.11. ^{13}C NMR COSY spectrum of $[CpWIr_3(\mu\text{-}CO)_3(CO)_6(PPh_3)_2]$ (**5**).....209

Figure 3.2.12. ^{13}C NMR EXSY spectrum of $[CpWIr_3(\mu\text{-}CO)_3(CO)_6(PPh_3)_2]$ (**5**).....210

Figure 3.2.13. Variable temperature ^{31}P NMR spectroscopic study of $[CpWIr_3(\mu\text{-}CO)_3(CO)_7(PMe_3)]$ (**7**).....214

Figure 3.2.14. Variable temperature ^{13}C NMR spectroscopic study of $[CpWIr_3(\mu\text{-}CO)_3(CO)_7(PMe_3)]$ (**7**).....215

Figure 3.2.15. ^{13}C NMR COSY spectrum of $[CpWIr_3(\mu\text{-}CO)_3(CO)_7(PMe_3)]$ (**7**).....216

Figure 3.2.16. ^{13}C NMR EXSY spectrum of $[CpWIr_3(\mu\text{-}CO)_3(CO)_7(PMe_3)]$ (**7**).....217

Figure 3.2.17. Variable temperature ^{31}P NMR spectroscopic study of $[CpWIr_3(\mu\text{-}CO)_3(CO)_6(PMe_3)_2]$ (**8**).....218

Figure 3.2.18. Variable temperature ^{13}C NMR spectroscopic study of $[CpWIr_3(\mu\text{-}CO)_3(CO)_6(PMe_3)_2]$ (**8**).....219

Figure 3.2.19. ^{13}C NMR COSY spectrum of $[CpWIr_3(\mu\text{-}CO)_3(CO)_6(PMe_3)_2]$ (**8**).....220

Figure 3.2.20. ^{13}C NMR EXSY spectrum of $[CpWIr_3(\mu\text{-}CO)_3(CO)_6(PMe_3)_2]$ (**8**).....221

Figure 3.2.21. Variable temperature ^{31}P NMR spectroscopic study of $[CpWIr_3(\mu\text{-}CO)_3(CO)_5(PMe_3)_3]$ (**9**).....223

Figure 3.2.22. Variable temperature ^{13}C NMR spectroscopic study of $[CpWIr_3(\mu\text{-}CO)_3(CO)_5(PMe_3)_3]$ (**9**).....224

Figure 3.2.23. Variable temperature ^{31}P NMR spectroscopic study of

$[CpWIr_3(\mu\text{-}CO)_3(CO)_7(PMePh_2)]$ (**10**).....228

Figure 3.2.24. Variable temperature ^{31}P NMR spectroscopic study of $[CpWIr_3(\mu\text{-}CO)_3(CO)_7(PMe_2Ph)]$ (**13**).....229

Figure 3.2.25. Configurations of $[CpWIr_3(\mu\text{-}CO)_3(CO)_{8-n}(L)_n]$ (L = $PMePh_2$, PMe_2Ph; n = 1 - 3).....230

Figure 3.2.26. Variable temperature ^{31}P NMR spectroscopic study of $[CpWIr_3(\mu\text{-}CO)_3(CO)_7\{P(OPh)_3\}]$ (**16**).....233

Figure 3.2.27. Variable temperature ^{31}P NMR spectroscopic study of $[CpWIr_3(\mu\text{-}CO)_3(CO)_7\{P(OMe)_3\}]$ (**19**).....234

Figure 3.2.28. Configurations of $[CpWIr_3(\mu\text{-}CO)_3(CO)_{8-n}(L)_n]$ [L = $P(OPh)_3$, $P(OMe)_3$; n = 1-3].....237

Figure 3.2.29. Variable temperature ^{31}P NMR spectroscopic study of $[CpWIr_3(\mu\text{-}CO)_3(\mu\text{-}dppe)(CO)_6]$ (**22**).....239

Figure 3.2.30. Variable temperature ^{13}C NMR spectroscopic study of $[CpWIr_3(\mu\text{-}CO)_3(\mu\text{-}dppe)(CO)_6]$ (**22**) 240

Figure 3.2.31. Partial ^{13}C NMR spectroscopic study (line broadening 10 Hz) of $[CpWIr_3(\mu\text{-}CO)_3(\mu\text{-}dppe)(CO)_6]$ (**22**) in CD_2Cl_2 emphasizing configuration **22c**.....241

Figure 3.2.32.(a) Configurations of $[CpWIr_3(\mu\text{-}CO)_3(\mu\text{-}dppe)(CO)_6]$ (**22**); (b) Projection of configurations **22a** and **22b** onto the Ir_3 plane.....242

Figure 3.2.33. ^{13}C NMR COSY spectrum of $[CpWIr_3(\mu\text{-}CO)_3(\mu\text{-}dppe)(CO)_6]$ (**22**).....243

Figure 3.2.34. ^{13}C NMR EXSY spectrum of $[CpWIr_3(\mu\text{-}CO)_3(\mu\text{-}dppe)(CO)_6]$ (**22**).....244

Figure 3.2.35. ^{13}C NMR EXSY spectrum of $[CpWIr_3(\mu\text{-}CO)_3(\mu\text{-}dppe)(CO)_6]$ (**22**).....246

Figure 3.2.36. Variable temperature ^{31}P NMR spectroscopic study of $[CpWIr_3(\mu\text{-}CO)_3(\mu\text{-}dppm)(CO)_6]$ (**23**).....248

Figure 3.2.37. Variable temperature ^{13}C NMR spectroscopic study of $[CpWIr_3(\mu\text{-}CO)_3(\mu\text{-}dppm)\ (CO)_6]$ (**23**).....249

Figure 3.2.38. Configurations of $[CpWIr(\mu\text{-}CO)_3(\mu\text{-}dppm)(CO)_6]$ (**23**).....250

Figure 3.2.39. ^{13}C NMR EXSY spectrum of $[CpWIr_3(\mu\text{-}CO)_3(\mu\text{-}dppm)(CO)_6]$ (**23**).....251

Figure 3.2.40. ^{13}C NMR EXSY spectrum of $[CpWIr_3(\mu\text{-}CO)_3(\mu\text{-}dppm)(CO)_6]$ (**23**).....252

Figure 3.2.41. Variable temperature ^{31}P NMR spectroscopic study of $[CpWIr_3(\mu\text{-}CO)_3(\mu\text{-}pdpp)(CO)_6]$ (**24**).....254

Figure 3.2.42. Configuration of $[CpWIr_3(\mu\text{-}CO)_3(\mu\text{-}pdpp)(CO)_6]$ (**24**).....255

Figure 3.2.43. Variable temperature ^{31}P NMR spectroscopic study of $[Cp_2W_2Ir_2(\mu\text{-}CO)_3(CO)_6(PMe_3)]$ (**33**).....257

Figure 3.2.44. Variable temperature ^{13}C NMR spectroscopic study of $[Cp_2W_2Ir_2(\mu\text{-}CO)_3(CO)_6(PMe_3)]$ (**33**).....258

Figure 3.2.45. HSQC NMR spectrum of $[Cp_2W_2Ir_2(\mu\text{-}CO)_3(CO)_6(PMe_3)]$ (**33**).....259

Figure 3.2.46. Triple resonance ^{1}H-^{31}P-^{13}C NMR spectroscopic study of $[Cp_2W_2Ir_2(\mu\text{-}CO)_3(CO)_6(PMe_3)]$ (**33**).....260

Figure 3.2.47. Configurations of $[Cp_2W_2Ir_2(\mu\text{-}CO)_3(CO)_{7-n}(L)_n]$ [L = PPh_3, PMe_3; n = 1-2].....261

Figure 3.2.48. ^{13}C NMR EXSY spectrum of $Cp_2W_2Ir_2(\mu\text{-}CO)_3(CO)_6(PMe_3)$ (**4**).....262

Figure 3.2.49. Variable temperature ^{31}P NMR spectroscopic study of $[Cp_2W_2Ir_2(\mu\text{-}CO)_3(CO)_6(PPh_3)]$ (**31**).....264

Figure 3.2.50. (a) Variable temperature ^{13}C NMR spectroscopic study of $[Cp_2W_2Ir_2(\mu\text{-}CO)_3(CO)_6(PPh_3)]$ (**31**; (b) ^{13}C NMR spectrum of $[Cp_2W_2Ir_2(\mu\text{-}CO)_3(CO)_6(PPh_3)]$ (**31**).....265-266

Figure 3.2.51. Variable temperature ^{31}P NMR spectroscopic study of $[Cp_2W_2Ir_2(\mu\text{-}CO)_3(CO)_5(PMe_3)_2]$ (**34**).....269

Figure 3.2.52. Variable temperature ^{31}C NMR spectroscopic study of $[Cp_2W_2Ir_2(\mu\text{-}CO)_3(CO)_5(PMe_3)_2]$ (**34**).....270

Figure 3.2.53. Triple resonance ^{1}H- ^{31}P-^{13}C NMR spectrum of $[Cp_2W_2Ir_2(\mu\text{-}CO)_3(CO)_5(PMe_3)_2]$ (**34**).....271

Figure 3.2.54. HSQC NMR spectrum of $[Cp_2W_2Ir_2(\mu\text{-}CO)_3(CO)_5(PMe_3)_2]$ (**34**).....273

Figure 3.2.55. Partial ^{13}C NMR spectrum (line broadening = 10 Hz) of $[Cp_2W_2Ir_2(\mu\text{-}CO)_3(CO)_5(PMe_3)_2]$ (**34**) emphasizing configuration **34c**.....274

Figure 3.2.56. ^{13}C NMR EXSY spectrum of $[Cp_2W_2Ir_2(\mu\text{-}CO)_3(CO)_5(PMe_3)_2]$ (**5**).....276

Figure 3.2.57. Variable temperature ^{31}P NMR spectroscopic study of $[Cp_2W_2Ir_2(\mu\text{-}CO)_3(CO)_5(PPh_3)_2]$ (**32**).....276

Figure 3.2.58. Variable temperature ^{13}C NMR spectroscopic study of $[Cp_2W_2Ir_2(\mu\text{-}CO)_3(CO)_5(PPh_3)_2]$ (**32**).....277

Figure 3.2.59. ^{183}W-^{13}C correlation NMR spectrum of $[Cp_2W_2Ir_2(\mu\text{-}CO)_3(CO)_6(PMe_3)]$ (**33**).....279

Figure 3.2.60. ^{183}W-^{1}H correlation NMR spectrum of $[Cp_2W_2Ir_2(\mu\text{-}CO)_3(CO)_6(PMe_3)]$ (**33**).....280

Figure 3.2.61. ^{31}P NMR spectroscopic study of $[Cp_2W_2Ir_2(\mu\text{-}CO)_3(CO)_5\{P(OMe)_3\}_2]$ (**36**).....282

Figure 3.2.62. Variable temperature ^{13}C NMR spectroscopic study of $[Cp_2W_2Ir_2(\mu\text{-}CO)_3(CO)_6\{P\{OMe)_3\}]$ (**35**).....285

Figure 3.2.63. Configurations of $[Cp_2W_2Ir_2(\mu\text{-}CO)_3(CO)_{7-n}\{P(OMe)_3\}_n]$ (n = 1-2).....286

Figure 3.2.64. ^{13}C NMR COSY spectrum of $[Cp_2W_2Ir_2(\mu\text{-}CO)_3(CO)_6\{P(OMe)_3\}]$ (**35**).....286

Figure 3.2.65. ^{13}C NMR EXSY spectrum of $[Cp_2W_2Ir_2(\mu\text{-}CO)_3(CO)_6\{P(OMe)_3\}]$ (**35**).....287

Figure 3.2.66. ^{13}C NMR spectroscopic study of $[Cp_2W_2Ir_2(\mu\text{-}CO)_3(CO)_5\{P(OMe)_3\}_2]$ (**35**).....288

Figure 3.2.67. Variable temperature 31P NMR spectroscopic study of $[Cp_2W_2Ir_2(\mu\text{-}CO)_3(\mu\text{-dppm})(CO)_5]$ (**37**).....291

Figure 3.2.68. Variable temperature ^{13}C NMR spectroscopic study of $[Cp_2W_2Ir_2(\mu\text{-}CO)_3(\mu\text{-dppm})(CO)_5]$ (**37**).....292

Figure 3.2.69. Configurations of $[Cp_2W_2Ir_2(\mu\text{-}CO)_3(\mu\text{-L})(CO)_5]$ [L = dppm (**37**), dppe (**38**)].....293

Figure 3.2.70. ^{183}W-^{13}C correlation NMR spectroscopic study of $[Cp_2W_2Ir_2(\mu\text{-}CO)_3(\mu\text{-dppm})(CO)_5]$ (**37**).....294

Figure 3.2.71. ^{183}W-^{1}H correlation NMR spectroscopic study of $[Cp_2W_2Ir_2(\mu\text{-}CO)_3(\mu\text{-dppm})(CO)_5]$ (**37**).....295

Figure 3.2.72. Variable temperature ^{31}P NMR spectroscopic study of $[Cp_2W_2Ir_2(\mu\text{-}CO)_3(\mu\text{-dppe})(CO)_5]]$ (**38**).....297

Figure 3.2.73. Variable temperature ^{13}C NMR spectroscopic study of $[Cp_2W_2Ir_2(\mu\text{-}CO)_3(\mu\text{-dppe})(CO)_5]$ (**38**).....298

Figure 3.2.74. ^{13}C NMR EXSY spectrum of $[Cp_2W_2Ir_2(\mu\text{-}CO)_3(\mu\text{-dppe})(CO)_5]$ (**38**).....300

Figure 3.2.75. ^{13}C chemical shifts for carbonyl ligands on derivatives of $[CpWIr_3(CO)_{11}]$ (**2**) 302

Figure 3.2.76. ^{31}P chemical shifts for *P*-donor ligands on derivatives of $[CpWIr_3(CO)_{11}]$ (**2**) 302

Figure 3.2.77. ^{13}C chemical shifts for carbonyl substitution on derivatives of $[Cp_2W_2Ir_2(CO)_{10}]$ (**3**) 303

Figure 3.2.78. ^{31}P chemical shifts for *P*-donor ligand derivatives of $[Cp_2W_2Ir_2(CO)_{10}]$ (**3**).....303

Figure 3.2.79. Coordination Geometries for derivatives of $[CpWIr_3(CO)_{11}]$ (**2**) 305-306

Figure 3.2.80. Coordination Geometries for derivatives of $[Cp_2W_2Ir_2(CO)_{10}]$ (**3**) 307

Figure 3.4.1. Pulse sequence used for triple resonance HPCO experiment.....314

List of Tables

Table 3.1.1. CO Exchange Pathways of Tetrairidium Clusters.....185

Table 3.1.2. Exchange pathways of Derivatives of $[Ir_4(CO)_{12}]$, $[Ir_3Rh(CO)_{12}]$ and $[Ir_2Rh_2(CO)_{12}]$.....191

Table 3.2.1. Steric and Electronic Parameters for Phosphines in $[CpWIr_3(\mu\text{-}CO)_3(CO)_{8-n}(L)_n]$.....226

Table 3.2.2. ^{31}P NMR Data for $[CpWIr_3(\mu\text{-}CO)_3(CO)_{8-n}(L)_n]$ (L = $PMePh_2$, PMe_2Ph; n = 1, 2 or 3).....227

Table 3.2.3. ^{31}P NMR Data for $[CpWIr_3(\mu\text{-}CO)_3(CO)_{8-n}(L)_n]$ [L = $P(OPh)_3$, $P(OMe_3)$; n = 1, 2 or 3].....235

List of Schemes

Scheme 3.1.1. "Merry - go - round" process in $[Ir_4(\mu\text{-}CO)_3(CO)_8(L)]$.....184

Scheme 3.1.2. Change-of-basal face process in $[Ir_4(\mu\text{-}CO)_3(CO)_8(L)]$.....184

Scheme 3.1.3. Change-of-basal face process in $[Ir_4(\mu\text{-}CO)_3(CO)_8(\eta^4\text{-cod})]$ (unbridged intermediate).....188

Scheme 3.1.4. Change-of-basal face process in $[Ir_4(\mu\text{-}CO)_3(CO)_8(\eta^4\text{-diars})]$ (synchronous face change).....188

Scheme 3.1.5. CO mobility in $[Ir_4(\mu\text{-}CO)_3(CO)_8(L)]$ [L = $P(OMe)_3$, $P(OPh)_3$, $P(OCH_2)_3CEt$].....188

Scheme 3.1.6. CO exchange pathways in $[Ir_4(\mu\text{-}CO)_3(\mu\text{-}L)(CO)_7]$ [L = dppm, dppp, dpam].....190

Scheme 3.2.1. "Merry - go - round" process in **4a** and **7a**.....205

Scheme 3.2.2. CO mobility about the Ir_3 face in **5a** and **8a**.....211

Scheme 3.2.3. CO mobility about the WIr_2 face in **5a** and **8a**.....212

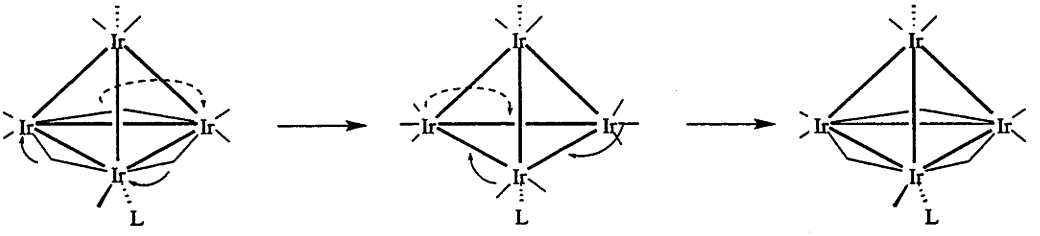
Scheme 3.2.4. CO exchange processes of $[CpWIr_3(\mu\text{-}CO)_3(\mu\text{-dppe})(CO)_6]$ (**22**) and $[CpWIr_3(\mu\text{-}CO)_3(\mu\text{-dppm})(CO)_6]$ (**23**).....253

Scheme 3.2.5. CO mobility about a WIr_2 face in **33b** and **35**.....263

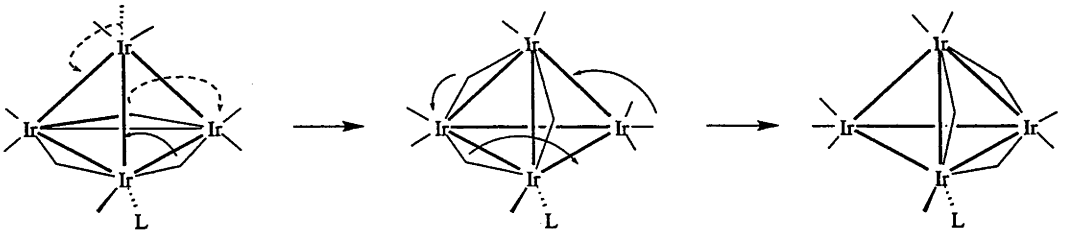
Scheme 3.2.6. CO mobility about a W_2Ir face in **34a**.....275

3.1 Carbonyl Migration on Tetrairidium Clusters

Ligand fluxionality on metal clusters has been the subject of many studies, with the majority of reports focussing on carbonyl migration on homometallic tri- and tetranuclear clusters.[1-10] The tetrahedral tetrairidium cluster core is robust, and facile routes into specifically substituted derivatives have been developed; not surprisingly, then, ligand-substituted derivatives of $[Ir_4(CO)_{12}]$ (**1**) form one of the most extensively investigated systems (Table 3.1.1.).[11-31] Carbonyl scrambling on $[Ir_4(CO)_{11}(L)]$ derivatives is well-defined, and proceeds by way of a Cotton merry-go-round process (Scheme 3.1.1.) or a mechanism with face-bridged intermediates (Scheme 3.1.2.).



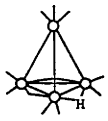
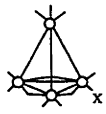
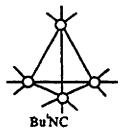
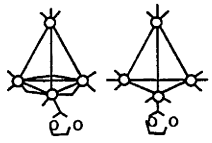
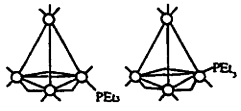
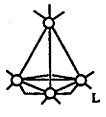
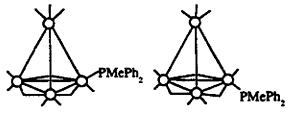
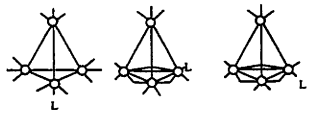
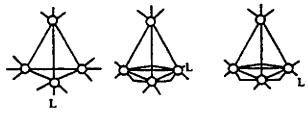
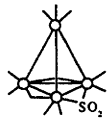
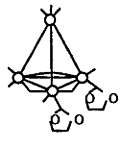
Scheme 3.1.1. "Merry - go - round" process in $[Ir_4(\mu\text{-}CO)_3(CO)_8(L)]$.

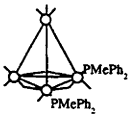
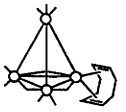
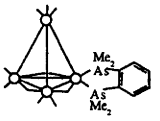
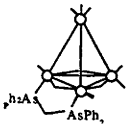
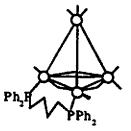
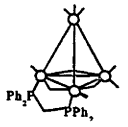
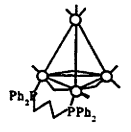
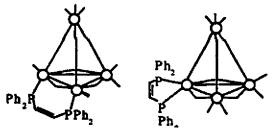
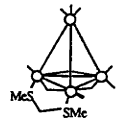
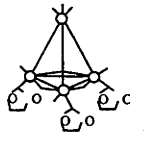
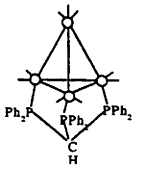
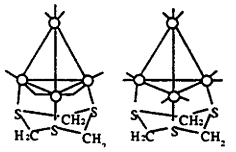
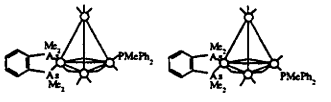


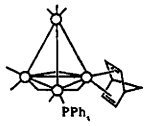
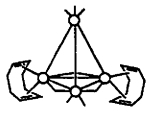
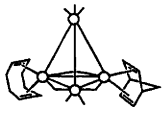
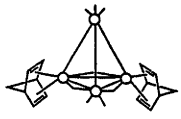
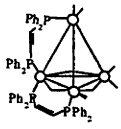
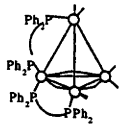
Scheme 3.1.2. Change-of-basal-face process in $[Ir_4(\mu\text{-}CO)_3(CO)_8(L)]$.

Carbonyl fluxionality on $[Ir_4(CO)_{10}(L)_2]$ derivatives is a function of the carbonyl ligand distribution, specifically, the nature of the edge-bridging carbonyls. For $[Ir_4(CO)_{10}(\eta^4\text{-cod})]$ with a symmetric edge-bridged structure, carbonyl scrambling proceeded to give an unbridged intermediate, followed by reformation of bridges about a different face (Scheme 3.1.3.).[25] For clusters with asymmetric bridges, carbonyl scrambling occurred via a synchronous face change, as the short Ir-CO bridging bond is too strong to permit access to an unbridged intermediate (Scheme 3.1.4.).

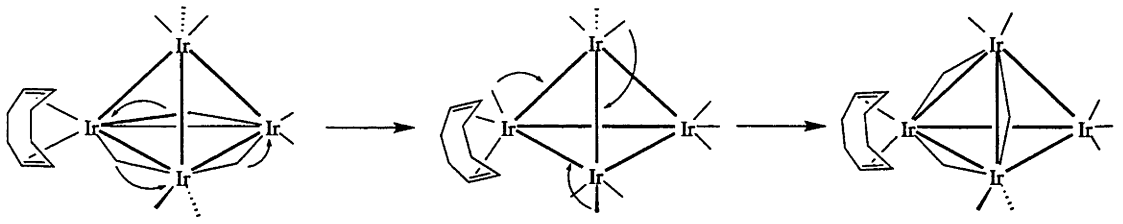
Table 3.1.1. CO Exchange pathways of Tetrairidium Clusters.

Ir_4 Cluster	*Ligand Coordination Geometries of Isomers*	*Fluxional Pathway* [a]	*Ref.(s)*
$[Ir_4(\mu\text{-}H)(\mu\text{-}CO)_2(CO)_9]^-$		synchronous change-of-basal-face	18
$[Ir_4(\mu\text{-}CO)_3(CO)_9X]^-$ (X = Br, I)		merry-go-round	14, 24
$[Ir_4(CO)_{11}(CNBu^t)]$		merry-go-round	29
$[Ir_4(CO)_{11}(\overline{COCH_2CH_2O})]$ $[Ir_4(\mu\text{-}CO)_3(CO)_8(\overline{COCH_2CH_2O})]$		1. merry-go-round 2. tripodal rotation	16
$[Ir_4(\mu\text{-}CO)_3(CO)_8(PEt_3)]$		1. merry-go-round 2. change-of-basal-face	23, 28
$[Ir_4(\mu\text{-}CO)_3(CO)_8(L)]$ [L = PPh_3, $P(C_6H_4NMe_2\text{-}4)_3$, $P(C_6H_4Cl\text{-}4)_3$, $P(C_6H_4OMe\text{-}4)_3$]		1. merry-go-round 2. synchronous change-of-basal-face	14
$[Ir_4(\mu\text{-}CO)_3(CO)_8(PMePh_2)]$		1. merry-go-round 2. change-of-basal-face	30
$[Ir_4(CO)_{11}(PH_{3-n}Ph_n)]$		modified merry-go-round	19
$[Ir_4(\mu\text{-}CO)_3(CO)_8(L)]$ [L = $P(OMe)_3$, $P(OPh)_3$, $P(OCH_2)CEt$]		change-of-basal-face	15
$[Ir_4(\mu\text{-}CO)_2(\mu\text{-}SO_2)(CO)_9]$		synchronous change-of-basal-face	27
$[Ir_4(\mu\text{-}CO)_3(CO)_7(\overline{COCH_2CH_2O})_2]$		1. merry-go-round 2. tripodal rotation	16

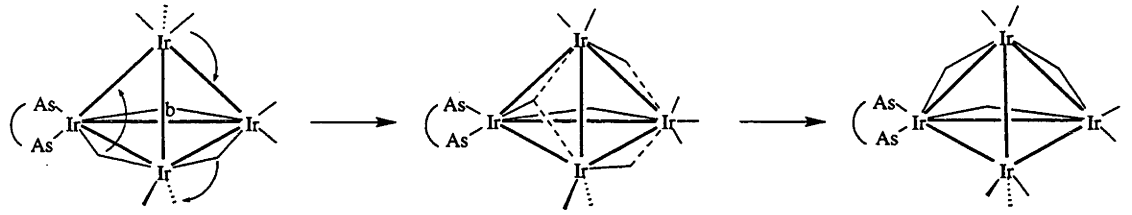
$[Ir_4(\mu\text{-}CO)_3(CO)_7(PMePh_2)_2]$		synchronous change-of-basal-face	14
$[Ir_4(\mu\text{-}CO)_3(CO)_7(\eta^4\text{-cod})]$		change-of-basal-face	25
$[Ir_4(\mu\text{-}CO)_3(CO)_7(\eta^4\text{-diars})]$		synchronous change-of-basal-face	25
$[Ir_4(\mu\text{-}CO)_3(\mu\text{-dpam})(CO)_7]$		merry-go-round	14
$[Ir_4(\mu\text{-}CO)_3(\mu\text{-dppb})(CO)_7]$		dppb chain flipping	21, 26
$[Ir_4(\mu\text{-}CO)_3(\mu\text{-dppm})(CO)_7]$		1. merry-go-round 2. tripodal rotation	14
$[Ir_4(\mu\text{-}CO)_3(\mu\text{-dppp})(CO)_7]$		merry-go-round	14
$[Ir_4(\mu\text{-}CO)_3(cis\text{-dppee})(CO)_7]$		tautomerization	11
$[Ir_4(\mu\text{-}CO)_3(\mu\text{-}MeSCH_2SMe)(CO)_7]$		merry-go-round	14
$[Ir_4(\mu\text{-}CO)_3(CO)_6(\overline{COCH_2CH_2O}\,)_3]$		merry-go-round	16
$[Ir_4\{\mu_3\text{-}HC(PPh_2)_3\}(\mu\text{-}CO)_3(CO)_6]$		merry-go-round	32]
$[Ir_4\{\mu_3\text{-}3S(SCH_2)_3\}(CO)_9]$		merry- go-round	20, 22
$[Ir_4(\mu\text{-}CO)_3(CO)_6(PMePh_2)(\eta^4\text{-diars})]$		synchronous change-of-basal-face	13

$[Ir_4(\mu\text{-}CO)_3(CO)_6(PPh_3)(\eta^4\text{-nbd})]$		change-of-basal-face	13
$[Ir_4(\mu\text{-}CO)_3(CO)_5(\eta^4\text{-cod})_2]$		tripodal rotation	13
$[Ir_4(\mu\text{-}CO)_3(CO)_5(\eta^4\text{-cod})(\eta^4\text{-nbd})]$		tripodal rotation	13
$[Ir_4(\mu\text{-}CO)_3(CO)_5(\eta^4\text{-nbd})_2]$		tripodal rotation	13
$[Ir_4(\mu\text{-}CO)_3(cis\text{-dppee})_2(CO)_5]$		synchronous change-of-basal-face	11
$[Ir_4(\mu\text{-}CO)_3(\mu\text{-L})(CO)_5]$ (L = dppm, dppm)		change-of-basal-face	13

[a] 1. Low energy process. 2. High energy process

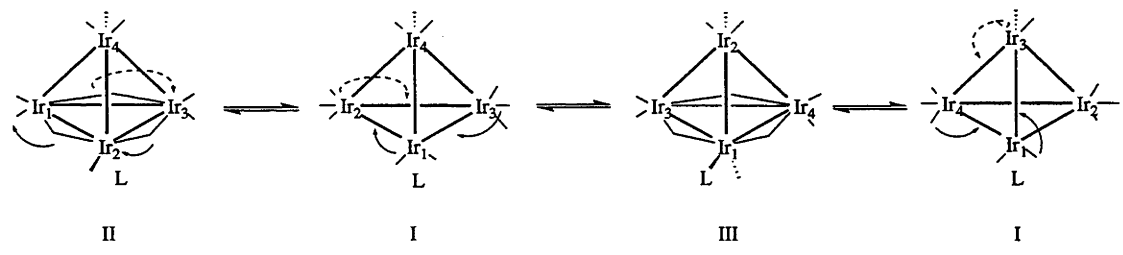


Scheme 3.1.3. Change-of-basal-face process in $[Ir_4(\mu\text{-}CO)_3(CO)_8(\eta^4\text{-cod})]$ (unbridged intermediate)



Scheme 3.1.4. Change-of-basal-face process in $[Ir_4(\mu\text{-}CO)_3(CO)_7(\eta^2\text{-diars})]$ (synchronous face change).

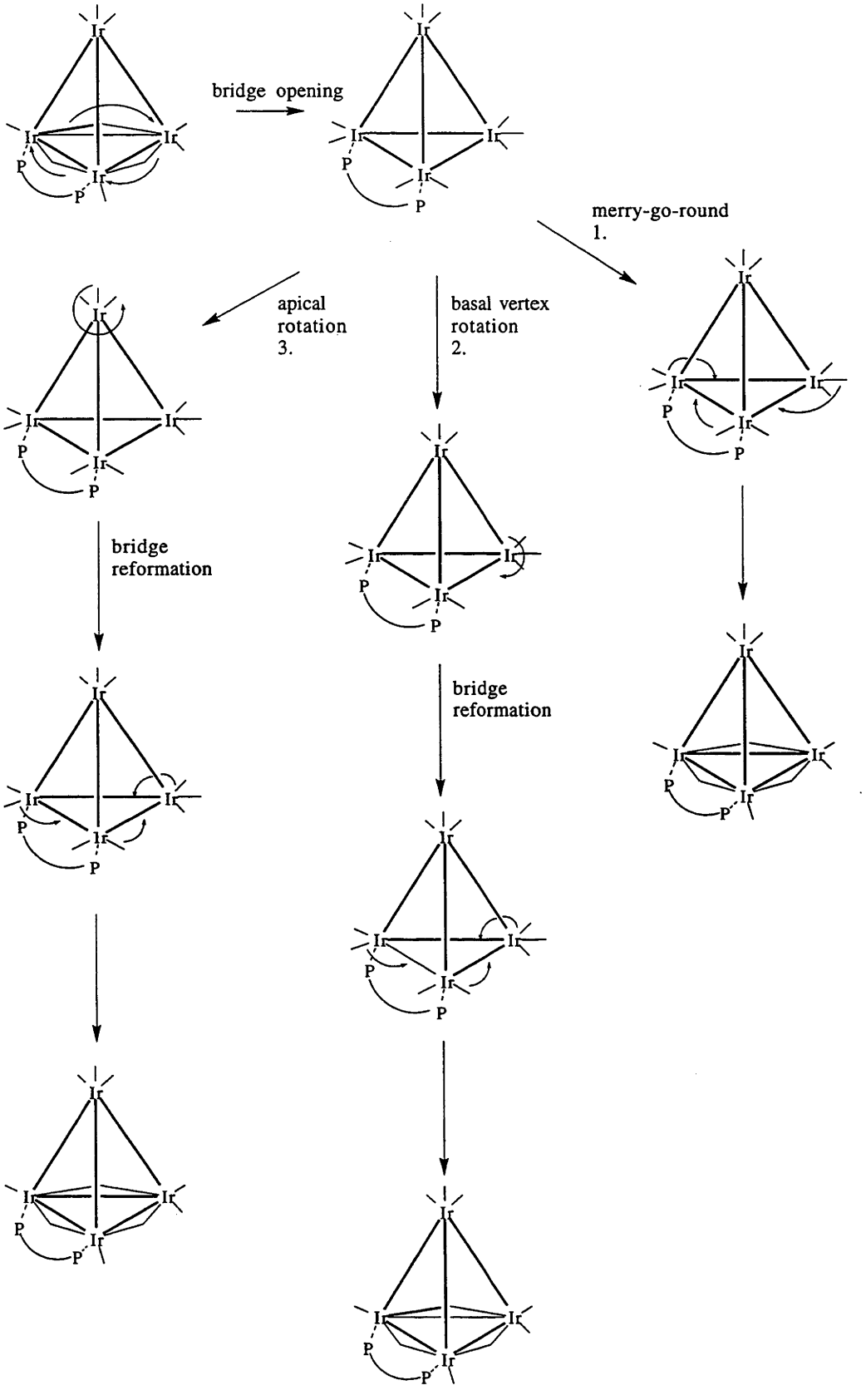
In addition to the extensive studies of phosphine substitution at tetrairidium clusters, phosphite substitution has also been of interest. The phosphite ligand in $[Ir_4(CO)_{11}\{P(OPh)_3\}]$[33] is proposed to be axially ligated on the basis of IR spectroscopy, whereas the tripodal phosphite $P(OCH_2)_3CEt$ affords a structurally characterized mono-substituted derivative with an all-terminal carbonyl geometry.[15] Detailed studies have revealed that these mono-substituted derivatives consist of three interconverting configurations in solution possessing the all-terminal ligand geometry, or an edge-bridged structure with the phosphite ligand occupying radial or axial sites (Scheme 3.1.5.), which correspond to three minima on the kinetic pathway of CO scrambling, and whose relative energies vary independently within a small range (1-9 kJ mol^{-1} at 298 K).[15] Darensbourg and co-workers have obtained $[Ir_4(CO)_8\{P(OMe)_3\}_4]$ and have suggested that it adopts an unusual triaxial, apical geometry.[38]



Scheme 3.1.5. CO mobility in $[Ir_4(\mu\text{-}CO)_3(CO)_8(L)]$ [L = $P(OMe)_3$, $P(OPh)_3$, $P(OCH_2)_3CEt$].

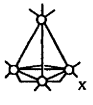
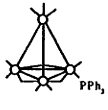
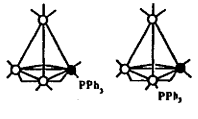
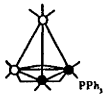
Fluxionality studies of tetrairidium complexes with one edge-bridging bidentate ligand have also been reported.[14] Studies of $[Ir_4(\mu\text{-}CO)_3(\mu\text{-}L)(CO)_7]$ [L = dppm, dppp, dpam] reveal fluxionality consistent with the lowest energy process being the "merry-go-round" of the six CO's about the basal plane perpendicular to the diaxially-coordinated ligands (Scheme 3.1.6., process 1). Upon raising the temperature, tripodal rotation at the non-phosphorus-ligated iridium in the basal plane of the bridge-opened intermediate occurs (process 2). Tripodal rotation at the apical iridium is the highest energy process observed (process 3). All site exchange processes are faster in the dppm-ligated cluster than in the dppp-containing cluster, rationalized by a greater relief of ring strain in proceeding to the unbridged intermediate (the Ir_4 core is smaller with an all-terminal ligand geometry than with an edge-bridged structure).

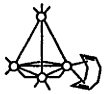
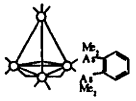
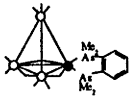
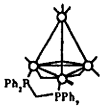
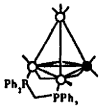
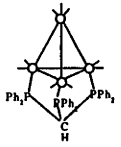
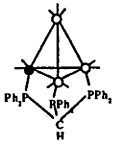
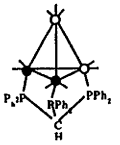
Carbonyl migration on heterometallic clusters has been the subject of significantly fewer studies than carbonyl mobility on homometallic clusters, although useful advantages accrue in the mixed-metal system. Introduction of a heterometal lowers the molecular symmetry and may provide a label to facilitate assignment and to monitor carbonyl scrambling (particularly with NMR-active nuclei). As metals have differing propensities to stabilize the putative edge-bridged, face-capped, or all-terminal intermediates, heterometallic clusters should exhibit different activation energies for the various mechanisms of carbonyl migration, so that ligand mobility at specific ligated derivatives becomes accessible on the NMR timeframe, or thermal discrimination of scrambling at specific faces or metals becomes possible. The studies of $[Ir_4(CO)_{12}]$ have been extended to $[Ir_3Rh(CO)_{12}]$ and $[Ir_2Rh_2(CO)_{12}]$,[34-37] with differences to the parent clusters ascribed to the differing electropositivities of the metals (Table 3.1.2.). The incorporation of a significantly more electropositive metal should accentuate such differences, but fluxionality studies of mixed-metal clusters incorporating iridium and an early transition metal have not thus far been promulgated. The tetrahedral mixed-metal clusters $[CpWIr_3(CO)_{11}]$ (**2**) and $[Cp_2W_2Ir_2(CO)_{10}]$ (**3**), conceptually derived from $[Ir_4(CO)_{12}]$, contain the electropositive tungsten; studies of ligand fluxionality at **2** and **3** and their derivatives are therefore of significant interest, and have been the focus of part of the current work.

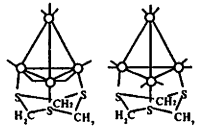
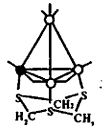
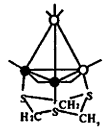
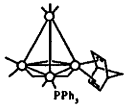
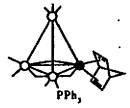
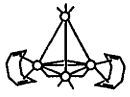
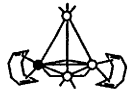
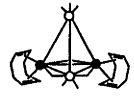
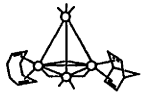
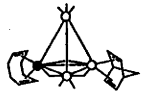
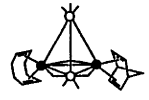
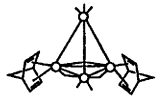
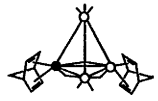
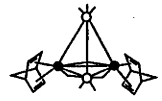


Scheme 3.1.6. CO exchange pathways in $[Ir_4(\mu\text{-}CO)_3(\mu\text{-}L)(CO)_7]$ (L = dppm, dppp, dpam).

Table 3.1.2. Exchange Pathways of Derivatives of $[Ir_4(CO)_{12}]$, $[Ir_3Rh(CO)_{12}]$ and $[Ir_2Rh_2(CO)_{12}]$

Ir_4 Cluster	*Fluxional Pathway*	*Ref.*	*Ir_3Rh Cluster*	*Fluxional Pathway*	*Ref.*	*Ir_2Rh_2 Cluster*	*Fluxional pathway*	*Ref.*
						$[Ir_2Rh_2(\mu\text{-}CO)_3(CO)_9]$ 	synchronous change-of-basal-face	37
$[Ir_4(\mu\text{-}CO)_3(CO)_8X]^-$ (X = Br, I) 	merry-go-round	14,24	$[Ir_3Rh(\mu\text{-}CO)_3(CO)_8X]^-$ (X = Br, I) 	1. merry-go-round 2. change of basal face	34	$[Ir_2Rh_2(\mu\text{-}CO)_3(CO)_8X]^-$ (X = Br, I) 	tripodal rotation	37
$[Ir_4(\mu\text{-}CO)_3(CO)_8(L)]$ [L = PPh_3, $P(C_6H_4Cl\text{-}4)_3$, $P(C_6H_4OMe\text{-}4)_3$, $P(C_6H_4NMe_2\text{-}4)_3$] 	1. merry-go-round 2. synchronous change-of-basal-face	14	$[Ir_3Rh(\mu\text{-}CO)_3(CO)_8(PPh_3)]$ 	1. merry-go-round 2. change-of-basal-face 3. migration of PPh_3 above room temperature	34	$[Ir_2Rh_2(\mu\text{-}CO)_3(CO)_8(PPh_3)]$ 	migration of PPh_3 above room temperature	36
			$[Ir_3Rh(\mu\text{-}CO)_3(CO)_8(\eta^2\text{-}nbd)]$ 	1. merry-go-round 2. change-of-basal-face	34			

$[Ir_4(\mu\text{-}CO)_3(CO)_7(\eta^4\text{-}cod)]$ 	change-of-basal-face	25	$[Ir_3Rh(\mu\text{-}CO)_3(CO)_7(\eta^4\text{-}cod)]$ 	change-of-basal-face	34	$[Ir_2Rh_2(\mu\text{-}CO)_3(CO)_7(\eta^4\text{-}cod)]$ 	tripodal rotation	37
$[Ir_4(\mu\text{-}CO)_3(CO)_7(\eta^4\text{-}diars)]$ 	synchronous change-of-basal-face	25	$[Ir_3Rh(\mu\text{-}CO)_3(CO)_7(\eta^4\text{-}diars)]$ 	synchronous change-of-basal-face	34			
			$[Ir_3Rh(\mu\text{-}CO)_3(CO)_7(\eta^4\text{-}nbd)]$ 	1. tripodal rotation 2. change-of-basal-face	34	$[Ir_2Rh_2(\mu\text{-}CO)_3(CO)_7(\eta^4\text{-}nbd)]$ 	1. tripodal rotation, 2. change-of-basal-face	37
$[Ir_4(\mu\text{-}CO)_3(\mu\text{-}dppm)(CO)_7]$ 	1. merry-go-round 2. tripodal rotation	14	$[Ir_3Rh(\mu\text{-}CO)_3(\mu\text{-}dppm)(CO)_7]$ 	merry-go-round	34			
$[Ir_4\{\mu_3\text{-}HC(PPh_2)_3\}(\mu\text{-}CO)_3(CO)_6]$ 			$[Ir_3Rh\{\mu_3\text{-}HC(PPh_2)_3\}(\mu\text{-}CO)_3(CO)_6]$ 	1. tripodal rotation 2. merry-go-round	34	$[Ir_2Rh_2\{\mu_3\text{-}HC(PPh_2)_3\}(\mu\text{-}CO)_3(CO)_6]$ 	tripodal rotation	37

$[Ir_4\{\mu_3\text{-}3S\text{-}c\text{-}(SCH_2)_3\}(CO)_9]$ 	merry-go-round	20,22	$[Ir_3Rh\{\mu_3\text{-}3S\text{-}c\text{-}(SCH_2)_3\}(\mu\text{-}CO)_3(CO)_6]$ 	tripodal rotation, merry-go-round	34	$[Ir_2Rh_2\{\mu_3\text{-}3S\text{-}c\text{-}(SCH_2)_3\}(\mu\text{-}CO)_3(CO)_6]$ 	tripodal rotation	37
$[Ir_4(\mu\text{-}CO)_3(CO)_6(PPh_3)(\eta^4\text{-nbd})]$ 	change-of-basal-face	13	$[Ir_3Rh(\mu\text{-}CO)_3(CO)_6(PPh_3)(\eta^4\text{-nbd})]$ 	tripodal rotation	34			
$[Ir_4(\mu\text{-}CO)_3(CO)_5(\eta^4\text{-cod})_2]$ 	tripodal rotation	13	$[Ir_3Rh(\mu\text{-}CO)_3(CO)_5(\eta^4\text{-cod})_2]$ 	tripodal rotation	34,35	$[Ir_2Rh_2(\mu\text{-}CO)_3(CO)_5(\eta^4\text{-cod})_2]$ 	tripodal rotation	37
$[Ir_4(\mu\text{-}CO)_3(CO)_5(\eta^4\text{-cod})(\eta^4\text{-nbd})]$ 	tripodal rotation	13	$[Ir_3Rh(\mu\text{-}CO)_3(CO)_5(\eta^4\text{-cod})(\eta^4\text{-nbd})]$ 	tripodal rotation	34	$[Ir_2Rh_2(\mu\text{-}CO)_3(CO)_5(\eta^4\text{-cod})(\eta^4\text{-nbd})]$ 	tripodal rotation	37
$[Ir_4(\mu\text{-}CO)_3(CO)_5(\eta^4\text{-nbd})_2]$ 	tripodal rotation	13	$[Ir_3Rh(\mu\text{-}CO)_3(CO)_5(\eta^4\text{-nbd})_2]$ 	tripodal rotation	34	$[Ir_2Rh_2(\mu\text{-}CO)_3(CO)_5(\eta^4\text{-nbd})_2]$ 	tripodal rotation	37

● = Rh, o = Ir

3.2. NMR Studies of Tungsten-Iridium Clusters

3.2.1. NMR Spectra of [$CpWIr_3(CO)_{11}$] (2) and [$Cp_2W_2Ir_2(CO)_{10}$] (3)

The room temperature ^{13}C NMR spectrum of **2** in $CDCl_3$ consists of a singlet at 178.2 ppm. On cooling to 156 K ($CD_2Cl_2/CHFCl_2$), the spectrum splits into two broad signals (Figure 3.2.1.), which could not be fully resolved due to solvent restrictions, solubility and other experimental problems. Similarly, the room temperature ^{13}C NMR spectrum of **3** in $CDCl_3$ consists of one averaged signal at 180.0 ppm. On cooling to 148 K ($CDFCl_2$) the spectrum splits into two broad and one sharp resonances (Figure 3.2.2.), which again could not be completely resolved. The exchange mechanism(s) for both clusters **2** and **3** are very fast, and appear to involve all the carbonyls on the clusters. This is unusual; in $[Ir_4(CO)_{11}L]$,[30] the carbonyl *trans* to the substituted ligand is not involved in exchange either by the merry-go-round or face centred exchange mechanisms. The presence of one averaged signal in the NMR spectra for clusters **2** and **3**, however, indicate all carbonyls are involved in the scrambling process. The ^1H NMR spectrum for **3** at 148 Kreveals one broad signal for the η^5-cyclopentadienyl ligand(s) (5.18 ppm $CDFCl_2$), reinforcing the suggestion that the exchange process is very fast.

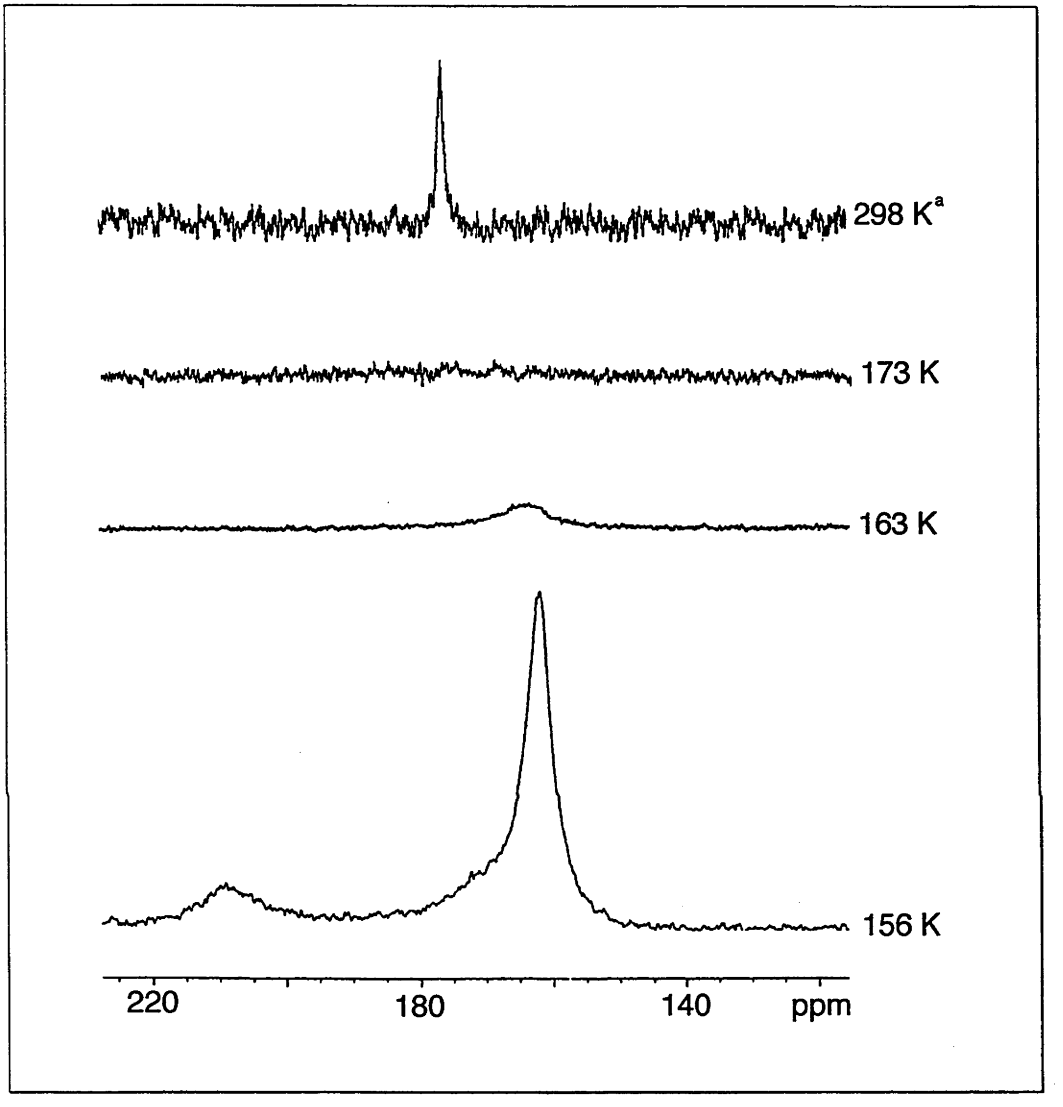


Figure 3.2.1. Variable temperature ^{13}C NMR spectroscopic study of $[CpWIr_3(CO)_{11}]$ (**2**) in $CD_2Cl_2/CHFCl_2$ ([a] in $CDCl_3$).

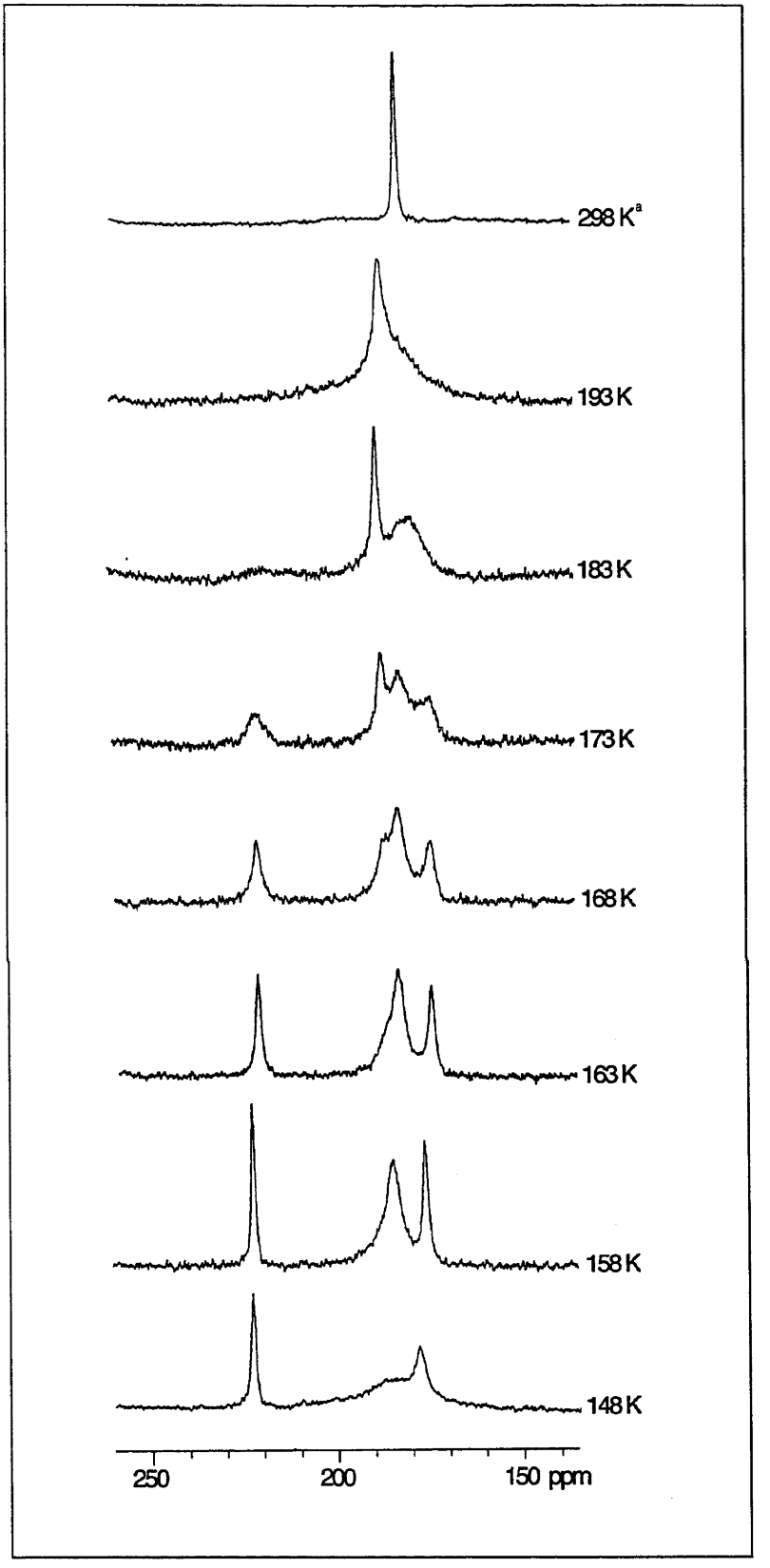


Figure 3.2.2. Variable temperature ^{13}C NMR spectroscopic study of $[Cp_2W_2Ir_2(CO)_{10}]$ (**3**) in $CDFCl_2$ ([a] in $CDCl_3$).

3.2.2. NMR studies of PPh_3 and PMe_3 derivatives of $[CpWIr_3(CO)_{11}]$ (**2**)

The synthesis and characterization of the ligand-substituted derivatives $[CpWIr_3(\mu\text{-}CO)_3(CO)_{8-n}(L)_n]$ [L = PPh_3, n = 1 (**4**), 2 (**5**), 3 (**6**); L = PMe_3, n = 1 (**7**), 2 (**8**), 3 (**9**)] were reported in Chapter 2, benchmarking the reaction rates in a qualitative sense against those of the "parent" cluster $[Ir_4(CO)_{12}]$; for the "very mixed"-metal system, reactions proceeded in a stepwise fashion in minutes at room temperature, in contrast to the homometallic cluster where reaction has been reported as requiring forcing conditions or use of activated precursors. The clusters usually exist as mixtures of interconverting isomers in solution, as shown by the IR and NMR spectra. The present Section contains assignment of the configurations of these interconverting isomers and, where possible, comment on the ligand scrambling processes.

NMR studies of $[CpWIr_3(\mu\text{-}CO)_3(CO)_7(PPh_3)]$ (4)

The room temperature ^{31}P NMR spectrum of **4** in CD_2Cl_2 contains a broad singlet at 0.5 ppm. On cooling to 173 K, three signals are resolved at 24.9, 5.3 and -4.9 ppm in the ratio 3 : 5 : 2 (Figure 3.2.3.). Shapley has previously noted that the ^{31}P NMR chemical shift sequence radial > axial is observed with tetrairidium clusters,[30] and its application to **4** suggests the resonance at 24.9 ppm can be assigned to the crystallographically characterized configuration with phosphine occupying a radial site, and the resonances at 5.3 and -4.9 ppm to configurations with phosphines in axial sites. The room temperature ^{13}C NMR spectrum of **4** consists of a broad singlet at 192.8 ppm. On cooling to 181 K, the spectrum splits into signals corresponding to three configurations in the approximate ratio 3 : 5 : 2 (Figure 3.2.4.), consistent with the ^{31}P NMR spectra. Due to solubility, relative abundance and other experimental problems, studies of only one of the three configurations (**4a**: see below) have been completed; the ^{13}C NMR assignments for **4b** and **4c** are tentative.

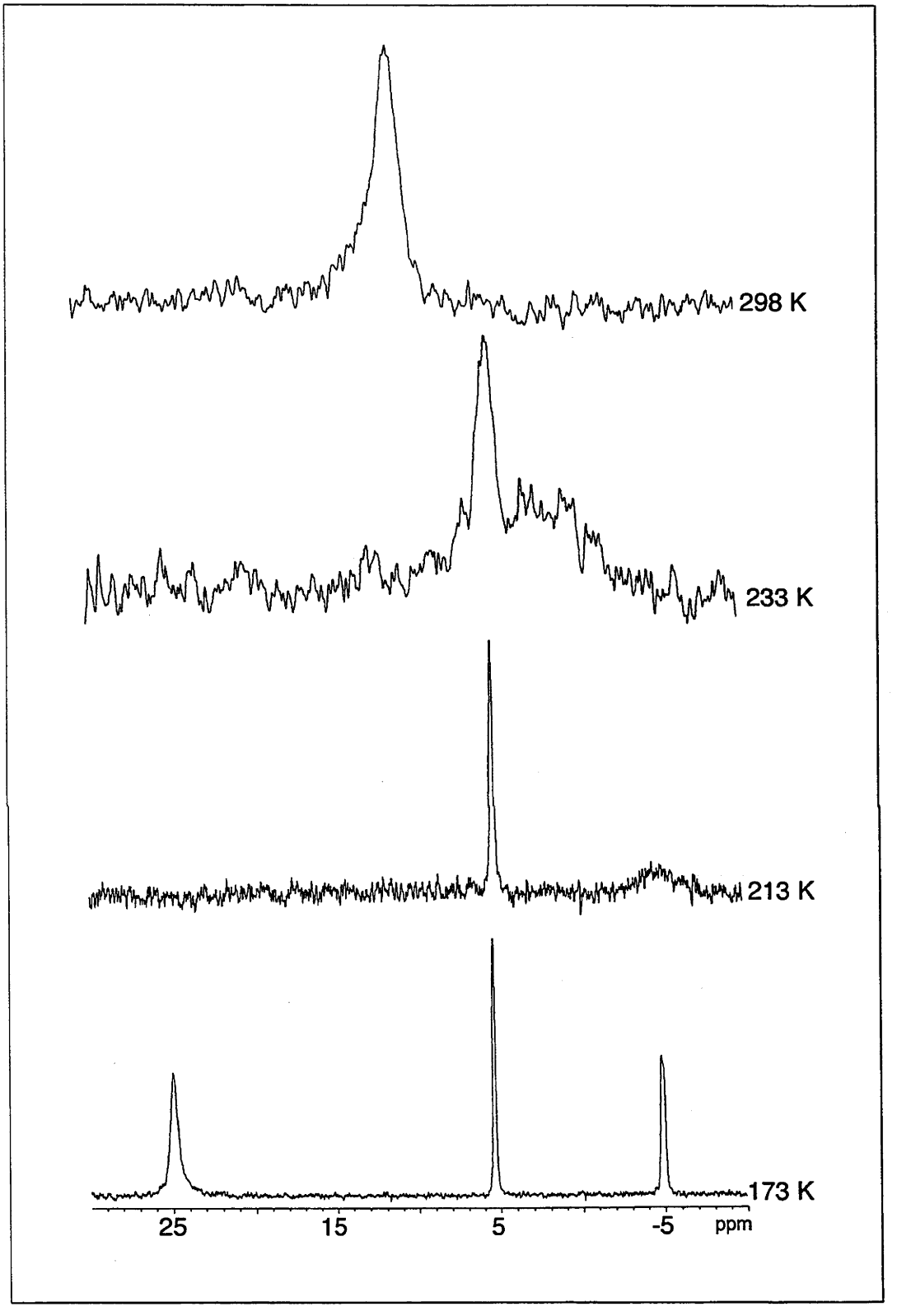


Figure 3.2.3. Variable temperature ^{31}P NMR spectroscopic study of $[CpWIr_3(\mu\text{-}CO)_3(CO)_7(PPh_3)]$ (**4**) in CD_2Cl_2.

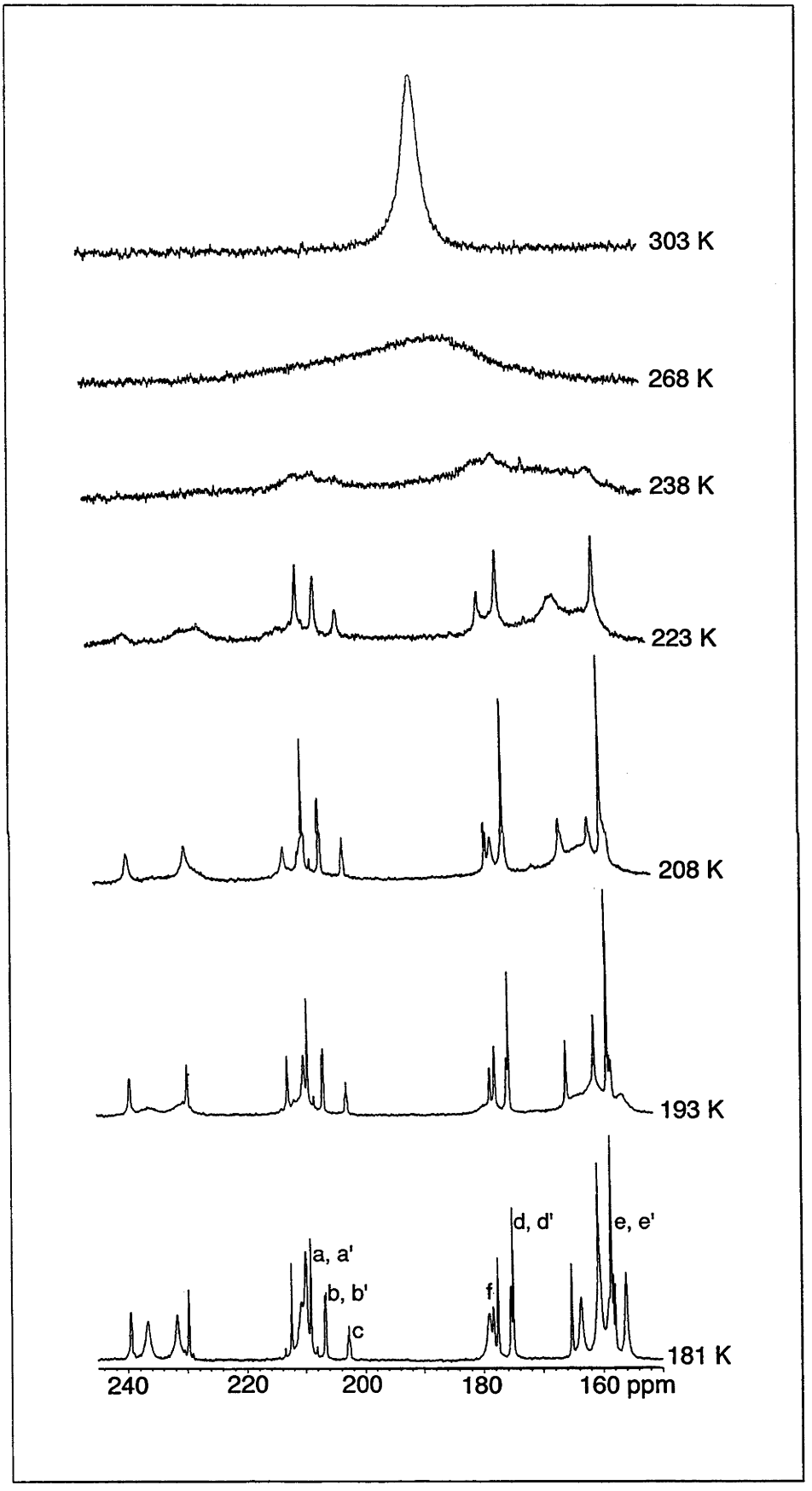
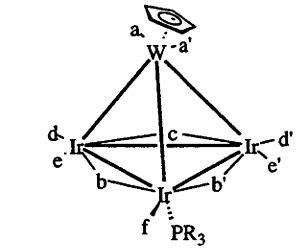


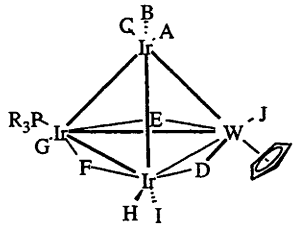
Figure 3.2.4. Variable temperature ^{13}C NMR spectroscopic study of [$CpWIr_3(\mu\text{-}CO)_3(CO)_7(PPh_3)$] (**4**) in CD_2Cl_2.

The structures of the three configurations of **4** can be assigned from the ^{31}P NMR data and ^{13}C NMR data (Figure 3.2.5.). The NMR chemical shift positional sequence established with tetrairidium clusters (bridging > radial > axial ≈ apical[26]) can be extended to the mixed-metal regime, affording the chemical shift sequence W-W bridging CO > W-Ir bridging CO > Ir-Ir bridging CO ≈ W terminal CO > Ir radial CO > Ir axial CO ≈ Ir apical CO; it is possible to distinguish Ir-Ir bridging carbonyls from W terminal carbonyls due to the 15% abundant ^{183}W-coupled satellites of the latter. With this information, it is then possible to assign the spectrum of **4a** and confirm its coordination geometry. At 181 K, resonances for configuration **4a** are observed at 208.3 (a, a'), 205.4 (b, b'), 201.9 (c), 177.6 (f), 174.9 (d, d') and 158.0 (e, e') ppm with the relative intensities 2 : 2 : 1 : 1 : 2 : 2, and the signal for the W-ligated a, a' at 208.3 ppm showing the expected coupling to ^{183}W. The signals at 205.4 and 201.9 ppm are assigned to the Ir-Ir bridging carbonyls b, b' and c, respectively. The signals at 177.6 and 174.9 ppm are assigned to the Ir-ligated radial carbonyls f and d, d', respectively, with the remaining signal at 158.0 ppm being assigned to the Ir-coordinated axial carbonyls e, e'. A ^{13}C-^{13}C correlation spectroscopy (COSY) experiment (Figure 3.2.6.) reveals coupling between the Ir-Ir bridging carbonyls b, b' and c. Long-range *trans* coupling between the Ir-Ir bridging carbonyls a, a' and e', e, respectively, was not observed. The coordination geometry of **4a** is analogous to that of a structurally characterized configuration of the trimethylphosphine-containing cluster **7** (**7a**: see below and Chapter 2). The crystallographically characterized **4b** (Chapter 2) has a basal WIr_2 plane with Cp occupying an axial site and PPh_3 occupying a radial site (radial, axial configuration), and is responsible for the most downfield signal in the ^{31}P NMR spectrum (see above). At 163 K, in the ^{13}C NMR in CS_2/CD_2Cl_2 (Figure 3.2.7.), resonances for configuration **4b** are observed, and cautiously assigned at 236.4 (E), 230.5 (D), 210.2 (F), 208.4 (J), 178.5 (H) and 160.3 (C) ppm. Discrimination between the remaining axial and apical carbonyl resonances was not possible. A gaussian weighting function was used to identify the ^{183}W satellites on carbonyls E, D and J. The signal at 210.2 ppm is assigned to the Ir-Ir bridging carbonyl F due to its coupling with the W-Ir bridging carbonyls D and E, as shown in the COSY experiment. The signal at 178.5 ppm is assigned the the Ir-ligated radial carbonyl H. The remaining signal in the axial phosphine region of the ^{31}P NMR spectrum (-4.9 ppm) is assigned to configuration **4c**, with an axial PPh_3, radial Cp coordination geometry. Diaxial coordination is unlikely with bulky ligands (cone angles: Cp 136°, PPh_3 145°). At 163 K in the ^{13}C NMR, resonances for configuration **4c** are observed at 238.9 (*e*), 228.6 (*d*), 211.8 (*j*), 208.4, (*f*), 177.1 (*h*), 174.9 (*g*), 164.9 (*b*), 160.3 (*i*), 160.0 (*c*) and 157.7 (*a*) ppm, all of relative intensity 1. A gaussian weighting function was used to identify the ^{183}W satellites on carbonyls *e*, *d* and *j*. The signal at 208.4 ppm is assigned to the Ir-Ir bridging carbonyl *f* by its coupling to the W-Ir bridging carbonyls *d* and *e* as observed in the COSY spectrum. The signals at 177.1 and 174.9 ppm are assigned to the Ir-ligated radial carbonyls *h* and *g* by their respective lack or

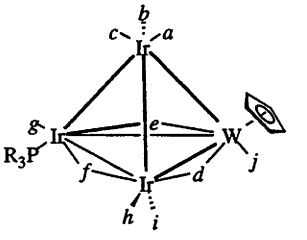
presence of *cis* P-C coupling. The signal at 157.7 ppm is assigned to the apical carbonyl *a* by its long-range *trans* coupling to PPh_3. The COSY spectrum (Figure 3.2.6.) reveals coupling between the W-Ir bridging carbonyls E, D and F (**4b**), and *e*, *d* and *f* (**4c**). Coupling between carbonyls D and E (**4b**) and *d* and *e* (**4c**), however, is not present, presumably due to the asymmetric bridging of the W-Ir carbonyls. Configuration **4a**, however, does reveal coupling between the Ir-Ir bridging carbonyls b, b' and c.



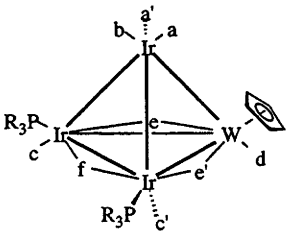
$[CpWIr_3(\mu\text{-}CO)_3(CO)_7(PPh_3)]$ **4a**
$[CpWIr_3(\mu\text{-}CO)_3(CO)_7(PMe_3)]$ **7a** XRS
ax, ap



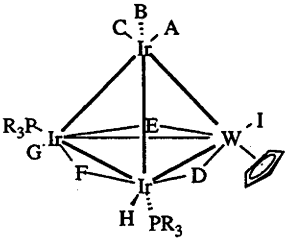
$[CpWIr_3(\mu\text{-}CO)_3(CO)_7(PPh_3)]$ **4b** XRS
$[CpWIr_3(\mu\text{-}CO)_3(CO)_7(PMe_3)]$ **7b**
r, ax



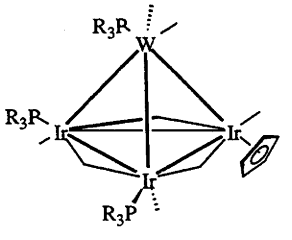
$[CpWIr_3(\mu\text{-}CO)_3(CO)_7(PPh_3)]$ **4c**
ax, r



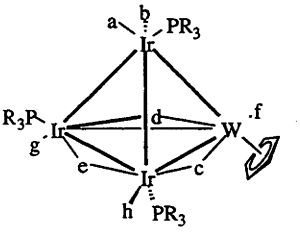
$[CpWIr_3(\mu\text{-}CO)_3(CO)_6(PPh_3)_2]$ **5a**
$[CpWIr_3(\mu\text{-}CO)_3(CO)_6(PMe_3)_2]$ **8a**
r, r, r



$[CpWIr_3(\mu\text{-}CO)_3(CO)_6(PPh_3)_2]$ **5b** XRS
$[CpWIr_3(\mu\text{-}CO)_3(CO)_6(PMe_3)_2]$ **8b**
r, ax, ax



$[CpWIr_3(\mu\text{-}CO)_3(CO)_5(PPh_3)_3]$ **6**
r, r, ax, ap



$[CpWIr_3(\mu\text{-}CO)_3(CO)_5(PMe_3)_3]$ **9**
r, ax, ax, ap

Figure 3.2.5. Configurations of $[CpWIr_3(\mu\text{-}CO)_3(CO)_{8-n}(L)_n]$ (L = PPh_3, PMe_3; n = 1 - 3); r = radial, ax = axial, ap = apical. XRS ≡ structurally characterized configuration.

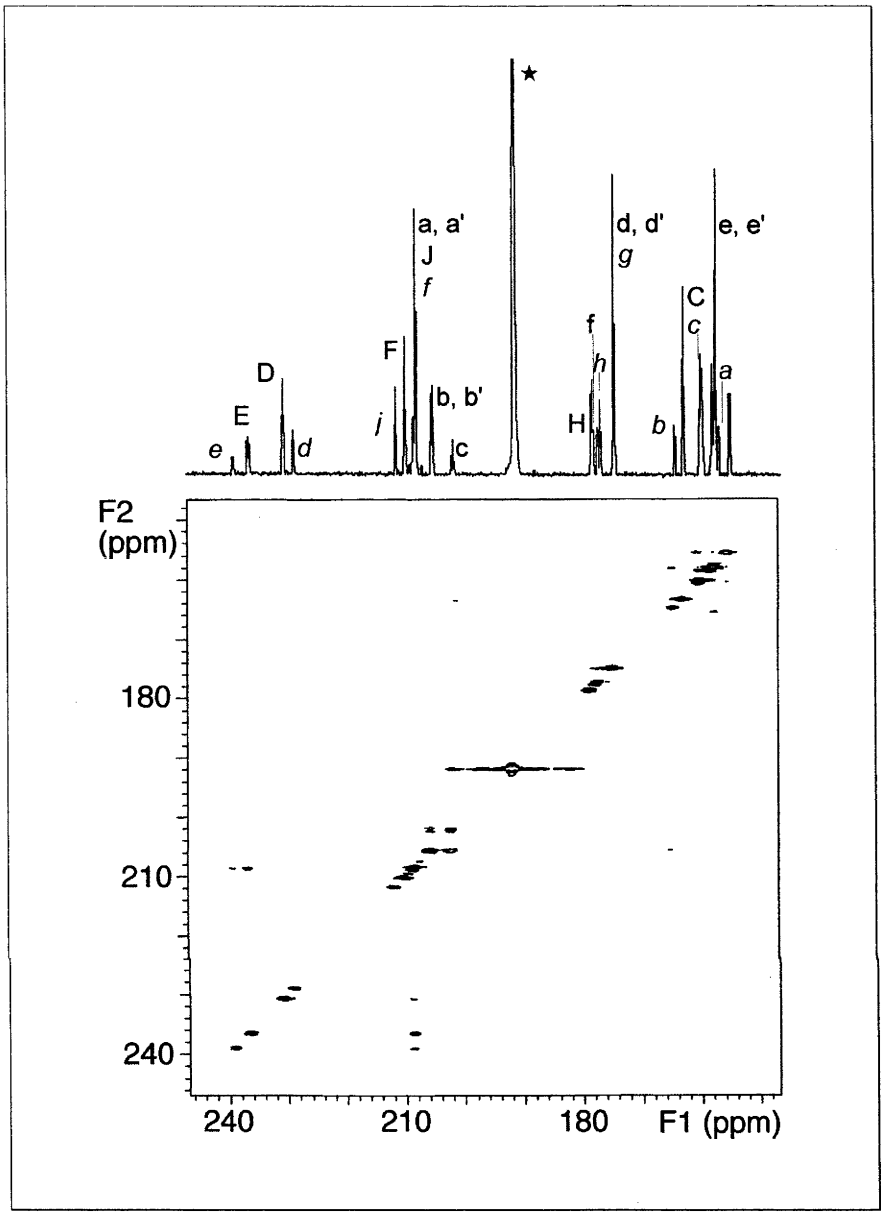


Figure 3.2.6. ^{13}C NMR COSY spectrum of $[CpWIr_3(\mu\text{-}CO)_3(CO)_7(PPh_3)]$ (**4**) in CS_2/CD_2Cl_2 at 173 K (★ ≡ CS_2).

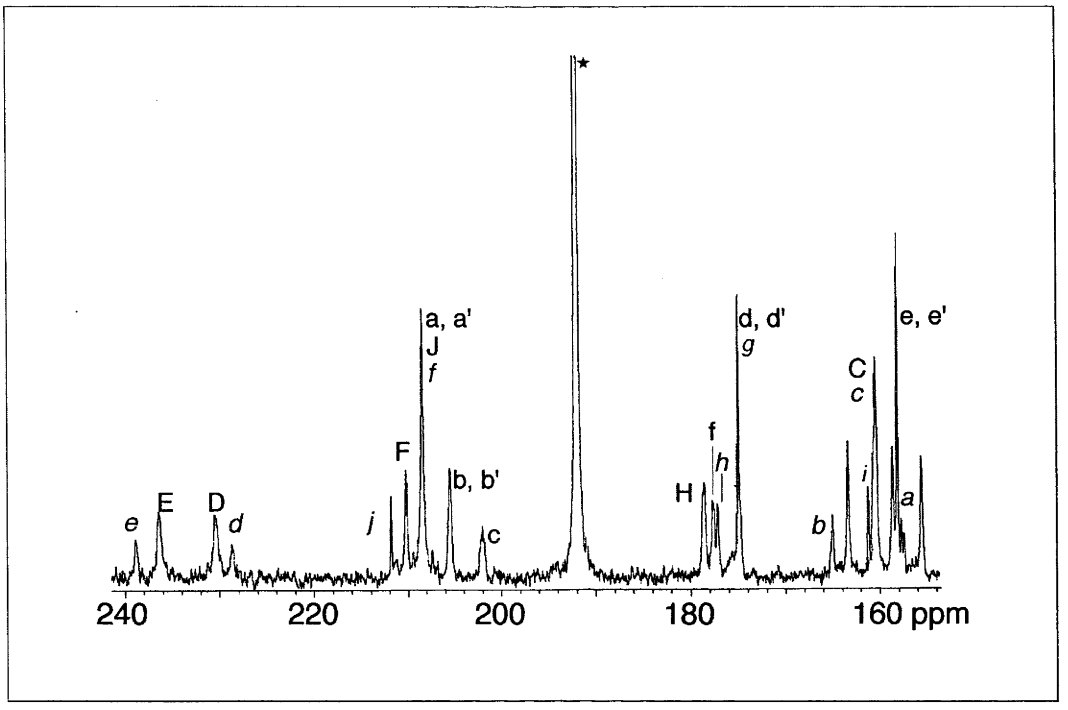


Figure 3.2.7. ^{13}C NMR spectrum of $[CpWIr_3(\mu\text{-}CO)_3(CO)_7(PPh_3)]$ (**4**) in CS_2/CD_2Cl_2 at 163 K (★ ≡ CS_2, other carbonyls not assigned)

Ligand fluxionality commences upon warming the mixture of configurations of **4**. A $^{13}C\text{-}\{^1H\}$ EXSY study at 218 K is shown in Figure 3.2.8. EXSY experiments use a NOESY sequence which allows for a "mixing time" during which the observed nuclei may migrate to another site. The contour plot for configuration **4a** (218 K) reveals site exchanges corresponding to a, a' ↔ b, b'; a, a' ↔ d, d'; a, a' ↔ e, e'; b, b' ↔ d, d'; b, b' ↔ e, e'; b, b' ↔ f; d, d' ↔ e, e' and c ↔ d, d'. This is consistent with the carbonyls exchanging via a concerted "merry - go – round" process, by way of an all-terminal intermediate (Scheme 3.2.1.). All carbonyls are involved in the exchange process, either by reformation of the Ir_3 bridged face or by formation of a WIr_2 bridged face. The only position blocked for "merry - go - round" exchange is that *trans* to the phosphine (occupied by the cyclopentadienyl ligand). The exchange process is thus analogous to that observed in $[Ir_4(CO)_{11}(PMe_2Ph)]$, where all carbonyls are fluxional with the exception of the unique carbonyl *trans* to the phosphine.[30] The integrated EXSY cross-peaks could not be utilized to afford rate data and confirm that the CO scrambling which affords the WIr_2 bridged intermediate has the same activation energy as reformation of the Ir_3-bridged structure; however, a qualitative inspection revealed no evidence for Ir_3 bridge reforming being a lower energy process than WIr_2 bridge formation (incorporation of the electropositive tungsten may polarize cluster electron density toward the Ir_3 face, and thereby stabilize bridging carbonyls about this face).

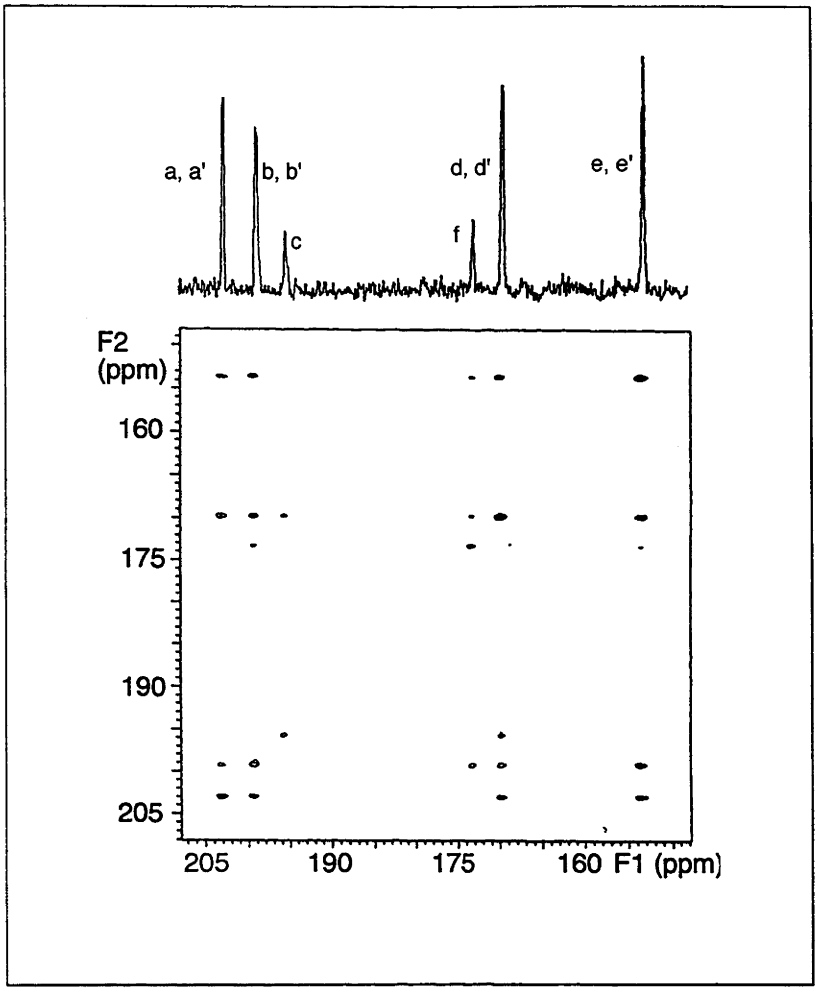
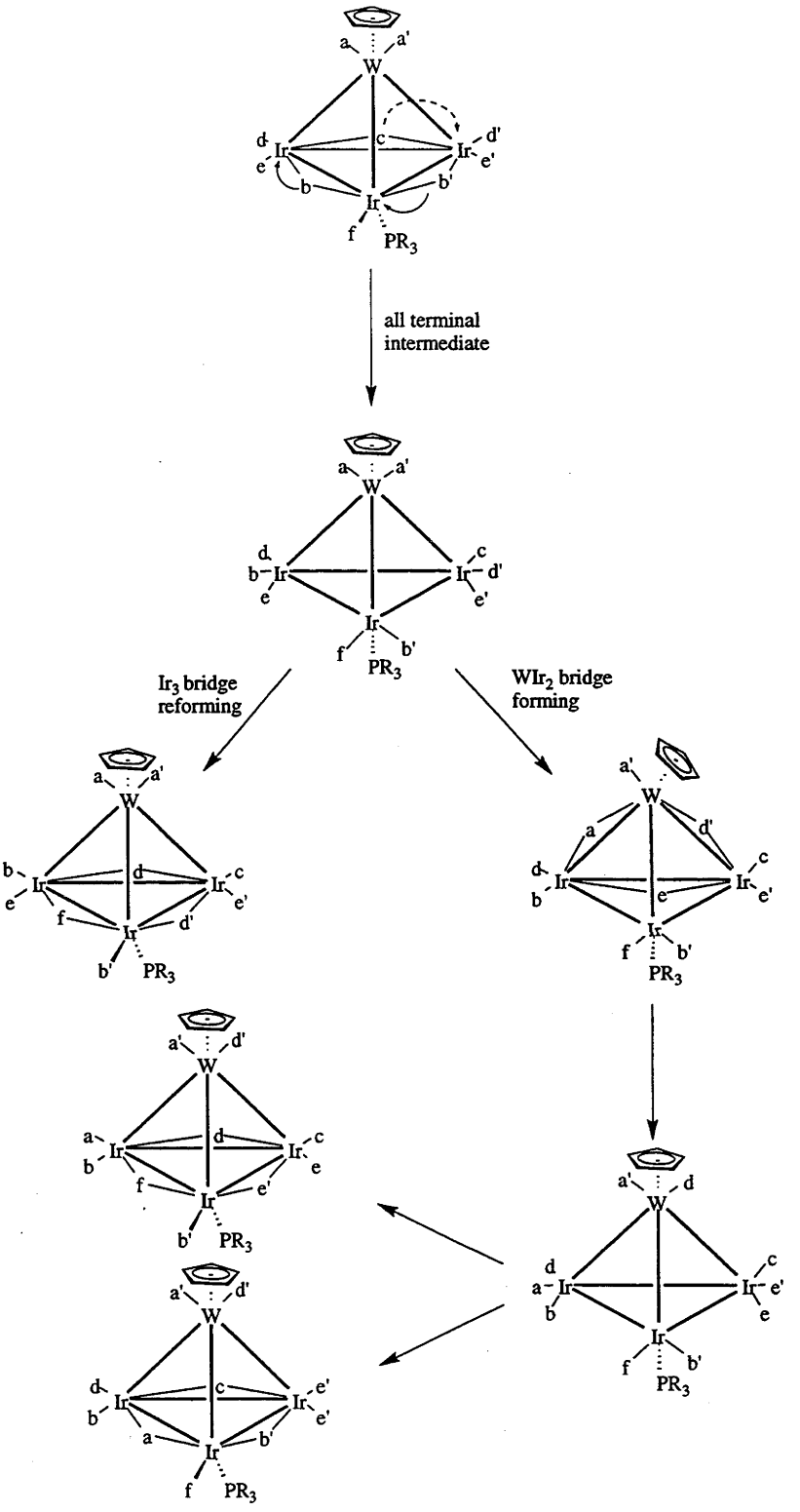


Figure 3.2.8. ^{13}C NMR EXSY spectrum of $[CpWIr_3(\mu\text{-}CO)_3(CO)_7(PPh_3)]$ (**4**) in toluene-d^8 at 218 K



Scheme 3.2.1. "Merry - go - round" process in **4a** and **7a**.

NMR studies of [CpWIr$_3$(μ-CO)$_3$(CO)$_6$(PPh$_3$)$_2$] (5).

The room temperature ^{13}C and ^{31}P NMR spectra of **5** in CD_2Cl_2 reveal broadened resonances, but at 191 K the fluxional processes have slowed sufficiently to reveal three signals in the ^{31}P NMR spectrum (ratio 16 : 1 : 1) and distinguish resonances corresponding to two configurations in the ^{13}C NMR spectrum (Figures 3.2.9. and 3.2.10.). The ^{31}P NMR spectrum suggests the presence of a major configuration with two radially coordinated phosphines (**5a**) and a minor configuration with radial and axial coordinated phosphines (**5b**) (Figure 3.2.5.). At 191 K, resonances for the more abundant configuration are observed in the ^{13}C NMR spectrum at 241.0 (e, e'), 217.0 (f), 212.8 (d), 167.5 (b), 162.2 (a, a') and 157.3 (c, c') ppm, with intensities 2 : 1 : 1 : 1 : 2 : 2. The signals at 241.0 and 212.8 ppm show satellite coupling to ^{183}W, and were therefore assigned as W-Ir bridging and W-ligated terminal carbonyls, respectively. A ^{13}C-^{13}C correlation spectroscopy (COSY) experiment was used to establish the position of the cyclopentadienyl ligand in **5a** (Figure 3.2.11.); the presence of a long-range *trans* coupling between carbonyls b and d revealed that d was axially ligated and therefore showed the Cp ligand to be radially coordinated. Configuration **5a** is therefore an example of a trisubstituted tetrahedral cluster with an unprecedented triradial geometry (Figure 3.2.5.). The signal at 217.0 ppm is assigned to the Ir-Ir bridging carbonyl f. The signal at 157.3 ppm is assigned to the iridium-coordinated axial carbonyls c, c'; carbonyls c, c' are distinguished from carbonyls a, a' by the presence of couplings in the ^{13}C-^{13}C COSY experiment [the signal at 157.3 ppm (c, c') shows a cross-peak with the signal at 241.0 ppm (the adjacent bridging carbonyls e, e'), and a long-range *trans* coupling with the signal at 162.2 ppm (a, a')]. The signals at 167.5 and 162.2 ppm are assigned to the apical carbonyls b and a, a', respectively. Resonances for the minor, and structurally characterized (Chapter 2), configuration **5b** are observed in the ^{13}C NMR spectrum at 243.1 (D or E), 237.4 (E or D), 228.0 (F), 214.1 (I), 177.6 (H), 164.7 (C or B), 161.5 (G), 161.5 (A) and 156.2 (B or C) ppm, all with intensity 1. The signals I, D or E and E or D are assigned by comparison of their chemical shifts to those of comparable carbonyls in configuration **5a** (the expected satellite coupling to ^{183}W of these low intensity signals could not be resolved). The signal at 228.0 ppm is assigned to the Ir-Ir bridging carbonyl F and the resonance at 177.6 ppm is assigned to the iridium-coordinated radial carbonyl H, the latter showing *cis* and *trans* P-C coupling to the axial- and radial-ligated phosphines, respectively. Carbonyl G is assigned on the basis of its *cis* P-C coupling to the radial phosphine ligand.

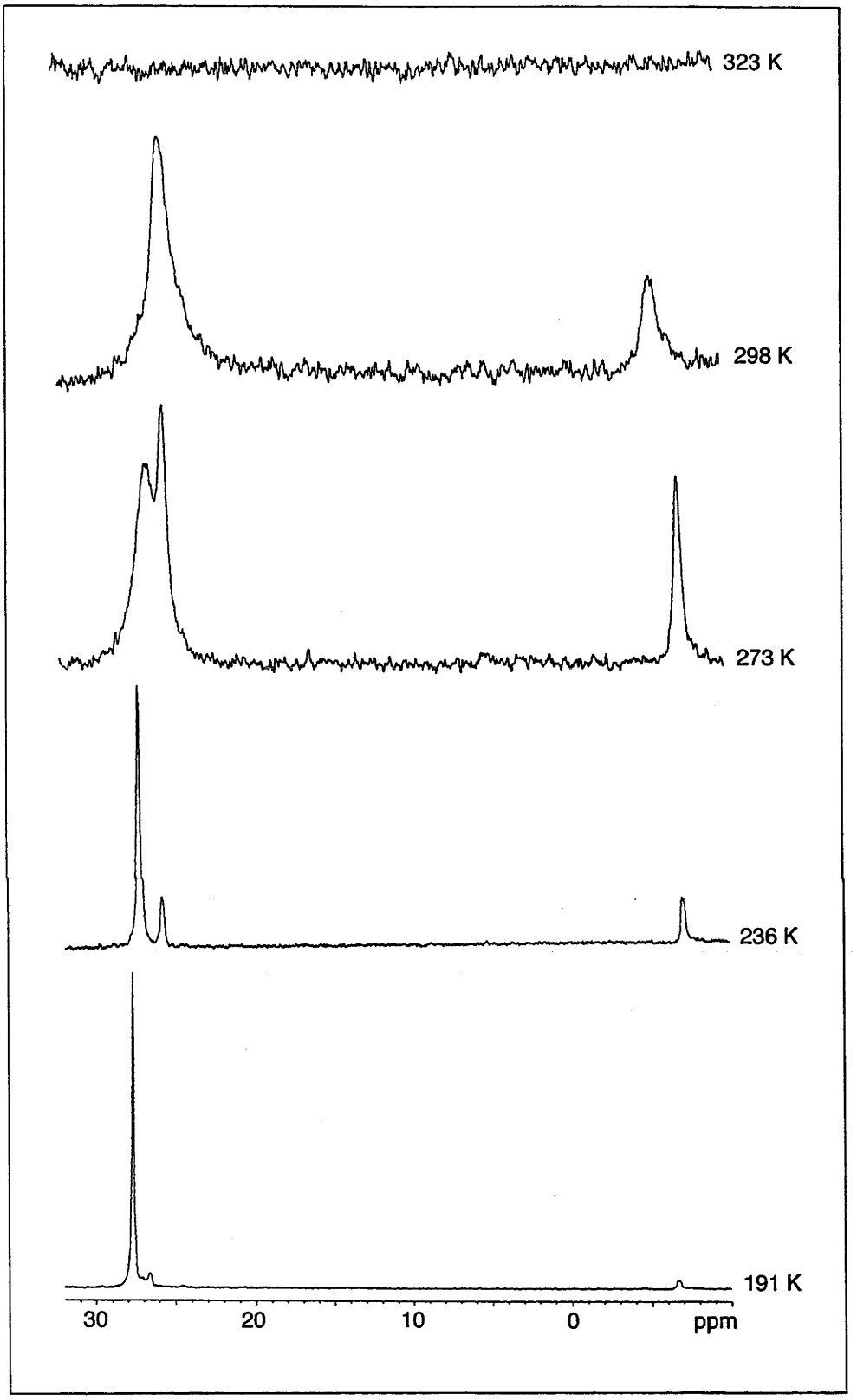


Figure 3.2.9. Variable temperature ^{31}P NMR spectroscopic study of $[CpWIr_3(\mu\text{-}CO)_3(CO)_6(PPh_3)_2]$ (**5**) in CD_2Cl_2.

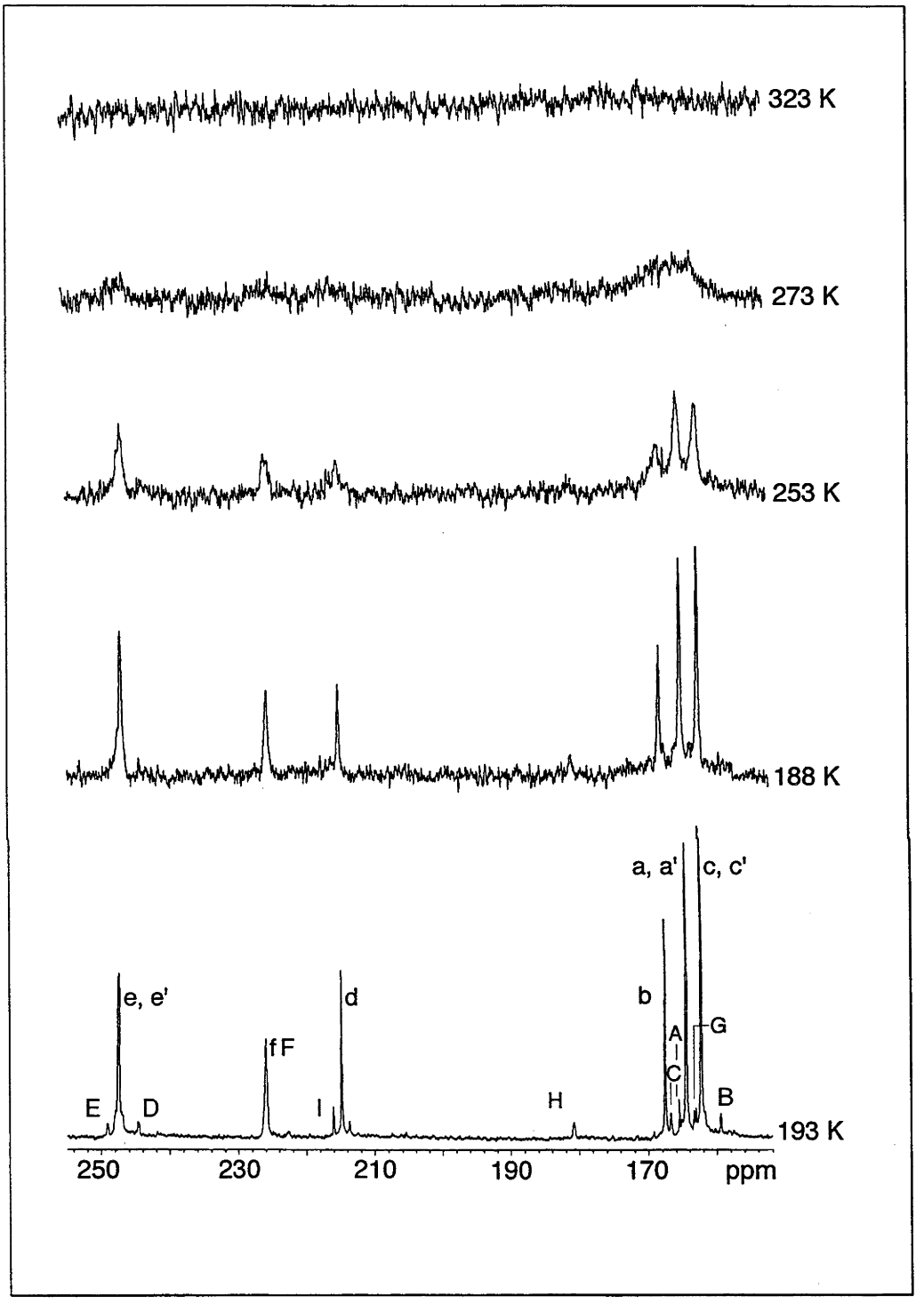


Figure 3.2.10. Variable temperature ^{13}C NMR spectroscopic study of $[CpWIr_3(\mu\text{-}CO)_3(CO)_6(PPh_3)_2]$ (**5**) in CD_2Cl_2.

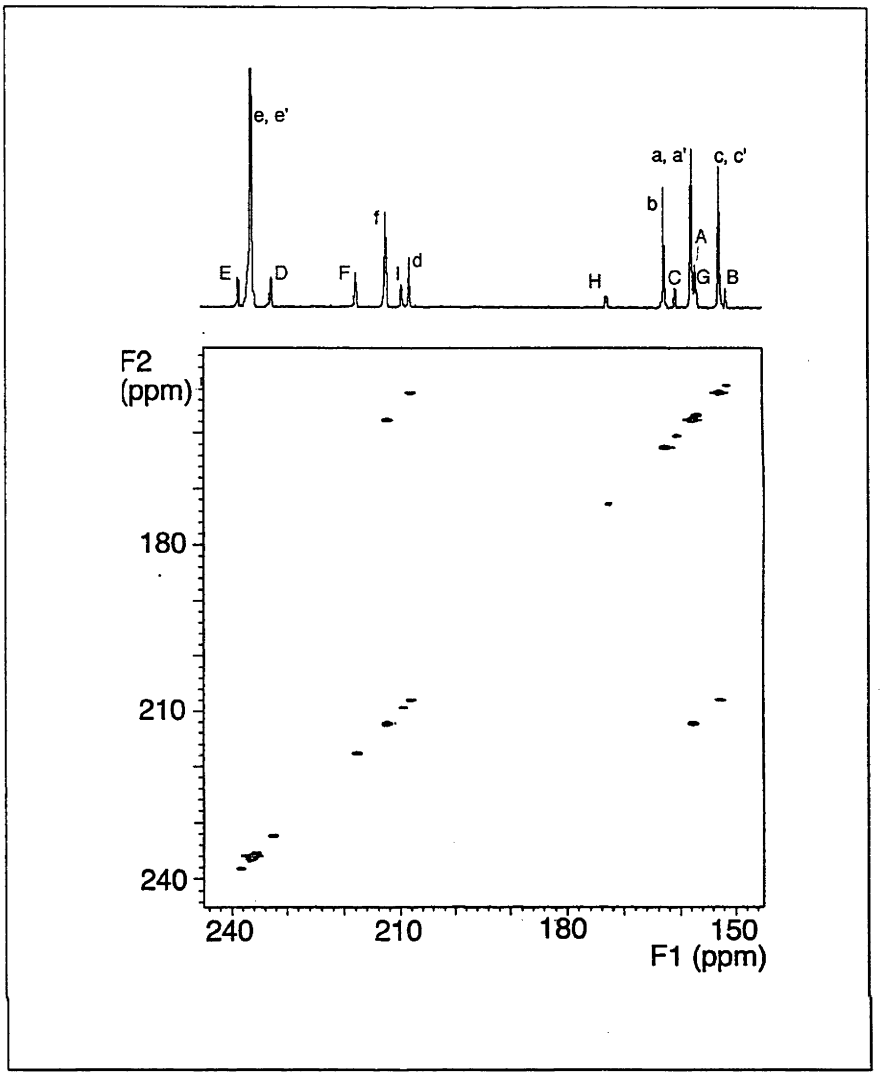


Figure 3.2.11. ^{13}C NMR COSY spectrum of $[CpWIr_3(\mu\text{-}CO)_3(CO)_6(PPh_3)_2]$ (**5**) in CD_2Cl_2 at 191 K.

The COSY experiment confirms the assignment of A, with the resonance at 161.5 ppm showing long range *trans* coupling to G. Carbonyls B and C are *trans* to PPh_3 (through Ir) and Cp (through W), respectively, and it is not possible to conclusively distinguish between these resonances at present.

Ligand fluxionality commences upon warming **5** above 191 K. The contour plot for **5** at 211 K (Figure 3.2.12.) reveals site exchanges for the major configuration (**5a**) only (the minor configuration **5b** is not sufficiently abundant to afford cross-peaks, restricting the utility of the EXSY data to postulating exchange pathways for the more abundant configuration). Exchanges corresponding to a, a' $\leftrightarrow$ f and c $\leftrightarrow$ d are observed, which are proposed to be due to two separate processes (note, however, that these processes could not be distinguished energetically by lowering the temperature at which the EXSY spectrum was attained). The

exchange a, a' ↔ f is consistent with ligand mobility about the Ir_3 face with a carbonyl distribution in the intermediate reminiscent of the D_{2d} intermediate implicated in the $[M_4(CO)_{12}]$ exchange pathway[7] (Scheme 3.2.2.). The exchange of carbonyls c and d probably involves scrambling about a WIr_2 face (Scheme 3.2.3.) for which the direct pathway (two steps) requires an intermediate with six bridging carbonyls; the longer pathway, which proceeds through two all-terminal intermediates in which the phosphines and Cp ligand prevent a "merry-go-round" process, is therefore preferred.

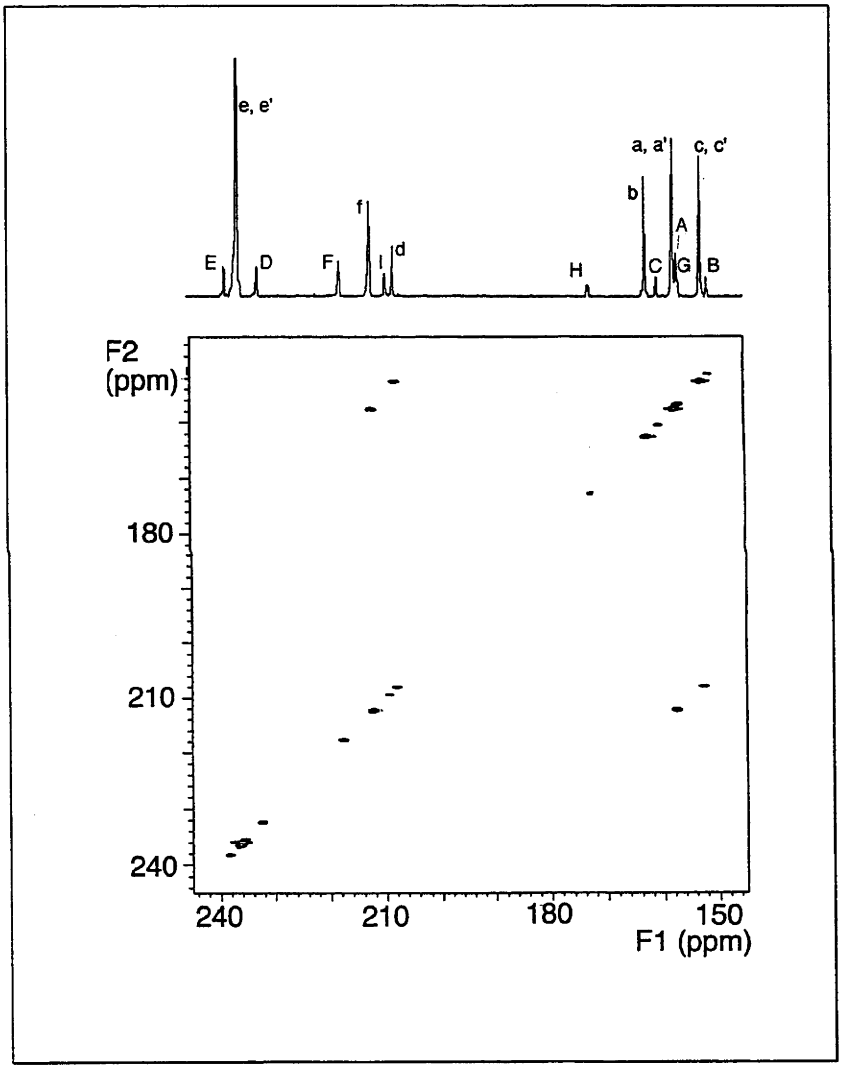
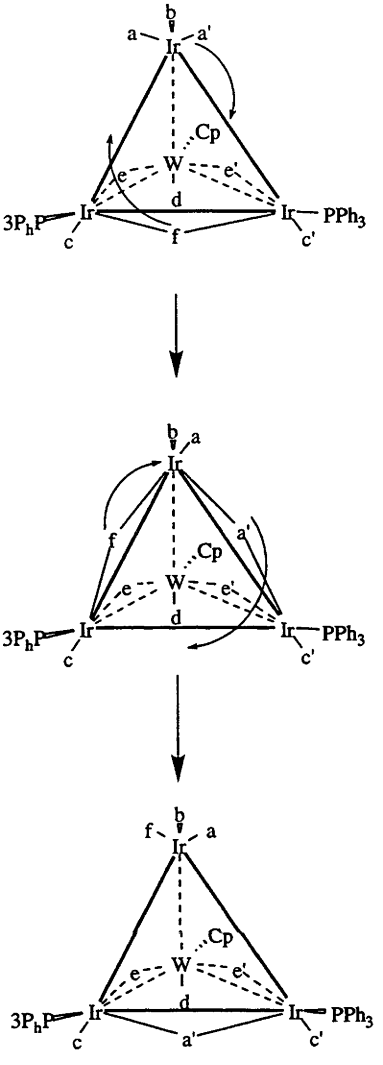
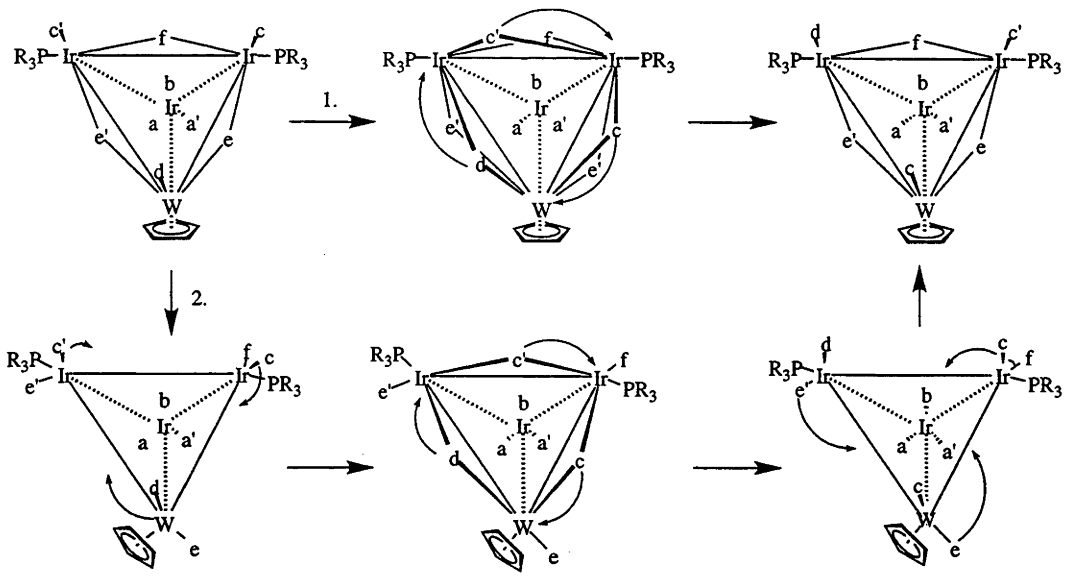


Figure 3.2.12. ^{13}C NMR EXSY spectrum of $[CpWIr_3(\mu\text{-}CO)_3(CO)_6(PPh_3)_2]$ (**5**) in CD_2Cl_2 at 211 K.



Scheme 3.2.2. CO mobility about the Ir_3 face in **5a** and **8a**



Scheme 3.2.3. CO mobility about the [WIr_2] face in **5a** and **8a**.

NMR studies of [$CpWIr_3(\mu\text{-}CO)_3(CO)_5(PPh_3)_3$] (6).

Unfortunately, carbonyl exchange at [$CpWIr_3(\mu\text{-}CO)_3(CO)_5(PPh_3)_3$] (**6**) could not be observed due to the instability of this cluster in solution; over a period of one hour at room temperature, essentially quantitative transformation of **6** into **5** was observed by ^{13}C NMR spectroscopy. The previously structurally confirmed monodentate tetrasubstituted tetrahedral tetrairidium clusters adopt radial, diaxial, apical geometries.[38,39] The ^{31}P NMR spectrum of **6** in $CDCl_3$ at 230 K shows a signal of intensity two, downfield of a signal of intensity one. The most likely configuration configuration consistent with this data involves a new tetrasubstituted coordination geometry with diradial, apical phosphines and the Cp occupying an axial site (Figure 3.2.5.). This configuration involves greater steric repulsion of phosphine ligands than that in the ideal tetrasubstituted radial, diaxial, apical geometry; consistent with the assignment of **6** is that the cluster (i) loses phosphine in solution and (ii) does not have a molecular ion in the MS but rather [M-PPh_3]$^+$.

NMR studies of [$CpWIr_3(\mu\text{-}CO)_3(CO)_7(PMe_3)$] (7).

[$CpWIr_3(\mu\text{-}CO)_3(CO)_7(PMe_3)$] (**7**) is fluxional on the NMR timescale, all ligands becoming equivalent above 298 K (^{13}C NMR, CD_2Cl_2/CS_2) or 273 K (^{31}P NMR, CD_2Cl_2). On cooling to 173 K in CD_2Cl_2, two signals are resolved in the ^{31}P NMR spectrum at -25.0 and -31.8 ppm (ratio 5 : 3, Figure 3.2.13.). On cooling to 163 K, the ^{13}C NMR spectrum in CD_2Cl_2/CS_2 splits into signals corresponding to two configurations (Figure 3.2.14.). One configuration of **7** has previously been structurally characterized (Chapter 2), and information from the structural study together with the NMR data has been used to assign geometries for the configurations of **7** (Figure 3.2.5). The crystallographically observed **7a** has Cp occupying an apical site and PMe_3 occupying an axial site (axial, apical configuration), corresponding to the upfield signal in the ^{31}P NMR spectrum. The resonances in the ^{13}C NMR spectrum corresponding to configuration **7a** exhibit a similar pattern to that of **4a**, and the clusters [$CpWIr_3(\mu\text{-}CO)_3(\mu\text{-}L)(CO)_6$] [L = dppe (**22**), dppm (**23**); Section 3.2.4.]. At 163 K, resonances for configuration **7a** are observed at 209.5 (a, a'), 206.6 (b, b'), 202.2 (c), 177.7 (f), 174.9 (d, d') and 158.0 (e, e') ppm, with the relative intensities 2 : 2 : 1 : 1 : 2 : 2. The signal at 209.5 ppm shows the expected coupling to ^{183}W. The signals at 206.6 and 202.2 ppm are assigned to the bridging carbonyls b, b' and c, respectively. The signals at 177.7 and 174.9 ppm are assigned to the radial carbonyls f and d, d', respectively, and the signal at 158.0 ppm is assigned to the axially coordinated carbonyls e, e'. The downfield signal in the ^{31}P NMR spectrum is assigned to configuration **7b**, a radial phosphine, axial Cp configuration. The signals in the ^{13}C NMR spectrum corresponding to **7b** are fully analogous to those of the structurally characterized **4b**, and correspond to a radial, axial configuration. As with configuration **4b**, the ^{13}C NMR spectrum of **7b** is as yet incompletely assigned. At 163 K, resonances for configuration **7b** are observed at 240.6 (E), 232.2 (D), 211.6 (F), 210.8 (J) and 179.4 (H) ppm. Again, discrimination between axial and apical carbonyl resonances was not possible. A COSY spectrum (Figure 3.2.15.) again reveals coupling between the W-Ir bridging carbonyls E and the Ir-Ir bridging carbonyl F, presumably due to the asymmetric bridging of the W-Ir carbonyls. A small crosspeak between the signals in the COSY spectrum at 158.4 ppm and 160.8 ppm can tentatively be assigned to the axially ligating carbonyls G or I and the apical carbonyls A or B, respectively; both pairs of carbonyls are situated in a transoid arrangement. The remaining specific assignments follow those for configuration **4**, above.

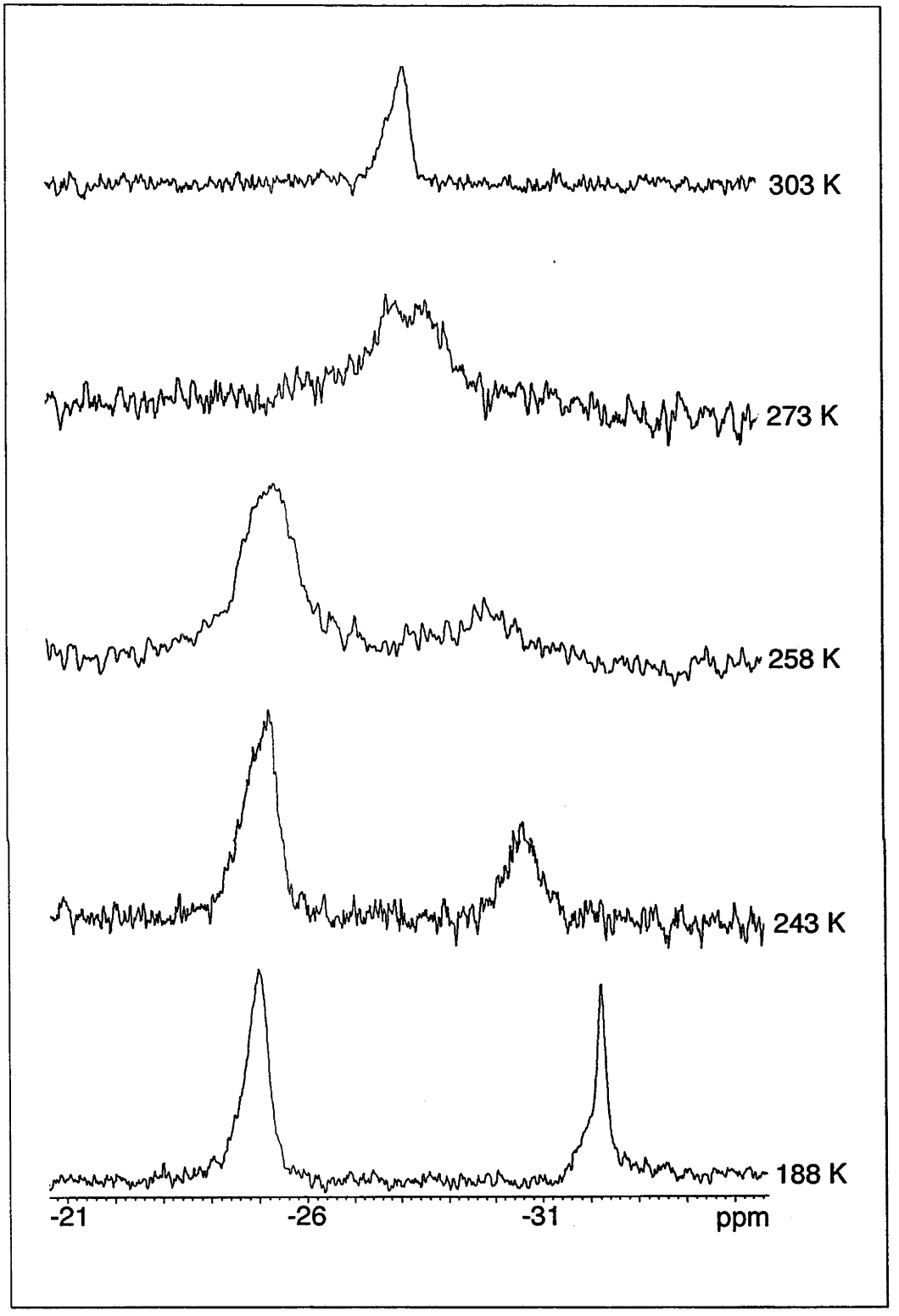


Figure 3.2.13. Variable temperature ^{31}P NMR spectroscopic study of $[CpWIr_3(\mu\text{-}CO)_3(CO)_7(PMe_3)]$ (**7**) in CS_2/CD_2Cl_2

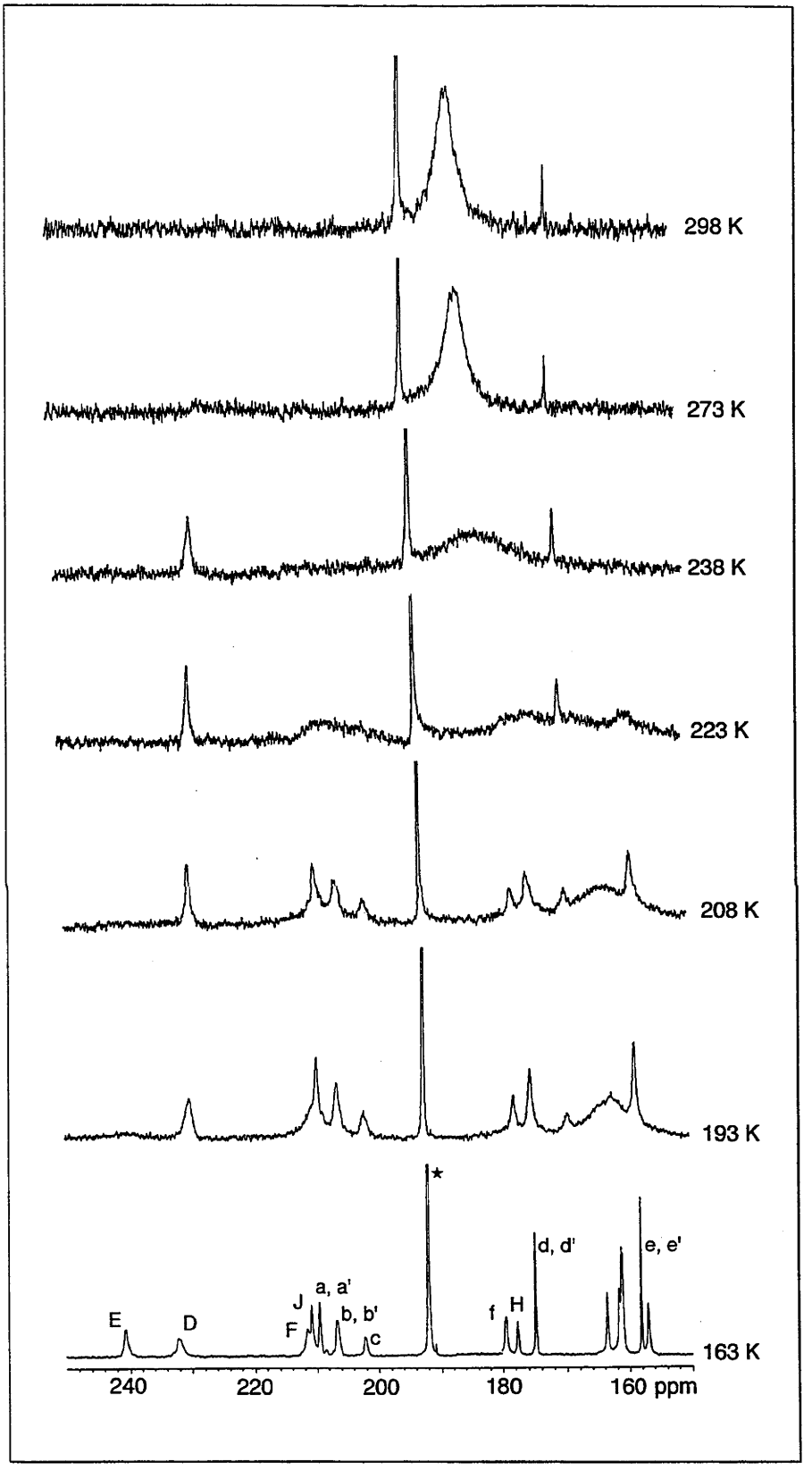


Figure 3.2.14. Variable temperature ^{13}C NMR spectroscopic study of $[CpWIr_3(\mu\text{-}CO)_3(CO)_7(PMe_3)]$ (**7**) in CS_2/CD_2Cl_2 (★ ≡ CS_2, other carbonyls not assigned)

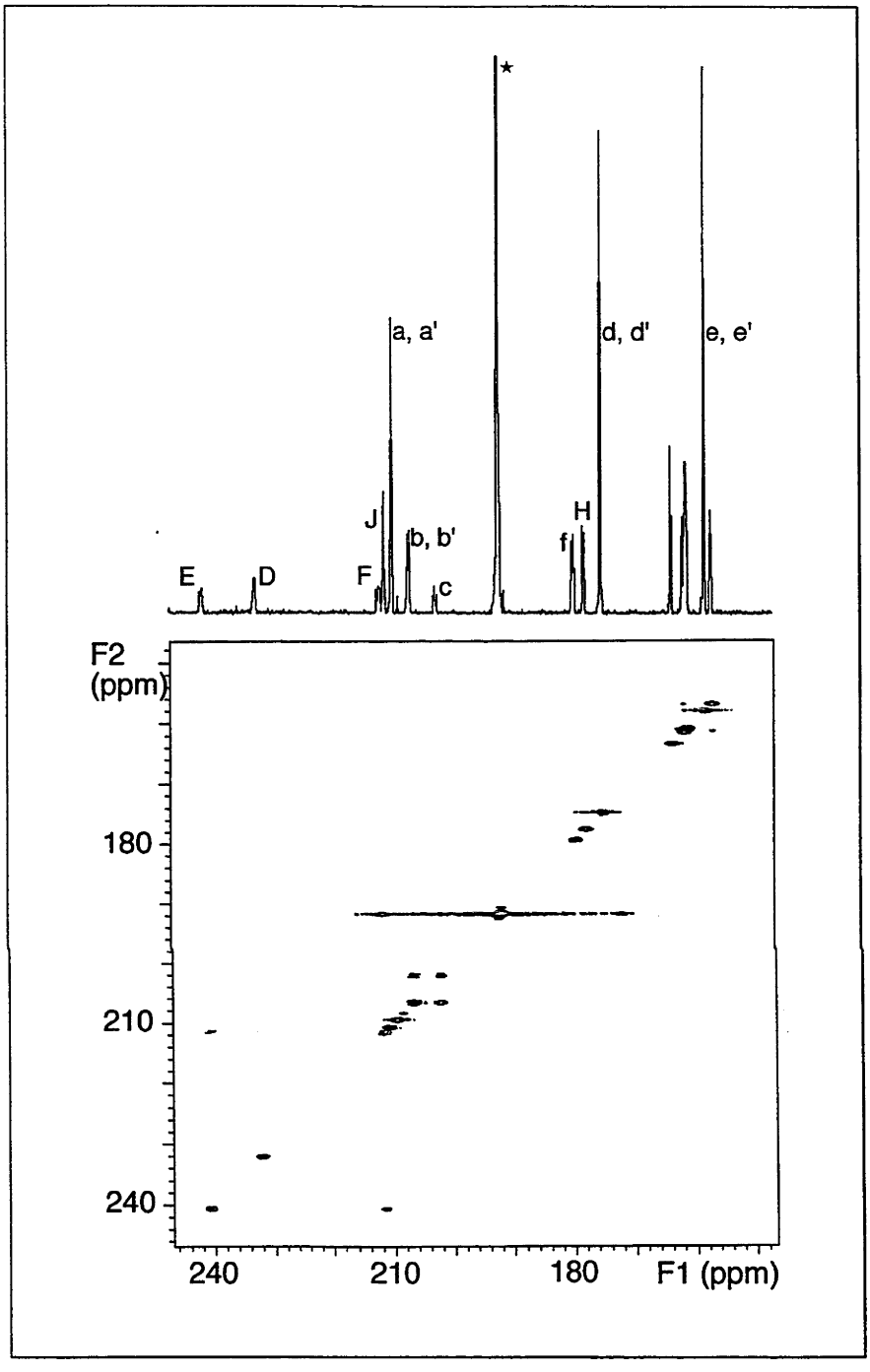


Figure 3.2.15. ^{13}C NMR COSY spectrum of $[CpWIr_3(\mu\text{-}CO)_3(CO)_7(PMe_3)]$ (**7**) in CS_2/CD_2Cl_2 at 163 K (★ = CS_2)

An EXSY spectrum of **7** at 178 K (Figure 3.2.16.) reveals site exchanges corresponding to a, a' ↔ b, b'; a, a' ↔ d, d'; a, a' ↔ e, e'; b, b' ↔ d, d'; b, b' ↔ e, e'; b, b' ↔ f; d, d' ↔ e, e' and c ↔ d, d' for configuration **7a**, observed previously with the carbonyl exchange of **4a**; the carbonyls of **7a** are therefore proposed to exchange via a concerted "merry - go - round" process as shown in Scheme 3.2.1.

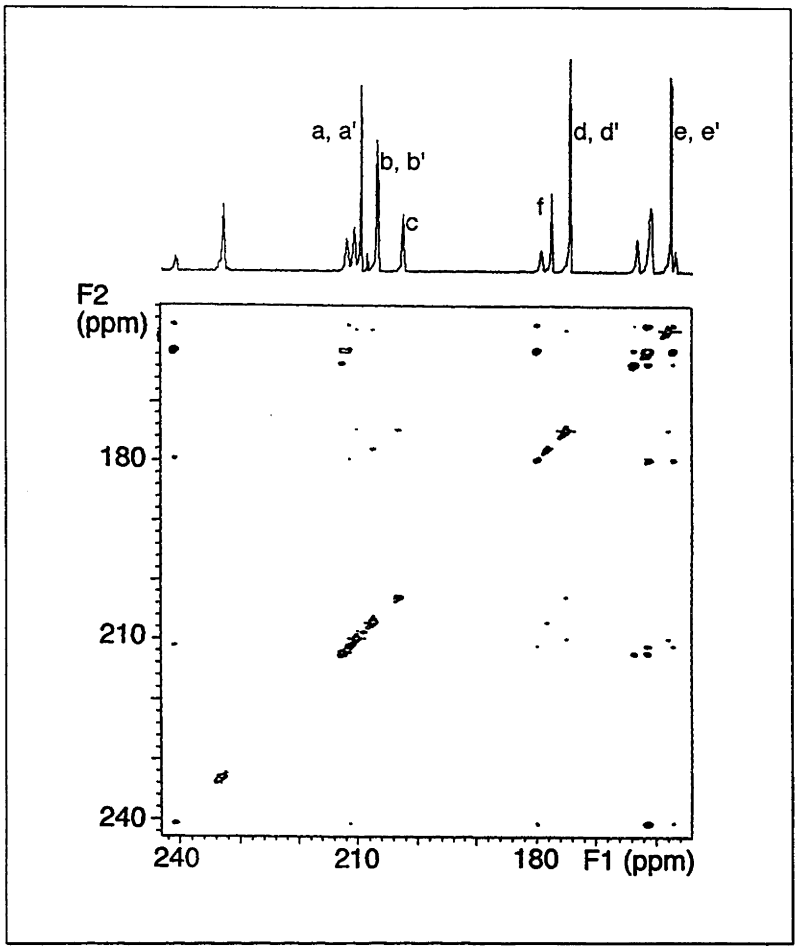


Figure 3.2.16. ^{13}C NMR EXSY spectrum of $[CpWIr_3(\mu\text{-}CO)_3(CO)_7(PMe_3)]$ (**7**) in CD_2Cl_2 at 178 K

NMR studies of $[CpWIr_3(\mu\text{-}CO)_3(CO)_6(PMe_3)_2]$ (8).

The room temperature ^{13}C and ^{31}P NMR spectra of **8** in CD_2Cl_2 are above coalescence, but all exchange processes are stopped at 193 K (Figures 3.2.17. and 3.2.18.). At this temperature, the ^{31}P NMR spectrum shows three resonances (ratio 20 : 1 : 1) corresponding to two configurations. Similarly, the ^{13}C NMR spectrum at 193 K displays signals corresponding to two configurations. A comparison of the ^{13}C and ^{31}P NMR spectra of **8** at this temperature with those of **5** at 191 K (Figure 3.2.9.) suggests that configurations **8a** and **8b** have the same triradial and radial, diaxial geometries as **5a** and **5b**, respectively. At 193 K, resonances in the ^{13}C NMR spectrum are observed for **8a** at 247.4 (e, e'), 225.9 (f), 214.8 (d), 167.5 (b), 164.0 (a, a') and 162.2 (c, c') ppm, with the relative intensities 2 : 1 : 1 : 1 : 2 : 2. A COSY experiment was used to establish the position of the cyclopentadienyl ligand in **8a** (Figure 3.2.19.). The presence of a long-range *trans* coupling between b and d demonstrated the radial coordination of the cyclopentadienyl ligand; **8a** is thus, like **5a**, an example of a cluster with a heretofor unobserved triradial coordination geometry. Resonances for the minor configuration **8b** are observed in the ^{13}C NMR spectrum at 249.0 (D or E), 244.7 (E or D), 225.8 (F), 216.1 (I),

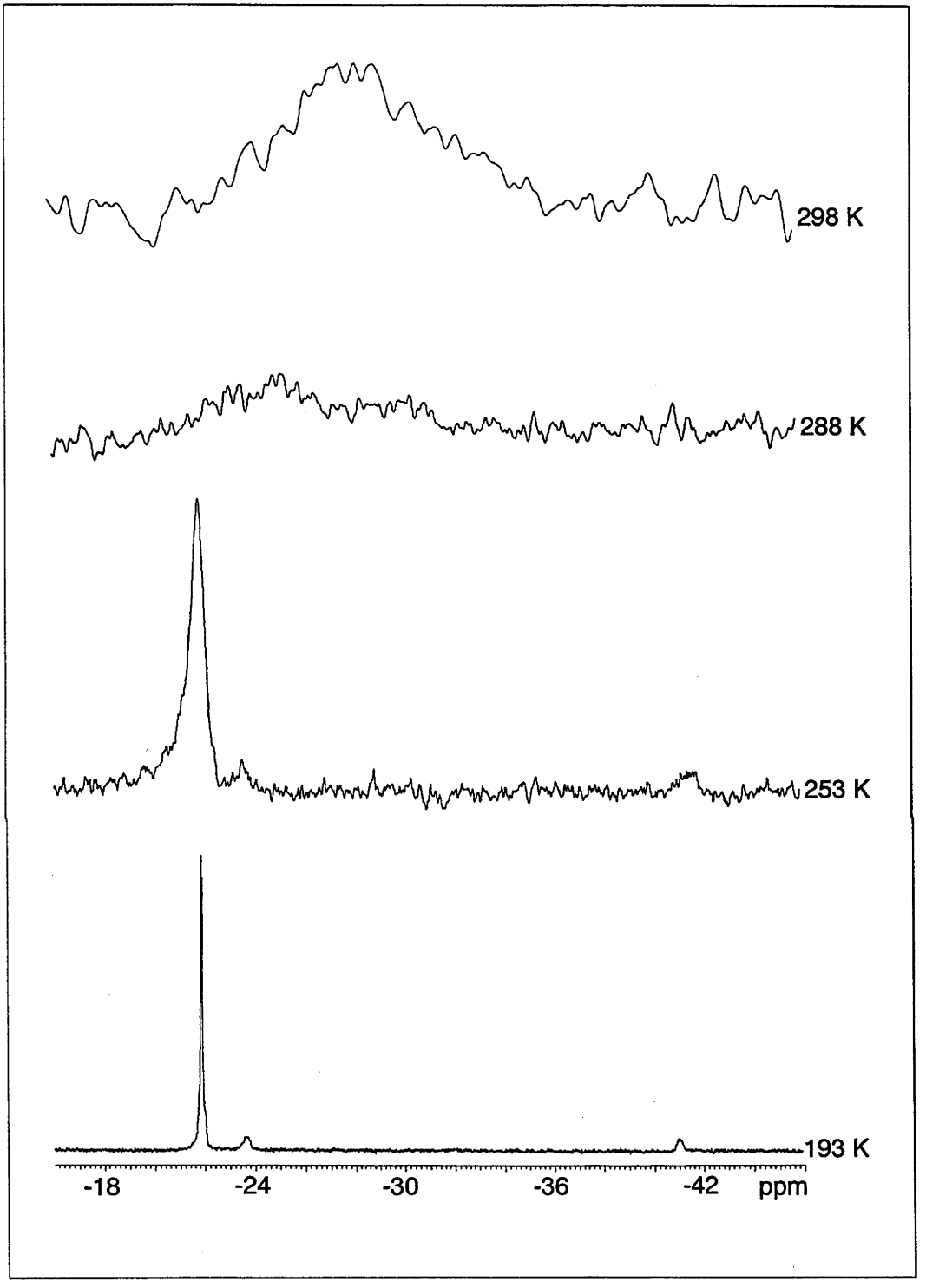


Figure 3.2.17. Variable temperature ^{31}P NMR spectroscopic study of $[CpWIr_3(\mu\text{-}CO)_3(CO)_6(PMe_3)_2]$ (**8**) in CD_2Cl_2

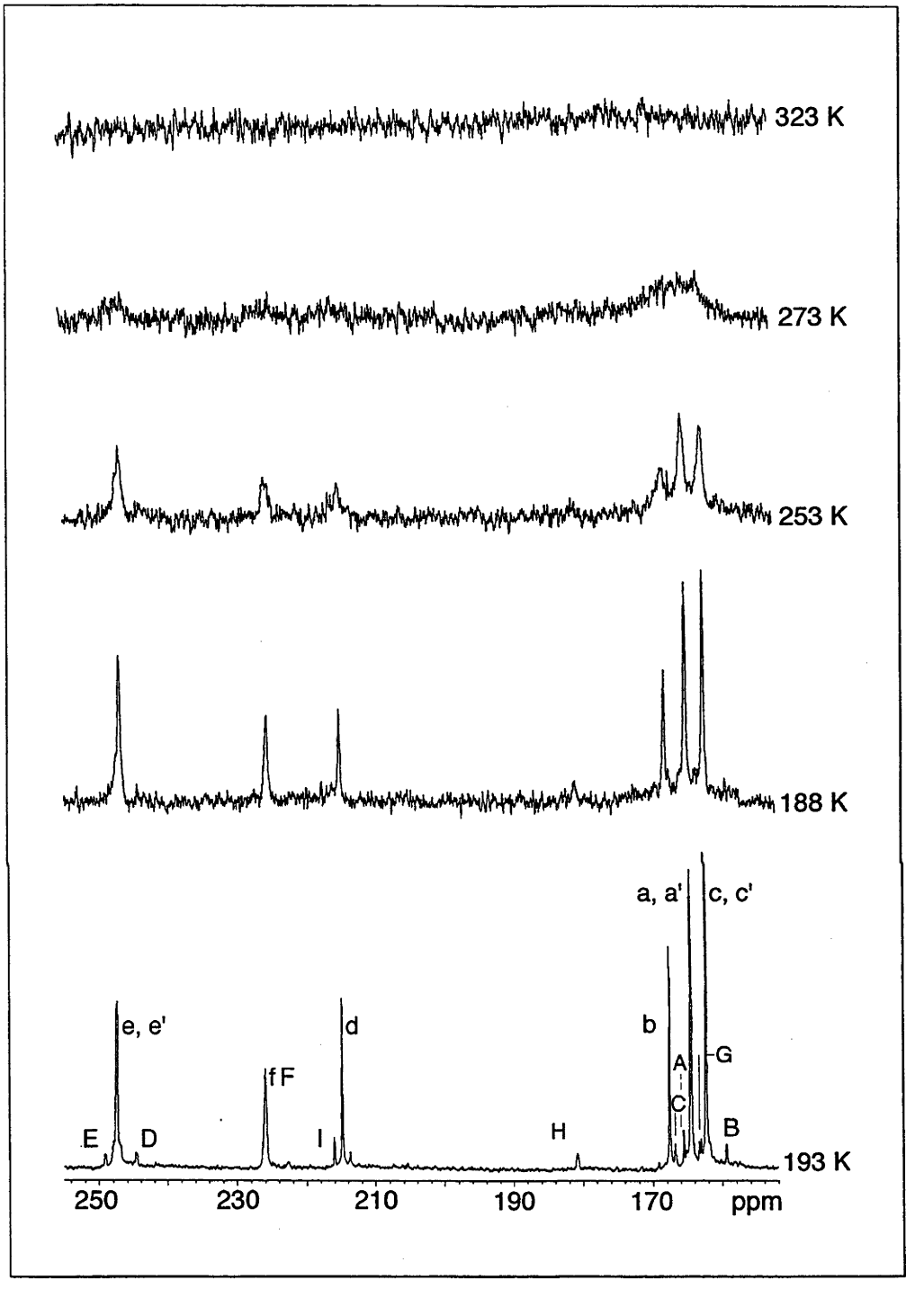


Figure 3.2.18. Variable temperature ^{13}C NMR spectroscopic study of $[CpWIr_3(\mu\text{-}CO)_3(CO)_6(PMe_3)_2]$ (**8**) in CD_2Cl_2.

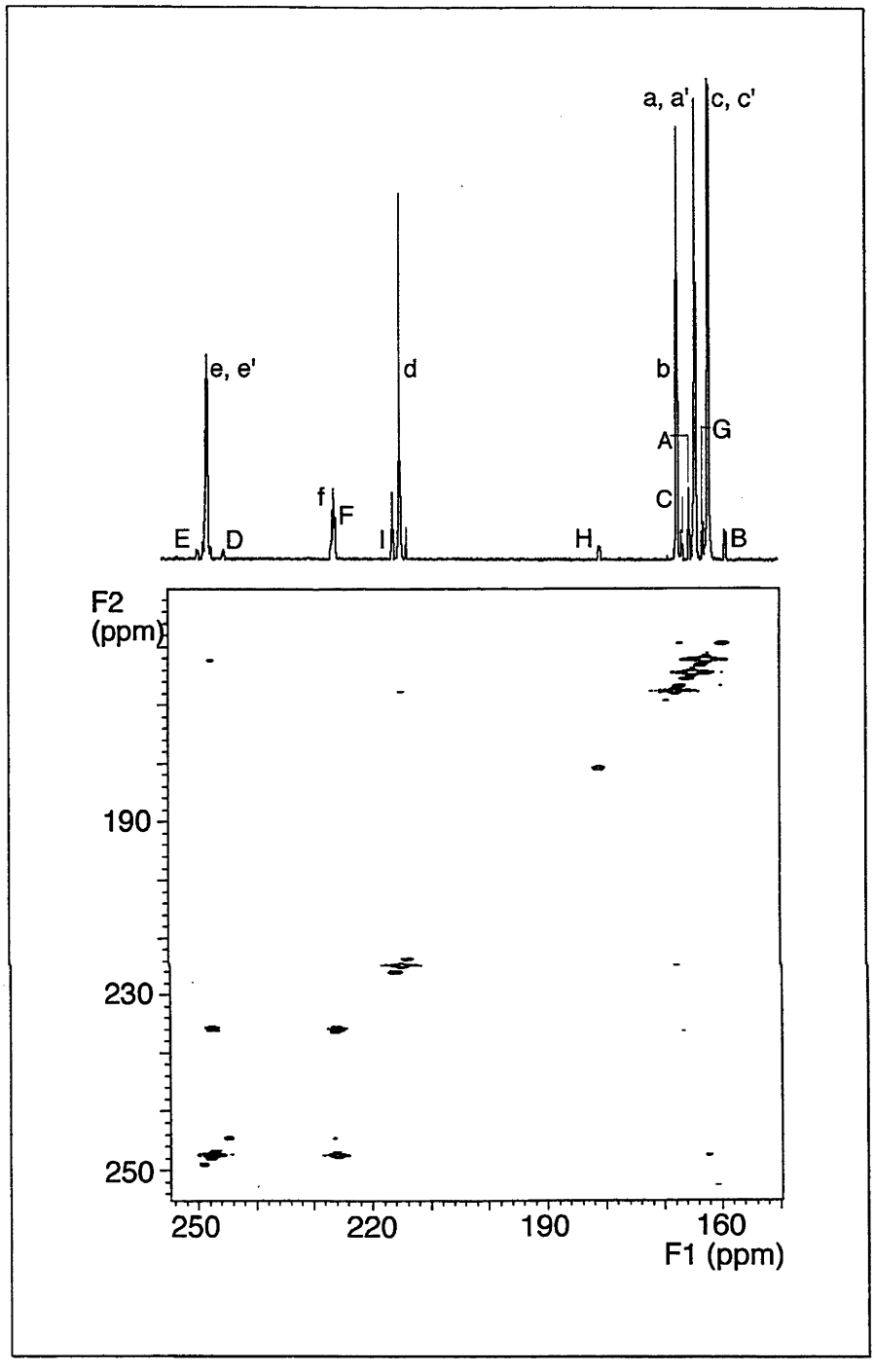


Figure 3.2.19. ^{13}C NMR COSY spectrum of $[CpWIr_3(\mu\text{-}CO)_3(CO)_6(PMe_3)_2]$ (**8**) in CD_2Cl_2 at 193 K.

Resonances for the minor configuration **8b** are observed in the ^{13}C NMR spectrum at 249.0 (D or E), 244.7 (E or D), 225.8 (F), 216.1 (I), 180.8 (H), 166.7 (C or B), 163.5 (G), 165.9 (A) and 159.2 (B or C) ppm, all with intensity 1, the specific assignments of which follow those outlined above for **5b**.

An EXSY spectrum of **8** (Figure 3.2.20.) reveals site exchanges corresponding to a, a' ↔ f and c ↔ d for **8a**, observed earlier with the analogous configuration **5a**. The proposed exchanges

follow those outlined for **5a**, the mechanisms being shown in Schemes 3.2.2. and 3.2.3. As with **5b**, configuration **8b** was present in insufficient amounts to allow exchange processes to be observed and identified.

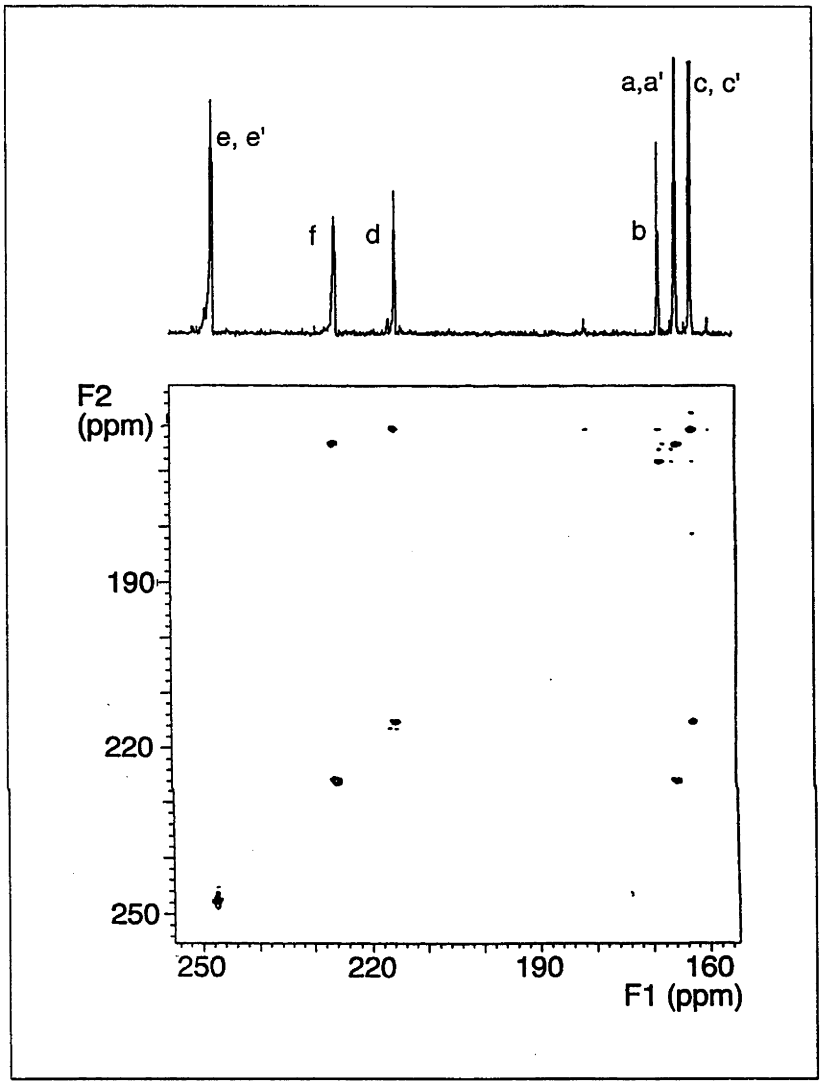


Figure 3.2.20. ^{13}C NMR EXSY spectrum of $[CpWIr_3(\mu\text{-}CO)_3(CO)_6(PMe_3)_2]$ (**8**) in CD_2Cl_2 at 228 K.

NMR studies of $[CpWIr_3(\mu\text{-}CO)_3(CO)_5(PMe_3)_3]$ (9).

The ^{31}P NMR spectrum of $[CpWIr_3(\mu\text{-}CO)_3(CO)_5(PMe_3)_3]$ (**9**) in CD_2Cl_2 at room temperature is close to coalescence. On cooling to 188 K three signals are resolved at -27.2, -45.8 and -83.2 ppm, in the ratio 1 : 1 : 1 (Figure 3.2.21.). The ^{13}C NMR spectrum of **9** in CD_2Cl_2 at room temperature is also close to coalescence. On cooling to 188 K the spectrum splits into eight resonances of equal intensity (Figure 3.2.22.). The combination of ^{31}P and ^{13}C NMR data indicates the presence of one configuration of **9** with the Cp occupying an axial site and the phosphines occupying radial, axial and apical sites. All previously structurally characterized

tetrasubstiuted tetrahedral tetrairidium clusters adopt this geometry, with the apical ligand inclined to the bond between axial-ligated iridiums to minimize steric effects. At 188 K the ^{13}C NMR spectrum shows resonances for **9** at 257.3 (c), 245.1 (d), 229.5 (e), 227.9 (f), 184.6 (h), 172.6 (a), 168.0 (b) and 166.0 (g) ppm, with the signals at 257.3, 245.1 and 227.9 ppm showing the expected satellite coupling to ^{183}W. The signal at 229.5 ppm is assigned to the bridging carbonyl e and the signal at 184.6 ppm to the radial carbonyl h. The resonance at 166.0 ppm shows *cis* and *trans* coupling to the radial and axial phosphines, respectively, and is assigned to axial carbonyl g. The carbonyls a and b are assigned by their respective lack or presence of long-range coupling to phosphines; the signal at 168.0 ppm shows *trans* coupling to the axial phosphine, and is assigned to carbonyl b, and the remaining signal is thus assigned to carbonyl a.

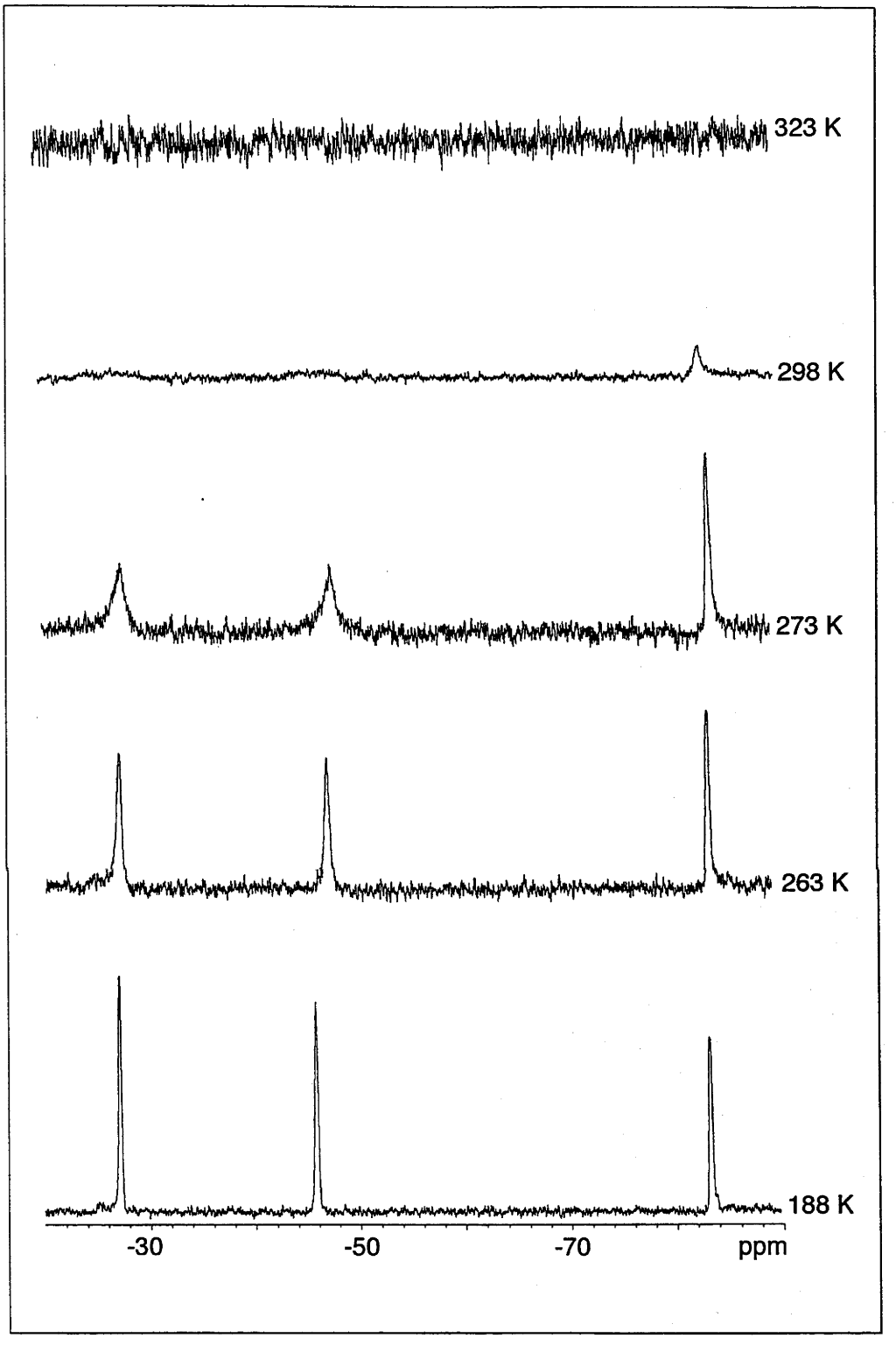


Figure 3.2.21. Variable temperature ^{31}P NMR spectroscopic study of $[CpWIr_3(\mu\text{-}CO)_3(CO)_5(PMe_3)_3]$ (**9**) in CD_2Cl_2

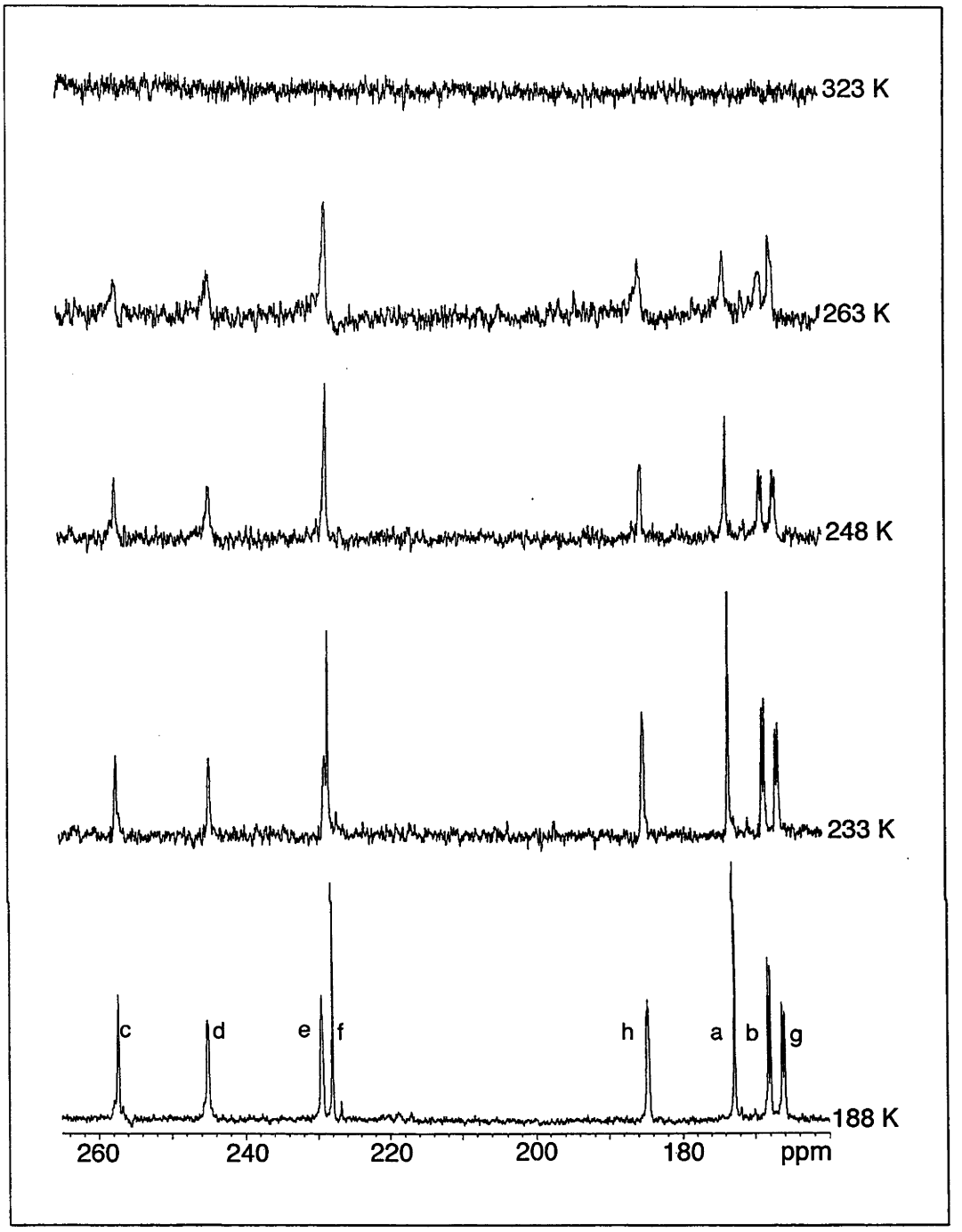


Figure 3.2.22. Variable temperature ^{13}C NMR spectroscopic study of $[CpWIr_3(\mu\text{-}CO)_3(CO)_5(PMe_3)_3]$ (**9**) in CD_2Cl_2

Discussion

Heterometal incorporation into a well-studied homometallic cluster is of primary importance, and the present study has afforded the possibility of examining its influence upon such fundamentally important properties as reaction kinetics, product distribution, and ligand fluxionality. The studies in Chapter 2 have shown vastly increased reaction rates for ligand substitution upon introduction of the mid-transition metal. The studies in this Chapter permit a comparison of configuration distribution and carbonyl scrambling pathways. These studies have

conclusively established the coordination geometries of many of the configurations of $[CpWIr_3(\mu\text{-}CO)_3(CO)_{8-n}(L)_n]$ (R = PPh_3, PMe_3; n = 1, 2). Replacement of PPh_3 by the more basic and sterically less demanding PMe_3 has essentially no impact on configuration structure or ratio for $[CpWIr_3(\mu\text{-}CO)_3(CO)_6(L)_2]$. For the mono-phosphine derivatives, PPh_3 affords significant amounts of three configurations with the axial PPh_3, apical Cp form the most abundant, while PMe_3 affords two configurations with the radial PMe_3, axial Cp form present in greater amounts; PPh_3 uniquely affords a radial Cp, axial PPh_3 configuration, a result which can perhaps be rationalized on steric grounds as the cone angles decrease in the order PPh_3 (145°) > Cp (136°) > PMe_3 (118°). The coordination geometries of the $[CpWIr_3(\mu\text{-}CO)_3(CO)_{8-n}(L)_n]$ can be contrasted with those of $[Ir_4(\mu\text{-}CO)_3(CO)_{8-n}(PR_3)_{n+1}]$. For n = 1, examples of radial, axial coordination in the iridium system are extant, but the axial, apical mode of **2a** and **4a** is unprecedented with tetrairidium clusters. For n = 2, the radial, diaxial mode of **3b** and **5b** is only observed in the iridium system with polydentate ligands (for monodentate ligands, diradial, axial coordination geometry is preferred); the triradial geometry of **3a** and **5a** is unprecedented with tetrairidium clusters. There are clearly dramatic differences in configuration preference for monodentate ligand derivatives in the Ir_4 and WIr_3 series of clusters.

These differences in configuration distribution between the Ir_4 and WIr_3 systems render comparisons of CO mobility difficult. The structural study of **4a** reveals a symmetric bridging carbonyl distribution. $[Ir_4(\mu\text{-}CO)_3(CO)_7(L)_2]$ examples with this carbonyl geometry exchange CO ligands by a "merry-go-round" process at all faces, which proceed by way of an unbridged intermediate (Scheme 3.1.1.), a process observed with the structurally similar **2a** and **4a**. The novel geometries observed with **3a** and **5a** obviously preclude comparisons with related derivatives in the tetrairidium system, but the pathway postulated in Scheme 6 for carbonyl fluxionality in mixed-metal clusters provides an interesting analogue of the D_{2d}-symmetry intermediate implicated in $[Ir_4(CO)_{12}]$ fluxionality.

3.2.3. NMR studies of $PMePh_2$ and PMe_2Ph derivatives of $[CpWIr_3(CO)_{11}]$

The room temperature ^{31}P NMR spectra of those complexes contain either a broadened weighted average resonance, or no signal at all. In all cases, lowering the temperature sharpened the resonances, suggesting fluxionality in each derivative. The triphenylphosphine- and trimethylphosphine-ligated tungsten-triiridium clusters exhibit different isomer configurations, differing particularly in the structural characterizatons. To assess the importance of steric and electronic factors in governing isomer distribution, phosphines with cone angles and electronic parameters between the two outliers were investigated. The steric and electronic parameters of these phosphines are listed in Table 3.2.1. Resonances of the

methyldiphenyl and dimethylphenylphosphine-substituted tungsten-iridium clusters are listed in Table 3.2.2. The substitution sites of the clusters $[CpWIr_3(\mu\text{-}CO)_3(CO)_{8-n}(L)_n]$ [L = $PMePh_2$, n = 1 (**10**), 2 (**11**), 3 (**12**); L = PMe_2Ph, n = 1 (**13**), 2 (**14**), 3 (**15**)], as reported in Chapter 2, have been assigned utilizing information from (a) the crystallographically-verified isomer, (b) the substitution geometries found in the analogous triphenylphosphine- or trimethylphosphine-substituted tungsten-iridium clusters **4** - **9**, and (c) chemical shifts in the ^{31}P NMR spectra. Figures 3.2.23. and 3.2.24. are indicative of the difference in isomer distribution. The room temperature ^{31}P NMR spectrum of **10** contains one averaged resonance at -11.8 ppm. a low temperature limiting spectrum of three signals (-3.2, -2.7 and -22.9 ppm in CD_2Cl_2; ratio 4 : 5 : 2) is obtained at 178 K (Figure 3.2.23.). Similarly, the room temperature ^{31}P NMR spectrum of **13** contains a broad resonance at -28.0 ppm. however, lowering the temperature to 178 K reveals a spectrum containing two singlets (-20.8 and -28.5 ppm in CD_2Cl_2; ratio 5 : 4; Figure 3.2.24.).

Table 3.2.1. Steric and Electronic Parameters for Phosphines in $[CpWIr_3(\mu\text{-}CO)_3(CO)_{8-n}(L)_n]$

Phosphine	Electronic Parameter ν (cm^{-1})	Cone Angle θ (°)
PPh_3	2068.9	145
$PMePh_2$	2067.0	136
PMe_2Ph	2065.3	122
PMe_3	2064.1	118

Table 3.2.2. ^{31}P NMR Data for $[CpWIr_3(\mu\text{-}CO)_3(CO)_{8-n}(L)_n]$ (L = $PMePh_2$, PMe_2Ph; n = 1, 2 or 3)

Complex		*^{31}P NMR shifts*	*Suggested site of phosphine substitution with respect to (μ-CO)$_3$ plane*	*Cp substitution*	*Isomer ratio*
n = 1, R = $PMePh_2$	**10a**	-12.7[a]	axial	apical	4
	10b	-3.2[a]	radial	axial	5
	10c	-22.9[a]	axial	radial	2
n = 2, R = $PMePh_2$	**11a**	0.6[b]	diradial	radial	2
	11b	-0.5, -22.9 (1:1)[b]	radial, axial	axial	3
n = 3, R = $PMePh_2$	**12a**	-3.6, -30.1, -55.3 (1:1:1)[b]	radial, axial, apical	axial	6
	12b	-8.9. -9.2 (1:2)[b]	triradial	apical	1
n = 1, R = PMe_2Ph	**13a**	-28.5[a]	axial[c]	apical	5
	13b	-20.8[a]	radial	axial	4
n = 2, R = PMe_2Ph	**14a**	-16.8[b]	diradial	radial	6
	14b	-18.9, -37.8 (1:1)[b]	radial, axial	axial	1
n = 3, R = PMe_2Ph	**15a**	-21.2, -44.0, -72.8 (1:1:1)[b]	radial, axial, apical	axial	

[a] CD_2Cl_2, 178 K. $CDCl_3$, 230 K. [c] Crystallographically confirmed

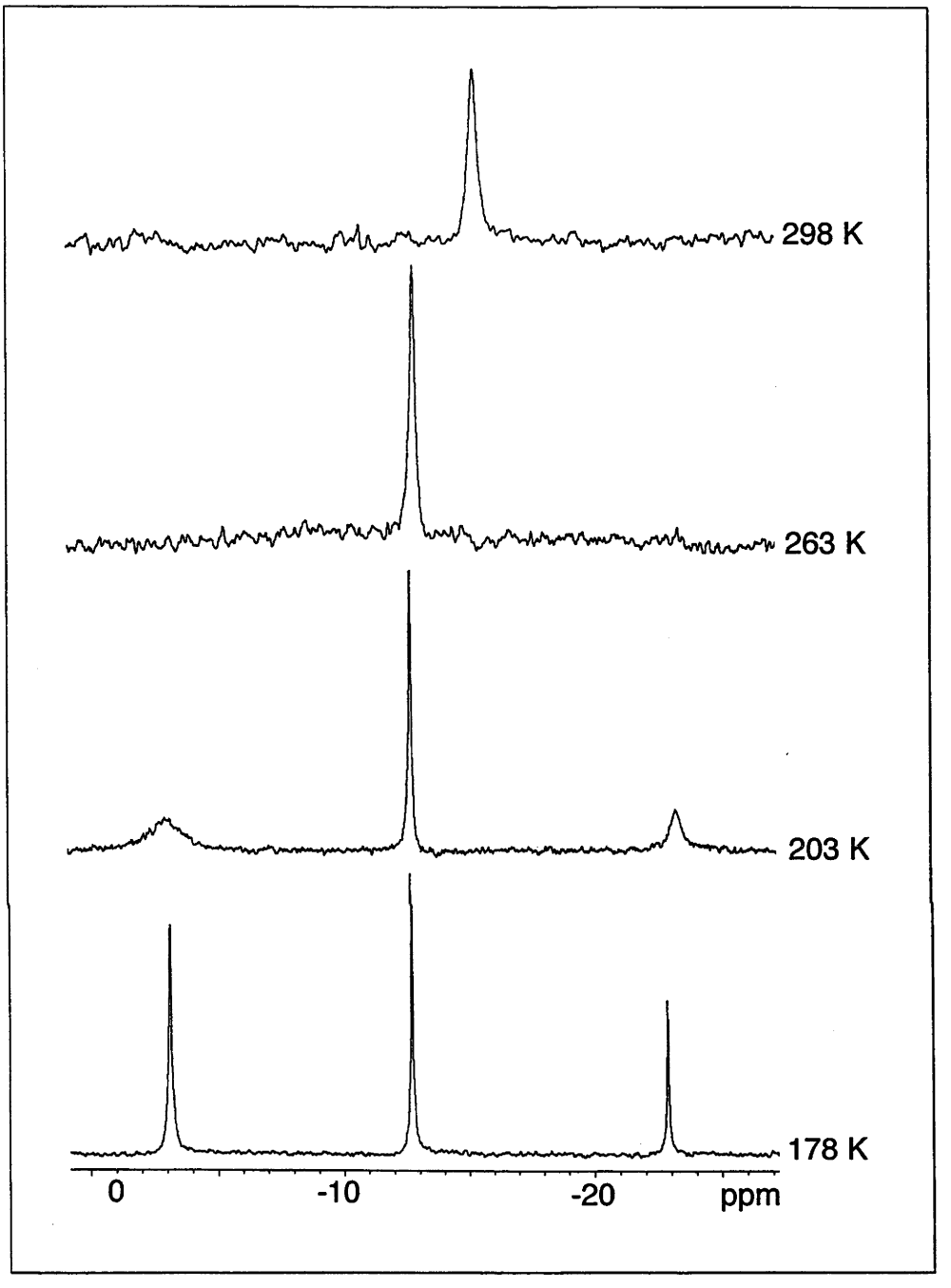


Figure 3.2.23. Variable temperature ^{31}P NMR spectroscopic study of $[CpWIr_3(\mu\text{-}CO)_3(CO)_7(PMePh_2)]$ (**10**) in CD_2Cl_2.

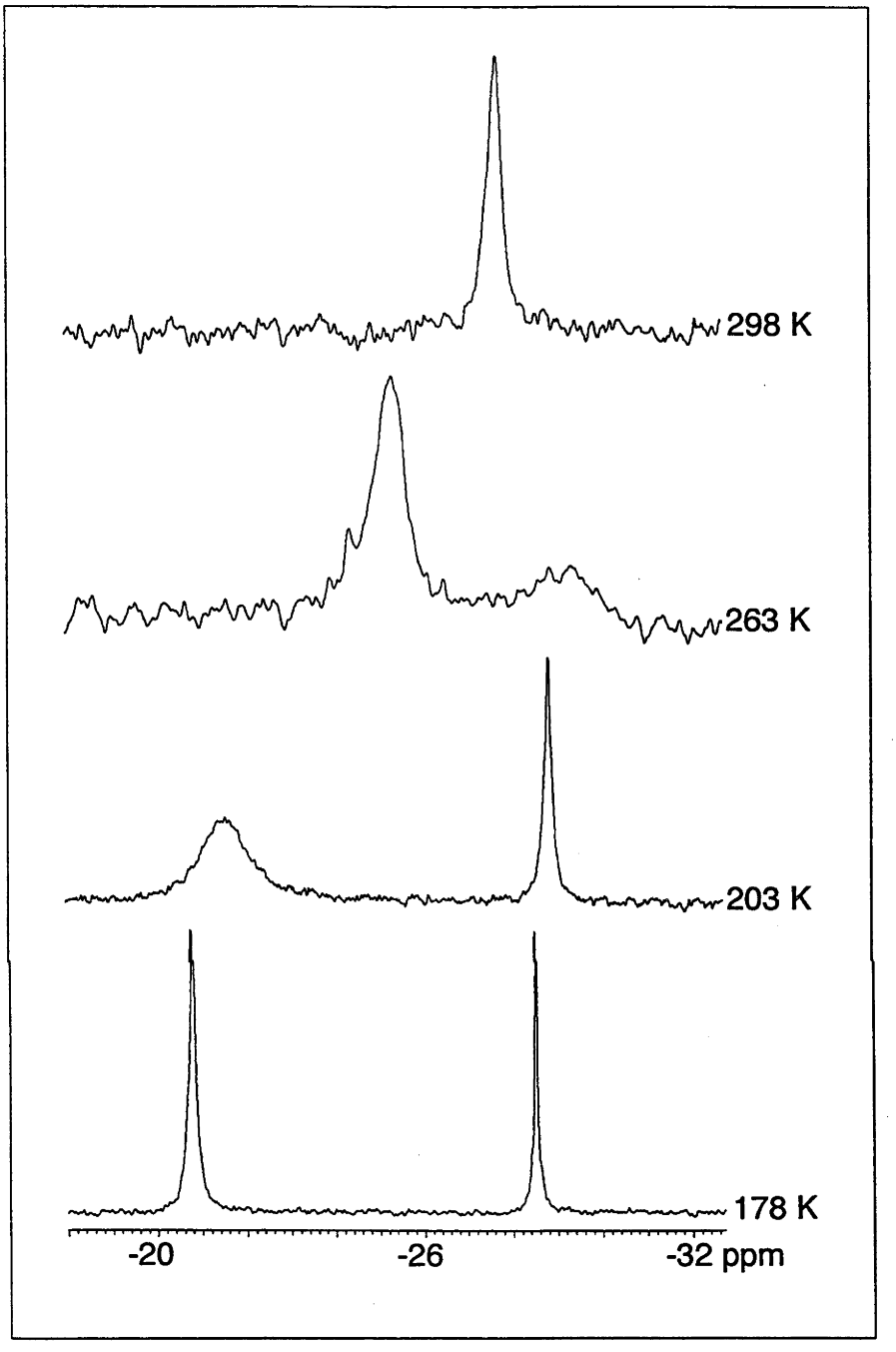
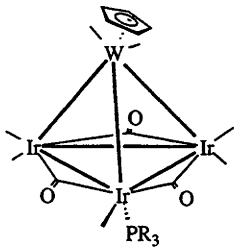
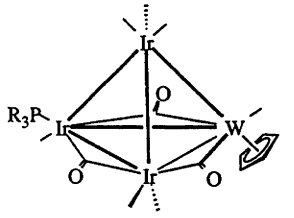


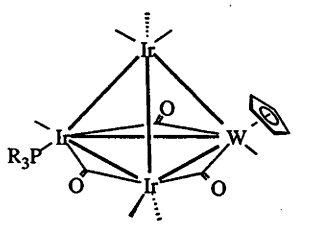
Figure 3.2.24. Variable temperature ^{31}P NMR spectroscopic study of $[CpWIr_3(\mu\text{-}CO)_3(CO)_7(PMe_2Ph)]$ (**13**) in CD_2Cl_2.



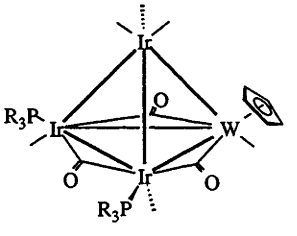
[CpWIr$_3$(μ-CO)$_3$(CO)$_7$(PMePh$_2$)] **10a**
[CpWIr$_3$(μ-CO)$_3$(CO)$_7$(PMe$_2$Ph)] **13a** XRS
ax, ap



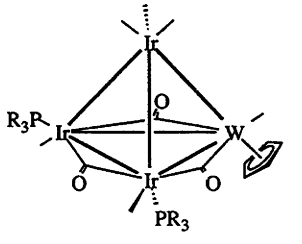
[CpWIr$_3$(μ-CO)$_3$(CO)$_7$(PMePh$_2$)] **10b**
[CpWIr$_3$(μ-CO)$_3$(CO)$_7$(PMe$_2$Ph)] **13b**
r, ax



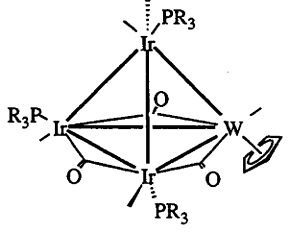
[CpWIr$_3$(μ-CO)$_3$(CO)$_7$(PMePh$_2$)] **10c**
ax, r



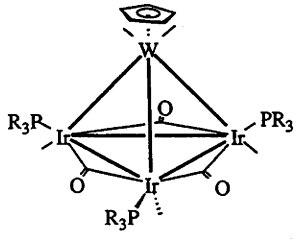
[CpWIr$_3$(μ-CO)$_3$(CO)$_6$(PMePh$_2$)$_2$] **11a**
[CpWIr$_3$(μ-CO)$_3$(CO)$_6$(PMe$_2$Ph)$_2$] **14a**
r, r, r



[CpWIr$_3$(μ-CO)$_3$(CO)$_6$(PMePh$_2$)$_2$] **11b**
[CpWIr$_3$(μ-CO)$_3$(CO)$_6$(PMe$_2$Ph)$_2$] **14b**
r, ax, ax



[CpWIr$_3$(μ-CO)$_3$(CO)$_6$(PMePh$_2$)$_3$] **12a**
[CpWIr$_3$(μ-CO)$_3$(CO)$_5$(PMe$_2$Ph)$_3$] **15**
r, ax, ax, ap



[CpWIr$_3$(μ-CO)$_3$(CO)$_5$(PMePh$_2$)$_3$] **12b**
r, r, r, ap

Figure 3.2.25. Configurations of [CpWIr$_3$(μ-CO)$_3$(CO)$_{8-n}$(L)$_n$]
(L = PMePh$_2$, PMe$_2$Ph; n = 1 - 3); r = radial, ax = axial, ap = apical.
XRS ≡ structurally confirmed characterization.\

Suggested geometries of the alkylarylphosphine-substituted derivatives of **2** are given in Figure 3.2.25. The crystallographically observed **13a** has Cp occupying an apical site and PMe_2Ph occupying an axial site. This axial, apical geometry has previously been observed in the PPh_3- and PMe_3-substituted derivatives, **4a** and **7a**. The second isomer **13b**, with a radially coordinated phosphine, is consistent with the isomer adopting radial, axial geometry to minimize phosphine-cyclopentadienyl repulsion. This radial, axial isomer is found in both $[CpWIr_3(\mu\text{-}CO)_3(CO)_7(PPh_3)]$ (**4b**) and $[CpWIr_3(\mu\text{-}CO)_3(CO)_7(PMe_3)]$ (**7b**). The shifts in the ^{31}P NMR spectrum of **14** combined with the trisubstituted geometries characterized for $[CpWIr_3(\mu\text{-}CO)_3(CO)_6(PPh_3)_2]$ (**5**) and $[CpWIr_3(\mu\text{-}CO)_3(CO)_6(PMe_3)_2]$ (**8**) lead to the assignment of isomer **14a** with triradial geometry and isomer **14b** with radial, diaxial geometry. In contrast, clusters **22** - **24** (Section 3.2.5.), with insufficiently flexible diphosphine backbones, adopt diaxial, apical geometries. The geometries adopted by the monodentate phosphine - containing clusters **14** and bidentate phosphine-containing clusters **22** and **23** are consistent with configuration discrimination based on ligand size, as previously observed for homometallic clusters (see above); it should be noted, though, that NMR data for **15** shows the presence of one configuration, the shifts being consistent with a radial, diaxial, apical assignment, previously observed with $[CpWIr_3(\mu\text{-}CO)_3(CO)_5(PMe_3)_3]$ (**9**). The suggested configurations for **10** - **12** follow similarly. Configuration **10a**, with an axially coordinated phosphine, is proposed to adopt an axial, apical geometry. Isomer **10b**, with a radially coordinated phosphine, presumably adopts the radial, axial geometry common to these systems. The third configuration, with axial phosphine, is proposed to adopt the axial, radial geometry identified in the ^{31}P NMR spectra of **4** (configuration **4c**). Chemical shifts in the ^{31}P NMR spectrum of **11** again suggests the triradial geometry (**11a**) and the radial, diaxial geometry (**11b**). The ^{31}P NMR spectrum of **12** unusually suggests the presence of two configurations. The major isomer **12a**, with radial, axial and apical coordinated phosphines, is again consistent with a radial, diaxial, apical assignment, as seen with $[CpWIr_3(\mu\text{-}CO)_3(CO)_5(PMe_3)_3]$ (**9**). The ^{31}P NMR resonances for the minor configuration **12b** (two signals in the radial region of the spectrum in the ratio 2:1) can only be consistent with the configuration adopting triradial, apical geometry; the Cp adopts an apical position and is inclined over a WIr_2 face such that two of the phosphines are equivalent. This geometry was not observed with either $[CpWIr_3(\mu\text{-}CO)_3(CO)_8(PPh_3)_3]$ (**6**) or $[CpWIr_3(\mu\text{-}CO)_3(CO)_8(PMe_3)_3]$ (**9**), and is thus far unprecedented in structurally characterized tetrahedral clusters.

3.2.4. NMR studies of $P(OPh)_3$ and $P(OMe)_3$ derivatives of $[CpWIr_3(CO)_{11}]$

The ^{31}P NMR spectra of the clusters $[CpWIr_3(\mu\text{-}CO)_3(CO)_{8-n}(L)_n]$ [L = $P(OPh)_3$, n = 1 (**16**), 2 (**17**), 3 (**18**); L = $P(OMe)_3$, n = 1 (**19**), 2 (**20**), 3 (**21**)] are also consistent with mixtures of configurations which interconvert on the NMR timescale. The room temperature ^{31}P NMR spectrum of **16** contains a sharp averaged resonance at 71.0 ppm. A low temperature limiting spectrum of three signals (103.2, 78.1 and 64.8 ppm in CS_2/CD_2Cl_2; ratio 1 : 2 : 1) is obtained at 173 K (Figure 3.2.26.). Likewise, the room temperature ^{31}P NMR spectrum of **19** contains a broad resonance at 86.6 ppm. A low temperature limiting spectrum of two singlets (91.8 and 81.7 ppm, ratio 1 : 7) is obtained at 163 K. The variable temperature spectra of **19** (Figure 3.2.27..) reveal that these signals coalesce at 216 K (CS_2/CD_2Cl_2, 300 MHz). The room temperature ^{31}P NMR spectra of the tetrasubstituted complexes **18** and **21** contain no signal at all. Lowering the temperature at which the spectra are obtained for each derivative sharpens the ^{31}P NMR resonances, suggesting fluxionality in each case.

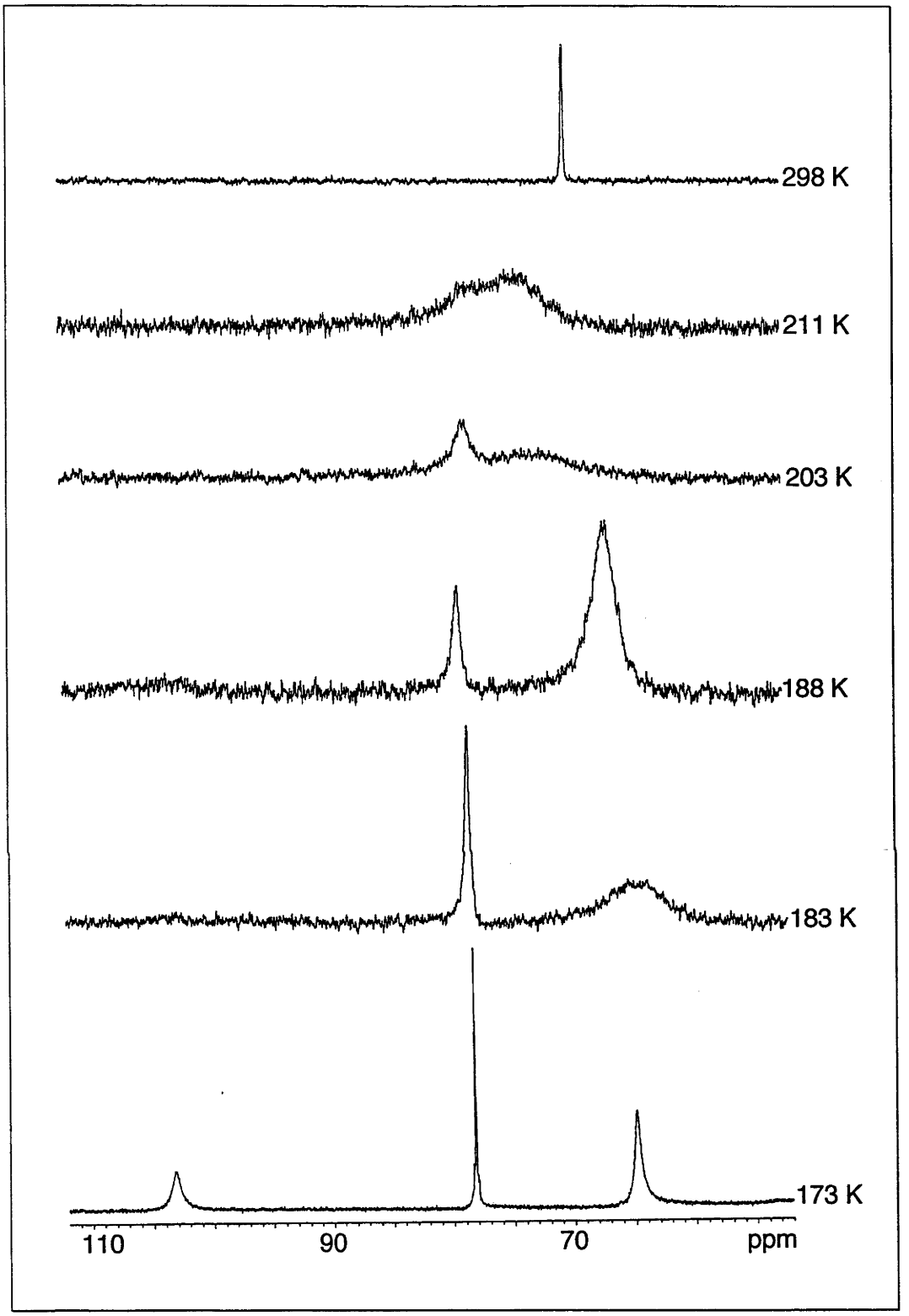


Figure 3.2.26. Variable temperature ^{31}P NMR spectroscopic study of $[CpWIr_3(\mu\text{-}CO)_3(CO)_7\{P(OPh)_3\}]$ (**16**) in CS_2/CD_2Cl_2.

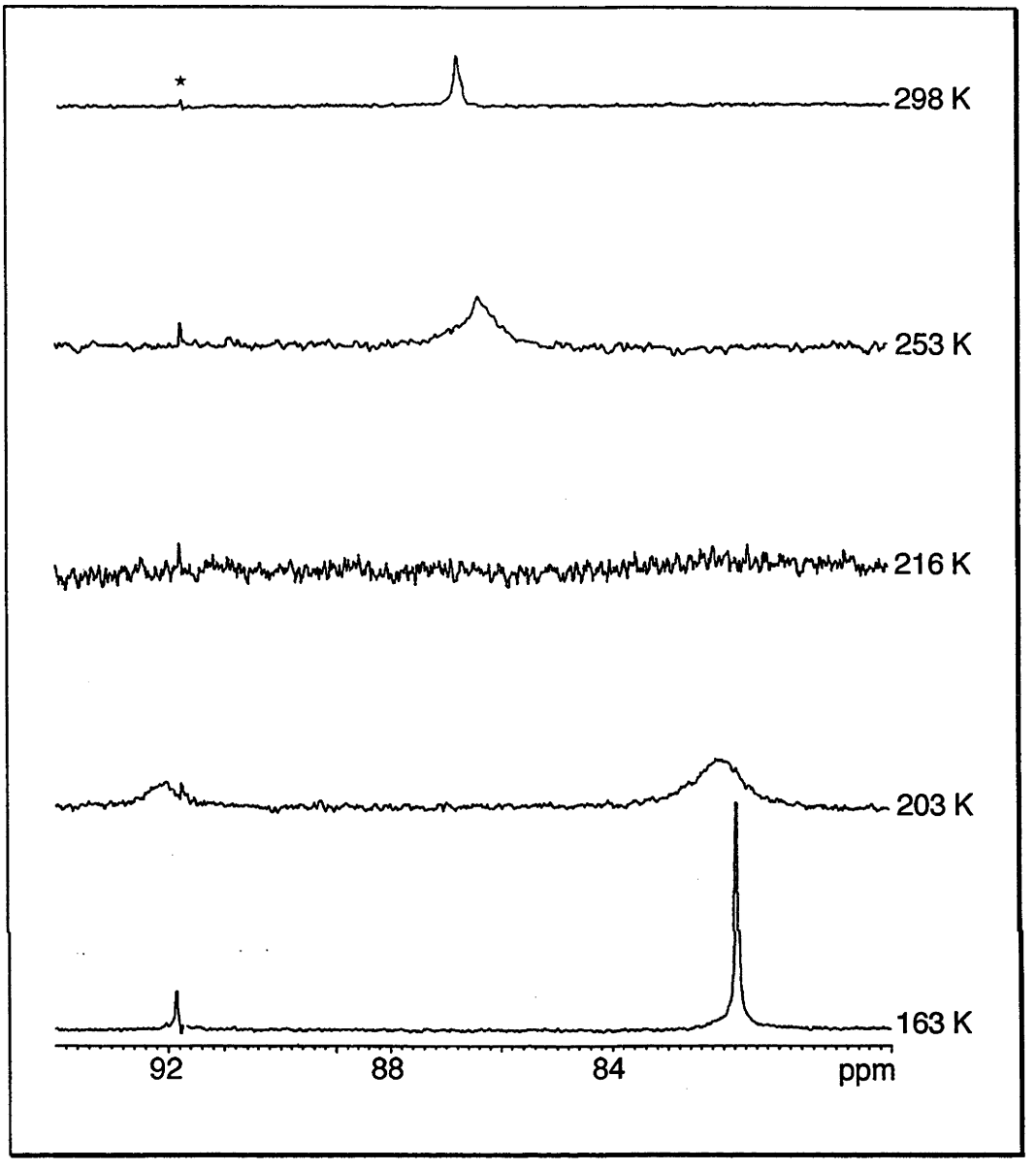


Figure 3.2.27. Variable temperature ^{31}P NMR spectroscopic study of $[CpWIr_3(\mu\text{-}CO)_3(CO)_7\{P(OMe)_3\}]$ (**19**) in CS_2/CD_2Cl_2 (* ≡ "spurious electronic artefact")

Resonances of the phosphite-substituted tungsten-iridium clusters are listed in Table 3.2.3., together with suggested coordination geometries. The substitution sites have been assigned utilizing information from (a) the crystallographically-verified configuration, (b) the substitution geometries found in the analogous phosphine - substituted tungsten - iridium clusters and the tetrairidium system, and (c) chemical shifts in the ^{31}P NMR spectra, assuming that the positional sequence is applicable to phosphite clusters.

Table 3.2.3. ^{31}P NMR Data for $[CpWIr_3(\mu\text{-}CO)_3(CO)_{8-n}(L)_n]$ [L = $P(OPh)_3$, $P(OMe)_3$; n = 1, 2 or 3]

Complex		^{31}P NMR shifts	Suggested site of phosphite substitution, with respect to $(\mu\text{-}CO)_3$ plane	Suggested site of Cp substitution	isomer ratio
n = 1, L = $P(OPh)_3$	**16a**	78.1[a]	axial	apical	2
	16b	103.2[a]	radial	axial	1
	16c	64.8[a]	axial	radial	1
n = 2, L = $P(OPh)_3$	**17**	109.5, 65.9 (1:1)[b]	radial, axial[c]	axial	
n = 3, L = $P(OPh)_3$	**18a**	107.7, 58.1, 35.2 (1:1:1)[b]	radial, axial, apical	axial	3
	18b	100.9, 78.8 (2:1)[b]	diradial, axial	apical	1
n = 1, L = $P(OMe)_3$	**19a**	91.8[a]	axial	apical	1
	19b	81.7[a]	axial	radial	7
n = 2, L = $P(OMe)_3$	**20**	124.4, 83.8 (1:1)[b]	radial, axial	axial	
n = 3, L = $P(OMe)_3$	**21a**	118.2, 97.1, 78.3 (1:1:1)[b]	radial, axial, apical	axial	2
	21b	118.5, 95.6 (2:1)[b]	diradial, axial	apical	1

[a] 4 CS_2/ 1 CD_2Cl_2, 163 K. [b] Acetone-d_6, 230K. [c] Crystallographically confirmed

Suggested geometries for the configurations of **16 - 18** are given in Figure 3.2.29. The crystallographically observed cluster **17** (isomer **17b**) has triphenylphosphite ligands occupying radial and axial sites and Cp occupying an axial site (radial, diaxial geometry). Assuming that the predominant isomer of **18** in solution adopts the geometry common to these systems, isomer **18a** has Cp occupying an axial site, and phosphites in radial, axial, apical sites (radial, diaxial, apical geometry). Utilizing the positional sequence of the ^{31}P NMR shifts, the minor isomer **18b** is therefore of diradial, axial, apical geometry with the Cp in an apical site. The assignments of **17** and **18** permit discrimination of axially-ligated triphenylphosphite when Cp is in the basal plane (~ 60 ppm) or in an apical site (~ 80 ppm). The configurations of **16** may therefore be assigned. Configuration **16a** is assigned an axial phosphite, apical Cp geometry, and isomer **16b** a radial phosphite, axial Cp geometry; the former geometry has been observed previously with a crystallographically characterized isomer of $[CpWIr_3(\mu\text{-}CO)_3(CO)_7(PMe_3)]$ (**7**), the latter geometry with a crystallographically confirmed isomer of $[CpWIr_3(\mu\text{-}CO)_3(CO)_7(PPh_3)]$ (**4**). The cone angle of $P(OPh)_3$ (121°) would suggest an axial phosphite, radial Cp geometry is proposed for isomer **16c**.

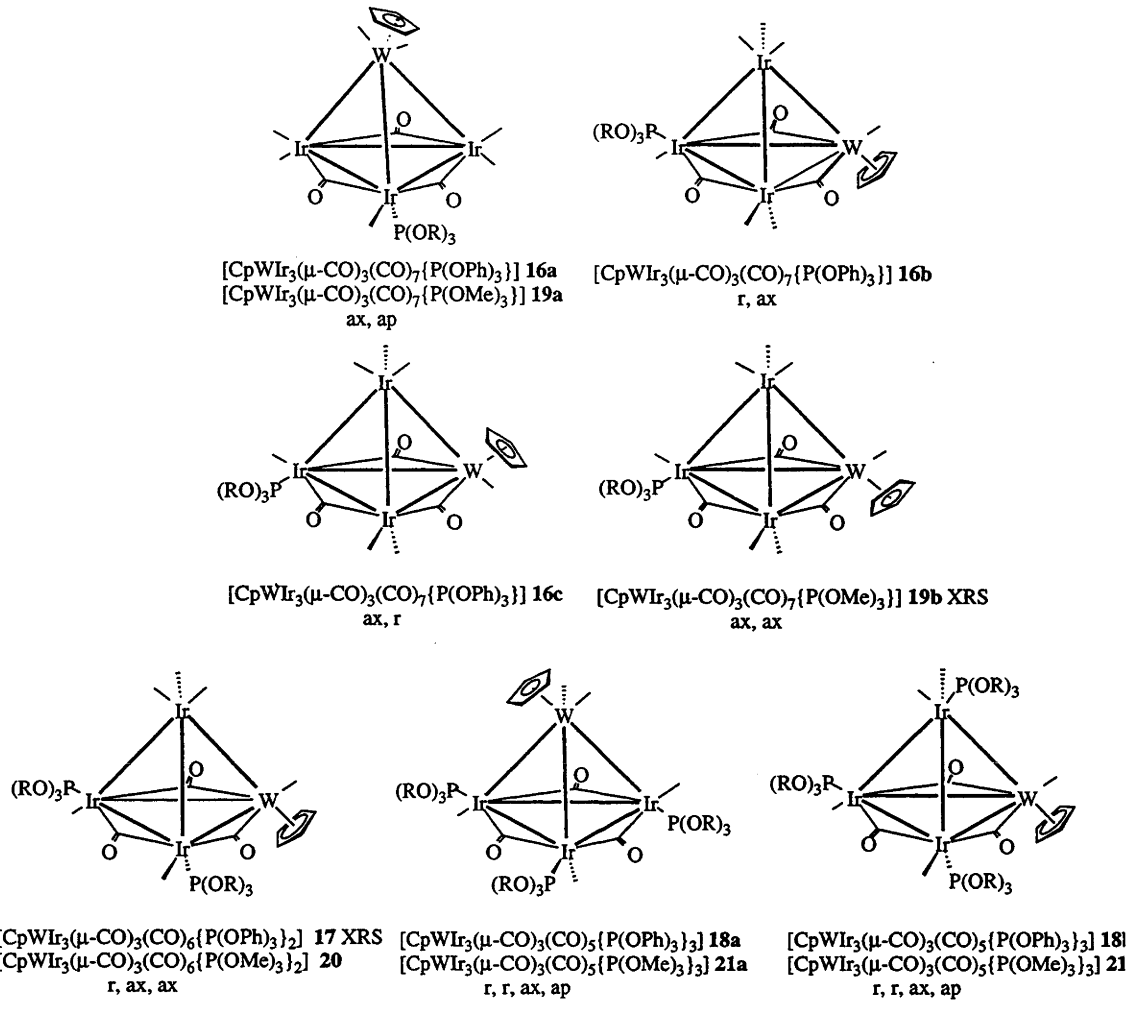


Figure 3.2.28. Isomers of $[CpWIr_3(\mu\text{-}CO)_3(CO)_{8-n}(L)_n]$

[L = $P(OPh)_3$, $P(OMe)_3$; n = 1 – 3]; r = radial, ax = axial, ap = apical]

XRS ≡ structurally confirmed configuration

Geometries of possible configurations of **19** - **21** are given in Figure 3.2.28. The major isomer of **21** in solution is assigned a radial, diaxial, apical geometry with axial Cp, and the minor isomer a diradial, axial, apical geometry with apical Cp, both analogous to that observed with **18**. Cluster **20** is assigned a radial, diaxial geometry with axial Cp, analogous to that observed with the crystallographically characterized **17**. Replacing triphenylphosphite by trimethylphosphite in progressing from **17**, **18** to **20**, **21** results in a shift to low field of 15 - 20 ppm. The observed configurations of **19** can be assigned axial phosphite, apical Cp (**19a**) and axial Cp, axial phosphite (**19b**) geometries. The crystallographically observed **19b** has a trimethylphosphite ligand occupying an axial site and the Cp also occupying an axial site (diaxial geometry, see Section *3.2.8.*) because of the small cone angle of the $P(OMe)_3$ ligand.

It should be emphasized that these assignments are cautious, requiring a crystallographic

underpinning to be solid. While many of these geometries have been structurally verified in the mixed - metal or "parent" tetrairidium systems, the diradial, axial, apical geometry is crystallographically unprecedented, and corroborating data is required to establish its existence. ^{31}P NMR chemical shifts have been utilized to assign many of the geometries in the present work, but it is not certain that the positional sequence of chemical shifts radial > axial > apical consists of mutually exclusive chemical shift ranges; in particular instances, for example, it is possible that radial and axial shifts may be similar, rendering assigment speculative. With these caveats in mind, it has been possible to assign coordination geometries to all configurations observed in the phosphite system. Comparison to the results with triphenylphosphine and trimethylphosphine reveals some differences. Unlike the bis-phosphite clusters, bis-phosphine clusters are observed as a mixture of two configurations, one of which has the three ligands in radial sites. The tris-trimethylphosphine derivative exists with a radial, diaxial, apical geometry (Cp axial) only, unlike the tris-phosphite clusters. A configuration of the mono-trimethylphosphite derivative exists with a diaxial geometry, not seen in the triphenylphosphite or phosphine substituted systems. The other geometries are observed in both phosphine and phosphite systems.

3.2.5. NMR studies of dppe, dppm and pdpp derivatives of [CpWIr$_3$(CO)$_{11}$]

The syntheses and X-ray structural characterizations of [CpWIr$_3$(μ-L)(μ-CO)$_3$(CO)$_6$] [L = dppe **22**, dppm **23**] have been reported previously.[40] In light of the discovery of interconverting configurations for the monodentate phosphine adducts, the bidentate phosphine complexes were reinvestigated, with their variable temperature ^{13}C and ^{31}P NMR spectra which are reported herein, revealing the presence of interconverting configurations, one of which (in each case) has the crystallographically-identified geometry. The ^{13}C NMR EXSY studies which have enabled elucidation of the pathways for ligand fluxionality in these complexes are also reported. The coordination geometry of [CpWIr$_3$(μ-pdpp)(μ-CO)$_3$(CO)$_6$] (**24**) was also investigated by ^{31}P NMR studies.

NMR studies of [CpWIr3(μ-dppe)(μ-CO)3(CO)6]

The variable temperature ^{31}P and ^{13}C NMR studies of **22** have been carried out, the results of which are displayed in Figures 3.2.29. and 3.2.30.

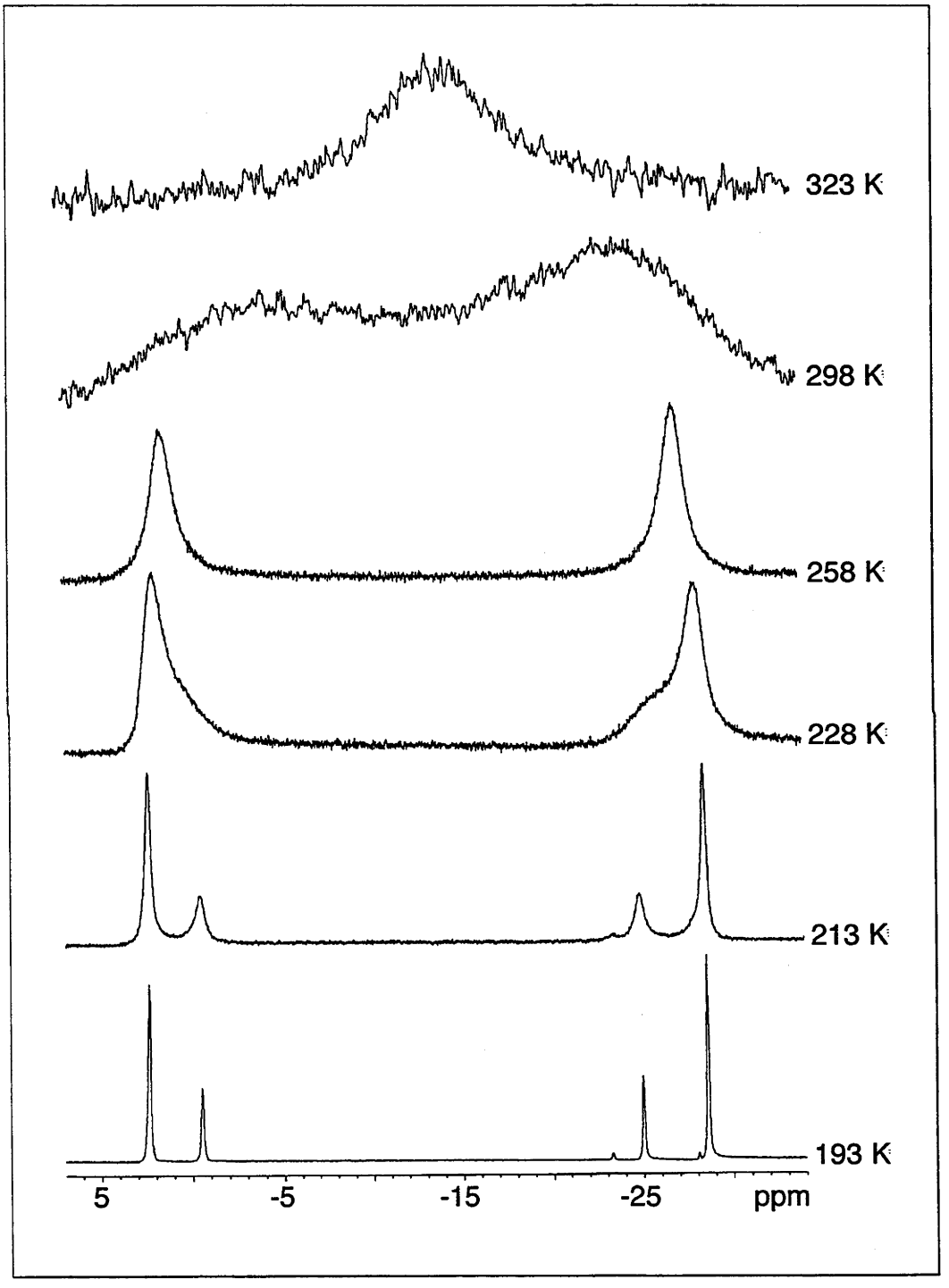


Figure 3.2.29. Variable temperature ^{31}P NMR spectroscopic study of $[CpWIr_3(\mu\text{-dppe})(\mu\text{-CO})_3(CO)_6]$ (**22**) in CD_2Cl_2.

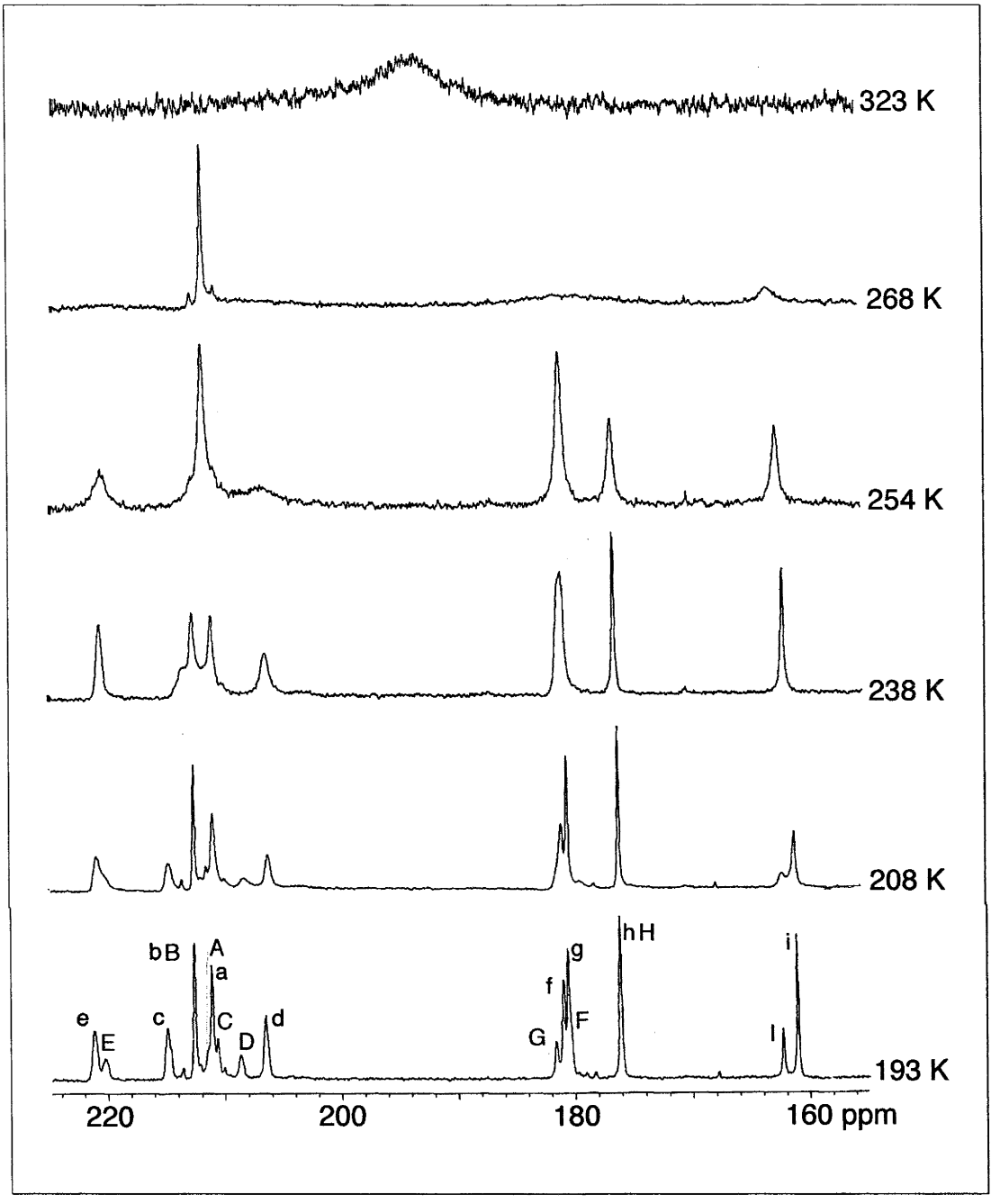


Figure 3.2.30. Variable temperature ^{13}C NMR spectroscopic study of $[CpWIr_3(\mu\text{-dppe})(\mu\text{-CO})_3(CO)_6]$ (**22**) in CD_2Cl_2

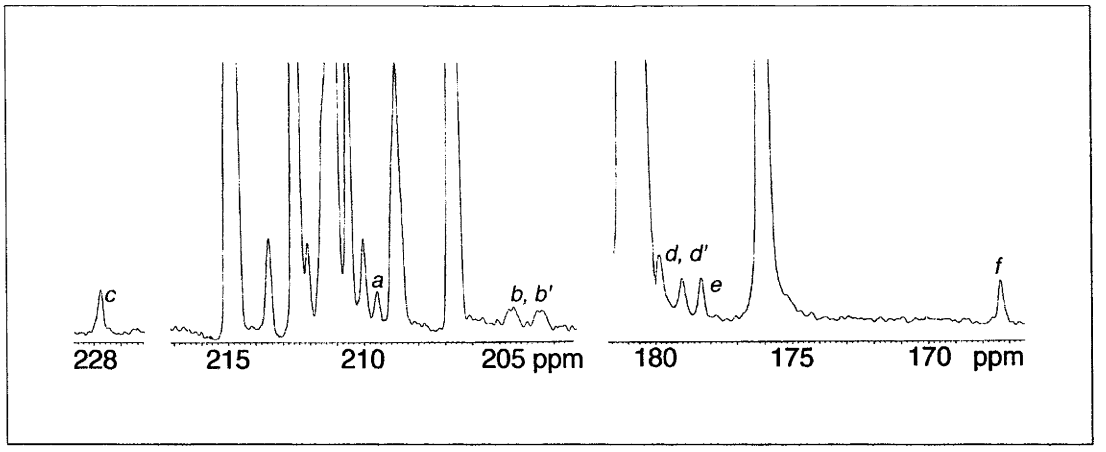
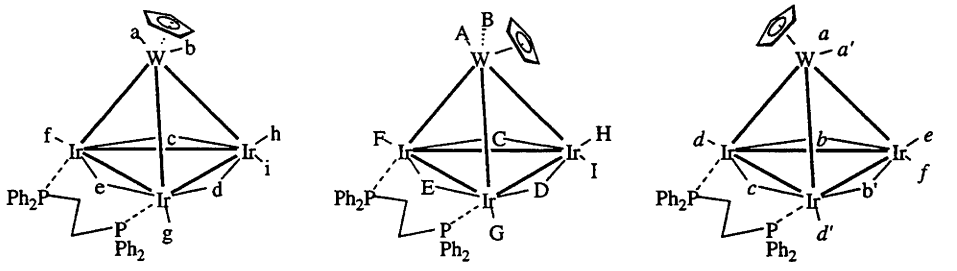


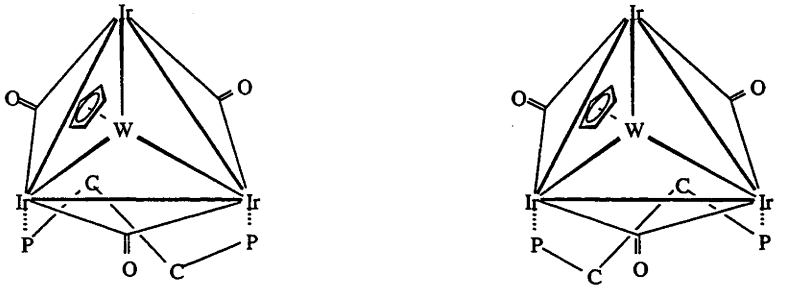
Figure 3.2.31. Partial ^{13}C NMR spectrum (line broadening = 10Hz) of $[CpWIr_3(\mu\text{-dppe})(\mu\text{-CO})_3(CO)_6]$ (**22**) in CD_2Cl_2 emphasizing isomer **22c**.

The ^{31}P NMR spectrum of **22** in $CDCl_3$ at 323 K consists of a broad singlet at -14.7 ppm (Figure 3.2.29.). On cooling to 193 K (in CD_2Cl_2), six signals are resolved, corresponding to the presence of three configurations in the ratio 1.00 : 0.40 : 0.01. The considerable difference in chemical shifts in the ^{31}P NMR spectra for axially-ligated phosphines is unusual and is noteworthy. The ^{13}C NMR spectrum of **22** at 323 K shows a single peak at 173 ppm, but at 193 K the fluxional processes are sufficiently slow to distinguish resonances corresponding to three different configurations (Figure 3.2.30.); the least abundant isomer becomes visible upon applying a line broadening of 10 Hz to the ^{13}C NMR spectrum at 193 K, to enhance the signal : noise ratio (Figure 3.2.31.). The chemical shifts of the two most abundant configurations in the ^{31}P NMR spectrum suggest that they are very similar to each other. Complex **22** has been structurally characterized; with respect to the carbonyl-bridged triiridium plane, it has a diaxially-ligated diphosphine and an apically coordinated cyclopentadienyl ligand.[40] The NMR spectra are consistent with the structural study, suggesting the presence of the three configurations displayed in Figure 3.2.32. Configurations **22a** and **22b** are similar, having the Cp ligand inclined to the WIr_2 faces remote from the diphosphine, whereas minor isomer **22c** has the Cp inclined to the WIr_2 face adjacent to the diphosphine. Isomers **22a** and **22b** differ in the conformation of the diphosphine backbone with respect to the location of the cyclopentadienyl ligands. Isomer **22b** is the crystallographically observed form, with the methylene attached to the phosphorus which is ligated to an iridium in the WIr_2 face containing the cyclopentadienyl ligand being "out" rather than "in": see Figure 33.2.32(b).



22a **22b** (XRS) **22c**

Figure 3.2.32. (a) Isomers of $[CpWIr_3(\mu\text{-dppe})(\mu\text{-}CO)_3(CO)_6]$
XRS ≡ structurally characterized configuration



22a **22b** XRS

(b) Projection of isomers **22a** and **22b** onto the Ir_3 plane
Phenyls, terminal carbonyls and ethylene protons omitted for clarity

Utilizing the information regarding the positional sequence established for the mixed-metal regime (Section *3.2.1.*), it is possible to assign the spectrum of **22a-c**. At 193 K, resonances for the most abundant isomer (**22a**) are observed at 221.5 (e), 215.0 (c or d), 212.4 (a or b), 211.0 (b or a), 207.0 (d or c), 181.0 (f or g), 180.5 (g or f), 176.0 (h) and 161.0 (i) ppm, all of relative intensity 1, with the signals at 212.4 and 211.0 ppm showing the expected satellite coupling to ^{183}W. An attempt to establish the assignments of a and b from the possible presence of long-range *trans* coupling from a to i in a complementary ^{13}C-^{13}C correlation spectroscopy (COSY) experiment was unsuccessful (Figure 3.2.35.). Fortunately, however, a more precise assignment of a or b is of no importance for the discussion of the fluxionality of **22**. The COSY experiment (Figure 3.2.33.) did, however reveal interesting coupling between Ir-Ir bridging carbonyls, not present in the clusters with coordination geometries with WIr_2 basal planes. The coupling between the bridging carbonyls e and c, e and d and c and d, as well as E and C, E and D and C and D was observed. The signals at 181.0, 180.5 and 176.0 ppm are assigned to the radial carbonyls f or g, g or f, and h, respectively, due to the similar chemical environments of the first two.

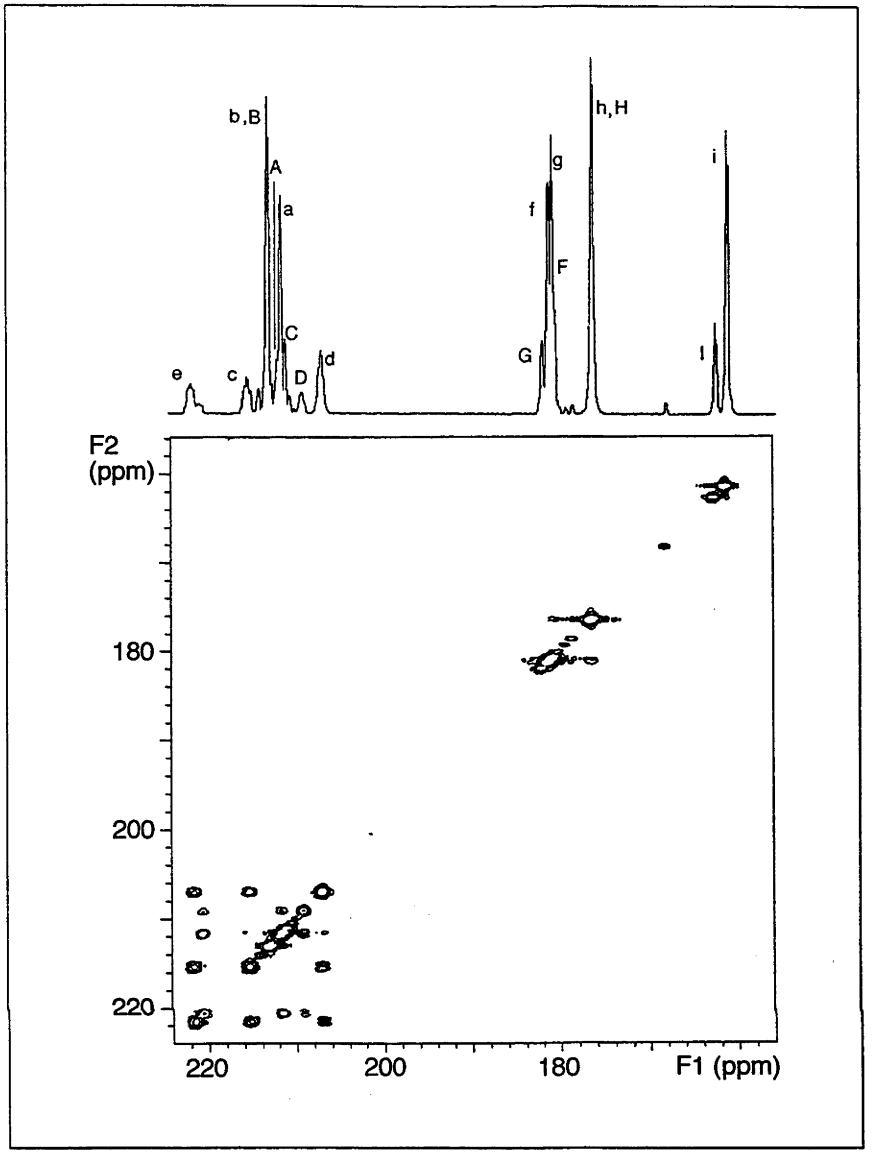


Figure 3.2.33. ^{13}C NMR COSY spectrum of $[CpWIr_3(\mu\text{-dppe})(\mu\text{-CO})_3(CO)_6]$ (**22**) in CD_2Cl_2 at 183 K.

Again, a precise assignment of f and g is not required to understand the fluxional processes of **22**. The signal at 221.5 ppm is assigned to bridging carbonyl e, by analogy to the assignment of the equivalent carbonyl in isomer **23b**: see below. Carbonyls c and d cannot be distinguished based on available information. Resonances for the least abundant isomer (**22c**) are observed at 227.9 (*c*), 210.1 (*a*, *a'*), 204.5 and 203.3 (*b*, *b'*), 179.5 and 178.9 (*d*, *d'*), 178.1 (*e*) and 167.7 (*f*) ppm, with relative intensities 1 : 2 : 1 : 1 : 1 : 1: 1: 1. The dppe backbone methylenes, one of which is "out", the other of which is "in" (Figure 3.2.34b.), result in slightly different magnetic environments for *d* and *d'* and for *b* and *b'*, an effect which is attenuated for the more remote *a* and *a'* resulting in the sole signal of intensity 2. The specific assignments follow those outlined above for the most abundant isomer. Signals for isomer **22b** are observed at 220.5 (E), 211.2 (A), 210.7 (C or D), 209.0 (D or C), 181.8 (F or G), 180.2 (G or F), 176.0 (H), and 162.2 (I) ppm, all of relative intensity 1, assigned analogously to isomer **22a**. In the figures, an arbitrary

assignment has been adopted for carbonyl resonances which cannot be unambiguously assigned, to enhance clarity of presentation; it does not affect arguments regarding ligand fluxionality.

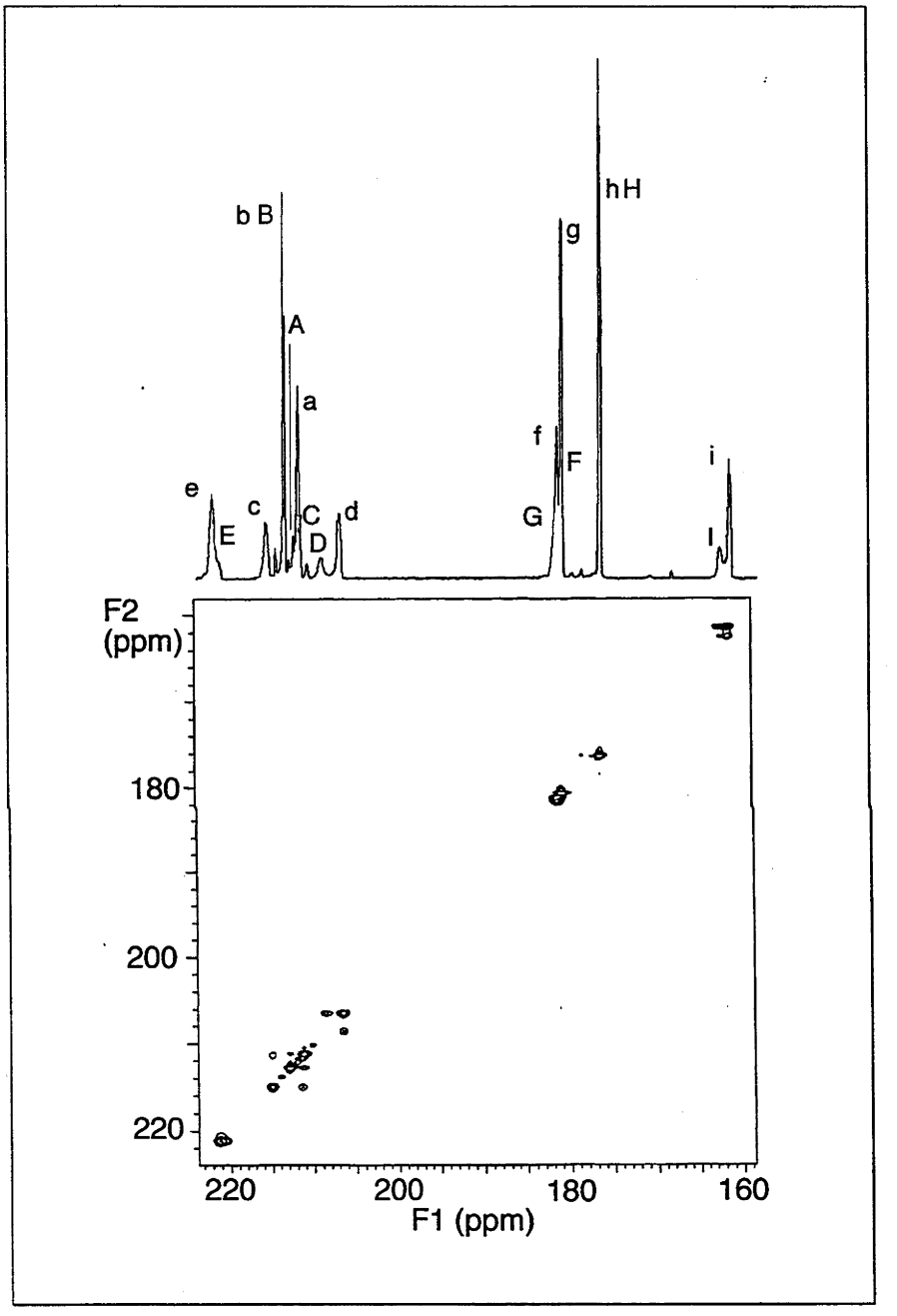


Figure 3.2.34. ^{13}C NMR EXSY spectrum of $[CpWIr_3(\mu\text{-dppe})(\mu\text{-CO})_3(CO)_6]$ (**22**) in CD_2Cl_2 at 208 K.

Ligand fluxionality commences upon warming the mixture of isomers of **22**. The contour plot for cluster **22** shown in Figure 3.2.34. reveals site exchanges at 208 K corresponding to i ↔ I, c or d ↔ C or D, d or c ↔ D or C, a ↔ b or B and/or A ↔ b or B, suggestive of interconversion of **22a** and **22b**. In principle, flexing of the diphosphine backbone, a

"waggling" of the $CpW(CO)_2$ group so as to place the Cp ligand over both WIr_2 faces remote from the diphosphine, or complete tripodal rotation will all interconvert **22a** and **22b**. However, the ^{31}P NMR spectrum at 258 K, which reveals two distinct P environments, is consistent with diphosphine backbone flexing being a very high energy process (coalescence of phosphorus resonances is not observed until >300 K). Confirmatory evidence is provided by studies in the related tetrairidium system, which have shown that, for phosphines with variable oligomethylene backbone, flexing as proposed here does not become important until the backbone is lengthened to that of a butylene linkage.[21] Diphosphine backbone flexing as the source of the low energy process is therefore rejected. The presence of an h, H ↔ *e* crosspeak, indicating a **22a**, **22b** ↔ **22c** interconversion, is inconsistent with "waggling" of the $[CpW(CO)_2]$ group at this temperature; although is is possible that complete tripodal rotation (which involves placing the cyclopentadienyl ligand over the diphosphine-containing WIr_2 face) is slightly higher in energy than "waggling" over the non-diphosphine-containing WIr_2 faces, no evidence for an energetic discrimination could be obtained with **22**. The EXSY data are thus consistent with tripodal rotation as the lowest energy process.

At 233 K a second process is observed, involving basal site exchange only (Figure 3.2.35.). The exchange e ↔ f ↔ c ↔ h ↔ d ↔ g ↔ y is consistent with the carbonyls exchanging via a concerted "merry-go-round" process. [Note: the additional exchanges c or c ↔ d or c and f or g ↔ h suggest that the long mixing time used for the experiment is such as to permit site exchange to succeeding sites].

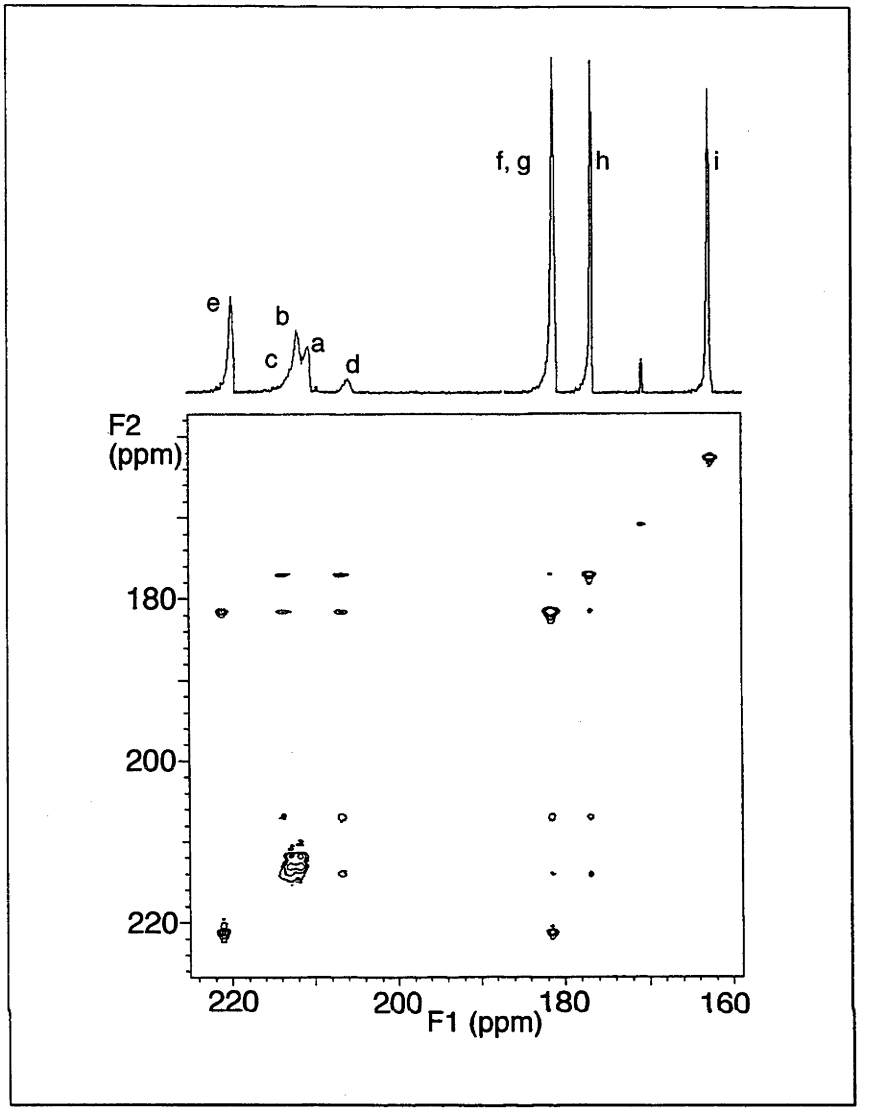


Figure 3.2.35. ^{13}C NMR EXSY spectrum of $[CpWIr_3(\mu\text{-}CO)_3(\mu\text{-}dppe)(CO)_6]$ (**22**) in CD_2Cl_2 at 233 K.

NMR studies of $[CpWIr_3(\mu\text{-}CO)_3(\mu\text{-}dppm)(CO)_6]$

The related cluster $[CpWIr_3(\mu\text{-}CO)_3(\mu\text{-}dppm)(CO)_6]$ (**23**) has also been crystallographically characterized; it is isostructural with **22**, having a diaxially-ligated diphosphine and an apically-coordinated cyclopentadienyl ligand.[40] The ^{31}P NMR spectrum of **23** at 298 K shows a broad singlet, which decoalesces upon cooling (Figure 3.2.36.). The spectrum at 181 K contains three signals, consistent with the presence of two configurations in the ratio 7 : 1. Similarly, the ^{13}C NMR spectrum of **3** at 298 K is also very broad, but cooling to 181 K reveals resonances consistent with the presence of two configurations (Figure 3.2.37.). As with **22**, the signals in the ^{31}P and ^{13}C NMR spectra were assigned using the relationship between chemical shift and ligand position. The relative intensities of the resonances are consistent with the major configuration possessing geometry **23a**, the Cp ligand being inclined over the WIr_2 faces away from the diphosphine, and the minor configuration having geometry **23b**, with the

Cp ligand inclined over the WIr_2 face including the diphosphine ligand (Figure 3.2.38.). At 181 K, resonances for the more abundant configuration **23a** are observed at 218.2 (e), 215.5 (a or b), 212.3 (c), 208.2 (b or a), 206.7 (d), 182.2 (f and g), 176.1 (h) and 164.1 (i) ppm, with relative intensities 1 : 1 : 1 : 1 : 1 : 2 : 1. Signals at 215.5 and 208.2 ppm show the expected satellite coupling to tungsten, and are therefore assigned to a and b. Carbonyl e, at 218.2 ppm, is assigned by analogy with the comparable carbonyl in **23b**. Resonances at 212.3 and 206.7 ppm are assigned to c and d, and labelled arbitrarily (as above). Assignments of f, g, h and i follow from the earlier discussion. Resonances for the least abundant configuration **23b** are observed at 228.4 (C), 210.2 (A and A'), 202.1 (B and B'), 180.4 (D and D'), 179.9 (E) and 170.6 (F) ppm, with relative intensities 1 : 2 : 2 : 2 : 1 : 1; the signals corresponding to A, A' and B, B' were assigned by comparison of their linewidths to previously assigned configurations above (resonances of bridging carbonyls are significantly broader than those of terminal carbonyls), and all other assignments follow logically from the earlier discussion. The assignment of the most downfield resonance as corresponding to C is straightforward (from its relative intensity); it confirms the assignment of the analogous carbonyl in the other configurations above. The assignment of configurations **23a** and **23b** is thus consistent with that of configurations **22a-c**. Significantly, the dppm ligand in **23** can only be configured symmetrically across the Ir-Ir bond, resulting in inequivalent *P* atoms in configuration **23a** and equivalent *P* atoms in **23b**.

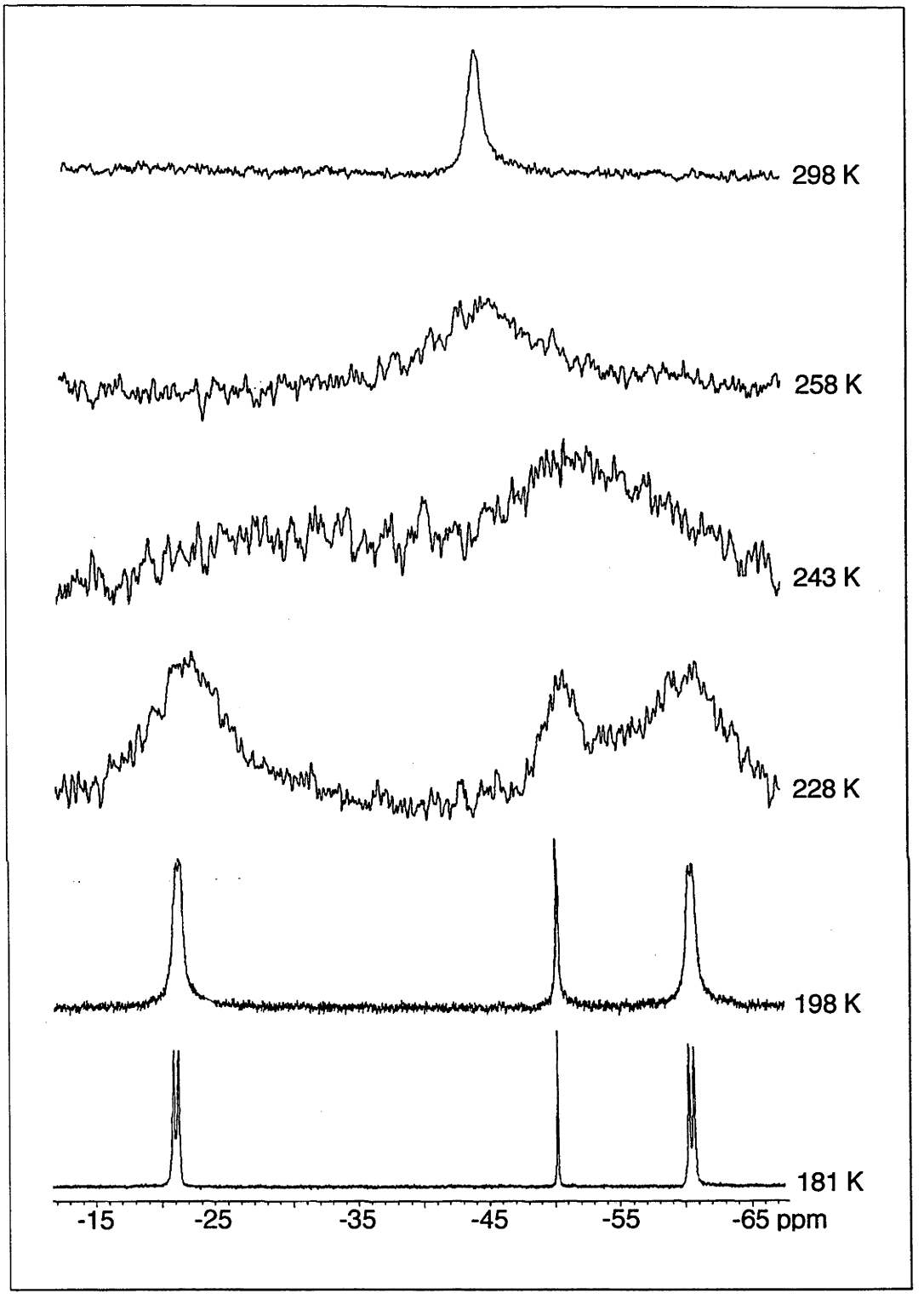


Figure 3.2.36. Variable temperature ^{31}P NMR spectroscopic study of $[CpWIr_3(\mu\text{-dppm})(\mu\text{-CO})_3(CO)_6]$ (**23**) in CD_2Cl_2.

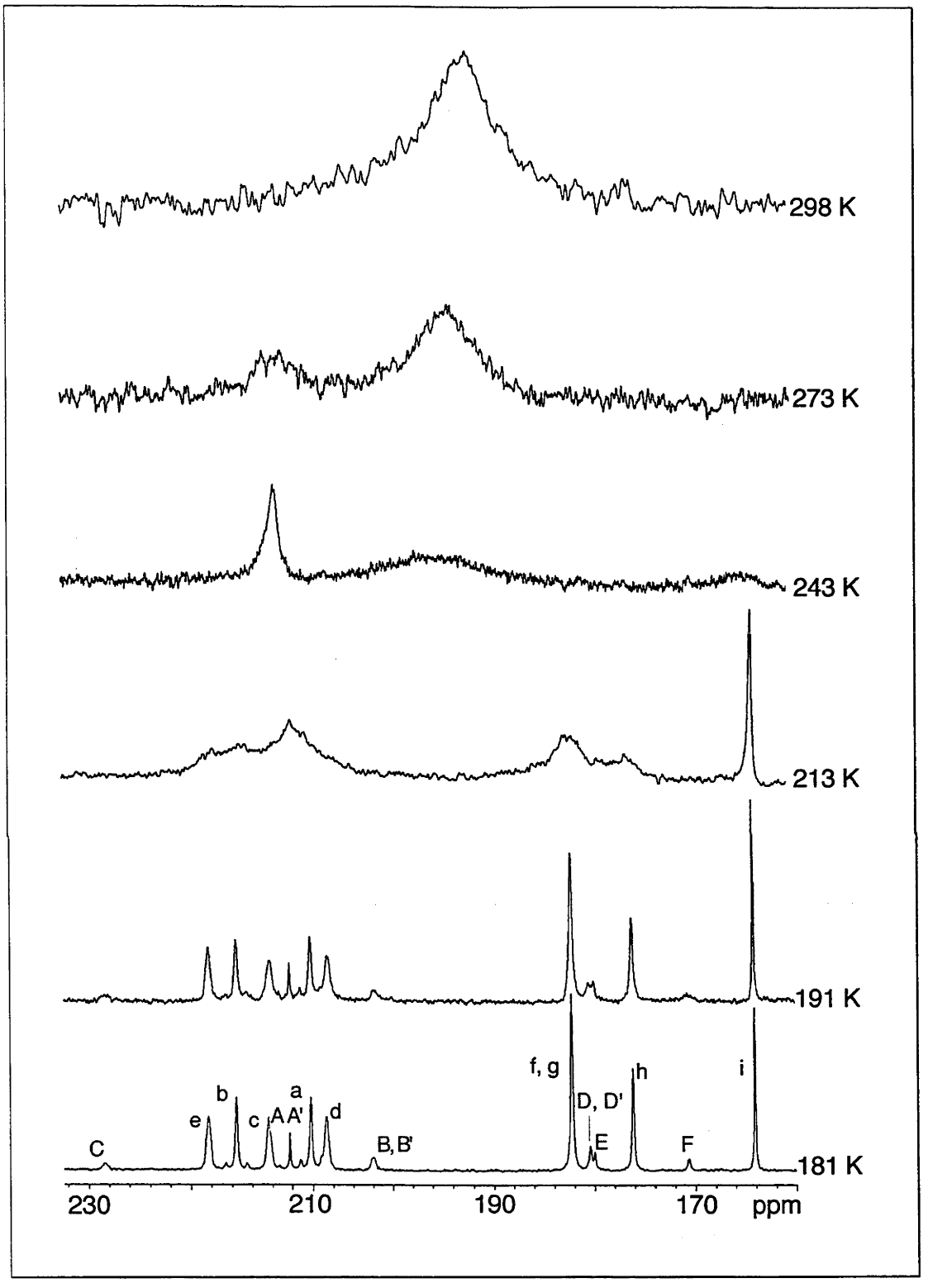
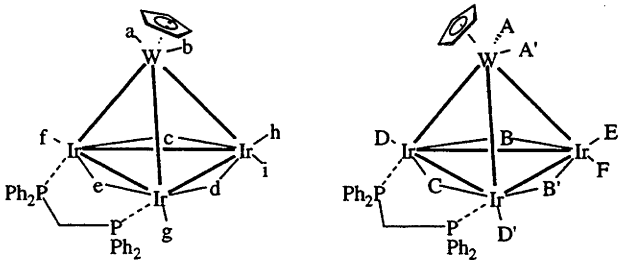


Figure 3.2.37. Variable temperature ^{13}C NMR spectroscopic study of $[CpWIr_3(\mu\text{-dppm})(\mu\text{-}CO)_3(CO)_6]$ (**23**) in CD_2Cl_2.



23a (XRS) **23b**

Figure 3.2.38. Isomers of $[CpWIr_3(\mu\text{-}CO)_3(\mu\text{-}dppm)(CO)_6]$ (**23**) XRS ≡ structurally characterized configuration

An EXSY spectrum at 183 K (Figure 3.2.39.) reveals the exchange pathway e ↔ f ↔ c ↔ h ↔ d ↔ g ↔ e in **23a**, and the analogous exchange (though less well resolved due to the decreased concentration) in **23b**, consistent with a merry - go - round of the six basal CO's. The exchanges a ↔ b and c ↔ d, and the lack of **23a** ↔ **23b** cross-peaks, are consistent with "waggling" of the $CpW(CO)_2$ group so as to place the Cp ligand over both WIr_2 faces remote from the diphosphine, but inconsistent with the onset of full tripodal rotation. Raising the temperature to 193 K results in the onset of full tripodal rotation, rendering configurations **23a** and **23b** equivalent (Figure 3.2.40.).

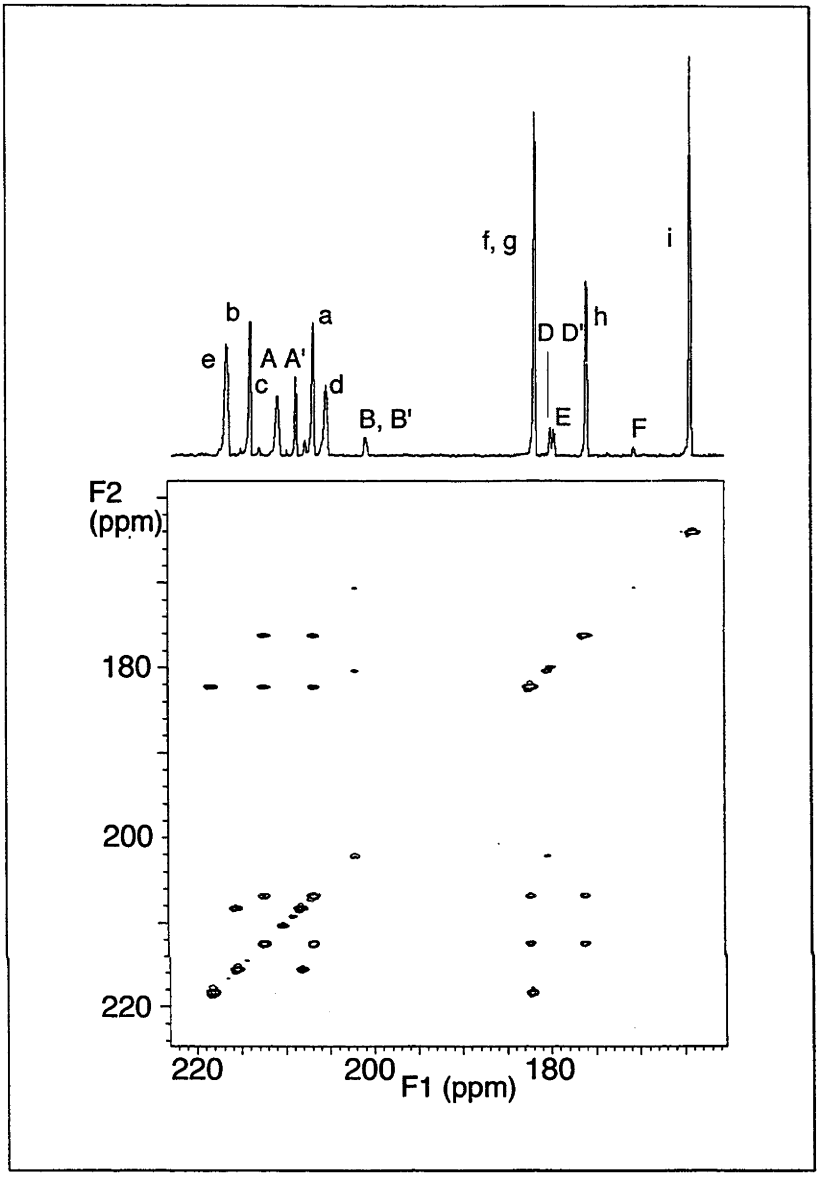


Figure 3.2.39. ^{13}C NMR EXSY spectrum of $[CpWIr_3(\mu\text{-}CO)_3(\mu\text{-}dppm)(CO)_6]$ (**23**) in CD_2Cl_2 at 183 K.

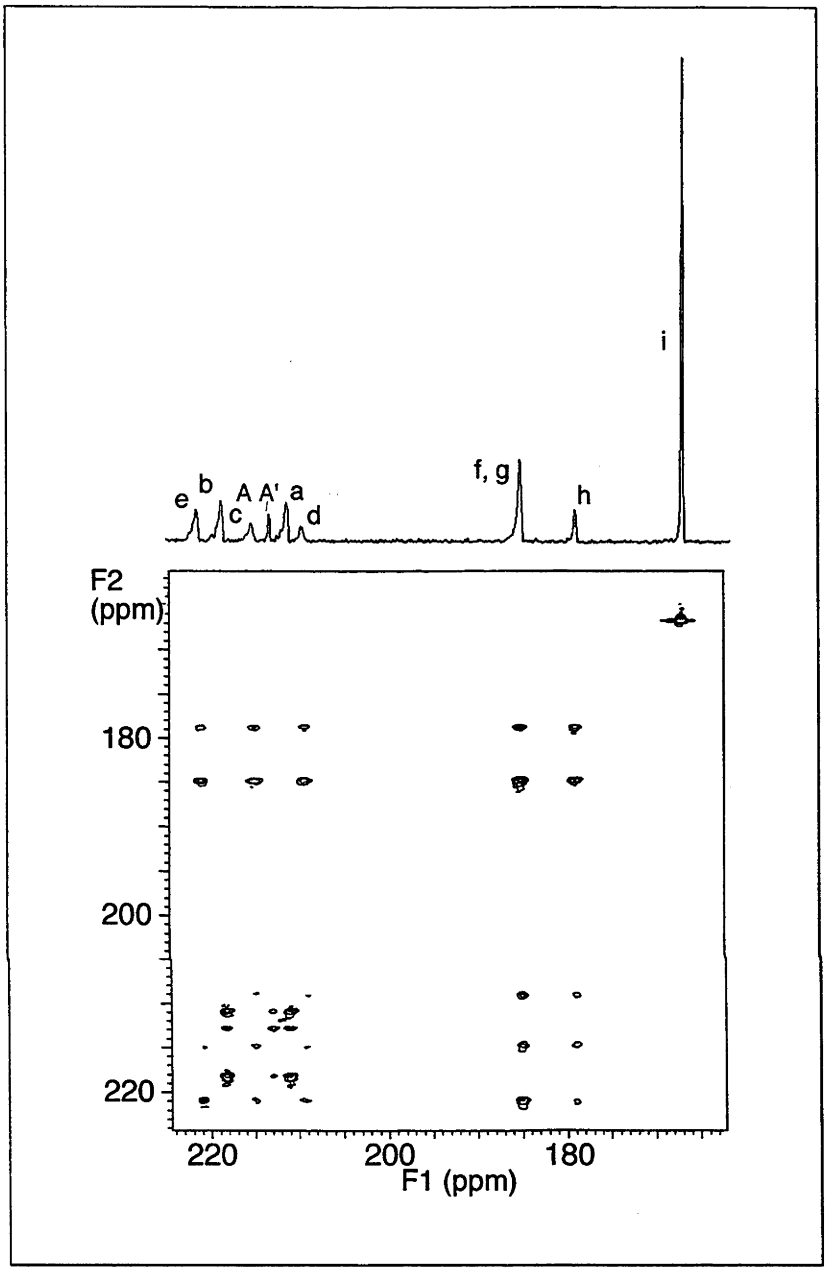
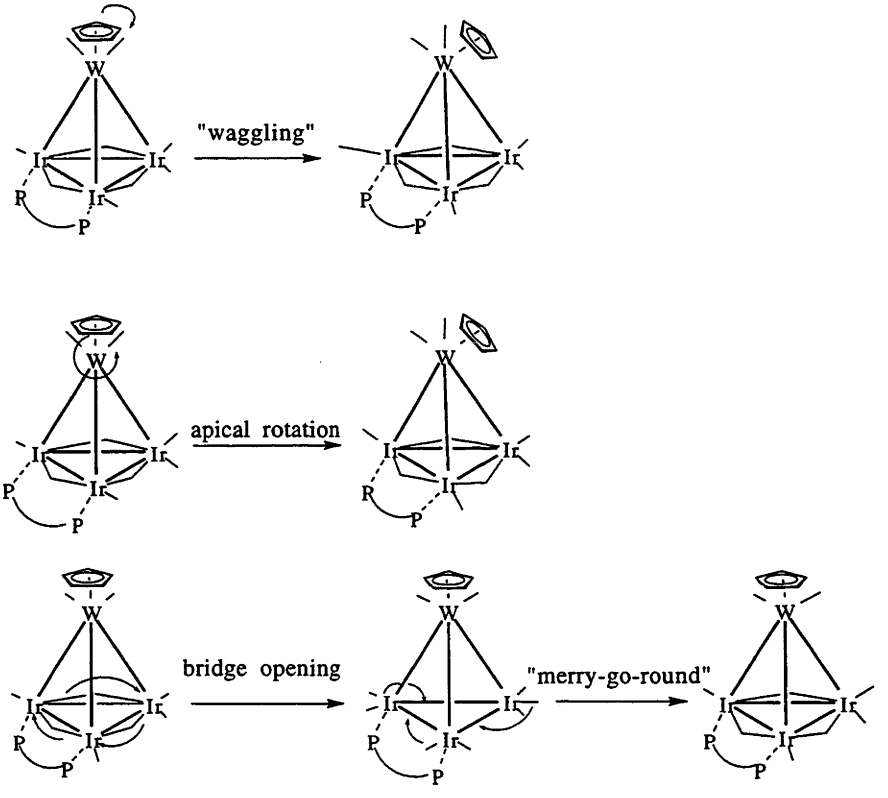


Figure 3.2.40. ^{13}C NMR EXSY spectrum of $[CpWIr_3(\mu\text{-}CO)_3(\mu\text{-}dppm)(CO)_6]$ (**23**) in CD_2Cl_2 at 193 K.

Discussion

A qualitative comparison of **22** and **23** reveals that signal broadening in the ^{13}C spectra occurs at a lower temperature in the dppm-containing cluster **23** than in its dppe-containing analogue **22**, consistent with results in the tetrairidium system. However, the lack of h $\leftrightarrow$ i crosspeaks in the ^{13}C-EXSY spectra of **22** and **23** suggests that exchange pathway 2 in the tetrairidium system (Scheme 3.1.6.) is not followed with these mixed-metal clusters (in the temperature range investigated); unlike the tetrairidium examples, it must be much higher in energy than process 3 (Scheme 3.1.6.), a direct consequence of (conceptual) apical replacement of

$[Ir(CO)_3]$ by $[CpW(CO)_2]$. Exchange pathway 3 is a lower energy process than or comparable energy process to pathway 1 in the mixed-metal system, and can be resolved into two processes in the case of **23**, the easier of which involves a "waggling" of the $[CpW(CO)_2]$ vertex, an the more difficult of which involves placing the Cp ligand over the diphosphine-ligated WIr_2 face (Scheme 3.2.4.) to effect complete tripodal rotation; again, the contrasting behaviour to that observed in the homometallic system is a consequence of apical metal replacement.



Complex	Exchange Process	(relative energy)
22	Tripodal rotation	(lower)
	"Merry-go-round"	(higher)
23	"Merry-go-round", "Waggling"	(lower)
	Tripodal rotation	(higher)

Scheme 3.2.4. CO exchange processes of **22** and **23**

NMR studies of $[CpWIr_3(\mu\text{-}CO)_3(\mu\text{-}pdpp)(CO)_6]$

The variable temperature ^{31}P NMR spectra of $[CpWIr_3(\mu\text{-}CO)_3(\mu\text{-}pdpp)(CO)_6]$ (**24**) were also investigated, as the rigid backbone of the bis(1,2-diphenylphosphino)benzene ligand may influence the coordination geometry. The ^{31}P NMR spectrum of **24** at room temperature reveals the presence of a broad signal at 15.0 ppm. Signals at 22.2 and 6.1 ppm, ratio 1 : 1, are

resolved on cooling to 181 K (Figure 3.2.41.). By analogy to the ^{31}P NMR spectra of **22** and **23**, **24** is assigned a geometry as shown in Figure 3.2.42., with the Cp ligand inclined over the WIr_2 faces away from the diphosphine. The configuration with the Cp inclined over the WIr_2 face including the diphosphine, a key feature of the NMR spectra of **22** and **23**, does not appear to be present in the NMR spectrum of **24**, a result signifying the importance of the phosphine ligand in controlling conformational preference.

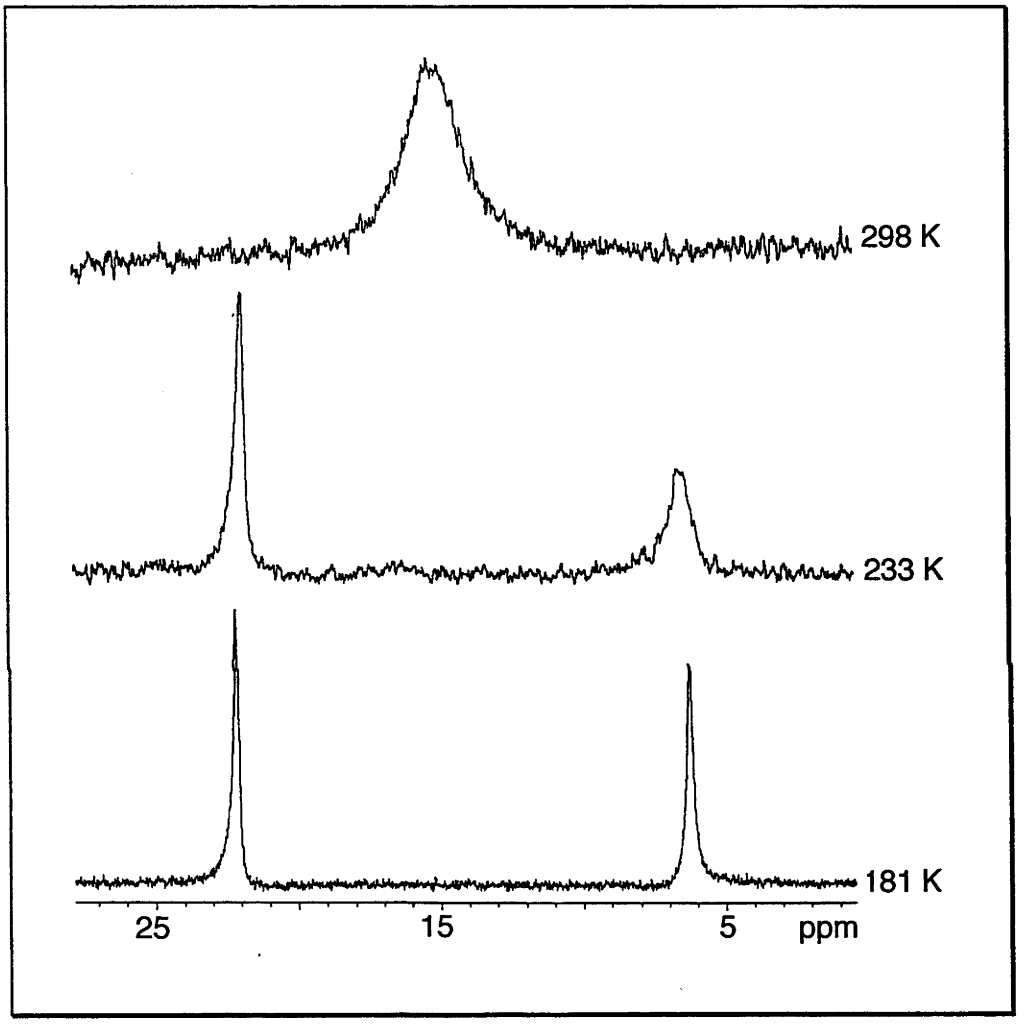
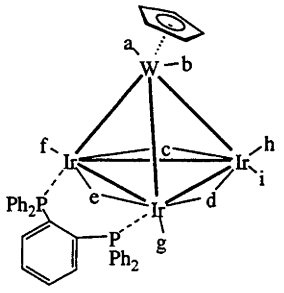


Figure 3.2.41. Variable temperature ^{31}P NMR spectroscopic study of $[CpWIr_3(\mu\text{-}CO)_3(\mu\text{-}pdpp)(CO)_6]$ (**24**) in CD_2Cl_2.



24

Figure 3.2.42. Configuration of $[CpWIr_3(\mu\text{-}CO)_3(\mu\text{-}pdpp)(CO)_6]$ (**24**)

3.2.6. NMR studies of isocyanide derivatives of $[CpWIr_3(CO)_{11}]$

As mentioned in Chapter 2, the IR spectra of the complexes $[CpWIr_3(CNXy)_2(CO)_9]$ (**26**), $[CpWIr_3(CNXy)_3(CO)_8]$ (**27**), $[CpWIr_3(CNBu^t)_2(CO)_9]$ (**29**), and $[CpWIr_3(CNBu^t)_3(CO)_8]$ (**30**) are indicative of the presence of different configurations, with the mono-(isocyanide) substituted derivatives displaying carbonyl frequencies arising from terminal carbonyls only. For all the clusters **25** - **30**, only infrared absorptions appropriate for terminal isocyanide ligands are observed [ν(CN) 2179 - 2155 cm^{-1}] (this is not unexpected; previous studies have revealed that the electron withdrawing R = CF_3 group is required to encourage the CNR ligand to adopt an edge-bridging coordination mode [41]). These results, in combination with the structural characterization of **26**, suggest that the clusters $[CpWIr_3(CNXy)(CO)_{10}]$ (**25**) and $[CpWIr_3(CNBu^t)(CO)_{10}]$ (**28**) adopt structures with all-terminal ligand coordination geometries, analogous to the structurally characterized precursor cluster **2**,[42] and the "parent" cluster $[Ir_4(CO)_{12}]$[43] and its mono-(isocyanide) substituted derivative $[Ir_4(CNBu^t)(CO)_{11}]$.[44] The complexity of the IR spectra of **26**, **27**, **29** and **30** indicates the presence of configurations, weak absorptions in the bridging carbonyl region suggesting that the clusters exist as mixtures of configurations with all-terminal ligand geometries and configurations incorporating a plane of bridging carbonyls. The IR spectra of **25** - **30** and unusual solid-state structure of **26** prompted the investigation of the configuration distribution and fluxionality of **28** - **30**. The ^{13}C NMR spectra of **28** - **30** each display a single carbonyl resonance at room temperature. Cooling the samples to 143 K reveals broadened resonances only, and solubility problems precluded a study at lower temperatures. The variable-temperature NMR results suggest that the carbonyls are undergoing much faster exchange than that observed in their phosphine-ligated counterparts (for which low temperature limiting spectra were obtained in the range 163 - 193 K).

3.2.7. NMR studies of PPh_3 and PMe_3 derivatives of $[Cp_2W_2Ir_2(CO)_{10}]$

The syntheses and characterization of the ligand-substituted derivatives $[Cp_2W_2Ir_2(\mu\text{-}CO)_3(CO)_{7-n}(L)_n]$ [L = PPh_3, n = 1 (**31**), 2 (**32**); L = PMe_3, n = 1 (**33**), 2 (**34**)] were reported in Chapter 2. The clusters exist as mixtures of interconverting isomers in solution, as shown by the IR and NMR spectra. This Section contains assignment of the configurations of these interconverting isomers, comment on ligand scrambling (where possible), and a comparison to the homometallic tetrairidium analogues.

NMR studies of $[Cp_2W_2Ir_2(\mu\text{-}CO)_3(CO)_6(PMe_3)]$ (33)

The room temperature ^{31}P NMR spectrum of **33** in CD_2Cl_2 consists of a broad singlet at -26.8 ppm (Figure 3.2.43.). On cooling to 183 K, one sharp signal at -26.2 ppm and a very broad singlet at -20.3 ppm are resolved, in the approximate ratio 4 : 1. Similarly, the ^{13}C NMR spectrum of **33** at 298 K (Figure 3.2.44.) shows a single broad resonance at 205.3 ppm, but at 183 K the fluxional processes are sufficiently slow to distinguish the nine carbonyl resonances of **33**, with one signal at 220.0 ppm belonging to (an) isomer(s) undergoing very fast exchange, and presumably correlated with the broad phosphorus resonance at -20.3 ppm. The proposed configuration of **33**, with axial phosphine, radial Cp and apical Cp, has been assigned utilizing information from the ^{13}C NMR spectrum, a HSQC experiment (Figure 3.2.45.) and a triple resonance ^{1}H-^{31}P-^{13}C experiment (Figure 3.2.46.). ^{1}H-^{31}P-^{13}C triple resonance experiments were acquired using the pulse sequence shown in Figure 3.4.1. The experiment consists of an initial INEPT transfer from ^{1}H to ^{31}P followed by creation of a two spin ^{31}P-^{13}C coherence with ^{13}C frequency labelling and a final reverse INEPT transfer from ^{31}P to ^{1}H. In terms of coherence transfer, this experiment is, in essence, the same as a reduced dimensionality version of early implementations of the 3D HNCO experiment[45] used in the determination of protein structures. As a result the term 2D HPCO experiment is required to determine through which phosphorus the carbon information was relayed in these experiments. The information obtained from the HPCO experiment is basically the same as can be extracted from 2D ^{31}P-^{13}C-{^{1}H} experiments which have been employed in the literature.[46] However, greater sensitivity is obtained using the double INEPT transfer to and from ^{31}P from ^{1}H. The PMe_3 ligand, with nine protons per phosphorus, is particularly well suited to these experiments since the ^{1}H resonance is a simple doublet due to phosphorus coupling. With PPh_3, the presence of homonuclear couplings, $^{3}J_{HH}$, of similar magnitude to $^{3}J_{HP}$ complicates the coherence transfer and a simpler 2D ^{31}P-^{13}C-{^{1}H} HMQC approach is more easily implemented.[47]

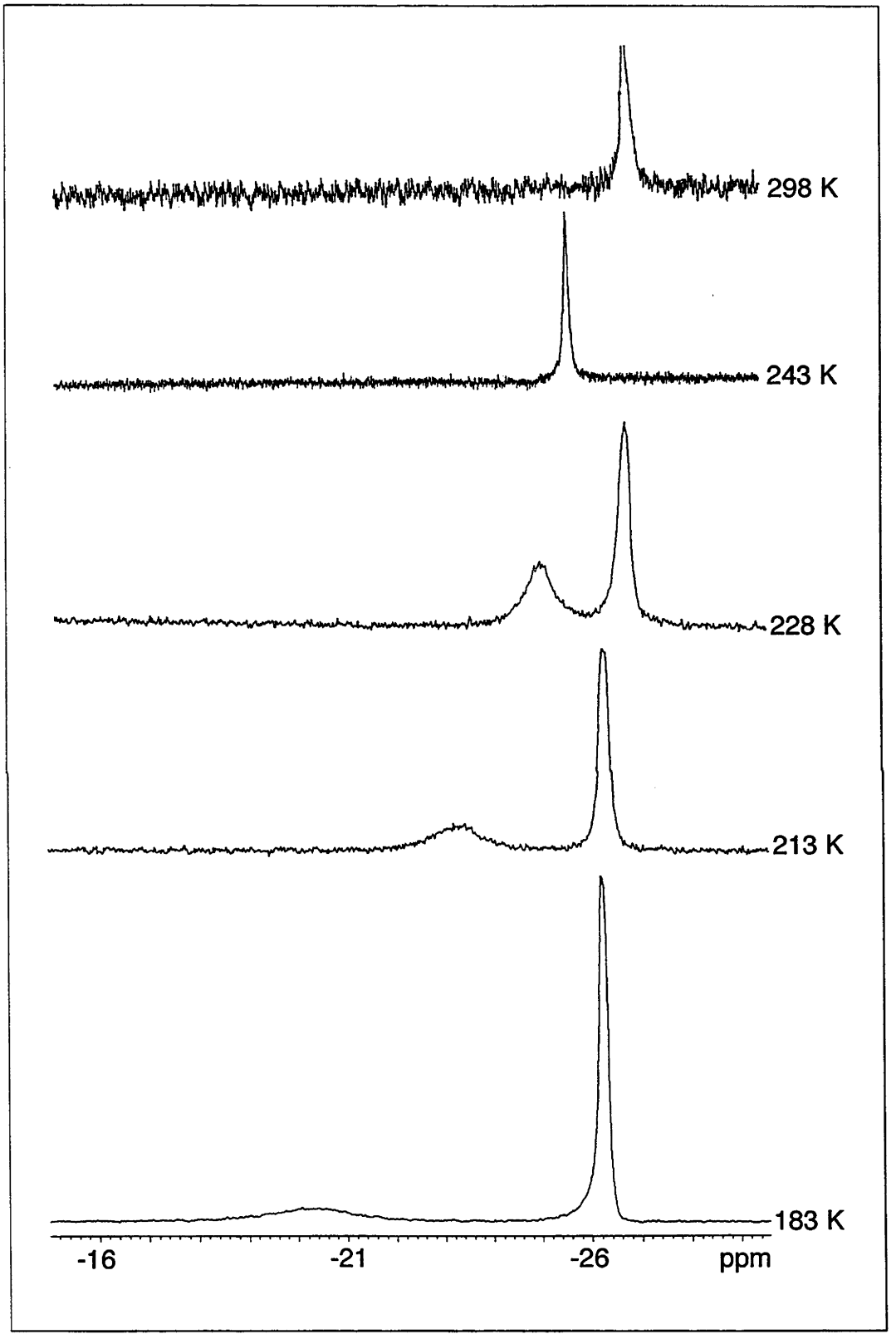


Figure 3.2.43. Variable temperature ^{31}P NMR spectroscopic study of $[Cp_2W_2Ir_2(\mu\text{-}CO)_3(CO)_6(PMe_3)]$ (**33**) in CD_2Cl_2

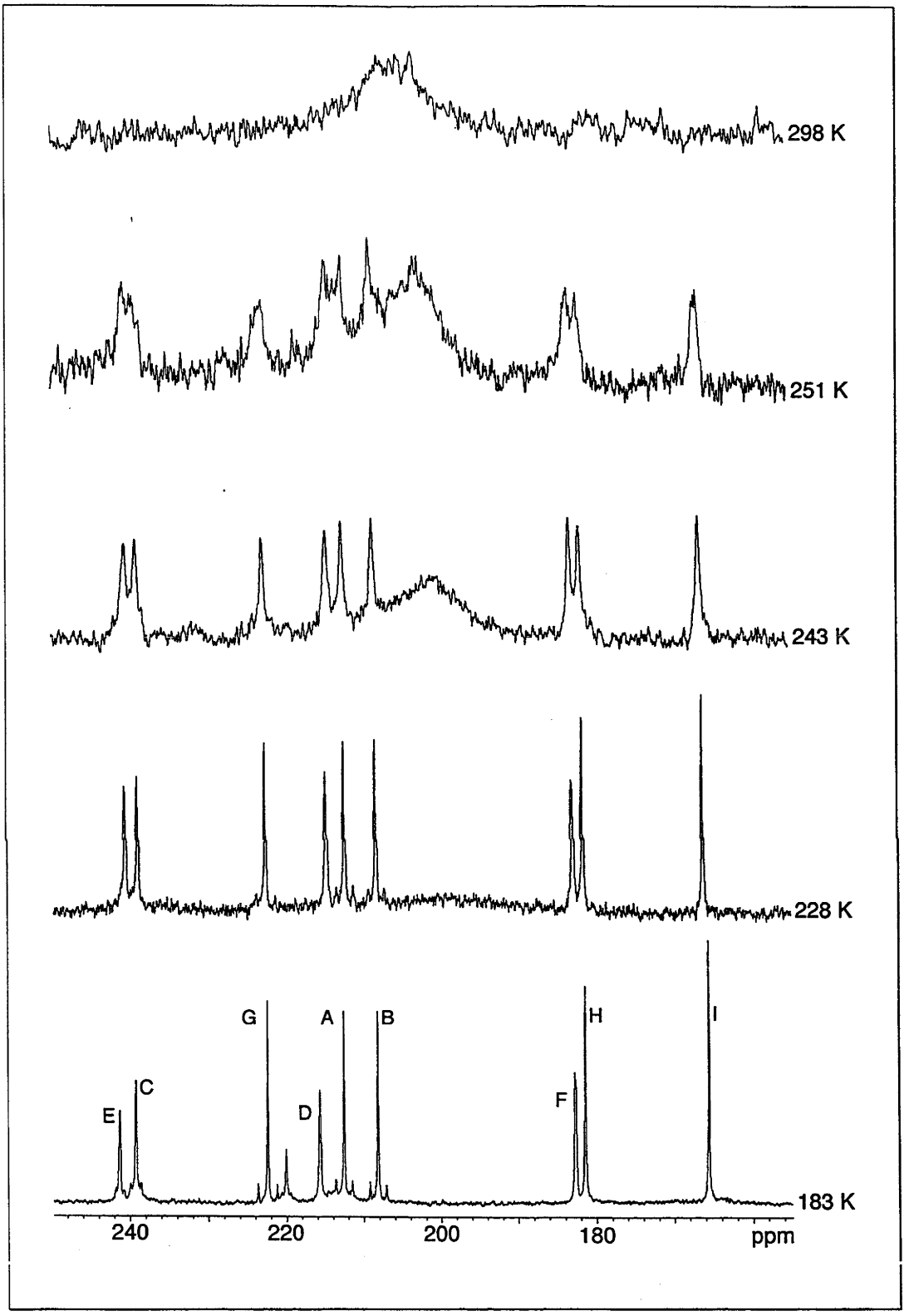


Figure 3.2.44. Variable temperature ^{13}C NMR spectroscopic study of $[Cp_2W_2Ir_2(\mu\text{-}CO)_3(CO)_6(PMe_3)]$ (**33**) in CD_2Cl_2

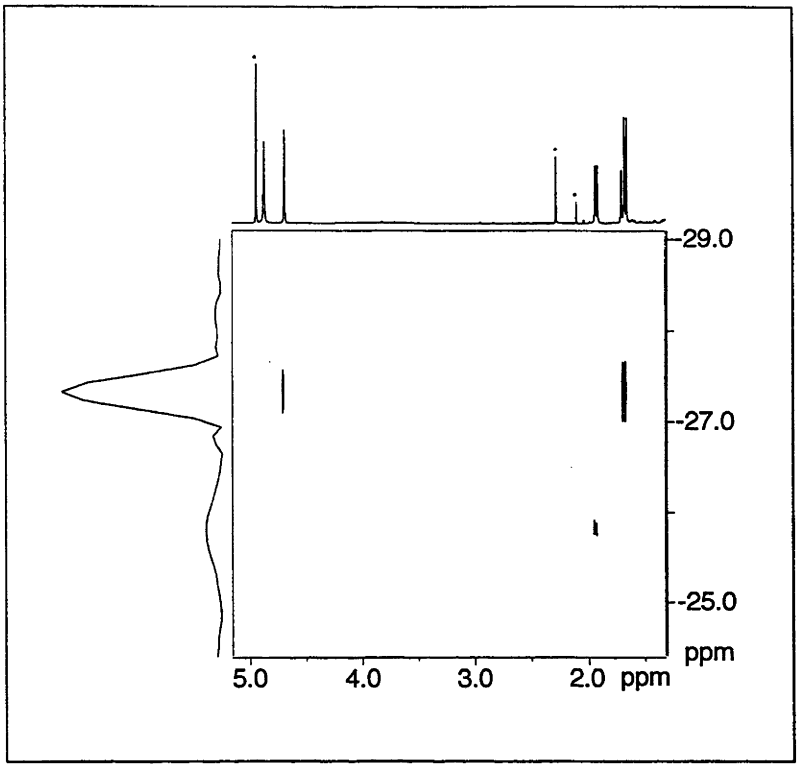


Figure 3.2.45. HSQC NMR spectrum of $[Cp_2W_2Ir_2(\mu\text{-}CO)_3(CO)_6(PMe_3)]$ (**33**) in CD_2Cl_2.

In the low temperature limiting ^{13}C NMR spectrum, the presence of at least one carbonyl resonance in the bridging carbonyl region and only one carbonyl resonance at high field in the apical/axial region excludes both an all terminal ligand configuration and the possibility of a W_2Ir basal plane. This isomer must therefore have a WIr_2 basal plane. There are two Ir-ligated axial sites, but only one is occupied by carbonyl, so the other must be occupied by phosphine. There are six possible configurations which are consistent with this information, corresponding to differing sites for the Cp ligands: the apical Cp ligand can be sited over any of the three non-basal faces, and the basal Cp can be axial or radial. The ^1H-^{31}P HSQC experiment of **31** at 213 K in CD_2Cl_2 (Figure 3.2.45.) reveals a cross peak between the apical Cp signal at 4.69 ppm in the ^1H NMR and the axial PMe_3 signal at -27.3 ppm in the ^{31}P NMR spectra, corresponding to a *trans* coupling from the protons on the apical Cp to the phosphorus of the PMe_3 ligand. The apical Cp is therefore inclined over the $[W_2\{Ir(CO)_2\}]$ face. The remaining ambiguity is the basal Cp, which can be radially or axially disposed. A ^1H NOESY experiment of **33** in CD_2Cl_2 at 183 K reveals the presence of through space interactions between the protons on the basal cyclopentadienyl ligand of **33** at 4.94 ppm and the protons on the axially-ligating PMe_3 at 1.65 ppm, combined with an absence of through space interactions between the apical Cp signal at 4.68 ppm and the axial PMe_3 signal at 1.65 ppm; these data strongly suggest that the basal Cp is axially ligating. Furthermore, thermodynamic considerations suggest that the basal Cp

should be axially ligated to minimize interligand repulsion with the apical Cp (Figure 3.2.47., configuration **33b**). It is significant that this configuration has previously been seen in the structurally characterized $[Cp_2Mo_2Ir_2(\mu\text{-}CO)_3(CO)_6(PMe_3)]$.[48] As mentioned above, the NMR chemical shift positional sequence established with tetrairidium clusters (bridging > radial > axial ≈ apical[26]) has been extended in the current studies to the mixed-metal regime, affording the chemical shift sequence W-W bridging CO > W-Ir bridging CO > Ir-Ir bridging CO ≈ W terminal CO > Ir radial CO > Ir axial CO ≈ Ir apical CO; it is possible to distinguish Ir-Ir bridging CO's from W terminal CO's due to the 15% abundant ^{183}W-coupled satellites of the latter.

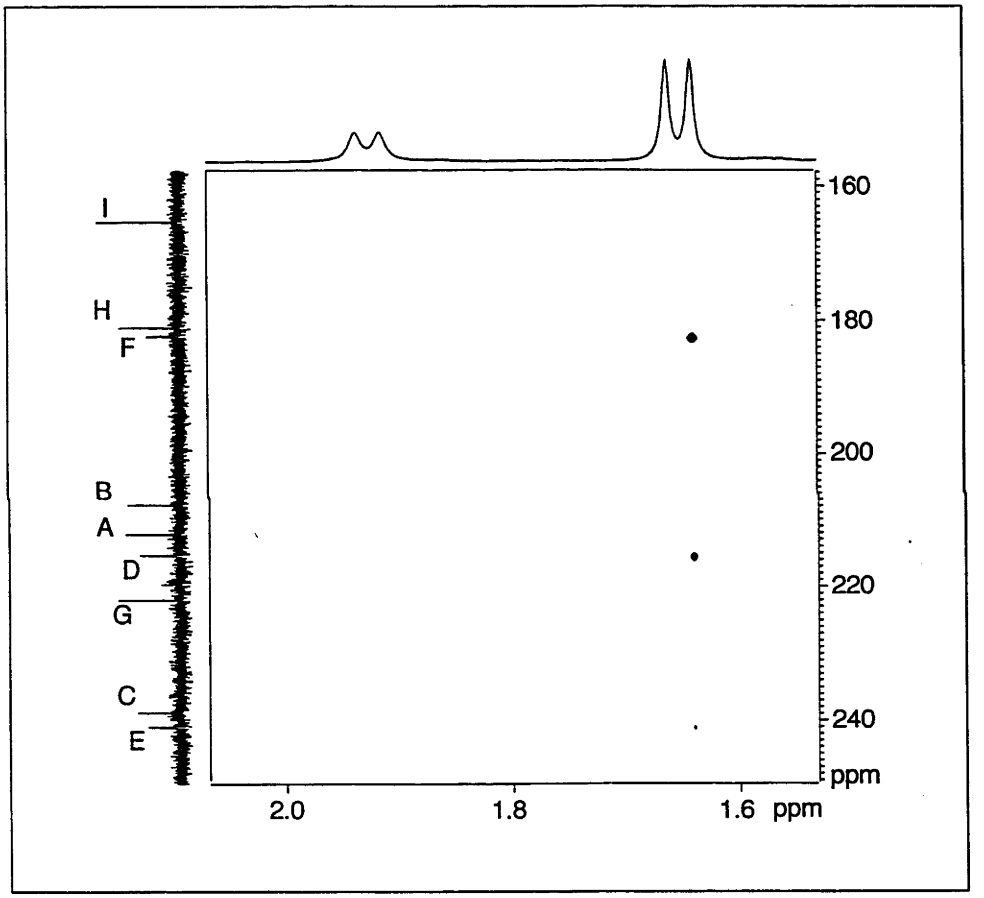
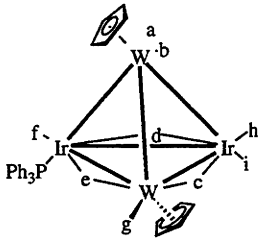


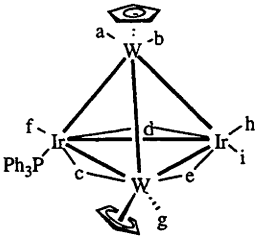
Figure 3.2.46. Triple resonance ^{1}H-^{31}P-^{13}C NMR spectroscopic study of $[Cp_2W_2Ir_2(\mu\text{-}CO)_3(CO)_6(PMe_3)]$ (**33**) in CD_2Cl_2 at 203 K.

With this information, it is possible to assign the spectrum of **33**, which consists of nine signals of equivalent intensity at 183 K. ^{183}W-coupled satellites are observed for the resonances at 241.3 (E, 71 Hz), 239.2 (C, 97 Hz), 222.4 (G, 183 Hz), 212.5 (A or B, 164 Hz) and 208.1 ppm (B or A, 158 Hz), the assignments following logically from (i) coupling between the axial phosphine and E rather than C observed in the triple resonance experiment (Figure 3.2.46.) and (ii) the observation that coupling constants for terminal carbonyls are significantly larger than those for bridging carbonyls. Regarding (i), a similar (μ-CO)-axial CO coupling was noted in a

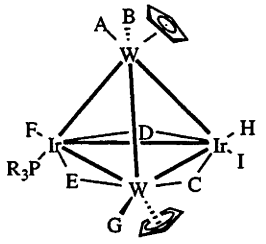
^{13}C-^{13}C correlation study of $[CpWIr_3(\mu\text{-}CO)_3(CO)_6(PPh_3)_2]$ (Figure 3.2.11.). Assignment of the remaining signals at 215.6 (D), 182.7 (F, J_{CP} = 10 Hz), 181.4 (H) and 165.6 ppm (I) is straightforward because of the *cis* coupling observed at carbonyl F.



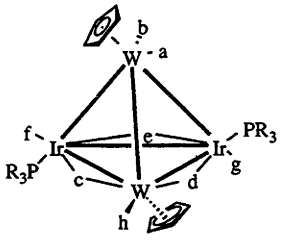
$[Cp_2W_2Ir_2(\mu\text{-}CO)_3(CO)_6(PPh_3)]$ **31a** XRS
axial PPh_3, axial Cp, apical Cp



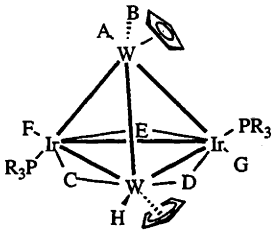
Alternative configuration consistent with spectral data of **31a** (**31c**)
axial PPh_3, radial Cp, apical Cp



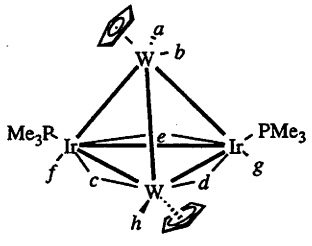
$[Cp_2W_2Ir_2(\mu\text{-}CO)_3(CO)_6(PPh_3)]$ **31b**
$[Cp_2W_2Ir_2(\mu\text{-}CO)_3(CO)_6(PMe_3)]$ **33b**
axial PR_3, axial Cp, apical Cp



$[Cp_2W_2Ir_2(\mu\text{-}CO)_3(CO)_5(PMe_3)_2]$ **34a**
axial PMe_3, radial PMe_3, axial Cp, apical Cp



$[Cp_2W_2Ir_2(\mu\text{-}CO)_3(CO)_5(PMe_3)_2]$ **34b**
axial PMe_3, radial PMe_3, axial Cp, apical Cp



$[Cp_2W_2Ir_2(\mu\text{-}CO)_3(CO)_5(PMe_3)_2]$ **34c**
diradial PMe_3, axial Cp, apical Cp

Figure 3.2.47. Isomers of $[Cp_2W_2Ir_2(\mu\text{-}CO)_3(CO)_{7-n}(L)_n]$
[L = PPh_3, PMe_3; n = 1 – 2; XRS ≡ X-ray study exists]

Ligand fluxionality commences upon warming the solution. A $^{13}C\{^1H\}$-EXSY study at 208 K is shown in Figure 3.2.48. and reveals site exchanges corresponding to H ↔ B or A, H ↔ D and B or A ↔ D. The carbonyl exchanges are consistent with assignment of the signal at 208.1 ppm to carbonyl B and ligand mobility about the WIr_2 face, with the carbonyl distribution in the intermediate reminiscent of the D_{2d} species implicated in an $M_4(CO)_{12}$ exchange pathway[7] (Scheme 3.2.5.). Carbonyl F is attached to the electron-rich phosphine-ligated iridium, and would be expected to have a higher activation energy for participation in an exchange of this type.

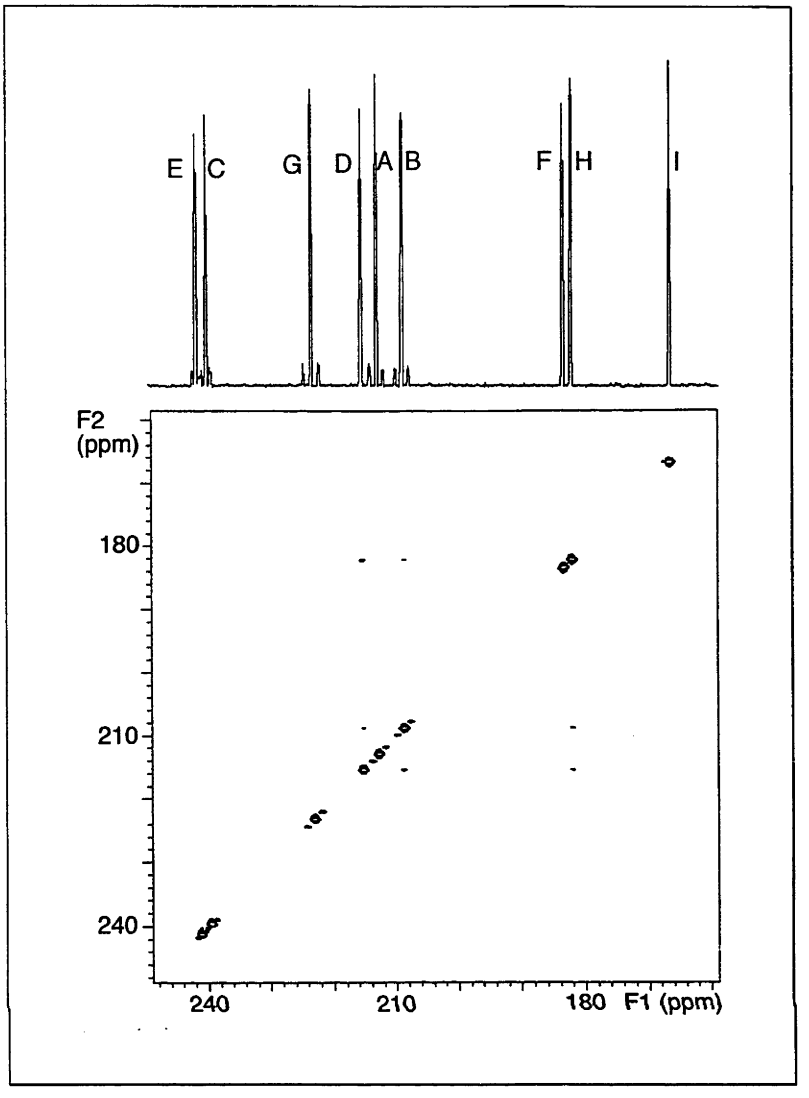
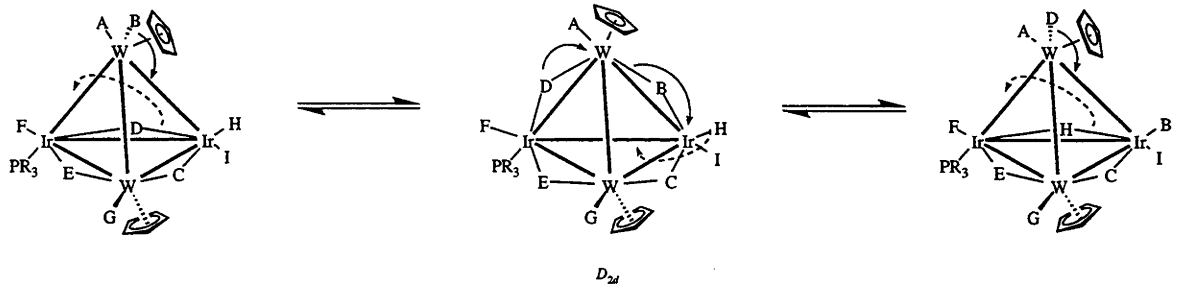


Figure 3.2.48. ^{13}C NMR EXSY spectrum of $[Cp_2W_2Ir_2(\mu\text{-}CO)_3(CO)_6(PMe_3)]$ (**33**) in CD_2Cl_2 at 208 K.



Scheme 3.2.5. CO mobility about a WIr_2 face in **33b** and **35**.

NMR spectra of $[Cp_2W_2Ir_2(\mu\text{-}CO)_3(CO)_6(PPh_3)]$ (31)

The ^{31}P NMR spectrum of **31** at 303 K is near coalescence. On cooling to 183 K two signals are resolved in the ratio of 3 : 2 (Figure 3.2.49.). Similarly, the ^{13}C NMR spectrum of **31** at 298 K reveals the presence of two average carbonyl signals, whereas cooling to 153 K resolves signals corresponding to the presence of two isomers in the ratio of 3 : 2 (Figure 3.2.50.). A broad signal at 221.5 ppm, observed in some preparations, suggests the presence of a minor unidentifiable species. The structures of the two resolvable isomers of **31** can be assigned from the ^{13}C NMR data. The minor isomer **31b** has a similar set of resonances in the ^{13}C NMR spectrum to that observed with **33**, and all resonances are assigned analogously. As with **33**, the presence of only one high field resonance confirms a configuration with a WIr_2 basal plane, and an axially ligated phosphine (9.2 ppm). The spectrum at 183 K reveals ^{183}W-coupled satellites for the resonances at 237.7 (E or C, 80 Hz), 237.5 (C or E, 80 Hz), 222.7 (G, 178 Hz), 211.3 (A, 165 Hz) and 206.1 ppm (B, 163 Hz), together with signals at 214.1 (D), 182.4 (F, J_{CP} = 13 Hz), 181.2 (H) and 167.3 (I), with the only ambiguity the assignment of E and C (it is assumed that carbonyl A resonates 4-5 ppm downfield of carbonyl B, as observed in **33**).

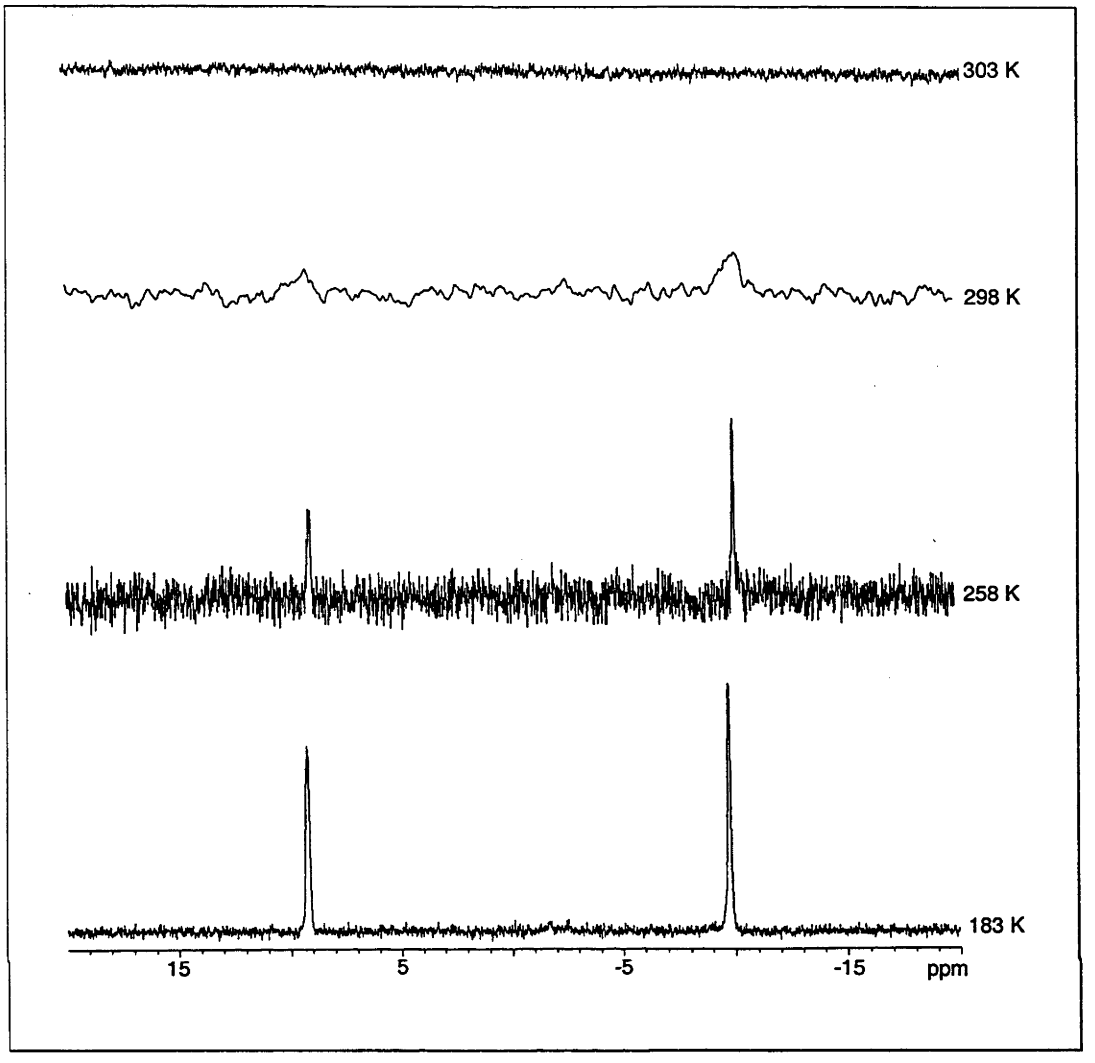


Figure 3.2.49. Variable temperature ^{31}P NMR spectroscopic study of $[Cp_2W_2Ir_2(\mu\text{-}CO)_3(CO)_6(PPh_3)]$ (**31**) in CD_2Cl_2.

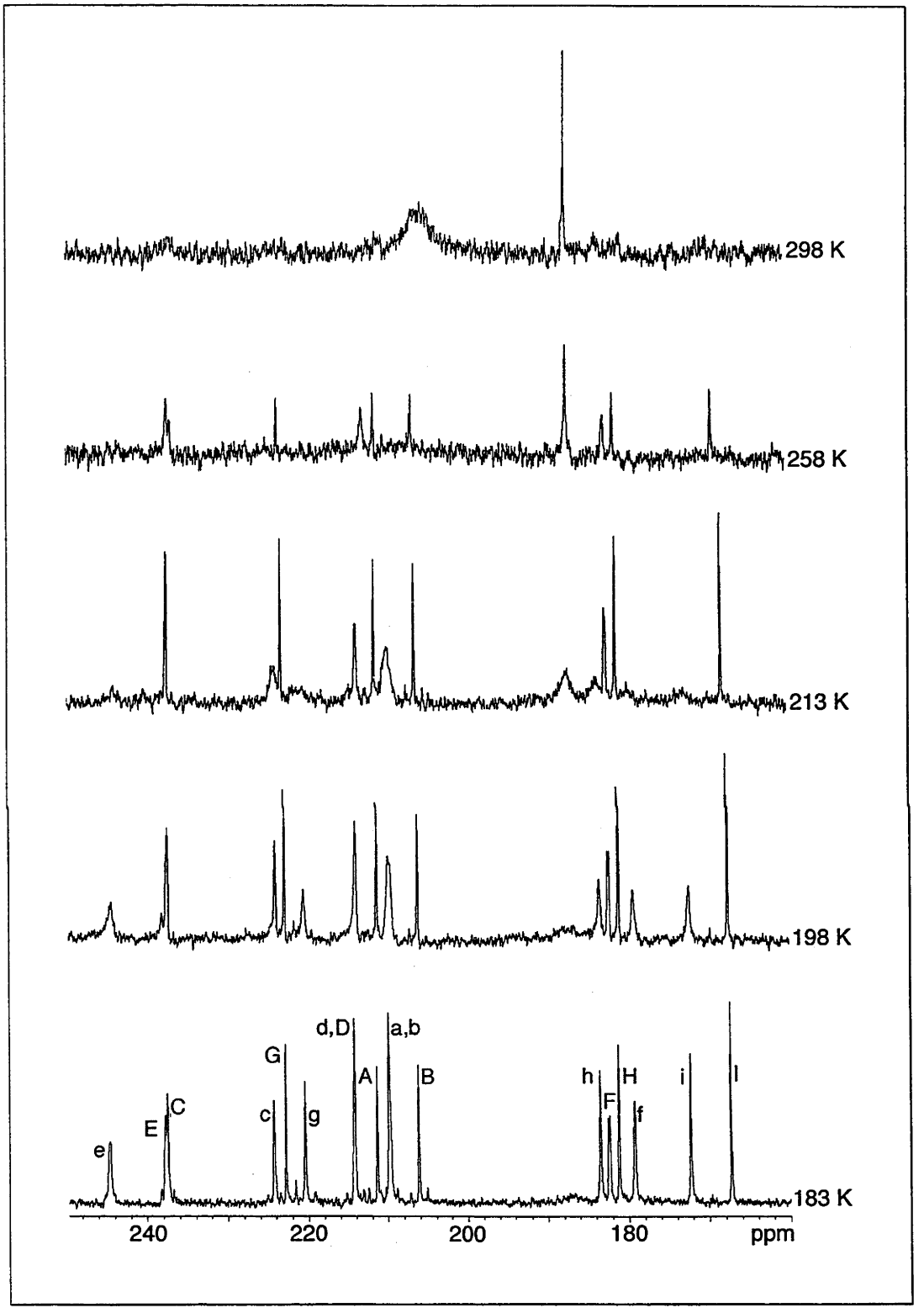
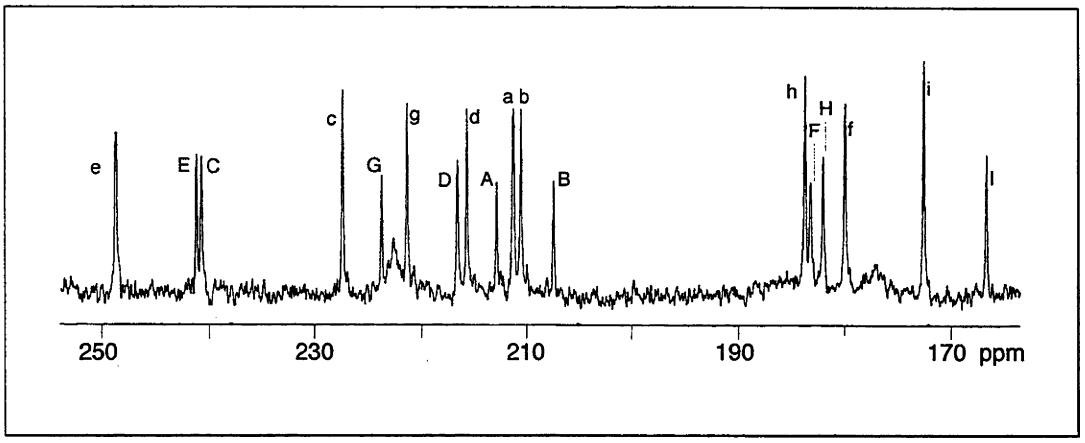


Figure 3.2.50. (a) Variable temperature ^{13}C NMR spectroscopic study of $[Cp_2W_2Ir_2(\mu\text{-}CO)_3(CO)_6(PPh_3)]$ (**31**) in CD_2Cl_2.



(b) ^{13}C NMR spectrum of $[Cp_2W_2Ir_2(\mu\text{-}CO)_3(CO)_6(PPh_3)]$ (**31**) in $CDFCl_2$ at 153 K.

The major isomer, **31a**, almost certainly corresponds to the crystallographically characterized form. As with **31b** and **33**, the presence of at least one carbonyl resonance in the bridging carbonyl region and only one carbonyl resonance at high field in the apical/axial region of **31a** excludes both an all-terminal ligand configuration and the possibility of a W_2Ir basal plane for either isomer; **31a** must therefore have a WIr_2 basal plane. As with **31b** and **33**, there are two Ir-ligated axial sites, but only one is occupied by carbonyl; the other must therefore be occupied by phosphine (^{31}P NMR -9.8 ppm). As mentioned above with **31b** and **33**, there are six possible configurations which are consistent with this information, corresponding to differing sites for the Cp ligands: the apical Cp ligand can be sited over any of the three non-basal faces, and the basal Cp can be axial or radial. Steric considerations militate against a radial Cp when the apical Cp is inclined to either W_2Ir face; in these circumstances axial Cp is favoured. As with **33**, a ^1H NOESY experiment of **31** in CD_2Cl_2 at 183 K shows the presence of a crosspeak between the axial PPh_3 protons at 7.68 - 7.05 ppm and the signal assigned to the protons of the axially-ligating Cp for **31a** at 4.79 ppm, suggesting an axial phosphine, axial Cp, apical Cp coordination geometry. These two configurations are **31a** and **31b** in Figure 3.2.47. The other two possibilities which are not sterically disfavoured have apical Cp inclined to the non-basal WIr_2 face. On steric grounds, the basal Cp can be radial or axial. An all *trans* [CpWWCp] arrangement is disfavoured on electronic grounds. The remaining possibility (radial Cp, axial phosphine, apical Cp) depicted in Figure 3.2.47. (**31c**) cannot be excluded on steric or electronic grounds, but the NOESY results as well as the significant difference in chemical shift of the [W-Ir(μ-CO)] resonances suggests that **31a** is the configuration observed for the major isomer [a significant (>10 ppm) difference between the chemical shift of the bridging carbonyls when one is at the face to which the apical Cp is inclined, and this face also contains two large axial ligands, was noted in Section *3.2.5.*]. The resonance at 244.3 ppm for the major isomer **31a** therefore corresponds to a W-Ir bridging carbonyl at a face to which the apical Cp is inclined, and which contains axially coordinated phosphine and cyclopentadienyl

ligands. Isomer **31a** thus adopts the axial phosphine, axial Cp, apical Cp configuration seen in the solid-state study (Figure 2.2.10.). The spectrum at 193 K reveals ^{183}W-coupled satellites for the resonances at 244.3 (e, 81 Hz), 224.2 (c, 83 Hz), 220.3 (g, 180 Hz) and 209.8 ppm (a and b, 171 Hz), the assignments for which follow logically from the fact that terminal carbonyl coupling constants are significantly larger than those for bridging carbonyls. The coincident signals for carbonyls a and b are resolved in the spectrum in $CDFCl_2$ at 153 K [Figure 3.2.50(b).], and a ^{31}P-^{13}C HMQC at 173 K shows a correlation between the axial phosphine and one of the apical CO resonances at 210.8 ppm, which is assigned as b assuming a linear three bond relationship will give rise to the larger *J* coupling. Assignment of the remaining signals at 214.1 (d), 183.5 (h), 179.2 (f, J_{CP} = 13 Hz) and 172.2 ppm (i) is straightforward because of the *cis* coupling observed at carbonyl f.

Ligand fluxionality for **31** commences upon warming its mixture of isomers, but due to poor signal to noise, suitable ^{13}C{^{1}H}-EXSY spectra could not be established for isomer **31a** or **31b**; an appropriate carbonyl exchange mechanism for this cluster was thus unable to be proposed.

NMR spectra of $[Cp_2W_2Ir_2(\mu\text{-}CO)_3(CO)_5(PMe_3)_2]$ (34)

The coalescence point in the NMR spectra of **34** could not be reached due to decomposition of the cluster above 300 K. The room temperature ^{31}P NMR spectrum of **34** consists of two signals in the ratio 1 : 1 at -27.7 and -29.8 ppm and a very broad resonance. On cooling to 193 K, six signals are resolved, corresponding to three isomers in the ratio 20 : 12 : 1 in CD_2Cl_2 (Figure 3.2.51.). Similarly, on cooling the sample of **34** to 193 K, signals corresponding to three isomers in the ratio 20 : 12 : 1 in CD_2Cl_2 can be identified in the ^{13}C NMR spectrum (Figure 3.2.52.). The structures of two of the three isomers of **34** (Figure 3.2.47.) can be assigned from the ^{13}C NMR data. Isomer **34a**, the most abundant in CD_2Cl_2, contains eight signals of equivalent intensity. The carbonyl resonances in the [W-Ir(μ-CO)] region, and single resonance in the apical/axial region, indicate a WIr_2 basal plane. There are two Ir-ligated axial sites, one occupied by carbonyl, the other occupied by phosphine. The lack of ^{31}P-^{31}P and ^{31}P-^{183}W coupling is only consistent with the second phosphine occupying a radial site at the axial carbonyl-ligated iridium atom. Six configurations corresponding to the differing Cp locations are consistent with these data. A HSQC experiment reveals a cross peak between the axial phosphine and an apical carbonyl (Figure 3.2.54.); the apical Cp is thus located inclined to the $[W_2Ir(P_{ax})]$ or WIr_2 face. There are four remaining possible configurations (the basal Cp may be radial or axial), but the low field signal at 253.8 ppm (which shows a cross peak to the axial PMe_3 in the ^{1}H-^{31}P-^{13}C triple resonance experiment: Figure 3.2.53.) is significantly downfield of the other [W-Ir(μ-CO)] resonance, and is thus indicative of a carbonyl bridging a bond

between two axially-ligated metals, with an apical Cp ligand inclined over the resultant face; configuration **34a** (Figure 3.2.47.) is therefore the only remaining possibility. A ^{1}H NOESY experiment of **34** in CD_2Cl_2 at 183 K reveals a crosspeak between the signal at 4.87 ppm corresponding to the protons on the axially-ligating Cp and the signal at 1.54 ppm corresponding to the axially-ligating PMe_3 protons, strengthening this assignment. This radial, diaxial, apical geometry is the only configuration structurally characterized thus far (for monodentate ligands) in the tetrairidium system.[38,39] The ^{13}C NMR spectrum at 183 K reveals ^{183}W-coupled satellites for the resonances at 253.8 (c, 90 Hz), 242.2 (d, 88 Hz), 223.0 (h, 185 Hz), 218.5 (a or b, 180 Hz) and 216.5 ppm (b or a, 180 Hz), with the assignments following from (i) coupling constant magnitude, (ii) the a-P_{ax} cross peak in the HSQC NMR spectrum (see above) and (iii) the cross peak between c and P_{ax} in the triple resonance study (see above). Assignment of the remaining signals at 227.6 (e), 183.5 (f, $^{2}J_{PC}$ = 22 Hz, $^{3}J_{PC}$ =10 Hz) and 169.1 ppm (g, $^{2}J_{PC}$ =10 Hz) is straightforward because of the *cis* and *trans* coupling to the phosphines.

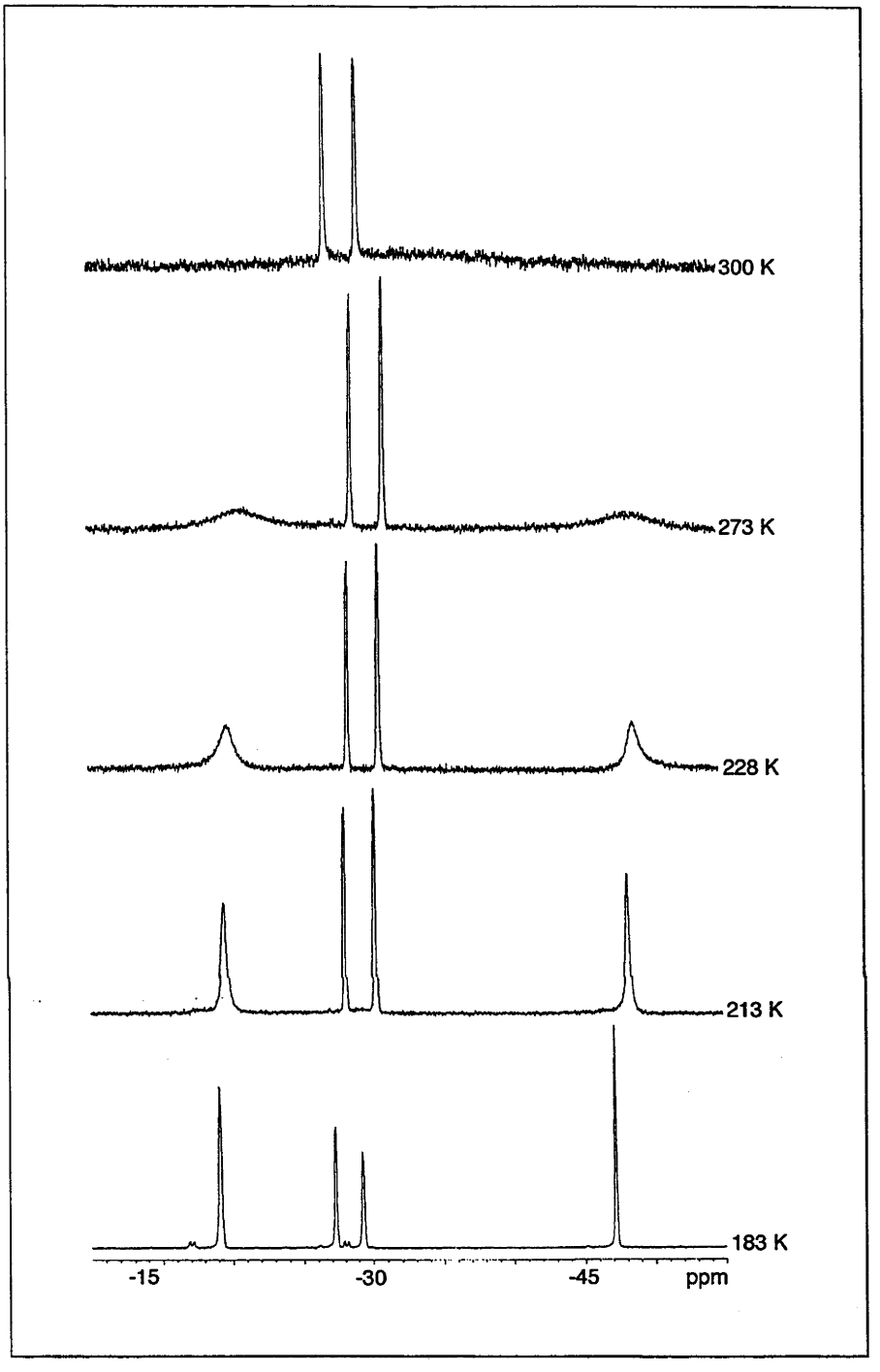


Figure 3.2.51. Variable temperature ^{31}P NMR spectroscopic study of $[Cp_2W_2Ir_2(\mu\text{-}CO)_3(CO)_5(PMe_3)_2]$ (**34**) in CD_2Cl_2.

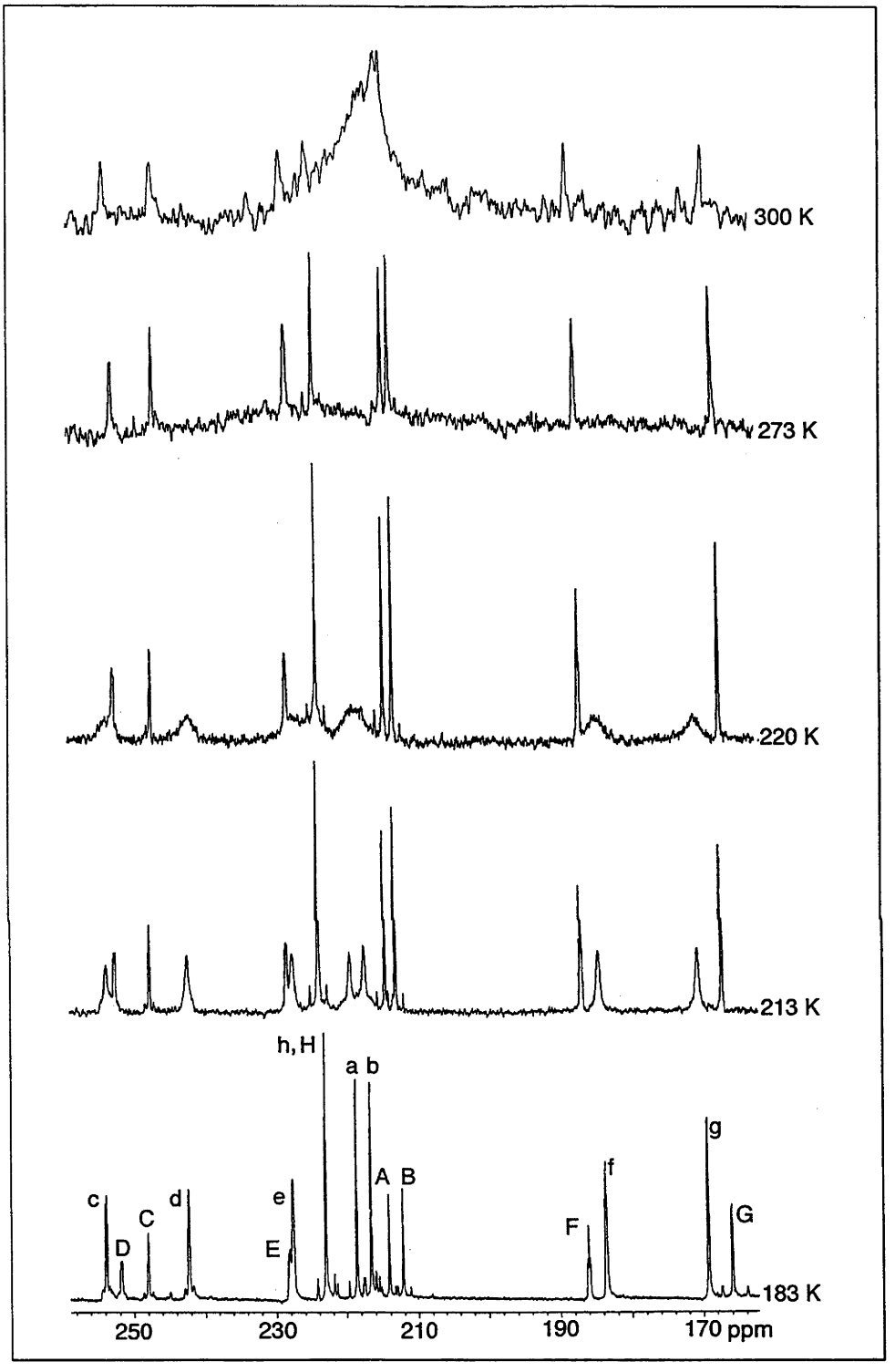


Figure 3.2.52. Variable temperature ^{31}C NMR spectroscopic study of $[Cp_2W_2Ir_2(\mu\text{-}CO)_3(CO)_5(PMe_3)_2]$ (**34**) in CD_2Cl_2.

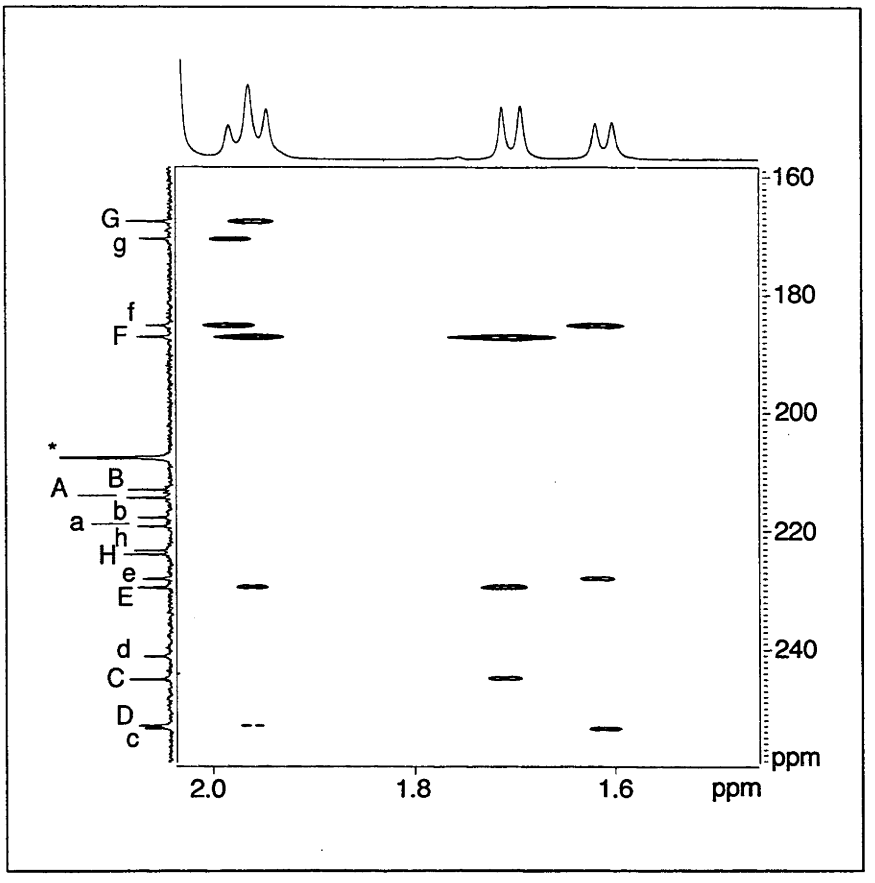


Figure 3.2.53. Triple resonance ^{1}H-^{31}P-^{13}C NMR spectrum of $[Cp_2W_2Ir_2(\mu\text{-}CO)_3(CO)_5(PMe_3)_2]$ (**34**) in acetone-d^6.

Isomer **34b** contains eight signals of equivalent intensity, and must also possess a WIr_2 basal plane with one phosphine axially ligated and the other radially disposed. A ^{1}H-^{31}P-HSQC experiment reveals a cross peak between the axial phosphine and the apical cyclopentadienyl (Figure 3.2.54.); the apical Cp is thus located inclined to the $[W_2Ir(P_{rad})]$ face. There are two remaining possible configurations (the basal Cp may be radial or axial), but a radially disposed basal Cp is highly unlikely on steric grounds, suggesting that configuration **34b** in Figure 3.2.47. is correct. The configuration of **34b** is strengthened by the presence of through space interactions, revealed in the ^{1}H NOESY experiment at 183 K. A crosspeak between the signal at 4.41 ppm, assigned to the apical Cp protons, and the signal at 1.89 ppm, assigned to the radially-ligating PMe_3 protons, strengthens the suggestion that the apical Cp is inclined to the $[W_2Ir(P_{rad})]$ face. Significantly, the structurally characterized bis-$P(OMe)_3$ derivative (**36**) also possesses this configuration (Figure 2.2.11.). The ^{13}C NMR spectrum at 183 K reveals ^{183}W-coupled satellites for the resonances at 251.7 (D, 92 Hz), 247.9 (C, 90 Hz), 223.0 (H, 183 Hz), 214.0 (A or B, 185 Hz) and 212.2 ppm (B or A, 188 Hz), with the assignments following from (i) coupling constant magnitude and (ii) a cross peak between C and P_{ax} in the triple resonance study. An attempt to establish the assignments of A and B from the possible long-range *trans* coupling between A and G in a complementary ^{13}C-^{13}C correlation spectroscopy (COSY)

experiment was unsuccessful, but a precise assignment of A and B is (fortunately) not required for the discussion of the fluxionality of **34b**. The low relative abundance (3 %) of **34c** in solution has frustrated efforts to definitively assign its coordination geometry. The ^{31}P-^{31}P coupling (and lack of ^{31}P-^{183}W coupling or any examples in which phosphine ligates to tungsten in this system) is only consistent with a *trans*-disposed [$P_{rad}IrIrP_{rad}$] arrangement. Steric arguments then militate against the apical Cp being inclined to the WIr_2 face. Inclination of the apical Cp to either of the W_2Ir faces favours an axially-ligated basal Cp. The likely configuration is thus **34c** (Figure 3.2.47.), for which six signals of equivalent intensity were observed at 193 K, with the remaining two resonances presumably concealed by signals from the more abundant isomers. Resonances were not sufficiently intense to observe ^{183}W-coupled satellites; consequently, the assignment is with extreme caution. The presence of W-Ir bridging carbonyl signals, axial/apical Ir-ligated carbonyl resonances, and two radially-ligated phosphines is only consistent with a WIr_2 basal plane and an apical tungsten atom. The two resonances at high field (167.2, 10 Hz; 163.8, 10 Hz) both display $^2J_{CP}$ coupling and are therefore assigned to *f* and *g*. The remaining resonances at 244.9 (*c* or *d*), 228.2 (*e*), 221.3 (*h*) and 215.9 (*a* or *b*) can be assigned by analogy with related clusters discussed above.

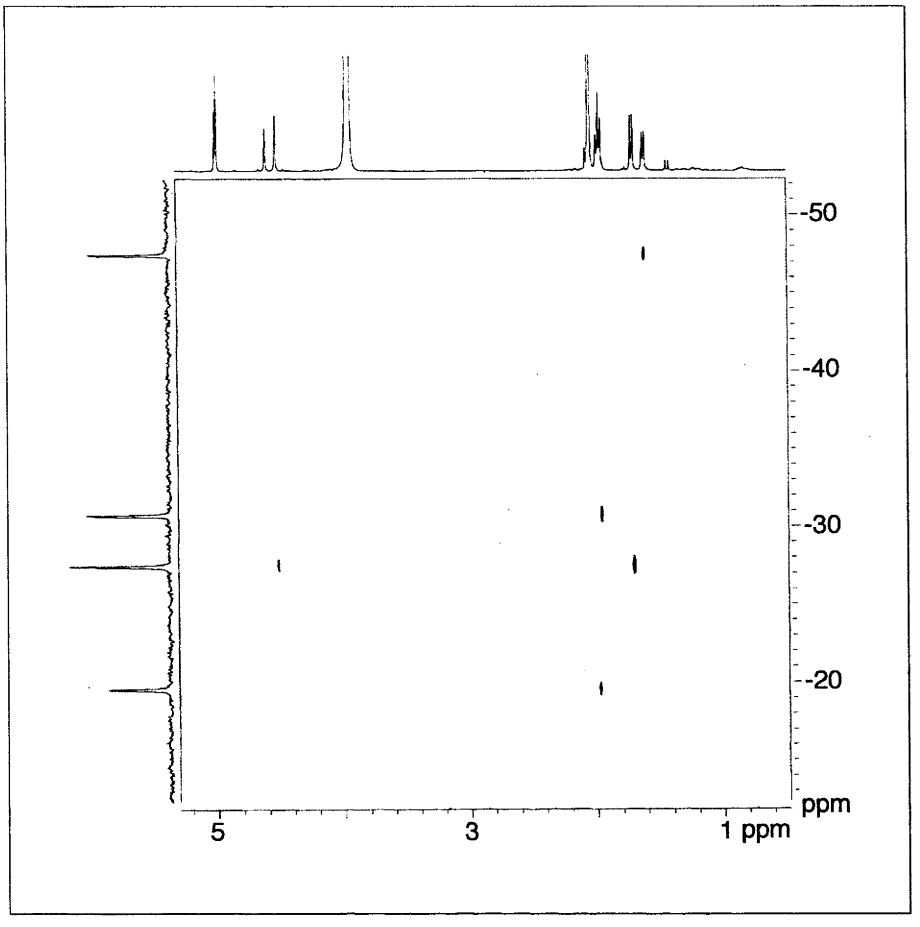


Figure 3.2.54. HSQC NMR spectrum of $[Cp_2W_2Ir_2(\mu\text{-}CO)_3(CO)_5(PMe_3)_2]$ (**34**) in acetone-d^6 at 203 K.

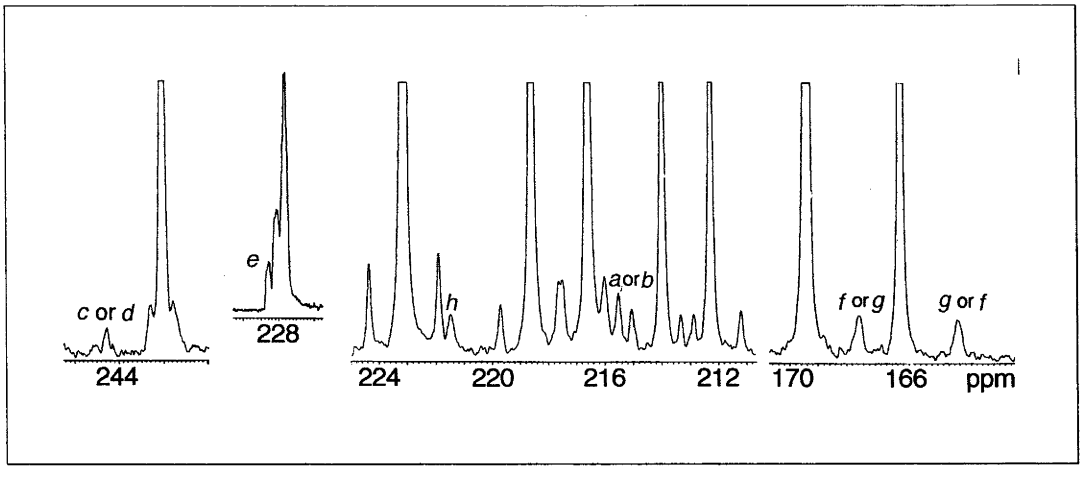


Figure 3.2.55. Partial ^{13}C NMR spectrum (line broadening = 10 Hz) of $[Cp_2W_2Ir_2(\mu\text{-}CO)_3(CO)_5(PMe_3)_2]$ (**34**) emphasizing isomer **34c**.

Ligand fluxionality commences upon warming the mixture of isomers. The contour plot for **34a** shown in Figure 3.2.56. reveals a site exchange at 203 K corresponding to h ↔ d. The exchange is consistent with ligand mobility about one of the W_2Ir faces with carbonyl distributions again reminiscent of the D_{2d} intermediate implicated in the $[M_4(CO)_{12}]$ exchange pathway (Scheme 3.2.6.). Useful carbonyl exchange data for the other isomers could not be obtained due to the low relative abundance in solution (isomer **34c**) or decomposition of the cluster in solution above 300 K (isomer **34b**).

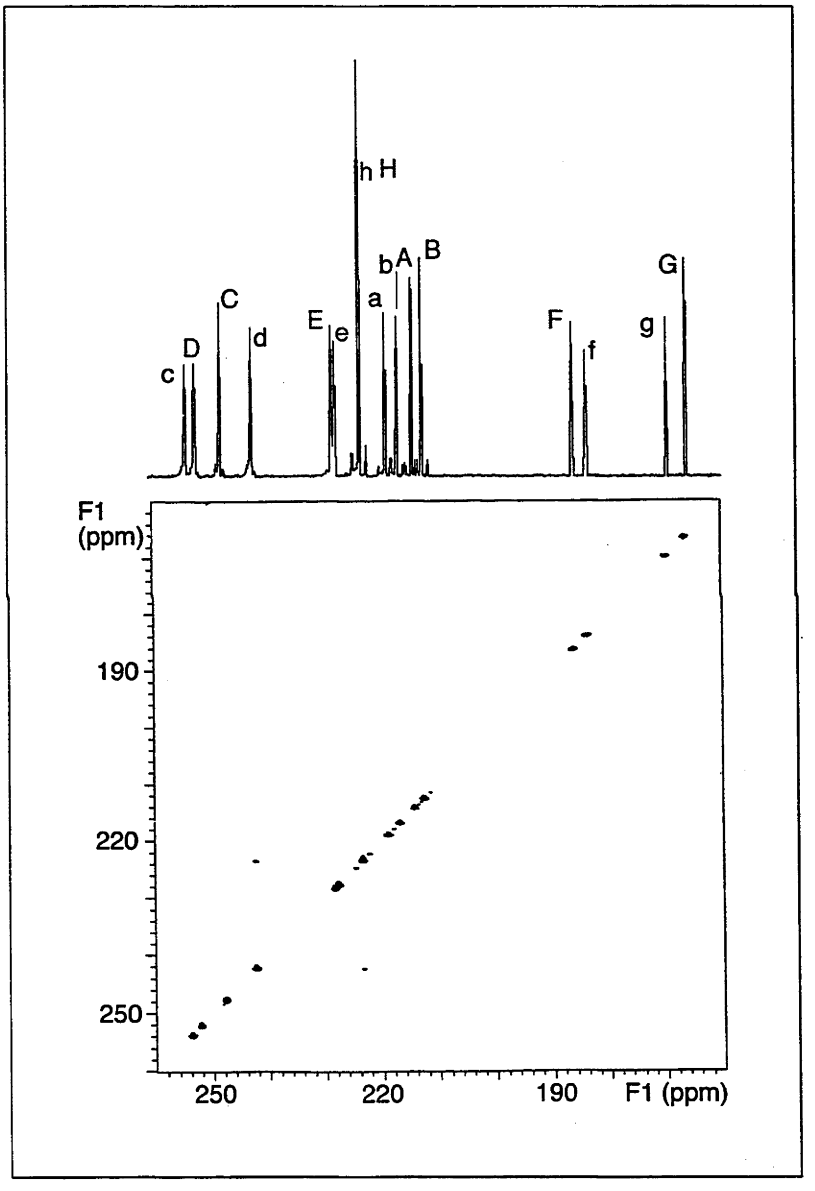
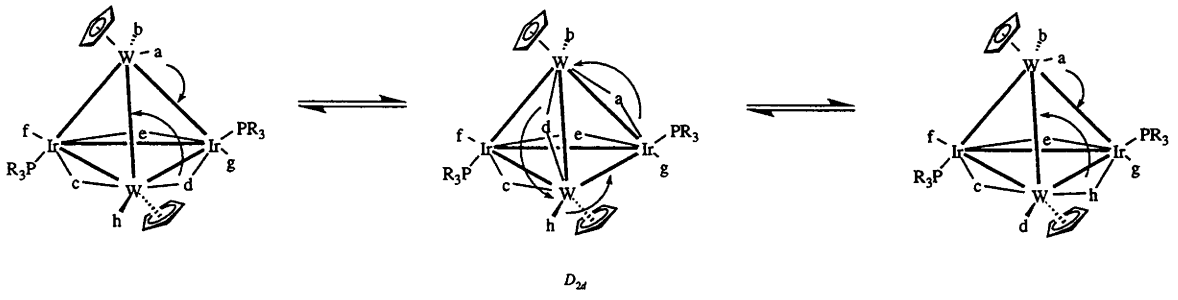


Figure 3.2.56. ^{13}C NMR EXSY spectrum of $[Cp_2W_2Ir_2(\mu\text{-}CO)_3(CO)_5(PMe_3)_2]$ (**34**) in CD_2Cl_2 at 203 K.



Scheme 3.2.6. CO mobility about a W_2Ir face in **34a**

NMR spectra of [$Cp_2W_2Ir_2(\mu$-CO)$_3$(CO)$_5$(PPh_3)$_2$] (32)

The coalescence point in the ^{31}P and ^{13}C NMR spectra of **32** could not be reached due to decomposition of the cluster above 273 K. Due to this poor thermal stability, well-resolved NMR spectra of **32** were difficult to obtain. The ^{31}P and ^{13}C NMR spectra at 203 K (Figures 3.2.57. and 3.2.58.) reveal resonances corresponding to two isomers in the ratio 4 : 1. Both isomers contain eight resonances of equal intensity in the ^{13}C NMR spectrum at 203 K. Following the arguments above, signals in the [W-Ir(μ-CO)] region and only one resonance in the apical/axial Ir-CO region are consistent with a WIr_2 basal plane and Ir-ligated phosphines in radial and axial sites for both isomers. Resonances are not sufficiently sharp to resolve ^{183}W-^{13}C coupling; as with **34c**, assignments are therefore cautious. The major isomer contains resonances at 249.1, 240.1, 226.9, 223.1, 211.5, 210.7, 185.0 and 164.6 ppm, while the minor isomer contains signals at 249.8, 238.0, 229.9, 223.9, 214.0, 212.9, 181.2 and 158.0 ppm. There are six configurations consistent with the phosphine disposition (inclining the apical Cp to any of three accessible faces, and siting the basal Cp axial or radial), one of which is electronically disfavoured (the transoid [CpWWCp] arrangement), and one of which is sterically disfavoured (inclining the apical Cp to a [$WCp_{ap}WCp_{rad}IrP_{rad}$] face). Of the remaining four possible configurations, two are analogues of **34a** and **34b**, the third involves interchanging Cp_{ax} and h in **34a**, and the fourth involves exchanging Cp_{ap} and b in **34a**. While PPh_3 analogues of **34a** and **34b** minimize steric repulsion, the other two possibilities cannot be excluded at present. Although ligand fluxionality commences upon warming the solution above 203 K, useful carbonyl exchange data could not be obtained due to the instability of the cluster in solution.

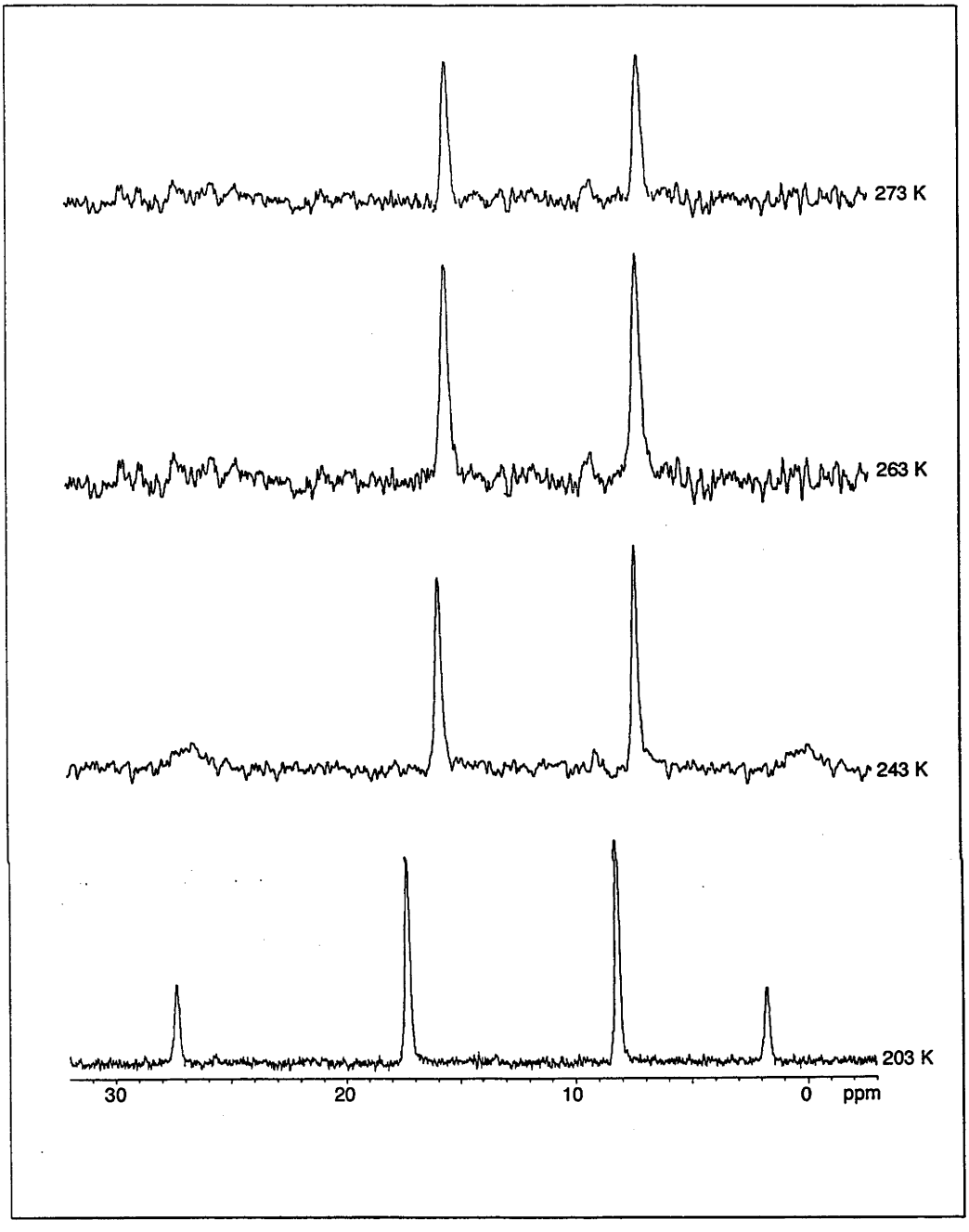


Figure 3.2.57. Variable temperature ^{31}P NMR spectroscopic study of $[Cp_2W_2Ir_2(\mu\text{-}CO)_3(CO)_5(PPh_3)_2]$ (**32**) in CD_2Cl_2 at 121.4 MHz.

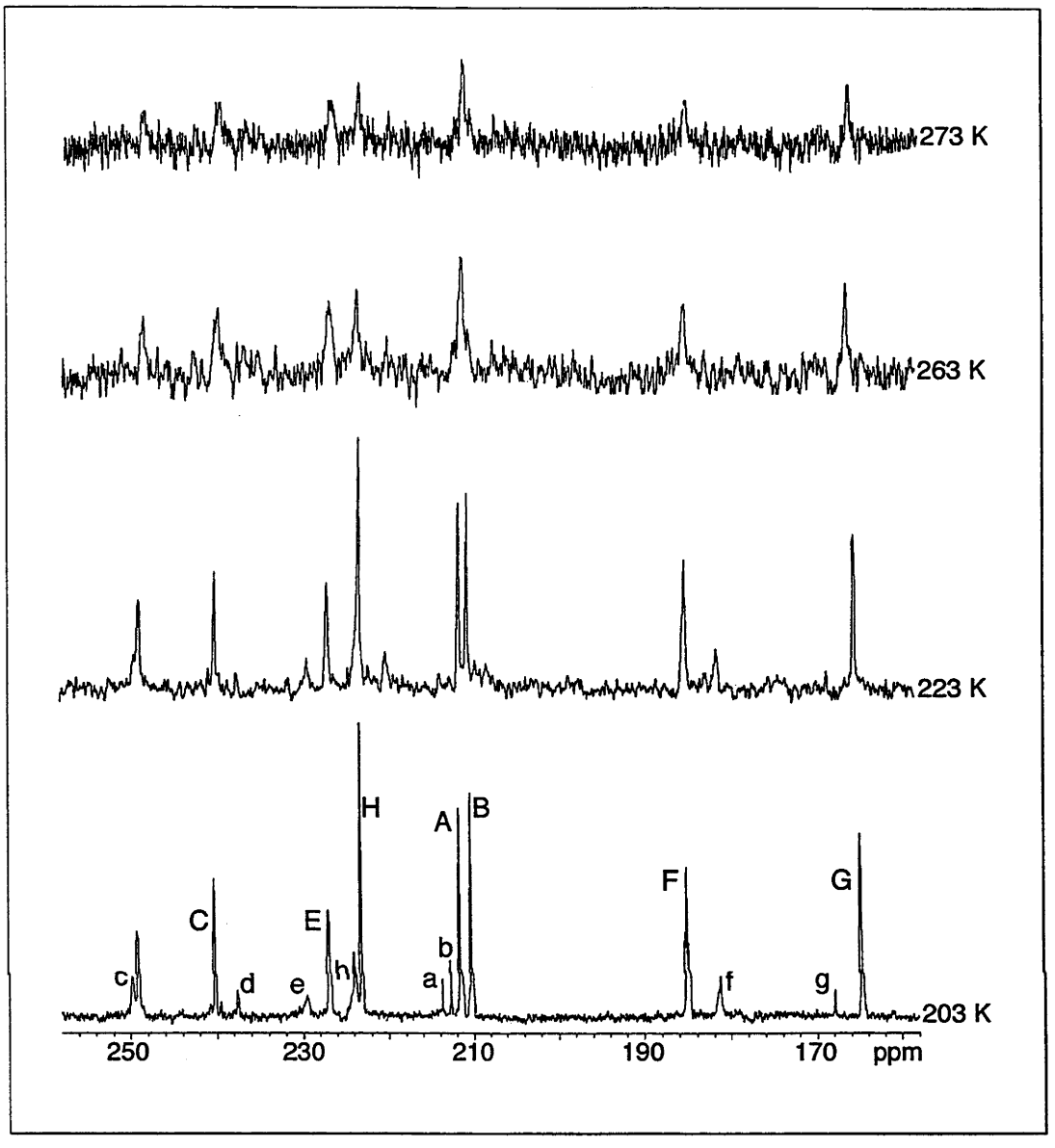


Figure 3.2.58. Variable temperature ^{13}C NMR spectroscopic study of $[Cp_2W_2Ir_2(\mu\text{-}CO)_3(CO)_5(PPh_3)_2]$ (**32**) in CD_2Cl_2 at 121.4 MHz.

Discussion

The studies above demonstrate the difficulty of definitively assigning carbonyl resonances in transition metal clusters. Replacement of iridium by tungsten in proceeding from homometallic $[Ir_4(CO)_{12}]$ (**1**) to heterometallic $[CpWIr_3(CO)_{11}]$ (**2**) and $[Cp_2W_2Ir_2(CO)_{10}]$ (**3**) leads to a significantly increased dispersion in chemical shifts of the carbonyl ligands: W-Ir bridging CO (221 - 257 ppm) > Ir-Ir bridging CO (205 - 231 ppm) ≈ W terminal CO (206 - 228 ppm) > Ir radial CO (175 - 187 ppm) > Ir axial CO (158 - 166 ppm) ≈ Ir apical CO (159 - 173 ppm), which facilitates assignment. The presence of the NMR-active 15% abundant ^{183}W isotope permits discrimination of Ir-Ir bridging CO and W terminal CO resonances. Nevertheless, ambiguities remain: the ^{13}C NMR spectra of the clusters reveal no logical way of

distinguishing between radial and axial ligated W-bound carbonyls, or of determining over which WMIr face (M = W or Ir) apical W-bound carbonyls are inclining. 2D NMR techniques (including triple resonance experiments) have been useful in assigning spectra in the present work. The identification of long-range *trans* coupling between axial ligated W-bound carbonyls and apical carbonyls in ^{13}C-^{13}C COSY experiments has also been useful in some instances, although poor sensitivity and small coupling constants have rendered this experiment unsatisfactory on many occasions. In the present studies ^{183}W-^{13}C and ^{183}W-^{1}H correlation spectra of **33** have been utilized to identify the appropriate coupling (^{1}J for the ^{183}W-^{13}C experiment, ^{2}J and ^{3}J for the ^{183}W-^{1}H experiment). 2D experiments with the ^{183}W nucleus have been examined in an attempt to obtain further useful information. A considerable difference in chemical shifts between the apical tungsten atom (-1657 ppm, CD_2Cl_2) and tungsten atoms ligated by cyclopentadienyl groups in axial sites (-2247 ppm) was noted. The experiment was thus consistent with the assignment of an axial, apical configuration of the η^5-cyclopentadienyl ligands (Figures 3.2.59. and 3.2.60., respectively). The lack of ^{183}W NMR data for a definitively assigned radial Cp-ligated tungsten atom and the general unpredictability of transition metal NMR chemical shifts means that, at present, no comment can be made on the utility of this procedure in distinguishing axial/radial Cp.

^{1}H-^{31}P-^{13}C triple resonance NMR spectroscopy and HSQC experiments have proven very useful. A number of ligand-substituted derivatives of **2** and **1** have been structurally characterized with a η^5-cyclopentadienyl ligand and a *P*-donor ligand located in a transoid arrangement with respect to a W-Ir vector (e.g. $[CpWIr_3(\mu\text{-}CO)_3(CO)_7(PMe_3)]$ (**7**), $[CpWIr_3(\mu\text{-}CO)_3(CO)_7(PMe_2Ph)]$ (**13**), $[CpWIr_3(\mu\text{-dppm})(\mu\text{-}CO)_3(CO)_6]$,[40] $[CpWIr_3(\mu\text{-dppe})(\mu\text{-}CO)_3(CO)_6]$,[40] $[Cp_2W_2Ir_2(\mu\text{-}CO)_3(CO)_5\{P(OMe)_3\}_2]$ (**36**) and $[Cp_2W_2Ir_2(\mu\text{-dppm})(\mu\text{-}CO)_3(CO)_5]$ (**37**): see Chapter 2). These instances should be amenable to study by a 2D (^{31}P-^{13}C) correlation. However, the proton detected ^{1}H-^{31}P-^{13}C triple resonance experiment is more useful due to its increased sensitivity over the ^{31}P detected technique, particularly when PMe_3 ligands are present. A review containing phosphorus detected ^{1}H-^{31}P-^{13}C triple resonance experiments has recently been published.[46] In the present study, the HSQC experiment was utilized to confirm the linear arrangement of axial phosphine and apical η^5-cyclopentadienyl ligand in **33b** and **34b**. Coupling from the axially-ligated phosphine to the adjacent W-Ir bridging carbonyl detected in the triple resonance study was utilized in the assignment of carbonyl E in **33b**, and carbonyls c and C in **33a** and **33b**, respectively.

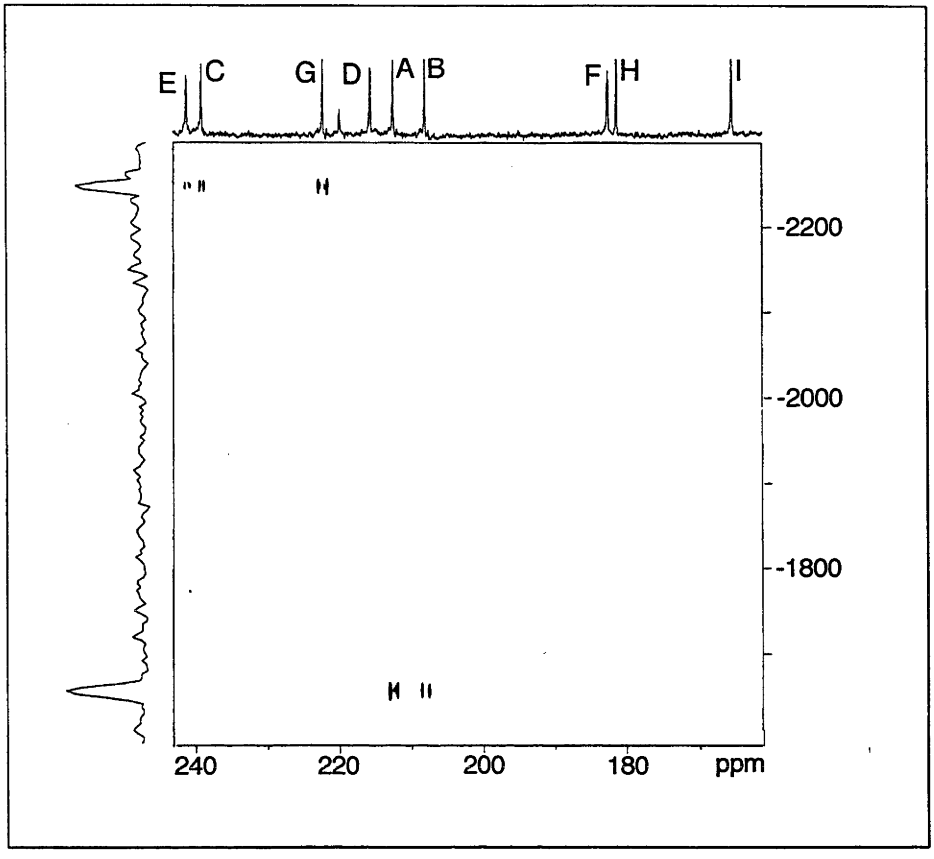


Figure 3.2.59. ^{183}W-^{13}C correlation NMR spectrum of $[Cp_2W_2Ir_2(\mu\text{-}CO)_3(CO)_6(PMe_3)]$ (**33**) in CD_2Cl_2 at 203 K (after skyline projection)

The configurations assigned to the PMe_3 derivatives seem secure, but the geometry of the mono-PPh_3 isomers is not completely certain, and that of the bis-PPh_3 isomers remains uncertain. A combination of steric and electronic arguments suggests that the major isomer of **32b** adopts the configuration of **34b**, while the minor isomer likely has the ligand disposition of **34a**, but this remains speculative. Experimental difficulties precluded the comprehensive NMR studies which are required, as shown by the work with the PMe_3-derivatives.

The geometries adopted by the crystallographically and spectroscopically well-defined isomers of **21** - **34** can be contrasted with those of related derivatives from the tungsten-triiridium and tetrairidium systems. Trisubstituted derivatives of **1** usually adopt diradial, axial geometries with monodentate ligands (radial, diaxial ligation is preferred with bidentate ligands), whereas trisubstituted derivatives of **2** (considering Cp as a ligand, i.e. bis-phosphine/phosphite derivatives) adopt radial, diaxial or triradial coordination modes (Section *3.2.2-4.*). Trisubstituted derivatives of **3** (i.e. mono-phosphine derivatives) adopt diaxial, apical coordination geometries, variants enforced by the fact that a W_2Ir basal plane is unfavourable. Tetrasubstituted derivatives of **1** adopt radial, diaxial, apical ligation (with the apical ligand oriented toward the axial substituents) to minimize unfavourable steric

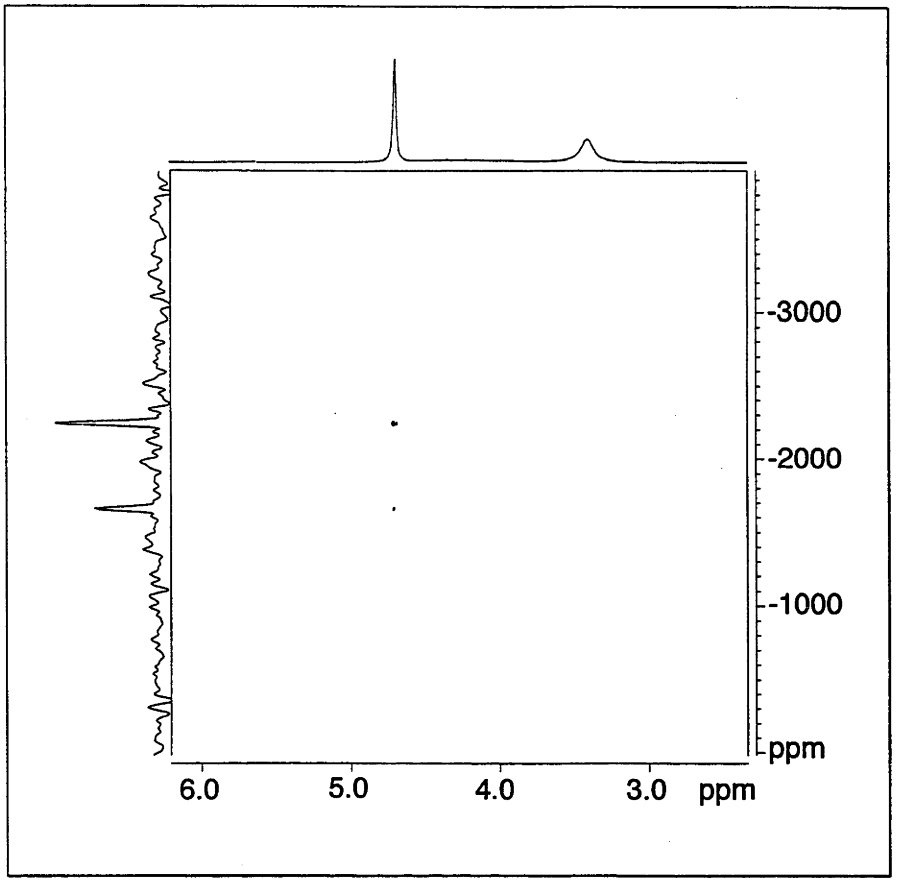


Figure 3.2.60. ^{183}W-^{1}H correlation NMR spectrum of $[Cp_2W_2Ir_2(\mu\text{-}CO)_3(CO)_6(PMe_3)]$ (**33**) in CD_2Cl_2 at 203 K

interactions, the preferred ligand disposition at tris-phosphine derivatives of **2**. Tetrasubstituted derivatives of **3** (i.e. bis-phosphine derivatives) from the studies described above favour this geometry, but also adopt a configuration corresponding to rotation at the apical tungsten atom, placing the bulky Cp over a radial phosphine-containing W_2Ir face. This latter geometry has been shown conclusively only for the sterically less demanding PMe_3 ligand.

Significantly less is known of fluxional processes across clusters of this type. Studies with tris- and tetra-substituted tetrairidium clusters have focussed on polydentate ligand derivatives.[11,13] Tripodal ligand derivatives scramble CO ligands by way of a Cotton merry-go-round, whereas bis(bidentate ligand) derivatives exchange CO ligands by a change-of-basal-face process. No reports of studies at monodentate ligand derivatives are extant. Bis-phosphine derivatives of this cluster exchange CO ligands by (i) scrambling about an Ir_3 face, by way of a pseudo-D_{2d} intermediate as postulated in the ligand fluxionality of derivatives of **1**, and (ii) rotation of the axial ligands about a WIr_2 face by way of a conical surface merry-go-round. The trisubstituted derivative of **3** which has afforded mechanistic insight (**33b**) exchanges CO ligands by scrambling about a WIr_2 face, by way of a pseudo-D_{2d} intermediate. A similar process is

operative to that observed in the bis-phosphine derivative of **2** for scrambling about an Ir_3 face. For the latter, however, two iridium atoms are phosphine ligated and, as a consequence, the terminal carbonyl ligands at each do not participate in the site exchange. For the former, the absence of phosphine at site I facilitates exchange involving carbonyl H. The tetrasubstituted derivative of **3** from the present work for which mechanistic insight has been gained (**34a**) has no comparators across the tetrairidium or tungsten-triiridium system. As observed with the other examples, terminal carbonyl ligands at phosphine-ligated iridium atoms do not site exchange. If carbonyl fluxionality by way of pseudo-D_{2d} intermediates is favoured, the question naturally arises as to why the b $\leftrightarrow$ e and a $\leftrightarrow$ d exchanges are not observed within the temperature range of investigation. The fact that no evidence for these exchanges was detected under the conditions employed may indicate that semi-bridging interactions are involved in the pseudo-D_{2d} intermediate depicted in Scheme 3.2.6.

3.2.8. NMR studies of $P(OMe)_3$ derivatives of $[Cp_2W_2Ir_2(CO)_{10}]$

The syntheses and characterization of the ligand-substituted derivatives $[Cp_2W_2Ir_2(\mu\text{-}CO)_3(CO)_{7-n}\{P(OMe)_3\}_n]$ [n = 1 (**35**), 2 (**36**)] were reported in Chapter 2 providing a further comparison of the reactivity, product configuration(s) and fluxional pathway(s) with the "parent" cluster **1** and the tungsten-triiridium cluster **2**. Unusually, clusters **35** and **36** were found to exist as one configuration each, as shown by the IR and NMR spectra. As mentioned in Chapter 2, the bis-phosphite derivative underwent an unusual decomposition in solution affording the tungsten-triiridium cluster **19**; a study of this decomposition is described first.

Decomposition of 36 to 19 by ^{31}P NMR Spectroscopy

A $^{31}P\{^1H\}$ NMR spectroscopic study of **36** in CD_2Cl_2 at 298 K was undertaken to monitor its decomposition into $[CpWIr_3(\mu\text{-}CO)_3(CO)_7\{P(OMe)_3\}]$ (**19**) in solution. ^{31}P NMR spectra of **19** were measured every 2 h over a 72 h period, selected results of which are summarized in Figure 3.2.61. The initial ^{31}P NMR spectrum (0 h) reveals two signals at 123.5 and 99.5 ppm, corresponding to the radial and axial phosphites of **36**. After 12 h, a small signal at 87.1 ppm appears. After 72 h, a very minor signal at 98.5 ppm can be seen, in addition to the signal at 87.1 ppm and the major signals corresponding to **36**. A ^{31}P NMR spectrum of pure **19** in CD_2Cl_2 at 298 K under the same experimental conditions reveals a signal at 87.1 ppm, and the corresponding signal in Figure 3.2.61., is therefore assigned to $[CpWIr_3(\mu\text{-}CO)_3(CO)_7\{P(OMe)_3\}]$ (**19**). Cluster **19** is known to be fluxional on the NMR timescale (Section *3.2.4.*), but an attempt to resolve the constituent isomers of **19** by lowering the temperature to 178 K was unsuccessful due to the low concentration of **19** in solution. The minor signal at 98.5 ppm may possibly correspond to **35**, another possible decomposition

product, although the concentration is too low for this to be confirmed. After 72 h, the ^{31}P NMR spectrum of **36** shows that the relative abundance of the components is (**36**) 92: (**19**) 7: (**35**) 1. Although the sample of **36** was left in solution for a further 28 days, ^{31}P NMR spectroscopy did not reveal significant additional conversion of **36** to **19**.

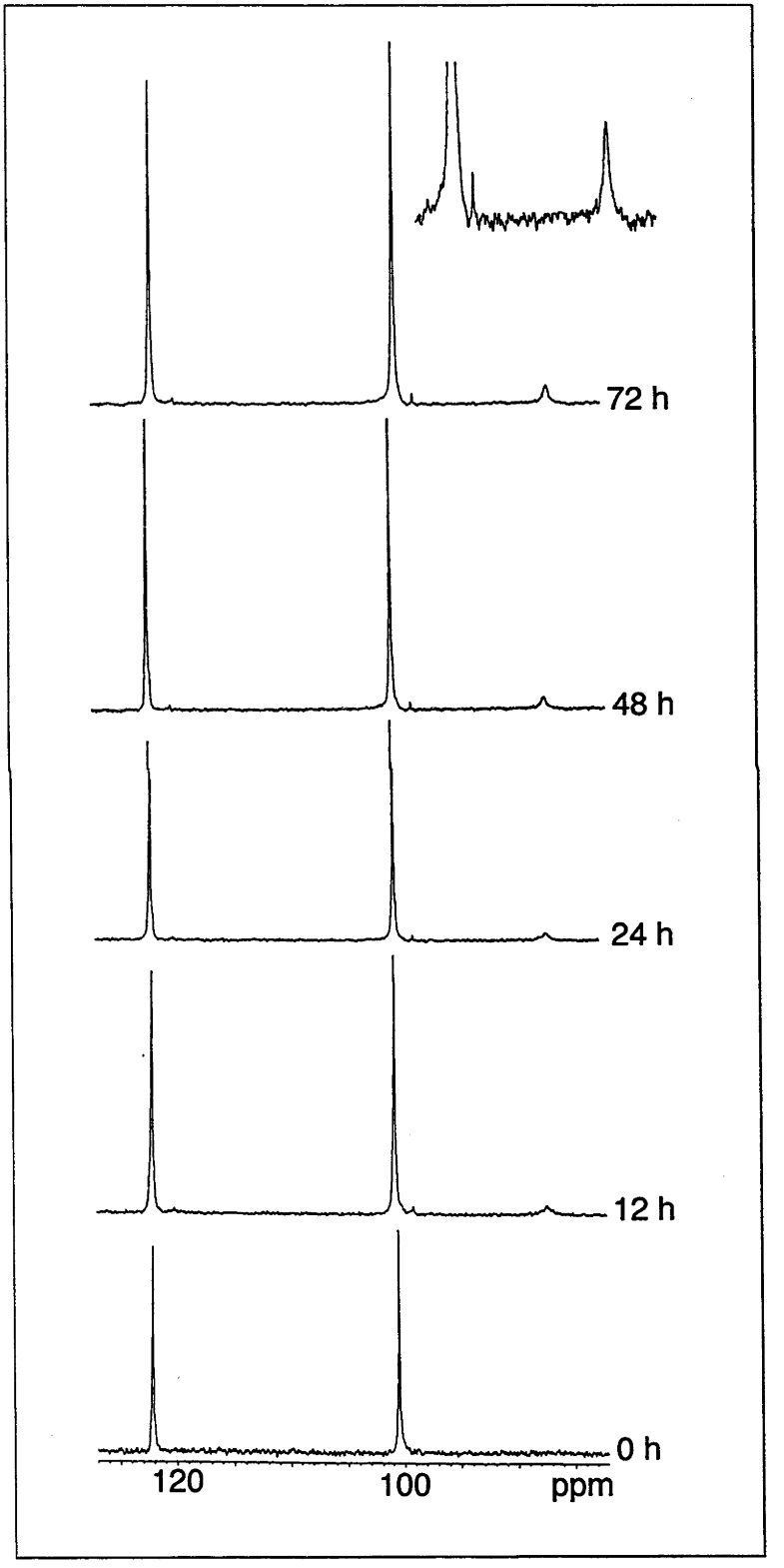


Figure 3.2.61. ^{31}P NMR spectroscopic study of $[Cp_2W_2Ir_2(\mu\text{-}CO)_3(CO)_5\{P(OMe)_3\}_2]$ (**36**) in CD_2Cl_2 at 298 K.

Decomposition-induced modifications to the coordination sphere have been noted before in ligand-substituted tungsten-iridium clusters. As mentioned above, the sterically-encumbered clusters $[CpWIr_3(\mu\text{-}CO)_3(CO)_5(PPh_3)_3]$ (**6**) and $[Cp_2W_2Ir_2(\mu\text{-}CO)_3(CO)_5(PPh_3)_2]$ (**32**) decompose rapidly in solution at room temperature or on a preparative thin-layer chromatographic plate affording $[CpWIr_3(\mu\text{-}CO)_3(CO)_6(PPh_3)_2]$ (**5**) or $[Cp_2W_2Ir_2(\mu\text{-}CO)_3(CO)_6(PPh_3)]$ (**31**), respectively, but these reactions proceed by the more conventional route of bulky ligand loss and retention of cluster core metals. The conversion of **36** into **19** must involve break-up of the ditungsten-diiridium core into metal fragments followed by recondensation into the tungsten-triiridium framework of **19**. Kinetic studies on several binuclear and polynuclear compounds have shown that when metal-metal bond fragmentation occurs, complex equilibria can exist between the species of different nuclearity.[49] In the present case, the presence of a bulky ligand at all four cluster vertices is crucial to effect this core transformation.

NMR studies of $[Cp_2W_2Ir_2(\mu\text{-}CO)_3(CO)_6\{P(OMe)_3\}]$ (35)

The ^{13}C NMR spectrum of **35** at 320 K reveals one broad signal (200.1 ppm in $CDCl_3$) corresponding to rapid exchange of all ligands. On cooling to 248 K in CD_2Cl_2, one $P(OMe)_3$ signal in the ^{31}P NMR spectrum and nine carbonyl resonances of equal intensity in the ^{13}C NMR spectrum (Figure 3.2.62.) are resolved, corresponding to the configuration of **35** shown in Figure 3.2.63. With this information, it is possible to assign the spectrum of **35**. The presence of at least one carbonyl resonance in the bridging carbonyl region, and only one carbonyl resonance at high field in the apical/axial region of **35** excludes both an all-terminal ligand configuration and the possibility of a W_2Ir basal plane; **35** must therefore have a WIr_2 basal plane. There are two Ir-ligated axial sites, but only one is occupied by carbonyl; the other must therefore be occupied by phosphite. There are six possible configurations which are consistent with this information, corresponding to differing sites for the Cp ligands: the apical Cp ligand can be sited over any of the three non-basal faces, and the basal Cp can be axial or radial. A ^1H-^1H NOESY experiment of **35** in CD_2Cl_2 at 248 K reveals the presence of a crosspeak between the signals at 4.99 ppm and 3.72 ppm, which can be assigned to through space interactions between an axially-disposed Cp and an axially-ligating $P(OMe)_3$, respectively. The chemical shifts of the carbonyl resonances in the ^{13}C NMR spectrum of **35** are very similar to those for $[Cp_2W_2Ir_2(\mu\text{-}CO)_3(CO)_6(PMe_3)]$ (**33**), strengthening the assignment of a diaxial, apical coordination geometry (it is also significant that this configuration has previously been seen in the structurally characterized $[Cp_2Mo_2Ir_2(\mu\text{-}CO)_3(CO)_6(PMe_3)]$[48]); all NMR resonances can be assigned analogously to those of **33**. ^{183}W-

coupled satellites are observed for the resonances at 238.5 (e, 80 Hz), 237.5 (c, 80 Hz), 221.1 (g, 181 Hz), 212.5 (a or b, 154 Hz) and 209.3 ppm (b or a, 156 Hz), corresponding to W-Ir bridging carbonyls, radially-ligating W-bound carbonyls and the apical carbonyls. The assignment of carbonyls e and c are confirmed by the presence of a coupling between the axial carbonyl i and the bridging carbonyl c in a ^{13}C-^{13}C correlation spectroscopy (COSY) experiment (Figure 3.2.64.); a similar (μ-CO)-axial CO coupling was noted in a COSY experiment of $[CpWIr_3(\mu\text{-}CO)_3(CO)_6(PPh_3)_2]$ (**5**) (Figure 3.2.11.). Assignment of the remaining signals in the ^{13}C NMR spectrum of **35**, namely 213.3 (d), 182.8 [f, $^2J(CP)$ = 14 Hz], 182.4 (h) and 162.2 ppm (i), is straightforward because of the *cis* coupling observed at carbonyl f. ^{183}W-coupled satellites are observed in the ^{31}P NMR spectrum of **35**, in contrast to the studies with phosphine-substituted clusters. This result is consistent with an iridium-coordinated $P(OMe)_3$ which ligates axially with respect to the basal plane and is effectively *trans* to the apical tungsten atom (Figure 3.2.63.). The $^2J_{PW}$ coupling is possibly due to the fact that Ir-(phosphite) bonds are somewhat shorter than the corresponding Ir-(phosphine) bonds in the related phosphine-substituted tungsten-iridium clusters, but an alternative explanation is that the slow exchange of the ligands surrounding the cluster core (as compared with the related phosphine-substituted derivatives) results in onset of fluxionality at higher temperatures. These higher temperatures afford better resolution for experimental reasons (less viscous solvents, and hence more effective shimming).

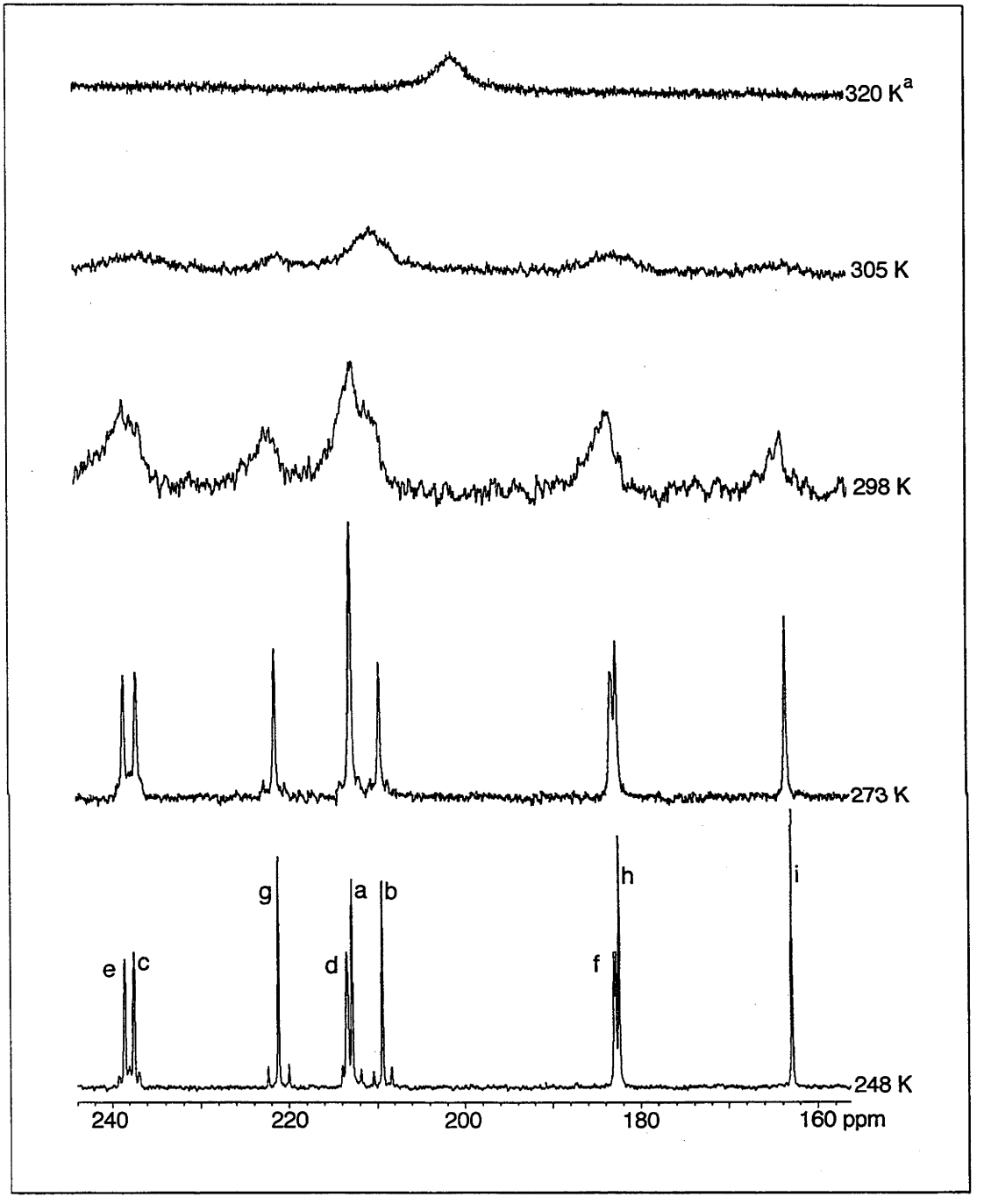
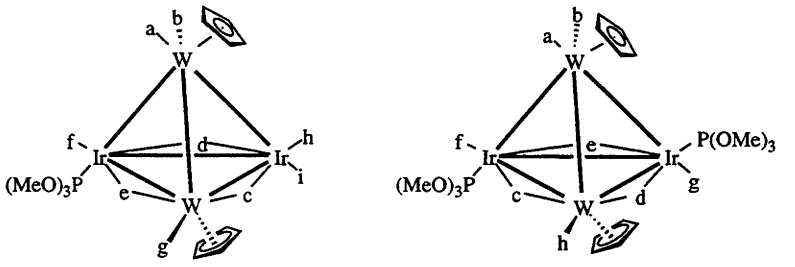


Figure 3.2.62. Variable temperature ^{13}C NMR spectroscopic study of $[Cp_2W_2Ir_2(\mu\text{-}CO)_3(CO)_6\{P(OMe)_3\}]$ (**35**) in CD_2Cl_2.



$[Cp_2W_2Ir_2(\mu\text{-}CO)_3(CO)_6\{P(OMe)_3\}]$ (35)
axial phosphite, axial Cp, apical Cp

$[Cp_2W_2Ir_2(\mu\text{-}CO)_3(CO)_5\{P(OMe)_3\}_2]$ (36)
radial phosphite, axial phosphite, axial Cp, apical Cp

Figure 3.2.63. Configurations of $[Cp_2W_2Ir_2(\mu\text{-}CO)_3(CO)_{7-n}\{P(OMe)_3\}_n]$ [n = 1 or 2]

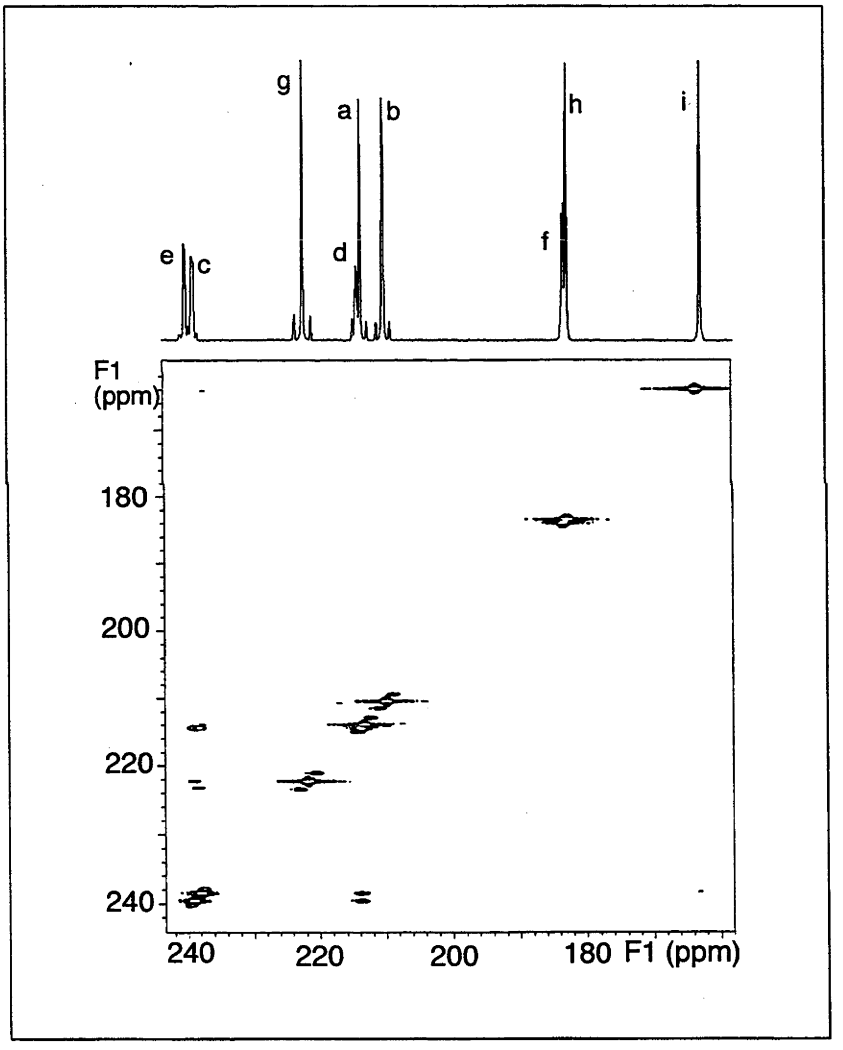


Figure 3.2.64. ^{13}C NMR COSY spectrum of $[Cp_2W_2Ir_2(\mu\text{-}CO)_3(CO)_6\{P(OMe)_3\}]$ (**35**) in CD_2Cl_2 at 248 K.

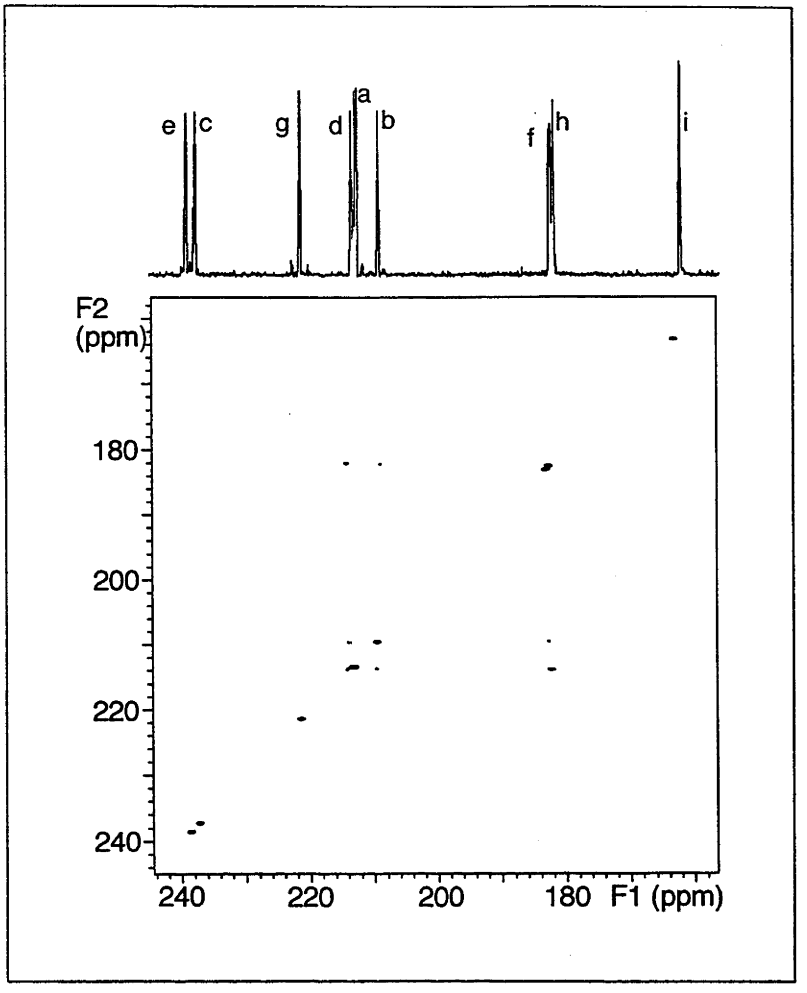


Figure 3.2.65. ^{13}C NMR EXSY spectrum of $[Cp_2W_2Ir_2(\mu\text{-}CO)_3(CO)_6\{P(OMe)_3\}]$ (**35**) in CD_2Cl_2 at 273 K.

Ligand fluxionality commences upon warming the solution. A $^{13}C\{^1H\}$-EXSY study of **35** at 273 K is shown in Figure 3.2.65. and reveals site exchanges corresponding to h ↔ b or a, h ↔ d and b or a ↔ d. This sequence of carbonyl exchanges has been identified previously in the analogous PMe_3-substituted cluster (**33b**) (Section *3.2.7.*). Exchanges are consistent with assignment of the signal at 209.3 ppm to carbonyl b, with ligand mobility about the $[WIr_2]$ face. The carbonyl distribution in the intermediate is reminiscent of the D_{2d} species implicated in an $[M_4(CO)_{12}]$ exchange pathway [7] (Scheme 3.2.5.). Carbonyl f is attached to the electron-rich phosphite-ligated iridium and, as described for **33b**, is expected to have a higher activation energy for participation in an exchange of this type.

Unlike other *P*-substituted derivatives of **3**, the NMR spectra of **36** reveal the carbonyls are undergoing very slow exchange; at room temperature, resonances corresponding to the configuration of **36** shown in Figure 3.2.63. can be identified. Raising the temperature results in broadening of the resonances but the coalescence point could not be reached due to slow decomposition of the cluster in solution above 303 K. The carbonyl resonances in the ^{13}C NMR spectrum of **36** (Figure 3.2.66.) are very similar to those of an isomer of $[Cp_2W_2Ir_2(\mu\text{-}CO)_3(CO)_5(PMe_3)_2]$ (**34**), assigned a radial, diaxial, apical configuration with the Cp inclined to a $W_2Ir(P_{rad})$ face, in agreement with the structural characterization of **36**. A ^1H-^1H NOESY experiment of **36** at 298 K indicates the presence of a crosspeak between the signals at 4.53 ppm and 3.75 ppm, corresponding to through space interactions between the apically-disposed Cp (4.53 ppm) and the radially-ligating $P(OMe)_3$ (3.75 ppm).

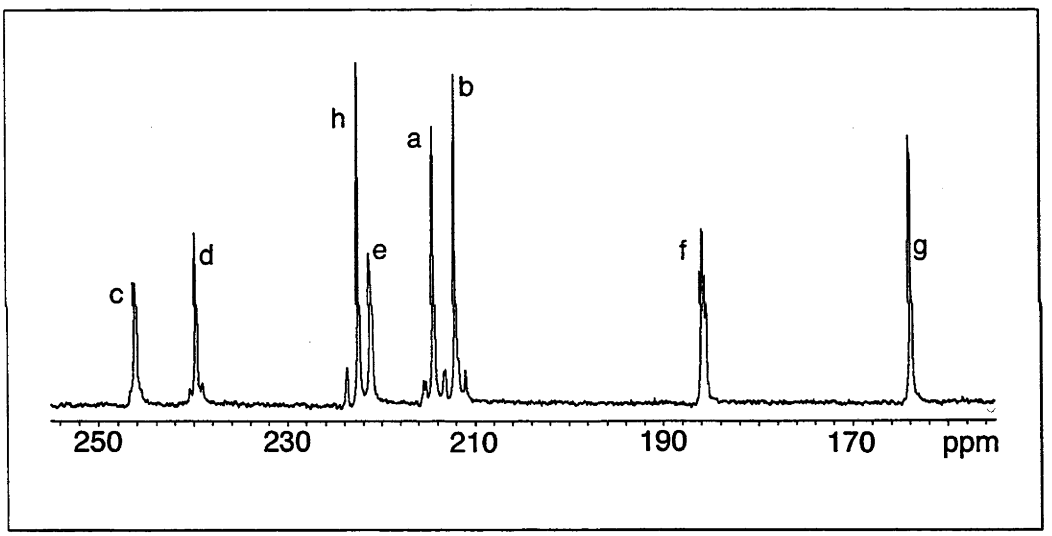


Figure 3.2.66. ^{13}C NMR spectroscopic study of $[Cp_2W_2Ir_2(\mu\text{-}CO)_3(CO)_5\{P(OMe)_3\}_2]$ (**36**) in CD_2Cl_2.

All resonances can therefore be assigned by comparison with the literature data for the trimethylphosphine-containing analogue. ^{183}W-coupled satellites in the ^{13}C NMR spectrum of **36** are observed for the resonances at 246.0 (c, 70 Hz), 239.0 (d, 80 Hz), 222.7 (h, 185 Hz), 214.2 (a or b, 172 Hz) and 212.0 ppm (b or a, 158 Hz), which identifies the W-Ir bridging carbonyls, the radially-ligating W-bound carbonyl and the apical carbonyls. Assignment of the remaining signals at 220.5 (e), 185.8 [f, $^2J_{CP}$ = 40 Hz, $^3J_{CP}$ = 8 Hz] and 164.3 ppm [g, $^2J_{CP}$ = 42 Hz] is straightforward due to the *cis* and *trans* coupling observed at carbonyl f, and the *cis* coupling at carbonyl g. ^{183}W-coupled satellites are also observed in the ^{31}P NMR spectrum of **36**. Both phosphites are effectively *trans* to a tungsten atom; the $^2J_{WP}$ coupling not seen in the NMR spectra of related phosphine-substituted clusters is attributed, as above, to the shorter Ir-

P bonds in **36**, and the improved resolution of the ^{31}P NMR spectrum. Ligand fluxionality for **36** commences upon warming the solution, but due to complications arising from the decomposition of **36** to give **19** and other products, an appropriate exchange mechanism was not able to be proposed for this cluster.

Discussion

The geometries adopted by **35** and **36** can be compared with those of related derivatives from the tungsten-triiridium and tetrairidium systems. Trisubstituted derivatives of **1** usually adopt diradial, axial geometries with monodentate ligands (radial, diaxial ligation is preferred with bidentate ligands), whereas the results in Section *3.2-4.* reveals trisubstituted derivatives of **2** (i.e. bis-phosphine/phosphite derivatives) adopt radial, diaxial or triradial coordination modes. Trisubstituted (mono-phosphine) derivatives of **3** adopt diaxial, apical coordination geometries ($[Cp_2W_2Ir_2(\mu\text{-}CO)_3(CO)_6(PPh_3)]$ **31**, two isomers; $[Cp_2W_2Ir_2(\mu\text{-}CO)_3(CO)_6(PMe_3)]$ **33**, one configuration); the coordination geometry and carbonyl exchange pathway proposed for **35** is analogous to that of **33**. Tetrasubstituted derivatives of **1**, **2** and **3** most frequently adopt radial, diaxial, apical ligation (with the apical ligand oriented toward the axial substituents) to minimize unfavourable steric interactions. One isomer of **34** has also been assigned a radial, diaxial, apical configuration, but with rotation at the tungsten atom, placing the Cp over a radial phosphine-containing W_2Ir face; this configuration is also seen with **36**, and it seems that this configuration becomes increasingly accessible with small ligands for which steric considerations are less important.

3.2.9. NMR studies of dppm and dppe derivatives of $[Cp_2W_2Ir_2(CO)_{10}]$ (3)

The syntheses and characterization of the ligand-substituted derivatives $[Cp_2W_2Ir_2(\mu\text{-}CO)_3(\mu\text{-}dppm)(CO)_5]$ and $[Cp_2W_2Ir_2(\mu\text{-}CO)_3(\mu\text{-}dppe)(CO)_5]$ were reported in Chapter 2. This Section considers the configurations of these products, and their ligand fluxionality.

NMR spectra of $[Cp_2W_2Ir_2(\mu\text{-}CO)_3(\mu\text{-}dppm)(CO)_5]$ (37)

The ^{31}P NMR spectrum of **37** in CD_2Cl_2 measured at 273 K shows two broad signals at -22.1 and -45.9 ppm which coalesce at 303 K ($CDCl_3$, Figure 3.2.67.). On cooling to 213 K (in CD_2Cl_2), the signals are resolved into two doublets. Similarly, the ^{13}C NMR spectrum of **37** measured at 318 K contains a broad signal which decoalesces at 298 K (Figure 3.2.68.). At 213 K, the fluxional processes are sufficiently slow to distinguish eight resonances of equal intensity, corresponding to one configuration in solution (Figure 3.2.69.). The presence of

carbonyl resonances in the bridging carbonyl region (254.4, 245.5 ppm) exclude the possibility of an all-terminal carbonyl geometry. W-bound terminal carbonyls have much larger $^1J_{WC}$ coupling (160 - 190 Hz) than W-bound bridging carbonyls (70 - 100 Hz). The presence of three resonances in the W-bound terminal carbonyl region with large coupling (224.0 ppm, $^1J_{WC}$ 191 Hz; 214.0 ppm, $^1J_{WC}$ 156 Hz; 211.9 ppm, $^1J_{WC}$ 158 Hz) excludes a carbonyl-bridged W_2Ir basal plane (for which only two W-bound terminal carbonyls would be observed). This configuration must therefore possess a WIr_2 basal plane, with the diphosphine coordinated to the iridium atoms. The lack of carbonyl resonances in the Ir axial/apical CO region is consistent with the diphosphine bridging the Ir-Ir linkage and diaxially coordinated. The remaining ambiguities concern the location of the W-bound cyclopentadienyl ligands. The apical cyclopentadienyl ligand cannot be located inclined to the $W_{ap}Ir_2$ face as this renders the phosphorus atoms equivalent, in conflict with the ^{31}P NMR spectrum at 213 K. The apical Cp must therefore be inclined to either of the equivalent W_2Ir faces. The basal Cp can in principle be radially or axially ligated. A radial Cp would result in sterically unfavourable Cp-Cp interactions which in this case would result in the apical Cp being located over the $W_{ap}Ir_2$ face, a possibility already discounted. An axial site for this Cp ligand is therefore more likely. The configuration of **37** is shown in Figure 3.2.72(a). It is significant that the X-ray structural study of **37**, described in Chapter 2, but not concluded satisfactorily, has shown one of the cyclopentadienyl ligands to be axially-coordinated. With this information, it is then possible to assign the spectrum of **37**. At 213 K, resonances are observed at 254.4 (c or d), 245.5 (d or c) , 226.2 (e), 224.0 (h), 214.0 (a or b), 211.9 (b or a), 188.5 (f or g) and 187.9 (g or f) ppm, all of relative intensity 1, with the signals at 254.4, 245.5, 224.0, 214.0 and 211.9 ppm showing the expected satellite coupling to ^{183}W.

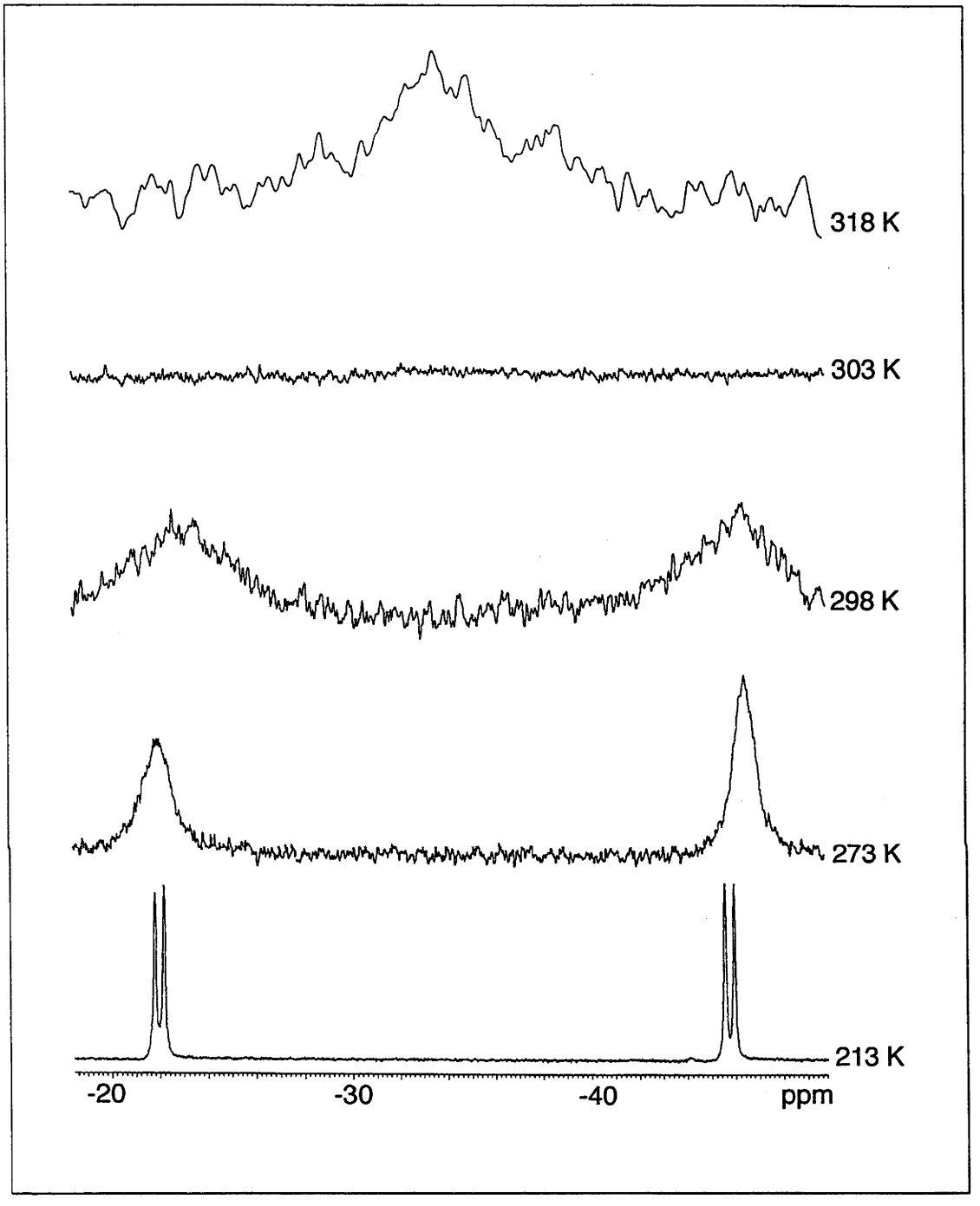


Figure 3.2.67. Variable temperature ^{31}P NMR spectroscopic study of $[Cp_2W_2Ir_2(\mu\text{-}CO)_3(\mu\text{-}dppm)(CO)_5]$ (**37**) in CD_2Cl_2.

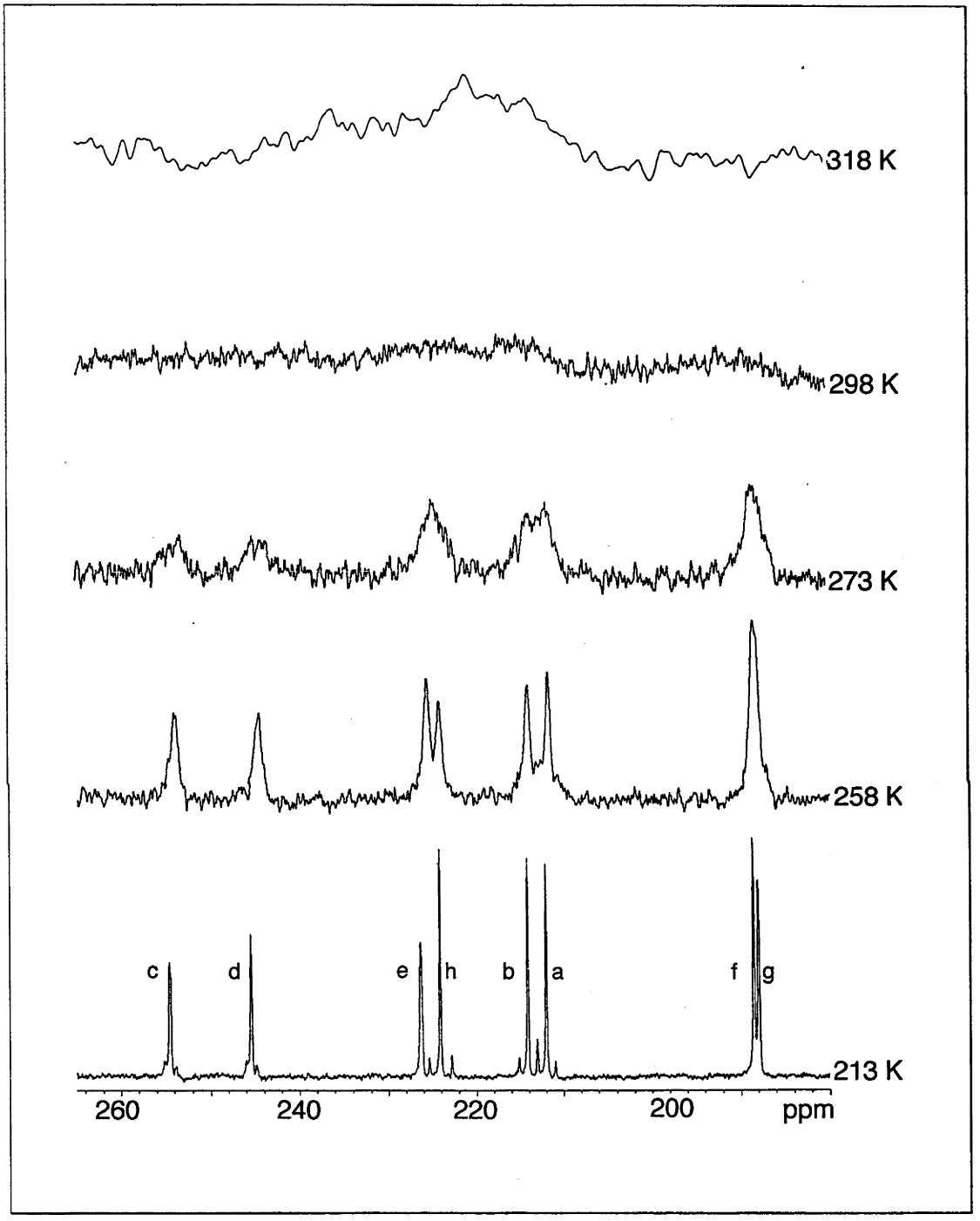


Figure 3.2.68. Variable temperature ^{13}C NMR spectroscopic study of $[Cp_2W_2Ir_2(\mu\text{-}CO)_3(\mu\text{-}dppm)(CO)_5]$ (**37**) in CD_2Cl_2.

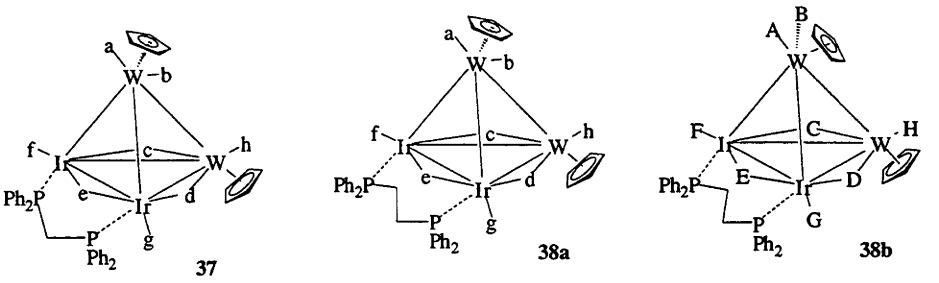
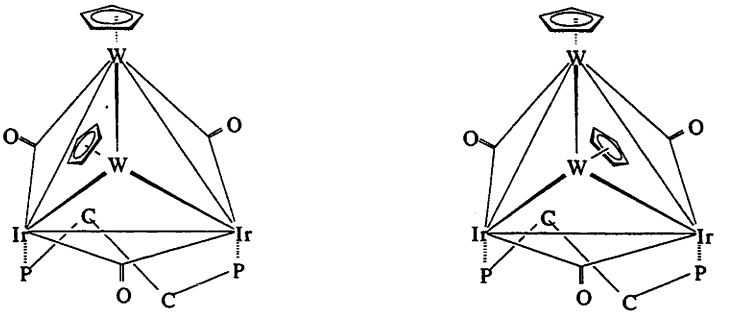


Figure 3.2.69. (a) Configuration of $[CpWIr_3(\mu\text{-}CO)_3(\mu\text{-}dppm)(CO)_5$ **37** and isomers of $[CpWIr_3(\mu\text{-}CO)_3(\mu\text{-}dppe)(CO)_5]$ **38**.



(b) Projection of isomers **38a** and **38b** onto the basal WIr_2 plane. Phenyls, terminal carbonyls and ethylene protons omitted for clarity

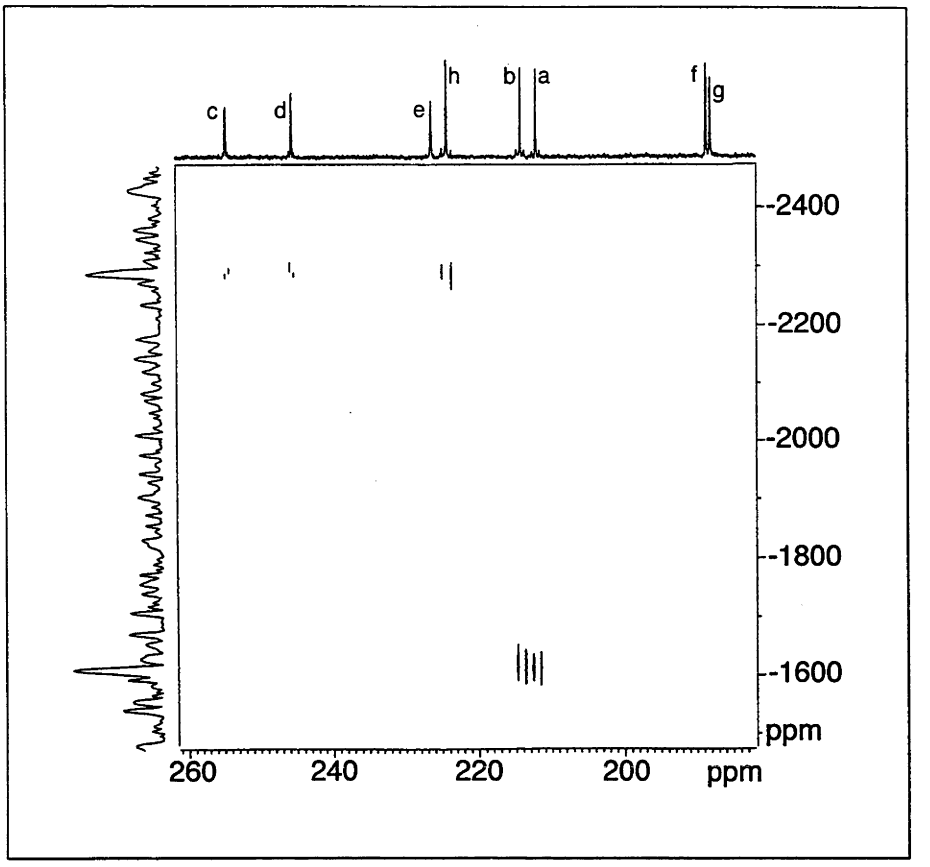


Figure 3.2.70. ^{183}W-^{13}C correlation NMR spectroscopic study of $[Cp_2W_2Ir_2(\mu\text{-}CO)_3(\mu\text{-}dppm)(CO)_5]$ (**37**) in CD_2Cl_2.

In the figures, an arbitrary assignment has been adopted for the carbonyl resonances which cannot be unambiguously assigned, to enhance clarity of presentation; a definitive assignment of the ambiguous resonances is unnecessary, as it does not affect ligand fluxionality discussion. In solution, raising the temperature results in equivalence of the phosphorus atoms (Figure 3.2.70.). In principle, this could arise from either (i) a "waggling" of the apical $CpW(CO)_2$ group, so as to place the apical cyclopentadienyl ligand over both W_2Ir faces, or (ii) inclining the apical Cp to the WIr_2 face, but the latter configures the two Cp ligands *trans* to each other; this configuration has not been observed in solution across the range of ditungsten-diiridium complexes studied thus far (clusters **31** – **36**) as it is unfavourable on electronic grounds and the preference of Cp ligands to avoid a mutually *trans* arrangement in these derivatives has been noted. These data cannot distinguish between apical $[CpW(CO)_2]$ "waggling" or complete tripodal rotation. As the configuration of **37** has been defined, it was of interest to determine whether ^{183}W chemical shifts could provide useful spectroscopic information. ^{183}W-^{13}C and ^{183}W-^{1}H correlation experiments were used to identify the coupling (^1J for ^{183}W-^{13}C, ^2J and ^3J for ^{183}W-^{1}H experiments) in **37** (Figure 3.2.70. and 3.2.71., respectively). There is a considerable difference in chemical shifts between apical tungsten atoms (-1613 ppm, CD_2Cl_2) and tungsten atoms ligated by cyclopentadienyl groups in axial

sites (-2289 ppm, CD_2Cl_2). ^{183}W data for a well-defined basal tungsten atom with a radailly-ligated cyclopentadienyl group is needed to judge whether or not tungsten NMR will be a useful technique to assign configurations of clusters of this type.

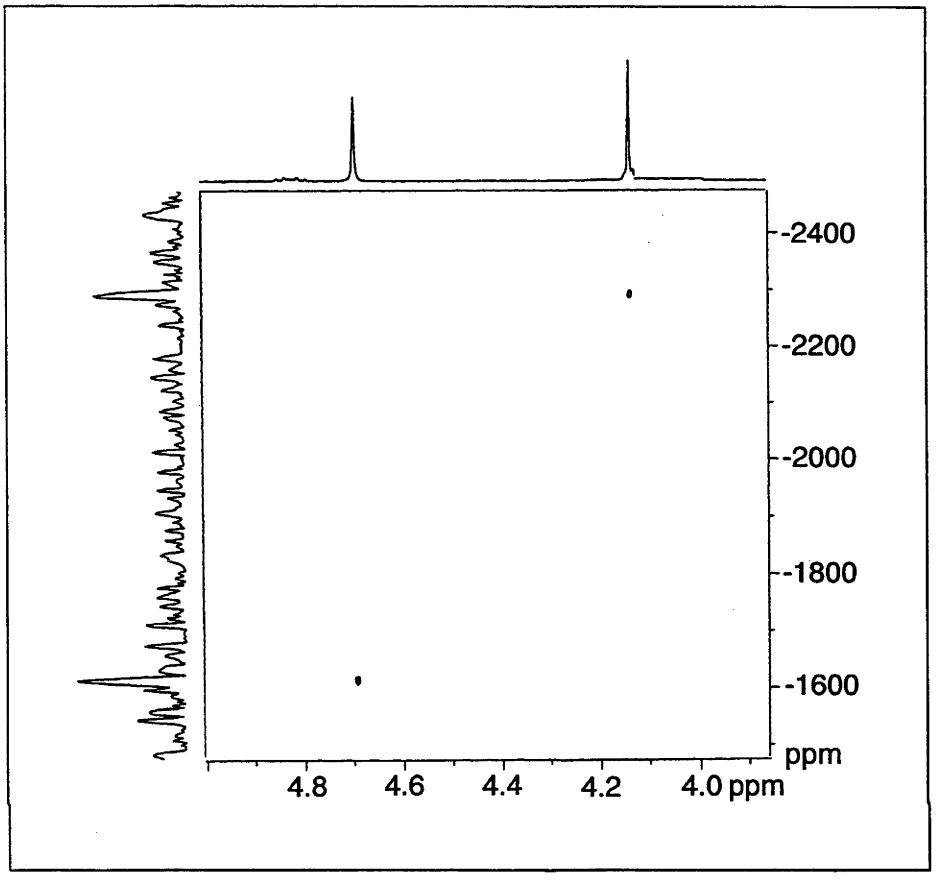


Figure 3.2.71. ^{183}W-^{1}H correlation NMR spectroscopic study of $[Cp_2W_2Ir_2(\mu\text{-}CO)_3(\mu\text{-}dppm)(CO)_5]$ (**37**) in CD_2Cl_2.

NMR spectra of $[Cp_2W_2Ir_2(\mu\text{-}CO)_3(\mu\text{-}dppe)(CO)_5]$ (38)

Cluster **38** is also fluxional on the NMR timescale, with scrambling commencing above 213 K in CD_2Cl_2. However, it slowly decomposes above 318 K, preventing a complete study by variable temperature NMR. In the ^{31}P and ^{13}C spectra of **38** in CD_2Cl_2 (Figures 3.2.72. and 3.2.73., respectively), all exchange processes are stopped at 213 K. At this temperature four resonances are observed in the ^{31}P NMR spectrum corresponding to the presence of two configurations. The ^{13}C NMR spectrum at this temperature contains thirteen resonances, with the upfield resonance integrating as four coincident resonances, two from each configuration. As with **37**, the presence of carbonyl resonances in the bridging carbonyl region (254.5, 242.9 ppm major isomer; 250.5, 246.9 ppm minor isomer) exclude the possibility of an all-terminal carbonyl geometry, and the lack of carbonyl resonances in the Ir axial/apical region is

consistent with a WIr_2 basal plane and diaxially bridging dppe ligands. The location of the cyclopentadienyl ligands is, as above, the remaining ambiguity but, following the arguments above, an apical Cp, axial Cp geometry is likely for both isomers, with the apical Cp inclined to the W_2Ir faces. The NMR spectra suggest the presence of the two isomers displayed in Figure 3.2.69(a). The isomers **38a** and **38b** are similar, having the Cp ligand inclined to the W_2Ir faces. Isomers **38a** and **38b** differ in the conformation of the diphosphine backbone with respect to the location of the cyclopentadienyl ligands; isomer **38a** has the methylene attached to the phosphorus which is ligated to the iridium in the W_2Ir face containing the cyclopentadienyl ligand located "out" rather than "in", with respect to the basal plane: see Figure 3.2.68(b).

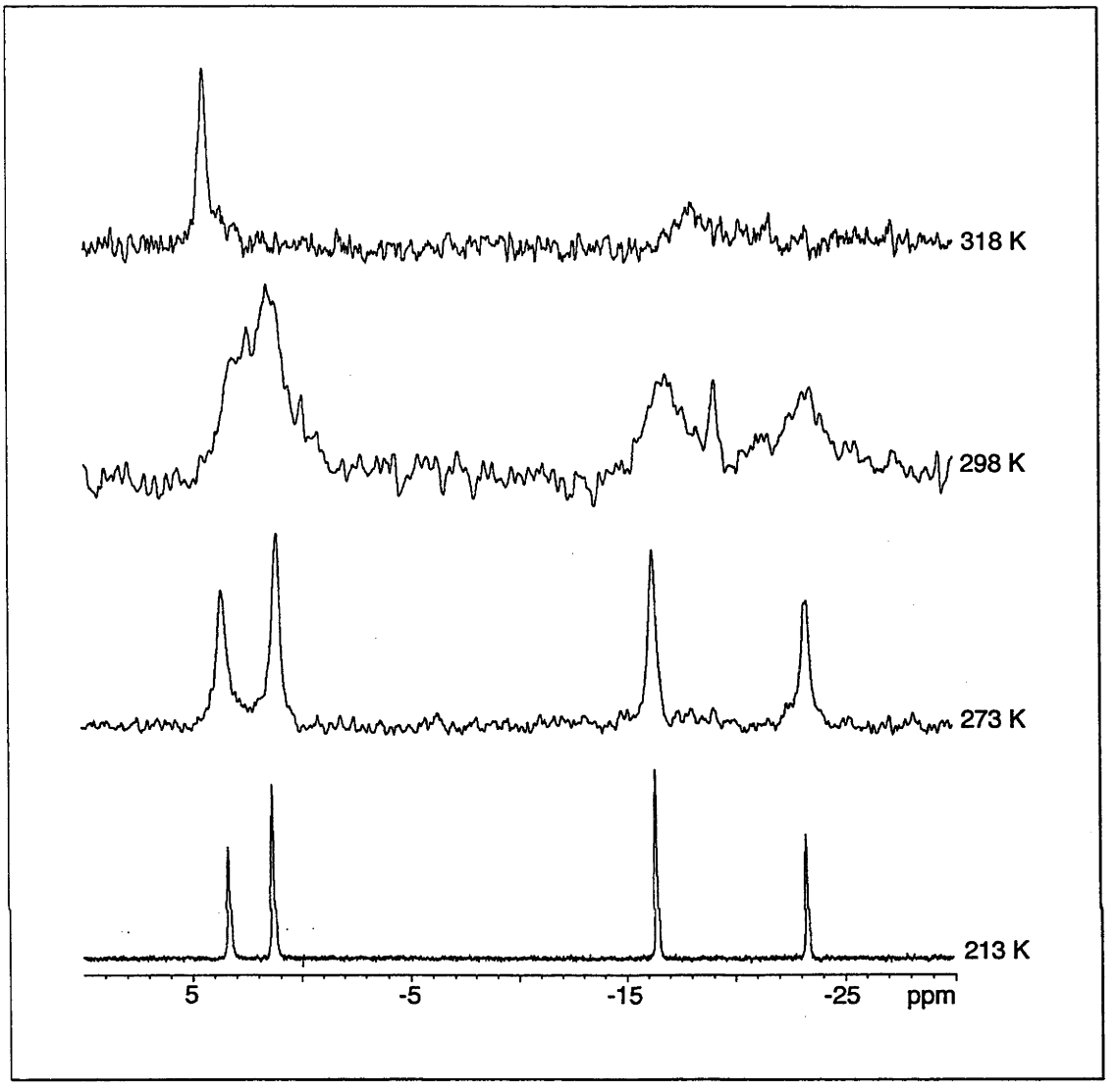


Figure 3.2.72. Variable temperature ^{31}P NMR spectroscopic study of $[Cp_2W_2Ir_2(\mu\text{-}CO)_3(\mu\text{-}dppe)(CO)_5]$ (**38**) in CD_2Cl_2.

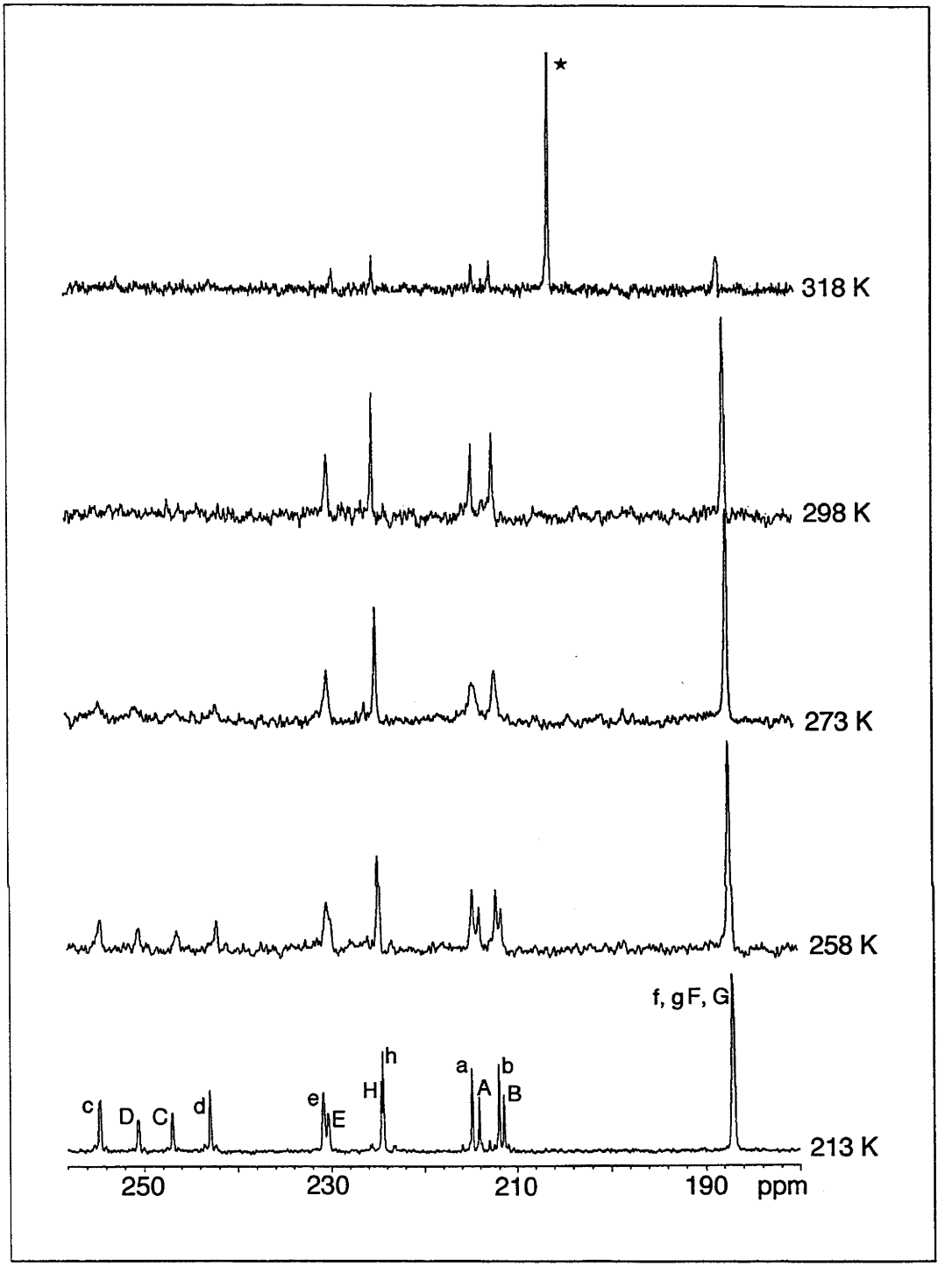


Figure 3.2.73. Variable temperature ^{13}C NMR spectroscopic study of $[Cp_2W_2Ir_2(\mu\text{-}CO)_3(\mu\text{-}dppe)(CO)_5]$ (**38**) in CD_2Cl_2 ($^a \equiv CDCl_3$)

Ligand fluxionality commences upon warming the mixture of isomers of **38**. A ^{13}C-{^1H} EXSY study at 208 K is shown in Figure 3.2.74. A contour plot of **38** reveals site exchanges at 208 K corresponding to c or d ↔ D or C, d or c ↔ C or D, a or b ↔ A or B and b or a ↔ B or A, suggestive of interconversion of **38a** and **38b**. In principle, flexing of the diphosphine backbone, a "waggling" of the $[CpW(CO)_2]$ group so as to place the Cp ligand over both W_2Ir faces, or complete tripodal rotation will all interconvert **38a** and **38b**. However, diphosphine

backbone flexing has been shown to be a very high energy process in related tetrairidium clusters; for phosphines with variable oligomethylene backbone, flexing as proposed here does not become important until the backbone is lengthened to that of a butylene linkage.[21] Diphosphine backbone flexing as the source of the low energy process is therefore rejected. It may also be significant that the processes rendering the phosphorus atoms equivalent occur at a similar temperature for **37** and **38** which, though not conclusive, suggests the same process is operative. Complete tripodal rotation is unlikely, as the apical cyclopentadienyl ligand would be placed over the diphosphine - containing face, and *trans* to the basal cyclopentadienyl ligand, an electronically unfavourable configuration (see above). The EXSY data are thus consistent with a "waggling" of the apical [$CpW(CO)_2$] group as the lowest energy process, although once again complete tripodal rotation cannot be excluded. For clusters such as these with triaxial, apical geometries, a second process, exchange via a "merry-go-round" of the basal carbonyls, could be expected. This process has been well-documented in tetrairidium clusters with tripodal face-capping ligands.[13,20,22,32] Surprisingly, this was not observed up to the temperature at which the compound begins to decompose. Tripodal ligands are held in a fixed geometric relationship which is truly triaxial, but a bidentate ligand and monodentate ligand occupying axial sites would be expected to be displaced somewhat to minimize steric repulsion, and a consequent "semiaxial" ligand would raise the energy barrier for the putative "merry-go-round" process. A number of derivatives with cyclopentadienyl ligands in formally axial, but effectively semiaxial, sites have been structurally characterized; significantly, no examples with a "merry-go-round" fluxional process have thus far been identified.

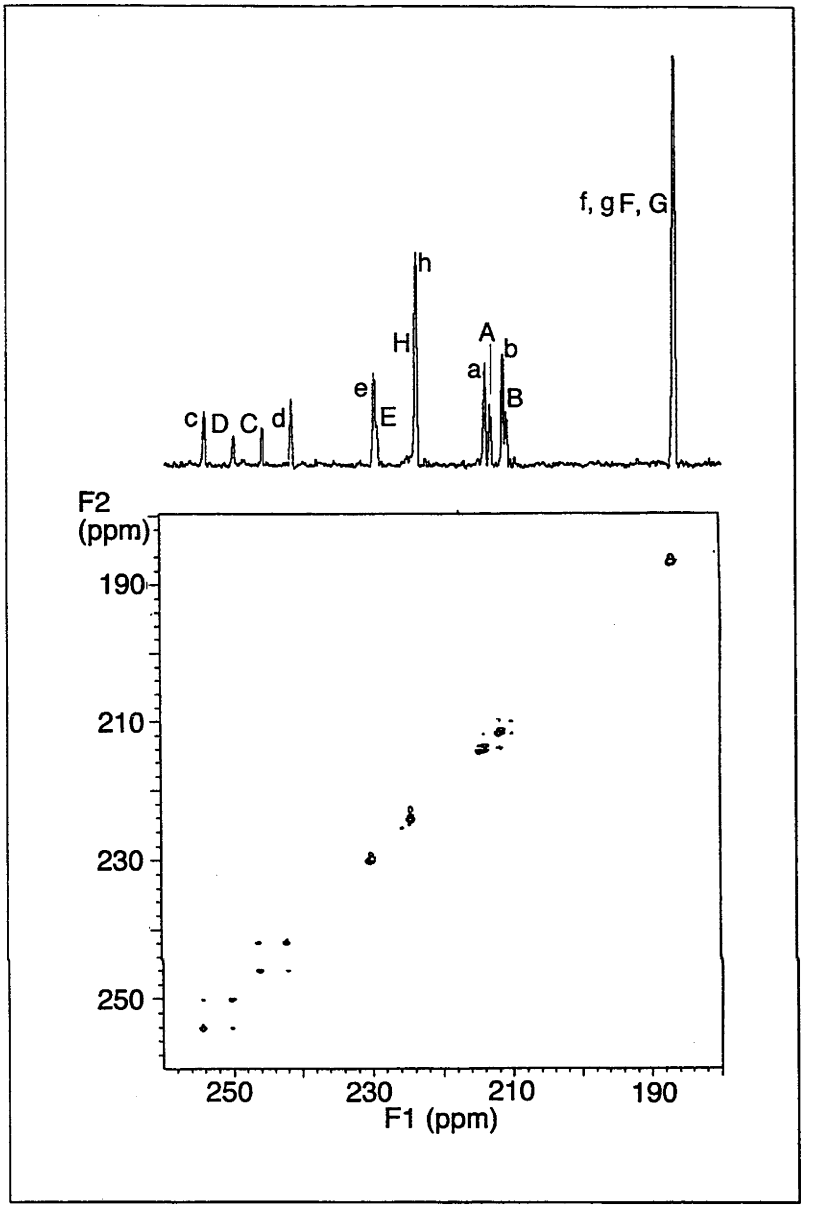


Figure 3.2.74. ^{13}C NMR EXSY spectrum of $[Cp_2W_2Ir_2(\mu\text{-}CO)_3(\mu\text{-}dppe)(CO)_5]$ (**38**) in CD_2Cl_2 at 233 K.

2.2.10. Discussion and Summary

The coordination geometries of the tungsten-iridium clusters **4-24** and **31-38** were assigned utilizing a combination of ^1H, ^{13}C and ^{31}P NMR spectroscopies and 2D techniques including ^{13}C-^{13}C correlation experiments, ^1H-^1H NOESY experiments, ^{31}P-^{13}C correlation experiments, ^{183}W-^{13}C correlation experiments, ^{183}W-^1H correlation experiments, ^{31}P-^1H HSQC experiments and ^1H-^{31}P-^{13}C triple resonance experiments. In the ^1H, ^{13}C and ^{31}P NMR spectra

of the analogous tetrairidium system the chemical shifts of the ligands have previously[26] been reported to decrease in the positional sequence:

bridging ≥ radial ≥ axial ≈ apical

Extending this to the tungsten-iridium mixed-metal regime afforded the ^{13}C NMR chemical shift sequence:

W-W bridging CO ≥ W-Ir bridging CO ≥ Ir-Ir bridging CO ≈ W terminal CO ≥ Ir radial CO ≥ Ir axial CO ≈ Ir apical CO

Although not as well defined, the above chemical shift sequence can be further divided into

W radial CO ≥ W axial CO ≥ W apical CO

The chemical shift sequence in the ^{31}P NMR spectra remained as:

Ir radial *P*-donor ligand ≥ Ir axial *P*-donor ligand ≈ Ir apical *P*-donor ligand

A summary of the results of the ^{13}C and ^{31}P NMR chemical shifts for the tungsten-triirdium and ditungsten-diiridium clusters investigated is given in Figures 3.2.75.-3.2.78. It should be noted that the ^{31}P NMR chemical shift sequence for the ditungsten-diiridium clusters **31** - **38** is not as well-defined as those of the related tungsten-triiridium or tetrairidium compounds. This is possibly ascribed to the preference of the derivatives of **3** for a WIr_2 basal plane, one cyclopentadienyl ligand in the derivatives always being apically substituted. A considerable difference in chemical shift of carbonyls in the proximity of the WMIr (M = W, Ir) face over which the apical Cp ligand inclines has been noted. This anomaly in the chemical shift sequence may extend to the ^{31}P NMR data.

A comparison between the different coordination geometries identified for the derivatives of **1**, **2** and **3** is useful. A summary of the coordination geometries of the configurations of the *P*-donor ligand substituted derivatives of **2** and **3** reported in this Chapter are shown in Figures 3.2.79. and 3.2.80., respectively.

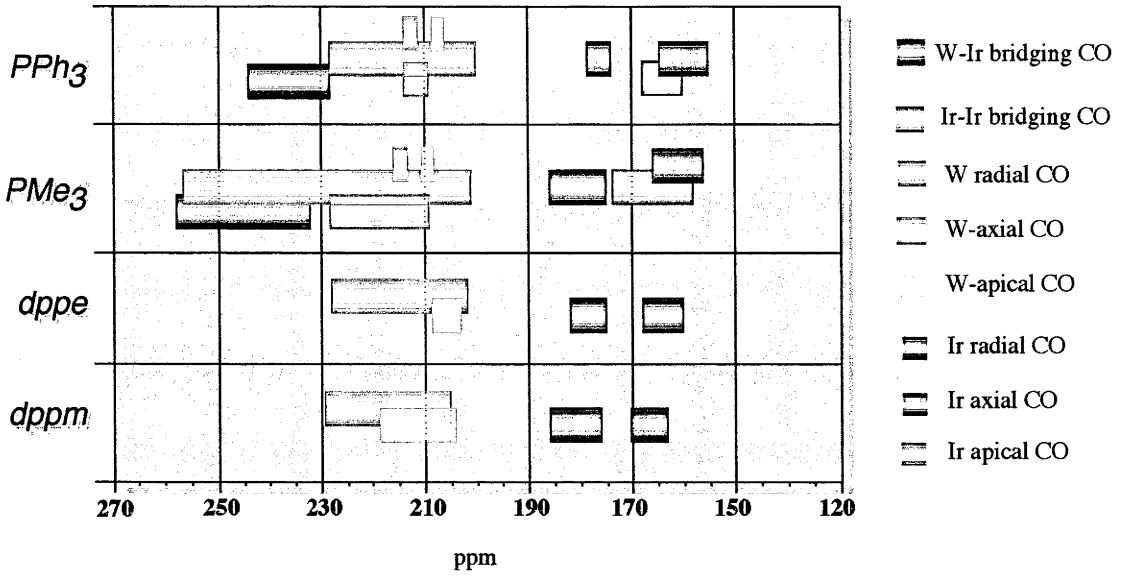


Figure 3.2.75. ^{13}C NMR chemical shifts for carbonyl ligands on derivatives of $[CpWIr_3(CO)_{11}]$ (**2**)

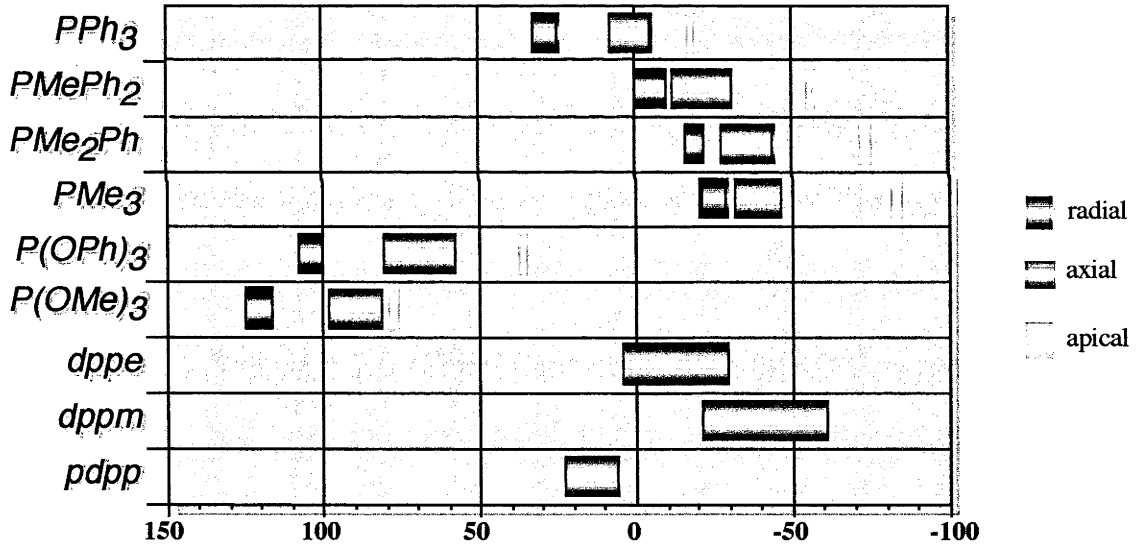


Figure 3.2.75. ^{131}P NMR chemical shifts for *P*-donor ligands on derivatives of $[CpWIr_3(CO)_{11}]$ (**2**)

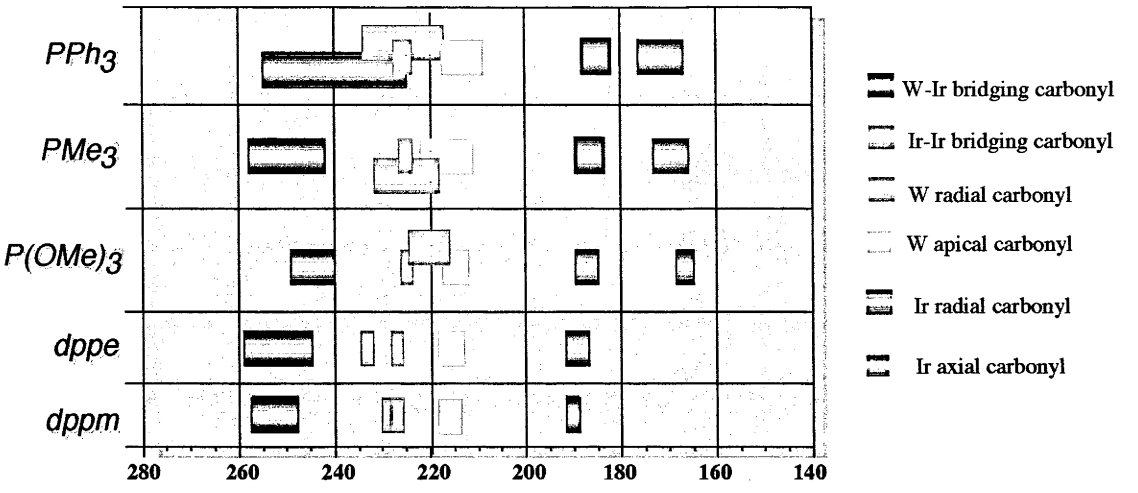


Figure 3.2.77. ^{13}C NMR chemical shifts for carbonyl ligands on derivatives of $[Cp_2W_2Ir_2(CO)_{10}]$ (**3**)

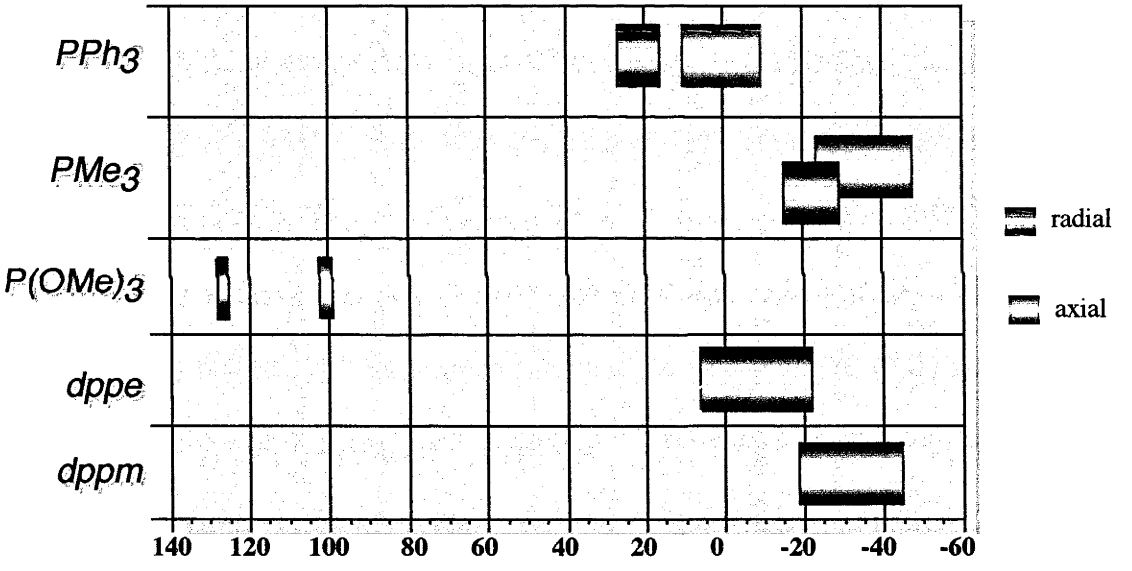
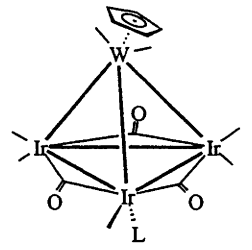


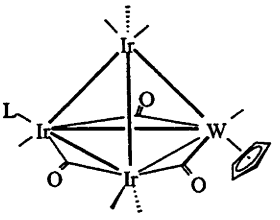
Figure 3.2.78. ^{13}C chemical shifts for *P*-donor ligands on derivatives of $[Cp_2W_2Ir_2(CO)_{10}]$ (**2**)

One configuration of all of the bis-substituted derivatives of **2** investigated was found to have an axial *P*-donor ligand, apical Cp coordination geometry. This geometry has not been seen in the tetrairidium system (Table 2.1.1.). A "merry-go-round" carbonyl exchange mechanism was proposed from exchange spectroscopy (EXSY) for the PPh_3- and PMe_3-ligated derivatives with this geometry (**4a** and **7a**, respectively). One configuration of all of the bis-substituted derivatives of **2** [except the $P(OMe)_3$-substituted derivative **19b**] were assigned radial *P*-donor ligand, axial Cp coordination geometry. A suitable exchange mechanism could not be proposed for either the PPh_3- or PMe_3-ligated derivatives (**4b** and **7b**, respectively). A derivative of **1** ($[Ir_4(\mu\text{-}CO)_3(CO)_7(PMePh_2)_2]$, Table 2.1.1.) with radial, axial geometry has been reported as exchanging via a synchronous change of basal face mechanism.[14] Perhaps not surprisingly, a diaxial coordination geometry was proposed (and confirmed by an X-ray study) for $[CpWIr_3(\mu\text{-}CO)_3(CO)_7[P(OMe)_3]$ (**19b**); this geometry was also proposed for derivatives of **1** only where the entering ligand has a small cone angle (as in that of **19b**). Complexes $[CpWIr_3(\mu\text{-}CO)_3(CO)_7(L)]$ containing the sterically more demanding ligands [L = PPh_3 (**4c**), $PMePh_2$ (**10c**) and $P(OPh)_3$ (**16c**)] were proposed to exist in a third configuration with an axial *P*-donor ligand, radial Cp coordination geometry.

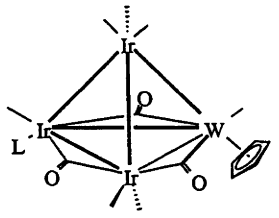
Trisubstituted derivatives of **1** usually exist with diradial, axial or radial, diaxial coordination geometries. Derivatives of **2** (**5b**, **8b**, **11b**, **14b**, **17** and **20**) were also assigned radial, axial *P*-donor ligand, axial Cp (radial, diaxial) coordination geometries, but existed in insufficient amounts for an exchange mechanism to be proposed. A novel diradial phosphine, radial Cp (triradial) configuration, not seen thus far in the tetrairidium system, was proposed for the bis-phosphine substituted derivatives (**5a**, **8a**, **11a**, **14a**). Two exchange pathways were proposed for the derivatives **5a** and **8a**, one providing an interesting analogue of the D_{2d}-symmetry intermediate implicated in the fluxionality of derivatives of **1**. The complexes $[CpWIr_3(\mu\text{-}CO)_3(\mu\text{-}L)(CO)_6]$ [L = dppe (**22**), dppm (**23**)] were found to exist as three (**22**) or two (**23**) configurations with diaxial bridging diphosphine, apical Cp (diaxial, apical) coordination geometries; again, these have not been seen in the tetrairidium system. Carbonyl exchange proceeded to interconvert the configurations by way of a "waggling" of the $[CpW(CO)_2]$ group so as to place the Cp ligand over both WIr_2 faces remote from the diphosphine, followed by a tripodal rotation at the tungsten apex, along with a "merry-go-round" of carbonyls in the basal plane. Trisubstituted derivatives of **3** were found to exist as different (**31**, 2; **33**, 1; **35**, 1) configurations of axial *P*-donor ligand, axial Cp, apical Cp (diaxial, apical) coordination



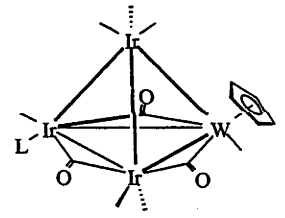
axial *P*-donor ligand (L), apical Cp:
$[CpWIr_3(\mu\text{-}CO)_3(CO)_7(PPh_3)]$ **4a**
$[CpWIr_3(\mu\text{-}CO)_3(CO)_7(PMePh_2)]$ **10a**
$[CpWIr_3(\mu\text{-}CO)_3(CO)_7(PMe_2Ph)]$ **13a**
$[CpWIr_3(\mu\text{-}CO)_3(CO)_7(PMe_3)]$ **7a**
$[CpWIr_3(\mu\text{-}CO)_3(CO)_7\{P(OPh)_3\}]$ **16a**
$[CpWIr_3(\mu\text{-}CO)_3(CO)_7(P(OMe_3\}]$ **19a**



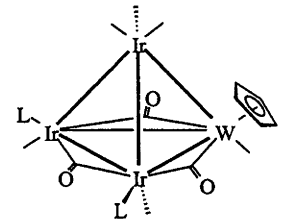
radial *P*-donor ligand (L), axial Cp:
$[CpWIr_3(\mu\text{-}CO)_3(CO)_7(PPh_3)]$ **4b**
$[CpWIr_3(\mu\text{-}CO)_3(CO)_7(PMePh_2)]$ **10b**
$[CpWIr_3(\mu\text{-}CO)_3(CO)_7(PMe_2Ph)]$ **13b**
$[CpWIr_3(\mu\text{-}CO)_3(CO)_7(PMe_3)]$ **7b**
$[CpWIr_3(\mu\text{-}CO)_3(CO)_7\{P(OPh)_3\}]$ **16b**



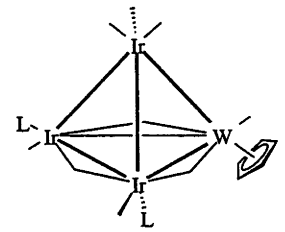
axial *P*-donor ligand (L), axial Cp:
$[CpWIr_3(\mu\text{-}CO)_3(CO)_7(P(OMe_3\}]$ **19b**



axial *P*-donor ligand (L), radial Cp:
$[CpWIr_3(\mu\text{-}CO)_3(CO)_7(PPh_3)]$ **4c**
$[CpWIr_3(\mu\text{-}CO)_3(CO)_7(PMePh_2)]$ **10c**
$[CpWIr_3(\mu\text{-}CO)_3(CO)_7\{P(OPh)_3\}]$ **16c**

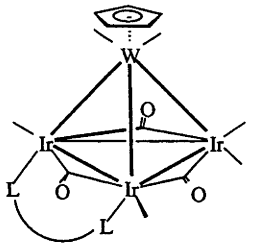


diradial *P*-donor ligands (L), radial Cp:
$[CpWIr_3(\mu\text{-}CO)_3(CO)_6(PPh_3)_2]$ **5a**
$[CpWIr_3(\mu\text{-}CO)_3(CO)_6(PMePh_2)]$ **11a**
$[CpWIr_3(\mu\text{-}CO)_3(CO)_6(PMe_2Ph)]$ **14a**
$[CpWIr_3(\mu\text{-}CO)_3(CO)_6(PMe_3)]$ **8a**

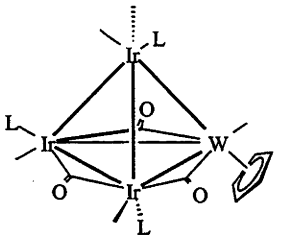


radial, axial *P*-donor ligands (L), axial Cp
$[CpWIr_3(\mu\text{-}CO)_3(CO)_6(PPh_3)_2]$ **5b**
$[CpWIr_3(\mu\text{-}CO)_3(CO)_6(PMePh_2)_2]$ **11b**
$[CpWIr_3(\mu\text{-}CO)_3(CO)_6(PMe_2Ph)_2]$ **14b**
$[CpWIr_3(\mu\text{-}CO)_3(CO)_6(PMe_3)_2]$ **8b**
$[CpWIr_3(\mu\text{-}CO)_3(CO)_6\{P(OPh)_3\}_2]$ **17b**
$[CpWIr_3(\mu\text{-}CO)_3(CO)_6\{P(OMe)_3\}_2]$ **20b**

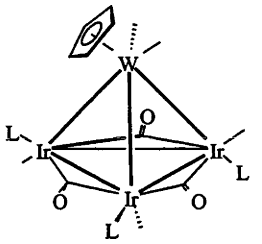
Figure 3.2.79. Coordination geometries for derivatives of $[CpWIr_3(CO)_{11}]$ (**2**).



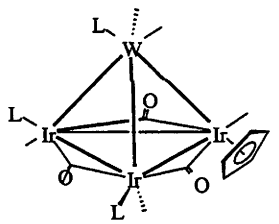
diaxial bridging *P*-donor ligand (L⌒L), apical Cp
$[CpWIr_3(\mu\text{-}CO)_3(\mu\text{-}dppe)(CO)_6]$ **22a, 22b, 22c**
$[CpWIr_3(\mu\text{-}CO)_3(\mu\text{-}dppm)(CO)_6]$ **23a, 23b**
$[CpWIr_3(\mu\text{-}CO)_3(\mu\text{-}pdpp)(CO)_6]$ **24**



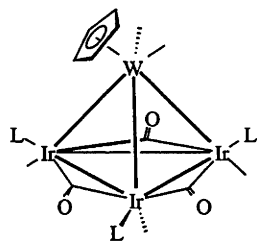
radial, axial apical *P*-donor ligands (L), axial Cp:
$[CpWIr_3(\mu\text{-}CO)_3(CO)_5(PMePh_2)_3]$ **12a**
$[CpWIr_3(\mu\text{-}CO)_3(CO)_5(PMe_2Ph)_3]$ **15**
$[CpWIr_3(\mu\text{-}CO)_3(CO)_5(PMe_3)_3]$ **7**
$[CpWIr_3(\mu\text{-}CO)_3(CO)_5\{P(OPh)_3\}_3]$ **18a**
$[CpWIr_3(\mu\text{-}CO)_3(CO)_5\{P(OMe)_3\}_3]$ **21a**



diaradial, axial *P*-donor liands (L), apical Cp:
$[CpWIr_3(\mu\text{-}CO)_3(CO)_5(PPh_3)_3]$ **6**

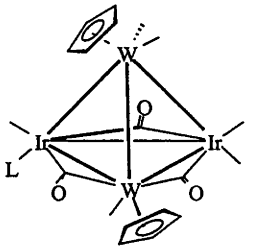


diradial, apical *P*-donor ligands (L), axial Cp:
$[CpWIr_3(\mu\text{-}CO)_3(CO)_5\{P(OPh)_3\}_3]$ **18b**
$[CpWIr_3(\mu\text{-}CO)_3(CO)_5\{P(OMe)_3\}_3]$ **21b**

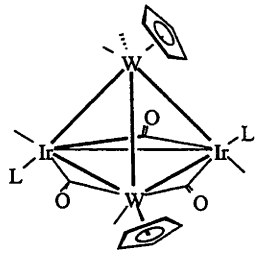


triradial *P*-donor liands (L), apical Cp:
$[CpWIr_3(\mu\text{-}CO)_3(CO)_5(PMePh_2)_3]$ **12b**

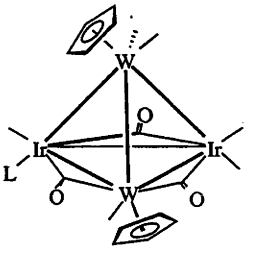
Figure 3.2.79.(cont.) Coordination geometries for derivatives of $[CpWIr_3(CO)_{11}]$ (**2**).



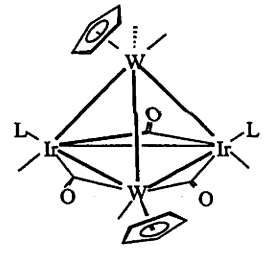
axial *P*-donor ligand (L), apical, axial Cp:
$[Cp_2W_2Ir_2(\mu\text{-}CO)_3(CO)_6(PPh_3)]$ **31a**



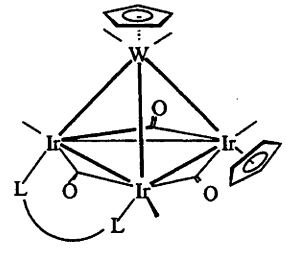
axial *P*-donor ligand (L), apical, axial Cp:
$[Cp_2W_2Ir_2(\mu\text{-}CO)_3(CO)_6(PPh_3)]$ **31b**
$[Cp_2W_2Ir_2(\mu\text{-}CO)_3(CO)_6(PMe_3)]$ **33**
$[Cp_2W_2Ir_2(\mu\text{-}CO)_3(CO)_6\{P(OMe)_3\}]$ **35**



radial, axial *P*-donor ligand, axial, apical Cp:
$[Cp_2W_2Ir_2(\mu\text{-}CO)_3(CO)_5(PMe_3)]$ **34a**



diradial *P*-donor ligand, axial, apical Cp:
$[Cp_2W_2Ir_2(\mu\text{-}CO)_3(CO)_5(PMe_3)]$ **34c**



diaxial bridging *P*-donor ligand (L⌒L), axial, apical C
$[Cp_2W_2Ir_3(\mu\text{-}CO)_3(\mu\text{-dppe})(CO)_5]$ **38a, 38b**
$[Cp_2W_2Ir_2(\mu\text{-}CO)_3(\mu\text{-dppm})(CO)_6]$ **37**

Figure 3.2.80. Coordination geometries for derivatives of $[Cp_2W_2Ir_2(CO)_{10}]$ (**3**).

geometries, variants perhaps enforced by the fact that a W_2Ir basal plane is unfavourable. Derivatives **33** and **35** were found to exchange carbonyls about a WIr_2 face by way of a pseudo-D_{2d} intermediate.

Tetrasubstituted derivatives of **1** usually exist with radial, diaxial, apical coordination geometries, although the carbonyl exchange pathway of clusters with this type has not been investigated. Previously reported studies with tetrairidium derivatives have concentrated on polydentate ligand derivatives,[13,24] with the exchange of carbonyls proceeding by way of either a Cotton merry-go-round or a change-of-basal-face process. The radial, axial, apical *P*-donor ligand, axial Cp (radial, diaxial, apical) coordination geometry (with the apical ligand oriented toward the axial substituents) is also the favoured configuration for tetrasubstituted derivatives of **2**. A suitable exchange process could not be proposed for the clusters with this configuration. Other tetrasubstituted derivatives of $[CpWIr_3(\mu\text{-}CO)_3(CO)_5(L)_3]$ were assigned with diradial, apical phosphine, axial Cp (diradial, axial, apical) geometry [L = PPh_3 (**5**)], triradial phosphine, apical Cp (triradial, apical) geometry [L = $PMePh_2$ (**12b**)] or diradial, axial phosphite, apical Cp (diradial, axial, apical) geometry [L = $P(OPh)_3$ (**18b**), $P(OMe)_3$ (**21b**)]. The tetrasubstituted derivatives of **3** were also identified with different (**34**, 2; **36**, 1) radial, axial *P*-donor ligand, axial, apical Cp (radial, diaxial, apical) configuration coordination geometries. A minor isomer of $[Cp_2W_2Ir_2(\mu\text{-}CO)_3(CO)_5(PMe_3)_2]$ (**34c**) was also assigned a diradial phosphine, axial, apical Cp (diradial, axial, apical) coordination geometry. Configuration **34a** was proposed to exchange carbonyls about a W_2Ir face via a pseudo-D_{2d} intermediate. The complexes $[Cp_2W_2Ir_2(\mu\text{-}CO)_3(\mu\text{-}L)(CO)_5]$ [L = dppe (**38**), dppm (**37**)] were found to exist as two (**38**) or one (**37**) configurations with diaxial bridging diphosphine, axial, apical Cp coordination geometries, not identified previously in the trairidium system. Configurations **38a** and **38b** were found to interconvert by way of a "waggling" of the $[CpW(CO)_2]$ group, placing the Cp ligand over both W_2Ir faces.

3.3. Conclusions

The impact upon ligand coordination geometry and carbonyl fluxionality of heterometal incorporation into the prototypical tetrahedral cluster $[Ir_4(CO)_{12}]$ (**1**) has been assessed. The isostructural $[CpWIr_3(CO)_{11}]$ (**2**) and $[Cp_2W_2Ir_2(CO)_{10}]$ (**3**) are related to **1** by conceptual replacement of one or two late transition metal-containing $[Ir(CO)_3]$ vertices by one or two mid-transition metal $[CpW(CO)_2]$ units, respectively. These "very mixed"-metal clusters have been derivatized by phosphines, phosphites and isocyanides, the ligand fluxionality of the resultant clusters examined, and both the coordination geometry and CO mobility of the tungsten-iridium clusters contrasted with those of derivatives of the "parent" homometallic cluster.

The tetrahedral clusters $[CpWIr_3(\mu\text{-}CO)_3(CO)_{8-n}(L)_n]$ [L = PPh_3, n = 1 (**4**), 2 (**5**), 3 (**6**); L = PMe_3, n = 1 (**7**), 2 (**8**), 3 (**9**)] are shown to exist as mixtures of interconverting isomers in solution. The structures of the isomers, together with those of $[CpWIr_3(\mu\text{-}CO)_3(CO)_5(L)_3]$ [L = PPh_3 (**6**), PMe_3 (**9**)], have been assigned using a combination of variable temperature ^{31}P and ^{13}C NMR, COSY spectra and X-ray structural studies. All phosphine-containing clusters contain a carbonyl-bridged basal plane and an apical metal; ligands can be approximately coplanar (radial) to the basal plane or below the plane (axial). The configurations of **4a** and **7a** (axial phosphine, apical Cp, Ir_3 basal plane), and **4b** and **7b** (radial phosphine, axial Cp, WIr_2 basal plane) are consistent with structural determinations of **7a** and **4b**, with a third configuration (**4c**; axial phosphine, radial Cp, WIr_2 basal plane) observed only with the larger phosphine. The configurations of **5b** and **8b** (radial phosphine, axial phosphine, axial Cp, WIr_2 basal plane) are consistent with a structural determination of **5b**, while a further configuration (**5a** and **8a**; diradial phosphines, radial Cp, WIr_2 basal plane) possesses a triradial coordination geometry. While cluster **9** (with a WIr_2 basal plane) possesses the radial phosphine, axial phosphine, axial Cp, apical phosphine geometry which minimizes steric repulsion, cluster **4** (with an Ir_3 basal plane) has an unusual diradial phosphine, axial phosphine, apical Cp geometry. The configurations of **4a** and **7a**, **5a** and **8a**, and **6** are without precedent in monodentate ligand-substituted derivatives of the parent tetrairidium system. In contrast to reports with rhodium-iridium clusters, the presence of the more electropositive tungsten does not polarize the electron distribution toward the iridiums, and thereby favour an Ir_3 basal plane; rather, the WIr_2-bridged form is predominant across the isomers in the tungsten-iridium system. Suggested mechanisms of carbonyl fluxionality in the abundant isomers of **4** - **9**, assigned using ^{13}C exchange spectroscopy (EXSY) spectra, are proposed. Clusters **4a** and **7a**, with mutually *trans* phosphine and Cp, exchange carbonyls via a "merry - go – round" at Ir_3

and WIr_2 faces. Clusters **5a** and **8a** exchange all carbonyls by way of two processes: scrambling about the Ir_3 face to afford an intermediate with the carbonyl distribution of the D_{2d} form implicated in carbonyl mobility at $Ir_4(CO)_{12}$, and scrambling about a WIr_2 face by way of an all-terminal intermediate in which the putative "merry - go – round" process is blocked by phosphines and Cp. The ligand mobility process in **5a** and **8a** involving the intermediate with a pseudo-D_{2d} ligand distribution has not been observed with analogous $Ir_4(CO)_9(L)_3$ clusters.

The clusters $[CpWIr_3(\mu\text{-}CO)_3(CO)_{8-n}(L)_n]$ [L = $PMePh_2$, n = 1 (**10**), 2 (**11**), 3 (**12**); L = PMe_2Ph, n = 1 (**13**), 2 (**14**), 3 (**15**)] are fluxional in solution, with the interconverting isomers resolvable at low temperatures. Information from the crystal structure of **13a**, ^{31}P NMR data, and comparison with the analogous PPh_3- and PMe_3-ligated tungsten-triiridium clusters **4 - 9** have been employed to suggest coordination geometries for the isomers of **10 - 15**. The geometries of the $PMePh_2$-derivatives **10** and **11** follow those of the PPh_3-derivatives **4** and **5**, while geometries of the PMe_2Ph-derivatives **13 - 15** follow those of the PMe_3-derivatives **7 - 9**. Cluster **12** is the exception, with isomer **12a** possessing the configuration of the PMe_3-derivative **9**, and **12b** which has an unprecedented triradial, apical substitution geometry.

The clusters $[CpWIr_3(\mu\text{-}CO)_3(CO)_{8-n}(L)_n]$ [L = $P(OPh)_3$, n = 1 (**16**), 2 (**17**), 3 (**18**); L = $P(OMe)_3$, n = 1 (**19**), 2 (**20**), 3 (**21**)] are fluxional in solution, with the interconverting isomers resolvable at low temperatures. Information from the crystal structures of **19b** and **17b**, ^{31}P NMR data, and comparision with analogous phosphine-substituted clusters have been employed to suggest coordination geometries for the isomers. Some differences to the phosphine-substituted clusters are noted. The bis-phosphite clusters **17** and **20** exist with a radial, diaxial configuration, unlike the bis-phosphine clusters with two isomers. The tris-phosphite clusters **18** and **21** exist as isomers with the radial, diaxial configuration found in **9**, **12** and **15**, as well as a diradial, axial, apical configuration unique to these derivatives. Isomers of the mono-triphenylphosphite cluster **16** follow those of the PPh_3- and $PMePh_2$-derivatives **4** and **10**. The mono-trimethylphosphite derivative **19** exists as an axial, apical isomer, as found in **4**, **7**, **10**, **13** and **16** and an unprecedented (for W-Ir clusters) diaxial coordination geometry.

Variable temperature ^{31}P and ^{13}C NMR spectra for $[CpWIr_3(\mu\text{-}CO)_3(\mu\text{-dppe})(CO)_6]$ (**22**) and $[CpWIr_3(\mu\text{-}CO)_3(\mu\text{-dppm})(CO)_6]$ (**23**) enable structural assignment of the isomers, revealing a triiridium face spanned by bridging carbonyls, a diaxially-ligated diphosphine and an apical tungsten-coordinated cyclopentadienyl ligand situated over differing WIr_2 faces in the configurations. EXSY spectra reveal that these isomers interconvert by tripodal rotation at the apical $[CpW(CO)_2]$ resolvable (in the case of **23**) into a "waggling" of the $[CpW(CO)_2]$ group over the non-diphosphine ligated WIr_2 faces before the onset of complete tripodal rotation. A

"merry-go-round" of carbonyl ligands in the basal $Ir(\mu\text{-}CO)_3(CO)_3$ plane occurs at a similar temperature to that of tripodal rotation for **23**, but at a higher temperature for **22**. For **22**, flexing of the diphosphine backbone is the highest energy process observed.

The clusters $[CpWIr_3(CO)_{11-n}(CNR)_n]$ [R = Xy ($C_6H_3Me_2$-2,6), n = 1 (**25**), 2 (**26**), 3 (**27**); R = ^{t}Bu, n = 1 (**28**), 2 (**29**), 3 (**30**)] exhibit ligand fluxionality in solution, with the ^{13}C NMR spectra of **28** - **30** revealing that the carbonyls are undergoing fast exchange at 143 K solubility and other experimental problems precluded a study at lower temperatures.

The clusters $[Cp_2W_2Ir_2(\mu\text{-}CO)_3(CO)_{7-n}(PPh_3)_n]$ [n = 1 (**31**) or 2 (**32**)] or $[Cp_2W_2Ir_2(\mu\text{-}CO)_3(CO)_{7-n}(PMe_3)_n]$ [n = 1 (**33**) or 2 (**34**)] exhibit ligand fluxionality in solution, resolvable at low temperature into the constituent interconverting isomers. Information from the crystal structure of **2a**, and ^{13}C and ^{31}P NMR spectral data have been employed to assign coordination geometries for the isomers of **31** - **34**. All the isomers of clusters contain a carbonyl-bridged WIr_2 basal plane and an apical tungsten atom; ligands can be approximately coplanar (radial) to the basal plane or below the plane (axial). The configuration of **31a** (axial phosphine, axial Cp, apical Cp), as assigned by NMR spectroscopy, is consistent with the structural determination. A second configuration (**31b**, **33b**: axial phosphine, axial Cp, apical Cp) is the only configuration identified (within the temperature range 183 - 293 K) for the PMe_3-substituted cluster, **33**. Two isomers, both with radial phosphine, axial phosphine, axial Cp, apical Cp configurations have been identified for **34**, namely **34a** and **34b**; it is likely that isomers of **32** adopt the same configurations. The WIr_2-bridged form is seen exclusively across the isomers, indicating that the presence of two electropositive tungsten atoms may be polarizing the electron distribution towards the iridiums, although steric factors may also be involved. The mechanisms of fluxionality in the clusters **33** and **34** have been assigned using ^{13}C exchange spectroscopy (EXSY) spectra. The clusters **33b** and **34a** exchange carbonyls by scrambling about a WIr_2 face (**33b**) or a W_2Ir face (**34a**), affording intermediates with the pseudo-D_{2d} carbonyl distributions implicated in carbonyl mobility at $[Ir_4(CO)_{12}]$.

An unusual decomposition reaction was observed during the crystallization of $[Cp_2W_2Ir_2(\mu\text{-}CO)_3(CO)_5\{P(OMe)_3\}_2]$ (**36**). A single-crystal X-ray study from one of the two types of crystals from a solution of **36** was identified as $[CpWIr_3(\mu\text{-}CO)_3(CO)_7\{P(OMe)_3\}]$ (**19**). Monitoring a solution of **36** by ^{31}P NMR spectroscopy reveals slow formation of **19** (93 % **36** : 7 % **19** over four days) at room temperature. One configuration only of clusters $[Cp_2W_2Ir_2(\mu\text{-}CO)_3(CO)_6\{P(OMe)_3\}]$ (**35**) and **36** was observed in the ^{13}C and ^{31}P NMR spectra (between 183 K and 303 K), with no evidence for the presence of additional isomers undergoing very fast exchange. The NMR spectra of **36** are consistent with the formulation given in the X-ray

crystallographic study. The NMR spectra of **35** suggest a configuration with axial phosphite, axial Cp, apical Cp, analogous to the related cluster $[Cp_2W_2Ir_2(\mu\text{-}CO)_3(CO)_6(PMe_3)]$ (**33**). Cluster **35** exchanges carbonyls by scrambling about a WIr_2 face, in the same manner as **33**.

The clusters $[Cp_2W_2Ir_2(\mu\text{-}CO)_3(\mu\text{-}L)(CO)_5]$ [L = dppm (**37**), dppe (**38**)] are fluxional in solution, with the interconverting isomers of **38** resolvable at low temperatures. Variable temperature ^{31}P and ^{13}C NMR spectra for **37** and **38** enable structural assignment of the radial Cp, diaxial phosphine, apical Cp isomers. ^{13}C NMR exchange spectroscopy (EXSY) spectra reveal that these isomers interconvert by tripodal rotation at the apical $CpW(CO)_2$, resolvable (in the case of **38**) into a "waggling" of the $[CpW(CO)_2]$ group over the W_2Ir faces.

3.4. Experimental

3.4.1. Instruments and Reagents

3.4.1.1. Instruments

NMR spectra were recorded on a Varian VXR300S spectrometer (^{13}C at 75.4 MHz and ^{31}P at 121.4 MHz) or a Bruker DMX500 (^{13}C at 125.7 MHz) and are proton decoupled. ^{1}H-^{31}P-^{13}C triple resonance experiments were recorded on a Bruker DMX500 (^{1}H at 500.1 MHz, ^{31}P at 202.5 MHz, ^{13}C at 125.7 MHz) or a Bruker DMX600 (^{1}H at 600.1 MHz, ^{31}P at 242.9 MHz, ^{13}C at 150.9 MHz). ^{183}W-^{13}C and ^{183}W-^{1}H correlation experiments were recorded on a Bruker DMX600 (^{183}W at 24.9 MHz, ^{1}H at 600.1 MHz, ^{13}C at 150.9 MHz). Spectra were run in $CDCl_3$ (Cambridge Isotope Laboratories), CD_2Cl_2 (Cambridge Isotope Laboratories), acetone-d_6 (Cambridge Isotope Laboratories), $CDFCl_2$[50], $4CS_2$:$1CD_2Cl_2$ (CS_2: Univer; CD_2Cl_2: Cambridge Isotope Laboratories) or toluene-d^8 (Fluorochem). References for the ^{13}C NMR spectra are the residual solvent peak resonances, with their chemical shifts relative to $SiMe_4$ = 0.0 ppm. Chemical shifts in ppm are referenced to internal residual solvent (^{1}H, $CHCl_3$ = 7.26 ppm; ^{13}C, CD_2Cl_2 = 53.8 ppm, acetone-d_6 = 29.8 ppm, $CDCl_3$ = 77.0 ppm) or external 85% H_3PO_4 (^{31}P, H_3PO_4 = 0.0 ppm). On the 500 and 600 MHz instruments, ^{31}P shifts were measured relative to hypothetical external 85% H_3PO_4 using Ξ = 40.480737 and ^{183}W shifts were measured relative to hypothetical external WF_6 (WF_6 = 0 ppm) using Ξ = 4.161733 using the formula X nucleus reference frequency = Ξ x ^{1}H zero ppm frequency/100.[51] Small differences in ^{31}P shifts obtained on 300 and 500 MHz instruments are ascribed to the differences in referencing techniques used.

Resonances are reported in the form: ppm (assignment; multiplicity; relative intensity), with the specific assigned sites shown in Figure 7. The ^{13}C-{^{1}H} EXSY experiments were carried out using the standard NOESY pulse sequence with the mixing time set to 0.05 s. The ^{1}H NOESY experiments were carried out using the standard pulse sequence with the mixing time set to 0.2 s. The integrated ^{13}C NMR spectra were recorded with a recycle delay of 3-5 timesthe longest T_1 of the carbonyl ligands. 2D NMR spectra were recorded utilizing a recycle delay of 1-3 times the longest T_1 of the carbonyl ligands. T_1 measurements were carried out employing the standard inversion-recovery procedure. ^{1}H-^{31}P HSQC experiments were recorded using the standard sequence including refocussing and decoupling. Typically, delays were optimized for a 12 Hz coupling to emphasize $^{2}J_{PH}$ correlations or 4 Hz to

emphasize long range correlations to the Cp protons. ^{1}H-^{31}P-^{13}C triple resonance experiments were acquired using the pulse sequence shown in Figure 3.4.1.

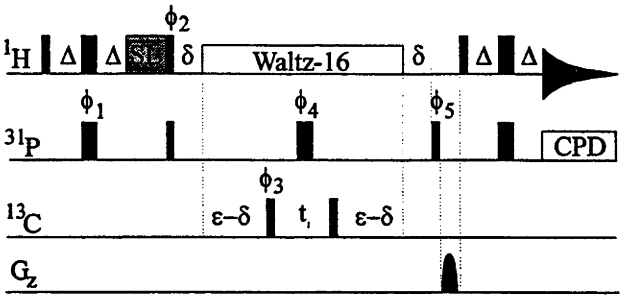


Figure 3.4.1. Pulse sequence used for triple resonance HPCO experiment. Narrow bars represent 90° pulses and wide bars 180° pulses. SL denotes a spin lock pulse (1.5 ms). Typical delays used were Δ = 20.8 ms ($\approx \frac{1}{4} J_{PH}$), δ = 9.8 ms and ε = 38.5 ms ($\approx \frac{1}{2} J_{PC}$, optimized for $^{n}J_{PC}$ = 13 Hz in this case). Phase cycles used were ϕ_1 = x, -x; ϕ_2 = y, -y; ϕ_3 = 2x, 2(-x); ϕ_4 = 8x, 8y, 8(-x), 8(-y); ϕ_5 = 4x, 4(-x); Receiver = x, -x, -x, x, -x, x, x, -x, -x, x, x, -x, x, -x, -x, x. A minimum of 8 scans per increment was employed. Inclusion of the gradient pulse (1 ms, sine shaped, ca. 28 Gauss cm^{-1}) is optional and more gradients should be incorporated in cases where the ^{13}C is not labeled and suppression of unwanted signals is important. In a typical experiment at a temperature of 183 K, 256 FID were collected in t_1 of 1024 t_2 points each. Spectral widths were 2.24 ppm in F_2 (^{1}H), resulting in an aquisition time of 0.46 s and 92.0 ppm in F_1 (^{13}C). A recycle delay of 0.3 s was used. High power 90° pulse widths were 9.4, 7.8 and 10.4 μs for ^{1}H, ^{31}P and ^{13}C, respectively.*3.4.1.2.*

Reagents

$[CpWIr_3(CO)_{11}]$ (**2**),[52] $[Cp_2W_2Ir_2(CO)_{10}]$ (**3**),[52] and $[CpWIr_3(\mu\text{-}CO)_3(CO)_7(PPh_3)]$ (**4**)[40] were synthesized according to literature procedures. All other clusters were prepared as described in Chapter 2. ^{13}CO enriched samples were prepared from ^{13}CO-enriched (65 %) **2** (obtained by stirring a solution of the cluster in CH_2Cl_2 under 1.2 atm ^{13}CO at 60 °C for 48 h) or from ^{13}CO-enriched (90 %) **3** (obtained by stirring a solution of the cluster in CH_2Cl_2 under 1.2 atm ^{13}CO at room temperature for 60 h).

3.4.2. Spectroscopic Data for $[CpWIr_3(\mu\text{-}CO)_3(CO)_7(PPh_3)]$ (4)

^{13}C NMR (CD_2Cl_2, 181 K) **4a** 208.3 (a, a'; s, 85%, d, 15%, J_{WC} = 154.3 Hz; 1.0), 205.4 (b, b'; s; 1.0), 201.9 (c; s; 0.5), 177.6 (f; s; 0.5), 174.9 (d, d'; s; 1.0), 158.0 (e, e'; s; 1.0) ppm; **4b** 238.9 (E; br s; 0.3), 230.9 (D; br s; 0.3), 209.9 (F; br s; 0.3), 209.2 (J; s; 0.3), 178.6 (H; br s; 0.3), 160.3 (C; s; 0.3), other signals not assigned; **4c** 238.6 (*e*; s, 85%, d, 15%, J_{WC} = 71.5 Hz; 0.2), 228.9 (*d*; s, 85%, d, 15%, J_{WC} = 71.8 Hz; 0.2), 211.6 (*j*; s, 85%, d, 15%, J_{WC} = 171.5 Hz;

0.2), 209.2 (*f*; s, 0.2), 177.2 (*h*; s; 0.2), 174.9 (*g*; s; 0.2), 162.5 (*b*; s; 0.2), 160.3 (*c*; s; 0.2), 157.9 (*a*; d J_{PC} = 15 Hz; 0.2). ^{13}C NMR (CS_2/CD_2Cl_2, 163 K) **4a** 208.4 (a, a'; s; 1.0), 205.7 (b, b'; s; 1.0), 202.0 (c; s; 0.5), 177.7 (f; s; 0.5), 174.9 (d, d'; s; 1.0), 157.9 (e, e'; s; 1.0) ppm; **4b** 235.6 (E; s; 0.3), 230.5 (D; s; 0.3), 210.2 (F; s; 0.3), 208.4 (J; s; 0.3), 178.5 (H; br s, 0.3), 160.3 (C; s; 0.3), other signals not assigned; **4c** 238.9 (*e*; s; 0.2), 228.6 (*d*; s; 0.2), 211.8 (*j*; s; 0.2), 208.4 (*f*; s, 0.2), 177.1 (*h*; s; 0.2), 174.9 (*g*; s; 0.2), 164.9 (*b*; s; 0.2), 160.3 (*i*; s; 0.2), 160.0 (*c*; s; 0.2), 157.7 (*a*; d J_{PC} = 15 Hz; 0.2). ^{31}P NMR (CD_2Cl_2, 173 K) 24.9 (0.3P, **4b**), 5.3 (0.5P, **4a**), -4.9 (0.2P, **4c**) ppm.

3.4.3. Spectroscopic Data for [$CpWIr_3(\mu\text{-}CO)_3(CO)_6(PPh_3)_2$] (5)

^{13}C NMR (CD_2Cl_2, 191 K) **5a** 241.0 (e, e'; s, 85%, d, 15%, J_{WC} = 73.4 Hz; 1.8), 217.0 (f; s; 0.9), 212.8 (d; s, 85%, d, 15%, J_{WC} = 172.4 Hz; 0.9), 167.5 (b; s; 0.9), 162.2 (a, a'; s; 1.8), 157.3 (c, c'; s; 1.8) ppm. **5b** 243.1 (D or E; s; 0.1), 237.4 (E or D; s; 0.1), 228.0 (F; s; 0.1), 214.1 (I; s; 0.1), 177.6 (H; dd $^2J_{CP}$ = 22 Hz, $^3J_{CP}$ = 10 Hz; 0.1), 164.7 (C or B; s; 0.1), 161.5 (G; d $^2J_{CP}$ = 22 Hz; 0.1), 161.5 (A; s; 0.1), 156.2 (B or C; s; 0.1) ppm. ^{31}P NMR (CD_2Cl_2, 191 K) 27.4 (1.8P, **5a**), 26.1 (0.1P, **5b**), -7.0 (0.1P, **5b**) ppm.

3.4.4. Spectroscopic Data for [$CpWIr_3(\mu\text{-}CO)_3(CO)_5(PPh_3)_3$] (6)

^{31}P NMR ($CDCl_3$, 230 K) 31.8 (2P, **6**), -17.9 (1P, **6**) ppm.

3.4.5. Spectroscopic Data for [$CpWIr_3(\mu\text{-}CO)_3(CO)_7(PMe_3)$] (7)

^{13}C NMR ($4CS_2$:$1CD_2Cl_2$, 163 K) **4a** 209.5 (a, a'; s, 85%, d, 15%, J_{WC} = 152.2 Hz; 0.76), 206.6 (b, b' ; s; 0.76), 202.2 (c'; s; 0.38), 177.7 (f; s; 0.38), 174.9 (d, d'; s; 0.76), 158.0 (e, e'; s; 0.76) ppm. **7b** 240.6 (E; s, 85%, d, 15%, J_{WC} = 71.5 Hz; 0.38), 232.2 (D; s, 85%, d, 15%, J_{WC} = 71.3 Hz; 0.38), 211.6 (F; s; 0.38), 210.8 (J; s, 85%, d, 15%, J_{WC} = 152.2 Hz; 0.38), 179.4 (H; s; 0.38), other signals not assigned. ^{31}P NMR (CD_2Cl_2, 173 K) -31.8 (0.38P, **7a**), -25.0 (0.62P, **7b**) ppm.

3.4.6. Spectroscopic Data for [$CpWIr_3(\mu\text{-}CO)_3(CO)_6(PMe_3)_2$] (8)

^{13}C NMR (CD_2Cl_2, 193 K) **8a** 247.4 (e, e'; s, 85%, d, 15%, J_{WC} = 72.7 Hz; 1.82), 225.9 (f; s; 0.91), 214.8 (d; s, 85%, d, 15%, J_{WC} = 177.5 Hz; 0.91), 167.5 (b; s; 0.91), 164.0 (a, a'; s; 1.82), 162.2 (c, c'; s; 1.82) ppm. **8b** 249.0 (D or E; s; 0.09), 244.9 (E or D; s; 0.09), 255.8 (F; s; 0.09), 216.0 (I; s; 0.09), 180.8 (H; dd $^2J_{CP}$ = 22 Hz, ^3J = 10 Hz; 0.09), 166.7 (C or B; s; 0.09), 165.4 (A; s; 0.09), 163.2 (G, d $^2J_{CP}$ = 22 Hz; 0.09), 159.4 (B or C; s; 0.09). ^{31}P NMR (CD_2Cl_2, 193 K) -21.8 (1.82P, **8a**), -23.6 (0.09P, **8b**), - 41.0 (0.09P, **8b**) ppm.

3.4.7. Spectroscopic Data for [CpWIr$_3$(μ-CO)$_3$(CO)$_5$(PMe$_3$)$_3$] (9)

^{13}C NMR (CD_2Cl_2, 188 K) 257.3 (c; s; 1), 245.1 (d; s; 1), 229.5 (e; s; 1), 227.9 (f; s; 1), 184.6 (h; dd ^2J = 18 Hz, ^3J = 9 Hz; 1), 172.6 (a; s; 1), 168.0 (b; d ^3J = 10 Hz; 1), 166.0 (g; dd ^2J = 20 Hz, ^3J = 10 Hz; 1) ppm. ^{31}P NMR (CD_2Cl_2, 188 K) -27.2 (1P), -45.8 (1P), -83.2 (1P) ppm.

3.4.8. Spectroscopic Data for [CpWIr$_3$(μ-CO)$_3$(CO)$_7$(PMePh$_2$)] (10)

^{13}C NMR ($CDCl_3$) δ 134.2-128.7 (Ph), 85.8 (C5H5), 20.3 (Me); ^{31}P NMR (CD_2Cl_2, 178 K) δ -3.2 (0.36P), -2.7 (s, 0.45P), -22.9 (s, 0.18P).

3.4.9. Spectroscopic Data for [CpWIr$_3$(μ-CO)$_3$(CO)$_6$(PMePh$_2$)$_2$] (11)

^{13}C NMR ($CDCl_3$) δ 131.9-128.3 (Ph), 87.1 (C_5H_5), 20.2 (Me); ^{31}P NMR ($CDCl_3$, 230 K) δ 0.6 (s, 0.8P), -0.5 (s, 0.6P), -22.9 (s, 0.6P).

3.4.10. Spectroscopic Data for [CpWIr$_3$(μ-CO)$_3$(CO)$_5$(PMePh$_2$)$_3$] (12)

^{13}C NMR ($CDCl_3$) δ 131.9-128.3 (Ph), 87.1 (C_5H_5), 53.4 (CH_2Cl_2), 20.7 (Me); ^{31}P NMR ($CDCl_3$, 230 K) δ -3.6 (s, 0.86P), -30.1 (s, 0.86P), -55.3 (s, 0.86P); -8.9 (s, 0.14P), -9.2 (s, 0.28P).

3.4.11. Spectroscopic Data for [CpWIr$_3$(μ-CO)$_3$(CO)$_7$(PMe$_2$Ph)] (13)

^{13}C NMR ($CDCl_3$) δ 130.5-128.6 (Ph), 86.3 (C_5H_5), 20.0 (Me); ^{31}P NMR (CD_2Cl_2, 178 K) δ -20.8 (s, 0.55P), -28.5 (s, 0.44P).

3.4.12. Spectroscopic Data for [CpWIr$_3$(μ-CO)$_3$(CO)$_6$(PMe$_2$Ph)$_2$] (14)

^{13}C NMR ($CDCl_3$) ($CDCl_3$) δ 132.2-123.4 (Ph), 86.3 (C_5H_5), 20.4 (Me); ^{31}P NMR ($CDCl_3$, 230 K) δ -16.8 (s, 1.72P), -18.9 (s, 0.14P), -37.8 (s, 0.14P).

3.4.13. Spectroscopic Data for [CpWIr$_3$(μ-CO)$_3$(CO)$_5$(PMe$_2$Ph)$_3$] (15)

^{13}C NMR ($CDCl_3$) δ 129.5-127.8 (Ph), 87.1 (C_5H_5), 53.4 (CH_2Cl_2), 20.4 (Me); ^{31}P NMR ($CDCl_3$, 230 K) δ -21.2 (s, 1P), -44.0 (s, 1P), -72.8 (s, 1P).

3.4.14. Spectroscopic Data for [CpWIr$_3$(μ-CO)$_3$(CO)$_7${P(OPh)$_3$}] (16)

^{31}P NMR (CS_2/CD_2Cl_2 188 K) δ 103.2 (s, 0.25P), 78.1 (s, 0.50P), 64.8 (s, 0.25P).

3.4.15. Spectroscopic Data for [CpWIr$_3$(μ-CO)$_3$(CO)$_6${P(OPh)$_3$}$_2$] (17)

^{31}P NMR (acetone-d_6, 230 K) δ 109.5 (s, 1P), 65.9 (s, 1P).

3.4.16. Spectroscopic Data for [CpWIr$_3$(μ-CO)$_3$(CO)$_5${P(OPh)$_3$}$_3$] (18)

^{31}P NMR (acetone-d_6, 230 K) δ 107.7 (s, 0.75P), 58.1 (s, 0.75P), 35.2 (s, 0.75P); 100.9 (s, 0.50P), 78.8 (s, 0.25P).

3.4.17. Spectroscopic Data for [CpWIr$_3$(μ-CO)$_3$(CO)$_7${P(OMe)$_3$}] (19)

^{31}P NMR (CS_2/CD_2Cl_2, 188 K) δ 91.8 (s, 0.13P), 81.7 (s, 0.87P).

3.4.18. Spectroscopic Data for [CpWIr$_3$(μ-CO)$_3$(CO)$_6${P(OMe)$_3$}$_2$] (20)

^{31}P NMR (acetone-d_6, 230 K) δ 124.4 (s, 1P), 83.8 (s, 1P).

3.4.19. Spectroscopic Data for [CpWIr$_3$(μ-CO)$_3$(CO)$_5${P(OMe)$_3$}$_3$] (21)

^{31}P NMR (acetone-d_6, 230 K) δ 118.2 (s, 0.67P), 97.1 (s, 0.67P), 78.3 (s, 0.67P); 118.5 (s, 0.67P), 95.6 (s, 0.33P).

3.4.20.Spectroscopic data for [CpWIr$_3$(μ-CO)$_3$(μ-dppe)(CO)$_6$] (22)

^{13}C NMR (CD_2Cl_2, 183 K) **22a** 221.5 (e; s; 0.70), 215.0 (c; s; 0.70), 212.5 (b; s, 85%, d, 15%, J_{WC} = 152.2 Hz; 0.70), 211.0 (a; s, 85%, d, 15%, J_{WC} = 154.5 Hz; 0.70), 208.2 (a, s, 85%, d, 15%, J_{WC} = 149.5 Hz; 0.87), 207.0 (d; s; 0.70), 181.0 (f; s; 0.70), 180.5 (g; s; 0.70), 176.0 (h; s; 0.70), 161.0 (i; s; 0.70). **22b** 220.5 (E; s; 0.28), 212.4 (B; s, 85%, d, 15%, J_{WC} = 152.1 Hz; 0.28), 211.2 (A; s; 0.28), 210.4 (C; s; 0.28), 209.0 (D; s; 0.28), 181.8 (G; s; 0.28), 180.2 (F; s; 0.28), 176.0 (H, s, 0.28), 162.2 (i; s; 0.28). **22c** 227.0 (*c*; s; 0.01), 210.1 (*a*, *a'*; s; 0.01), 210.1 (*b*, *b'*; s; 0.01), 179.5 and 178.9 (*d* and *d'*; s; 0.01), 178.1 (*e*; s; 0.01), 167.7 (*f*; s; 0.01). ^{31}P NMR (CD_2Cl_2, 183 K) δ -21.1 [d, *J*(PP) = 44 Hz, 0.87P, **23a**], -50.2 (s, 0.13P, **23b**), -60.5 [d, *J*(PP) = 45 Hz, 0.87P, **23a**.

3.4.21. Spectroscopic data for [CpWIr$_3$(μ-CO)$_3$(μ-dppm)(CO)$_6$] (23)

^{13}C NMR (CD_2Cl_2, 183 K) **23a** 218.2 (e; s; 0.87), 215.5 (b; s, 85%, d, 15%, J_{WC} = 154.4 Hz; 0.87), 212.3 (c; s; 0.87), 208.2 (a, s, 85%, d, 15%, J_{WC} = 149.5 Hz; 0.87), 206.7 (d; s; 0.87), 182.2 (f and g; s; 0.87). 176.1 (h; s; 0.87), 164.1 (i; s; 0.87). **23b** 228.4 (C; s; 0.13), 210.2 (A and A'; s, 85%, d, 15%, J_{WC} = 155.0 Hz; 0.13), 202.1 (B and B'; s; 0.13), 180.4 (D and D's;

0.13), 179.9 (E; s; 0.13), 170.6 (F; s; 0.13). ^{31}P NMR (CD_2Cl_2, 183 K) δ -21.1 [d, J(PP) = 44 Hz, 0.87P, **23a**], -50.0 (s, 0.13P, **23b**), -60.5 [d, J(PP) = 45 Hz, 0.87P, **23a**.

3.4.22. Spectroscopic data for [$CpWIr_3(\mu\text{-}CO)_3(\mu\text{-}pdpp)(CO)_6$] (24)

^{31}P NMR (CD_2Cl_2, 183 K) δ 22.1 (s, 1P, **24**), 6.1 (s, 1P, **24**).

3.4.23. Spectroscopic data for [$Cp_2W_2Ir_2(\mu\text{-}CO)_3(CO)_6(PPh_3)$] (31)

^1H NMR (CD_2Cl_2, 183 K) 7.68 - 7.05 (m, 15H, Ph), 4.79 (s, 3H, C_5H_5), 4.68 (s, 2H, C_5H_5), 4.40 (s, 3H, C_5H_5), 4.30 (s, 2H, C_5H_5). ^{13}C NMR ($CDFCl_2$, 153 K) **31a** 248.8 (e; s; 0.6), 227.5 (c; s; 0.6), 221.5 (g; s; 0.6), 215.8 (d; s; 0.6), 211.4 (a or b; s; 0.6), 210.7 (b or a; s; 0.6), 183.9 (h; s; 0.6), 180.1 (f; s; 0.6), 172.7 (i; s; 0.6) ppm. **31b** 241.4 (E; s; 0.4), 240.9 (C; s; 0.4), 223.9 (G; s; 0.4), 216.7 (D; s; 0.4), 213.0 (A; s; 0.4), 207.5 (B; s; 0.4), 183.3 (F; s; 0.4), 182.2 (H; s; 0.4), 166.8 (I; s; 0.4) ppm. ^{13}C NMR (CD_2Cl_2, 183 K) **31a** 244.3 (e; s, 85%, d, 15% $^1J_{WC}$ = 81 Hz; 0.6), 224.2 (c; s, 85%, d, 15% $^1J_{WC}$ = 83 Hz; 0.6), 220.3 (g; s, 85%, d, 15% $^1J_{WC}$ = 180 Hz; 0.6), 214.1 (d; s; 0.6), 209.8 (a, b; s, 85%, d, 15% $^1J_{WC}$ = 171 Hz; 1.2), 183.5 (h; s; 0.6), 179.2 (f; d ^2J = 13 Hz; 0.6), 172.2 (i; s; 0.6) ppm. **31b** 237.7 (E; s, 85%, d, 15% $^1J_{WC}$ = 80 Hz; 0.4), 237.5 (C; s, 85%, d, 15% $^1J_{WC}$ = 80 Hz; 0.4), 222.7 (G; s, 85%, d, 15% $^1J_{WC}$ = 178 Hz; 0.4), 214.1 (D; s; 0.4), 211.3 (A or B; s, 85%, d, 15% $^1J_{WC}$ = 165 Hz; 0.4), 206.1 (B or A; s, 85%, d, 15% $^1J_{WC}$ = 163 Hz; 0.4), 182.4 (F; d $^2J_{PC}$ = 13 Hz; 0.4), 181.2 (H; s; 0.4), 167.3 (I; s; 0.4) ppm. ^{13}C NMR (CD_2Cl_2, 183 K) 133.0-128.2 (Ph), 88.2 (s, C_5H_5), 87.8 (s, C_5H_5), 87.3 (s, C_5H_5), 85.4 (s, C_5H_5). ^{31}P NMR (CD_2Cl_2, 183 K) 9.2 (0.4P, **31b**), -9.8 (0.6P, **31a**) ppm.

3.4.24. Spectroscopic data for [$Cp_2W_2Ir_2(\mu\text{-}CO)_3(CO)_5(PPh_3)_2$] (32)

^1H NMR (CD_2Cl_2, 203 K) 7.80-7.31 (m, 30H, Ph), 4.68 (s, 5H, C_5H_5, both isomers), 4.55 s 4H, C_5H_5, major isomer), 4.42 (s, 1H, C_5H_5, minor isomer). ^{13}C NMR (CD_2Cl_2, 203 K) **32a** 249.8 (s; 0.2), 238.0 (s; 0.2), 229.9 (s; 02), 223.9 (s; 0.2), 214.0 (s; 0.2), 212.9 (s; 0.2), 181.2 (s; 0.2), 158.0 (s; 0.2) ppm. **32b** 249.1 (s; 0.8), 240.1 (s; 0.8), 226.9 (s; 0.8), 223.1 (s; 0.8), 211.5 (s; 0.8), 210.7 (s; 0.8), 185.0 (s; 0.8), 164.6 (s; 0.8). ^{13}C NMR (CD_2Cl_2, 203 K) 135.0-128.3 (Ph), 88.5 (s, C_5H_5), 87.4 (s, C_5H_5), 87.1 (s, C_5H_5), 85.9 (s, C_5H_5). ^{31}P NMR (CD_2Cl_2, 203 K) 27.3 (s, 0.2P, **32a**), 17.2 (s, 0.8P, **32b**), 8.1 (s, 0.8P, **32b**), 1.9 (s, 0.2P, **32a**) ppm.

3.4.25. Spectroscopic data for [$Cp_2W_2Ir_2(\mu\text{-}CO)_3(CO)_6(PMe_3)$] (33)

Major isomer **33b**: ^1H NMR (CD_2Cl_2, 183 K) 4.94 (d, $^4J_{HP}$ = 2 Hz, 5H, C_5H_5), 4.68 (s, 5H, C_5H_5), 1.65 (d, $^2J_{HP}$ = 11 Hz, 1.0); ^{13}C NMR (CD_2Cl_2, 183 K) 241.3 (E; s, 85%, d, 15% $^1J_{WC}$ = 71 Hz; 1.0), 239.2 (C; s, 85%, d, 15% $^1J_{WC}$ = 97 Hz; 1.0), 222.4 (G; s, 85%, d, 15% $^1J_{WC}$ =

183 Hz; 1.0), 215.6 (D; s; 1.0), 212.4 (A or B; s, 85%, d, 15% $^1J_{WC}$ = 164 Hz; 1.0), 208.1 (B or A; s, 85%, d, 15% $^1J_{WC}$ = 158 Hz; 1.0), 182.7 (F; d $^2J_{PC}$ = 10 Hz; 1.0), 181.4 (H; s; 1.0), 165.6 (I; s; 1.0) ppm. ^{13}C NMR (CD_2Cl_2, 183 K) 88.4 (s, C_5H_5), 88.0 (s, C_5H_5), 19.6 (d, $^1J_{CP}$ = 37 Hz). ^{31}P NMR (CD_2Cl_2, 183 K) -26.2 (s). Unidentified minor isomer(s): ^{1}H NMR (CD_2Cl_2, 183 K) 4.87 [s (br)], 1.92 (d, $^2J_{HP}$ = 11 Hz); ^{13}C NMR (CD_2Cl_2, 183 K) 220.0 (s) ppm; ^{31}P NMR (CD_2Cl_2, 183 K) -26.2 (br s) ppm.

3.4.26. Spectroscopic data for [$Cp_2W_2Ir_2(\mu$-CO)$_3$(CO)$_5$(PMe_3)$_2$] (34)

^{1}H NMR (CD_2Cl_2, 183 K) 4.98 (s, 2H, C_5H_5), 4.87 (s, 3H, C_5H_5), 4.56 (s, 3H, C_5H_5), 4.41 (s, 2H, C_5H_5), 1.94 (d, J_{HP} = 10 Hz, 5.4H, Me), 1.89 (d, J_{HP} = 10 Hz, 3.6H, Me), 1.64 (d, J_{HP} = 10 Hz, 3.6H, Me), 1.54 (d, J_{HP} = 10 Hz, 5.4H, Me). ^{13}C NMR (CD_2Cl_2, 183 K) **34a** 253.8 (c; s, 85%, d, 15% $^1J_{WC}$ = 90 Hz; 0.60), 242.2 (d; s, 85%, d, 15% $^1J_{WC}$ = 88 Hz; 0.60), 227.6 (e; s; 0.60), 223.0 (h; s, 85%, d, 15% $^1J_{WC}$ = 185 Hz; 0.60), 218.5 (a or b; s, 85%, d, 15% $^1J_{WC}$ = 180 Hz; 0.60), 216.5 (b or a; s, 85%, d, 15% $^1J_{WC}$ = 180 Hz; 0.60), 183.5 (f; dd $^2J_{PC}$ = 22 Hz, $^3J_{PC}$ = 10 Hz; 0.60), 169.1 (g, d $^2J_{PC}$ = 10 Hz; 0.60). **34b** 251.7 (D; s, 85%, d, 15% $^1J_{WC}$ = 92 Hz; 0.35), 247.9 (C; s, 85%, d, 15% $^1J_{WC}$ = 90 Hz; 0.35), 228.1 (E; s; 0.36), 223.0 (H; s, 85%, d, 15% $^1J_{WC}$ = 183 Hz; 0.35), 214.0 (A or B; s, 85%, d, 15% $^1J_{WC}$ = 185 Hz; 0.35), 212.2 (B or A; s, 85%, d, 15% $^1J_{WC}$ = 188 Hz; 0.35), 186.0 (F; dd $^2J_{PC}$ = 22 Hz, $^3J_{PC}$ = 10 Hz; 0.35), 165.9 (G, d ^2J = 10 Hz; 0.35). **34c** 244.9 (*c* or *d*; s; 0.05), 228.2 (*e*; s; 0.05), 221.3 (*h*; s; 0.05), 215.9 (*a* or *b*; s; 0.05), 167.2 (*f* or *g*; d $^2J_{PC}$ = 10 Hz; 0.05), 163.8 (g or f; d $^2J_{PC}$ = 10 Hz; 0.05), other signals not observed. ^{13}C NMR (CD_2Cl_2, 183 K) 9.2 (s, C_5H_5), 88.4 (s, C_5H_5), 87.9 (s, C_5H_5), 87.5 (s, C_5H_5), 20.5 (d, ^1JCP = 35 Hz), 19.3 (d, ^1JCP = 35 Hz), 17.7 (d, ^1JCP = 35 Hz). ^{31}P NMR (CD2Cl2, 183 K) -47.7 (s, 0.60P, **34a**), -29.8 (s, 0.35P, **34b**), -28.5 (d ^3J = 10 Hz, 0.05P, **34c**), -27.7 (s, 0.35P, **34b**), -19.4 (s, 0.60P, 34a), -12 (d ^3J = 10 Hz, 0.05P, **34c**) ppm.

3.4.27. Spectroscopic data for [$Cp_2W_2Ir_2(\mu$-CO)$_3$(CO)$_6${P(OMe)$_3$}] (35)

^{1}H NMR ($CDCl_3$, 248 K) 4.99 (s, 5H, C_5H_5), 4.68 (s, 5H, C_5H_5), 3.74 [d, $^3J_{PH}$ = 12 Hz, 9H, OMe]; ^{13}C NMR (CD_2Cl_2, 248 K) **35** 238.5 [e, s, 85%, d, 15% $^1J_{WC}$ = 80 Hz, 1.0], 237.5 [c, s, 85%, d, 15% $^1J_{WC}$= 80 Hz, 1.0], 221.1 [g, s, 85%, d, 15% $^1J_{WC}$ = 181 Hz, 1.0], 213.3 (d, s, 1.0), 212.5 [a, s, 85%, d, 15% $^1J_{WC}$= 154 Hz, 1.0], 209.3 [b, s, 85%, d, 15% $^1J_{WC}$ = 156 Hz, 1.0], 182.8 [f, d, $^2J_{CP}$ = 14 Hz, 1.0], 182.4 (h, s, 1.0), 162.8 (i, s, 1.0) ppm; ^{13}C NMR (CD_2Cl_2, 298 K) 89.2 (s, Cp), 88.6 (s, Cp) ppm; ^{31}P NMR (CD_2Cl_2, 248 K) 98.8 [s, 85%, d, 15% $^2J_{PW}$= 43 Hz, 1P; **35**].

3.4.28. Spectroscopic data for $[Cp_2W_2Ir_2(\mu\text{-}CO)_3(CO)_5\{P(OMe)_3\}_2]$ (36)

^{13}C NMR (CD_2Cl_2, 298 K) **36** 246.0 [c, s, 85%, d, 15% $^1J_{WC}$ = 70 Hz, 1.0], 239.0 [d, s, 85%, d, 15% $^1J_{WC}$ = 80 Hz, 1.0], 222.7 [h, s, 85%, d, 15% $^1J_{WC}$ = 185 Hz, 1.0], 220.5 (e, s, 1.0), 214.2 [a or b, s, 85%, d, 15% $^1J_{WC}$ = 172 Hz, 1.0], 212.0 [b or a, s, 85%, d, 15% $^1J_{WC}$ = 80 Hz, 1.0], 185.8 [f, dd, $^2J_{CP}$ = 40 Hz, $^3J_{CP}$ = 8 Hz, 1.0], 164.3 [g, d, $^2J_{CP}$ = 8 Hz, 1.0] ppm; ^{13}C NMR (CD_2Cl_2, 298 K) 89.5 (s, Cp), 89.3 (s, Cp); ^{31}P NMR (CD_2Cl_2, 248 K) 125.3 [s, 85%, d, 15% $^2J_{PW}$ = 42 Hz, 1P, **36**], 99.5 [s, 85%, d, 15% $^2J_{PW}$ = 42 Hz, 1P, **36**].

3.4.29. Spectroscopic data for $[Cp_2W_2Ir_2(\mu\text{-}CO)_3(\mu\text{-}dppm)(CO)_5]$ (37)

^1H NMR (CD_2Cl_2, 213 K) 7.82 - 6.95 (m, 20H, C_6H_5), 4.69 (s, 5H, C_5H_5), 4.15 (s, 5H, C_5H_5), 3.44 (s, 2H, CH_2). ^{13}C NMR (CD_2Cl_2, 213 K) **37** 254.4 (c or d; s, 85%, d, 15%, $^1J_{WC}$ = 99.8 Hz; 1), 245.5 (d or c; s, 85%, d, 15%, $^1J_{WC}$ = 84.4 Hz;), 226.2 (e), 224.0 (hs, 85%, d, 15%, $^1J_{WC}$ = 190.8 Hz; 1), 214.0 (a or b; s, 85%, d, 15%, $^1J_{WC}$ = 156.4 Hz;), 211.9 (b or a; s, 85%, d, 15%, $^1J_{WC}$ = 157.7 Hz;), 188.5 (f or g) and 187.9 (g or f) ppm. ^{13}C NMR (CD_2Cl_2, 213 K) δ 133.2-127.9 (Ph), 88.7 (C_5H_5), 87.6 (C_5H_5), other signals not observed. ^{31}P NMR (CD_2Cl_2, 213 K) δ -21.9 (d, $^2J_{PP}$ = 48 Hz, 1P, **37**), -45.8 (d, $^2J_{PP}$ = 48 Hz, 1P, **37**).

3.4.30. Spectroscopic data for $[Cp_2W_2Ir_2(\mu\text{-}CO)_3(\mu\text{-}dppe)(CO)_5]$ (38)

^1H NMR (CD_2Cl_2, 213 K) 8.05 – 7.02 (m, 20H, C_6H_5), 4.69 (s, 5H C_5H_5), 4.34 (s, 3.3H, C_5H_5), 4.06 (s, 1.6H, C_5H_5), 3.85 (s, 2H, CH_2).^{13}C NMR (CD_2Cl_2, 213 K) **38a** 254.5 (d or c; s, 85%, d, 15%, $^1J_{WC}$ = 92.2 Hz; 0.67), 242.9 (c or d; s, 85%, d, 15%, $^1J_{WC}$ = 92.1 Hz; 0.67), 230.8 (e; s; 0.67), 224.5 (h; s, 85%, d, 15%, $^1J_{WC}$ = 183.7 Hz; 0.67), 214.8 (a or b; s, 85%, d, 15%, $^1J_{WC}$ = 157.2 Hz; 0.67), 211.9 (b or a; s, 85%, d, 15%, $^1J_{WC}$ = 163.1 Hz; 0.67), 186.9 (f and g; s; 1.34) ppm. **38b** 250.5 (C or D; s, 85%, d, 15%, $^1J_{WC}$ = 92.2 Hz; 0.33), 246.9 (D or C; s, 85%, d, 15%, $^1J_{WC}$ = 92.2 Hz; 0.33), 230.3 (E; s; 0.33), 224.3 (H; s, 85%, d, 15%, $^1J_{WC}$ = 183.7 Hz; 0.33), 214.0 (A or B; s, 85%, d, 15%, $^1J_{WC}$ = 159.4 Hz; 0.33), 211.4 (B or A; s, 85%, d, 15%, $^1J_{WC}$ = 154.2 Hz; 0.33) and 186.9 (F and G; s; 0.66) ppm. ^{13}C NMR (CD_2Cl_2, 213 K) δ 131.3-128.5 (Ph), 88.7 (C_5H_5), 88.4 (C_5H_5), 87.9 (C_5H_5), 87.6 (C_5H_5), other signals not observed. ^{31}P NMR (CD_2Cl_2, 213 K) δ 3.3 (s, 0.33P, **38b**), 1.3 (s, 0.67P, **38a**), -16.4 (s, 0.67P, **38a**), -23.3 (s, 0.33P, **38b**).

3.5. References

(1) Farrugia, L. J. *J. Chem. Soc., Dalton Trans.* **1997**, 1783.
(2) Roulet, R. *Chimia* **1996**, *50*, 629.
(3) Johnson, B. F. G.; Roberts, Y. V.; Parisini, E.; Benfield, R. E. *J. Organomet. Chem.* **1994**, *478*, 21.
(4) Orrell, K.; Sik, V. *Ann. Rep. NMR Spectroscopy* **1993**, *27*, 103.
(5) Orrell, K.; Sik, V. *Ann. Rep. NMR Spectroscopy* **1987**, *19*, 79.
(6) Mann, B. E. *Ann. Rep. NMR Spectroscopy* **1982**, *12*, 263.
(7) Band, E.; Muetterties, E. L. *Chem. Rev.* **1978**, *78*, 639.
(8) Johnson, B. F. G.; Benfield, R. E. *J. Chem. Soc., Dalton Trans.* **1978**, 1554.
(9) Shriver, D. F.; Kaesz, H. D.; Adams, R. D. *The Chemistry of Metal Cluster Complexes*; V.C.H.: New York, 1990.
(10) *Transition Metal Clusters*; Johnson, B. F. G. Ed.; John Wiley: Cambridge, 1980.
(11) Laurenczy, G.; Bondietti, G.; Ros, R.; Roulet, R. *Inorg. Chim. Acta* **1996**, *247*, 65.
(12) Roberts, Y. V.; Johnson, B. F. G.; Benfield, R. E. *Inorg. Chim. Acta* **1995**, *229*, 221.
(13) Strawczynski, A.; Hall, C.; Bondietti, G.; Ros, R.; Roulet, R. *Helv. Chim. Acta* **1994**, *77*, 754.
(14) Strawczynski, A.; Suardi, G.; Ros, R.; Roulet, R. *Helv. Chim. Acta* **1993**, *76*, 2210.
(15) Besançon, K.; Laurenczy, G.; Lumini, T.; Roulet, R. *Helv. Chim. Acta* **1993**, *76*, 2926.
(16) Bondietti, G.; Ros, R.; Roulet, R.; Musso, F.; Gervasio, G. *Inorg. Chim. Acta* **1993**, *213*, 301.
(17) Johnson, B. F. G.; Roberts, Y. V. *Inorg. Chim. Acta* **1993**, *205*, 175.
(18) Davis, M. J.; Roulet, R. *Inorg. Chim. Acta.* **1992**, *197*, 15.
(19) Mann, B. E.; Vargas, M. D.; Khadar, R. *J. Chem. Soc., Dalton Trans.* **1992**, 1725.
(20) Orlandi, A.; Frey, U.; Suardi, G.; Merbach, A. E.; Roulet, R. *Inorg. Chem.* **1992**, *31*, 1304.
(21) Strawczynski, A.; Ros, R.; Roulet, R.; Braga, D.; Gradella, C.; Grepioni, F. *Inorg. Chim. Acta* **1990**, *170*, 17.
(22) Suardi, G.; Strawczynski, A.; Ros, R.; Roulet, R. *Helv. Chim. Acta* **1990**, *73*, 154.
(23) Mann, B. E.; Pickup, B. T.; Smith, A. K. *J. Chem. Soc., Dalton Trans.* **1989**, 889.
(24) Strawczynski, A.; Ros, R.; Roulet, R. *Helv. Chim. Acta* **1988**, *71*, 867.
(25) Strawczynski, A.; Ros, R.; Roulet, R. *Helv. Chim. Acta* **1988**, *71*, 1885.
(26) Ros, R.; Scrivanti, A.; Albano, V. G.; Braga, D. *J. Chem. Soc., Dalton Trans.* **1986**, 2411.
(27) Braga, D.; Ros, R.; Roulet, R. *J. Organomet. Chem.* **1985**, *286*, C8.
(28) Mann, B. E.; Spencer, C. M.; Smith, A. K. *J. Organomet. Chem.* **1983**, *244*, C17.
(29) Stuntz, G. F.; Shapley, J. R. *J. Organomet. Chem.* **1981**, *213*, 389.
30) Stuntz, G. F.; Shapley, J. R. *J. Am. Chem. Soc.* **1977**, *99*, 607.
(31) Cattermole, P. E.; Orrell, K. G.; Osborne, A. G. *J. Chem. Soc., Dalton Trans.* **1974**, 328.
(32) Clucas, J. A.; Harding, M. M.; Nicholls, B. S.; Smith, A. K. *J. Chem. Soc., Chem. Commun.* **1984**, 319.
(33) Stuntz, G. F.; Shapley, J. R. *Inorg. Chem.* **1976**, *15*, 1994.
(34) Bondietti, G.; Laurenczy, G.; Ros, R.; Roulet, R. *Helv. Chim. Acta* **1994**, *77*, 1869.
(35) Bondietti, G.; Ros, R.; Roulet, R.; Grepioni, F.; Braga, D. *J. Organomet. Chem.* **1994**, *464*, C45.
(36) Laurenczy, G.; Bondietti, G.; Merbach, A. E.; Moullet, B.; Roulet, R. *Helv. Chim. Acta* **1994**, *77*, 547.
(37) Bondietti, G.; Suardi, G.; Ros, R.; Roulet, R.; Grepioni, F.; Braga, D. *Helv. Chim. Acta* **1993**, *76*, 2913.
(38) Darensbourg, D. J.; Baldwin-Zuschke, B. J. *Inorg. Chem.* **1981**, *20*, 3846.
(39) Blake, A. J.; Osborne, A. G. *J. Organomet. Chem.* **1984**, *260*, 227.
(40) Lee, J.; Humphrey, M. G.; Hockless, D. C. R.; Skelton, B. W.; White, A. H. *Organometallics* **1993**, *12*, 3468.
(41) Lentz, D. *Angew. Chem. Int. Ed. Engl.* **1994**, *33*, 1315.
(42) Churchill, M. R.; Hutchinson, J. P. *Inorg. Chem.* **1981**, *20*, 4112.
(43) Churchill, M. R.; Hutchinson, J. P. *Inorg. Chem.* **1978**, *17*, 3528.
(44) Churchill, M. R.; Hutchinson, J. P. *Inorg. Chem.* **1979**, *18*, 2451.
(45) Kay, L. E.; Ikura, M.; Tschudin, R.; Bax, A. *J. Magn. Reson.* **1990**, *89*, 496.
(46) López-Ortiz, F.; Carbajo, R. J. *Current Org. Chem.* **1998**, *2*, 97.
(47) Bast, P.; Berger, S.; Günther, H. *Magn. Reson. Chem.* **1992**, *30*, 587.

(48) Lucas, N. T.; Humphrey, M. G.; Healy, P. C.; Williams, M. L. *J. Organomet. Chem.* **1997**, *545*, 519.
(49) Pöe, A. *Chem. Brit.* **1983**, *19*, 997.
(50) Siegel, J. S.; Anet, F. A. L. *J. Org. Chem.* **1988**, *53*, 2629.
(51) Harris, R. K. *Nuclear Magnetic Resonance Spectroscopy: a physicochemical view*; Pitman, 1983, p 230.
(52) Shapley, J. R.; Hardwick, S. J.; Foose, D. S.; Stucky, G. D. *J. Am. Chem. Soc.* **1981**, *103*, 7383.

Chapter 4

Other Chemistry of Tungsten - Iridium Clusters

Chapter 4

Other Chemistry of Tungsten-Iridium Clusters

Contents

4.1. Thermolyses of Tungsten-Iridium Clusters....328

4.1.1. Activation of Homonuclear Clusters....328
4.1.2. Thermolyses of Phosphine adducts of $[CpWIr_3(CO)_{11}]$ (**2**)....335
4.1.3. Thermolyses of Phosphine adducts of $[Cp_2W_2Ir_2(CO)_{10}]$ (**3**)....343
4.1.4. Thermolyses of Isocyanide adducts of $[CpWIr_3(CO)_{11}]$ (**2**)....343
4.1.5. Thermolyses of $[Cp_2W_2Ir_2(CO)_{10}]$ (**3**) 344

4.2. Some Alkyne Chemistry of Tungsten-Iridium Clusters....351

4.2.1. Acetylene Chemistry of $[Ir_4(CO)_{12}]$ (**1**). $[CpWIr_3(CO)_{11}]$ (**2**) and $[Cp_2W_2Ir_2(CO)_{10}]$ (**3**)....351
4.2.2. Syntheses and Characterization of $[Cp_2W_2Ir_2(\mu_4\text{-}\eta^2\text{-}HC_2R)(\mu\text{-}CO)_4(CO)_4]$ (**18 - 21**)....353
4.2.3. Syntheses and Characterization of $[Cp_2W_2Ir_2\{\mu_4\text{-}\eta^2\text{-}HC_2C{\equiv}CW(CO)_3Cp\}(\mu\text{-}CO)_4(CO)_4]$ (**24**)....356
4.2.4. Syntheses and Characterization of $[Cp_2W_2Ir_3(\mu_4\text{-}\eta^2\text{-}C_2R)(\mu\text{-}CO)(CO)_9]$ (**26 - 29**)....359
4.2.5. Reaction of $[CpWIr_3(CO)_{11}]$ (**2**) and $[Cp_2W_2Ir_2(CO)_{10}]$ (**3**) with $[CpW(CO)_3(C{\equiv}CC{\equiv}C)(CO)_3WCp]$....361
4.2.6. Discussion....362

4.3. Conclusions....366

4.4. Experimental....368

4.4.1. General Conditions, Instruments, Reagents and Chromatography....368
4.4.2. Crystal Preparation....369
4.4.3. Thermolysis of $[CpWIr_3(\mu\text{-}CO)_3(CO)_7(PPh_3)]$ (**4**)....369
4.4.4. Thermolysis of $[CpWIr_3(\mu\text{-}CO)_3(CO)_6(PPh_3)_2]$ (**5**)....370
4.4.5. Thermolysis of $[CpWIr_3(\mu\text{-}CO)_3(CO)_5(PPh_3)_3]$ (**6**)....370
4.4.6. Thermolysis of $[CpWIr_3\{\mu_3\text{-}\eta^2\text{-}PPh(C_6H_4)\}(\mu\text{-}CO)_2(CO)_7]$ (**12**)....371
4.4.7. Photolysis of $[CpWIr_3\{\mu_3\text{-}\eta^2\text{-}PPh(C_6H_4)\}(\mu\text{-}CO)_2(CO)_7]$ (**12**)....371

4.4.8. Reaction of [$CpWIr_3\{\mu_3$-η^2-$PPh(C_6H_4)\}(\mu$-$CO)_2(CO)_7$] (**12**) with Me_3NO 371
4.4.9. Reaction of [$CpWIr_3\{\mu_3$-η^2-$PPh(C_6H_4)\}(\mu$-$CO)_2(CO)_7$] (**12**) with PhC≡CPh 371
4.4.10. Thermolysis of [$CpWIr_3(\mu$-$CO)_3(CO)_7(PMe_3)$] (**7**) 371
4.4.11. Thermolysis of [$Cp_2W_2Ir_2(\mu$-$CO)_3(CO)_6(PPh_3)$] (**8**) 371
4.4.12. Thermolysis of [$Cp_2W_2Ir_2(\mu$-$CO)_3(CO)_5(PPh_3)_2$] (**9**) 372
4.4.13. Thermolysis of [$CpWIr_3(CO)_{10}(CNBu^t)$] (**10**) 372
4.4.14. Thermolysis of [$CpWIr_3(CO)_9(CNBu^t)_2$] (**11**), I 372
4.4.15. Thermolysis of [$CpWIr_3(CO)_9(CNBu^t)_2$] (**11**), II 372
4.4.16. Reaction of [$Cp_2W_2Ir_2(CO)_{10}$] (**3**) and NPh_3 372
4.4.17. Reaction of [$Cp_2W_2Ir_2(CO)_{10}$] (**3**) with HC≡CPh 373
4.4.18. Reaction of [$Cp_2W_2Ir_2(CO)_{10}$] (**3**) with HC≡CC_6H_4Me-4 373
4.4.19. Reaction of [$Cp_2W_2Ir_2(CO)_{10}$] (**3**) with HC≡$CC_6H_4NO_2$-4 374
4.4.20. Reaction of [$Cp_2W_2Ir_2(CO)_{10}$] (**3**) with HC≡CBu^t 374
4.4.21. Reaction of [$Cp_2W_2Ir_2(CO)_{10}$] (**3**) with [$CpW(CO)_3$(C≡CC≡CH)] 374
4.4.22. Thermolysis of [$Cp_2W_2Ir_2\{\mu_4$-η^2-$HC_2C{\equiv}CW(CO)_3Cp\}(\mu$-$CO)_4(CO)_4$] (**24**) 375
4.4.23. Reaction of [$Cp_2W_2Ir_2\{\mu_4$-η^2-$HC_2C{\equiv}CW(CO)_3Cp\}(\mu$-$CO)_4(CO)_4$] (**24**) with Me_3NO 375
4.4.24. Reaction of [$CpWIr_3(CO)_{11}$] (**2**) with HC≡CPh 375
4.4.25. Reaction of [$CpWIr_3(CO)_{11}$] (**2**) with HC≡$CC_6H_4NO_2$-4 375
4.4.26. Reaction of [$CpWIr_3(CO)_{11}$] (**2**) with [$CpW(CO)_3$(C≡CC≡CH)] 375
4.4.27. Reaction of [$Cp_2W_2Ir_2(CO)_{10}$] (**3**) with [$CpW(CO)_3$(C≡CR)] 376
4.4.28. Reaction of [$CpWIr_3(CO)_{11}$] (**2**) with [$CpW(CO)_3$(C≡CPh)] 376
4.4.29. Reaction of [$CpWIr_3(CO)_{11}$] (**2**) with [$CpW(CO)_3$(C≡CC_6H_4Me-4)] 376
4.4.30. Reaction of [$CpWIr_3(CO)_{11}$] (**2**) with [$CpW(CO)_3$(C≡$CC_6H_4NO_2$-4)] 377
4.4.31. Reaction of [$CpWIr_3(CO)_{11}$] (**2**) with [$CpW(CO)_3$(C≡CC≡CPh)] 377
4.4.32. Reaction of [$CpWIr_3(CO)_{11}$] (**2**) with [$CpW(CO)_3$(C≡CC≡C)$(CO)_3$WCp] 377
4.4.33. Reaction of [$Cp_2W_2Ir_2(CO)_{10}$] (**2**) with [$CpW(CO)_3$(C≡CC≡C)$(CO)_3$WCp] 378

4.5. References 379

List of Figures

Figure 4.1.1 - 2. Activation of Phosphine-substituted tetrairidium clusters by thermolysis.....320
Figure 4.1.3. Activation of an Isocyanide-substituted cluster by thermolysis.....332
Figure 4.1.4. Molecular structure and atomic labelling scheme for $[CpWIr_3(\mu\text{-}PPhC_6H_4)(\mu\text{-}CO)_2(CO)_7]$ (**12**).....337
Figure 4.1.5. Molecular structure and atomic labelling scheme for $[CpWIr_3(\mu\text{-}PPhC_6H_4)(\mu\text{-}CO)_2(CO)_6(PPh_3)]$ (**13**).....338
Figure 4.1.6. Molecular structure and atomic labelling scheme for $[Cp_3W_3Ir_4(\mu\text{-}H)(CO)_{12}]$ (**16**).....345
Figure 4.1.7. Bicapped trigonal bipyramidal core isomers, and crystallographically verified examples of heptametallic clusters consisting of transition metal core atoms.....349
Figure 4.1.8. Repesentations of diffferent PSEPT geometries.....350
Figure 4.2.1. $[Ir_4\{\mu\text{-}\eta^4\text{-}Me(O)OCC_2C(O)OMe\}_2\{\mu\text{-}Me(O)OCC_2C(O)OMe\}_2(CO)_8]$.....351
Figure 4.2.2. Molecular structure and atomic labelling scheme for $[Cp_2W_2Ir_2(\mu_4\text{-}\eta^2\text{-}HC_2Ph)(\mu\text{-}CO)_4(CO)_4]$ (**18**).....354
Figure 4.2.3. Molecular structure and atomic labelling scheme for $[Cp_2W_2Ir_3(\mu_4\text{-}\eta^2\text{-}C_2C_6H_4Me\text{-}4)(\mu\text{-}CO)(CO)_9]$ (**27**).....359

List of Tables

Table 4.1.1. Selected Bond Lengths (Å) for Complexes $[CpWIr_3(\mu\text{-}PPhC_6H_4)(\mu\text{-}CO)_2(CO)_7]$ (**12**) and $[CpWIr_3(\mu\text{-}PPhC_6H_4)(\mu\text{-}CO)_2(CO)_6(PPh_3)]$ (**13**).....339
Table 4.1.2. Selected Bond Angles (°) for Complexes $[CpWIr_3(\mu\text{-}PPhC_6H_4)(\mu\text{-}CO)_2(CO)_7]$ (**12**) and $[CpWIr_3(\mu\text{-}PPhC_6H_4)(\mu\text{-}CO)_2(CO)_6(PPh_3)]$ (**13**).....340
Table 4.1.3. Selected Bond Lengths (Å) for Complex $[Cp_3W_3Ir_4(\mu\text{-}H)(CO)_{12}]$ (**16**).....346
Table 4.1.4. Selected Bond Angles (°) for Complex $[Cp_3W_3Ir_4(\mu\text{-}H)(CO)_{12}]$ (**16**).....347
Table 4.2.1. Selected Bond Lengths (Å) for $[Cp_2M_2Ir_2(\mu_4\text{-}\eta^2\text{-}HC_2Ph)(\mu\text{-}CO)_4(CO)_4]$ [M = W (**18**), Mo (**22**)].....355
Table 4.2.2. Selected Bond Angles (°) for $[Cp_2M_2Ir_2(\mu_4\text{-}\eta^2\text{-}HC_2Ph)(\mu\text{-}CO)_4(CO)_4]$ [M = W (**18**), Mo (**22**)].....356
Table 4.2.3. IR Data for $[Cp_2W_2Ir_2(\mu_4\text{-}\eta^2\text{-}HC_2R)(\mu\text{-}CO)_4(CO)_4]$ [R = Ph (**18**), C_6H_4Me-4 (**19**), $C_6H_4NO_2$-4 (**20**), Bu^t (**21**)], $Cp_2W_2Ir_2(\mu_4\text{-}\eta^2\text{-}HC_2C{\equiv}CW(CO)_3Cp)(\mu\text{-}CO)_4(CO)_4$ (**24**) and $CpW(CO)_3(C{\equiv}CC{\equiv}CH)$ (**23**).....358
Table 4.2.4. Selected Bond Lengths (Å) for $[Cp_2W_2Ir_3(\mu_4\text{-}\eta^2\text{-}C_2C_6H_4Me\text{-}4)(\mu\text{-}CO)(CO)_9]$ (**27**).....360
Table 4.2.5. Selected Bond Angles (°) for $[Cp_2W_2Ir_3(\mu_4\text{-}\eta^2\text{-}C_2C_6H_4Me\text{-}4)(\mu\text{-}CO)(CO)_9]$ (**27**).....360

List of Schemes

Scheme 4.1.1. Fragmentation pathway for $PRPh_2$ (R = Ph or Me) on triosmium clusters.....329

Schemes 4.1.2 - 4. Activation of isocyanide-substituted clusters by thermolyses.....331-332

Schemes 4.1.5 - 7. Routes to higher nuclearity iridium clusters.....333-335

Scheme 4.1.8. Thermolyses of $[CpWIr_3(CO)_{11-n}(PPh_3)_n]$ (n = 1, 2 or 3).....342

Scheme 4.2.1. Reactivity of $[CpWIr_3(CO)_{11}]$ (**2**) and $[Cp_2W_2Ir_2(CO)_{10}]$ (**3**) with diphenylacetylene.....352

Scheme 4.2.2. Reactivity of $[CpWIr_3(CO)_{11}]$ (**2**) and $[Cp_2W_2Ir_2(CO)_{10}]$ (**3**) with terminal alkynes and alkynyltungsten complexes.....364

Scheme 4.2.3. Reaction of $[Cp_2M_2Co_2(\mu\text{-}CO)_3(CO)_7]$ (M = Mo, W) with HC_2Ph.....364

Scheme 4.2.4. Group 6 - Group 8 mixed-metal cluster chemistry with metal acetylides.....366

Chapter 4

Other Chemistry of Tungsten-Iridium Clusters

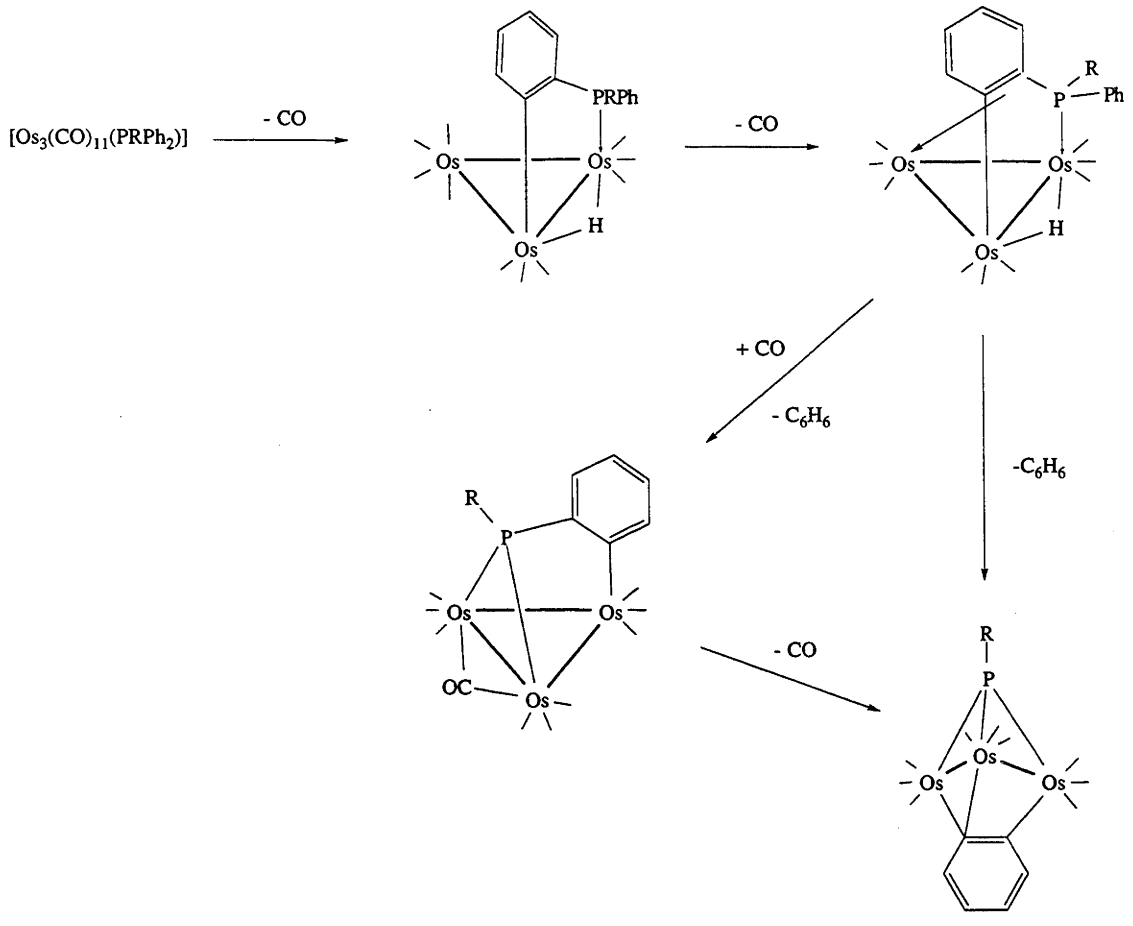
4.1. Thermolyses of Tungsten-Iridium Clusters

As mentioned in Chapter 1, significant progress has recently been made in understanding the reactivity and transformation of clusters. Organic ligands, such as phosphines or isocyanides, can undergo bond activation by thermolysis, photolysis, chemically-induced ligand elimination or hydrogenation which may lead to novel coordination modes. This section includes some examples of condensation reactions leading to clusters with ligands in interesting coordination modes.

The majority of medium- and high-nuclearity clusters are prepared from lower-nuclearity cluster precursors, usually by thermolysis. Although many improvements to cluster syntheses have been made since the mid-1960's, the syntheses of higher-nuclearity clusters remains somewhat of an art. This section also briefly outlines some controlled routes to higher-nuclearity tungsten-iridium clusters.

4.1.1. Activation of Homonuclear Clusters

Transition-metal mediated phosphorus-carbon bond cleavage is of intrinsic interest, as well as relevant to homogeneous catalyst deactivation.[1] The fragments resulting from P-C cleavage are frequently stabilized on multimetallic frameworks, and so clusters with phosphine ligands have been an abundant source of such species. Not surprisingly, then, thermolyses of ruthenium[2-5] or osmium[3,6-15] clusters proceed by P-C bond-breaking, although the chemistry of the lighter metal is complicated by competitive Ru-Ru cleavage. More recent work by Deeming and coworkers has delineated the fragmentation pathway for $PRPh_2$ (R = Me, Ph) on triosmium clusters, with reaction proceeding by way of orthometalated reaction intermediates as in Scheme 4.1.1.[16]



Scheme 4.1.1. Fragmentation pathway for $PRPh_2$ (R = Ph or Me) on triosmium clusters

Thermolysis of $[Ir_4(CO)_{12}]$ (**1**) with triphenylphosphine gave a cluster bearing a phenylphosphido ligand (Figure 4.1.1.);[17] however, no orthometalated phenylphosphinidene ligands have been identified thus far in the tetrairidium system, although $[Ir_4(\mu\text{-}H)\{\mu_3\text{-}\eta^2\text{-}cis\text{-}Ph_2PCHCHPPh(C_6H_4)\}(\mu\text{-}CO)_3(CO)_4(\eta^2\text{-dppee})]$ with an orthometalated phenyl group has been reported (Figure 4.1.1.).[18] On thermolysis, the $Ph_2PC(H)CPh$ ligand in $[Ir_4\{\mu_3\text{-}\eta^4\text{-}Ph_2PC(H)CPh\}(\mu\text{-}PPh_2)(CO)_8]$ underwent selective bond scission affording two isomers of $[Ir_4\{\mu_4\text{-}\eta^3\text{-}PhPC(H)CPh\}(\mu\text{-}PPh_2)(CO)_8(\eta^1\text{-Ph})]$ (Figure 4.1.2.), differing only in the position of the η^1-Ph ligand with respect to the butterfly core.[19]

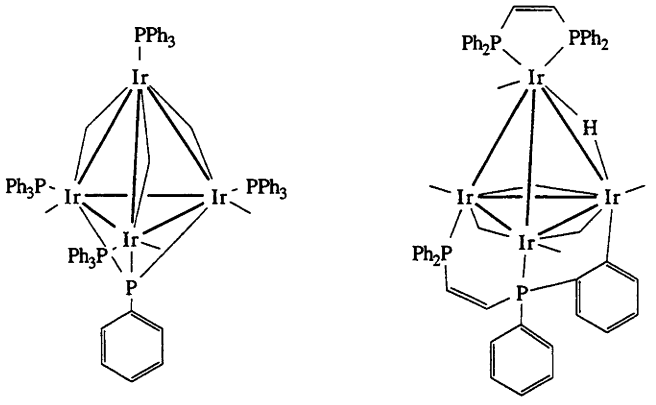


Figure 4.1.1.

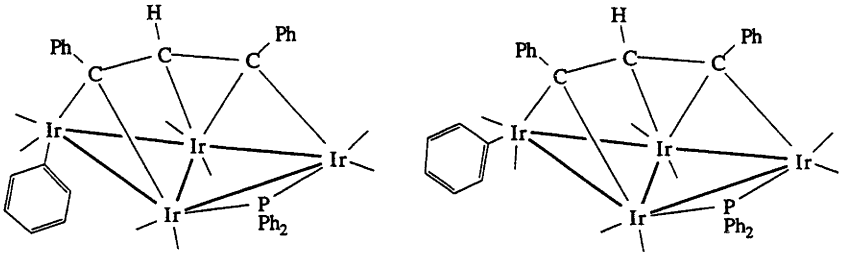
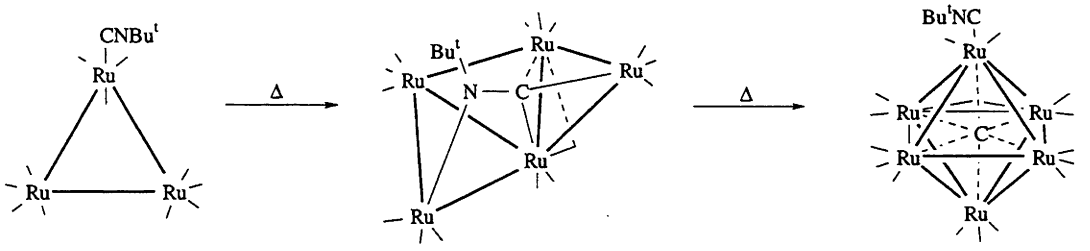


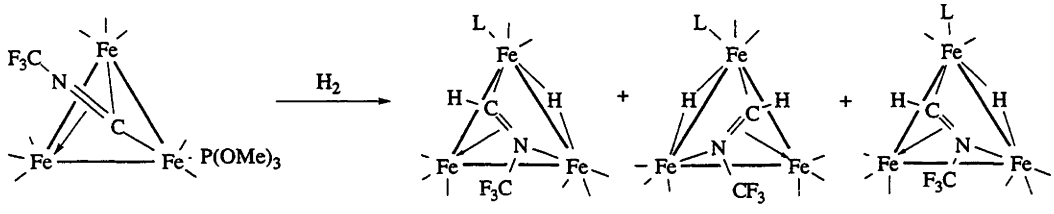
Figure 4.1.2.

Although the syntheses and characterization of the clusters $[Ir_4(CNBu^t)_n(CO)_{11-n}]$ (n = 1-3) have been reported,[20] their thermolyses have not been investigated, and so a comparison to the related tungsten-iridium compounds is not possible. Previous investigation of the thermolyses of isocyanide-derived clusters has been largely confined to trinuclear systems. As well as the common η^1 bonding mode, isocyanide ligands have the propensity for μ_n-η^2-CNR coordination in clusters. Thermolysis of the triangular ruthenium cluster $[Ru_3(CNBu^t)(CO)_{11}]$, which has an all-terminal geometry, has been reported to afford the cluster $[Ru_5(\mu_5\text{-}\eta^2\text{-}CNBu^t)(CNBu^t)(CO)_{14}]$,[21] with an edge-bridged butterfly ("swallow") core geometry and a quintuply bridging isocyanide ligand. More vigorous thermolysis (Scheme 4.1.2.) affords two products, one unidentified, and the other structurally characterized as $[Ru_6(\mu_6\text{-}C)(\mu\text{-}CO)(CNBu^t)(CO)_{15}]$,[22] with an octahedral core geometry and a terminal isocyanide ligand.



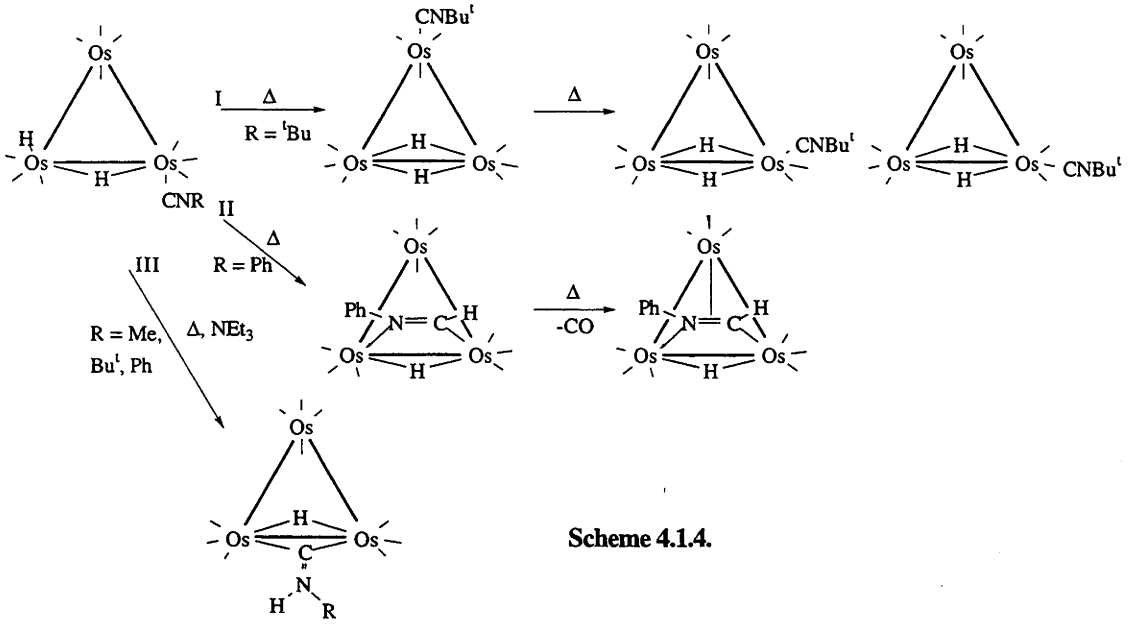
Scheme 4.1.2.

Thermolysis of the clusters $[Fe_3(\mu\text{-}CNCF_3)(CO)_{10}(L)]$ [L = $P(OMe)_3$, $P(OEt)_3$, PMe_3, PEt_3] gave $[Fe_3(\mu_3\text{-}\eta^2\text{-}CNCF_3)(CO)_8(L)]$;[23] reaction of the latter cluster with H_2 afforded $[Fe_3(\mu\text{-}H)(\mu_3\text{-}\eta^2\text{-}HC{=}NCF_3)(CO)_8(L)]$, existing as a mixture of three isomers.



Scheme 4.1.3.

Thermolysis of the cluster $[Os_3(\mu\text{-}H)(H)(CNBu^t)(CO)_{10}]$ in hexane afforded $[Os_3(\mu\text{-}H)_2(CNBu^t)(CO)_9]$ with an axially-ligated isocyanide group coordinated to the osmium not associated with the bridging hydrides.[24] Further heating of this cluster gave two different isomers of $[Os_3(\mu\text{-}H)_2(CNBu^t)(CO)_9]$ [25] with the isocyanide bound either axially or equatorially to an osmium ligated by the two bridging hydride ligands (Scheme 4.1.4, I). In contrast, thermolysis of $[Os_3(\mu\text{-}H)(H)(CNR)(CO)_{10}]$ (R = Me, Bu^t, Ph) in chloroform in the presence of base afforded $[Os_3(\mu\text{-}H)\{\mu\text{-}\eta^1\text{-}C{=}NC(H)R\}(CO)_{10}]$ involving proton transfer to the nitrogen atom (Scheme 4.1.4., III).[25,26] Thermolysis of $[Os_3(\mu\text{-}H)(H)(CNPh)(CO)_{10}]$ in di-*n*-butylether gave $[Os_3(\mu\text{-}H)(\mu\text{-}\eta^2\text{-}HC{=}NPh)(CO)_{10}]$ with an edge-bridging formimidoyl ligand. On further heating this was converted to $[Os_3(\mu\text{-}H)(\mu_3\text{-}\eta^2\text{-}HC{=}NPh)(CO)_9]$, the formimidoyl ligand rolling onto the face of the cluster (Scheme 4.1.4., II).[25]



Scheme 4.1.4.

Reaction of the rhenium cluster $[Re_3(\mu\text{-}H)_4(CO)_{10}]^-$ with cyclohexyl- or *p*-tolylisocyanide afforded $[Re_3(\mu\text{-}H)_3(\mu\text{-}\eta^2\text{-}HC{=}NR)(CO)_{10}]^-$. Upon heating, this was converted to $[Re_3(\mu\text{-}H)_3(\mu_3\text{-}\eta^2\text{-}HC{=}NR)(CO)_9]^-$,[27] a similar conversion to process II in Scheme 4.1.3. Heating the ruthenium cluster $[Ru_3(\mu\text{-dppm})(CO)_{10}]$ in the presence of CyNC afforded $[Ru_3(\mu_3\text{-}\eta^2\text{-CyNC})(\mu_3\text{-}\eta^2\text{-}PhPCH_2PPh_2)(\mu\text{-CO})(CO)_5(\eta^1\text{-Ph})]$[28] with an open core geometry and one isocyanide ligand in a novel bonding mode (Figure 4.1.3.).

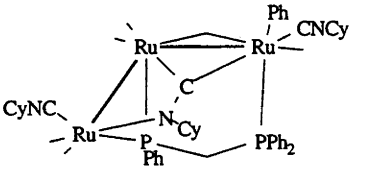
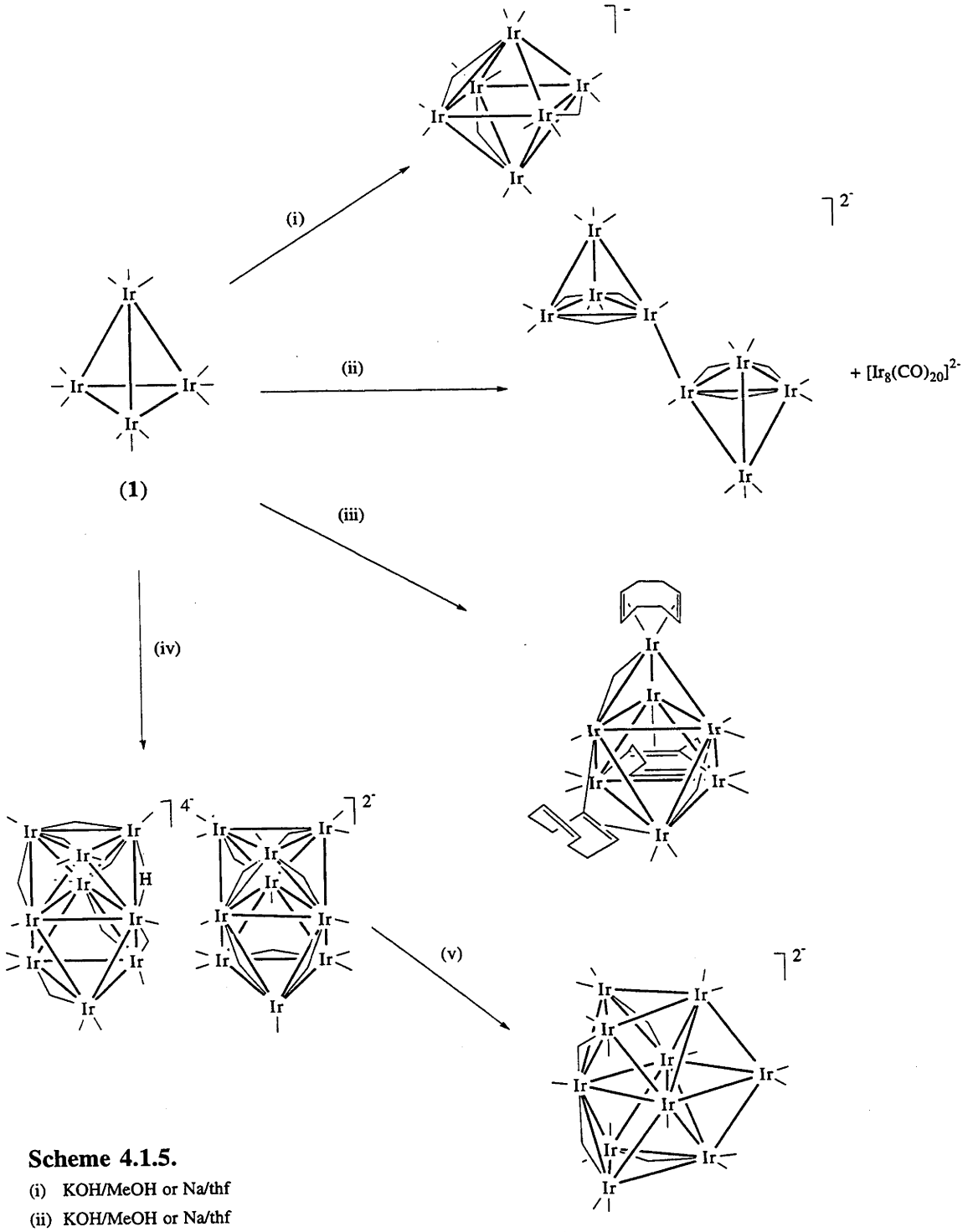


Figure 4.1.3.

The majority of medium- and high-nuclearity clusters of iridium have been prepared from lower nuclearity cluster precursors, thermolysis or base-assisted reactions being the most common routes. In some cases, other transition metals have also been incorporated into the iridium cluster core. The number of structurally characterized clusters has increased significantly in the last ten years. Several higher-nuclearity clusters of iridium have been prepared from $[Ir_4(CO)_{12}]$ (**1**) (Scheme 4.1.5.). Reaction of **1** with potassium hydroxide in methanol or sodium in thf afforded $[Ir_6(\mu\text{-}CO)_3(CO)_{12}]^{2-}$, $[Ir_8(CO)_{20}]^{2-}$, $[Ir_8(\mu\text{-}CO)_6(CO)_{16}]^{2-}$ and some lower nuclearity by-products.[29,30] The dianion $[Ir_6(\mu\text{-}CO)_3(CO)_{12}]^{2-}$ has an octahedral core geometry,[31] whereas $[Ir_8(\mu\text{-}CO)_6(CO)_{16}]^{2-}$ has two inversion-related tetrahedra.[32] Treatment of **1** with potassium carbonate in methanol afforded the structurally characterized $[Ir_9(\mu\text{-}H)(\mu\text{-}CO)_7(CO)_{12}]^{4-}$ [33] and $[Ir_9(\mu\text{-}CO)_7(CO)_{13}]^{2-}$,[34] with core geometries of face-sharing bioctahedra. Under acidic conditions, $[Ir_9(\mu\text{-}CO)_7(CO)_{13}]^{2-}$ gave $[Ir_9(CO)_{20}]^{2-}$ which was subsequently oxidized to the structurally characterized $[Ir_{10}(\mu\text{-}CO)_4(CO)_{17}]^{2-}$.[33] A minor product of the thermolyses of **1** and 1,5-cyclooctadiene was structurally identified as $[Ir_7(CO)_{12}(\eta^4\text{-}cod)(C_8H_{11})(C_8H_{10})]$,[35,36] with a capped octahedral core geometry and one coordinated, one singly and one doubly dehydrogenated cyclooctadiene residue. The hexanuclear



Scheme 4.1.5.

(i) KOH/MeOH or Na/thf

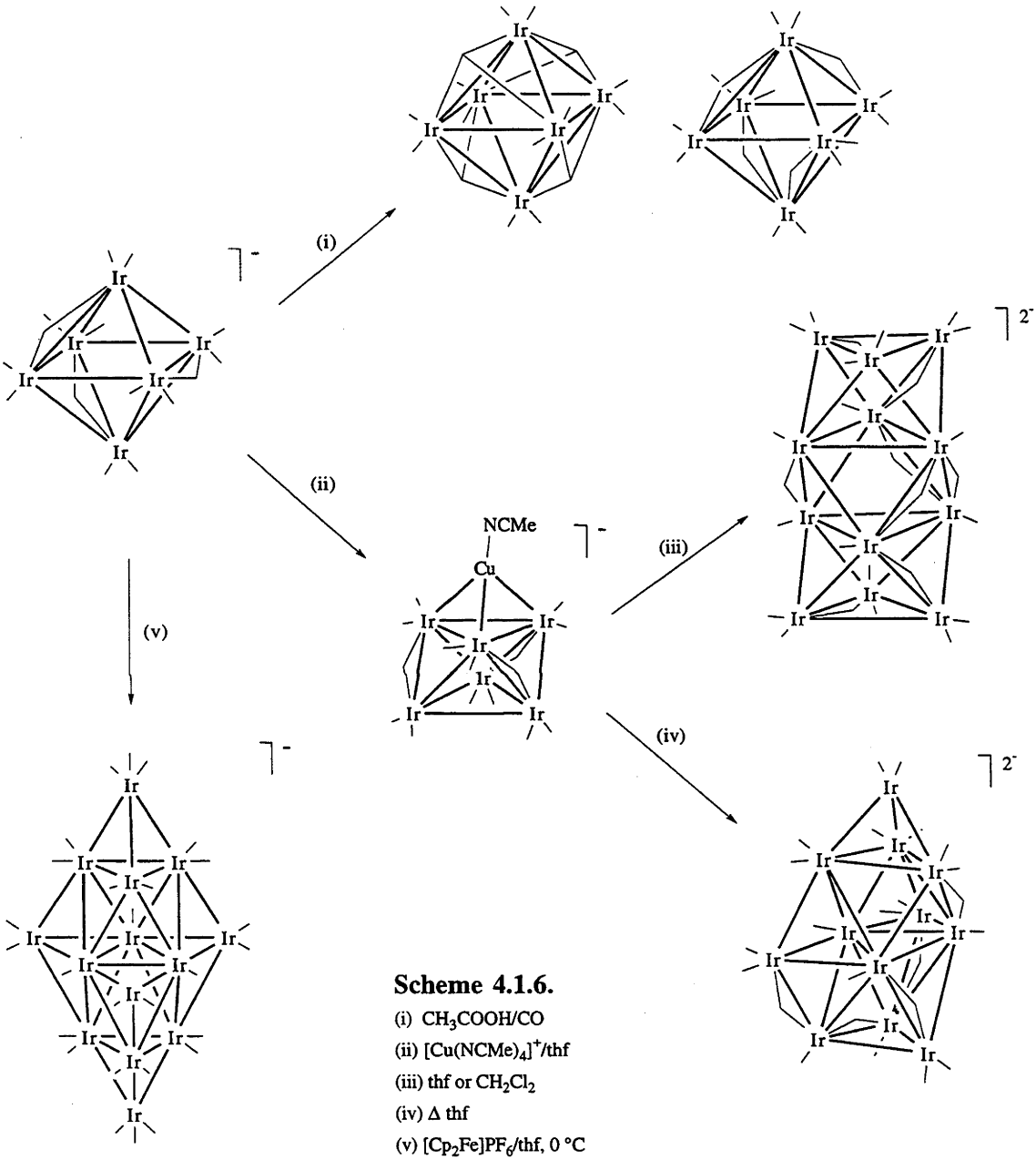
(ii) KOH/MeOH or Na/thf

(iii) cod/ Δ C_6H_5Cl

(iv) K_2CO_3/MeOH

(v) H^+

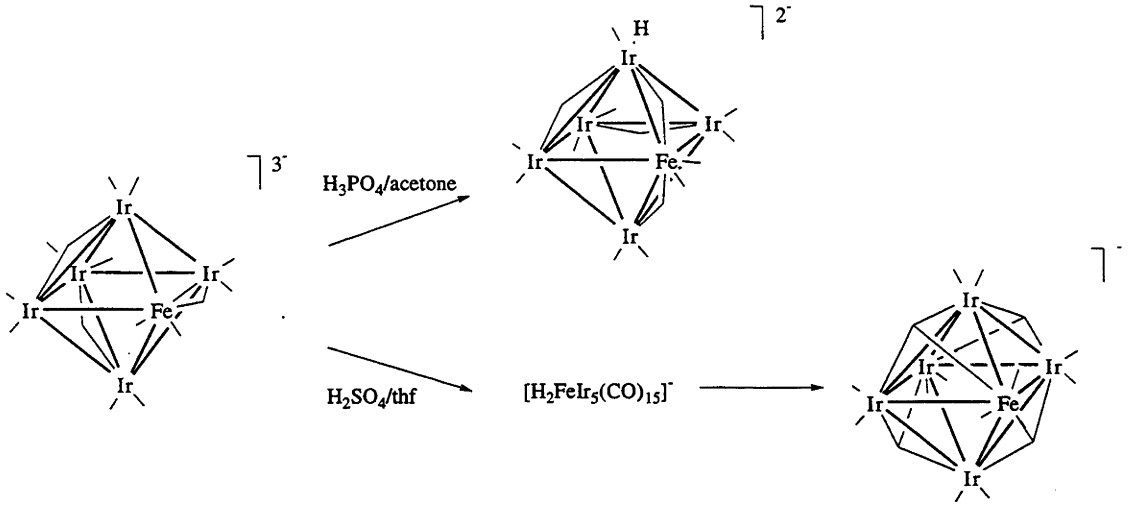
dianion. $[Ir_6(\mu\text{-}CO)_3(CO)_{12}]^{2-}$ is also a precursor to higher-nuclearity clusters (Scheme 4.1.6.). $[Ir_6(\mu\text{-}CO)_3(CO)_{12}]^{2-}$ reacted under acidic conditions forming $[Ir_6(CO)_{16}]$. Two octahedral isomers of $[Ir_6(CO)_{16}]$ have been structurally characterized, the "red" isomer with four face capping carbonyls, analogous to the structures of $[Rh_6(CO)_{16}]$ and $[Co_6(CO)_{16}]$ and the "black" isomer with four bridging carbonyls.[37]



Scheme 4.1.6.
(i) CH_3COOH/CO
(ii) $[Cu(NCMe)_4]^+$/thf
(iii) thf or CH_2Cl_2
(iv) Δ thf
(v) $[Cp_2Fe]PF_6$/thf, 0 °C

Reaction of $[Ir_6(\mu\text{-}CO)_3(CO)_{12}]^{2-}$ with $[Cu(NCMe)_4]^+$ afforded $[Ir_6(\mu\text{-}CO)_3(CO)_{12}Cu(NCMe)]^-$[38] which slowly oxidized to $[Ir_{12}(\mu\text{-}CO)_8(CO)_{18}]^{2-}$, identified as face-fused octahedra.[39] Alternatively, thermolysis in thf afforded $[Ir_{12}(\mu\text{-}CO)_5(CO)_{19}]^{2-}$.[40] Oxidation of $[Ir_6(CO)_{15}]^{2-}$ with $[Cp_2Fe]^+$ afforded $[Ir_{14}(CO)_{27}]^-$ with the novel geometry shown in Scheme 4.1.6.[41]

Reaction of **1** with $[Fe(CO)_5]$ or $[RuCl_3.xH_20]$ afforded $[MIr_4(\mu\text{-}CO)_3(CO)_{12}]^{2-}$ (M = Fe, Ru respectively) with the incoming metal atom capping the tetrahedral tetrairidium core.[42,43] Thermolyses of the iron-iridium derivative $[FeIr_4(\mu\text{-}CO)_3(CO)_{12}]^{2-}$ with $[Ir(CO)_4]^-$ afforded $[FeIr_5(\mu\text{-}CO)_3(CO)_{12}]^{3-}$.[44] A number of structurally characterized octahedral clusters were formed from the latter by protonation (Scheme 4.1.7.).[44]



Scheme 4.1.7.

In summary, the thermolyses of homonuclear clusters have been extensively investigated. Reactions of phosphine- or isocyanide-substituted homometallic clusters afford a significant number of different clusters with ligands in novel coordination modes. The majority of medium- and high-nuclearity iridium clusters were prepared by thermolysis or other methods of bond activation, the most common precursor being $[Ir_4(CO)_{12}]$ (**1**). This leadsto the medium-nuclearity cluster $[Ir_6(\mu\text{-}CO)_3(CO)_{12}]^{2-}$, which in turn was reacted under a variety of conditions to form higher nuclearity clusters.

Although comprehensive thermolytic investigations of homometallic clusters have been carried out, comparatively less is known about thermolyses of mixed-metal clusters. As part of the investigations contrasting reactivity of tetrahedral tungsten-iridium clusters with that of the parent tetrairidium clusters, the thermolyses of the $[CpWIr_3(CO)_{11}]$ (**2**), $[Cp_2W_2Ir_2(CO)_{10}]$ (**3**), $[CpWIr_3(\mu\text{-}CO)_3(CO)_{7-n}(PR_3)]$ [R = Ph, n = 1 - 3, (**4** - **6**); R = Me, n = 1 (**7**)], $[Cp_2W_2Ir_2(\mu\text{-}CO)_3(CO)_{6-n}(PPh_3)]$ [n = 1 (**8**) or 2 (**9**)], $[CpWIr_3(CO)_{10}(CNBu^t)]$ (**10**) and $[CpWIr_3(CO)_9(CNBu^t)_2]$ (**11**) have been investigated.

4.1.2. Thermolyses of P-adducts of [CpWIr3(CO)11] (2)

Heating $[CpWIr_3(\mu\text{-}CO)_3(CO)_7(PPh_3)]$ (**4**) in toluene for 15 min afforded one major and one minor product on purification by preparative thin layer chromatography. The minor band, $[CpWIr_3(CO)_{11}]$ (**2**), was isolated in 32 % yield, and its identity confirmed by FTIR spectroscopy. The major product was obtained in 56 % yield as dark purple crystals of

$[CpWIr_3\{\mu_3\text{-}\eta^2\text{-}PPh(C_6H_4)\}(\mu\text{-}CO)_2(CO)_7]$ (**12**). The spectral data are sufficient to establish the molecular composition but not the specific ligation sites. The solution IR spectrum of **12** contains seven terminal carbonyl bands between 2066 and 1943 cm^{-1}; a band at 1864 cm^{-1}, characteristic of edge-bridging carbonyl, is also present. The ^1H NMR spectrum exhibits an ABCD pattern of resonances suggesting the presence of an orthometalated C_6H_4 ring. The ^{31}P NMR spectrum contains a singlet at 309.6 ppm, characteristic of a phosphinidene ligand. The FAB mass spectrum has peaks corresponding to the parent ion (at 1262 mass units) and loss of nine successive CO ligands.

Similarly, thermolysis of $[CpWIr_3(\mu\text{-}CO)_3(CO)_6(PPh_3)_2]$ (**5**) in toluene for 15 min afforded two major products on workup by preparative thin-layer chromatography. One product was characterized as $[CpWIr_3\{\mu_3\text{-}\eta^2\text{-}PPh(C_6H_4)\}(\mu\text{-}CO)_2(CO)_7]$ (**12**) in 23 % yield. The other major product was isolated in 39 % yield as brown crystals of $[CpWIr_3\{\mu_3\text{-}\eta^2\text{-}PPh(C_6H_4)\}(\mu\text{-}CO)_2(CO)_6(PPh_3)]$ (**13**), and characterized by a combination of FTIR, ^1H NMR, ^{13}C NMR and ^{31}P NMR spectroscopies and FAB MS. The solution FTIR spectrum contains five terminal carbonyl bands between 2046 and 1963 cm^{-1}. A weak intensity absorption at 1814 cm^{-1} suggests the presence of edge-bridging carbonyls. The ^1H NMR spectrum features an ABCD pattern of signals in the aromatic region consistent with the presence of an orthometalated C_6H_4 ring, as well as resonances in the expected regions indicating the presence of phenyl and cyclopentadienyl groups. The FAB mass spectrum contains the parent ion at 1496 mass units and sequential loss of seven CO ligands. In an analogous fashion, heating $[CpWIr_3(\mu\text{-}CO)_3(CO)_5(PPh_3)_3]$ (**6**) gave **12** (15 %) and **13** (44 %). X-ray structural studies of **12** and **13** were carried out to confirm the identities of the orthometalated products, and to determine the coordination sites of the phosphine ligand (**13**) and phosphinidene species (**12** and **13**); significant bond lengths are collected in Table 4.1.1., and selected angles displayed in Table 4.1.2. Figures 4.1.4. (**12**) and 4.1.5. (**13**) contain plots of the molecular geometries and show the atomic numbering scheme.

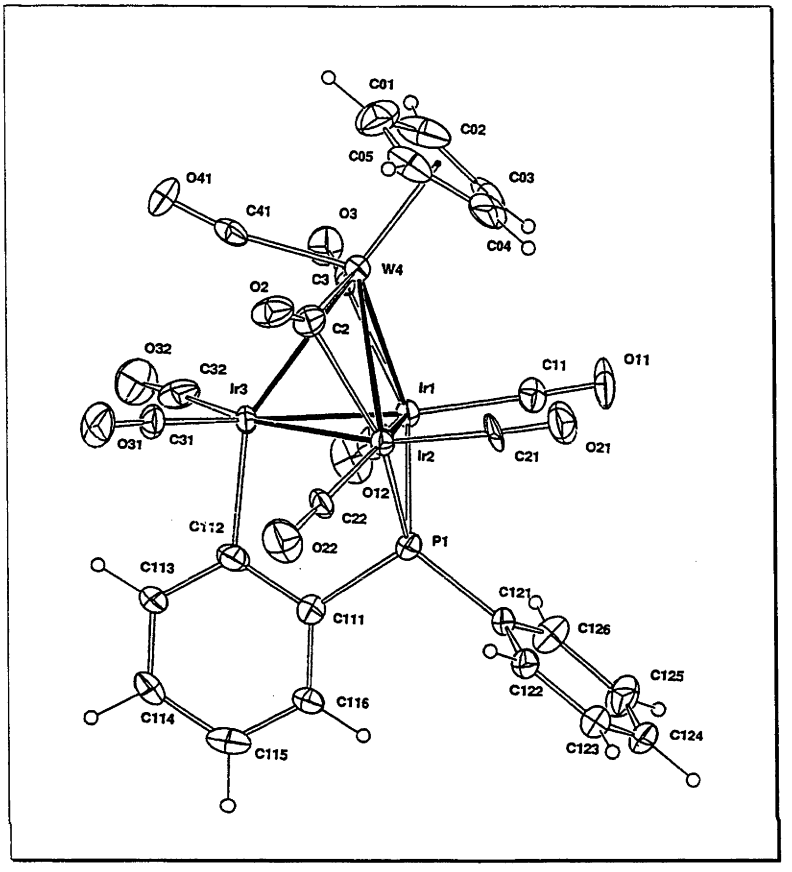


Figure 4.1.4. Molecular structure and atomic labelling scheme for $[CpWIr_3\{\mu_3\text{-}\eta^2\text{-}PPh(C_6H_4)\}(\mu\text{-}CO)_2(CO)_7]$, (**12**). Thermal envelopes of 20 % probability are shown for the non-hydrogen atoms; hydrogen atoms have arbitrary radii of 0.1 Å.

(By Brian W. Skelton, Vicki-Anne Tolhurst and Allan H. White)

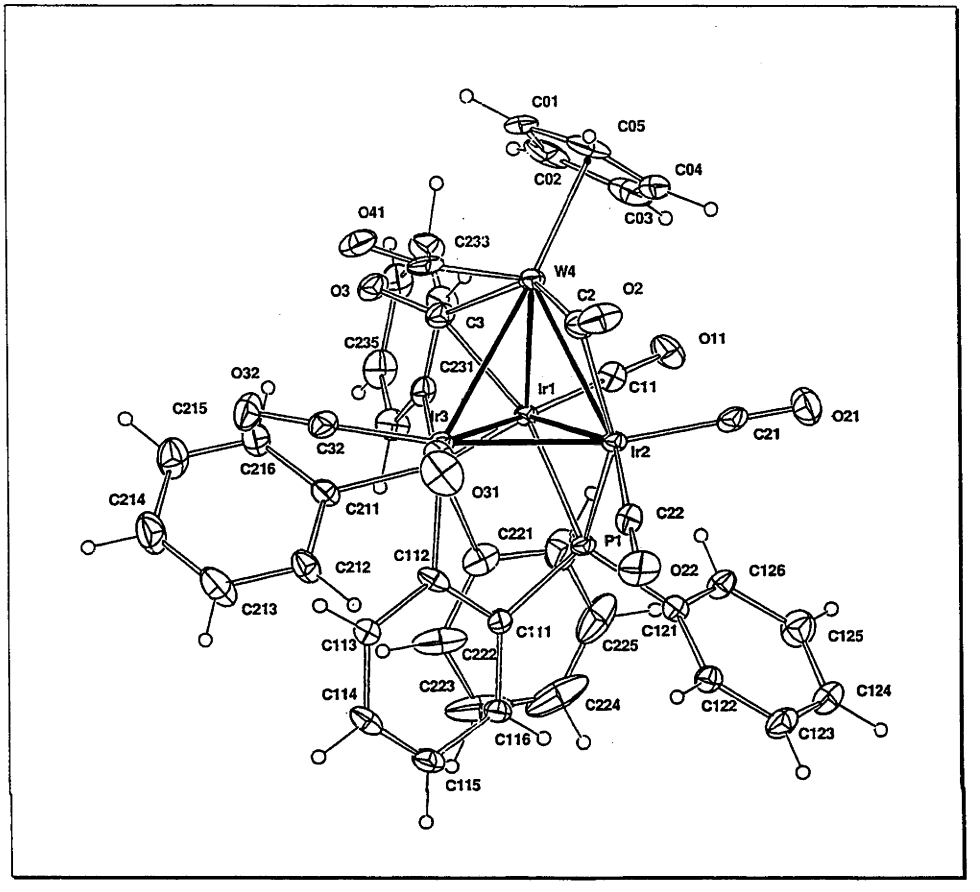


Figure 4.1.5. Molecular structure and atomic labelling scheme for $[CpWIr_3\{\mu_3\text{-}\eta^2\text{-}PPh(C_6H_4)\}(\mu\text{-}CO)_2(CO)_6(PPh_3)]$, (**13**). Thermal envelopes of 20 % probability are shown for the non-hydrogen atoms; hydrogen atoms have arbitrary radii of 0.1 Å.

(By Brian W. Skelton and Allan H. White)

Table 4.1.1. Selected Bond Lengths (Å) for Complexes **12** and **13**

Bond	12	13	Bond	12	13
Ir(1)-Ir(2)	2.741(1)	2.743(1)	Ir(1)-Ir(3)	2.676(1)	2.721(2)
Ir(1)-W(4)	2.813(1)	2.839(1)	Ir(2)-Ir(3)	2.670(2)	2.654(2)
Ir(2)-W(4)	2.800(1)	2.803(1)	Ir(3)-W(4)	2.907(1)	2.880(1)
W(4)-C(01)	2.30(2)	2.32(2)	W(4)-C(02)	2.32(2)	2.33(2)
W(4)-C(03)	2.28(3)	2.36(2)	W 4)-C(04)	2.36(3)	2.33(2)
W(4)-C(05)	2.29(2)	2.30(1)	Ir(1)-P(1)	2.279(4)	2.308(3)
Ir(2)-P(1)	2.28(5)	2.285(3)	Ir(1)-P(2)		2.337(4)
Ir(2)-C(2)	2.24(2)	2.34(2)	Ir(1)-C(3)	2.22(2)	2.05(1)
W(4)-C(2)	2.07(2)	2.06(2)	W(4)-C(3)	2.07(2)	2.20(1)
C(2)-O(2)	1.17(3)	1.15(2)	C(3)-O(3)	1.21(3)	1.19(2)
C(01)-C(02)	1.32(4)	1.42(4)	C(02)-C(03)	1.34(5)	1.39(3)
C(03)-C(04)	1.45(5)	1.32(3)	C(04)-C(05)	1.45(5)	1.37(3)
C(01)-C(05)	1.30(4)	1.36(3)	P(1)-C(111)	1.81(3)	1.82(1)
P(1)-C(121)	1.83(2)	1.78(1)	P(2)-C(211)		1.83(1)
P(2)-C(221)		1.82(2)	P(2)-C(231)		1.82(1)
Ir(3)-C(112)	2.12(2)	2.11(1)	C(111)-C(112)	1.42(4)	1.41(2)
Ir(1)-C(11)	1.93(3)	1.87(2)	Ir(1)-C(12)	1.81(3)	
Ir(2)-C(21)	1.87(3)	1.86(2)	Ir(2)-C(22)	1.86(2)	1.94(2)
Ir(3)-C(31)	1.88(3)	1.85(2)	Ir(3)-C(32)	1.89(3)	1.87(1)
W(4)-C(41)	2.01(3)	1.87(2)	C(11)-O(11)	1.10(4)	1.14(2)
C(12)-O(12)	1.18(3)		C(21)-O(21)	1.17(4)	1.16(2)
C(22)-O(22)	1.13(3)	1.09(2)	C(31)-O(31)	1.12(3)	1.15(2)
C(32)-O(32)	1.14(4)	1.16(2)	C(41)-O(41)	1.11(3)	1.22(2)

Table 4.1.2. Selected Bond Angles (°) for Complexes **12** and **13**.

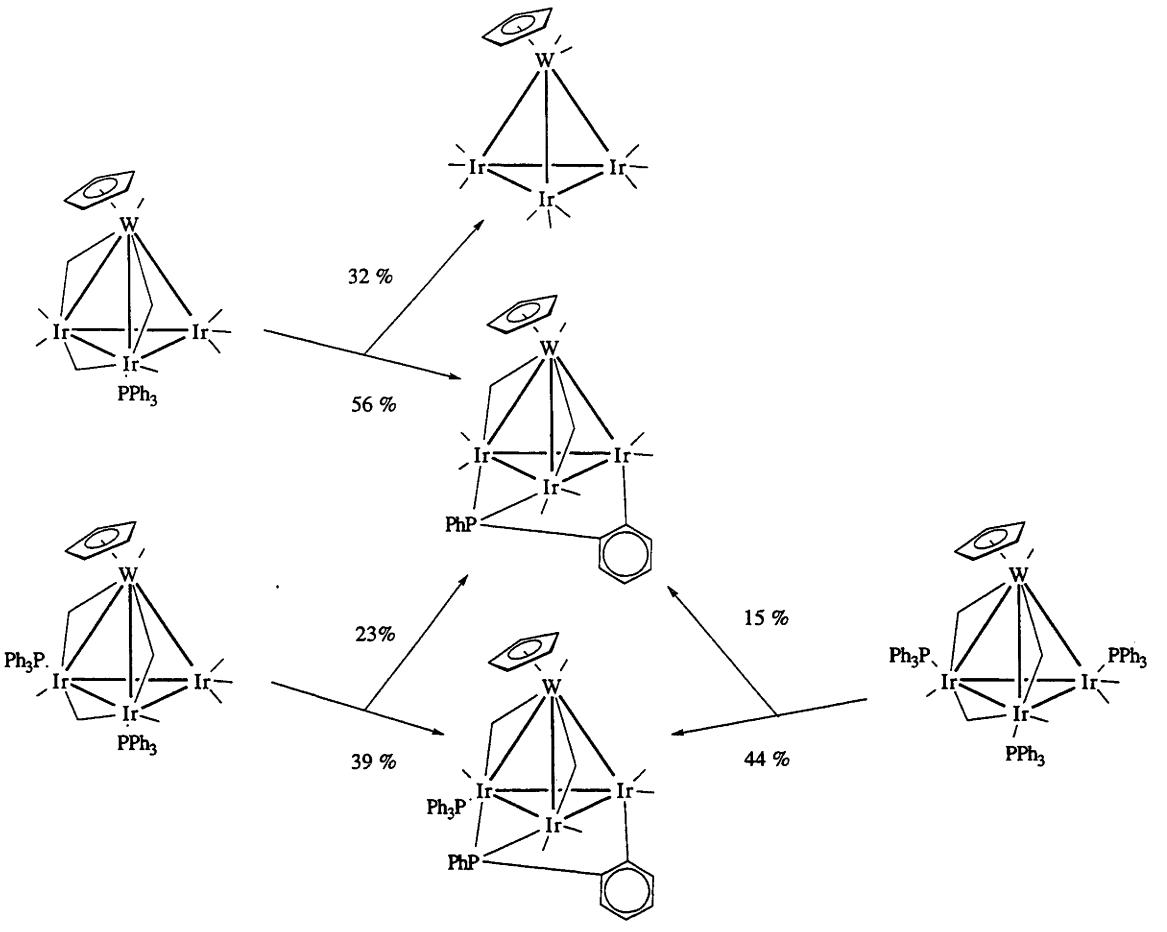
Angle	12	13
Ir(2)-Ir(1)-Ir (3)	59.06 (3)	58.12(4)
Ir(2)-Ir(1)-W(4)	60.53 (3)	60.24(3)
Ir(3)-Ir (1)-W(4)	63.91(3)	62.34(3)
Ir(1)-Ir (2)-Ir(3)	59.26(4)	60.52(3)
Ir(3)-Ir (2)-W(4)	64.17(4)	63.64(4)
Ir(1)-Ir (3)-Ir(2)	61.68(4)	61.36(5)
Ir(1)-Ir (3)-W(4)	60.34(3)	60.85(3)
Ir(2)-Ir (3)-W(4)	60.09(3)	60.69(3)
Ir(1)-W (4)-Ir(2)	58.45(3)	58.17(3)
Ir(1)-W(4)-Ir(3)	55.75(3)	56.81(4)
Ir(2)-W(4)-Ir(3)	55.75(3)	55.67(4)
Ir(2)-C(2)-W(4)	80.8(8)	78.9(6)
Ir(2)-C(2)-O(2)	128(1)	125(1)
W(4)-C(2)-O(2)	150(1)	156(1)
Ir(1)-C(3)-W(4)	82.0(7)	83.9(5)
Ir(1)-C(3)-O(3)	129(1)	138(1)
W(4)-C(3)-O(3)	148(1)	138(1)
W(4)-C(41)-O(41)	167(2)	170(1)
Ir(1)-P(1)-Ir(2)	73.9(1)	73.33(9)
Ir(1)-Ir(2)-P(1)	53.0(1)	53.73(8)
Ir(2)-Ir(1)-P(1)	53.1(1)	52.94(9)
Ir(1)-P(1)-C(111)	112.7(7)	112.9(4)
Ir(2)-P(1)-C(111)	111.5(7)	111.8(5)
P(1)-C(111)-C(112)	113(1)	112.3(8)
Ir(3)-C(112)-C(111)	118(2)	118.5(9)
Ir(1)-Ir(3)-C(112)	93.8(7)	94.1(4)
Ir(2)-Ir(3)-C(112)	92.4(7)	93.6(4)

Complexes **12** and **13** have the WIr_3 pseudotetrahedral framework of the precursor clusters $[CpWIr_3(\mu\text{-}CO)_3(CO)_{8-n}(PPh_3)_n]$ [n = 1 (**4**), 2 (**5**) and 3 (**6**)] and possess η^5-cyclopentadienyl groups, two bridging carbonyls spanning W-Ir vectors, seven (**12**) or six (**13**) terminal carbonyl ligands, a triphenylphosphine ligand (**13**), and a μ_3-η^2-bound orthometalated phosphinidene moiety capping the triiridium faces. The WIr_3 core distances in **12** and **13** are inequivalent, with the longest [2.907(1) Å (**12**), 2.880(1) Å (**13**)] being

those not bearing a bridging carbonyl ligand; as with other phosphine-substituted tungsten-iridium clusters, the longest W-Ir vectors are those effectively *trans* to the cyclopentadienyl groups.[45] The bridging carbonyl ligands in **12** and **13** bridge asymmetrically; in **12**, both ligands are displaced toward the tungsten, whereas in **13**, CO(3) is closer to Ir(1), the latter presumably resulting from the ligation of triphenylphosphine at Ir(1), and the consequent increase in electron density at this metal. Distances and angles involving the phosphines are not unusual. Those involving the terminal carbonyl ligands are relatively imprecise; the most dramatic difference between **12** and **13** is in the geometry about CO(4) [W(4) - C(41) 2.01(3) Å **12**, 1.87(2) Å **13**], with the shorter bond in **13** possibly a result of compensation for the asymmetry of CO(3). The phosphinidene ligands cap the triiridium faces, with the phosphorus atom bridging an Ir-Ir vector symmetrically in both **12** and **13**; the corresponding WIr_2 face thus has bridging ligands about all edges, and it is over this face that the cyclopentadienyl ligands sit. The orthometalated phenyl interacts with the remaining iridium. Electron counting procedures reveal that both **12** and **13** have 60 e, electron precise for clusters possessing tetrahedral cores.

Crystallographically-verified clusters containing orthometalated phenylphosphinidene groups are comparatively rare; there are no precedents in the tetrairidium system for clusters of this type, with previous examples being confined to the iron subgroup,[4,46-50] and a mixed ruthenium-iridium cluster $[Ru_3Ir(\mu\text{-}H)_2\{\mu_3\text{-}\eta^2\text{-}PPh(C_6H_4)\}(\mu\text{-}PPh_2)(\mu\text{-}CO)(CO)_7(PPh_3)]$ (**14**).[46] In the ruthenium-iridium cluster **14**, the $PPhC_6H_4$ group face-caps at a Ru_2Ir face with the phosphorus bridging a Ru-Ru bond and the orthometalated phenyl group bound to the iridium. The Ir-C(*ortho*) linkage is shorter in **14** than in **12** or **13** [2.086(7) Å **14** vs 2.12(2) Å **12**, 2.11(1) Å **13**], although these differences are within 3σ error margins. The phosphine ligates at the orthometalated phenyl-bound iridium in **14**, unlike in **13**, where it coordinates to a phosphido-bound iridium. Phosphido bridges in the tetrairidium system are rare; in $[Ir_4(\mu\text{-}H)(\mu\text{-}PPh_2)(\mu\text{-}CO)(CO)_8(PPh_3)]$, the phosphido bridges symmetrically, with Ir-P_{av} 2.30 Å similar to the corresponding distances in **12** and **13**.[51] In contrast to **13**, $[Ir_4(\mu\text{-}H)(\mu\text{-}PPh_2)(\mu\text{-}CO)(CO)_8(PPh_3)]$ contains a phosphine ligand at a non-phosphido-ligated iridium.

The results of the thermolytic investigations detailed above are summarized in Scheme 4.1.8. All three reactions proceeded to give a mixture of products, with the identified components of the reaction mixtures accounting for 60-90 % of the theoretical yields. Thermolyses of related phosphine-substituted triosmium clusters proceeded by initial loss of CO to generate a vacant coordination site, and subsequent oxidative addition of a phenyl *ortho*-C-H bond across the Os-Os bond.[16] Subsequent loss of CO, rearrangement, addition of CO and loss of benzene form triosmium complexes bearing phosphinidene ligands analogous to **12** and **13** (Scheme 4.1.1.).



Scheme 4.1.8. Thermolyses of $[CpWIr_3(CO)_{11-n}(PPh_3)_n]$ (n = 1, 2 or 3). Reaction conditions: toluene, 110 °C, 15 min.

While a similar process may be operative in the tungsten-iridium system in the conversion of $[CpWIr_3(\mu\text{-}CO)_3(CO)_7(PPh_3)]$ (**4**) into **12** and $[CpWIr_3(\mu\text{-}CO)_3(CO)_6(PPh_3)_2]$ (**5**) into **13**, the mixtures of products suggest that other pathways are accessible; the transformation of **4** into **2**, and **5** into **12**, and the formation of **12** and **13** from heating $CpWIr_3(\mu\text{-}CO)_3(CO)_5(PPh_3)_3]$ (**6**), is consistent with the loss of PPh_3 being competitive with loss of CO for the system under investigation. The product distributions also suggest that this pathway becomes increasingly important on proceeding from **4** through **5** to **6**. Indeed, for the last mentioned cluster, initial loss of PPh_3 seems specific, chemistry which is mirrored in its FAB MS where $[M\text{-}PPh_3]^+$ rather than $[M]^+$ is observed, and in its solution chemistry, where it tranforms into **5** at room temperature over an hour.

The relatively good yield of the orthometalated product **12** prompted the examination of its derivative chemistry, in a bid to generate benzyne fragments on a mixed-metal cluster, analogous to those described previously for homometallic systems; clusters similar to **12** which have phenylphosphido ligands react to form benzyne derivatives, by way of decarbonylation (Scheme 4.1.1.), so attempted elimination of CO was pursued. All rational attempts proved fruitless, however, with thermolysis, photolysis, and the attempted

generation of a vacant coordination site by employing trimethylamine-*N*-oxide all affording intractable mixtures.

It is well known that P-C(aryl) cleavage is favoured over P-C(methyl). However, double C-H activation of coordinated trimethylphosphine has been achieved, in converting $[Os_3(CO)_{11}(PMe_3)]$ into $[Os_3(\mu\text{-}H)_2(\mu_3\text{-}\eta^2\text{-}Me_2PCH)(CO)_9]$.[10] This pathway does not seem accessible in the tungsten-iridium system; heating $[CpWIr_3(\mu\text{–}CO)_3(CO)_7(PMe_3)]$ (**7**) (refluxing thf, 15 min) did not lead to any tractable products.

The results in Chapter 2 reveal that (conceptual) isolobal replacement of one $Ir(CO)_3$ vertex in **1** by $CpW(CO)_2$ to give $[CpWIr_3(CO)_{11}]$ (**2**) facilitated phosphine substitution at iridium; whereas reaction of **1** with phosphine requires forcing conditions (heating at 80-110 °C)[52] to proceed, phosphines react with **2** at room temperature. Differences in reactivity extend to thermolyses, with the mixed tungsten-iridium system affording examples of orthometalation of the phenylphosphine-substituted clusters, cluster types not thus far identified in the tetrairidium system (it has been reported that, in contrast to the triosmium system, thermolysis of $[Ir_4(\mu\text{-}H)(\mu\text{-}PPh_2)(\mu\text{-}CO)(CO)_8(PPh_3)]$ does not afford orthometalated products).[51]

4.1.3. Thermolyses of Phosphine adducts of $[Cp_2W_2Ir_2(CO)_{10}]$ (3)

Heating $[Cp_2W_2Ir_2(\mu\text{-}CO)_3(CO)_6(PPh_3)]$ (**8**) in thf for 1 h afforded one band on purification by preparative thin layer chromatography. IR spectroscopy identified the product as the precursor cluster **3** in 34 % yield, formed presumably by disproportionation of the reactant cluster. All other attempts at activation of the core afforded the same result, or caused decomposition of the cluster. The sterically congested cluster $[Cp_2W_2Ir_2(\mu\text{-}CO)_3(CO)_5(PPh_3)_2]$ (**9**) is known to convert to $[Cp_2W_2Ir_2(\mu\text{-}CO)_3(CO)_6(PPh_3)]$ (**8**) in solution at room temperature. Not surprisingly then, mild thermolysis of **9** in dichloromethane causes conversion to the mono-substituted derivative, followed by further disproportionation to the parent cluster, **3**, as monitored by IR. This type of disproportionation reaction is not uncommon in the ditungsten-diiridium cluster system; crystals of **8** suitable for X-ray diffraction studies were grown from a solution of **9**.

4.1.4. Thermolyses of Isocyanide adducts of $[CpWIr_3(CO)_{11}]$ (2)

Refluxing $[CpWIr_3(CO)_{10}(CNBu^t)]$ (**10**) in thf for 30 h afforded two minor bands on purification by preparative thin layer chromatography, however a substantial amount of decomposition of the cluster was noted. The first band was isolated in 15 % yield and identified as unreacted **10** by IR spectroscopy. The second band was isolated in 10 % yield and its identity confirmed by spectroscopic methods as $[CpWIr_3(CO)_9(CNBu^t)_2]$ (**11**). Heating $[CpWIr_3(CO)_9(CNBu^t)_2]$ (**11**) in thf for 30 h afforded a green solution.

Purification by preparative thin layer chromatography gave one minor band of **10** and one major band of unreacted **11**, identified by IR spectroscopy, with the origin of the green colour as yet unknown. Thermolysis of **11** under more forcing conditions (refluxing toluene, 30 h) afforded a brown solution. Purification by preparative thin layer chromatography afforded three minor bands, identified spectroscopically as **10** (9 %), **11** (16 %) and $[CpWIr_3(CO)_8(CNBu^t)_3]$ (**15**, 4 %). It would appear that activation of the isocyanide ligand(s) on the clusters to afford μ_n-η^2-CNR coordination is not, as yet, accessible in the tungsten-iridium system.

4.1.5. Thermolyses of $[Cp_2W_2Ir_2(CO)_{10}]$ (3)

Refluxing $[Cp_2W_2Ir_2(CO)_{10}]$ with triphenylamine in tetrahydrofuran for 30 h afforded a complex mixture of products, separated by preparative thin layer chromatography. The first two bands were characterized as **2** (formed by disproportionation of the cluster core, 7 %) and **3** (unreacted starting material, 40 %), respectively. Band 5 was identified as the previously characterized cluster $[Cp_3W_3Ir_2(\mu\text{-}H)(CO)_{10}]$ (**17**) (< 1 %).[53] The third band was conclusively identified as $[Cp_3W_3Ir_4(\mu\text{-}H)(CO)_{12}]$ (**16**) by a combination of NMR spectroscopy and an X-ray structural study. The presence of base in the reaction mixture is not critical in affecting the products formed, although it does influence the product distribution. Refluxing **3** in thf in the absence of base generated the aforementioned complexes, but in slightly lower yields, with additional unidentified byproducts making the purification of complexes **3** and **5** more difficult.

Compound **16** has seven IR-active bands and a ^1H NMR spectrum consistent with the presence of three inequivalent tungsten-bound cyclopentadienyl ligands, and a signal assigned to a hydride bridging a tungsten-iridium bond.

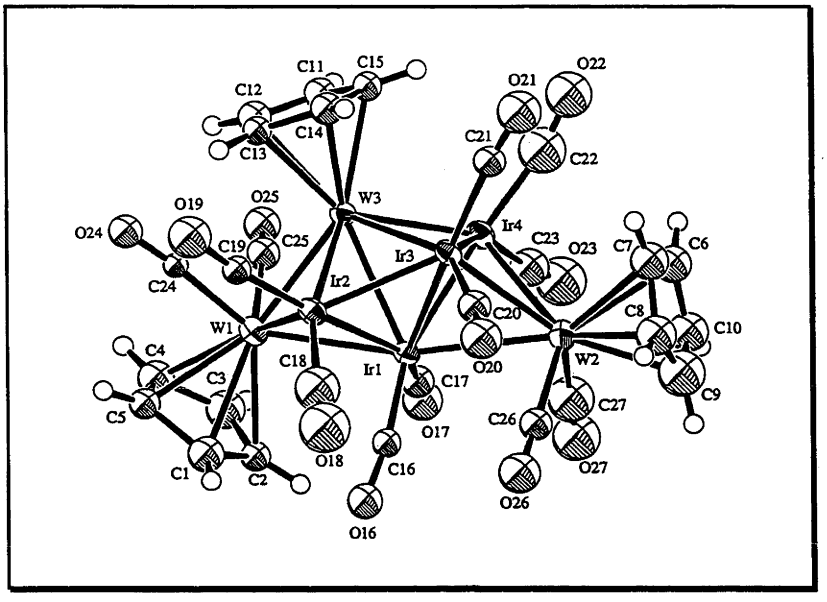
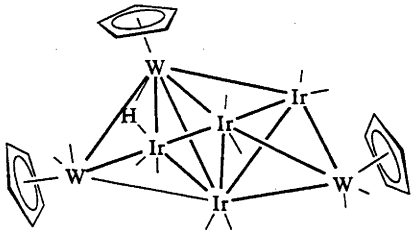


Figure 4.1.6. (a) Molecular structure and atomic labelling scheme for $[Cp_3W_3Ir_4(\mu\text{-}H)(CO)_{12}]$ (**16**). Thermal envelopes of 20 % probability are shown for the non-hydrogen atoms; hydrogen atoms have arbitrary radii of 0.1 Å.

(By David C. R. Hockless)



(b) Schematic representation of **16** with postulated location (potential energy calculations) of the spectroscopically identified bridging hydride.

Table 4.1.3. Selected Bond Lengths (Å) for Complex **16**.

Bond	Length	Bond	Length
Ir(1)-Ir(2)	2.751(2)	Ir(1)-Ir(3)	2.687(2)
Ir(1)-Ir(4)	2.695(2)	Ir(1)-W(1)	2.864(2)
Ir(1)-W(2)	2.889(2)	Ir(1)-W(3)	2.824(2)
Ir(2)-Ir(3)	2.715(2)	Ir(2)-W(1)	2.832(2)
Ir(2)-W(3)	2.713(2)	Ir(3)-Ir(4)	2.704(2)
Ir(3)-W(2)	2.763(2)	Ir(3)-W(3)	2.682(2)
Ir(4)-W(2)	2.786(2)	Ir(4)-W(3)	2.684(2)
W(1)-W(3)	2.784(2)	Ir(1)-C(16)	1.86(3)
Ir(1)-C(17)	1.90(3)	Ir(2)-C(18)	1.96(4)
Ir(2)-C(19)	1.81(3)	Ir(3)-C(20)	1.82(3)
Ir(3)-C(21)	1.92(3)	Ir(4)-C(22)	1.91(4)
Ir(4)-C(23)	1.90(4)	W(1)-C(24)	1.98(3)
W(1)-C(24)	1.98(3)	W(1)-C(25)	2.01(3)
W(2)-C(26)	1.96(3)	W(2)-C(27)	2.01(5)
W(3)...C(25)	2.63(3)	W(1)-C(1)	2.45(3)
W(1)-C(2)	2.40(3)	W(1)-C(3)	2.30(4)
W(1)-C(4)	2.29(3)	W(1)-C(5)	2.36(3)
W(2)-C(6)	2.37(3)	W(2)-C(7)	2.46(4)
W(2)-C(8)	2.34(4)	W(2)- C(9)	2.31(4)
W(2)-C(10)	2.29(3)	W(3)-C(11)	2.38(3)
W(3)-C(12)	2.40(3)	W(3)-C(13)	2.38(3)
W(3)-C(14)	2.39(3)	W(3)-C(15)	2.39(3)

Table 4.1.4. Selected Bond Angles (°) for Complex **16**.

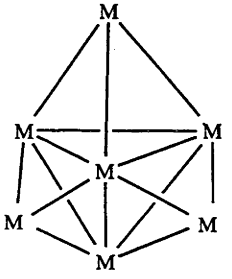
Bond	Angle	Bond	Angle
Ir(2)-Ir(1)-Ir(3)	59.88(4)	Ir(2)-Ir(1)-Ir (4)	108.01(6)
Ir(2)-Ir(1)-W(1)	60.52(4)	Ir(2)-Ir(1)-W(2)	113.49(6)
Ir(2)-Ir(1)-W(3)	58.22(4)	Ir(3)-Ir(1)-Ir(4)	60.33(4)
Ir(3)-Ir(1)-W(1)	108.40(6)	Ir(3)-Ir(1)-W(2)	59.28(5)
Ir(3)-Ir(1)-W(3)	58.19(4)	Ir(4)-Ir(1)-W(1)	107.71(6)
Ir(4)-Ir(1)-W(2)	59.74(5)	Ir(4)-Ir(1)-W(3)	58.14(4)
W(1)-Ir(1)-W(2)	165.07(6)	W(1)-Ir(1)-W(3)	58.61(4)
W(2)-Ir(1)-W(3)	106.47(5)	Ir(1)-Ir(2)-Ir(3)	58.89(4)
Ir(1)-Ir(2)-W(1)	61.71(5)	Ir(1)-Ir(2)-W(3)	62.24(5)
Ir(3)-Ir(2)-W(1)	108.57(5)	Ir(3)-Ir(2)-W(3)	59.24(4)
W(1)-Ir(2)-W(3)	60.24(5)	Ir(1)-Ir(3)-Ir(2)	61.24(4)
Ir(1)-Ir(3)-Ir(4)	59.99(4)	Ir(1)-Ir(3)-W(2)	64.00(5)
Ir(1)-Ir(3)-W(3)	63.47(5)	Ir(2)-Ir(3)-Ir(4)	108.82(6)
Ir(2)-Ir(3)-W(2)	118.88(6)	Ir(2)-Ir(3)-W(3)	60.35(4)
Ir(4)-Ir (3)-W(2)	61.25(5)	Ir(4)-Ir(3)-W(3)	59.77(5)
W(2)-Ir(3)-W(3)	114.36(6)	Ir(1)-Ir(4)-Ir(3)	59.69(4)
Ir(1)-Ir(4)-W(2)	63.59(5)	Ir(1)-Ir(4)-W(3)	63.34(4)
Ir(3)-Ir(4)-W(2)	60.41(5)	Ir(3)-Ir(4)-W(3)	59.71(4)
W(2)-Ir (4)-W(3)	113.57(6)	Ir(1)-W(1)-Ir(2)	57.77(4)
Ir(1)-W(1)-W(3)	59.98(4)	Ir(2)-W(1)-W(3)	57.77(4)
Ir(1)-W(2)-Ir(3)	56.72(4)	Ir(1)-W(2)-Ir(4)	56.68(4)
Ir(3)-W(2)-Ir(4)	58.33(5)	Ir(1)-W(3)-Ir(2)	59.55(4)
Ir(1)-W(3)-Ir(3)	58.34(4)	Ir(1)-W(3)-Ir(4)	58.52(4)
Ir(1)-W(3)-W(1)	61.41(5)	Ir(2)-W(3)-Ir(4)	109.48(6)
Ir(2)-W(3)-Ir(3)	60.41(4)	Ir(3)-W(3)-W(1)	110.92(6)
Ir(3)-W(3)-Ir(4)	60.52(5)	Ir(4)-W(3)-W(1)	110.39(6)
Ir(2)-W(3)-W(1)	61.99(5)	W(1)-C(25)-O(25)	161(3)
W(3)-C(25)-O(25)	125(2)	Ir-C-O	168(3) - 177(2)
W-C-O	171(2) - 177(3)		

An ORTEP diagram of the crystallographically determined molecular structure of **16** is shown in Figure 4.1.6., selected bond lengths are listed in Table 4.1.3. and selected bond angles are collected in Table 4.1.4. The seven-vertex cluster **16** is comprised of four iridium and three tungsten atoms arranged as four face-sharing catenated tetrahedra. The four iridiums and a tungsten define the central trigonal bipyramidal unit; the iridiums each bear two terminal carbonyl ligands, and the tungsten is coordinated by an η^5-

cyclopentadienyl group. The remaining two tungstens occupy capping sites, with both possessing two terminal carbonyl groups and an η^5-cyclopentadienyl ligand. The spectroscopically-identified hydride could not be located crystallographically; potential energy calculations suggest that it is possibly located on W(3)-Ir(2),[54] although this is not the longest M-M vector in the molecule. The structural characterization of a number of tri- and tetra-nuclear tungsten-iridium clusters have been reported; including those mentioned in Chapter 2 [45,55-60] the title complex is the largest cluster by far in the W-Ir system. W-Ir distances in **16** [2.682(2) - 2.889(2) Å] fall within the range of those previously reported [2.665(2) - 2.9023(9) Å]. Similarly, the Ir-Ir distances [2.687(2) - 2.751(2) Å] are not unprecedented, with published structures exhibiting values in the range 2.5976(7) - 2.814(3) Å. Interestingly, the shortest W-Ir [2.682(2) Å] and Ir-Ir [2.687(2) Å] distances in **16** involve the pentametallic-coordinate Ir(3) while the longest W-Ir [2.889(2) Å] and Ir-Ir [2.751(2) Å] bonds in **16** involve the hexametallic-coordinate Ir(1); unlike capped octahedral structures where all metals are bound to 4 or 5 other metals, the core geometry observed here contains a hexametallic-coordinate metal, and steric considerations may possibly explain bond lengthening associated with this metal (although it is formally a 19 e metal, localized bonding considerations are probably inappropriate). The W-W distance [2.784(2) Å] is rather short; previously reported values span the range 2.951(1)-3.080(1) Å, with a distance of 2.666(1) Å in $[Cp_2W_2Ir\{\mu_3\text{-}\eta^2\text{-}C_2(C_6H_4Me\text{-}4)_2\}(Cl)(CO)_4]$ assigned to W=W. For the trinuclear cluster, a W=W double bond gives each metal an 18 electron configuration. In **16**, a W=W would give W(1) 19 e and W(3) 17 e. Although the existence of a dative bond could possibly be invoked to explain the electronic anomaly, and the semibridging CO(25) (see below) also serves to redistribute electron density, it is most likely for a heptametallic cluster that localized bonding arguments are overly simplistic and that the unsaturation is delocalized over the cluster. Other interactions are normal, except W(1)-C(25)-O(25) [161(3)°], the latter possibly indicating some semibridging character; W(3)-C(25) [2.63(3) Å] and W(3)-C(25)-O(25) [125(2)°] are consistent with this idea, as is the presence of a weak low-frequency carbonyl stretch in the IR spectrum [ν(CO) 1839w cm^{-1}] in a similar region to one observed in the precursor **3** [ν(CO) 1833w cm^{-1}], which was also assigned to that of a crystallographically observed semibridging interaction.[57]

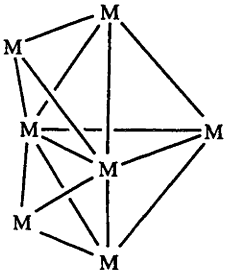
Complex **16** has a highly unusual bicapped trigonal bipyramidal heptametallic core geometry. Other structurally characterized heptametallic cores incorporating iridium all have the conventional face-capped octahedral geometry and are all homometallic in nature.[36,38,61] All but one of the crystallographically authenticated hexametallic cores incorporating iridium possess octahedral core geometries[31,37,44,62-72] ($[Ir_3Pt_3(\mu\text{-}CO)_3(CO)_3(\eta^5\text{-}C_5Me_5)_3]$[73] has a "raft" geometry); cluster **16** thus has a new core geometry for iridium that is not related by simple capping to previously characterized core geometries involving this metal.

For heptametallic clusters, there is little (5.5 %) energetic difference between the bicapped trigonal bipyramidal and the common capped octahedral core geometries.[74] It is possible that the former has only rarely been observed because its high metal-metal connectivity requirements are not compatible with clusters consisting of central d-block metals; these metals have greater ligation needs to achieve a stable electron count than the coinage metals. Consequently, the majority of reports of clusters with this core geometry are gold-rich, some markedly so. All reported transition metal clusters with bicapped trigonal bipyramidal cores and the three possible core isomers are summarized in Figure 4.1.7.



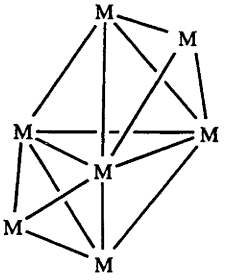
(A)

$[Au_3CoRu_3(CO)_{12}(PPh_3)_3]$[a] 96 CVE
$[Au_3(\mu\text{-}H)Ru_4(CO)_{12}(PPh_3)_3]$[b,c,d] 96 CVE



(B)

No examples



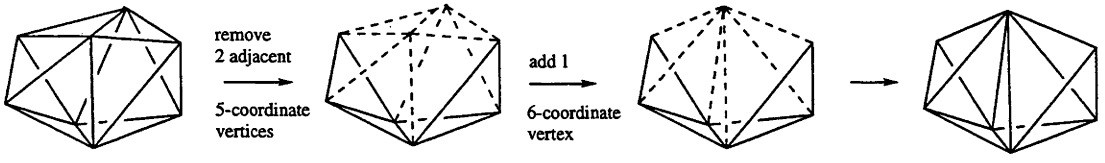
(C)

$[Au_6V(CO)_4(PPh_3)_6]^{+}$[e] 90 CVE
$[Au_6Pt(CO)(PPh_3)_7]^{2+}$[f] 90 CVE
$[Au_6Co(CO)_2(PPh_3)_6]^{+}$[g] 90 CVE
$[Cp_3W_3Ir_4(\mu\text{-}H)(CO)_{12}]$[h] 94 CVE
$[Os_7(CO)_{17}(\eta^6\text{-}C_6H_6)]$[i] 96 CVE
$[Cp_2Ru_2Os_5(CO)_{15}]$[j] 96 CVE

Figure 4.1.7. Bicapped trigonal bipyramidal core isomers, and crystallographically verified examples of heptametallic clusters consisting of transition metal core atoms. [a]Reference 75 , [b]Reference 74, [c]Reference 76, [d]Reference 77, [e]Reference 78, [f]Reference 79, [g]Reference 80, [h]this work, [i]Reference 81, [j]Reference 82.

The EAN rule predicted electron count for bicapped trigonal bipyramidal transition metal clusters is 96 CVE [4 × 60(tetrahedra) - 3 × 48(shared faces)]. The two clusters of core isomer (A) are thus electron precise with 96 CVE. No examples of core isomer (B) are extant. Cluster **16** was the first transition metal example of isomer (C) without coinage metals, although three 90 CVE clusters incorporating six gold atoms each have been reported previously. Two examples of transition metal carbonyl clusters of type (C) have been reported subsequently ($[Os_7(CO)_{17}(\eta^5\text{-}C_6H_6)]$[81] and $[Cp_2Ru_2Os_5(CO)_{15}]$[82]), both being electron precise with 96 CVE. Cluster **16** has 94 CVE [15(3Cp) + 18(3W) + 36(4Ir) + 1(H) + 24(12CO)]. The reason for the formal electron deficiency is not certain, but should be consistent with the fact that the examples of isomer (A) are electron precise whereas **16**, an example of isomer (C), is a "rule-breaker". It is well known that simple electron counting rules break down for columnar clusters, as the assumption that each

metal fragment has three nonbonding *d* orbitals is no longer valid.[83] The catenated nature of **16** may be responsible for the lack of success in applying conventional counting rules. Columnar clusters based on the octahedron have an electron count of 50 for the shared triangular face, due to an additional electron pair occupying an a'_2 antibonding molecular orbital.[84] Thus, $[Rh_9(CO)_{19}]^{3-}$, a face-sharing bioctahedron, has an electron count of 122 rather than 124. The same idea may be operative with the title cluster, which unlike isomer (A) could be alternatively visualized as a face-sharing trigonal bipyramid.



closo-triangulated dodecahedron *arachno*-triangulated dodecahedron *isocloso* -7-vertex geometry

18

Figure 4.1.8.

Alternatively, vertices W(1-3) and Ir(2-4) define an *arachno*-triangulated dodecahedron, derived from the *closo*-geometry by removal of two adjacent 5-coordinate vertices. Addition of vertex Ir(1) (6 coordinate) constructs an *isocloso*-7-vertex geometry (Figure 4.1.8.), previously observed for main group-transition metal clusters $[Au_2Fe_4(\mu_6\text{-}B)(H)(CO)_{12}(PPh_3)_2]$,[85,86] $[Co(\mu_6\text{-}P)(\mu\text{-}CO)_2(CO)_{14}]^-$,[87] $[Ru_6(\mu_6\text{-}P)(\mu\text{-}H)_6(\mu\text{-}PHBu^n)(\mu\text{-}PBu^n_2)_2(CO)_{10}(PBu^n_3)_2]$,[88] $[Au_3Fe_3(\mu_6\text{-}P)(CO)_9(PPh_3)_3]$,[89] $[Au_2Fe_4(\mu_6\text{-}B)(H)(CO)_{12}\{P(C_6H_4Me\text{-}4)_3\}_2]$[90] and $[Au_2Fe_4(\mu_6\text{-}B)(H)(CO)_{12}(AsPh_3)_2]$[91] (note that in each case the six-coordinate vertex is occupied by the main group atom, emphasizing the unusual nature of **16**). Wade has stated that the *closo*-triangulated dodecahedron geometry is compatible with 8 and 10 cluster bonding pairs as well as the 9 expected from PSEPT, due to the nondegeneracy of the HOMO and LUMO;[92] this electronic flexibility could extend to the *isocloso* derivative. From this viewpoint, the "anomalous" electron count of **16**, and electron precise nature of the recent osmium and mixed ruthenium-osmium clusters with the same core geometry, is a consequence of the capability of this structural type to accommodate both PSEPT and non PSEPT-predicted electron counts.

4.2. Some Alkyne Chemistry of Tungsten-Iridium Clusters

Acetylenes are the prototypical C_x ligands; their cluster chemistry is of interest, not only in its own right, but also in modelling Fischer-Tropsch and other catalyzed processes.[93-96] This section includes a summary of previously reported acetylene chemistry of $[Ir_4(CO)_{12}]$ (**1**), $[CpWIr_3(CO)_{11}]$ (**2**) and $[Cp_2W_2Ir_2(CO)_{10}]$ (**3**), together with the results of reactivity studies of **2** and **3** towards other acetylenes and metal acetylides, and a comparison across these clusters.

4.2.1 Acetylene Chemistry of $[Ir_4(CO)_{12}]$ (1), $[CpWIr_3(CO)_{11}]$ (2) and $[Cp_2W_2Ir_2(CO)_{10}]$ (3)

The acetylene chemistry of **1** has been summarized;[97] excluding phosphinoalkynes which initially react by way of P-coordination, the only tetranuclear product isolated thus far is the rectangular $[Ir_4\{\mu\text{-}\eta^4\text{-}Me(O)OCC_2C(O)OMe\}_2\{\mu\text{-}Me(O)OCC_2C(O)OMe\}_2(CO)_8]$ (Figure 4.2.1.).[98]

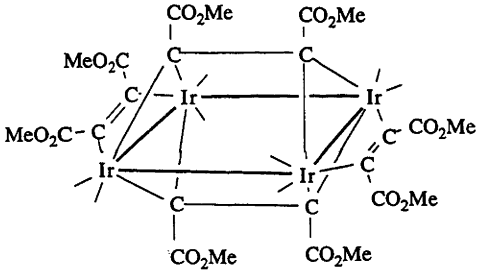
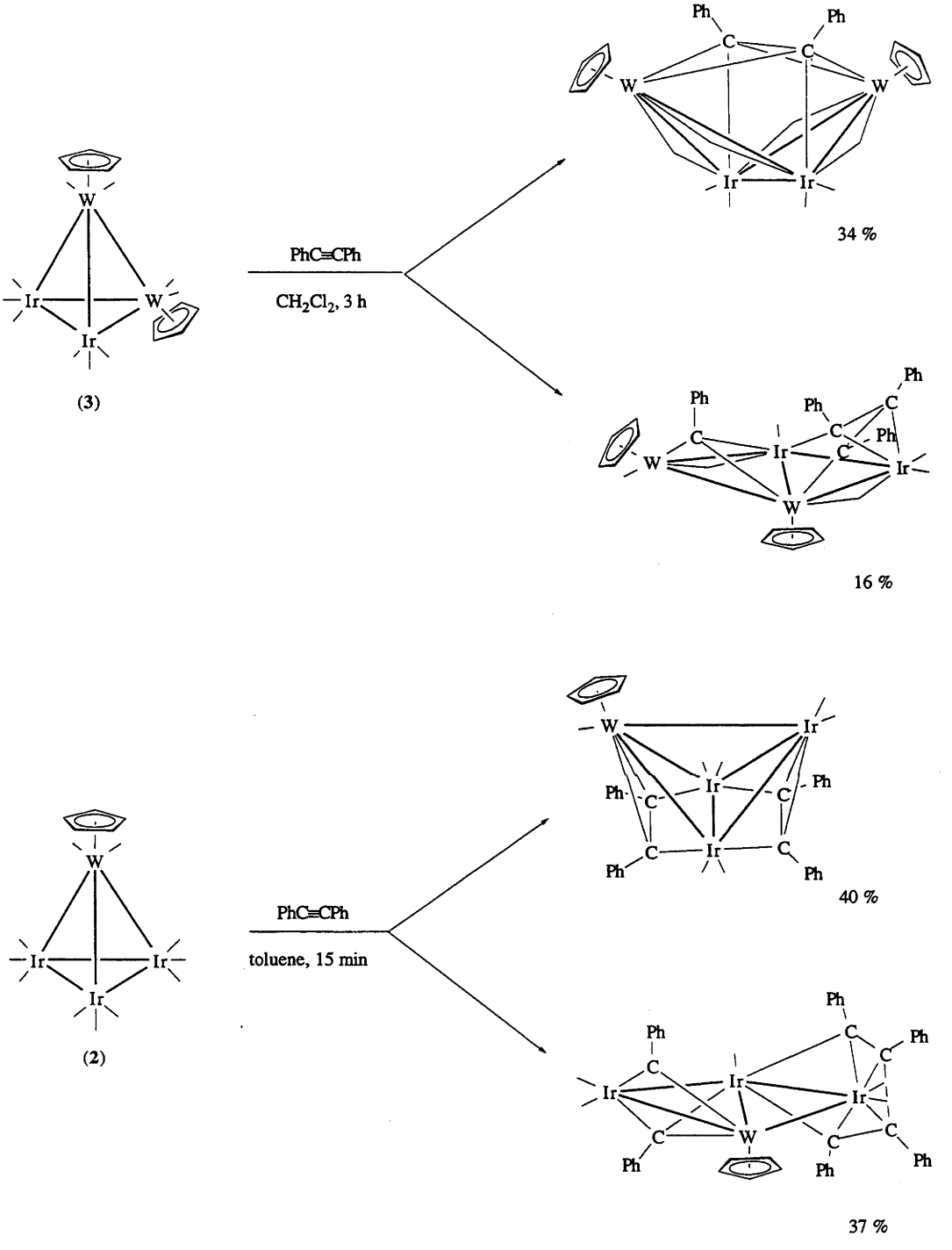


Figure 4.2.1.

The mixed-metal system shows significantly enhanced reactivity. Shapley and co-workers have reported the reactions of $[Cp_xW_xIr_{4-x}(CO)_{12-x}]$ [x = 1 (**2**), 2 (**3**)] with internal acetylenes. The addition of diphenylacetylene to **3** afforded $[Cp_2W_2Ir_2(CO)_8(PhC_2Ph)]$ (34 %) and the structurally verified $[Cp_2W_2Ir_2(\mu_3\text{-}CPh)\{\mu_3\text{-}\eta^3\text{-}C(Ph)C(Ph)C(Ph)\}(CO)_6]$ (16 %).[59] In contrast, diphenylacetylene reacted with **2** to give the crystallographically confirmed clusters $[CpWIr_3(\mu_3\text{-}\eta^2\text{-}PhC_2Ph)_2(CO)_7]$ (40 %) and $[CpWIr_3(\mu_3\text{-}CPh)(\mu\text{-}CPh)\{\mu\text{-}\eta^4\text{-}C(Ph)C(Ph)C(Ph)C(Ph)\}(CO)_5]$ (37 %) [99] (Scheme 4.2.1.).



Scheme 4.2.1. Reactivity of $[CpWIr_3(CO)_{11}]$ (**2**) and $[Cp_2W_2Ir_2(CO)_{10}]$ (**3**) with diphenylacetylene.

The reactions of these mixed tungsten - iridium clusters with terminal alkynes have been investigated in the current work. The results of reacting **2** and **3** with HC≡CR [R = Ph, C_6H_4Me-4, $C_6H_4NO_2$-4, Bu^t and C≡CW(CO)$_3$Cp] are reported, together with the results of a single crystal X-ray study of a representative adduct $[Cp_2W_2Ir_2(\mu_4\text{-}\eta^2\text{-}HC_2Ph)(\mu\text{-}CO)_4(CO)_4]$. Extension of the earlier studies to include "inorganic acetylenes" such as alkynylmetal complexes is also logical. Reaction of **2** and **3** with tungsten acetylide complexes potentially affords a method of expanding the metal core nuclearity under controlled conditions. With this idea in mind, the results of treating **2** and **3** with tungsten acetylides are reported, together with characterization by single crystal X-ray study of the reaction product $[Cp_2W_2Ir_3(\mu_4\text{-}\eta^2\text{-}C_2C_6H_4Me\text{-}4)(\mu\text{-}CO)(CO)_9]$ (**27**).

4.2.2. Syntheses and Characterization of $[Cp_2W_2Ir_2(\mu_4\text{-}\eta^2\text{-}HC_2R)(\mu\text{-}CO)_4(CO)_4]$ [R = Ph (18), C_6H_4Me-4 (19), $C_6H_4NO_2$-4 (20), Bu^t (21)]

The reactions of **3** with the terminal alkynes HC≡CR (R = Ph, C_6H_4Me-4, $C_6H_4NO_2$-4) proceeded either in CH_2Cl_2 at room temperature overnight, or in 1 h at 50 °C in toluene. Purification by preparative thin-layer chromatography afforded clusters with the composition $[Cp_2W_2Ir_2(HC_2R)(CO)_8]$ [R = Ph (**18**), C_6H_4Me-4 (**19**), $C_6H_4NO_2$-4 (**20**)] in excellent yields (56 - 70 %). The comparatively more sterically encumbered 3,3-dimethyl-1-butyne required significantly more forcing conditions (refluxing toluene, 1 h) for reaction to proceed, and the analogous product $[Cp_2W_2Ir_2(HC_2Bu^t)(CO)_8]$ (**21**) was isolated in much lower yield (20 %). The products have been characterized by a combination of IR and ^{1}H NMR spectroscopies, FAB MS, satisfactory microanalyses and, in the case of **19**, a single crystal X-ray diffraction study. The infrared spectra are consistent with the presence of edge-bridging carbonyl ligands in all complexes [ν(CO) 1835 - 1821 cm^{-1}], which contrasts with the all-terminal precursor **3**. The ^{1}H NMR spectra contain characteristic resonances at 9.77 - 8.95 ppm corresponding to the acetylenic protons ≡CH, and signals assigned to Cp (**18** - **21**), Ph (**18** - **20**) and Me (**19** and **21**) groups in the appropriate ratios. The mass spectra of all complexes (**18** - **21**) show molecular ions, followed by stepwise loss of carbonyls, and particularly intense fragment ions $[M\text{-}3CO]^+$ and $[M\text{-}6CO]^+$; isotope patterns are consistent with the presence of two iridium atoms and two tungsten atoms.

A single crystal X-ray diffraction study of **18** was undertaken to confirm the acetylene coordination mode and carbonyl disposition in these complexes. Selected bond distances (Table 4.2.1.) and angles (Table 4.2.2.) are listed, together with those of the isostructural, previously reported, molybdenum analogue $[Cp_2Mo_2Ir_2(\mu_4\text{-}\eta^2\text{-}HC_2Ph)(\mu\text{-}CO)_4(CO)_4]$ (**22**).[100] An ORTEP plot showing the molecular geometry and atomic numbering scheme is shown in Figure 4.2.2.

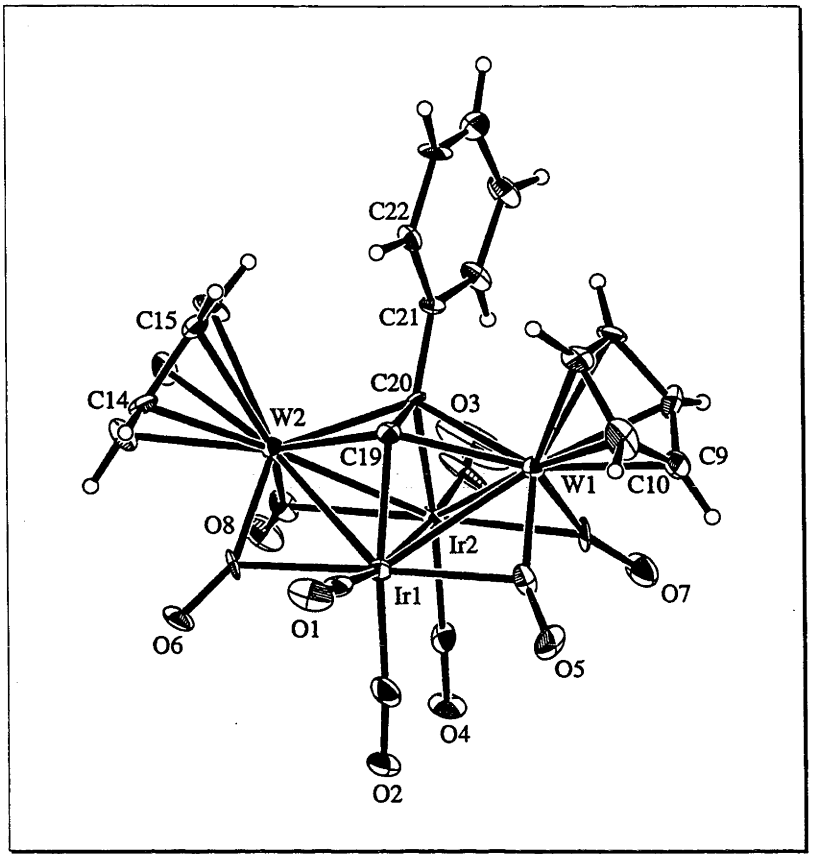


Figure 4.2.2. Molecular structure and atomic labelling scheme for $[Cp_2W_2Ir_2(\mu_4\text{-}\eta^2\text{-}HC_2Ph)(\mu\text{-}CO)_4(CO)_4]$ (**18**). Thermal envelopes of 20 % probability are shown for the non-hydrogen atoms; hydrogen atoms have arbitrary radii of 0.1 Å.

(By David C. R. Hockless)

Table 4.2.1. Selected Bond Lengths (Å) for $[Cp_2M_2Ir_2(\mu_4\text{-}\eta^2\text{-}HC_2Ph)(\mu\text{-}CO)_4(CO)_4]$ [M = W (**18**), Mo (**22**)].

Bond	18	22[100]
Ir(1)-Ir(2)	2.688(1)	2.6982(6)
Ir(1)-M(1)	2.813(1)	2.8199(9)
Ir(1)-M(2)	2.802(1)	2.8146(9)
Ir(2)-M(1)	2.812(1)	2.8209(9)
Ir(2)-M(2)	2.813(1)	2.8222(9)
Ir(1)-C(19)	2.07(2)	2.074(8)
Ir(2)-C(20)	2.09(2)	2.107(9)
M(1)-C(19)	2.25(2)	2.299(8)
M(1)-C(20)	2.34(2)	2.298(8)
M(2)-C(19)	2.29(2)	2.290(8)
M(2)-C(20)	2.28(2)	2.340(8)
Ir(1)-C(1)	1.97(3)	1.91(1)
Ir(1)-C(2)	1.90(3)	1.91(1)
Ir(1)-C(5)	2.33(2)	2.333(9)
Ir(1)-C(6)	2.33(2)	2.314(9)
Ir(2)-C(3)	1.88(3)	1.92(1)
Ir(2)-C(4)	1.93(2)	1.93(1)
Ir(2)-C(7)	2.38(2)	2.35(1)
Ir(2)-C(8)	2.42(2)	2.37(1)
M(1)-C(5)	1.95(2)	1.98(1)
M(1)-C(7)	1.97(2)	1.98(1)
M(2)-C(6)	1.97(2)	2.00(1)
M(2)-C(8)	2.03(3)	1.99(1)
M(1)-C(9)	2.27(2)	2.28(1)
M(1)-C(10)	2.30(2)	2.28(1)
M(1)-C(11)	2.32(2)	2.32(1)
M(1)-C(12)	2.34(2)	2.334(10)
M(1)-C(13)	2.29(2)	2.313(10)
M(2)-C(14)	2.28(2)	2.29(1)
M(2)-C(15)	2.36(2)	2.32(1)
M(2)-C(16)	2.35(3)	2.35(1)
M(2)-C(17)	2.34(2)	2.33(1)
M(2)-C(18)	2.28(2)	2.284(9)

Table 4.2.2. Selected Bond Angles (°) for $[Cp_2M_2Ir_2(\mu_4\text{-}\eta^2\text{-}HC_2Ph)(\mu\text{-}CO)_4(CO)_4]$ [M = W (**18**), Mo (**22**)].

Angle	18	22
Ir(2)-Ir(1)-M(1)	61.44(3)	61.44(2)
Ir(2)-Ir(1)-M(2)	61.61(4)	61.54(2)
M(1)-Ir(1)-M(2)	94.83(4)	95.69(3)
Ir(1)-Ir(2)-M(1)	61.46(3)	61.40(2)
Ir(1)-Ir(2)-M(2)	61.19(3)	61.26(2)
M(1)-Ir(2)-M(2)	94.59(4)	95.50(3)
Ir(1)-M(1)-Ir(2)	57.10(3)	57.15(2)
Ir(1)-M(2)-Ir(2)	57.20(4)	57.20(2)

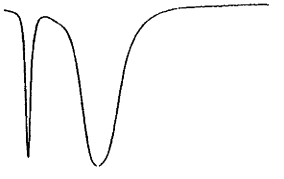
Complex **18** possesses a W_2Ir_2 core in which the metals adopt a butterfly geometry; the iridiums form the hinge and the tungstens occupy the wing-tip sites. Each iridium is ligated by two terminal carbonyls and each tungsten is coordinated by an η^5-cyclopentadienyl ligand. The four remaining carbonyl ligands bridge the W-Ir bonds. The spectroscopically-identified acetylenic proton could not be located crystallographically. The phenylacetylene ligand bridges all four metals in a μ_4-η^2-fashion, lying parallel to the Ir(1)-Ir(2) vector. This arrangement completes a *closo*-octahedral core consisting of the four metals and the two 'acetylenic' carbon atoms. The Ir-Ir bond length [2.688(1) Å] and the W-Ir distances [2.802(1)-2.813(1) Å] are "normal" and consistent with a marginal contraction of M_2Ir_2 butterfly core compared to the analogous distances in **22**. As with **22**, the core carbons C(19) and C(20) in **18** interact more closely with iridium [C-Ir 2.07(2)-2.09(2) Å] than with the group 6 metal [C-W 2.25(2) - 2.34(2) Å]. All tungsten - iridium bonds are spanned by an asymmetrically disposed bridging carbonyl ligand [W-C 1.95(2)-2.03(3) Å compared to Ir-C 2.33(2)-2.42(2) Å]; the asymmetry of the bridging carbonyl ligands increases slightly in proceeding from the molybdenum containing cluster **22** (Mo-C_{av} 1.99 Å; Ir-C_{av} 2.34 Å) to its tungsten analogue **18** (W-C_{av} 1.98 Å; Ir-C_{av} 2.37 Å). Cluster **18** has 7 bonding pairs by the polyhedral skeletal electron pair theory, electron precise for a *closo* octahedron.

4.2.3. Syntheses and Characterization of $[Cp_2W_2Ir_2\{\mu_4\text{-}\eta^2\text{-}HC_2C{\equiv}CW(CO)_3Cp\}(\mu\text{-}CO)_4(CO)_4]$ (24)

Compound **3** reacted with the buta-1,3-diynyl complex $[CpW(CO)_3(C{\equiv}CC{\equiv}CH)]$ (**23**) in CH_2Cl_2 at room temperature to afford $[Cp_2W_2Ir_2\{\mu_4\text{-}\eta^2\text{-}HC_2C{\equiv}CW(CO)_3Cp\}(\mu\text{-}CO)_4(CO)_4]$ (**24**), characterized by a combination of IR, ^1H and ^{13}C NMR spectroscopies, FAB MS, and satisfactory microanalyses. Spectroscopic evidence is consistent with the least hindered C≡C

triple bond (that remote from the tungsten) being coordinated to the cluster. The IR spectrum for **24** is suggestive of a superposition of the characteristic carbonyl absorption pattern of **18** - **21**, two carbonyl absorptions for the pendant $W(CO)_3Cp$ moiety (see Table 4.2.3.), and a weak absorption assigned to the uncomplexed alkynyl linkage (2155w cm^{-1}). Replacing the organic substituents (R = Ph, C_6H_4Me-4, $C_6H_4NO_2$-4, Bu^t) by the organometallic substituent [R = $CpW(CO)_3C{\equiv}C$] leads to a decrease in the weighted ν(CO) average for the W_2Ir_2 core. Coordinating [$CpW(CO)_3(C{\equiv}CC{\equiv}CH)$] to the ditungsten - diiridium cluster leads to a similar decrease in weighted ν(CO) average for the pendant group. The shift in both IR parameters indicated enhanced π back-donation to carbonyl ligands upon formation of the cluster-butadiynyl complex adduct. The ^1H NMR contains resonances assigned to ≡CH (8.40 ppm) and Cp (5.54 ppm and 5.29 ppm), ratio 1 : 5 : 10; the chemical shift of the acetylenic proton is similar to that in **18** - **21**, and thus consistent with coordination of the buta-1,3-diynyl complex to the cluster via the C≡CH unit. To facilitate assignment of the ^{13}C NMR spectrum of cluster **24**, the ^{13}C NMR spectrum of the X-ray crystallographically characterized cluster **18** has also been obtained. Some carbonyl resonances in the ^{13}C NMR spectrum of **24** (222.3, 221.7 ppm, ratio 2 : 2, W-Ir μ-CO; 177.9, 177.7, 173.5, 172.3 ppm, ratio 1 : 1 : 1 : 1, Ir-CO) are analogous to those of complex **18** (222.0, 220.9 ppm, ratio 2 : 2, W-Ir μ-CO; 177.9, 177.7, 175.7, 173.1 ppm, ratio 1 : 1 : 1 : 1, Ir-CO). The chemical shifts of the remaining two signals in the carbonyl region of the ^{13}C NMR spectrum of **24** (227.6, 212.9 ppm, ratio 1 : 2) are similar to those of the carbonyl ligands in **23** (227.4, 210.9 ppm, ratio 1 : 2 in $CDCl_3$ [101]), and are thus assigned to carbonyls of the pendant $CpW(CO)_3$ group. The signals at 99.2 ppm (**18**) and 109.6 ppm (**24**) are assigned to ≡CH with the aid of INEPT spectra. The signals at 78.0 ppm (WC≡*C*) and 106.2 ppm (W*C*≡C) are assigned by comparison to the equivalent carbons in **23** (71.6 ppm and 110.5 ppm in $CDCl_3$, respectively[101]). The remaining signal at 146.8 ppm (**24**) is assigned to *C*≡CH by comparison to the analogous resonance in **18** (152.8 ppm). These similar NMR shifts are a further indication that the $CpW(CO)_3C{\equiv}C$ linkage is a pendant group. The FAB mass spectrum of **24** contains a parent ion and stepwise loss of eleven carbonyl groups; the isotope patterns are consistent with the presence of two iridium atoms and three tungsten atoms. Attempts to coordinate the pendant group or activate the ≡C-H bond (thermolysis, prior activation with Me_3NO) resulted in decomposition of the cluster. The buta-1,3-diynyl complex coordination mode in **24** is the same as that of the product from the reaction between **23** and $[Ru_3(CO)_{10}(NCMe)_2]$,[102] namely $[Ru_3\{\mu_3\text{-}\eta^2\text{-}HC_2C{\equiv}CW(CO)_3Cp\}(\mu\text{-}CO)(CO)_9]$ (**25**). In contrast to **24**, thermolysis of **25** resulted in ≡C-H activation to afford $[Ru_3(\mu\text{-}H)\{\mu_3\text{-}\eta^2\text{-}C_2C{\equiv}CW(CO)_3Cp\}(CO)_9]$.

Table 4.2.3. IR Data for $[Cp_2W_2Ir_2(\mu_4\text{-}\eta^2\text{-}HC_2R)(\mu\text{-}CO)_4(CO)_4]$ [R = Ph (**18**), C_6H_4Me-4 (**19**), $C_6H_4NO_2$-4 (**20**), Bu^t (**21**)], $[Cp_2W_2Ir_2(\mu_4\text{-}\eta^2\text{-}HC_2C{\equiv}CW(CO)_3Cp)(\mu\text{-}CO)_4(CO)_4]$ (**24**) and $[CpW(CO)_3(C{\equiv}CC{\equiv}CH)]$ (**23**).[a]

Cluster	ν_{CO} (cm^{-1})	
	W_2Ir_2 core	$CpW(CO)_3$ fragment
		
$[Cp_2W_2Ir2(\mu_4\text{-}\eta^2\text{-}HC_2Bu^t))(\mu\text{-}CO)_4(CO)_4,]$ **21**	2065, 2036, 2010, 1990, 1835	-
$[Cp_2W_2Ir_2(\mu4\text{-}\eta^2\text{-}HC_2C_6H_4NO_2\text{-}4)(\mu\text{-}CO)_4(CO)_4]$, **20**	2064, 2036, 2006, 1991, 1829	-
$[Cp_2W_2Ir_2(\mu4\text{-}\eta^2\text{-}HC_2Ph)(\mu\text{-}CO)_4(CO)_4,]$ **18**	2061, 2032, 2008, 1986, 1821	-
$[Cp_2W_2Ir_2(\mu4\text{-}\eta^2\text{-}HC_2C_6H_4Me\text{-}4)(\mu\text{-}CO)_4(CO)_4,]$ **19**	2060, 2031, 2006, 1986, 1825	-
$[Cp_2W_2Ir_2\{\mu4\text{-}\eta^2\text{-}HC_2C{\equiv}C(CO)_3WCp\}(\mu\text{-}CO)_4(CO)_4]$, **24**	2058, 2033, 2003, 1984, 1823	2055, 1945
$[CpW(CO)_3(C{\equiv}CC{\equiv}CH)]$, **23**	-	2045, 1958[101]

[a]All spectra as solution in CH_2Cl_2

4.2.4. Syntheses and Characterization of [$Cp_2W_2Ir_3(\mu_4\text{-}\eta^2\text{-}C_2R)(\mu\text{-}CO)(CO)_9$] [R = Ph (26), C_6H_4Me-4 (27), $C_6H_4NO_2$-4 (28), C≡CPh (29)]

The reactions of **2** with [$CpW(CO)_3(C{\equiv}CR)$] (R = Ph, C_6H_4Me-4, $C_6H_4NO_2$-4, C≡CPh) proceeded slowly in dichloromethane at room temperature to afford clusters of composition [$Cp_2W_2Ir_3(CO)_{10}(C_2R)$] [R = Ph (**26**), C_6H_4Me-4 (**27**), $C_6H_4NO_2$-4 (**28**), C≡CPh (**29**)] as the major reaction product in fair yield (23 - 45 %). The products were characterized by a combination of IR and ^1H NMR spectroscopies, FAB MS, and satisfactory microanalyses. The ^1H NMR spectra contain signals assigned to cyclopentadienyl and phenyl groups for all complexes, and a methyl group for **27**. The mass spectra of **16, 27** and **28** contain molecular ions and all complexes show sequential loss of carbonyl ligands; isotope patterns are consistent with the presence of three iridium atoms and two tungsten atoms.

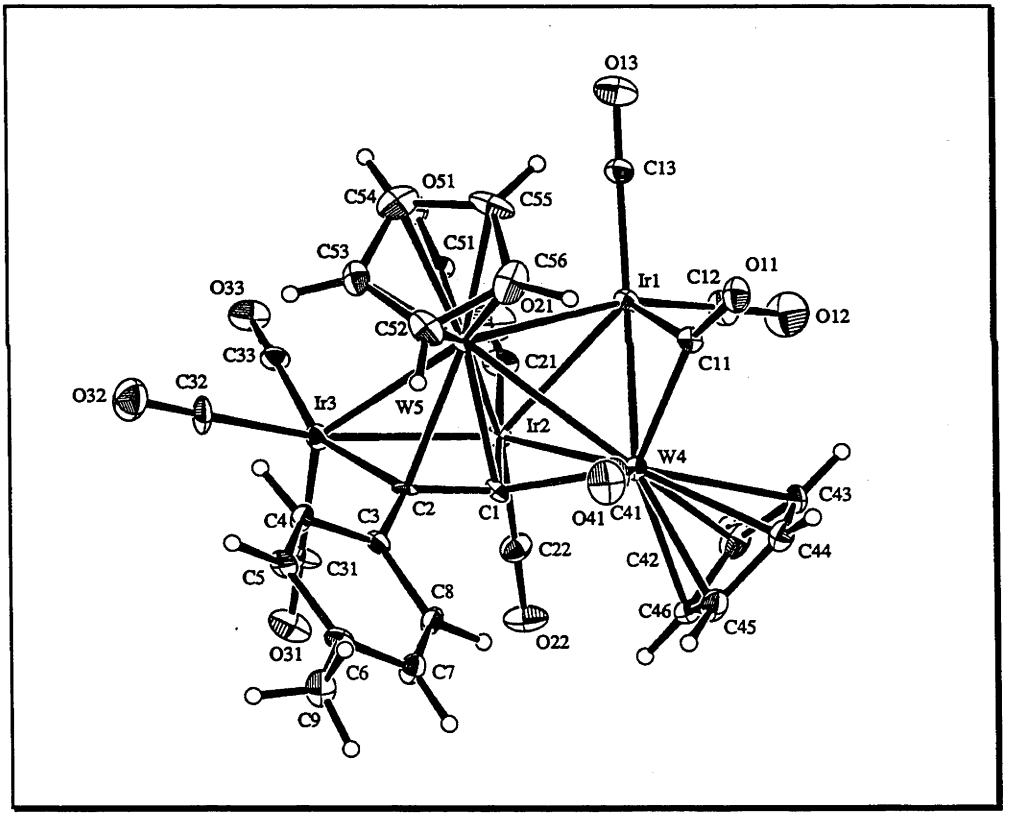


Figure 4.2.3. Molecular structure and atomic labelling scheme for [$Cp_2W_2Ir_3(\mu_4\text{-}\eta^2\text{-}C_2C_6H_4Me\text{-}4)(\mu\text{-}CO)(CO)_9$] (**27**). Thermal envelopes of 20 % probability are shown for the non-hydrogen atoms; hydrogen atoms have arbitrary radii of 0.1 Å.

(By David C. R. Hockless)

Table 4.2.4. Selected Bond Lengths (Å) for $[Cp_2W_2Ir_3(\mu_4\text{-}\eta^2\text{-}C_2C_6H_4Me\text{-}4)(\mu\text{-}CO)(CO)_9]$ (**27**).

Bond	Distance	Bond	Distance
Ir(1)-Ir(2)	2.7934(7)	Ir(1)-W(4)	2.7251(8)
Ir(1)-W(5)	2.8253(7)	Ir(2)-Ir(3)	2.7422(7)
Ir(2)-W(4)	2.8811(7)	Ir(2)-W(5)	2.7281(8)
Ir(3)-W(5)	2.8347(7)	W(4)-W(5)	3.0245(8)
Ir(1)-C(11)	2.05(1)	Ir(1)-C(12)	1.84(2)
Ir(1)-C(13)	1.86(1)	Ir(2)-C(1)	2.08(1)
Ir(2)-C(21)	1.89(1)	Ir(2)-C(22)	1.85(1)
Ir(3)-C(2)	2.07(1)	Ir(3)-C(31)	1.93(1)
Ir(3)-C(32)	1.89(1)	Ir(3)-C(33)	1.94(1)
W(4)-C(1)	2.00(1)	W(4)-C(11)	2.06(1)
W(4)-C(41)	1.97(1)	W(4)-C(42)	2.30(1)
W(4)-C(43)	2.34(1)	W(4)-C(44)	2.30(1)
W(4)-C(45)	2.25(2)	W(4)-C(46)	2.31(1)
W(5)-C(1)	2.22(1)	W(5)-C(2)	2.29(1)
W(5)-C(51)	1.96(1)	W(5)-C(52)	2.35(1)
W(5)-C(53)	2.35(1)	W(5)-C(54)	2.37(2)
W(5)-C(55)	2.32(1)	W(5)-C(56)	2.37(1)

Table 4.2.5. Selected Bond Angles (°) for $[Cp_2W_2Ir_3(\mu_4\text{-}\eta^2\text{-}C_2C_6H_4Me\text{-}4)(\mu\text{-}CO)(CO)_9]$ (**27**).

Bond	Angles	Bond	Angles
Ir(2)-Ir(1)-W(4)	62.93(2)	Ir(2)-Ir(1)-W(5)	58.09(2)
W(4)-Ir(1)-W(5)	66.01(2)	Ir(1)-Ir(2)-Ir(3)	121.12(3)
Ir(1)-Ir(2)-W(4)	57.38(2)	Ir(1)-Ir(2)-W(5)	61.54(2)
Ir(3)-Ir(2)-W(4)	111.38(2)	Ir(3)-Ir(2)-W(5)	62.42(2)
W(4)-Ir(2)-W(5)	65.19(2)	Ir(2)-Ir(3)-W(5)	58.54(2)
Ir(1)-W(4)-Ir(2)	59.69(2)	Ir(1)-W(4)-W(5)	58.59(2)
Ir(2)-W(4)-W(5)	54.96(2)		
Ir(1)-Ir(2)-C(1)	90.3(3)	Ir(3)-Ir(2)-C(1)	69.5(3)
W(4)-Ir(2)-C(1)	43.9(3)	W(5)-Ir(2)-C(1)	53.0(3)
Ir(2)-Ir(3)-C(2)	72.5(4)	W(5)-Ir(3)-C(2)	52.8(3)
Ir(1)-W(4)-C(1)	94.0(3)	Ir(2)-W(4)-C(1)	46.1(3)
W(5)-W(4)-C(1)	47.3(3)		

A single crystal X-ray diffraction study of $[Cp_2W_2Ir_3(\mu_4\text{-}\eta^2\text{-}C_2C_6H_4Me\text{-}4)(\mu\text{-}CO)(CO)_9]$ (**27**) was undertaken to ascertain the molecular geometry. Significant bond lengths and angles are collected in Tables 4.2.4. and 4.2.5. An ORTEP plot showing the molecular geometry is shown in Figure 4.2.3. The pentanuclear cluster **27** is comprised of three iridium atoms and two tungsten atoms arranged as an edge-bridged tetrahedron. The two tungstens and two of the iridium atoms define the core tetrahedral unit; the remaining iridium atom [Ir(3)] bridges the Ir(2)-W(5) vector. Terminal carbonyl ligands are coordinated to Ir(1) (two), Ir(2) (two), Ir(3) (three), W(4) (one) and W(5) (one), a carbonyl symmetrically bridges the Ir(1)-W(4) linkage [Ir(1)-C(11) 2.05(1), W(4)-C(11) 2.06(1) Å], and each tungsten is ligated by an η^5-cyclopentadienyl group. Core bond distances in **27** [W-Ir 2.7251(8)-2.8811(7) Å; Ir-Ir 2.7422(7)-2.7934(7) Å] fall within the range of those previously reported [W-Ir 2.665(2)[59]-2.9023(9)[45] Å; Ir-Ir 2.598(1)[99]-2.814(3)[99] Å] in mixed-metal tungsten-iridium clusters. The alkynyl ligand is coordinated in a $\mu_4\text{-}\eta^2$ ($3\sigma + \pi$) fashion, capping the Ir(2)Ir(3)W(4)W(5) butterfly cleft. This unusual coordination mode, with the alkynyl ligand π-bonded to a hinge rather than a wing-tip metal, has been observed previously only in $[Cp^*WOs_3(\mu_4\text{-}\eta^2\text{-}C_2Ph)(\mu_3\text{-}\eta^2\text{-}MeC_2Me)(CO)_9]$ ($Cp^* = \eta^5\text{-}C_5Me_5$),[103] although a similar coordination mode for benzonitrile was found in $[Fe_4(\mu_4\text{-}\eta^2\text{-}NCPh)(\mu\text{-}CO)(CO)_{11}]$.[104] The geometry of **27** is consistent with formal insertion of $CpW(CO)_3(C{\equiv}CC_6H_4Me\text{-}4)$ into an Ir-Ir bond in **2**, with concomitant elimination of CO ligands.

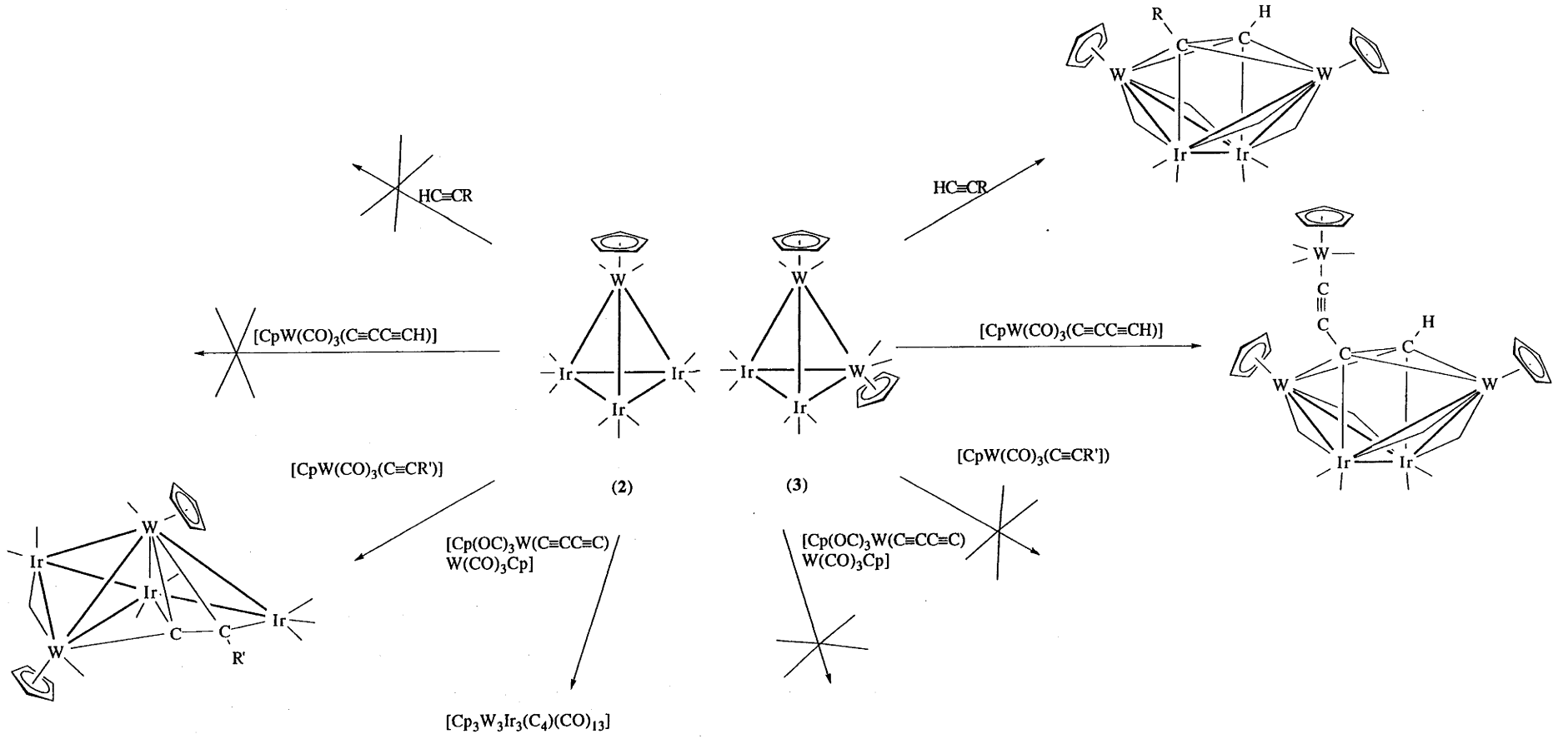
4.2.5. Reaction of $[CpWIr_3(CO)_{11}]$ and $[Cp_2W_2Ir_2(CO)_{10}]$ with $[Cp(OC)_3W(C{\equiv}CC{\equiv}C)W(CO)_3Cp]$

Refluxing **2** in toluene in the presence of $[Cp(OC)_3W(C{\equiv}CC{\equiv}C)W(CO)_3Cp]$ afforded a brown solution; purification by preparative thin-layer chromatography afforded a compound shown (by analytical and spectroscopic methods) to have the molecular composition $[Cp_3W_3Ir_3(C)_4(CO)_{13}]$ (**30**). The IR spectrum contains seven bands in the ν(CO) region, with no evidence for bridging carbonyl ligands. The ^1H NMR spectrum has three resonances of equal intensity assigned to cyclopentadienyl groups, while the ^{13}C NMR spectrum contains resonances in the carbonyl (nine), butadiynyl (six) and cyclopentadienyl (three) regions; the reason for six rather than four resonances in the butadiynyl region is, as yet, unclear. The mass spectrum is the most informative, containing a molecular ion at 1735 mass units and bands corresponding to sequential loss of thirteen carbonyl ligands. Attempts to grow crystals suitable for X-ray structural characterization were uniformly unsuccessful, invariably losing solvent and decomposing, so the geometry of **30** is unknown at present. In contrast to this relatively clean reaction, refluxing **3** in toluene in the presence of $[Cp(OC)_3W(C{\equiv}CC{\equiv}C)W(CO)_3Cp]$ caused decomposition of the cluster, with the poor solubility of $[Cp(OC)_3W(C{\equiv}CC{\equiv}C)W(CO)_3Cp]$ in most solvents precluding an investigation of this reaction under milder conditions.

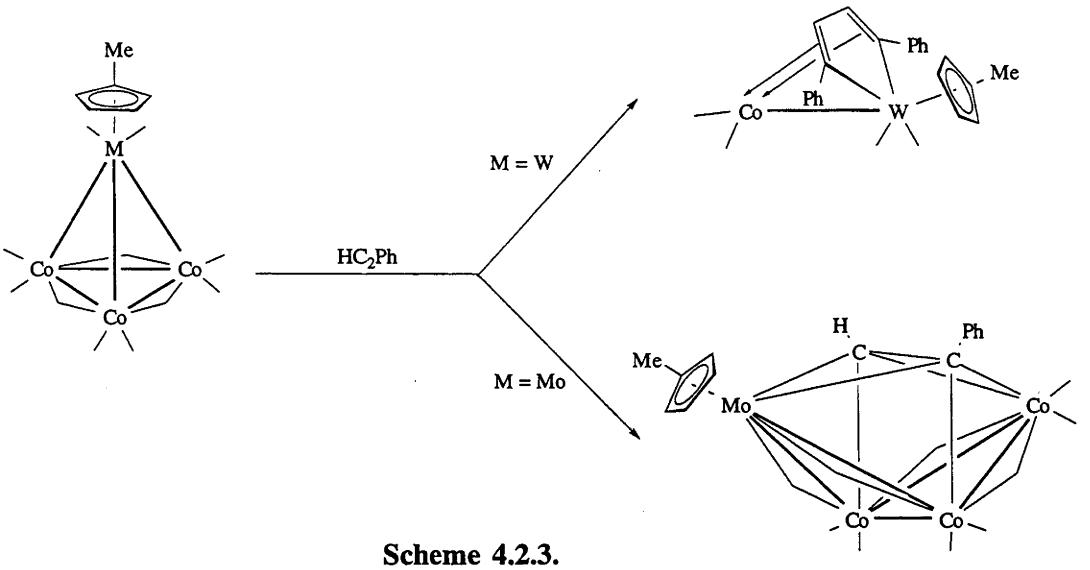
4.2.6. Discussion.

A summary of the results is given in Scheme 4.2.2. In contrast to the facile reactivity of **3** towards terminal alkynes, all attempts at reacting **2** with HC≡CR [R = Ph, $C_6H_4NO_2$-4, C≡CW(CO)$_3$Cp] have thus far proven unsuccessful. Terminal alkyne reactions at **3** occurred with bond selectivity; in addition to clusters **18 - 21, 24** arising from formal insertion into the W-W linkage, only trace quantities of thus-far-uncharacterized byproducts were obtained. Conceptual heterometal replacement in proceeding from **3** to **2** removes the preferred site of reactivity for terminal alkynes. Conversely, reactions of **2** with the alkynyltungsten complexes [CpW(CO)$_3$(C≡CR)] (R = Ph, C_6H_4Me-4, $C_6H_4NO_2$-4, C≡CPh) proceeded smoothly to afford the adducts [$Cp_2W_2Ir_3(\mu_4\text{-}\eta^2\text{-}C_2R)(\mu\text{-}CO)(CO)_9$] [R = Ph (**26**), C_6H_4Me-4 (**27**), $C_6H_4NO_2$-4 (**28**), C≡CPh (**29**)], whereas attempted reactions with **3** were all unsuccessful. Reactions of alkynyltungsten complexes with **2** afforded major products corresponding to bond-selective formal insertion into an Ir-Ir linkage (minor amounts of thus-far-uncharacterized products were also obtained in some cases). Although an analogous insertion is possible with **3**, it may be disfavoured sterically by the necessity to place bulky CpW(CO) units at the hinge position of the putative product. It is perhaps significant that **3** reacted with internal acetylenes by way of W-W and W-Ir cleavage, but not via formal Ir-Ir insertion (Scheme 4.2.1.). It is not clear at present why **2** does not react with [CpW(CO)$_3$(C≡CC≡CH)] at the W-C≡C unit.

Other tetrahedral group 6-group 9 mixed-metal clusters have been reacted with terminal acetylenes. [Cp'$WCo_3(\mu\text{-}CO)_3(CO)_8$] (Cp' = η^5-C_5H_4Me) reacted with phenylacetylene with cluster fragmentation and acetylene oligomerization to afford the binuclear derivative [Cp'$WCo\{\mu\text{-}\eta^2,\eta^4\text{-}C(Ph)C(H)C(H)C(Ph)\}_2(CO)_4$].[105] In contrast to the [WCo_3] cluster, and to the [WIr_3] cluster of the current studies, introduction of a 4d metal in proceeding to [Cp'$MoCo_3(\mu\text{-}CO)_3(CO)_8$] resulted in phenylacetylene reaction with retention of nuclearity, to afford [Cp'$MoCo_3(\mu_4\text{-}\eta^2\text{-}HC_2Ph)(\mu\text{-}CO)_2(CO)_6$], with formal insertion of acetylene into a Mo-Co bond (Scheme 4.2.3.).[105] Weakening the M-M' bond in proceeding to a 4d-3d linkage enables control over reactivity. [$Cp'_2W_2Co_2(\mu\text{-}CO)_3(CO)_7$] reacted with phenylacetylene to afford [$Cp'_2W_2Co_2(\mu_4\text{-}\eta^2\text{-}HC_2Ph)(\mu\text{-}CO)_4(CO)_4$] in very low yield,[105] in contrast to [$Cp_2Mo_2Ir_2(\mu\text{-}CO)_3(CO)_7$][100] and **3** in the present work which afford analogous acetylene adducts in good to excellent yields. Across this series of [$M_2M'_2$] clusters, insertion into the group 6 M-M bond is facile, and the stability conferred by the heavier group 9 metal is the most important consideration.

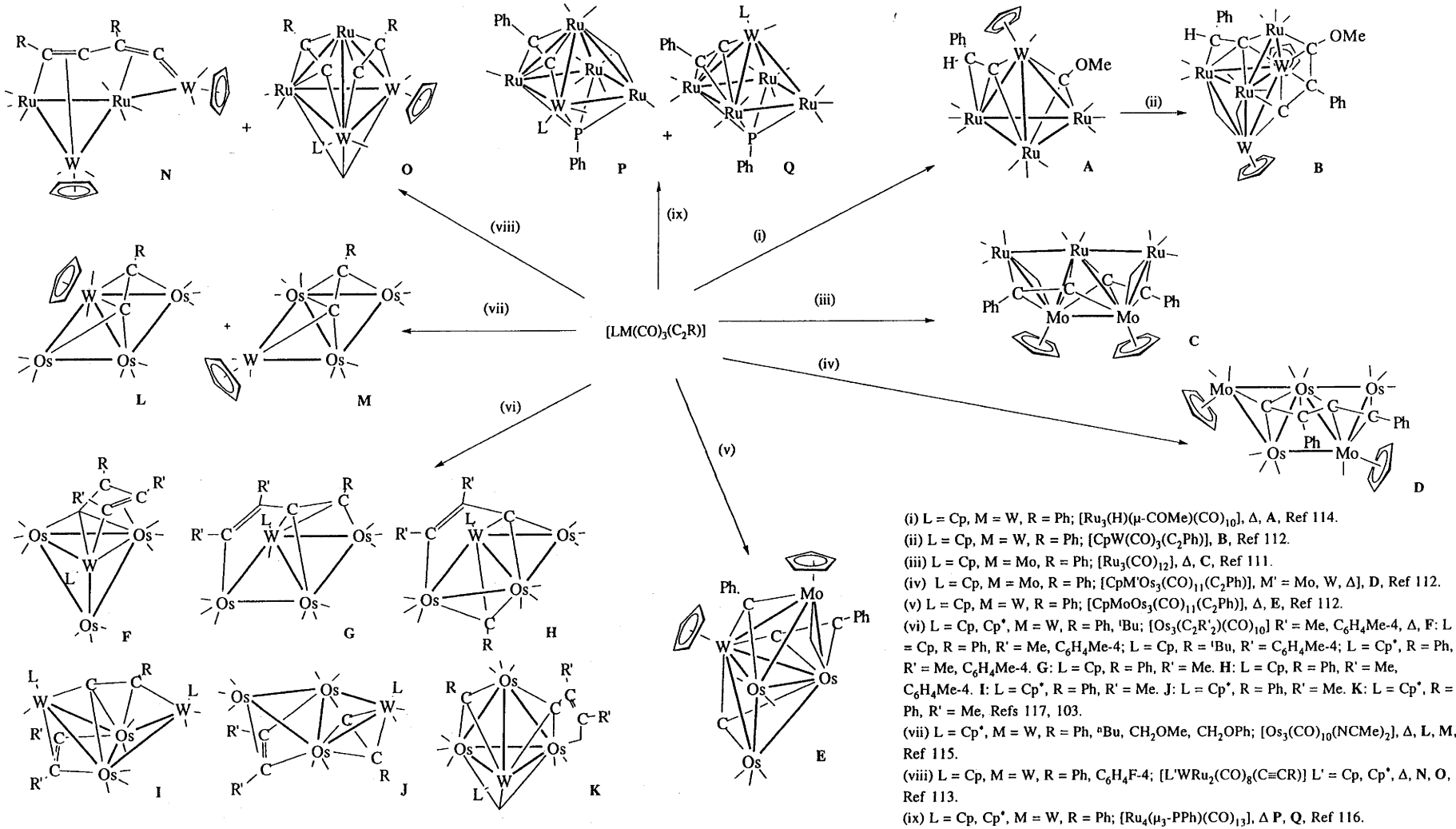


Scheme 4.2.2. Reactivity of $[CpWIr_3(CO)_{11}]$ (**2**) and $[Cp_2W_2Ir_2(CO)_{10}]$ (**3**) with terminal alkynes and alkynyltungsten complexes
(R = Ph, C_6H_4Me-4, $C_6H_4NO_2$-4, Bu^t; R' = Ph, C_6H_4Me-4, $C_6H_4NO_2$-4, C≡CPh).



Scheme 4.2.3.

The chemistry of group 6 transition metal acetylides is well established.[106,107] As well as being utilized in cluster formation,[108] and as metal exchange reagents in cluster chemistry,[109,110] they have been used extensively to expand the core nuclearity of the clusters in group 6 - group 8 mixed-metal cluster chemistry, the results of which are summarized in Scheme 4.2.4.[103,111-117] The reactions of "very mixed"-metal clusters with metal complexes frequently cause expansion of the cluster core (Chapter 1). This work is the first example of cluster core expansion of group 6 - group 9 clusters by reaction with group 6 metal acetylides. The majority of the reactions shown in Scheme 4.2.4. required forcing conditions to proceed (refluxing toluene), whereas reaction of **2** with $[CpW(CO)_3(C_2R)]$ proceeded at ambient temperatures in fair yields. In contrast, the reaction of **2** with the diynediyl complex $[Cp(OC)_3W(C{\equiv}CC{\equiv}C)W(CO)_3Cp]$ which afforded **30** required refluxing toluene, but this was due to the poor solubility of $[Cp(OC)_3W(C{\equiv}CC{\equiv}C)W(CO)_3Cp]$ in most solvents at room temperature. The nature of the acetylene significantly affects the product distribution; whereas cluster **3** reacted with internal acetylenes to afford *inter alia* a product involving C≡C cleavage and C-C formation (Scheme 4.2.1.), only products of general formula $[Cp_2W_2Ir_2(\mu_4\text{-}\eta^2\text{-}HC_2R)(\mu\text{-}CO)_4(CO)_4]$ were observed with terminal acetylenes. In combination with the above mentioned studies, the present work provides an interesting comparison of the effect of heterometal vertex replacement on the reactivity of a tetrahedral cluster, and the possibility of directing the chemistry of alkyne- or alkynyl-containing reagents towards specific sites by varying heterometal introduction and M-M' bond weakening. This differing alkyne reactivity of **2** and **3** does not extend to differing *P*-ligand substitution chemistry (Chapter 2), but differences in thermolytic ligand transformations of the adducts were observed (see Section 4.1.).



(i) L = Cp, M = W, R = Ph; $[Ru_3(H)(\mu\text{-}COMe)(CO)_{10}]$, Δ, **A**, Ref 114.
(ii) L = Cp, M = W, R = Ph; $[CpW(CO)_3(C_2Ph)]$, **B**, Ref 112.
(iii) L = Cp, M = Mo, R = Ph; $[Ru_3(CO)_{12}]$, Δ, **C**, Ref 111.
(iv) L = Cp, M = Mo, R = Ph; $[CpM'Os_3(CO)_{11}(C_2Ph)]$, M' = Mo, W, Δ], **D**, Ref 112.
(v) L = Cp, M = W, R = Ph; $[CpMoOs_3(CO)_{11}(C_2Ph)]$, Δ, **E**, Ref 112.
(vi) L = Cp, Cp*, M = W, R = Ph, ^{t}Bu; $[Os_3(C_2R'_2)(CO)_{10}]$ R' = Me, C_6H_4Me-4, Δ, **F**: L = Cp, R = Ph, R' = Me, C_6H_4Me-4; L = Cp, R = ^{t}Bu, R' = C_6H_4Me-4; L = Cp*, R = Ph, R' = Me, C_6H_4Me-4. **G**: L = Cp, R = Ph, R' = Me. **H**: L = Cp, R = Ph, R' = Me, C_6H_4Me-4. **I**: L = Cp*, R = Ph, R' = Me. **J**: L = Cp*, R = Ph, R' = Me. **K**: L = Cp*, R = Ph, R' = Me, Refs 117, 103.
(vii) L = Cp*, M = W, R = Ph, ^{n}Bu, CH_2OMe, CH_2OPh; $[Os_3(CO)_{10}(NCMe)_2]$, Δ, **L**, **M**, Ref 115.
(viii) L = Cp, M = W, R = Ph, C_6H_4F-4; $[L'WRu_2(CO)_8(C{\equiv}CR)]$ L' = Cp, Cp*, Δ, **N**, **O**, Ref 113.
(ix) L = Cp, Cp*, M = W, R = Ph; $[Ru_4(\mu_3\text{-}PPh)(CO)_{13}]$, Δ **P**, **Q**, Ref 116.

Scheme 4.2.4.

4.3. Conclusions

Some reactions leading to clusters with ligands in interesting coordination geometries were reported. The thermolysis of $[CpWIr_3(\mu\text{-}CO)_3(CO)_7(PPh_3)]$ (**4**) in refluxing toluene gave $[CpWIr_3\{\mu_3\text{-}\eta^2\text{-}PPh(C_6H_4)\}(\mu\text{-}CO)_2(CO)_7]$ (**12**) in good yield (56 %), together with $[CpWIr_3(CO)_{11}]$ (**2**) (32 %). An analogous reaction with $[CpWIr_3(\mu\text{-}CO)_3(CO)_6(PPh_3)_2]$ (**5**) gave **12** (23 %) and $[CpWIr_3\{\mu_3\text{-}\eta^2\text{-}PPh(C_6H_4)\}(\mu\text{-}CO)_2(CO)_6(PPh_3)]$ (**13**) (39 %). Products **12** and **13** (in 15 % and 44 % yield, respectively) were also obtained from heating $[CpWIr_3(\mu\text{-}CO)_3(CO)_5(PPh_3)_3]$ (**6**). Both **12** and **13** have been structurally characterized. The structural studies show that orthometallation has occurred, to afford products with (phenylphosphido)phenyl-*P*, *C* ligands capping the triiridium faces. In **13**, the intact PPh_3 resided at an iridium ligated by the phosphorus of the capping group. Attempts to effect further P-C cleavage of **12** (pyrolysis, photolysis, reaction with trimethylamine-*N*-oxide) were unsuccessful, as were attempts to effect C-H activation at the analogous $[CpWIr_3(\mu\text{-}CO)_3(CO)_7(PMe_3)]$ (**7**). Thermolyses of the related clusters $[Cp_2W_2Ir_2(\mu\text{-}CO)_3(CO)_6(PPh_3)]$ (**8**) and $[Cp_2W_2Ir_2(\mu\text{-}CO)_3(CO)_5(PPh_3)_2]$ (**9**) were less successful than those of **4** - **6**. Disproportionation of the clusters occurred, affording **3** in low yields (18 - 34 %). Previous reports have shown the ability of isocyanide ligands to adopt $\mu_n\text{-}\eta^2$-CNR coordination on clusters by activation of the ligand, usually by thermolysis. Thermolysis the isocyanide-substituted cluster $[CpWIr_3(CO)_{10}(CNBu^t)]$ (**10**), however, was found to afford $[CpWIr_3(CO)_9(CNBu^t)_2]$ (**11**) in low yield (15 %). Thermolysis of **11** afforded **10** (9 %), unreacted **11** (16 %) and **15** (4 %).

A controlled route to higher nuclearity clusters was also reported. Heating **3** with triphenylamine in refluxing tetrahydrofuran afforded $[Cp_3W_3Ir_4(\mu\text{-}H)(CO)_{12}]$ (**16**) in poor yield; an X-ray structural study revealed that the molecule consists of a trigonal bipyramidal $CpW\{Ir(CO)_2\}_4$ unit bicapped by $CpW(CO)_2$ fragments, generating a heptanuclear mixed-metal cluster of four face-sharing catenated tetrahedra.

The reactions of **2** and **3** with internal acetylenes have previously been reported to afford clusters with interesting coordination geometries. These earlier investigations were extended to include terminal alkynes and tungsten acetylides. Reactions of **3** with terminal arylalkynes HC≡CR afforded the complexes $[Cp_2W_2Ir_2(\mu_4\text{-}\eta^2\text{-}HC_2R)(\mu\text{-}CO)_4(CO)_4]$ [R = Ph (**18**), C_6H_4Me-4 (**19**), $C_6H_4NO_2$-4 (**20**)] in excellent yields (56 - 70 %). The analogous adduct with the terminal alkylalkyne HC≡CBu^t was obtained in much lower yield (20 %). An X-ray structural study of **19** revealed that the alkynes have formally inserted into the W-W bond of **3**, affording clusters with a pseudooctahedral geometry. The site of reactivity in **3** is consistent with the lack of reactivity towards terminal alkynes of the isostructural and isolobally-related **2**. Reaction of **3** with the buta-1,3-diynyl complex $[CpW(CO)_3(C{\equiv}CC{\equiv}CH)]$ (**23**) afforded the analogous adduct $[Cp_2W_2Ir_2\{\mu_4\text{-}\eta^2\text{-}$

$HC_2C{\equiv}CW(CO)_3Cp)(\mu\text{-}CO)_4(CO)_4]$ (**24**), shown spectroscopically to be attached via the C≡CH unit rather than by the [WC≡C] group. Attempts at condensing the pendant $CpW(CO)_3C{\equiv}C$ unit with the $[W_2Ir_2]$core in **24** have proven unsuccessful. Reactions of **2** with equimolar amounts of the tungsten acetylides $[CpW(CO)_3(C{\equiv}CR)]$ (R = Ph, C_6H_4Me-4, $C_6H_4NO_2$-4, C≡CPh) afforded the products $[Cp_2W_2Ir_3(\mu_4\text{-}\eta^2\text{-}C_2R)(\mu\text{-}CO)(CO)_9]$ [R = Ph (**26**), C_6H_4Me-4 (**27**), $C_6H_4NO_2$-4 (**28**), C≡CPh (**29**)] in fair yields (23-45 %). Product **27** has been structurally characterized, with the structural study revealing an edge-bridged tetrahedral metal core geometry and an unusual $\mu_4\text{-}\eta^2\,(3\sigma + \pi)$-coordinated alkynyl ligand. The reaction corresponds to formal insertion of the alkynyltungsten reagent into an Ir-Ir linkage of **2**. Reactions of **3** with these tungsten acetylides were not successful under the experimental conditions attempted, a result ascribed to steric constraints. A complex with the molecular composition $[Cp_3W_3Ir_3(C)_4(CO)_{13}]$ (**30**) is produced by refluxing **2** with the diynediyl complex $[Cp(OC)_3W(C{\equiv}CC{\equiv}C)W(CO)_3Cp]$, but a similar reaction of **3** caused decomposition of the cluster.

4.4. Experimental

4.4.1. General Conditions, Instruments, Reagents and Chromatography

4.4.1.1. General Conditions

These have been described in Chapter Two. The reaction solvent toluene was dried and distilled over sodium/benzophenone under an inert atmosphere prior to use.

4.4.1.2. Instruments

IR spectra, mass spectra and elemental analyses were performed as described in Chapter 2.

NMR spectra were recorded on either a Varian Gemini-300 or a Varian VXR300S spectrometer, the ^{1}H spectra at 300 MHz, the ^{13}C at 75 MHz using approximately 0.02 M $Cr(acac)_3$ as the relaxation agent and the recycle delay set to 0.5 s. References for the ^{1}H and ^{13}C NMR spectra were set to residual solvent peaks; the latter were proton decoupled. The INEPT experiments were run with a multiplicity of 2, selecting methine carbons only.

4.4.1.3. Reagents

The clusters $[CpWIr_3(CO)_{11}]$ (**2**) and $[Cp_2W_2Ir_2(CO)_{10}]$ (**3**) were prepared by literature methods.[55] The substituted clusters $[CpWIr_3(\mu\text{-}CO)_3(CO)_7(PPh_3)]$ (**4**), $[CpWIr_3(\mu\text{-}CO)_3(CO)_6(PPh_3)_2]$ (**5**), $[CpWIr_3(\mu\text{-}CO)_3(CO)_5(PPh_3)_3]$ (**6**), $[CpWIr_3(\mu\text{-}CO)_3(CO)_7(PMe_3)]$ (**7**), $[Cp_2W_2Ir_2(\mu\text{-}CO)_3(CO)_6(PPh_3)]$ (**8**), $[Cp_2W_2Ir_2(\mu\text{-}CO)_3(CO)_5(PPh_3)_2]$ (**9**), $[CpWIr_3(CNBu^t)(CO)_{10}]$ (**10**) and $[CpWIr_3(CNBu^t)_2(CO)_9]$ (**11**) were prepared as described in Chapter Two. 4-Nitrophenylacetylene[118] was prepared by the literature procedure. $[CpW(CO)_3(C{\equiv}CR)]$ (R = Ph, C_6H_4Me-4, $C_6H_4NO_2$-4, Bu^t) were prepared by modifications of the literature method.[119] Commercial reagents triphenylamine (Koch-Light), phenylacetylene (Aldrich), diphenylacetylene (Aldrich), 4-ethynyltoluene (Aldrich) and 3,3-dimethyl-1-butyne (Aldrich) were used as received. Trimethylamine-*N*-oxide dihydrate was purchased commercially (Aldrich) and sublimed before use. The complexes $[CpW(CO)_3(C{\equiv}CC{\equiv}CH)]$, $[CpW(CO)_3(C{\equiv}CC{\equiv}CPh)]$ and $[Cp(OC)_3W(C{\equiv}CC{\equiv}C)W(CO)_3Cp]$ were obtained from Prof. M. I. Bruce and Mr P. J. Low (University of Adelaide).

4.4.1.4. Chromatography

These conditions have been described in Chapter 2.

4.4.2. Crystal Preparation

Crystals suitable for diffraction analyses were grown as follows:

• $[CpWIr_3\{\mu_3\text{-}\eta^2\text{-}PPh(C_6H_4)\}(\mu\text{-}CO)_2(CO)_6(PPh_3)]$ (**13**) by slow diffusion of methanol into a solution of **13** in dichloromethane at room temperature.

• $[Cp_3W_3Ir_4(\mu\text{-}H)(CO)_{12}]$ (**16**) by slow evaporation of dichloromethane from a solution of **16** in dichloromethane / octane at room temperature.

• $[Cp_2W_2Ir_2(\mu_4\text{-}\eta^2\text{-}HC_2Ph)(\mu\text{-}CO)_4(CO)_4]$ (**18**) by slow diffusion of hexane into a solution of **18** in dichloromethane at -5 °C.

• $[Cp_2W_2Ir_3(\mu_4\text{-}\eta^2\text{-}C_2C_6H_4Me\text{-}4)(\mu\text{-}CO)(CO)_9]$ (**27**) by slow evaporation of dichloromethane from a solution of **27** in dichloromethane / octane at room temperature.

• $[CpWIr_3\{\mu_3\text{-}\eta^2\text{-}PPh(C_6H_4)\}(\mu\text{-}CO)_2(CO)_7]$ (**12**) (by V.-A. Tolhurst) by slow diffusion of methanol into a solution of **12** in dichloromethane at room temperature.

4.4.3. Thermolysis of $[CpWIr_3(\mu\text{-}CO)_3(CO)_7(PPh_3)]$

An orange solution of $[CpWIr_3(\mu\text{-}CO)_3(CO)_7(PPh_3)]$ (**4**) (20.0 mg, 0.0146 mmol) in toluene (15 mL) was slowly heated to 110 °C and refluxed for 15 min. The dark red solution obtained was evaporated to dryness. The deep red residue was then redissolved in CH_2Cl_2 (*ca* 1 mL) and chromatographed (1 CH_2Cl_2 : 2 petroleum ether eluant) to afford two products. The contents of the major purple band, R_f 0.40, were crystallized ($CHCl_3$/MeOH) to afford purple crystals of $[CpWIr_3\{\mu_3\text{-}\eta^2\text{-}PPh(C_6H_4)\}(\mu\text{-}CO)_2(CO)_7]$, **12** (12.2 mg, 56 %). Analytical data for **12**: IR (c-C_6H_{12}) 2065m, 2042s, 2030m, 2003s, 1995m, 1978w, 1943w, 1864w cm^{-1}; ^1H NMR ($CDCl_3$) δ 7.55 (m, 5H, Ph), 7.37 (m, 1H, C_6H_4), 6.91 (t, J_{HP} = 7 Hz, 1H, C_6H_4), 6.63-6.57 (m, 1H, C_6H_4), 6.15 (t, J_{HP} = 7 Hz, 1H, C_6H_4), 5.28 (s, 5H, C_5H_5); ^{13}C NMR ($CDCl_3$) δ 131-127 (Ph), 91.7 (C_5H_5), other signals not detected; ^{31}P NMR ($CDCl_3$) δ 309.6; FAB MS 1262 ($[M]^+$, 30), 1234 ($[M\text{-}CO]^+$, 44), 1206 ($[M\text{-}2CO]^+$, 18), 1178 ($[M\text{-}3CO]^+$, 100), 1150 ($[M\text{-}4CO]^+$, 22), 1122 ($[M\text{-}5CO]^+$, 26), 1094 ($[M\text{-}6CO]^+$, 54), 1066 ($[M\text{-}7CO]^+$, 47), 1038 ($[M\text{-}8CO]^+$, 45), 1010 ($[M\text{-}9CO]^+$, 32). Anal. Calcd for $C_{26}H_{14}Ir_3O_9PW$: C, 24.75; H, 1.12. Found: C, 24.50; H, 1.02 %.

The minor product, R_f 0.60, was recrystallized from CH_2Cl_2/MeOH to afford orange crystals of $[CpWIr_3(CO)_{11}]$, **2** (5.3 mg, 32 %). **2**: IR (c-C_6H_{12}) 2091m, 2054vs, 2049vs, 2029s, 1997m, 1981m, 1964w cm^{-1} (cf. lit. 2093m, 2053vs, 2049vs, 2031vs, 1996m, 1979m, 1967w [55,56]).

4.4.4. *Thermolysis of* $[CpWIr_3(\mu\text{-}CO)_3(CO)_6(PPh_3)_2]$

An orange solution of $[CpWIr_3(\mu\text{-}CO)_3(CO)_6(PPh_3)_2]$ (**5**) (20.0 mg, 0.0125 mmol) in toluene (20 mL) was heated to 110 °C and refluxed for 15 min. Solvent was removed *in vacuo* from the resulting brown solution. Subsequent purification by thin-layer chromatography (1 CH_2Cl_2: 1 petroleum ether eluant) afforded five bands, of which all but bands 2 and 5 were present in trace amounts. The contents of band 2, R_f 0.40, were crystallized from $CHCl_3$/MeOH to give purple crystals of $[CpWIr_3\{\mu_3\text{-}\eta^2\text{-}PPh(C_6H_4)\}(\mu\text{-}CO)_2(CO)_7]$, **12** (3.6 mg, 23 %), identified by IR spectroscopy. The contents of band 5, R_f 0.25, were crystallized from CH_2Cl_2/MeOH to afford $[CpWIr_3\{\mu_3\text{-}\eta^2\text{-}PPh(C_6H_4)\}(\mu\text{-}CO)_2(CO)_6(PPh_3)]$, **13** (7.3 mg, 39 %). Analytical data for **13**: IR (c-C_6H_{12}) 2046s, 2025vs, 1998m, 1984m, 1963vw, 1899w, 1814vw cm^{-1}; ^1H NMR ($CDCl_3$) δ 7.32-7.12 (s, 20H, Ph), 7.00 (t, J_{HP} = 7 Hz, 1H, C_6H_4), 6.82-6.71 (m, 2H, C_6H_4), 6.18 (t, J_{HP} = 7 Hz, 1H, C_6H_4), 5.38 (s, 5H, C_5H_5), 5.32 (s, 1.3H, CH_2Cl_2); ^{13}C NMR ($CDCl_3$) δ 222.0 (s, μ–CO), 178.7 (s, CO), 172.2 (s, CO), 170.7 (s, CO), 169.7 (s, C112, C_6H_4), 162.3 (s, CO), 143.9 (d, J_{CP} = 18 Hz, C111, C_6H_4), 135.7 (d, J_{CP} = 40 Hz, *i*-C, PPh_3), 135.7 (d, J_{CP} = 35 Hz, *i*-C, Ph), 133.9 (d, J_{CP} = 11 Hz, *m*-C, PPh_3), 130.2 (s, *p*-C, PPh_3), 129.7 (s, *p*-C, Ph), 129.4 (d, J_{CP} = 12 Hz, *m*-C, Ph), 128.3 (d, J_{CP} = 9 Hz, *o*-C, Ph), 128.1 (d, J_{CP} = 11 Hz, *o*-C, PPh_3), 127.3 (d, J_{CP} = 11 Hz, C116, C_6H_4), 122.3 (d, J_{CP} = 7.5 Hz, C115, C_6H_4), 91.5 (s, C_5H_5), 53.8 (s, CH_2Cl_2), C113, C114 not detected; ^{31}P NMR ($CDCl_3$) δ 267.5 (s, 1P, $PPhC_6H_4$), 7.9 (s, 1P, PPh_3); FAB MS 1496 ($[M]^+$, 24), 1468 ($[M\text{-}CO]^+$, 9), 1440 ($[M\text{-}2CO]^+$, 12), 1412 ($[M\text{-}3CO]^+$, 21), 1384 ($[M\text{-}4CO]^+$, 100), 1356 ($[M\text{-}5CO]^+$, 72), 1328 ($[M\text{-}6CO]^+$, 24). Anal. Calcd for $C_{43}H_{29}Ir_3O_8P_2W.0.68CH_2Cl_2$: C, 33.95; H, 1.96. Found: C, 34.03; H, 1.84 %.

4.4.5. *Thermolysis of* $[CpWIr_3(\mu\text{-}CO)_3(CO)_5(PPh_3)_3]$

An orange solution of $[CpWIr_3(\mu\text{-}CO)_3(CO)_5(PPh_3)_3]$ (**6**) (25.2 mg, 0.0137 mmol) in toluene (15 mL) was slowly heated to 110 °C and refluxed for 15 min. The brown solution obtained was evaporated to dryness. The resultant brown residue was redissolved in CH_2Cl_2 (*ca* 1 mL) and purified by thin layer chromatography (1 CH_2Cl_2 : 2 petroleum ether eluant) to afford seven bands. The contents of the second band, R_f 0.40, were crystallized from $CHCl_3$/MeOH and characterized as $[CpWIr_3\{\mu_3\text{-}\eta^2\text{-}PPh(C_6H_4)\}(\mu\text{-}CO)_2(CO)_7]$, **12** (2.3 mg, 15 %), by IR spectroscopy. The contents of the sixth, and major, band were crystallized from $CHCl_3$/MeOH to give brown crystals of $[CpWIr_3\{\mu_3\text{-}\eta^2\text{-}PPh(C_6H_4)\}(\mu\text{-}CO)_2(CO)_6(PPh_3)]$, **13** (9.0 mg, 44 %), characterized by IR spectroscopy. All other bands were present in trace amounts.

4.4.6. *Thermolysis of* $[CpWIr_3\{\mu_3\text{-}\eta^2\text{-}PPh(C_6H_4)\}(\mu\text{-}CO)_2(CO)_7]$

A solution of **12** (15.0 mg, 0.0119 mmol) in xylene (15 mL) was slowly heated to 120 °C and stirred for 15 min, at which stage a brown precipitate was evident in the dark reaction

mixture. The solvent was removed *in vacuo* and the residue taken up in dichloromethane (*ca* 1 mL). Purification by thin layer chromatography (1 acetone: 1 petroleum ether) eluted 3 bands in trace amounts.

4.4.7. Photolysis of [CpWIr$_3${μ_3-η^2-PPh(C_6H_4)}(μ-CO)$_2$(CO)$_7$]

A solution of **12** (15.0 mg, 0.0119 mmol) in acetonitrile (15 mL) was stirred and irradiated for 45 min with a 450 W mercury-arc lamp. The solvent was removed *in vacuo* leaving a brown residue. Subsequent purification by thin layer chromatography (1 CH_2Cl_2 : 1 petroleum ether eluant) gave 3 bands in trace amounts.

4.4.8. Reaction of [CpWIr$_3${μ_3-η^2-PPh(C_6H_4)}(μ-CO)$_2$(CO)$_7$] with Me_3NO

A solution of **12** (15.0 mg, 0.0119 mmol) and Me_3NO (0.89 mg, 0.012 mmol) in acetonitrile (15 mL) was stirred for 1 h. The solvent was removed *in vacuo*, leaving a brown residue. No tractable products were obtained.

4.4.9. Reaction of [CpWIr$_3${μ_3-η^2-PPh(C_6H_4)}(μ-CO)$_2$(CO)$_7$] with diphenylacetylene

A solution of **12** (2.9 mg, 0.23 μmol) and diphenylacetylene (0.4 mg, 0.23 μmol) in toluene (10 mL) was stirred at room temperature for 18 h. No reaction was observed. The solution was warmed and monitored by IR at 60 °C, 80 °C and 100 °C, stirring for 1 h at each interval. The solution was finally refluxed for 2 h. The solvent was removed *in vacuo*, leaving a brown residue. Subsequent purification by thin layer chromatography (1 CH_2Cl_2 : 1 petroleum ether eluant) afforded one band of starting material.

4.4.10. Thermolysis of [CpWIr$_3$(μ-CO)$_3$(CO)$_7$(PMe$_3$)]

An orange solution of [CpWIr$_3$(μ-CO)$_3$(CO)$_7$(PMe$_3$)] (**7**) (24.7 mg, 0.0201 mmol) in toluene (15 mL) was slowly heated to 110 °C and refluxed for 15 min. No reaction was apparent by IR monitoring of the reaction mixture. The solution was allowed to reflux for a further 45 min. Decomposition of the cluster was observed.

4.4.11. Thermolysis of [Cp$_2$W$_2$Ir$_2$(μ-CO)$_3$(CO)$_6$(PPh$_3$)]

A red solution of [Cp$_2$W$_2$Ir$_2$(μ-CO)$_3$(CO)$_6$(PPh$_3$)] (**8**) (20.0 mg, 0.0143 mmol) in thf (15 mL) was slowly heated to 65 °C and refluxed for 1 h with monitoring by IR spectroscopy. The solvent was removed *in vacuo*, leaving a red brown residue. Subsequent purification by thin layer chromatography (2 CH_2Cl_2 : 1 petroleum ether eluant) afforded one band of [Cp$_2$W$_2$Ir$_2$(CO)$_{10}$], **3** (5.5 mg, 34 %).

4.4.12. Thermolysis of $[Cp_2W_2Ir_2(\mu\text{-}CO)_3(CO)_5(PPh_3)_2]$

A red solution of $[Cp_2W_2Ir_2(\mu\text{-}CO)_3(CO)_5(PPh_3)_2]$ (**9**) (20.0 mg, 0.0121 mmol) in CH_2Cl_2 (15 mL) was slowly heated to 30 °C and stirred for 1 h. Monitoring the reaction by IR spectroscopy revealed complete conversion to $[Cp_2W_2Ir_2(\mu\text{-}CO)_3(CO)_6(PPh_3)]$, **8**. The solution was refluxed for 45 min. The solvent was removed *in vacuo*, leaving a red brown residue. Subsequent purification by thin layer chromatography (2 CH_2Cl_2 : 1 petroleum ether eluant) afforded one band of $[Cp_2W_2Ir_2(CO)_{10}]$, **3** (2.5 mg, 18 %).

4.4.13. Thermolysis of $[CpWIr_3(CO)_{10}(CNBu^t)]$

An orange solution of $[CpWIr_3(CO)_{10}(CNBu^t)]$ (**10**) (20.0 mg, 0.0168 mmol) in thf (15 mL) was slowly heated to 60 °C and refluxed for 30 h. A brown decomposition product was noted in the resultant orange solution. The solution was cooled and the solvent removed *in vacuo*, leaving a brown residue. Subsequent purification by thin layer chromatography (2 CH_2Cl_2 : 1 petroleum ether eluant) afforded two bands, identified by IR spectroscopy as **10** (3.3 mg, 15 %) and $[CpWIr_3(CO)_9(CNBu^t)_2]$, **11** (2.0 mg, 10 %).

4.4.14. Thermolysis of $[CpWIr_3(CO)_9(CNBu^t)_2]$, I

An orange solution of $[CpWIr_3(CO)_9(CNBu^t)_2]$ (**11**) (20.0 mg, 0.0164 mmol) in thf (15 mL) was slowly heated to 60 °C and refluxed for 30 h. The green solution obtained was evaporated to dryness. Subsequent purification by thin layer chromatography (2 CH_2Cl_2 : 1 petroleum ether eluant) afforded two bands, identified by IR spectroscopy as **10** (2.0 mg, 10 %) and **11** (7 mg, 30 %).

4.4.15. Thermolysis of $[CpWIr_3(CO)_9(CNBu^t)_2]$, II

An orange solution of $[CpWIr_3(CO)_9(CNBu^t)_2]$ (**11**) (20.0 mg, 0.0160 mmol) in toluene (15 mL) was slowly heated to 110 °C and refluxed for 30 h. The brown solution obtained was evaporated to dryness. Purification by thin layer chromatography (3 CH_2Cl_2 : 1 petroleum ether eluant) afforded three minor bands, identified by IR spectroscopy as **10** (2.3 mg, 12 %), **11** (6.0 mg, 30 %) and $[CpWIr_3(CO)_8(CNBu^t)_3]$, **15** (1.6 mg, 8 %).

4.4.16. Reaction of $[Cp_2W_2Ir_2(CO)_{10}]$ and NPh_3

A solution of $[Cp_2W_2Ir_2(CO)_{10}]$ (**3**) (50.0 mg, 0.0430 mmol) and NPh_3 (10.5 mg, 0.0430 mmol) in thf (15 mL) was refluxed for 30 h. Solvent was removed *in vacuo* to leave a brown residue. Subsequent purification by preparative thin-layer chromatography (7 CH_2Cl_2: 3 petroleum ether) resulted in six bands. Bands 1 and 2 were identified as

$[CpWIr_3(CO)_{11}]$ (3.6 mg, 7%) and $[Cp_2W_2Ir_2(CO)_{10}]$ (19.8 mg, 40%). Bands 4 and 6 were very minor and have not thus far been characterized. Band 3, R_f 0.51, was crystallized from CH_2Cl_2/octane to afford brown crystals of $[Cp_3W_3Ir_4(\mu\text{-}H)(CO)_{12}]$, **16** (1.1 mg, 1%). Analytical data for **16**: IR (c-C_6H_{12}) 2014vs, 2001vs, 1985m, 1969m, 1946w, 1940w, 1839w cm^{-1}. ^1H NMR δ(acetone-d_6) 5.67 (s, 5H, Cp), 5.60 (s, 5H, Cp), 5.55 (s, 5H, Cp), -6.37 (s, 1H, μ-H). The very small yields of **16** precluded microanalyses.

Band 5, R_f 0.25, was characterized as $[Cp_3W_3Ir_2(\mu\text{-}H)(CO)_{10}]$, **17** by comparison of its IR spectrum with previously reported data. Spectroscopic data for **17**: IR (c-C_6H_{12}): 2040s, 2000vs, 1985m, 1944m, 1875m, 1809w (lit: 2040s, 2000vs, 1985m, 1944m, 1876m, 1809w [53]).

4.4.17. Reaction of $[Cp_2W_2Ir_2(CO)_{10}]$ with HC≡CPh (with V.-A. Tolhurst)

A deep red solution of $[Cp_2W_2Ir_2(CO)_{10}]$ (20.0 mg, 0.0172 mmol) and HC≡CPh (3.2 μL, 0.03 mmol) in toluene (20 mL) was stirred at 50 °C for 1 h, after which time the reaction solution was allowed to cool to room temperature and the solvent removed *in vacuo*. Alternatively, the solution was stirred at room temperature for 16 h (the result and yield of product were approximately the same). The resultant brown residue was dissolved in CH_2Cl_2 (*ca* 1 mL) and chromatographed (3 CH_2Cl_2 : 1 petroleum ether eluant) to afford one product. The band, R_f 0.30, was crystallized from CH_2Cl_2/*n*-C_6H_{14} to afford dark green crystals of $[Cp_2W_2Ir_2(\mu_4\text{-}\eta^2\text{-}HC_2Ph)(\mu\text{-}CO)_4(CO)_4]$, **18** (14.5 mg, 70 %). Analytical data for **18**: IR (CH_2Cl_2) 2061vs, 2032vs, 2008m, 1986m, 1821br m cm^{-1}. ^1H NMR (acetone-d_6) δ 9.77 (s, 1H, ≡CH), 7.32-7.00 (m, 5H, Ph), 5.28 (s, 1H, CH_2Cl_2), 5.14 (s, 10H, C_5H_5); ^{13}C NMR (CD_2Cl_2) δ 222.0 (CO), 220.9 (CO), 177.9 (CO), 177.7 (CO), 175.7 (CO), 173.1 (CO), 152.8 (*C*Ph), 128.9 - 118.9 (Ph), 99.2 (≡CH), 93.5 (C_5H_5); FAB MS 1208 ($[M]^+$, 58), 1152 ($[M\text{-}2CO]^+$, 29), 1124 ($[M\text{-}3CO]^+$, 100), 1096 ($[M\text{-}4CO]^+$, 47), 1068 ($[M\text{-}5CO]^+$, 12), 1040 ($[M\text{-}6CO]^+$, 98), 1012 ($[M\text{-}7CO]^+$, 39). Anal. Calcd: C 25.84, H 1.33. Found: C 25.50, H 1.26 %.

4.4.18. Reaction of $[Cp_2W_2Ir_2(CO)_{10}]$ with HC≡CC$_6$H$_4$Me-4

Following the method of Section 4.4.17., $[Cp_2W_2Ir_2(CO)_{10}]$ (20.0 mg, 0.0172 mmol) and HC≡CC$_6$H$_4$Me-4 (3.5 mg, 0.03 mmol) in toluene (20 mL) afforded one product after chromatography (3 CH_2Cl_2 : 1 petroleum ether eluant). The band, R_f 0.32, was crystallized from CH_2Cl_2/c-C_6H_{12} to afford purple/green crystals of $[Cp_2W_2Ir_2(\mu_4\text{-}\eta^2\text{-}HC_2C_6H_4Me\text{-}4)(\mu\text{-}CO)_4(CO)_4]$, **19** (12.5 mg, 59 %). Analytical data for **19**: IR (CH_2Cl_2) 2060vs, 2031vs, 2006m, 1986m, 1825br m cm^{-1}. ^1H NMR (acetone-d_6) δ 9.12 (s, 1H, ≡CH), 7.00-6.45 (m, 4H, C_6H_4), 4.90 (s, 10H, C_5H_5), 2.22 (s, 3H, Me); FAB MS 1222 ($[M]^+$, 57), 1166 ($[M\text{-}2CO]^+$, 30), 1138 ($[M\text{-}3CO]^+$, 98), 1110 ($[M\text{-}4CO]^+$, 37), 1082 ($[M\text{-}5CO]^+$, 10), 1054

([M-6CO]$^+$, 100), 1026 ([M-7CO]$^+$, 42). Anal. Calcd: C 26.53, H 1.70. Found: C 26.82, H 1.90 %.

4.4.19. Reaction of $[Cp_2W_2Ir_2(CO)_{10}]$ with $HC{\equiv}CC_6H_4NO_2$-4

Following the method of Section 4.4.17., $[Cp_2W_2Ir_2(CO)_{10}]$ (20.0 mg, 0.0172 mmol) and $HC{\equiv}CC_6H_4NO_2$-4 (4.4 mg, 0.03 mmol) in toluene (20 mL) afforded two products after chromatography (3 CH_2Cl_2 : 1 petroleum ether eluant), one of which was in trace quantities. Crystallization of the contents of the second band, R_f 0.40, from CH_2Cl_2/c-C_6H_{12} afforded brown crystals of $[Cp_2W_2Ir_2(\mu_4\text{-}\eta^2\text{-}HC_2C_6H_4NO_2\text{-}4)(\mu\text{-}CO)_4(CO)_4]$, **20** (12.0 mg, 56 %). Analytical data for **20**: IR (CH_2Cl_2) 2064vs, 2036vs, 2006w, 1991m, 1829br m cm^{-1}; ^{1}H NMR ($CDCl_3$) δ 8.95 (s, 1H, ≡CH), 8.10-7.02 (m, 4H, C_6H_4), 4.95 (s, 10H, C_5H_5); FAB MS 1253 ([M]$^+$, 37), 1197 ([M-2CO]$^+$, 26), 1169 ([M-3CO]$^+$, 100), 1141 ([M-4CO]$^+$, 80), 1113 ([M-5CO]$^+$, 61), 1085 ([M-6CO]$^+$, 88), 1057 ([M-7CO]$^+$, 47). Anal. Calcd: C 24.91, H 1.21, N 1.12. Found: C 25.81, H 1.40, N 2.17 %.

4.4.20. Reaction of $[Cp_2W_2Ir_2(CO)_{10}]$ with $HC{\equiv}CBu^t$

A deep red solution of $[Cp_2W_2Ir_2(CO)_{10}]$ (20.0 mg, 0.0172 mmol) and $HC{\equiv}CBu^t$ (4 μL, 0.03 mmol) in toluene (20 mL) was refluxed for 1 h, after which time the reaction solution was allowed to cool to room temperature and the solvent removed *in vacuo*. The resultant brown residue was dissolved in CH_2Cl_2 (*ca* 1 mL) and chromatographed (3 CH_2Cl_2 : 1 petroleum ether eluant) to afford five bands, four of which were in minor amounts and not isolated. Band 3, R_f 0.30, was crystallized from CH_2Cl_2/c-C_6H_{12} to afford brown crystals of $[Cp_2W_2Ir_2(\mu_4\text{-}\eta^2\text{-}HC_2Bu^t)(\mu\text{-}CO)_4(CO)_4]$, **21** (4.0 mg, 20 %). Analytical data for **21**: IR (CH_2Cl_2) 2065vs, 2036vs, 2010m, 1990m, 1835br m cm^{-1}; ^{1}H NMR ($CDCl_3$) δ 9.64 (s, 1H, ≡CH), 4.73 (s, 10H, C_5H_5), 2.12 (s, 9H, Me); FAB MS 1192 ([M]$^+$, 35), 1164 ([M-CO]$^+$, 6), 1136 ([M-2CO]$^+$, 14), 1108 ([M-3CO]$^+$, 100), 1080 ([M-4CO]$^+$, 80), 1052 ([M-5CO]$^+$, 58). Anal. Calcd: C 24.25, H 1.70. Found: C 23.86, H 1.90 %.

4.4.21. Reaction of $[Cp_2W_2Ir_2(CO)_{10}]$ with $[CpW(CO)_3(C{\equiv}CC{\equiv}CH)]$

A deep red solution of $[Cp_2W_2Ir_2(CO)_{10}]$ (20.0 mg, 0.0172 mmol) and $CpW(CO)_3(C{\equiv}CC{\equiv}CH)$ (6.6 mg, 0.0172 mmol) in CH_2Cl_2 (20 mL) was stirred at room temperature for 16 h. The brown solution was evaporated to dryness. The resultant brown residue was redissolved in CH_2Cl_2 (*ca* 1 mL) and chromatographed (3 CH_2Cl_2 : 1 petroleum ether eluant) to afford one product. The band, R_f 0.28, was crystallized from CH_2Cl_2/c-C_6H_{12} to afford dark green crystals of $[Cp_2W_2Ir_2\{\mu_4\text{-}\eta^2\text{-}HC_2C{\equiv}CW(CO)_3Cp\}(\mu\text{-}CO)_4(CO)_4]$, **24** (15.3 mg, 62 %). Analytical data for **24**: IR (CH_2Cl_2) ν(C≡C) 2155w, ν(C≡O) 2058s, 2055sh, 2033vs, 2003m, 1984w, 1945br s, 1823 br m cm^{-1}; ^{1}H NMR ($CDCl_3$) δ 8.40 (s, 1H, ≡CH), 5.54 (s, 5H, C_5H_5), 5.29 (s, 10H, C_5H_5);

^{13}C NMR (CD_2Cl_2) δ 227.6 (CO), 222.3 (CO), 221.7 (CO), 212.9 (CO), 177.9 (CO), 177.7 (CO), 173.5 (CO), 172.3 (CO), 146.8 (*C*≡CH), 109.6 (≡CH), 106.2 (W*C*≡), 94.2 (C_5H_5), 92.3 (C_5H_5), 78.0 (s, WC≡*C*); FAB MS 1488 ($[M]^+$, 10), 1460 ($[M\text{-}CO]^+$, 4), 1432 ($[M\text{-}2CO]^+$, 6), 1404 ($[M\text{-}3CO]^+$, 13), 1376 ($[M\text{-}4CO]^+$, 3), 1348 ($[M\text{-}5CO]^+$, 7), 1320 ($[M\text{-}6CO]^+$, 17), 1292 ($[M\text{-}7CO]^+$, 65), 1264 ($[M\text{-}8CO]^+$, 37), 1236 ($[M\text{-}9CO]^+$, 42), 1208 ($[M\text{-}10CO]^+$, 35), 1180 ($[M\text{-}11CO]^+$, 100). Anal. Calcd: C 24.21, H 1.08. Found: C 24.31, H 0.84 %.

4.4.22. Thermolysis of $[Cp_2W_2Ir_2\{\mu_4\text{-}\eta^2\text{-}HC_2C{\equiv}CW(CO)_3Cp\}(\mu\text{-}CO)_4(CO)_4]$

A solution of **24** (15 mg, 0.010 mmol) in thf (15 mL) was slowly heated to 65 °C, and stirred for 15 min, the course of the reaction being monitored by IR spectroscopy. Intensities of the ν(CO) bands decreased with time. The solvent was removed *in vacuo*, leaving a brown residue from which no tractable products could be obtained.

4.4.23. Reaction of $[Cp_2W_2Ir_2\{\mu_4\text{-}\eta^2\text{-}HC_2C{\equiv}CW(CO)_3Cp\}(\mu\text{-}CO)_4(CO)_4]$ with Me_3NO

A solution of **24** (20 mg, 0.013 mmol) and Me_3NO (1.0 mg, 0.013 mmol) in acetonitrile (10 mL) was stirred for 1 h. The solution was evaporated to dryness leaving a brown residue from which no tractable products could be obtained.

4.4.24. Reaction of $[CpWIr_3(CO)_{11}]$ with HC≡CPh

An orange solution of $[CpWIr_3(CO)_{11}]$ (20.0 mg, 0.0176 mmol) and HC≡CPh (3 μL, 0.03 mmol) in toluene (20 mL) was slowly heated to 110 °C and refluxed for 15 min. No reaction was apparent by IR monitoring of the reaction mixture. The solution was allowed to reflux for a further 45 min, and the resultant brown solution was then evaporated to dryness. The brown residue was dissolved in CH_2Cl_2 (*ca.* 1 mL). Purification by thin-layer chromatography (3 CH_2Cl_2 : 1 petroleum ether) eluted three bands in trace amounts.

4.4.25. Reaction of $[CpWIr_3(CO)_{11}]$ with $HC{\equiv}CC_6H_4NO_2$-4

Following the method of Section 4.4.24., $[CpWIr_3(CO)_{11}]$ (20.0 mg, 0.0176 mmol) and $HC{\equiv}CC_6H_4NO_2$-4 (4.4 mg, 0.03 mmol) afforded three trace bands after chromatography (3 CH_2Cl_2 : 1 petroleum ether).

4.4.26. Reaction of $[CpWIr_3(CO)_{11}]$ with $[CpW(CO)_3(C{\equiv}CC{\equiv}CH)]$

Following the method of Section 4.4.24., $[CpWIr_3(CO)_{11}]$ (20.0 mg, 0.0176 mmol) and $CpW(CO)_3(C{\equiv}CC{\equiv}CH)$ (6.7 mg, 0.0176 mmol) afforded one trace band after chromatography (3 CH_2Cl_2 : 1 petroleum ether).

4.4.27. Reaction of $[Cp_2W_2Ir_2(CO)_{10}]$ with $[CpW(CO)_3(C{\equiv}CR)]$

An orange-red solution of $[Cp_2W_2Ir_2(CO)_{10}]$ (20.0 mg, 0.0172 mmol) and $[CpW(CO)_3(C{\equiv}CPh)]$ (7.6 mg, 0.0176 mmol) in CH_2Cl_2 (20 mL) was stirred at room temperature for 60 h in the absence of light. No reaction was apparent by IR monitoring of the reaction mixture. The solution was slowly heated to 40 °C and refluxed 15 min. No reaction was apparent by IR monitoring. The solvent was then removed *in vacuo*, and replaced with toluene (20 mL). The solution was slowly heated to 110 °C and finally refluxed for 15 min. The resultant dark brown solution was then evaporated to dryness. The brown residue obtained was dissolved in CH_2Cl_2 (*ca.* 1 mL). Purification by thin-layer chromatography (1 CH_2Cl_2 : 1 petroleum ether) eluted five bands in trace amounts. Related reactions of **2** with $[CpW(CO)_3(C{\equiv}CR)]$ (R = C_6H_4Me-4, $C_6H_4NO_2$-4 or C≡CPh) afforded similar results.

4.4.28. Reaction of $[CpWIr_3(CO)_{11}]$ with $[CpW(CO)_3(C{\equiv}CPh)]$

An orange solution of $[CpWIr_3(CO)_{11}]$ (20.0 mg, 0.0176 mmol) and $[CpW(CO)_3(C{\equiv}CPh)]$ (7.6 mg, 0.0176 mmol) in CH_2Cl_2 (20 mL) was stirred at room temperature for 60 h in the absence of light. The brown solution was then evaporated to dryness. The resultant brown residue was dissolved in CH_2Cl_2 (ca 1 mL) and chromatographed (3 CH_2Cl_2 : 2 petroleum ether eluant) to afford three bands. The contents of the first two bands were identified as starting materials by IR spectroscopy. The third band, R_f 0.43, was crystallized from CH_2Cl_2/*n*-hexane to afford brown crystals of $[Cp_2W_2Ir_3(\mu_4\text{-}\eta^2\text{-}C_2Ph)(\mu\text{-}CO)(CO)_9]$, **26** (11.5 mg, 45 %). Analytical data for **26**: IR (c-C_6H_{12}) 2080vs, 2037s, 2032vs, 2024s, 2017m, 2004s, 1996w, 1982w, 1968m, 1958br m cm^{-1}; ^1H NMR ($CDCl_3$) δ 7.69-7.34 (m, 5H, Ph), 5.59 (s, 5H, C_5H_5), 4.64 (s, 5H, C_5H_5); FAB MS 1456 ($[M]^+$, 15), 1428 ($[M\text{-}CO]^+$, 34), 1400 ($[M\text{-}2CO]^+$, 22), 1372 ($[M\text{-}3CO]^+$, 84), 1344 ($[M\text{-}4CO]^+$, 75), 1316 ($[M\text{-}5CO]^+$, 100), 1288 ($[M\text{-}6CO]^+$, 60), 1260 ($[M\text{-}7CO]^+$, 59), 1232 ($[M\text{-}8CO]^+$, 60), 1204 ($[M\text{-}9CO]^+$, 39), 1176 ($[M\text{-}10CO]^+$, 740). Anal. Calcd: C 23.21, H 1.04. Found: C 23.64, H 1.25 %.

4.4.29. Reaction of $[CpWIr_3(CO)_{11}]$ with $[CpW(CO)_3(C{\equiv}CC_6H_4Me\text{-}4)]$

Following the method of Section 4.4.28., $[CpWIr_3(CO)_{11}]$ (20.0 mg, 0.0176 mmol) and $[CpW(CO)_3(C{\equiv}CC_6H_4Me\text{-}4)]$ (7.9 mg, 0.0176 mmol) in CH_2Cl_2 (20 mL) afforded one product after purification by preparative thin-layer chromatography (1 CH_2Cl_2 : 1 petroleum ether eluant). The contents of the band, R_f 0.41, were crystallized from CH_2Cl_2/c-C_6H_{12} to afford brown crystals of $[Cp_2W_2Ir_3(\mu_4\text{-}\eta^2\text{-}C_2C_6H_4Me\text{-}4)(\mu\text{-}CO)(CO)_9]$, **27** (10.3 mg, 40 %). Analytical data for **27**: IR (c-C_6H_{12}) 2079vs, 2036s, 2031vs, 2024s, 2016m, 2003s, 1995w, 1981w, 1967m, 1958br m cm^{-1}; ^1H NMR ($CDCl_3$) δ

7.73-7.42 (m, 4H, C_6H_4), 5.58 (s, 5H, C_5H_5), 4.63 (s, 5H, C_5H_5), 2.40 (s, 3H, Me); FAB MS 1470 ($[M]^+$, 27), 1442 ($[M\text{-}CO]^+$, 34), 1414 ($[M\text{-}2CO]^+$, 3), 1386 ($[M\text{-}3CO]^+$, 90), 1358 ($[M\text{-}4CO]^+$, 66), 1330 ($[M\text{-}5CO]^+$, 100), 1302 ($[M\text{-}6CO]^+$, 95), 1274 ($[M\text{-}7CO]^+$, 90), 1246 ($[M\text{-}8CO]^+$, 60). Anal. Calcd: C 23.70, H 1.17. Found: C 24.14, H 0.73 %.

4.4.30. Reaction of [CpWIr$_3$(CO)$_{11}$] with [CpW(CO)$_3$(C≡CC$_6$H$_4$NO$_2$-4)]

Following the method of Section 4.4.28., $[CpWIr_3(CO)_{11}]$ (20.0 mg, 0.0176 mmol) and $[CpW(CO)_3(C{\equiv}CC_6H_4NO_2\text{-}4)]$ (8.4 mg, 0.0176 mmol) in CH_2Cl_2 (20 mL) afforded three products after purification by preparative thin-layer chromatography (1 CH_2Cl_2 : 1 petroleum ether eluant). Crystallization of the contents of the third band, R_f 0.38, from CH_2Cl_2/c-C_6H_{12} afforded brown crystals of $[Cp_2W_2Ir_3(\mu_4\text{-}\eta^2\text{-}C_2C_6H_4NO_2\text{-}4)(\mu\text{-}CO)(CO)_9].CH_2Cl_2$, **28** (11.6 mg, 44 %). Analytical data for **28**: IR (c-C_6H_{12}) 2082vs, 2040s, 2035vs, 2029s, 2019m, 2007s, 1972w, 1961m, 1955br m cm^{-1}; ^1H NMR ($CDCl_3$) δ 8.36 (d, $^3J_{HH}$ = 8 Hz, 2H, C_6H_4), 7.75 (d, $^3J_{HH}$ = 8 Hz, 2H, C_6H_4), 5.57 (s, 5H, C_5H_5), 5.28 (s, 2H, CH_2Cl_2), 4.66 (s, 5H, C_5H_5); FAB MS 1501 ($[M]^+$, 10), 1473 ($[M\text{-}CO]^+$, 25), 1445 ($[M\text{-}2CO]^+$, 26), 1417 ($[M\text{-}3CO]^+$, 71), 1389 ($[M\text{-}4CO]^+$, 67), 1361 ($[M\text{-}5CO]^+$, 100), 1333 ($[M\text{-}6CO]^+$, 59), 1305 ($[M\text{-}7CO]^+$, 51), 1277 ($[M\text{-}8CO]^+$, 48). Anal. Calcd: C 21.97, H 1.02, N 0.88. Found: C 21.50, H 0.89, N 1.02 %.

4.4.31. Reaction of [CpWIr$_3$(CO)$_{11}$] with [CpW(CO)$_3$(C≡CC≡CPh)]

Following the method of Section 4.4.28., $[CpWIr_3(CO)_{11}]$ (20.0 mg, 0.0176 mmol) and $[CpW(CO)_3(C{\equiv}CC{\equiv}CPh)]$ (8.0 mg, 0.0176 mmol) in CH_2Cl_2 (20 mL) afforded four bands after purification by preparative thin-layer chromatography (1 CH_2Cl_2 : 1 petroleum ether eluant). The contents of the first two bands were identified as starting material by IR spectroscopy. The third band was in trace amounts. The contents of the fourth band, R_f 0.29, were crystallized from CH_2Cl_2/c-C_6H_{12} to afford brown crystals of $[Cp_2W_2Ir_3(\mu_4\text{-}\eta^2\text{-}C_2C{\equiv}CPh)(\mu\text{-}CO)(CO)_9]$, **29** (6.1 mg, 23 %). Analytical data for **29**: IR (c-C_6H_{12}) 2085s, 2053w, 2037vs, 2019vs, 1980m, 1975w, 1967br w cm^{-1}; ^1H NMR ($CDCl_3$) δ 7.47-7.36 (m, 5H, Ph), 5.80 (s, 5H, C_5H_5), 4.80 (s, 5H, C_5H_5); FAB MS 1423 ($[M\text{-}2CO]^+$, 20), 1395 ($[M\text{-}3CO]^+$, 40), 1367 ($[M\text{-}4CO]^+$, 61), 1339 ($[M\text{-}5CO]^+$, 100), 1311 ($[M\text{-}6CO]^+$, 86), 1283 ($[M\text{-}7CO]^+$, 50), 1255 ($[M\text{-}8CO]^+$, 63). Anal. Calcd: C 24.35, H 1.02. Found: C 24.64, H 1.00 %.

4.4.32. Reaction of [CpWIr$_3$(CO)$_{11}$] with [CpW(CO)$_3$(C≡CC≡C)(CO)$_3$WCp]

An orange suspension of $[CpWIr_3(CO)_{11}]$ (**2**) (20.0 mg, 0.0176 mmol) and $[CpW(CO)_3(C_4)(CO)_3WCp]$ (12.6 mg, 0.0176 mmol) in toluene (20 mL) was slowly heated to 110 °C and refluxed for 15 min. The resulting dark brown solution was then cooled and

evaporated to dryness. The deep brown residue obtained was dissolved in CH_2Cl_2 (ca 1 mL) and chromatographed (2 CH_2Cl_2 : 1 petroleum ether eluant) affording one band. The contents of the band, R_f 0.30, were crystallized from CH_2Cl_2/c-C_6H_{12} to afford brown crystals of $[Cp_3W_3Ir_3(C)_4(CO)_{13}]$, **30** (12.2 mg, 40 %). Analytical data for **30**: IR (c-C_6H_{12}) 2079s, 2033vs, 2011m, 1976m, 1972w, 1962w, 1952w; ^{1}H NMR ($CDCl_3$) δ 5.75 (s, 5H, C_5H_5), 5.69 (s, 5H, C_5H_5), 4.70 (s, 5H, C_5H_5); ^{13}C NMR (CD_2Cl_2) 227.1 (s), 221.2 (s), 216.0 (s), 212.8 (s), 212.5 (s), 211.3 (s), 182.5 (s), 179.4 (s), 171.9 (s), 139.8 (s), 138.2 (s), 134.5 (s), 129.2 (s), 128.3 (s), 125.4 (s), 92.5 (s, Cp), 92.3 (s, Cp), 90.3 (s, Cp); FAB MS 1735 ($[M]^+$, 21), 1707 ($[M\text{-}CO]^+$, 45), 1679 ($[M\text{-}2CO]^+$, 40), 1651 ($[M\text{-}3CO]^+$, 95), 1623 ($[M\text{-}4CO]^+$, 97), 1595 ($[M\text{-}5CO]^+$, 100), 1567 ($[M\text{-}6CO]^+$, 29), 1539 ($[M\text{-}7CO]^+$, 28), 1511 ($[M\text{-}8CO]^+$, 54), 1483 ($[M\text{-}9CO]^+$, 59), 1455 ($[M\text{-}10CO]^+$, 38), 1427 ($[M\text{-}11CO]^+$, 58), 1399 ($[M\text{-}12CO]^+$, 55), 1371 ($[M\text{-}13CO]^+$, 65). Anal. Calcd: C 22.14, H 0.87. Found: C 22.05, H 1.16 %.

4.4.33. Reaction of $[Cp_2W_2Ir_2(CO)_{10}]$ with $[Cp(OC)_3W(C{\equiv}CC{\equiv}C)W(CO)_3Cp]$

An orange suspension of $[Cp_2W_2Ir_2(CO)_{10}]$ (**3**) (20.0 mg, 0.0172 mmol) and $[Cp(OC)_3W(C{\equiv}CC{\equiv}C)W(CO)_3Cp]$ (12.3 mg, 0.0172 mmol) in toluene (20 mL) was slowly heated to 110 °C and refluxed for 15 min. The solvent was removed *in vacuo*, leaving a brown residue. No tractable products were obtained, decomposition of the cluster having occurred.

4.5. References

(1) Garrou, P. E. *Chem. Rev.* **1985**, *85*, 171.
(2) Bruce, M. I.; Shaw, G.; Stone, F. G. A. *J. Chem. Soc., Dalton Trans.* **1972**, 2094.
(3) Bruce, M. I.; Guss, J. M.; Mason, R.; Skelton, B. W.; White, A. H. *J. Organomet. Chem.* **1983**, *251*, 261.
(4) Jungbluth, H.; Süss-Fink, G.; Pellinghelli, M. A.; Tiripicchio, A. *Organometallics* **1989**, *8*, 925.
(5) Knox, S. A. R.; Lloyd, B. R.; Orpen, A. G.; Vinas, J. M.; Weber, M. *J. Chem. Soc., Chem. Commun.* **1987**, 1498.
(6) Bradford, C. W.; Nyholm, R. S. *J. Chem. Soc., Dalton Trans.* **1973**, 529.
(7) Cullen, W. R.; Harbourne, D.; Leingme, B.; Sams, J. R. *Inorg. Chem.* **1970**, *9*, 702.
(8) Cullen, W. R. *Adv. Inorg. Chem. Radiochem.* **1972**, *15*, 323.
(9) Deeming, A. J.; Kimber, R. E.; Underhill, M. *J. Chem. Soc., Dalton Trans.* **1973**, 2589.
(10) Deeming, A. J.; Underhill, M. *J. Chem. Soc., Dalton. Trans.* **1973**, 2727.
(11) Gainsford, G. J.; Guss, J. M.; Ireland, P. R.; Mason, R.; Bradford, C. W.; Nyholm, R. S. *J. Organomet. Chem.* **1972**, *40*, C70.
(12) Bradford, C. W.; Nyholm, R. S.; Gainsford, G. J.; Guss, J. M.; Ireland, P. R.; Mason, R. *J. Chem. Soc., Chem. Commun.* **1972**, 87.
(13) Bradford, C. W.; Nyholm, R. S. *J. Chem. Soc., Chem. Commun.* **1972**, 2094.
(14) Deeming, A. J.; Rothwell, I. P.; Hursthouse, M. B.; Backer-Dirks, J. D. J. *J. Chem. Soc., Dalton Trans.* **1981**, 1879.
(15) Brown, S. C.; Evans, J.; Smart, L. *J. Chem. Soc., Chem. Commun.* **1980**, 1021.
(16) Deeming, A. J.; Kabir, S. E.; Powell, N. I. *J. Chem. Soc., Dalton Trans.* **1987**, 1529.
(17) Demartin, F.; Manassero, M.; Sansoni, M.; Garlaschelli, L.; Sartorelli, U. *J. Organomet. Chem.* **1981**, *204*, C10.
(18) Albano, V. G.; Braga, D.; Ros, R.; Scrivanti, A. *J. Chem. Soc., Chem. Commun.* **1985**, 866.
(19) Pereira, R. M. S.; Fujiwara, F. Y.; Vargas, M. D.; Braga, D.; Grepioni, F. *Organometallics* **1997**, *16*, 4833.
(20) Stuntz, G. F.; Shapley, J. R. *J. Organomet. Chem.* **1981**, *213*, 389.
(21) Bruce, M. I.; Matisons, J. G.; Rodgers, J. R.; Wallis, R. C. *J. Chem. Soc., Chem. Commun.* **1981**, 1070.
(22) Adams, R. D.; Mathur, P.; Segmüller, B. E. *Organometallics* **1983**, *2*, 1258.
(23) Lentz, D.; Marschall, R. *Chem. Ber.* **1991**, *124*, 497.
(24) Ma, A. K.; Einstein, F. W. B.; Johnston, V. J.; Pomeroy, R. K. *Organometallics* **1990**, *9*, 45.
(25) Adams, R. D.; Golembeski, N. M. *J. Am. Chem. Soc.* **1979**, *101*, 2579.
(26) Adams, R. D.; Golembeski, N. M. *Inorg. Chem.* **1979**, *18*, 2255.
(27) Beringhelli, T.; D'Alfonso, G.; Minoja, A.; Ciani, G.; Moret, M.; Sironi, A. *Organometallics* **1991**, *10*, 3131.
(28) Shawkataly, O. b.; Teoh, S.-G.; Fun, H.-K. *J. Organomet. Chem.* **1994**, *464*, C29.
(29) Malatesta, L.; Caglio, G.; Angoletta, M. *J. Chem. Soc., Chem. Commun.* **1970**, 532.
(30) Angoletta, M.; Malatesta, L.; Caglio, G. *J. Organomet. Chem.* **1975**, *94*, 99.
(31) Demartin, F.; Manassero, M.; Sansoni, M.; Garlaschelli, L.; Martinengo, S.; Canziani, F. *J. Chem. Soc., Chem. Commun.* **1980**, 903.
(32) Demartin, F.; Manassero, M.; Sansoni, M.; Garlaschelli, L.; Raimondi, C.; Martinengo, S.; Canziani, F. *J. Chem. Soc., Chem. Commun.* **1981**, 528.
(33) Della Pergola, R.; Cea, F.; Garlaschelli, L.; Masciocchi, N.; Sansoni, M. *J. Chem. Soc., Dalton Trans.* **1994**, 1501.
(34) Della Pergola, R.; Demartin, F.; Garlaschelli, L.; Manassero, M.; Martinengo, S.; Masciocchi, N.; Strumolo, D. *Inorg. Chem.* **1991**, *30*, 846.
(35) Pierpoint, C. G.; Stuntz, C. G.; Shapley, J. R. *J. Am. Chem. Soc.* **1978**, *100*, 616.
(36) Pierpoint, C. G. *Inorg. Chem.* **1979**, *18*, 2972.
(37) Garlaschelli, L.; Martinengo, S.; Bellon, P. L.; Demartin, F.; Manassero, M.; Chiang, M. Y.; Wei, C.-Y.; Bau, R. *J. Am. Chem. Soc.* **1984**, *106*, 6664.
(38) Della Pergola, R.; Garlaschelli, L.; Demartin, F.; Manassero, M.; Masciocchi, N. *J. Organomet. Chem.* **1992**, *436*, 241.

(39) Della Pergola, R.; Demartin, F.; Garlaschelli, L.; Manassero, M.; Martinengo, S.; Sansoni, M. *Inorg. Chem.* **1987**, *26*, 3487.
(40) Della Pergola, R.; Demartin, F.; Garlaschelli, L.; Manassero, M.; Martinengo, S.; Masciocchi, N.; Zanello, P. *Inorg. Chem.* **1993**, *32*, 3670.
(41) Della Pergola, R.; Garlaschelli, L.; Manassero, M.; Masciocchi, N.; Zanello, P. *Angew. Chem. Int. Ed. Engl.* **1993**, *32*, 1347.
(42) Della Pergola, R.; Garlaschelli, L.; Demartin, F.; Manassero, M.; Masciocchi, N.; Sansoni, M.; Fumagelli, A. *J. Chem. Soc, Dalton Trans.* **1989**, 1109.
(43) Fumagelli, A.; Koetzle, T. F.; Fusao, T. *J. Organomet. Chem.* **1981**, *213*, 365.
(44) Ceriotti, A.; Della Pergola, R.; Garlaschelli, L.; Laschi, F.; Manassero, M.; Masciocchi, N.; Sansoni, M.; Zanello, P. *Inorg. Chem.* **1991**, *30*, 3349.
(45) Lee, J.; Humphrey, M. G.; Hockless, D. C. R.; Skelton, B. W.; White, A. H. *Organometalllics* **1993**, *12*, 3468.
(46) Jungbluth, H.; Süss-Fink, G.; Pellinghelli, M.; Tiripicchio, A. *Organometallics* **1990**, *9*, 1670.
(47) Colbran, S. B.; Irele, P. T.; Johnson, B. F. G.; Lahoz, F. J.; Lewis, J.; Raithby, P. R. *J. Chem. Soc., Dalton Trans.* **1989**, 2023.
(48) Corrigan, J. F.; Doherty, S.; Taylor, N. J.; Carty, A. J.; Boroni, E.; Tiripicchio, A. *J. Organomet. Chem.* **1993**, *462*, C24.
(49) Deeming, A. J.; Hardcastle, K. I.; Kabir, S. E. *J. Chem. Soc., Dalton Trans.* **1988**, 827.
(50) Bruce, M. I.; Humphrey, P. A.; Shawkataly, O. b.; Snow, M. R.; Tiekink, E. R. T.; Cullen, W. R. *Organometallics* **1990**, *9*, 2910.
(51) Livotto, F. S.; Raithby, P. R.; Vargas, M. D. *J. Chem. Soc., Dalton Trans.* **1993**, 1797.
(52) Ros, R.; Scrivanti, A.; Albano, V. G.; Braga, D. *J. Chem. Soc., Dalton Trans.* **1986**, 2411.
(53) Lee, J. Honours Thesis, University of New England, Australia 1992.
(54) Orpen, A. G. *J. Chem. Soc., Dalton Trans.* **1980**, 2509.
(55) Shapley, J. R.; Hardwick, S. J.; Foose, D. S.; Stucky, G. D. *J. Am. Chem. Soc.* **1981**, *103*, 7383.
(56) Churchill, M. R.; Hutchinson, J. P. *Inorg. Chem.* **1981**, *20*, 4112.
(57) Churchill, M. R.; Bueno, C.; Hutchinson, J. P. *Inorg. Chem.* **1982**, *21*, 1359.
(58) Churchill, M. R.; Biondi, L. V.; Shapley, J. R.; McAteer, C. H. *J. Organomet. Chem.* **1985**, *280*, C63.
(59) Shapley, J. R.; McAteer, C. H.; Churchill, M. R.; Biondi, L. V. *Organometallics* **1984**, *3*, 1595.
(60) Jeffery, J. C.; Ruiz, M. A.; Stone, F. G. A. *J. Chem. Soc., Dalton Trans.* **1988**, 1131.
(61) Della Pergola, R.; Demartin, F.; Garlaschelli, L.; Manassero, M.; Martinengo, S.; Masciocchi, N.; Sansoni, M. *Organometallics* **1991**, *10*, 2239.
(62) Demartin, F.; Manassero, M.; Sansoni, M.; Garlaschelli, L.; Sartorelli, U.; Tagliabue, F. *J. Organomet. Chem.* **1982**, *234*, C39.
(63) Demartin, F.; Manassero, M.; Sansoni, M.; Garlaschelli, L.; Malatesta, M. C.; Sartorelli, U. *J. Organomet. Chem.* **1983**, *248*, C17.
(64) Demartin, F.; Manassero, M.; Sansoni, M.; Garlaschelli, L.; Raimondi, C.; Martinengo, S. *J. Organomet. Chem.* **1983**, *243*, C10.
(65) Garlaschelli, L.; Malatesta, M. C.; Martinengo, S.; Demartin, F.; Manassero, M.; Sansoni, M. *J. Chem. Soc., Dalton Trans.* **1986**, 777.
(66) Della Pergola, R.; Garlaschelli, L.; Martinengo, S.; Demartin, F.; Manassero, M.; Masciocchi, N. *J. Chem. Soc., Dalton Trans.* **1988**, 2307.
(67) Churchill, M. R.; Bexman, S. A. *Inorg. Chem.* **1974**, *13*, 1418.
(68) Della Pergola, R.; Ceriotti, A.; Garlaschelli, L.; Demartin, F.; Manassero, M.; Masciocchi, N.; Sansoni, M. *Inorg. Chem.* **1993**, *32*, 3277.
(69) Day, V. W.; Klemperer, W. G.; Main, D. J. *Inorg. Chem.* **1990**, *29*, 2345.
(70) Della Pergola, R.; Garlaschelli, L.; Martinengo, S.; Demartin, F.; Manassero, M.; Masciocchi, N.; Bau, R.; Zhao, D. *J. Organomet. Chem.* **1990**, *396*, 385.
(71) Ceriotti, A.; Della Pergola, R.; Demartin, F.; Garlaschelli, L.; Manassero, M.; Masciocchi, N. *Organometallics* **1992**, *11*, 756.
(72) Beringhelli, T.; Ciani, G.; D'Alfonso, G.; Garlaschelli, L.; Moret, M.; Sironi, A. *J. Chem. Soc., Dalton Trans.* **1992**, 1865.
(73) Freeman, M. J.; Miles, A. D.; Murray, M.; Orpen, A. G.; Stone, F. G. A. *Polyhedron* **1984**, *3*, 1093.

(74) Bruce, M. I.; Nicholson, B. K. *J. Organomet. Chem.* **1983**, *252*, 243.
(75) Bruce, M. I.; Nicholson, B. K. *J. Chem. Soc., Chem. Commun.* **1982**, 1141.
(76) Bateman, L. W.; Green, M.; Howard, J. A. K.; Mead, K. A.; Mills, R. M.; Salter, I. D.; Stone, F. G. A.; Woodward, P. *J. Chem. Soc., Chem. Commun.* **1982**, 773.
(77) Howard, J. A. K.; Slater, I. D.; Stone, F. G. A. *Polyhedron* **1984**, *5*, 567.
(78) Wurst, K.; Srähle, J.; Beuter, G.; Dell'Amico, D. B.; Calderazzo, F. *Acta. Chem. Scand.* **1991**, *45*, 844.
(79) Ito, L. N.; Sweet, J. D.; Mueting, A. M.; Pignolet, L. H.; Schoondergang, M. F. J.; Steggerda, J. J. *Inorg. Chem.* **1989**, *28*, 3696.
(80) Holzer, M.; Strähle, J.; Baum, G.; Fenske, D. *Z. anorg. allg. Chem.* **1994**, *620*, 192.
(81) Lewis, J.; Li, C.-K.; Morewood, C. A.; Ramirez de Arellano, M. C.; Raithby, P. R.; Wong, W.-T. *J. Chem. Soc., Dalton Trans.* **1994**, 2159.
(82) Lewis, J.; Morewood, C. A.; Raithby, P. R.; Ramirez de Arellano, M. C. *J. Chem. Soc., Dalton Trans.* **1996**, 4509.
(83) *The Chemistry of Metal Cluster Complexes*; Shriver, D. F.; Kaesz, H. D.; Adams, R. D., Ed.; V.C.H. Publishers: New York, 1990.
(84) Mingos, D. M. P.; Wales, D. J. *Introduction to Cluster Chemistry*; Prentice Hall: Englewood Cliffs, New Jersey, 1990.
(85) Housecroft, C. E.; Rheingold, A. L. *J. Am. Chem. Soc.* **1986**, *108*, 6420.
(86) Housecroft, C. E.; Rheingold, A. L. *Organometallics* **1987**, *6*, 1332.
(87) Chini, P.; Ciani, G.; Martinengo, S.; Sironi, A. *J. Chem. Soc., Chem. Commun.* **1979**, 188.
(88) Frediani, M.; Bianchi, M.; Salvani, A.; Piacenti, F.; Ianelli, S.; Nardelli, M. *J. Chem. Soc., Dalton Trans.* **1990**, 165.
(89) Sunick, D. L.; White, P. S.; Schauer, C. K. *Inorg. Chem.* **1993**, *32*, 5665.
(90) Housecroft, C. E.; Shongwe, M. S.; Rheingold, A. L. *Organometallics* **1989**, *8*, 2651.
(91) Housecroft, C. E.; Shongwe, M. S.; Rheingold, A. L.; Zanello, P. *J. Organomet. Chem.* **1991**, *408*, 7.
(92) O'Neill, M. E.; Wade, K. *Inorg. Chem.* **1982**, *21*, 461.
(93) Sappa, E.; Tiripicchio, A.; Carty, A. J.; Toogood, G. E. *Prog. Inorg. Chem.* **1987**, *35*, 437.
(94) Sappa, E.; Tiripicchio, A.; Braunstein, P. *Chem. Rev.* **1983**, *83*, 203.
(95) Raithby, P. R.; Rosales, M. J. *Adv. Inorg. Chem. Radiochem.* **1985**, *29*, 169.
(96) Carty, A. J. *Pure Appl. Chem.* **1982**, *54*, 113.
(97) Barnes, C. In *Comprehensive Organometallic Chemistry II*; Abel, E. W., Stone, F. G. A., Wilkinson, G., Ed.; Pergamon Press: Oxford, U.K.: 1995; Vol. 8, Chapter 4.
(98) Heveldt, P. F.; Johnson, B. F. G.; Lewis, J.; Raithby, P. R.; Sheldrick, G. M. *J. Chem. Soc., Chem. Commun.* **1978**, 340.
(99) Shapley, J. R.; Humphrey, M. G.; McAteer, C. H. In *Selectivity in Catalysis*; M. Davis and S. Suib, Eds.; ACS: Washington DC, 1993; Vol. 517; p 127.
(100) Lucas, N. T.; Humphrey, M. G.; Healy, P. C.; Williams, M. L. *J. Organomet. Chem.* **1997**, *545*, 519.
(101) Bruce, M. I.; Ke, M.; Low, P. J. *J. Chem. Soc., Chem. Commun.* **1996**, 2405.
(102) Bruce, M. I.; Skelton, B. W.; White, A. H.; Zaitseva, N. N. *J. Chem. Soc., Dalton Trans* **1996**, 3151.
(103) Chi, Y.; Lin, R.-C.; Chen, C.-C.; Peng, S.-M.; Lee, G.-H. *J. Organomet. Chem.* **1992**, *439*, 347.
(104) Keller, E.; Wolters, D. *Chem. Ber.* **1984**, *117*, 1572.
(105) Chetcuti, M. J.; Fanwick, P. E.; Gordon, J. C. *Inorg. Chem.* **1991**, *30*, 4710.
(106) Manna, J.; John, K. D.; Hopkins, M. D. *Adv. Organomet. Chem.* **1995**, *38*, 79.
(107) Bruce, M. I. *Pure Appl. Chem.* **1986**, *58*, 553.
(108) Peng, J.-J.; Horng, K.-M.; Cheng, P.-S.; Chi, Y.; Peng, S.-M.; Lee, G.-M. *Organometallics* **1994**, *13*, 2365.
(109) Chi, Y.; Liu, B.-J.; Lee, G.-H.; Peng, S.-M. *Polyhedron* **1989**, *8*, 2003.
(110) Hwang, D.-K.; Chi, Y.; Peng, S.-M.; Lee, G.-H. *Organometallics* **1990**, *9*, 2709.
(111) Hwang, D.-K.; Chi, Y.; Peng, S.-M.; Lee, G. H. *J. Organomet. Chem.* **1990**, *389*, C7.
(112) Wu, C.-H.; Chi, Y. *J. Chem. Soc., Chem. Commun.* **1990**, 3025.
(113) Hwang, D.-K.; Lin, P.-J.; Chi, Y.; Peng, S.-M.; Lee, G.-H. *J. Chem. Soc., Dalton Trans.* **1991**, 2161.
(114) Chi, Y.; Chuang, S.-H.; Liu, L.-K.; Wen, Y.-S. *Organometallics* **1991**, *10*, 2485.
(115) Chi, Y.; Chung, C.; Chou, Y.-C.; Su, P.-C.; Chiang, S.-J.; Peng, S.-M.; Lee, G.-H. *Organometallics* **1997**, *16*, 1702.

(116) Tseng, W.-C.; Chi, Y.; Su, C.-J.; Carty, A. J.; Peng, S.-M.; Lee, G.-H. *J. Chem. Soc., Dalton Trans.* **1998**, 1053.
(117) Chi, Y.; Hsu, H.-Y.; Peng, S.-M.; Lee, G.-H. *J. Chem. Soc., Chem. Commun.* **1991**, 1023.
(118) Takahashi, S.; Kuroyama, Y.; Sonogashira, K.; Hagihara, N. *Synthesis* **1980**, 627.
(119) Bruce, M. I.; Humphrey, M. G.; Matisons, J. G.; Roy, S. K.; Swincer, A. G. *Aust. J. Chem.* **1984**, *37*, 1955.